

Synthesis, Processing, and Properties of Silicon-Containing Phthalonitrile Resins

William Jacob Monzel

Dissertation submitted to the faculty of the Virginia Polytechnic Institute and State University in partial fulfillment of the requirements for the degree of

Doctor of Philosophy  
In  
Materials Science and Engineering

Guo-Quan Lu  
Gordon T. Yee  
Carlos Suchicital  
Thomas Staley  
Timothy Pruyn

December 10<sup>th</sup>, 2018  
Blacksburg, Virginia

Keywords: Phthalonitrile, Organosilicon, Polymer, High-Temperature, Degradation

Creative Commons, CC BY-NC



# Synthesis, Processing and Properties of Silicon-Containing Phthalonitrile Resins

William Jacob Monzel

## ABSTRACT

Hybrid inorganic-organic resins may provide higher temperature performance in oxidizing environments than their organic counterparts. Phthalonitrile (PN) polymers are excellent candidates for hybridization due to their high thermal stability and glass transition temperatures and their need for improved long-term oxidative stability and toughness. In this work phenyl-substituted organosilicon linkages were incorporated into PN monomers to investigate their effect on the processing, thermo-mechanical properties, and thermal and oxidative stability. Three hybrid silicon-containing phthalonitrile monomers were synthesized incorporating diphenoxydiphenylsilane, tetraphenylsilane, and hexaphenyldisiloxane moieties. Processability of the polymers was highly dependent on catalyst content and an ideal concentration was determined. The impact on glass transition, coefficient of thermal expansion, stability in TGA, and long-term oxidative stability at 250 °C was evaluated. As-synthesized materials performed significantly better than polymers produced from purified monomers. Degradation of the tetraphenylsilane phthalonitrile monomer was examined in detail via IR-TGA and analysis of aged samples. Multiple degradations were identified involving both the organic and hybrid sections of the polymer. Synthesized materials are compared with commercial phthalonitrile reference materials and to other silicon-phthalonitriles in recent literature. Explanations of behavior and suggestions for future improvements are provided.

# Synthesis, Processing and Properties of Silicon-Containing Phthalonitrile Resins

William Jacob Monzel

## GENERAL AUDIENCE ABSTRACT

High temperature plastics and plastic composites are needed for electronics and aerospace components. Phthalonitriles (PNs) are one chemistry that shows promise for these applications. PN materials show excellent stability and strength at high temperatures. In this work, the inclusion of silicon-containing linkages into PN plastics was investigated with the intention of improving the properties and long-term stability in air at high temperatures. Three silicon-containing PN compounds were produced. The processing of un-cured resins was characterized and optimized. Resins were then cured at high temperatures. Each polymer's softening point, thermal expansion, and stability in air and under inert conditions were evaluated. The effect of purity was considered, and it was found that as-produced PN plastics behaved better than highly purified PN plastics. The degradation reactions were studied during long-term exposure to high temperatures and short-term exposure to even higher temperatures. These silicon-containing PN materials were also compared with commercial PN plastics and with other PN literature. Explanations of behavior and suggestions for future improvements are provided.

## Dedication

I dedicate this dissertation to my dog, Winter. He kept me company during much of my PhD but passed away at a young age. Buddy, I'm sorry I was busy working and didn't spend more time with you. You were the best dog.



## Acknowledgements

I would like to thank my advisors Dr. Gordon Yee and Dr. GQ Lu and my committee members: Dr. Thomas Staley, Dr. Carlos Suchicital, and Dr. Tim Pruyn. I would especially like to thank Dr. Pruyn for his assistance in taking TOS data. I would also like to acknowledge the support of the Science, Mathematics and Research for Transformation (SMART) Scholarship for Service Program. Dr. Carla Slebodnick assisted with the X-ray characterization of CSPN. Dr. Kenneth Knott assisted with the NMR characterization. Dr. Kathleen Shugart assisted with SEM/EDS. Andrew Sharits conducted X-Ray CT experiments. Dr. Mehdi Ashraf-Khorassani conducted SFC, LC/MS, and LC/UV experiments. I am also grateful to Dr. Hilmar Koerner, Chris Houser, Thao Gibson, Dr. G.P. Tandon, Dr. Josh Kennedy, Kaitlin Rigitano, Dr. Jeff Baur, Isabella Ulate, and Steven Miller, for their assistance. Lastly, I would like to thank my wonderful wife, Rose Roberts, for her patience and support.

## Table of Contents

ABBREVIATIONS.....	VI
1 INTRODUCTION.....	1
2 BACKGROUND INFORMATION .....	1
2.1 High Temperature Polymers.....	5
2.2 Phthalonitriles .....	37
2.3 Silicon-Containing Polymers .....	59
3 SUMMARY OF DESIGN CONSIDERATIONS AND RESEARCH APPROACH .....	102
3.1 Research Approach .....	105
4 SYNTHETIC PROCEDURES FOR SILICON-CONTAINING PHTHALONITRILE MONOMERS	
109	
4.1 Introduction .....	109
4.2 Experimental .....	109
4.3 Results and Discussion .....	126
4.4 Summary and Conclusions.....	131
5 PROCESSING AND CHARACTERIZATION OF AS-SYNTHESIZED CARBOXYSILANE AND	
CARBOSILANE PHTHALONITRILES.....	132
5.1 Introduction .....	132
5.2 Experimental .....	133
5.3 Results and Discussion .....	135
5.4 Conclusions .....	158
6 PROCESSING AND CHARACTERIZATION OF PURIFIED CSPN AND CSOPN MATERIALS	160
6.1 Introduction .....	160
6.2 Experimental .....	161
6.3 Results and Discussion .....	163
6.4 Summary and Conclusions.....	187
7 LONG-TERM THERMO-OXIDATIVE STABILITY OF PHTHALONITRILE POLYMERS .....	189
7.1 Introduction .....	189
7.2 Experimental .....	190
7.3 Results and Discussion .....	190
7.4 Conclusions .....	202
8 SUMMARY AND CONCLUSIONS.....	204
9 OPPORTUNITIES FOR FUTURE WORK.....	211
10 BIBLIOGRAPHY .....	216
11 APPENDIX A: ANALYSIS OF SYNTHESIZED COMPOUNDS.....	231
11.1 <sup>1</sup> H NMR Spectra .....	231
11.2 Correlation Spectroscopy (COSY) NMR Spectra .....	239
11.3 <sup>13</sup> C NMR Spectra .....	242
11.4 Heteronuclear Single-Quantum Correlation Spectroscopy (HSQC) NMR Spectra...	246
11.5 Heteronuclear Multiple-Bond Correlation Spectroscopy (HMBC) NMR Spectra ....	249
11.6 FTIR Spectra.....	252
11.7 DSC Curves .....	256
11.8 SFC, LCMS and LCUV of COSPN .....	257
12 APPENDIX B: THERMOGRAVIMETRIC DATA.....	260

## List of Abbreviations

Acetone-d <sub>6</sub> : Deuterated acetone	DMA: Dynamic mechanical analysis
AEK-PN: Aromatic ether-ketone based oligomeric phthalonitrile	DMAc: N,N-Dimethylacetamide DMAc: N,N-Dimethylacetamide
AFRL: Air Force Research Laboratory	DMAP: 4-dimethylaminopyridine
APPH: 4-(Aminophenoxy) phthalonitrile	DMSO: Dimethyl sulfoxide
ArC: Aromatic carbon (NMR)	DMSO-d <sub>6</sub> : Deuterated dimethyl sulfoxide
ATF: Advanced Tactical Fighter	DMF: N,N-Dimethylformamide
ATR: Attenuated total reflectance	DMPS: Dimethyldiphenoxysilane
BADCy: Bisphenol A-based dicyanate ester	DPDSO: 4,4'-(1,1,3,3-Tetraphenyldisiloxane-1,3-diyl)diphenol
BAPh: 2,2-Bis[4-(3,4-dicyanophenoxy)phenyl]propane	DPPS: Diphenyldiphenoxysilane
BMI: Bismaleimide	DPSDP: 4,4'-(Diphenylsilanediyl)diphenol
BODPS: Bis(4-(benzyloxy)phenyl)diphenylsilane	DSC: Differential scanning calorimetry
BODSO: 1,3-Bis(4-(benzyloxy)phenyl)-1,1,3,3-tetraphenyldisiloxane	EDS: Energy dispersive spectroscopy
BOPOP: 4-(4-(Benzyloxy)phenoxy)phthalonitrile	FTIR: Fourier transform infrared spectroscopy
BTDA: 3,3',4,4'-Tetracarboxylic dianhydride	G <sup>''</sup> : Loss modulus
CDCl <sub>3</sub> : Deuterated chloroform	G <sup>'</sup> : Storage modulus
CHCl <sub>3</sub> : Chloroform	H <sub>2</sub> SO <sub>4</sub> : Sulfuric acid
COSPN: Carboxysilane phthalonitrile, 4,4'-(((Diphenylsilanediyl)bis(oxy))bis(4,1-phenylene))bis(oxy)diphthalonitrile	HCl: Hydrochloric acid
COSY: Correlation spectroscopy	HOPOP: 4-(4-Hydroxyphenoxy)phthalonitrile
CSOPN: Carbsiloxane phthalonitrile, 4,4'-(((1,1,3,3-Tetraphenyldisiloxane-1,3-diyl)bis(4,1-phenylene))bis(oxy))diphthalonitrile	HPLC: High pressure liquid chromatography
CSPN: Carbsilane phthalonitrile, 4,4'-(((Diphenylsilanediyl)bis(4,1-phenylene))bis(oxy))diphthalonitrile	HSCT: High-Speed Civil Transport
CTE: Coefficient of thermal expansion	HSQC: Heteronuclear multiple-bond correlation spectroscopy
Cu(AcAc)/TsOH: Cu(II) acetylacetonate (Cu(AcAc))/p-toluenesulfonic acid	HSQC: Heteronuclear single-quantum correlation spectroscopy
d: Doublet (NMR)	HT: High temperature
DCM: Dichloromethane	K <sub>2</sub> CO <sub>3</sub> : Potassium carbonate
dd: Doublet of doublets (NMR)	m: Multiplet (NMR)

<i>m</i> -APB: 1,3-Bis(3-Aminophenoxy) benzene	PTFE: Polytetrafluoroethene
<i>m</i> -BAPS: bis[4-(3-Aminophenoxy) phenyl]sulfone	RTM: Resin transfer molding
MDA: 4,4'-Methylenedianiline	s: Singlet (NMR)
MgSO <sub>4</sub> : Magnesium sulfate	<i>n</i> -BuLi: <i>n</i> -Butyllithium
mp: Melting Point	NMP: N-Methyl-2-pyrrolidinone
MPPS: Methylphenyldiphenoxysilane	SEM: Scanning electron microscopy
NaOH: Sodium hydroxide	SFC: Supercritical fluid chromatography
NMR: Nuclear magnetic resonance spectroscopy	SiC: Silicon carbide
ODA: 4,4'-Diaminodiphenyl ether	SiMCy: Methylphenyl silicon-containing cyanate ester
OPDA: 4,4'-Oxidiphtalic anhydride	SiO <sub>2</sub> : Silicon dioxide, silica
<i>p</i> -BAPS: bis[4-(4-Aminophenoxy) phenyl]-sulfone	T <sub>10%</sub> : Temperature at 10% weight loss
PDMS: Polydimethylsiloxane	T <sub>5%</sub> : Temperature at 10% weight loss
PDPS: Polydiphenylsiloxane	Tan (δ): Loss tangent
PEA: 3-(Phenylethynyl)aniline	TDPE: 1,1,1-tris-[4-(3,4-dicyanophenoxy)phenyl]ethane
PEEK: Polyetheretherketone	TEA: Triethylamine
PEK: Polyetherketone	T <sub>g</sub> : Glass transition temperature
PEN: Poly(arylene ether) nitrile	TGA: Thermogravimetric analysis
PEPA: 4-(Phenylethynyl)phthalic anhydride	T <sub>hd</sub> : Heat deflection temperature
PET: Phenylethynyl-terminated	THF: Tetrahydrofuran
PETI: Phenylethynyl terminated imide	TLC: Thin layer chromatography
Ph: Phenyl	TMA: Thermomechanical analysis
PI: Polyimide	TMPS: Poly(tetramethyl-silphenylene-siloxane)
PIS: Polyimide-siloxane	TOF: Time of flight
PMC: Polymer matrix composite	TOS: Thermo-oxidative stability
PMPS: Polymethylphenylsiloxane	TPPS: Poly(tetraphenyl-p-silphenylene-siloxane)
PMPS-M: Polymethylphenylsiloxane containing methacryloyl groups	UPLC/MS: Ultra-performance liquid chromatography/ mass spec
PN: Phthalonitrile	UPLC/UV: Ultra-performance liquid chromatography/ ultraviolet spectroscopy
POSS: Polyoctahedral silsesquioxane	

## 1 Introduction

The inclusion of organosilicon moieties into phthalonitrile resins may provide a feasible route to maintaining processing characteristics while improving thermo-oxidative stability for high temperature applications.

Since the onset of research into high temperature polymers in the 1950's, work has been governed by technological need, economic opportunity, and academic pursuit. Today, high temperature materials are a small but critical class of polymers, present in many applications that touch our daily lives. Applications for thermally and environmentally stable polymers include: 1) aerospace composites 2) electronics and microelectronics. 3) space applications 4) optoelectronics and other optical applications 5) structural reinforcements, 6) automotive parts including composites for high performance vehicles, brake pads binders, and filters, 7) other filters and membranes 8) structural and insulating foams, 9) fire resistant materials, 11) tooling, 12) moldings, 13) coatings, 14) gaskets, sealants, tubing, and pipes, and 15) components for the energy sector including geothermal, nuclear, and petroleum systems.<sup>1-9</sup>

Specifically, in this work, motivation is derived from aerospace composites and wide band-gap power modules. For aerospace composites, polymer matrix materials are needed for long-term use above 300 °C. High temperature polymers and polymer composites are required for advancement of supersonic and hypersonic aircraft as well as subsonic civilian transport.<sup>10</sup> Replacement of metal structures with polymer composites results in valuable weight savings, and in turn improvements in performance and fuel efficiency.<sup>11</sup> Similarly, polymer encapsulation compounds are an enabling technology for wide band-gap power modules for use above 250 °C. Such devices promise improved thermal and mechanical durability, lower power losses, higher switching speeds and current densities, increased durability and reliability, greater resistance to ionizing radiation, and reduced weight.<sup>12-14</sup> The operating temperatures for both applications are well above the useful range for other polymers including silicones and epoxies.

In polymers, continuous exposure at elevated temperatures or intermittent exposure to extreme temperatures results in chemical and physical aging and decomposition. Mass loss, volume shrinkage, cracking, discoloration, and a degradation of thermo-mechanical and mechanical properties can occur.<sup>10</sup> High temperature polymers must be able to resist degradation of their

properties during operation in extreme environments with long exposure times, cyclic heating, and intense temperature spikes.

Many different chemistries have been evaluated and developed including polyimides, bismaleimides, phenolics and benzoxazines, fluorinated polymers, poly(arylene ethers), cyanate esters, and phthalonitriles. However, opportunities for improvement exist as applications demand greater temperature capabilities and improved processing. Resins are sought with reduced cost, good solubility in common solvents, low softening temperatures, stable and easily controllable melt viscosities, large processing windows, lower cure temperatures, and minimal volatile evolution. For processed polymers, even greater thermal and oxidative stability, higher glass transition temperatures, improved toughness, excellent mechanical strength and modulus, and improved retention of mechanical properties at elevated temperatures are desired. A greater understanding of degradation and aging mechanisms is also needed.<sup>10</sup>

One resin system currently growing in popularity is phthalonitriles (PNs). PN based resins show great promise for high temperature applications and easier processing. Research into phthalonitrile polymers began in earnest at the U.S. Naval Research Lab in the 1980's. Phthalonitrile monomers possess low melt viscosities and are soluble in many common solvents. Curing occurs at elevated temperatures with the addition of a catalyst, usually a thermally stable aromatic amine. The curing reaction progresses by addition polymerization via the phthalonitrile cyano groups and does not produce volatile by-products, facilitating the fabrication of dense components.<sup>15</sup> State-of-the-art cured resins possess high flammability resistance, excellent mechanical and dielectric properties, and low water absorption.<sup>9, 16-19</sup>

Although these materials show exceptional thermal and oxidative stability in thermogravimetric experiments and during hours of exposure at temperatures between 250-400 °C,<sup>6, 9, 20-28</sup> their long-term thermo-oxidative stability requires improvement to meet the challenging demands of the extreme applications. During longer exposures to air at high temperatures, many phthalonitrile polymers experience significant weight losses, volume shrinkage and cracking.<sup>4, 19, 22-23, 26, 29</sup> Furthermore, oxidative aging studies of durations longer than 48 hours and subsequent analysis of degradation regions, are rarely reported in phthalonitrile literature. Such experiments are critical in gaining an understanding of material degradation modes and behavior in service.

The incorporation of inorganic groups into the organic monomer backbone of polymers often provides a viable route for improved stability and toughness during service at high temperatures in oxidizing environments.<sup>22, 30</sup> The inclusion of silicon moieties has been reported to improve oxidative stability and flammability of high temperature polymers including cyanate ester,<sup>31-33</sup> and polyimide systems.<sup>34-44</sup> As oxygen and free radicals cleave carbon-silicon bonds, siloxy units are formed. These siloxy moieties may interact to produce the inert phase SiO<sub>2</sub>. In this case, a silica-rich surface layer forms. This layer can act as a barrier, reducing the rates of degradation of the surface and oxygen diffusion into the bulk.<sup>45-49</sup>

Thus, it is of interest to evaluate the effects of the inclusion of silicon-containing linkages on the properties of high temperature polymers, including phthalonitriles. Phthalonitriles are good candidates for hybridization with organosilicon moieties due to their ease of processing and high glass transition temperatures.<sup>3-8, 15</sup> Prior to beginning investigations for this dissertation, little research existed on silicon-containing phthalonitrile resins. However, in the last few years several groups have produced and characterized silicon-containing phthalonitrile compounds. Examples include silane,<sup>50</sup> silazane,<sup>51</sup> oxysilane,<sup>30, 52</sup> siloxane,<sup>6, 53</sup> and silsesquioxane moieties.<sup>54</sup> Additional groups have synthesized silicon-containing phthalonitrile compounds but did not report their properties as neat phthalonitrile resins.<sup>55-57</sup> While the silicon-phthalonitrile materials synthesized by these groups exhibited high thermal and thermo-oxidative stability in short-term thermogravimetric experiments, emphasis was generally placed on developing resins with low softening points and long-term stability was not characterized.

Design of hybrid organic-inorganic polymers is not a trivial matter however. Inclusion of organosilicon moieties does not in itself guarantee improvements. Literature suggests there are a number of design considerations to keep in mind to achieve desirable properties. For example, avoiding the use of benzylic or methylene bridges, the presence of phenyl functional groups on the silicon, and limiting the length of silicon-containing linkages are a few approaches reported to achieve higher glass transitions and thermo-oxidative stabilities.

The purpose of this work is to investigate the processing, properties, and degradations of the silicon-containing phthalonitrile resins for high temperature applications. Background is provided on relevant properties and measurement techniques, high temperature polymers in general, phthalonitriles, and several classes of organosilicon polymers. While a plethora of similar

compounds to those discussed in this dissertation have been synthesized and evaluated in literature for other purposes, focus here is placed primarily on high temperature applications. Thus, this work is not intended to be comprehensive of all related compounds and chemistries. In addition, focus was placed on silane, oxysilane, and siloxane chemistries. While polymers containing poly octahedral silsesquioxane (POSS) or silazane (Si-N) linkages are discussed briefly, they are mostly outside the scope of this work. A thorough investigation of various chemical synthesis techniques is also not included, though some information is provided for phthalonitriles and polyimides.

Based on available literature, three monomer structures were selected containing carboxysilane (C-O-Si-O-C), carbosilane (C-Si-C), and carbosiloxane linkages (C-Si-O-Si-C). The processing and properties of these silicon-containing phthalonitriles were evaluated. While similar compounds with diphenyl-substitution have been recently investigated in literature the three monomers considered in this manuscript have not been investigated.<sup>30, 51-52</sup> Furthermore, this manuscript addresses the complex degradation mechanisms of silicon-containing phthalonitriles. It also includes information not often reported for phthalonitrile resins, such as coefficient of thermal expansion and long-term (~4000 hour) oxidative aging behavior. Synthetic routes were developed, and the monomers and their precursors were synthesized in high yields. Compounds were analyzed by nuclear magnetic resonance spectroscopy, Fourier transform infrared spectroscopy, elemental analysis, X-ray crystallography, and differential scanning calorimetry. The monomers were mixed with a catalytic amount of bis(4-(4-aminophenoxy)phenyl)sulfone. The pre-polymer mixtures were analyzed by differential scanning calorimetry and parallel plate rheology. The effect of purity and catalyst content were considered. The resins were cured to 350-375 °C under nitrogen. Cured polymer samples were characterized by acoustic density scans, Fourier transform infrared spectroscopy, differential scanning calorimetry, thermo-mechanical analysis, dynamic mechanical analysis, thermogravimetric analysis, infrared spectroscopy-thermogravimetric analysis, and an oxidative aging study. Glass transitions, coefficients of thermal expansion, and degradations in air and nitrogen are reported. After exposure to air for 5000 hours at 250 °C, aged carbosilane-phthalonitrile samples were removed and analyzed by optical microscopy, energy dispersive spectroscopy, Fourier transform infrared spectroscopy, Knoop hardness measurements, and X-ray micro-computed tomography. Four zones of degradation were identified. Chemical and physical changes were observed providing insight into degradation routes.

## 2 Background Information

### 2.1 High Temperature Polymers

In this section background information is provided on polymers for high temperature use, including a brief history of these materials, relevant properties and measurement techniques, specific polymer chemistries, design considerations, and commercial applications. Good reviews of high temperature polymers are provided by Hergenrother<sup>1</sup> (updated by Connell<sup>2</sup>), Lau<sup>58</sup>, and Tant et al.<sup>10</sup> Hergenrother<sup>1</sup> defines high temperature polymers as fitting the following criteria: 5 % weight loss in thermogravimetric analysis at temperatures higher than 450 °C, little weight loss (0.5 wt.%/hour) at temperatures above 450 °C, glass transition temperatures above 200 °C, heat deflection temperatures above 177 °C (10 % deflection at 1.52 MPa of load), retention and stability of properties at greater than 10,000 hours at 177 °C, and possessing adequate properties above 177 °C. Most of the materials discussed in this manuscript meet the majority of these criteria.

#### 2.1.1 Brief History of High Temperature Polymers

While some materials had been investigated prior, high temperature polymer research began in earnest in the 1950's, just after the Second World War. New materials were required for electronics and aerospace applications due to significant growth in those industries as well as the beginning of the Space Race and the Cold War.<sup>1, 58</sup> Over the next four decades, sporadic funding dictated ups and downs in the intensity of research. Many materials were investigated and developed that had outstanding properties at high temperatures, resistance to solvents and other chemicals, UV and radiation resistance, and excellent dielectric properties.<sup>58</sup> However, very few found commercial success. This was due to the difficulty and thus higher cost of processing, higher cost of feedstock materials and resins, and unstable and niche market. Some companies were successful in bringing their materials to market and overcoming the difficulties of higher temperature processing, component fabrication, and cost. Currently a sizable demand exists for these materials.<sup>58</sup>

In the 1960's a considerable amount of progress was made. Many high temperature polymers containing heterocyclic moieties were produced. At first, research focused on thermal stability with little regard to processing characteristics or mechanical properties.<sup>1</sup> Polysulfone, one of the first commercial poly(arylene ether) polymers, was introduced during this time period. The beginning of the 1960's also saw focus and subsequent development of polybenzimidazole. While polybenzimidazoles never found substantial commercial success, the research enabled

development of other polymers that cure by heterocyclic ring formation.<sup>1</sup> The most commercially successful class of high temperature polymers, polyimides, were developed and marketed by E. I. du Pont de Nemours and Company (DuPont) during this decade.<sup>58</sup> Among these materials was the polyimide film, Kapton<sup>TM</sup>. Since its introduction, it has retained the largest market value of any high temperature polymer material. Other polyimides were also introduced by Dupont and Monsanto for polymer composites, molding materials, and wire enamel.

In the 1970's several advances were made. Thermosetting polyimide polymers were developed at NASA Lewis Research Center. A thermoplastic polyimide, Ultem<sup>TM</sup> was first produced by General Electric. Polybenzoxazoles, and other various rigid-rod polymers were produced by the Air Force Research Laboratory at Wright Patterson and then further developed by Dow Chemical. A nadic endcapped polyimide, called PMR-15 was developed at NASA Glenn Research Center. For many years PMR-15 remained the standard material for use at temperatures greater than 250 °C. Additional materials emerged such as bismaleimides, a polyamide-imide produced by Amoco called Torlon<sup>TM</sup>, and poly (arylene ethers) including polyetherketone (PEK), polyetheretherketone (PEEK), and a polyphenylsulfone called Radel<sup>TM</sup>.<sup>1</sup>

Research focused on processing in the 1980's. Polymers were modified, and processes were developed to produce foams, ribbons, fibers, moldings, composites, and adhesives. Only a few new materials were produced, usually for specific applications for aerospace components, separation processes, and microelectronics. Ube Industries Ltd. introduced polyimide films under the tradename Upilex<sup>TM</sup>. These biaxially oriented films possessed low coefficients of thermal expansion and exceedingly high mechanical properties. Several programs, including the Advanced Tactical Fighter (ATF) program run by the Air Force, and NASA's High-Speed Civil Transport (HSCT) initiative, demanded extensive utilization of high temperature composites and adhesives. These materials needed to withstand temperatures above 371 °C for short periods of time.<sup>58</sup> Polymers were optimized for compression molding into high performing structural components capable of withstanding these conditions. Specifically, polyimides oligomers and other heterocyclic materials were endcapped with phenylethynyl groups.<sup>1</sup>

In the 1990's polybenzoxazoles were commercialized by Toyobo. Also around this time, concern arose over the health and environmental hazards of the diamine used in PMR-15, 4,4'-methylenedianiline (MDA). Due to its carcinogenic effects, research focused on finding

replacement diamines and several polyimide materials were produced including RP-46, and a series of resins by Maverick Corp. Work also continued on the High-Speed Civil Transport (HSCT) initiative, with the goal of developing civilian aircraft capable of Mach 2.4. Significant technology was developed in support of this program, including a phenylethynyl-terminated imide, PETI-5. However the HSCT was cancelled in 1999, and with it the work on PETI-5 was abandoned.<sup>1</sup>

Since the year 2000, work has continued on phenylethynyl terminated imide (PETI) systems with support of jet aircraft engine manufacturers, the Air Force, and NASA. Work has also continued on other polyimides, phthalonitriles, cyanate esters, benzoxazines, bismaleimides, and polyetherimides. At the recent 2017 High Temperature Polymeric Laminate Workshop focus was placed on inorganic and hybrid organic-inorganic resins with improved oxidative stability. Processing has also been a primary focus, and resins have been optimized for out-of-autoclave methods, such as resin transfer molding (RTM). These processes offer significant reduction in production cost of composite parts. This is due to the decreased energy use and emissions, shorter processing times, lower cost of tooling, effective elimination of volatiles, smooth part faces, versatility, and precision of dimensional tolerances.<sup>58</sup> Materials are also being evaluated and formulated for new processes such as additive manufacturing. The thermoplastic arylene ethers have been the first high temperature resins developed for additive processes to see commercial success.

In general, the quest continues for materials with ever higher thermal and oxidative stability and excellent high temperature mechanical properties, while maintaining or improving processing characteristics. Resins are being developed which target low monomer softening points, stable and controllable viscosities, good solubilities of monomers and oligomers, wide processing windows, lower cure temperatures, and low volatile evolution.

### **2.1.2 Relevant Properties and Experimental Techniques**

This section covers properties of interest for high temperature polymers and the commonly used methods of measuring these properties. The section is broken into two subsections. Monomer Processing, Properties, and Characterization deals with characterizations on feedstock materials including precursors, monomers, and oligomers. The following subsection, Polymer Properties and Characterizations focuses on properties of polymer materials after processing. Short-term and

long-term characterization of thermal and oxidative stability is considered. Thermo-mechanical properties including glass transitions, melting points, and heat deflection temperatures are also discussed. Mechanical experiments including dynamic bending, tensile, shear, and compression tests, as well as static creep tests are not directly discussed but are also commonly used to measure the properties of these materials at elevated or room temperature.

#### *2.1.2.1 Monomer Processing, Properties, and Characterizations*

Synthesized feedstock materials, including monomers and oligomers, are commonly characterized by nuclear magnetic resonance spectroscopy (NMR), Fourier transform infrared spectroscopy (FTIR), elemental analysis, mass spectroscopy, chromatography techniques, and melting point measurements. These methods are used to confirm the identity and purity of the material. Elemental analysis provides quantitative information on mass fractions of various elements including carbon, nitrogen, and hydrogen. NMR provides spectra corresponding to the atomic resonances ( $^1\text{H}$ ,  $^{13}\text{C}$ ,  $^{29}\text{Si}$  etc.) of the compound in deuterated solvents. The technique may be used to identify chemical groups and specific compounds as well as estimate purity. FTIR looks at the infrared absorption leading to vibrational excitations. Characteristic absorption peaks in the IR spectrum may relate to known bond deformations.

Melting observations may also be used to determine purity and confirm synthesis of a compound of known melting point. Pure crystalline compounds exhibit sharp endothermic melting peaks, whereas impure samples show smaller, broader, and less symmetric transitions. The melting point of a material may be measured using a melting point apparatus where a small sample is heated in a glass tube until melting. Differential scanning calorimetry (DSC) is also used. DSC measures temperature and heat flow to or from a sample and a reference while controlling the heating rate. In addition to endothermic melting points, glass transitions, crystallizations, exothermic polymerizations, and degradations may be evident in the plot of heat flow (or heat capacity) vs. temperature.<sup>59-60</sup> A more in-depth discussion of DSC and melting points and glass transitions is included in the following section, Polymer Properties and Characterizations.

The melting points, glass transitions, and minimum viscosities of feedstock materials (monomers, oligomers, and prepolymers) and their curing rates at different temperatures are critical to effective processing of the material. These properties determine which methods are well-suited and the required processing parameters including temperature, pressure, and time steps. For

example, melt viscosities of less than 10 Pa·s are important for resin infusion processes and other non-autoclave methods. Furthermore, mold filling requirements often demand melt viscosities to be stable for several hours at the processing temperature, which is often greater than 280 °C. The processing window is dictated by resin chemistry. Temperatures must be high enough to achieve the desired viscosity and curing rate, but low enough that the mold has time to fill before curing and to ensure degradation does not occur.<sup>58</sup> Parallel plate rheology, conducted in a temperature ramp, provides information on softening temperatures, minimum viscosity, and temperatures where viscosity increases from curing reactions. The temperature range between the softening point and curing temperatures defines a processing window. Isothermal rheometric tests provide data on the stability of viscosity at a given temperature. The pot life is defined as the time it takes for the viscosity to increase out of a workable range at this temperature. Since pre-polymer stability during high temperature processing is important,<sup>1</sup> thermogravimetric analysis (TGA) is often performed in addition to melt stability experiments. TGA is discussed in more detail in the following section.

#### *2.1.2.2 Polymer Properties and Characterizations*

High temperature polymers are commonly evaluated for retention of mechanical properties at high temperatures, resistance to moisture, solvents, acids, and bases, and of course short-term and long-term thermal and oxidative stability. Glass transitions, melting points, and heat deflection temperatures are measured and reported. Direct measurements of mechanical properties (elastic modulus, yield stress, strain etc.) at high temperatures are also commonly conducted. Thermal behavior is commonly analyzed by dynamic thermogravimetric analysis (TGA), differential scanning calorimetry (DSC), dynamic mechanical analysis (DMA), and thermomechanical analysis (TMA).

While colloquially, the term thermal stability concerns the general ability to withstand high temperatures, specifically it refers to ability to resist degradation under specific temperature conditions in inert environments. Thermo-oxidative or oxidative stability thus specifically covers resistance to degradation in oxidizing environments. The term heat resistance is also sometimes used to define circumstances where a material is unable to meet a certain criteria.

Dynamic TGA measures the weight loss of the sample as the temperature is increased. Temperatures corresponding to 5 and 10 % weight loss ( $T_{5\%}$  and  $T_{10\%}$ ) are commonly reported, as

is residual weight at 800-1000 °C.<sup>1</sup> Derivative weight loss curves are used to show mass loss peaks corresponding to one or more decomposition reactions. Initial and maximum decomposition temperatures, determined from the derivative curves, are also reported. Several experimental variables are important and significantly affect results. Tests may be conducted in an oxidizing or inert atmosphere. The form of the sample, and thus its surface area, also matters. Powders show lower oxidative stability than bulk pieces. The sample's processing and thermal history is also important. For example, the presence of solvents or absorbed moisture contributes to weight loss. Ramp rates and gas flow rates should be reported since the rate and location of degradations depends on these variables. Faster ramp rates result in higher  $T_{5\%}$  and  $T_{10\%}$  values. Higher flow rates also result in faster removal of volatile species and, in air, faster oxidation. A ramp rate of around 10 °C/min is commonly used for TGA. If multiple tests are run with different ramp rates, the activation energy for a given reaction may be calculated following the Ozawa theory. Arrhenius plots are constructed with the axes  $\log(\text{heating rate})$  vs  $1/\text{temperature}$ . Lines of constant weight % loss are plotted, their slope providing an activation energy.<sup>61</sup>

These tests may show the evolution of volatile compounds at specific temperatures or the gain of weight through oxidation. Reactions that do not affect the weight of the polymer, such as some rearrangement reactions, are not directly evident in TGA results but may affect the resulting stability of the compound. Reactions that occur at slower rates will be also be less evident than reactions that occur at faster rates, even if the slower reaction dominates at a specific temperature. FTIR or other spectroscopic techniques may be used in conjunction with TGA to provide information on chemical reactions, changes in structure, and degradation mechanisms, including oxidation. Analysis may be conducted of the residue or the volatile products. In air at high temperatures, FTIR analysis of volatiles is limited since many small molecules will continue to combust and decompose prior to reaching the IR detector.

TGA tests provide good indications of the behavior of polymers for short-term thermal exposure. However, during extended exposure to high temperatures, degradation and transitions occur at much lower temperatures and kinetically slow reactions become more evident. Chemical and physical aging processes occur. Chemical aging corresponds to changes in the polymer composition, including molecular weight and extent of crosslinking. This involves reactions forming or breaking chemical bonds. In addition to thermal exposure, these reactions may be

catalyzed by humidity, UV exposure, radiation, chemical exposure, stress, and other environmental effects.<sup>10</sup> Physical aging corresponds to non-chemical, structural changes due to the amorphous polymer not being in an equilibrium state. An increase in density occurs and the mobility of molecules decreases. Physical aging generally increases the glass transition temperature, and mechanical strength and modulus at high temperatures. At room temperature toughness, elastic modulus, and mechanical strength may decrease.<sup>10</sup>

Thus, if the material will see high service temperatures for long durations, short-term or accelerated tests may not provide accurate data. For long-term stability and behavior, isothermal TGA or extended aging studies are required to properly evaluate the polymers behavior during or after extended exposure to high temperatures. During extended aging tests, samples are exposed to harsh conditions for long periods of time. Volume and mass of the samples is often tracked. Weight loss does not necessarily correlate directly to a loss of mechanical properties but is often a good indicator. Polymer samples that have undergone more than 5% weight loss, likely have significantly reduced mechanical properties. However, this is not always the case, especially for some composites due to surface erosion, or polymers that are still undergoing curing reactions. Mechanical properties and other characteristics may be tested at temperature, or after the test at room temperature. Room temperature property measurements show evidence of permanent changes in the material from thermal aging, but of course do not quantify the behavior at high temperature. For the most accurate predictions of behavior, aging conditions should be selected to mimic expected service conditions. Increasing the temperature, atmospheric pressures, or mechanical stresses, or incorporating cyclic loading or temperature cycling, usually result in accelerated tests. Yet these conditions also likely change the rates of various degradations and may not provide the same results.<sup>1</sup>

Oxidatively aged samples may be analyzed by a variety of methods to identify degradation zones and local chemical and mechanical properties. Degradation of polymers and their composites generally begins at the exposed surfaces. Regions of high stress may also experience higher degradation rates. An oxidized surface layer forms. Oxygen is used up by reacting species, limiting the diffusion of oxygen into the bulk. The degradation layer grows as reacting species are consumed and oxygen continues to diffuse into the material. With increasing degradation, porosity and cracks form in the oxidized region. Cracks generally form from the surface and act as pathways

for oxygen diffusion into the bulk. A highly connected network of cracks eventually forms throughout the material. Various models exist to predict different aspects of oxidation behavior. These models make use of empirical Arrhenius rate curves, chemical degradation mechanisms combined with oxygen diffusion, laminated plate theory and micromechanics, or finite element models with regions of differing properties.<sup>10</sup> One such approach, a three-zone thermo-oxidative degradation model, is discussed by Tandon et al.<sup>62</sup> The model describes three regions commonly observed in degraded polymer samples. Zone 1 corresponds to a fully oxidized surface region. Oxidation and degradation reactions are completed, leaving a residual char layer. This zone accounts for the bulk of the mass loss of the sample. Zone 2 corresponds to an active region. In this zone oxygen has diffused into the material and reacted with the polymer and its degradation products. Cleavage and oxidation of the chain or functional groups as well as crosslinking mechanisms occur in this region. Zone 3 corresponds to an unoxidized bulk of the material. The polymer may still experience thermal degradation and physical or chemical aging in this region. Analysis of the thickness of these zones and their chemical compositions can provide insight into degradation mechanisms.

In addition to thermal and oxidative stability, the mechanical and thermo-mechanical properties are also of paramount importance. Glass transitions, melting points, and heat deflection temperatures indicate where the ability to support mechanical load is reduced. Other properties also change drastically around glass and melting transitions. For example, in addition to a loss of mechanical strength, glass transition and melting points also correlate with expansion and changes in thermal expansion coefficient. High tensile strength and high interfacial strength are required to resist thermal stresses and support loads. The elastic modulus and thermal expansion coefficient determine the magnitude of these thermal stresses. If cracks or delamination occur at high temperature the part may fail. For this reason, electronic encapsulants often require low stiffness and/or matched thermal expansion. In addition, resistance to other environmental factors is required. Polymers should have low moisture uptake and high solvent resistance when fully cured.

The glass transition is a kinetic or non-equilibrium transition that corresponds to a change in the molecular mobility of a polymer's amorphous regions. Below the glass transition temperature ( $T_g$ ), the material behaves like a glassy solid. The molecules in this range have limited mobility. Above this temperature the molecules are able to move more freely and the material exhibits

rubbery, elastomeric characteristics.<sup>59</sup> A decrease in density with an increase in free volume and kinetic energy is observed. Cooling from a melted or rubbery state to a glassy one, through a glass transition is defined as vitrification, whereas devitrification corresponds to crystallization from an amorphous state.<sup>10</sup>

While well-defined monomers may display precise and distinct amorphous transitions, the polydispersity (distribution of molecular weight) and overall length of polymer chains results in less defined and broader glass, crystallization, and melting transitions. These transitions depend on thermal history and a number of other factors.<sup>10</sup> The magnitude of modulus change during a glass transition is strongly effected by residual stresses, and the amount of crosslinking and crystallinity.<sup>59</sup> Highly crosslinked or highly crystalline materials may show only minor decreases in modulus at the glass transition temperature. However, the modulus and strength of less crosslinked and more amorphous materials may decrease by orders of magnitude at the glass transition temperature.<sup>10</sup> Since the glass transition does not correspond to chemical changes, the transition is reversible.<sup>1</sup> However, creep and other plastic deformations may occur due to the polymers increased mobility and inability to support load. Thus, viscous flow and irreversible shape changes occur under applied stress.<sup>63</sup> The loss of mechanical properties at the  $T_g$  is critical for many applications. Some load may be sustained by crystalline phases above the  $T_g$ . Melting of these crystalline regions, then coincides with a substantial drop in modulus and strength.<sup>1, 10</sup>

As mentioned previously, the value  $T_g$  is also increased by physical aging. The extent of physical aging is also affected by the proximity of the aging temperature to the  $T_g$ . When aging below the glass transition temperature, the mobility of polymer chains is reduced. However, motion still occurs as the molecules approach a more thermodynamically stable equilibrium state corresponding to greater packing density.<sup>10</sup> The rate of this motion increases as temperature is increased to the  $T_g$  and above. Thus, polymers with a higher  $T_g$  tend to experience slower physical aging at a given temperature. This is important since physical aging results in a decreased toughness of the material, which may be a significant problem, depending on application. However, polymers with lower  $T_g$  may also show increased toughness and dampening effect in the short-term.<sup>10</sup>

Melting corresponds to liquification of crystalline regions. Whereas the glass transition is an approximately second-order phase transition, melting is a first-order phase transition. Since

polymers are often comprised of amorphous and crystalline regions, they can exhibit both a melting point and a glass transition. Phase separated materials or block copolymers with blocks of significant length can exhibit multiple glass transitions. The melting point, if present, is generally observed above the glass transition temperature. For most polymers glass transitions and melting points occur below degradation. However, for highly crosslinked materials such as phthalonitrile polymers and some polyimides this may not be the case.<sup>10</sup>

Another characterization of interest is a material's heat deflection temperature ( $T_{hd}$ ), which depends on the glass and melting transitions but is not directly equivalent to them. The  $T_{hd}$  is not a fundamental material property but instead a measured engineering metric. Test parameters are defined by ASTM D 648 and ISO 75 standards. A load is applied to the sample, usually in three-point bending mode. The temperature is increased at a specified rate. The  $T_{hd}$  corresponds to the temperature at which a deflection of 0.25 mm occurs. Since creep occurs at these temperatures, ramp rate is highly important.<sup>10</sup>

Measurements of the glass transition and other thermo-mechanical properties may be conducted by DMA, TMA, and DSC methods. Since these methods use different approaches to measure the glass transition, slightly different values of  $T_g$  are observed. In addition to parameters discussed in the following paragraphs, heating rate and the thermal history of the sample are important for all of these methods. Measurements of the  $T_g$  are affected by these and other experimental variables and thus a universal, precise value of  $T_g$  does not exist for any given material.<sup>1</sup>

For highly crosslinked, high temperature materials specifically, DMA is usually the most accurate method of measuring the glass transition, since transitions may become less evident in TMA or DSC. However, these methods are also commonly reported. DMA studies the stress-strain relationships of the polymer as a function of temperature and frequency. Molecular relaxations including glass transitions and other transformations are visible. The test may be conducted in torsion, tension, or three-point bending. Cyclic loading is applied with a specified frequency. The displacement is recorded and the storage modulus ( $G'$ ), loss modulus ( $G''$ ), and loss tangent ( $\tan \delta$ ) are calculated. The sample dimensions, frequency of loading, and magnitude of load are important parameters. The frequency is especially important since chain motion and rotation are time-dependent.<sup>1</sup> The glass transition may be taken as the onset of decrease of  $G'$  or the peak of  $G''$  or  $\tan \delta$ . Generally speaking, the  $T_g$  from  $G'$  is less than when taken from  $G''$ , which in turn is

less than if taken from  $\tan \delta$ . The loss tangent and  $\tan \delta$  are also indicators of the materials ability to dampen and absorb force. Physical aging decreases the viscoelastic compliance and thus  $\tan \delta$  in DMA also decreases.<sup>10</sup>

TMA may be used in expansion mode to identify glass transitions. The temperature is increased and the change in sample dimension is measured. While DMA requires larger samples, TMA is capable of testing small pieces or thin films. The sample size and magnitude of applied load are important variables.<sup>1</sup> The glass transition may appear as an inflection or change of slope in the plot of dimension change vs temperature. The  $T_g$  is commonly measured by tangent lines<sup>59</sup> but can also be defined by derivative peaks. The slope of this plot, normalized by sample thickness, corresponds to the coefficient of thermal expansion (CTE). Thus, the CTE has units of  $1/^\circ\text{C}$ .<sup>64</sup> The CTE itself is highly important for certain applications such as electronic packaging. A CTE mismatch between contacting materials creates thermal stresses and increases the likelihood of failure. In addition to the expansion accompanying a glass transition, the CTE also increases substantially above the  $T_g$ . For these reasons glass transitions are often avoided even in non-structural applications. Residual stresses affect the magnitude and shape of the measured dimension change. Compressive residual stresses result in increased expansion, whereas tensile residual stresses result in contraction (decreased expansion). DMA and TMA may also be used to measure the heat deflection temperature in three-point bending or penetration modes.<sup>52-53</sup>

While DSC is commonly used to measure the melting temperature of chemical compounds and feedstock materials, it can also be used to identify transitions in cured polymer samples. The energy required to maintain equal temperature between sample and reference pans is recorded as a function of temperature. A ramp rate of 5-10  $^\circ\text{C}$  per minute is common. The reference material is usually inorganic and exhibits no thermal transitions and degradations. An empty aluminum pan is often used. The difference in energy necessary to hold the reference and sample at equal temperatures is measured. The sample amount and form are important. In DSC glass transitions show up as an endothermic step or inflection in heat flow due to rapid changes in the heat capacity of the material. In this temperature range, an increase in energy is required to maintain the sample temperature equal to the reference.<sup>10, 59</sup> The  $T_g$  is taken as the midpoint of this step transition. As mentioned in the previous section, Monomer Processing, Properties, and Characterization, since melting occurs at a mostly constant temperature, melting transitions appear as endothermic peaks.

The depth and sharpness of the peak is dependent on the amount, size, and quality of crystalline phases.<sup>59</sup> Physical aging is evident in DSC by an enthalpy recovery peak.<sup>10</sup> Also evident are endothermic loss of solvents or moisture, degradation and oxidation reactions, and residual curing reactions.

Dielectric properties, including permittivity, loss, and breakdown strength, are also important parameters for many applications. The dielectric permittivity is a materials ability to store energy through ionic, dipole, atomic, and electronic contributions when an external electric field is applied. Thus, glass transitions also appear in dielectric spectroscopy as changes in the dielectric permittivity and loss. There are several methods for measuring the permittivity of solid materials, including transmission line, free space, resonant cavity, and parallel plate methods.<sup>65-66</sup> An insulating material's resistance to failure under applied electrical field is referred to as its dielectric strength. When voltage is increased to a sufficient value exceeding the material's dielectric strength, breakdown occurs. A conduction path is formed resulting in the flow of current between electrodes. Dielectric strength is measured by placing the sample between two electrodes and applying a voltage difference. Static or dynamic breakdown tests may be conducted. Static tests involve samples being stressed under a constant applied voltage and the time to failure is measured. This test is useful in estimating the life of materials under specific conditions. For insulating materials, dynamic testing is more commonly used. In these tests, dielectric strength is measured by increasing the applied voltage until failure occurs and the peak voltage is measured.<sup>67</sup> Standard test details are provided in ASTM D149-09 (AC) and ASTM D3755-14 (DC).<sup>68-69</sup> Breakdown involves multiple failure mechanisms and is highly dependent on the sample and test method.<sup>70-71</sup>

### **2.1.3 Design of High Temperature Polymers**

This section discusses chemical and physical considerations in the design of high temperature polymers. Thermal, oxidative, and hydrolytic stability are discussed, as well as processing characteristics, thermo-mechanical properties, and dielectric properties. It is important to recognize that, in addition to chemical composition and structure, the processing, history of the sample, and environmental conditions have a significant effect on the properties discussed in the previous section. Attributes such as the extent of cure and amount of porosity are affected by the specific processing method and pressure, temperature, and time parameters. Storage environment and subsequent thermal and mechanical history also play a role in the thermal, oxidative, thermo-

mechanical, and dielectric properties. Thus, care must be taken in relating chemical composition to properties.<sup>33</sup>

It is of note that aspects that yield high thermal stability rarely contribute to easy processing of the material or high mechanical toughness.<sup>58</sup> Stronger, more rigid structures such as aromatic and heterocyclic compounds limit solubility, increase softening points, and result in brittle materials. Higher molecular weight polymers tend to be tougher and have higher stability but also have higher melt viscosities. Conversely, aspects that improve processing are usually detrimental to stability and mechanical and thermo-mechanical properties. For example, flexible linkages or asymmetric structures improve processability but usually decrease stability and  $T_g$ .<sup>10</sup> Low melting points and glass transitions are desirable for monomers and oligomers but not for resulting polymers.

Several attributes affect thermal and oxidative stability. These include: 1) the strength of primary chemical bonds, 2) mechanism of bond cleavage, 3) resonance contributions, 4) secondary bonding such as polar interactions, hydrogen-bonding, and van der Waals forces, 5) rigidity of structure, 6) crosslinking, 7) symmetry of chemical structures, 8) molecular weight and polydispersity, 9) quantity and nature of impurities, and 10) fillers and reinforcing media.<sup>1</sup>

Out of the considerations that effect thermal and oxidative stability, the primary bonding strength is the single biggest factor. High temperature polymers contain strong bonds such as C-O or Si-O bonds, aromatic compounds, or double bonds. Chemically, the resistance to degradation is dictated by backbone composition as well as functional groups. This is due to the thermal stability of constituents being somewhat affected by the molecular structures around it. Electronegative and steric effects impact effective bond strengths and thus must be considered. Table 1 provides approximate bonding strengths.<sup>2, 72-75</sup> This is contrasted with Table 2, which provides approximate thermal and oxidative energy for a given temperature.<sup>2</sup>

Table 1: Average bond dissociation energies.<sup>2, 72-75</sup>

Bond	Avg Bond Dissociation Energy kJ/mol	Bond	Avg Bond Dissociation Energy kJ/mol
C-Si	322	C-C	346
Si-O	397	C=C	607
Si-N	355	C-H	413
Si-Si	226	C-N	296
Si-H	357	C=N	615
B-O	707	C-O	354
B-B	293	C=O	630
B-N	421	C-F	466
B-C	356	O-H	462
B-H	389	N-H	388
P-C	265	N-N	162
P-Si	215	C-S	264
P-O	343	S=O	522
P=O	544	Ti-O	669

Table 2: Approximate energy for a given temperature.<sup>2</sup>

Temperature, °C	Energy kJ/mol
275	523
300	569
325	615
350	665
371	703

Multiple bonds are stronger than single bonds. Thus, double bonds or structures with resonance stabilization are common in high temperature polymers. Approximately 167-293 kJ/mol is contributed by resonance to provide aromatic and heterocyclic rings with a partial double bond character.<sup>2</sup> The Si-C bond is slightly weaker than the C-C bond, and thus is considered less thermally stable. However, as discussed in the subsequent section Silicon-Containing Polymers, silicon undergoes oxidation to SiO<sub>2</sub>. This inert phase can increase the thermal and oxidative stability of the system. The C-F bond is significantly stronger than the C-H bond and hence fluorinated compounds tend to have high thermal stability. Hydrolytic sensitivity is also however a concern. Many bonds, especially those containing silicon, boron, and phosphorous, are sensitive to degradation from moisture.

Significant stability is provided by polar interactions, hydrogen bonding, and van der Waals forces. Such secondary bonding increases the chain-chain interaction and attraction. Thermomechanical properties, including glass transition temperature, and mechanical properties, such as elastic modulus, are affected. In addition to thermal stability, the glass transition and resistance to combustion and oxidation are increased by the inclusion of polar groups, such as sulfone and phenylphosphine oxide.<sup>1</sup>

Polymers with narrow molecular weight distribution are usually more stable than those with a large polydispersity. Additionally, increasing the molecular weight of a polymer generally results in greater thermal stability, higher melt viscosity, greater toughness, and higher resistance to chemicals and environmental effects. Low molecular weight components result in decreased stability, lower mechanical properties, and a lower glass transition.<sup>1</sup> These trends may not hold true if increasing the molecular weight of a section decreases the crosslinking density.

Symmetry and crystallinity also play a large role in a polymer's properties. Polymers with greater crystallinity and more regular structure often have greater strength, higher modulus, improved thermal stability and creep resistance, and greater chemical resistance. The inclusion of bulky side groups may hinder the formation of crystalline regions<sup>76</sup> but can also provide rigidity and a barrier for oxygen diffusion.<sup>77</sup> Annealing a polymer above its glass transition or mechanical forming, such as bi-axial drawing, are methods used to improve the crystallinity, regularity, and molecular packing. Compared to unoriented films, biaxially drawn films have greater thermal and chemical stability.<sup>1</sup>

Symmetric structures tend to result in higher mechanical, thermo-mechanical, thermal, and oxidative properties as compared with asymmetric structures. However asymmetric structures result in improved processing characteristics.<sup>10</sup> When considering attachment of aromatic linkages, the resulting polymer properties usually follow the trend ortho < meta < para. Monomer and oligomer processability generally follow the reverse trend. Para-substituted backbone linkages usually exhibit the highest tensile strengths, thermal stability, glass transitions, and melting points, and lowest solubility. Ortho-substituted moieties tend to possess higher solubility and lower tensile strengths, thermal stability, melting points, and glass transitions. Occasionally this is not the case, where asymmetric structures result in greater volume and energy required for chain crankshaft motion. This results in a higher glass transition.<sup>1</sup>

Thermal and mechanical properties are generally increased with increasing rigidity. Rigid rod polymers, such as those containing phenylene, biphenylene, and heterocyclic moieties, are more stable, stiffer, and stronger than those containing more flexible linkages such as alkyl, isopropylidene, ether, carbonyl, and sulfone groups.<sup>1</sup> Flexible and less sterically hindered linkages improve processing characteristics. The addition of linkages such as  $-\text{Si-O-Si}-$ ,  $-\text{SO}_2-$ ,  $-\text{O}-$ ,  $-\text{CH}_2-$  and hexafluoroisopropylidene groups lower the energies of rotation of the polymer chain and introduce kinks which inhibit close chain packing. This lowers the  $T_g$  and melting temperatures, and results in increased toughness, and improved solubility.<sup>10, 39</sup>

Crosslinking significantly improves the stability of polymers. Additional bonds are formed which must be broken to result in a reduction in chain length. Similarly, star-shaped and branched materials display better stability than similar linear polymers; they also show lower melt viscosities and polymers with higher glass transitions.<sup>1</sup> As noted previously, more rigid and sterically hindered polymers often show improved stability and glass transition temperatures. This is not always the case however. For example, chain rigidity and steric bulk can interfere with polymerization and crosslinking, resulting in a lower molecular weight and smaller degree of networking.<sup>30, 52, 78-79</sup>

The degree of crosslinking can be somewhat self-limiting. With increasing crosslinking, steric hindrance is increased and chain mobility is decreased, which hinders further reaction. For phthalonitriles it is reported that complete curing is never achieved for this reason.<sup>21</sup> Unreacted endgroups may continue to react during service at elevated temperatures, due to overall increased mobility of the chain. This results in a drift of polymer properties. To alleviate this issue, several approaches are followed. Increasing the curing temperature and time may be appropriate but adds processing cost and curing temperatures are often already above 300 °C. Adding additional catalyst amounts and increasing reactivity may result in decreased hot-wet stability. As previously noted, decreasing steric hindrance and increasing chain flexibility may improve curing but can also decrease the stability and  $T_g$  of resins.<sup>31, 33</sup> It is also of note that while a lower degree of cure results in lower onsets of degradation, unreacted endgroups may slow down degradation once it begins to occur. Chain mobility is increased by bond cleavage, and thus unreacted groups may continue to react during degradation.<sup>21</sup>

Bond cleavage mechanisms also significantly affect the effective stability of the polymer. Many polymers considered in this manuscript degrade by random scission. However, some materials such as polydimethylsiloxane, experience chain folding and subsequent rearrangement and unzipping. These reactions propagate down the chain, releasing small oligomers and resulting in a reduction in molecular weight. Thus the effective bond strength of the Si-O bond is significantly diminished in this case.<sup>80</sup> In these cases, since unzipping occurs from the ends, proper endcapping can alleviate or eliminate this issue. Endcapping can also provide better melt stability.<sup>1</sup> Bond cleavage by interaction with moisture also occurs. Polyimide compounds cure through condensation reactions, which release water and alcohol compounds. These materials are susceptible to degradation in humid environments at high temperatures.<sup>81</sup> Aryoxysilanes<sup>53, 82-86</sup> and cyanate esters<sup>87</sup> are also known to degrade in the presence of moisture.

Purity also affects the properties and stability of polymer systems. Metal and organometallic compounds can catalyze degradation mechanisms, especially oxidation mechanisms. These contaminants may be present from synthesis or introduced during processing. The presence or formation of organic or inorganic compounds with hydroxyl groups are known to catalyze the degradation of Si-C and Si-O bonds.<sup>78</sup> Impurities can also act as plasticizers and lower the  $T_g$ . Low molecular weight impurities may also volatilize, contributing to weight loss. However, impurities containing hydroxyl or amine groups, transition metals and their salts, strong organic acids, strong organic acids/amine salts, are also known to catalyze the curing reaction of several resin systems, including phthalonitriles.<sup>5, 15, 88</sup> Thus, the presence of these impurities may improve the stability of the system. Purity also affects processing in that pure materials have higher softening points.

Many polymers require the use of catalysts for their respective curing reactions. Excessive amounts of catalyst can contribute to higher weight losses, where insufficient amounts result in decreased curing and crosslinking. Phthalonitrile compounds must be cured at high temperatures and often require curing additives to polymerize. These additives affect the final stability of the polymer.<sup>5, 15, 22, 88</sup> Other additives and fillers may also be used to affect the stability of the system. Inorganic fillers including clay, alumina, and silica, often improve the stability as well as affecting modulus, CTE, and other properties.<sup>1, 89-90</sup> Free radical scavengers and antioxidants can also increase stability and prevent oxidation.<sup>76</sup>

Thus far, discussion in this section has focused on attributes that effect stability, with additional properties mentioned briefly. The effect of chemistry on these and other properties should be considered. The glass transition is increased by increasing molecular weight and crosslinking, and the inclusion of polar groups, bulky substituents, and rigid groups. The incorporation of inorganic linkages containing silicon and phosphorous can improve oxidative stability, char yield, and flame resistance. Hexafluoroisopropylidene and other fluorinated groups result in lower permittivity, less color, and increased solubility. Specifically, the hexafluoroisopropylidene group provides high thermal and chemical stability, and is used in polymers for 371 °C exposure and improved processing.<sup>58</sup> Aromatic groups improve the solubility in chlorinated solvents, increase glass transition temperature, decrease the moisture absorption, and lower permittivity.<sup>1</sup>

To improve solubility and lower viscosity, several methods are used, many of which are intended to reduce chain-chain interactions, increase flexibility, and decrease chain packing efficiency. These include the addition of fluorine groups, flexible linkages, unsymmetrical linkages, or bulky, non-planar pendant groups. Bulky substituents, such as phenyl or fluorene, can increase the melting and glass transition temperatures and the thermo-oxidative stability in addition to increasing solubility. These large structures contort the backbone symmetry and restrict mobility, decreasing crystallinity and increasing chain spacing, and in turn lowering the melt viscosity and improving solubility.<sup>1</sup> Copolymers may also be used to disrupt symmetry and crystallinity, resulting in increased solubility.<sup>91-92</sup>

For applications such as radomes and electronics, the dielectric properties are important. Low permittivity (dielectric constant) and high breakdown strength are often desired. There are several ways to reduce the permittivity<sup>1-2</sup> including inclusion of: 1) fluorinated groups such as hexafluoroisopropylidene or perfluoroalkyl groups 2) siloxane segments, 3) bulky functional groups, 4) asymmetric structures, 5) low dielectric constant fillers, and 6) porosity. The inclusion of flexible siloxane backbone linkages, branches, or end groups reduces charge transfer between chains.<sup>93</sup> Bulky functional groups and disruptions in symmetry also reduce dipole-dipole interactions and charge transfer between chains by increasing the chain-chain distance. The presence of porosity or low permittivity fillers reduces the overall permittivity of the material. Unfortunately, most of these methods reduce properties such as stability, glass transition, mechanical modulus and strength, and breakdown strength.<sup>1</sup>

The relationship between dielectric breakdown strength and chemistry is more complex. It is difficult to define relationships between breakdown and specific chemical structures since the resulting dielectric strength is heavily influenced by other factors. The dielectric strength depends on 1) microstructural defects such as impurities and voids, 2) degree of crystallinity, 3) molecular free volume, 4) the presence of solvents or moisture, 5) thermal and electrical conductivity, 6) thermal and oxidative stability, and 7) mechanical strength. It is also heavily affected by test conditions such as electrode size and geometry, electrode contact, sample thickness and geometry, voltage rise rate, AC or DC applied current, temperature, and environment.<sup>65, 70-71</sup>

#### **2.1.4 Classes of High Temperature Polymers**

This section covers common groups of high temperature polymers, generally classified by their primary curing and crosslinking mechanisms. Polymers discussed briefly in this section include polyimides, bismaleimides, phenolics and benzoxazines, cyanate esters, fluorinated polymers, poly(arylene ethers), and phthalonitriles. Phthalonitriles are only briefly introduced and covered in more detail in the subsequent section. Here, greater focus is placed on polyimides than other resins due to their more extensive use and greater thermal and oxidative properties. Silicones are not considered in this section since they are limited to around 200 °C for long-term application and are not structural resins with little load bearing capability at high temperatures. However, silicones and other organosilicon polymers are discussed in the section Silicon-Containing Polymers. Similarly, polytetrafluoroethene (PTFE) is not considered in detail in this manuscript. PTFE is often considered a high temperature material, yet its glass transition temperature is only 115 °C, thus it does not retain mechanical properties at elevated temperatures. Thermal degradation also begins around 200 °C.<sup>94</sup>

The majority of high temperature polymers are thermosets, though some thermoplastic systems are discussed at the end of this section. For thermosetting resins, the lower viscosity of prepolymers results in easier fill of molds and impregnation of fiber preforms. The production of stable curing products and high crosslinking density results in high thermal stability and glass transition temperatures. However, curing cycles require longer times at high temperatures than simply melting and molding. Additionally, cured parts cannot be re-molded, and are generally insoluble and infusible. This makes repair and correction of dimensions difficult.<sup>10</sup>

#### 2.1.4.1 Phthalonitriles (PNs)

Phthalonitriles (PNs) are discussed in detail later in this manuscript but are introduced briefly here. PN resins were developed by the U.S. Navy as an alternative to polyimides. These materials cure via reaction of 1,2-dicyanobenzene groups. They have been shown often to retain their mechanical properties above 340 °C and have glass transition temperatures above 400 °C. Properties may equal or exceed most polyimides. In addition, they tend to be easier to process, absorb less moisture, and have lower melt viscosities than traditional polyimides.<sup>26, 95</sup> Since the phthalonitrile cure reaction does not produce volatiles, fabrication of dense components with negligible porosity is significantly easier than with polyimides. Similar TGA results are obtained with phthalonitriles and polyimides but phthalonitriles show lower long-term oxidative stability as compared with some polyimide systems.<sup>96</sup> Phthalonitriles also exhibit more moisture resistant monomers and more thermally and oxidatively stable polymers than cyanate esters.<sup>87</sup> One of the most defining features of phthalonitriles is their resistance to combustion. These resins are the only organic polymers which meet the U.S. Navy's MIL-STD-2031 standard for flammability of materials used in submarines.<sup>87</sup>

Phthalonitrile materials usually need to be cured at high temperature with the addition of curing additives. Much research has focused on improving processing by lowering the melting point of monomers, creating a larger processing window, and control of viscosity as a function of curing additive. In addition, self-curing materials have been produced by the addition of phenolic groups, amino or amine groups, or benzoxazine.<sup>15, 88, 97-98</sup> While the short-term thermal properties of phthalonitriles have been well characterized, there is less information available on their long-term performance and their dielectric properties, especially breakdown strength.

#### 2.1.4.2 Polyimides (PIs)

Polyimides are by far the most heavily researched and commercially successful class of high temperature polymers. These materials have become widely used for a variety of high temperature applications.<sup>58, 91</sup> They show excellent thermal and thermo-oxidative stability, being able to withstand short-term exposure up to 500 °C and service temperatures up to 340 °C. Glass transitions may be above 300 °C. They also have good chemical resistance, electrical and dielectric properties, and mechanical properties. These materials consist of nitrogen atoms bonded to

carbonyl groups, usually coupled with an aromatic backbone. Figure 1 and Figure 2 show cyclic and linear polyimides.

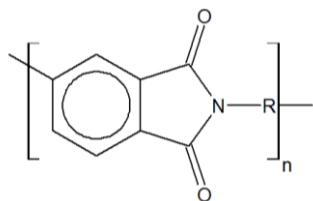


Figure 1: Cyclic polyimide.

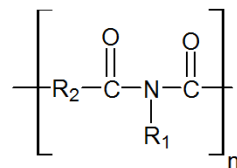


Figure 2: Linear polyimide.

Cyclic imides generally possess superior stability in comparison to linear materials. Thus, the bulk of high temperature polyimide resins use heterocyclic imide moieties. These groups provide additional stability and higher glass transitions in comparison to wholly aromatic chemistries.<sup>58</sup>

Liaw et al.<sup>92</sup> present a sizable review on synthesis, polymerization, and properties of various polyimides. Resins discussed include kink, spiro, and cardo structures, as well as aromatic, cyclic aliphatic, fluorinated, hetero, carbazole, perylene, chiral, and unsymmetrical structures. McKeen also provides several examples of polyimide chemical structures in his chapter on thermal exposure of polyimides.<sup>99</sup>

Polyimides are prepared by a variety of synthetic routes, generally from dianhydride and diamine monomers though other precursors are also used. Small changes in the chemical structure of the dianhydride or diamine yields significant changes in final properties.<sup>92</sup> The diamines and dianhydrides are reacted to form poly(amic acids), which are then chemically or thermally dehydrated, undergoing intramolecular cyclization (imidization).<sup>100</sup> Water and alcohol are released as a byproduct of the condensation reaction. An example reaction is shown in Figure 3.<sup>101</sup> Other synthesis methods include reactions of diisocyanates and dianhydrides, diamines and dithioanhydrides, Michael addition reactions containing diamines and bismaleimides, Diels–Alder reactions containing bisdiene and bidienophiles, silylated diamines and dianhydrides, and Mitsunobu reactions containing dihydroxyalkyl and diimide compounds.<sup>92</sup>

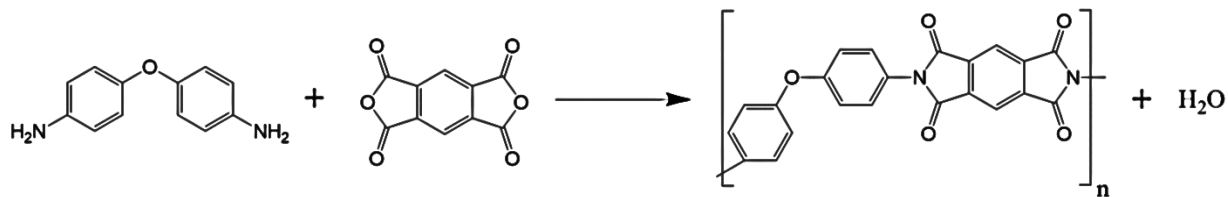


Figure 3: Example reaction of 4-4'-diaminodiphenyl ether oxydianiline and pyromellitic dianhydride to form polyimide and  $2n \text{ H}_2\text{O}$ .

Some issues with polyimide systems exist. Older polyimides absorb moisture after cure, which results in degradation and affects mechanical and thermal properties. For example their effective hot-wet  $T_g$  is significantly reduced.<sup>81</sup> Many older polyimide systems also contain the carcinogen methylenedianiline (MDA). Recent polyimide systems have been formulated to avoid this compound.<sup>1</sup>

There are a number of difficulties in processing polyimide resins, including high viscosities, volatile production, high processing temperatures, and cure shrinkage. Yao<sup>89</sup> investigated two commercial polyimides as electronic encapsulants. It was found that the viscosity was too high, the curing too slow, and the materials experienced volume shrinkages of greater than 40% during curing. This resulted in stress, cracking, and porosity.

The imidization step of thermally cured polyimides requires temperatures above 140 °C, however to ensure complete imidization curing temperatures at or above 300 °C are common.<sup>58</sup> Porosity issues arise since the imidization reaction produces alcohols and water. As curing progresses it becomes more difficult to remove these volatiles, resulting in the formation of voids. Thus polyimides are usually polymerized under pressure, which retains the volatiles within the resin until after curing.<sup>100</sup> Precise ramps and holds are also required to eliminate porosity.<sup>87</sup>

In addition to thermally curing, chemical dehydration is also possible with the use of ketenes, acid anhydrides, and strong Lewis acids. An intermediate isoimide forms. This isoimide may then be processed thermally without volatile production.<sup>58</sup> Chemical dehydration often yields more soluble polyimides compared to thermal imidization. However thermal imidization generally results in higher thermal stability and a higher glass transition temperature.<sup>92</sup> Another alternative route is the production of thermoplastic polyimides, which may be processed above their softening points without significant volatile production. However the modifications needed to result in thermoplastic processing result in lower stability and softening points.

Porosity issues can be also be solved by the development of mostly imidized monomers or prepolymers, which are encapped with reactive end groups for polymerization purposes. This approach entails the incorporation of imide linkages between terminal groups that are capable of polymerizing and forming cross-linked polymers. Lower molecular weight oligomers with additional crosslinking groups, including phenylethynyl and nadimide, have been developed and found some commercial success.<sup>26, 58</sup>

Phenylethynyl terminated imide (PETI) chemistries have received significant focus due to their improved processing, and high toughness and stability. In contrast, nadic terminated imides exhibit higher viscosities and lower stability. The nadic polymerization creates aliphatic moieties which reduce the thermo-oxidative stability. Furthermore, nadic-terminated prepolymers must be stored below room temperature to reduce the rate of polymerization.<sup>26</sup>

PETI oligomers have lower viscosities, higher solubilities, and are often fusible.<sup>58</sup> In these systems the majority of the imidization reaction, and thus most of the volatile evolution, occurs below the final crosslinking temperature.<sup>87</sup> This secondary curing reaction progresses by addition reactions that do not produce volatile products, yielding void-free polymeric materials.<sup>58, 100</sup> A large processing window is obtained and resulting polymers show high  $T_g$  values in the 300 °C range. A downside to this approach is the high curing temperature of the phenylethynyl groups, which pushes the final curing temperature to at or above 350 °C.<sup>26</sup> While imidized oligomers show lower melt viscosities, the viscosities are still higher than desirable for resin transfer molding and other non-autoclave processes. Thus to a degree, processing of these resins into composite parts has been limited to prepreg methods.<sup>26, 87</sup>

Solubility and viscosity issues are common across polyimides. Much of the recent research has focused on improving processing. It is desirable to have polymers with low viscosity that are dissolvable in common organic solvents. This facilitates processes such as spin coating, casting, and resin transfer molding.<sup>92</sup> However most polyimides are at least partially aromatic in nature. They contain strong bonds and symmetric structures, and highly polar groups. Strong interactions occur between chains and chain segments. Charge transfer complexes and electronic polarization are enhanced by the electron donor characteristics of amine segments and electron acceptor characteristics of imide segments. These interactions and stiff, strong backbones result in high

thermal stability. However, these characteristics also result in low solubility, viscosities, and high processing temperatures of the fully imidized polymers.

To improve solubility and lower viscosity, several methods are used, many of which are intended to reduce chain-chain interactions, increase flexibility, and decrease chain packing efficiency.<sup>10</sup> The use of flexible linkages, bulky side groups, and asymmetric structures has been discussed in the previous section Design of High Temperature Polymers. Today low viscosity resins are available.<sup>87, 102</sup>

#### *2.1.4.3 Bismaleimides-(BMIs)*

Bismaleimides (BMI) are a sub-class of polyimides. These materials are produced by reacting a diamine with a maleic anhydride. Linear polyimides are formed by a Michael addition reaction. This reaction progresses by free radical polymerization of double bonds. The use of an addition reaction instead of a condensation route, significantly reduces volatile products.<sup>87</sup> The curing temperature is also much lower than other polyimides. While the processing of these resins is similar to epoxies, BMI resins show higher modulus and higher thermal and hydrolytic stabilities. However, the toughness, and thermal and oxidative stability are lower than cyclic polyimides. Micro-cracking is common in such brittle resins.<sup>10</sup>

#### *2.1.4.4 Phenolics/Benzoxazines*

Phenol formaldehyde resins are some of the oldest polymers considered for elevated temperature applications, yet still find a sizable market. Phenolic resins cure by condensation reactions to produce methylene bridges with the release of water. The use of phenolic resins at high temperatures is limited by their  $T_g$ , which is around 160 °C. However, these resins provide char yields of 50-60% in air, higher than any other commercial organic resin. For this reason, they are used for ablative materials. The carbon pyrolyzes to an inert char. This char can still bear some load and insulates and protects the remainder of the material.<sup>87</sup>

A sub-group of phenolic resins are benzoxazines. These materials are produced by reaction of an aldehyde, an aromatic amine, and phenol groups. Polymerization occurs similar to epoxies, but results in materials with lower moisture absorption, low CTEs, low permittivity, and high retention of mechanical properties at elevated temperatures in the presence of moisture.<sup>87</sup>

#### 2.1.4.5 Cyanate Esters

A class of polymers related to phthalonitriles are polycyanurates (cyanate esters). These resins cure through reaction of terminal cyano groups to form triazine structures.<sup>58</sup> Thermal crosslinking may be accomplished at 170-270 °C for less than 2 hours.<sup>58</sup> These polymers may be mixed with epoxy resins and co-cure by polyetherification, triazine formation, and epoxy curing reactions.<sup>58</sup>

Cyanate esters are commonly used for radomes and space applications. They display low moisture absorption, high glass transition temperatures, good thermal stability, excellent flammability, resistance to microcracking, chemical resistance, strong adhesion to metals, smaller cure shrinkage and high dimensional stability, electromagnetic transparency, low permittivity and high dielectric breakdown strength.<sup>58, 87</sup> Cheaper resins display low toughness. In general cyanate esters are less thermally stable than BMI, polyimide, and phthalonitrile resins, with the triazine moieties of cyanate esters degrading below 500 °C.<sup>33</sup> The resins are also somewhat moisture sensitive.<sup>87</sup>

#### 2.1.4.6 Additional High Temperature Thermosets

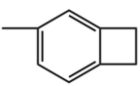
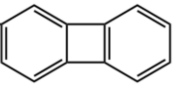
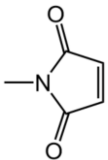
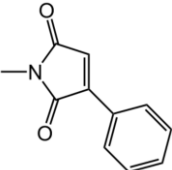
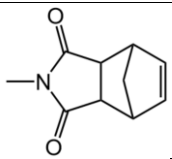
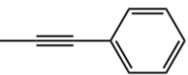
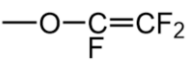
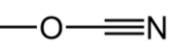
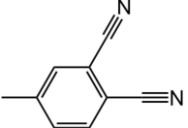
There are a number of additional high temperature polymer systems that have been investigated but had not found significant commercial success. These include polybenzimidazole, poly-N-phenylbenzimidazole, polybenzimidazoquinazoline, polybisbenzimidazobenzophenanthrolines, polyphenylquinoxaline, polybenzothiazole, and polybenzoxazole,<sup>1, 58</sup> as well as phthalocyanine polymers.<sup>103-106</sup> Generally most of these resins generally lack the softening temperatures, curing times and temperatures, viscosities, and solubilities required for effective processing.<sup>58</sup>

#### 2.1.4.7 Overview of Reactive Groups

As discussed briefly in the section on polyimides the use of oligomers of varying chemistry with terminated or functionalized with reactive groups, is a viable method of producing highly stable resins with improved processing. The use of oligomers, instead of higher molecular weight pre-polymers, results in lower melt viscosities and increased solubilities. This in turn results in better moldability and higher quality parts with decreased void content. The use of secondary, latent curing reactions allows for the removal of volatiles, and the subsequent production of thermally and chemically stable bonds without additional volatile production. The high degree of crosslinking results in high  $T_g$  and chemical resistance, but also lower toughness. The backbone composition and molecular weight can be tailored. Longer the backbone linkages between

crosslinking sites, results in a lower crosslinking density. The backbones may contain linkages from one class of polymer discussed previously, and the secondary reactive groups from another.<sup>1</sup> Hergenrother<sup>1</sup> and Connell<sup>2</sup> provide information on a variety of reactive end groups, Table 3.

Table 3: Example reactive end groups and crosslinking groups.<sup>1-2</sup>

Name	Chemical Structure	Approximate Cure (°C)	Comments
<b>Benzocyclobutene</b>		220	Low stability
<b>Biphenylene</b>		350	High cure temperature, brittle
<b>Maleimide</b>		230	Low stability
<b>Phenylmaleimide</b>		370	High cure temperature, unknown stability, not commercialized
<b>Nadimide</b>		325-350, postcured	Volatile evolution (cyclopentadiene), brittle
<b>Ethynyl</b>		250	High cost, small processing window, brittle
<b>Phenylethynyl</b>		350-370	High cost, high cure temperature, good toughness, excellent stability
<b>Trifluorovinylether</b>		250	High cost, small processing window, unknown stability
<b>Cyanate Ester</b>		200	Low stability
<b>Phthalonitrile</b>		250, postcure 330+	High cure temperature, brittle

During the HSCT program a number of chemistries were evaluated. Poor thermo-oxidative stability was observed for cyanate esters, maleimide, and benzocyclobutene terminated oligomers when tested at 177 °C. When aged in air for less than 5000 hours, these materials displayed

significant losses in mechanical properties. Losses were even higher when tested under applied stress.<sup>1</sup>

While other groups, such as phthalonitriles show promise, of these reactive groups, acetylene-terminated compounds have received much attention recently. These compounds undergo addition-type polymerizations at high temperatures. Several compounds have been investigated, including propargyl, ethynyl, and phenylethynyl. Of these, propargyl and ethynyl-terminated linkages show substantially lower stability than phenylethynyl linkages.<sup>1, 58</sup> Phenylethynyl-terminated (PET) polymers are generally highly stable but may exhibit slightly less oxidative stability than their corresponding parent polymers. Of the various crosslinking mechanisms in Table 3, PET systems result in polymers with high fracture toughness.<sup>1</sup> An example of phenylethynyl-containing polymers are the PETI systems discussed briefly in the section on polyimides. Phenylethynyl groups are stable under harsh synthetic conditions including aromatic nucleophilic displacement reactions. This allows for their use in a wide range of polymers. These compounds are commonly produced using endcapping agents, such as 3-(phenylethynyl)aniline (PEA), and 4-(phenylethynyl)phthalic anhydride (PEPA).<sup>58</sup> PET oligomers show excellent shelf lives and wide processing windows. The stability of linkages resulting from phenylethynyl groups is somewhat dependent on adjacent groups. Electron withdrawing groups, including benzophenone, sulfonyl, and imide moieties, increases the glass transition temperature and the modulus at this temperature.<sup>1</sup>

#### *2.1.4.8 High Temperature Thermoplastics*

High temperature thermoplastics incorporate flexible linkages between rigid aromatic and heterocyclic moieties. These materials do not generally undergo crosslinking reactions. The ability to melt process these materials without additional curing, results in lower cost, shorter molding times, and greater volume capabilities. Thermoplastic components may be softened and molded again to correct errors. Compared to thermosetting resins, these materials usually have greater toughness. Their thermal and oxidative stability tends to be somewhat lower however. In addition, these resins have high melting points (> 300 °C) and high melt viscosities. Their use is also limited by their glass transition temperatures which are often around of 140-240 °C.<sup>10, 107</sup>

The largest class of high temperature thermoplastics are the poly(arylene ethers), including polysulfone, polyphenylsulfone, polyethersulfone, and polyaryletherketones such as

polyetheretherketone (PEEK). These materials take up a large sector of the high temperatures polymers market. Poly(arylene ethers) have lower stability and strength compared with polyimides but are more easily processable.<sup>1</sup> Another thermoplastic material is an amorphous polyimide, Ultem™. This material may be melted and molded at 350-425 °C, and has a  $T_g$  of 220 °C<sup>10</sup>

### 2.1.5 Applications of High Temperature Polymers

As mentioned in the introduction of this manuscript, thermally stable polymers are used for a wide variety of applications. These include: 1) aerospace structural composites including radome, airframe parts, and ducts, engine cowls, thrust reversers and other turbine and jet engine components. 2) space applications including ablative materials and rocket engines, 3) electronics and microelectronics including wide band-gap power modules, induction motors, high voltage insulation, and capacitive sensors. 4) photoresists, 5) Langmuir–Blodgett films, 6) optical applications including liquid crystalline displays, electrochromic materials, solar cells, nonlinear optical devices, electroluminescent devices, and optical fibers, 7) memory devices, 8) fuel cells, 9) fire resistant materials for structural applications, 10) fire resistant and high-performance textiles, 11) tooling, 12) moldings, 13) heat resistant and environmental coatings, 14) solvent and temperature resistant gaskets, sealants, tubing, and pipes, 15) components for the energy sector including geothermal conversion systems, nuclear reactors, and oil and gas drilling and refining, 16) adhesives, 17) structural reinforcements, 18) automotive components including binders in brake pads, filters, and composite parts for high performance vehicles, 19) filters and membranes for other applications, 20) insulating, and structural foams, and 21) other industrial applications including conveyor belts, abrasive wheels, and cutting discs.<sup>1-9, 91-92, 108-109</sup>

Desirable properties vary depending on the specific high temperature application. All applications discussed here require high thermal and oxidative stability. The material must be able to resist long exposure times and cyclic heating without degradation of properties. In most applications it is preferred that the polymer's glass transition temperature be outside of its use range. Thus, in an electronic application demanding use from -30 to 300 °C the  $T_g$  should be either below or above this temperature range. This may be less critical for materials with multiple smaller transitions, such as copolymers or polymer blends. Most polymers with glass transitions below -30 °C, i.e. silicones, have limited thermal stability. Thus generally, the  $T_g$  needs to be above 300 °C for this application. In addition, polymers have limited load-bearing capabilities near or above

their  $T_g$ . Thus, for aerospace composites the  $T_g$  must be well above the use temperature. For example, supersonic aircraft applications also demand glass transitions above 300 °C.

Most applications require high tensile strength and high interfacial strength. If the material develops cracks or delaminates at high temperature, the part may fail. In addition, most applications also require resistance to other environmental factors. Polymers should have low moisture uptake and high solvent resistance in service. The elastic modulus is of interest; however, its desired values depend on application. Electronic encapsulants often require limited stiffness to compensate for thermal stresses. For aerospace composites, much higher matrix stiffness may be desired. Dielectric properties are of critical importance for electronics and for some composite applications. Encapsulants require low dielectric constant, low loss, and high dielectric strength. Low permittivity (dielectric constant) minimizes cross talk between components, minimizes power dissipation, and improves signal propagation speed. High dielectric strength prevents conduction through the insulating polymer.

The ease of processing and cost of materials also plays an important role. It is generally desirable to work with liquid resins or monomers with fairly low melting points. These solutions should possess low viscosity. Although the final product often requires solvent resistance, the pre-polymer resins should have good solubility in common solvents. This may be difficult to achieve since chemical structures that result in good solubility tend to decrease the thermal stability of the polymer. A large processing window should also exist between the melting point and the initiation of polymerization. The monomer should also not degrade or react in storage conditions.

The influence and motivation for this dissertation comes primarily from the applications of aerospace composites and wide band-gap power modules. Thus, these are discussed in more detail below.

#### *2.1.5.1 Aerospace Composites*

Since the 1950's, the aerospace industry has grown rapidly, with ever-higher requirements for performance and cost, and ever-increasing volumes of parts required. New materials were required to enable technological improvements of hot air and space vehicle structures and turbine engine components.<sup>10</sup> These polymer matrix composites (PMCs) needed to have low density, greater mechanical properties and retention of these properties at high temperatures, and higher thermal and oxidative stability. PMCs are increasingly used to replace metals in applications that see 200-

350 °C. Engine nozzles for military aircraft are exposed to temperatures of 400 °C and must operate for thousands of hours.<sup>110</sup> These temperatures are well above the operating temperatures of common industrial polymers such as epoxies. The use in space environments requires low moisture uptake and resistance to UV and ionizing radiation.<sup>58</sup> For missile applications, including air-launched stand-off missiles and air-to-air tactical missiles, polymer composite airframes must be capable of maintaining strength for several minutes at temperatures above 540 °C. Both space and missile applications also experience short exposure to temperatures as high as 816 °C during launch and re-entry.<sup>110</sup> Such composites may also find use in hypersonic applications, where structures are subject to high loads and heat fluxes for several minutes. Airframe structures for vehicles with cruise velocities of Mach 2 need to perform at temperatures around 180 °C for extended periods of time. This long-term performance requires materials with oxidative stability above 320 °C.<sup>58</sup> Long-range cruise missiles, stealth vehicles, space vehicles, also require high temperature polymer composites and adhesives. Though the fibers may play a role in oxidation and diffusion of oxygen, the majority of the mass loss and degradation of these composites is driven by the polymer matrix. Polymers with even higher stability and easier processing are continually the subject of research.<sup>58</sup>

#### *2.1.5.2 Polymer Encapsulation*

High-temperature power modules use wide-bandgap semiconductor materials such as silicon carbide (SiC) instead of silicon. Research on SiC-based power modules began in the early 1990's. Originally, SiC device research was driven by obtaining higher reliability in harsh environments. However it was discovered that SiC devices also offered significant advantages over silicon power modules.<sup>111</sup> These devices are only just becoming commercially available. Research and commercial application of this technology continue to grow and while many challenges have been overcome, several reliability issues remain.

Compared with silicon based modules, these next-generation devices may possess lower power losses, higher switching speeds, higher current densities, increased durability and reliability, greater resistance to ionizing radiation, reduced weight, and the ability to operate in high-temperature environments.<sup>12-14, 101</sup> Heat is produced by electronic devices as well as other sources in the system including engines, gear boxes, and the environment itself. This often creates high operating temperatures, especially for components for automotive, aerospace, nuclear power, and

down-hole oil and gas applications.<sup>112</sup> In addition, the device efficiency increases with temperature, and the removal of cooling considerations can result in reduced weight of the system.<sup>111</sup> Thus, all components of these devices must function together at temperatures above 150 to 200 °C.<sup>101, 113</sup> Encapsulation compounds are a critical component of these power modules. These encapsulation materials provide electrical insulation, and protect the devices from mechanical and environmental damage from thermal stresses, physical abrasion or impact, moisture, mobile ions, contaminants, and radiation.<sup>89</sup>

Polymeric encapsulation compounds may be broken into two classes: hard and soft materials. Hard materials have glass transition temperatures ( $T_g$ ) above the operating temperature, while soft materials operate above their  $T_g$ . Unfortunately, soft encapsulants degrade at lower temperatures while hard materials provide thermomechanical problems due to higher moduli, and brittle failure behavior. Usually, thermal properties, mechanical properties, and processing characteristics are all related to the rigidity of the polymer backbone. Polymers with more rigid backbones have higher  $T_g$ , higher stability, and higher elastic moduli. It is difficult to design polymeric materials that possess both high thermal stability and flexibility. Thus, the lack of reliable encapsulation compounds may be considered the greatest hurdle to the development and use of high-temperature electronics.<sup>14</sup>

Currently a variety of polymer materials are traditionally used as encapsulants for silicon power modules, including silicones, epoxies, polyimides, and benzocyclobutene.<sup>111, 113-114</sup> However, as discussed in previous sections, many of these materials cannot operate for extended periods above 200 °C without severe degradation. Yao,<sup>89</sup> Scofield,<sup>111</sup> and many other authors have shown that the properties of these materials degrade during prolonged exposure to these conditions. Materials harden through crosslinking reactions, and crack and delaminate due to thermal stresses. The increase in defects and degradation of the polymer chains causes a decrease in dielectric breakdown strength. Silicones and epoxies begin to degrade at temperatures above 170-200 °C.<sup>114</sup> Some stabilization of silicones up to 250 °C may be achieved by the addition of fillers, such as alumina nano-rods.<sup>115</sup> However, the inclusion of fillers increases the resin viscosity. Polyimide materials are stable above 250 °C, but are difficult to process into void free components and present significant thermomechanical reliability concerns.<sup>114</sup>

Several categories exist for encapsulants. For potting compounds, the device is covered in a liquid resin and the resin is cured. Underfills are used to encapsulate the bottom of chips by flowing between the chip and the substrate. Molding compounds are melted and injected around a chip or device. Conformal coatings are thin films that cover the surfaces of a printed circuit board. These categories each require different properties and serve slightly different functions. Ideal properties of uncured monomers and oligomers are given in Table 4.<sup>89, 116</sup>

*Table 4: Encapsulant prepolymer properties.*<sup>89, 116</sup>

Property	Conformal Coating	Underfill	Molding Compound	Potting Compound
Viscosity	N/A	< 20 Pa·s near 25 °C	Low at elevated temperature	<50 Pa·s near 25 °C
Pot Life	< 30 min	8-24 hours	N/A	8-24 hours

Once cured, encapsulation materials need to possess low dielectric constant, low dielectric loss and high dielectric strength, low electrical conductivity, low viscosity, and high thermal stability. The ideal properties of encapsulation polymers are given in Table 5.<sup>89, 116</sup>

*Table 5: Encapsulant polymer properties.*<sup>89, 116</sup>

Property	Conformal Coating	Underfill	Molding Compound	Potting Compound
Dielectric Breakdown	$\geq 20$ kV/mm	$\geq 10$ kV/mm		
Permittivity, $\epsilon$	$\leq 5$			
Moisture Absorption	< 1% weight gain in 85 °C RH			
Thermal Conductivity	> 1 W/m-K			
Max Temperature	>250-300 °C			
$T_g$	N/A	> 265-315 °C or < 0 °C		
CTE	N/A	20-30 ppm/°C	<20 ppm/ °C	N/A
Elastic Modulus	Varies	3-10 GPa		N/A

The coefficient of thermal expansion and elastic modulus must be such as to limit thermal stresses. The glass transition temperature must be avoided, since this can cause mechanical failure. The material must be able to resist long exposure times and cyclic heating without degradation of

properties, cracking, or delamination. Low permittivity minimizes cross talk between components, reduces power dissipation, and improves signal propagation speed. High dielectric strength prevents conduction through the insulating polymer.

## 2.2 Phthalonitriles

Phthalonitrile (PN) polymers have attracted attention for potential applications in extreme environments, e.g. as a high-performance structural composites, microelectronics, coatings, tooling, textiles, or high-temperature encapsulants for wide band-gap power modules.<sup>3-9</sup> These polymers are usually comprised of a short aromatic chain, end-capped with phthalonitrile groups, as shown in Figure 4. Bis-phthalonitrile compounds are the most common structure, though monomers with multiple branches are also produced. Phthalonitrile monomers possess low melt viscosities and are soluble in many common solvents. Monomers are melted and polymerize at high temperatures to form a heterocyclic cross-linked thermoset. Example structures formed are shown in Figure 5. Curing occurs in the presence of a catalyst, usually a thermally stable aromatic amine. The curing reaction progresses by addition polymerization via the phthalonitrile cyano groups and does not produce volatile by-products, facilitating the fabrication of dense components.<sup>15</sup> State-of-the-art cured PN polymers possess high flammability resistance, excellent mechanical and dielectric properties, and low water absorption.<sup>9, 16-19</sup> Although these materials show exceptional thermal and oxidative stability in thermogravimetric experiments and during hours of exposure at temperatures between 250-400 °C,<sup>6, 9, 20-28</sup> their long-term thermo-oxidative stability requires improvement to meet the challenging demands of the extreme applications. During longer exposures to air at high temperatures, many phthalonitrile polymers experience significant weight losses, volume shrinkage and cracking.<sup>4, 19, 22-23, 26, 29</sup> Furthermore, oxidative aging studies of durations longer than 48 hours and subsequent analysis of degradation regions, are rarely reported in the phthalonitrile literature. Such experiments are critical in gaining an understanding of material degradation modes and behavior in service.

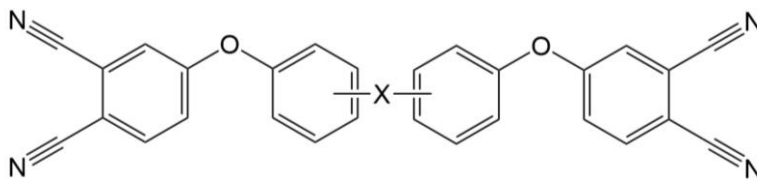


Figure 4: Bis-phthalonitrile monomer, where X represents a variety of backbone chemistries.

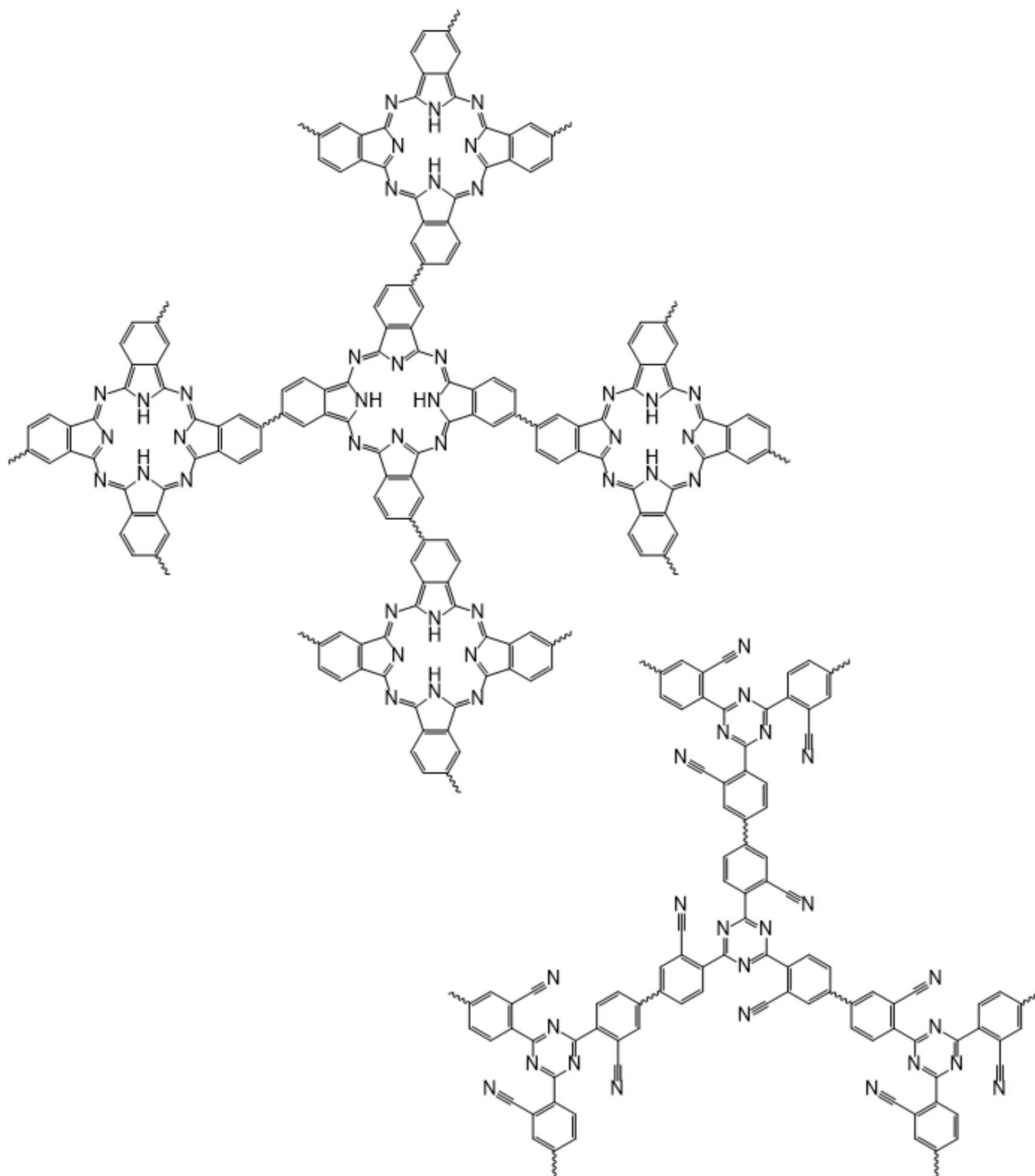


Figure 5: Example networked structures, phthalocyanine (top left) and triazine (bottom right).<sup>95</sup>

### 2.2.1 Brief History of Phthalonitrile (PN) Resins

Historically, phthalonitriles and subsequently phthalocyanines have been used in the production of paints and dyes. The first thermal evaluations were conducted in 1934 by Dent and Linstead.<sup>117</sup> It was observed that phthalocyanine sublimed at 560 °C without degrading. Marvel and Rassweiler<sup>118</sup> produced low molecular weight phthalocyanine polymers in 1957. In two 1968

papers by Leipins et al.<sup>119-120</sup> the production of various polymers via the polymerization of nitrile groups, including phthalonitrile is described. Polymerization occurred at elevated temperatures with the addition of tert-butyl hydroperoxide or di-tert-butyl peroxide. Figure 6 tracks numbers of publications phthalonitrile polymers starting around this time period. For reference, Figure 7 shows numbers of publications per year for polyimide polymers. It is of note that this data is skewed to what is available online and older publications are likely somewhat excluded. Still, differences are evident in the magnitude of research between phthalonitriles and polyimides.

Beginning in the 1980s phthalonitrile polymers gradually became the focus of increasing research and development. In the subsequent decades, extensive research on phthalonitrile-based polymers was conducted at the U.S. Naval Research Lab by Keller and his coworkers. The motivation of this research was to develop an alternative to polyimides that provided significantly easier processing, not requiring extremely diligent removal of volatiles by the use of complex curing cycles or autoclave processes.<sup>87</sup>

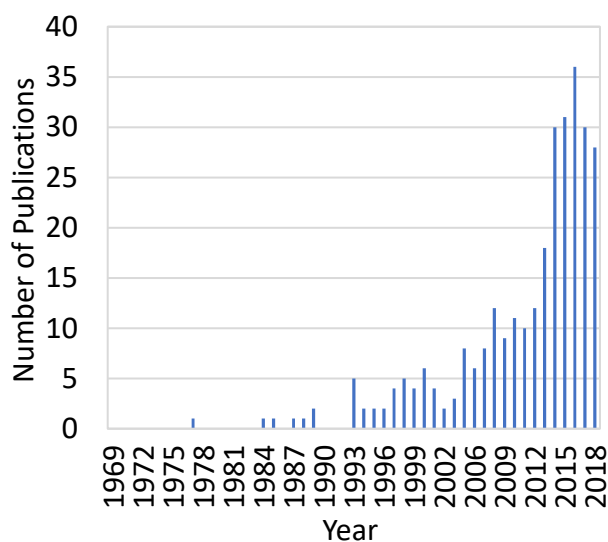


Figure 6: ISI Web of Knowledge search results for "phthalonitrile polymer."<sup>121</sup>

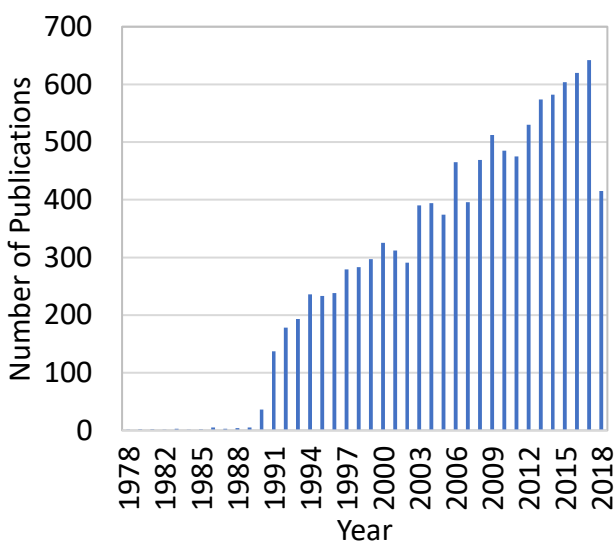


Figure 7: ISI Web of Knowledge search results for "polyimide polymer."<sup>121</sup>

Initially, phthalonitrile monomers consisted of short, highly-aromatic backbones with high melting points. Consequently, these compounds had high processing temperatures and small processing windows.<sup>52</sup> Subsequent research has been devoted to producing low melting point monomers and improving the processing of the polymers. Specifically, thermally stable, yet flexible linkages have been incorporated into a wide variety of monomers.<sup>6, 21-26</sup> In addition, oligomers were developed from flexible-linked phthalonitriles.<sup>5-6, 19, 24</sup> These oligomeric

monomers resulted in melting points as low as 41 °C and more stable viscosities, at the cost of a small decrease in thermal stability.<sup>52</sup> Another area of focus was diminishing the impact of moisture on the glass transition temperature.<sup>110</sup> Additional recent phthalonitrile research has focused on controlling the viscosity as a function of curing additive, and using self-curing materials to decrease the curing temperature.<sup>88, 97, 122-124</sup>

Microcracking has long been a problem in phthalonitrile monomers. The development of flexible-linked oligomeric monomers has alleviated this issue to some degree, resulting in tougher materials during short-term thermal experiments. However, microcracking is still a significant issue. In 2017 Koerner et al.<sup>96</sup> conducted a long-term oxidative stability study on two commercially available phthalonitriles at the Air Force Research Laboratory. The resins showed oxidative stabilities significantly lower than a reference polyimide material. Significant cracking and weight loss were observed. New chemistries and approaches are required to improve the oxidative stability and resistance to microcracking of phthalonitriles, while maintaining good processability.

Traditionally, phthalonitrile research has been driven primarily by polymer matrix composites, however the resins are also finding use for other applications. For example, recently Phua et al.<sup>125</sup> used a resorcinol-based phthalonitrile originally developed by Keller and Dominguez<sup>26</sup> for electronic encapsulation. Alumina and silica fillers were added to improve the thermo-oxidative stability and tailor the CTE to better match other components of the electronic package. A package encapsulated with silica-filled PN resin was able to withstand 310 °C and 190 MPa for 168 hours without failure.

### 2.2.2 Chemistries of Phthalonitriles

Monomers are commonly synthesized by reaction with and aromatic bisphenols involving the nucleophilic displacement of the nitro group on 4-nitrophthalonitrile.<sup>95</sup> This reaction yields low molecular weight chains end-capped with phthalonitrile groups as shown in Figure 8.

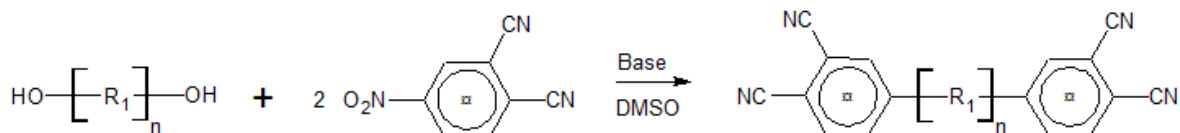


Figure 8: Monomer Synthesis.<sup>3</sup>

A large variety of phthalonitrile polymers have been produced by Keller and other groups, more than can be covered in this manuscript. Backbone linkages incorporated in literature include but are not limited to: bisphenol,<sup>3</sup> resorcinol,<sup>26</sup> pyrocatechol,<sup>126</sup> biphenyl,<sup>23, 126-127</sup> naphthyl,<sup>95</sup> triphenylmethane,<sup>128</sup> methyltriphenylmethane,<sup>124</sup> ketone,<sup>4-5, 28, 129</sup> imide,<sup>97, 100, 130</sup> bismaleimide,<sup>122, 131</sup> phosphine oxide,<sup>22</sup> phosphazene,<sup>18, 132</sup> oxadiazole,<sup>126</sup> benzonitrile,<sup>7, 21</sup> aminobenzene,<sup>88, 97</sup> benzoxazines,<sup>98, 133</sup> triazine,<sup>20, 134</sup> propargyl,<sup>135</sup> phenylethynyl<sup>130</sup> sulfone,<sup>16, 24</sup> phthalazinone,<sup>123</sup> phenol,<sup>136</sup> fluorene,<sup>137</sup> silazane,<sup>51</sup> carboxysilane,<sup>30, 52</sup> carbosilane,<sup>50</sup> siloxane,<sup>6, 53</sup> and silsesquioxane groups.<sup>54</sup>

### 2.2.3 Processing of Phthalonitriles

As mentioned previously in the section 2.2.1, the first generation of phthalonitrile resins involved short crystalline chains synthesized with bisphenols and 4-nitrophthalonitrile. These resins showed high melting points around 195–230 °C, and thus small processing windows. The initiation of polymerization, and thus increase in viscosity, usually occurs above 230 °C. Processing and curing are usually limited to temperatures between 10 °C above the melting point and 30 °C below the resin decomposition temperature. Highly thermally stable units, such as aromatic and heterocyclic segments, improve the stability of the polymer but also make the polymer difficult to process and the resulting material brittle.<sup>15</sup> These structures increase the melting point and melt viscosity, and make the material insoluble and infusible.<sup>133</sup> However, low melting points (< 200 °C), low melt viscosities, and large processing windows are required for non-autoclave processing techniques such as filament winding and resin transfer molding.<sup>3</sup> Recent research has focused on improving processing. Flexible linkages were incorporated and oligomeric polymers were developed with improved processing characteristics. This resulted in monomers and oligomers possessing softening points of 40-150 °C.<sup>5</sup> For example the incorporation of oligomeric aromatic ether-containing linkages into the phthalonitrile polymer chain resulted in low molecular weight monomers with melting points between 50 and 90 °C.<sup>5</sup> In general, phthalonitrile monomers also have low melt viscosities, with minimums on the order of 0.01-1 Pa·s.<sup>5-6, 23</sup> Most recent phthalonitrile monomers are also soluble in common solvents including toluene, tetrahydrofuran (THF), chloroform, methylene chloride (DCM), acetone, dimethylformamide (DMF), and dimethyl sulfoxide (DMSO).<sup>21-22</sup>

Polymerization of phthalonitrile materials is usually accomplished using several heating steps at a series of temperatures.<sup>3</sup> Depending on the chemical structure of the monomers, the softening point may be anywhere from 40-250 °C. The curing additive is often mixed into the melt. However, the additive may also be dry-mixed with the monomer powder, or wet-mixed by dissolving the monomer and catalyst and then removing the solvent. The polymerization rate may be controlled by controlling the processing temperatures, the specific curing additive selected, and amount of the curing additive used. Curing of monomers occurs via cyano groups on the phthalonitrile moiety. The curing reaction is shown in Figure 9. This occurs with the addition of a catalytic amount of a curing additive at temperatures above 200 °C. Initially, at 200–250 °C diimine and isoindoline intermediates are formed. These compounds react with additional phthalonitrile groups to form triazine and phthalocyanine macrocycles at 250– 375 °C.<sup>15, 79, 95</sup> This polymerization occurs via an addition-cyclization reaction to form a highly cross-linked network without the production of volatile byproducts.<sup>15</sup>

A general heating profile of a phthalonitrile/curing agent mixture involves initial gelation at 160-250 °C for 2-12 hours followed additional curing/post-curing steps at various temperatures up to 370-415 °C for 4-16 hours each. The use of multiple temperature steps allows the thermal stability to increase before being exposed to a higher curing temperature. Higher curing temperatures are required to overcome steric hindrance and form the triazine and phthalocyanine structures. Greater phthalocyanine formation is desirable, being more stable than triazine. In fact, the phthalocyanine moiety is reported to be among the most thermally and oxidatively stable known organic compounds.<sup>58</sup> As the reaction progresses, the resulting polymer linkages become more sterically constrained. This in turn reduces the rate of further curing and necessitates higher temperature steps. It has been shown that even after extensive post-curing some cyano groups remain unreacted due to steric hindrance.<sup>21</sup> Thus, unreacted intermediates, and incomplete phthalocyanine structures also likely exist.

At any stage in this process, the reaction may be quenched to form a partially cured, or b-staged prepolymer. This b-staged material may be kept in ambient conditions almost indefinitely without further reaction or degradation.<sup>58</sup> The prepolymer may then be melted and fully cured at a later time.<sup>3</sup> It may also be pulverized and molded into desired shapes.<sup>3</sup>

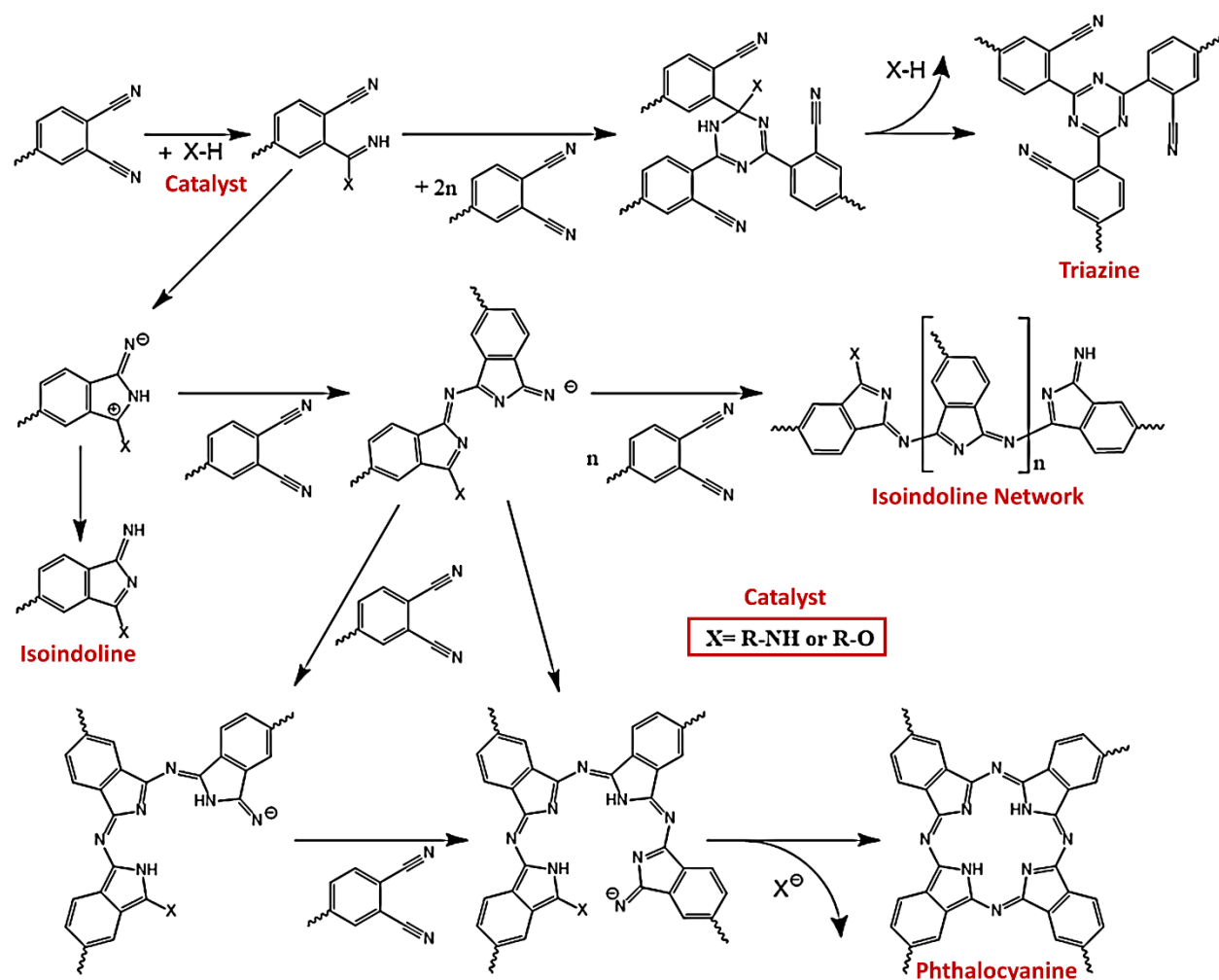


Figure 9: Polymerization of phthalonitrile groups, X-H denotes the curing additive containing active hydrogen.<sup>3, 15, 79</sup>

Pure phthalonitrile monomers often do not contain an active hydrogen or other nucleophilic moiety and thus the polymerization of these materials is difficult. Without a curing agent the reaction is extremely slow, requiring several days of heating at temperatures above 260-300 °C before any viscosity increase is observed.<sup>3,5</sup> Adding a small amount (<10 wt. %) of a nucleophilic compound results in a much greater degree of polymerization.<sup>3, 100</sup> The rate of conversion and specific products depend on the chemical structure of the monomer, and catalyst concentration and type. For example more basic amine compounds result in higher rates of polymerization.<sup>3</sup> Polymerization of phthalonitrile monomers with a bis[4-(4-aminophenoxy) phenyl]-sulfone (*p*-BAPS) curing agent occurs at temperatures above 200-270 °C, depending on monomer backbone chemistry and amount of catalyst.<sup>5</sup> Excess catalyst shortens the time the resin remains melted prior to polymerization. The use of too little curing additive results in incomplete curing within a

reasonable time period. Unreacted or incomplete structures are less thermally stable than triazine or phthalocyanine and result in a lower degree of crosslinking. Thus, it is desirable to optimize processing and chemistry to push the curing reaction to a high degree of conversion. The amount of curing additive must be tailored to specific processing requirements. It is believed that the curing additives do not remain bonded to the matrix, especially at high temperatures. Thus, the use of excess curing additive contributes to weight loss of the polymer. This has stimulated research into self-curing phthalonitrile monomers, which incorporate amines, hydroxyl groups, or other structures in the monomer.<sup>88, 97, 122-124</sup>

A curing agent needs to fit several criteria: 1) It should react with the phthalonitrile monomer to generate an intermediate species, 2) this intermediate should react with excess phthalonitrile monomers to form a polymer structure, 3) the resulting linkage should be thermally stable, 4) the reaction must occur under reasonable processing conditions and progress in a controlled manner, 5) the curing agent must be thermally stable and may not degrade under processing conditions, 6) the curing reaction may not produce volatile products, 7) the curing agent cannot volatilize or segregate during the polymerization, and 8) the curing agent must be soluble or easily dispersed in the monomer melt.<sup>3</sup> Regarding #5, any degradation of the curing agent not only reduces the polymerization but releases volatiles and creates products which decrease the thermal stability.<sup>98</sup> Several types of curing agents may meet these criteria depending on the specific phthalonitrile and processing conditions.<sup>87</sup> Some curing additives include: aromatic amines, transition metals and their salts, strong organic acids, strong organic acid/amine salts, and phenolic compounds.<sup>88</sup>

Thermally-stable aromatic amines are commonly used for this purpose due to their thermal stability, solubility in the polymer melt, and the stability of the resulting polymers.<sup>3, 5, 88, 98, 100</sup> The addition of only 2–3 wt. % can increase the curing rate significantly, allowing faster processing at lower temperatures.<sup>15</sup> Some specific amines used include *m*- and *p*-phenylenediamine, 4,4'-methylenedianiline, 4-aminophenyl ether, 4,4'-(*p*-phenylenedioxy) dianiline, 4-aminophenyl sulfone, 1,3-bis(3-aminophenoxy)benzene (*m*-APB), bis[4-(3-aminophenoxy)phenyl] sulfone (*m*-BAPS), and bis[4-(4-aminophenoxy)phenyl]sulfone (*p*-BAPS).<sup>3</sup> Work done at NRL found that *m*-APB exhibited some volatility. More thermally stable amines such as *p*-BAPS resulted in improved processing and the resulting properties.<sup>88</sup>

Metal salts are another class of curing additives that have received attention.<sup>4, 58, 133</sup> It was found that the addition of metal salts decreased the curing temperature significantly, however the thermal stability and the char yield also decreased. It is possible that they may be of great benefit if used in conjunction with other curing agents.

#### **2.2.4 Properties of Phthalonitrile Polymers**

Phthalonitriles possess excellent properties, often equal to or exceeding most polyimides. The glass transition temperature ( $T_g$ ) is related to the maximum cure temperature. Organic phthalonitrile polymers cured above 350 °C generally have glass transition temperatures above 400 °C, if observed at all. Polymers cured between 300-350 °C usually show glass transitions in the range of 200-360 °C.<sup>29</sup> The high  $T_g$  is due to the highly-cross-linked nature of the polymer and the rigidity of triazine and phthalocyanine moieties. This results in decreased backbone mobility even at elevated temperatures. They retain their mechanical properties and thermal stability during short-term exposure to temperatures greater than 340 °C in inert environments and 325 °C in oxidizing environments.<sup>4</sup> In thermogravimetric measurements phthalonitrile polymers exhibit a 5% weight loss in range of 410-580 °C in both nitrogen and air environments.<sup>6, 134</sup> The polymers also show high char yields due to unreacted nitrile groups reacting during degradation.

Although these materials show exceptional thermal and oxidative stability in TGA experiments and during hours of exposure at temperatures between 250-400 °C,<sup>6, 9, 20-28</sup> their long-term thermo-oxidative stability will require improvement to meet the challenging demands of the extreme applications. While significant information is available on short-term thermal properties, few studies are reported on extended thermal aging for more than 200 hours. At temperatures below 260 °C, less than 5% weight loss was observed up to 200 hours.<sup>23</sup> No degradation of mechanical properties was reported after aging samples at 205 °C for 100 hours.<sup>19</sup> Aging at temperatures above 300-320 °C resulted in higher weight losses, a 20-24% decrease in flexural strength, and the formation of cracks.<sup>4, 19, 22, 26, 29</sup> It is of note that higher curing temperatures almost always result in higher TGA results, but sometimes lower oxidative stability and mechanical properties.<sup>5, 19</sup> This may be due to degradation of the material at the curing temperatures and a decrease in toughness.

Phthalonitrile materials are particularly useful for applications demanding low flammability.<sup>95</sup> In fact, they are the only polymeric matrix composites to meet the U.S. Navy's MIL-STD-2031

flammability standard for submarine components. This is due to their lower evolution of smoke and toxic fumes and high char yield.<sup>87</sup>

Polymers show low moisture uptake on the order of 0.7-3% after long-term immersion in water.<sup>3-5, 124</sup> These materials also exhibit good adhesion to a variety of substrates,<sup>95</sup> even bonding to Teflon at high temperatures. Coefficients of thermal expansion are in the range of 50-60 ppm/°C.<sup>138</sup>

Phthalonitrile polymers mechanically behave like highly cross-linked brittle resins. In tensile tests, they undergo brittle failure with tensile strengths and elastic moduli in the range of 72-110 MPa and 1.7-4.3 GPa respectively.<sup>7, 19, 29</sup> For example, Warzel and Keller<sup>29</sup> investigated the tensile properties of an aromatic diether-linked phthalonitrile resin, 4,4'-bis (3,4-dicyanophenoxy)biphenyl, cured with 1,3-bis(3-amino phenoxy)benzene. They measured the tensile strengths and double torsion fracture of polymers after cure, post-cure, and thermal aging conditions. All samples were initially cured at 240 °C for 6 hours and 280 °C for 16 hours. Samples cured at 315 °C for an additional 24 hours in air or at 350 °C for an additional 12 hours in argon, had tensile strengths of 94 MPa. Aging samples at 315 °C in air for 100 hours gave a tensile strength of 72 MPa. Samples underwent brittle failure. Samples cured at 315 and 375 °C had elastic modulus ranging from 2.4-3.6 GPa.

#### 2.2.4.1 Thermal Properties

The thermal properties of phthalonitrile resins have been evaluated in a number of publications by Keller and his coworkers at the Naval Research Laboratory. Keller and Price<sup>3</sup> cured bisphenol-linked phthalonitrile monomers with various amines and post-cured at a maximum temperature of 280 °C. The use of amine curing agents results in lower curing times and temperatures. Thermal and oxidative properties and water absorption were measured. It was reported that curing in the presence of an amine results in more thermally stable polymers than curing of the material without a catalyst. The stability was dependent on the reactivity and amount of amine curing agent used. The use of 4,4'-(*p*-phenylenedioxy) dianiline and 4-aminophenyl ether curing agents resulted in rapid reactions. The use of 4,4'-methylene dianiline resulted in a somewhat slower reaction. The curing agent 4-aminophenyl sulfone corresponded to a slow reaction, and higher amine content was required to reach equivalent thermal stability. The polymers formed with 4,4' -methylene dianiline and *m*- and *p*-phenylenediamine showed porosity issues when the amine content was

higher than 10 wt.%. This was attributed to the curing agent volatilizing during cure. The temperature at which the polymers had experienced 10 wt.% weight loss ranged from 440-490 °C in air and 460-488 °C in N<sub>2</sub>. The polymers showed 0.7-1.5% water absorption after immersion in water for two months.

An imide-containing phthalonitrile resin was synthesized by Keller<sup>100</sup> from a di(amic acid) phthalonitrile intermediate. The monomers were imidized prior to polymerization. Addition polymerization occurred via the phthalonitrile cyano groups, at temperatures below the monomers melting point but above the glass transition temperature. As noted in the section Polyimides (PIs), porosity issues are associated with the evolution of volatiles during the imidization condensation reaction. By pre-imidizing the monomers and then polymerizing them via a different method with reactive end groups, the porosity may be avoided. The imide-phthalonitrile polymer showed excellent thermal stability. TGA graphs reveal T<sub>5%</sub> occurs between 500-540 °C in N<sub>2</sub>, and around 470-500 °C in air. The initial degradation was attributed to failure in the imide moiety.

Keller and Dominguez<sup>9, 26</sup> synthesized a resorcinol-based phthalonitrile polymer with a large processing window. The polymer was comprised of two aromatic ether linkages, end capped by phthalonitrile units. DSC was used to identify melting and reaction temperatures. The monomer was heated along with the amine curing additive 1,3-bis(3,4-dicyanophenoxy)benzene (*m*-APB). Melting occurred around 173–179 °C, and polymerization between 252-269 °C. The 5% weight loss occurred around 500-510 °C in N<sub>2</sub>, and around 520 °C in air.

Oligomeric versions of the resorcinol-based phthalonitrile were then synthesized.<sup>9</sup> The backbone length between the terminal phthalonitrile groups was varied. The *n* = 2 and *n* = 4 oligomers displayed softening points near 40 °C. The curing additives *p*-BAPS and *m*-APB were used, and polymerization was initiated around 200 °C. Polymer melts showed low complex melt viscosities in the range of (0.01–0.1 Pa·s at 200 °C. When cured to 375 °C for 8 hours, polymers showed 5% weight losses at 479-507 °C in air and 487-509 °C in nitrogen. When cured to a maximum temperature of 425 °C for 8 hours, T<sub>5%</sub> increased to 547-558 °C in air and 557-567 °C in nitrogen. When aged in air at 260 °C, the *n* = 4 oligomeric phthalonitrile polymer with 5 mol % *p*-BAPS retained 98 wt.% after 100 hours and 95 wt.% after 200 hours. Non-oligomeric resorcinol and biphenyl phthalonitriles retained 99-100 wt.%. The cured oligomeric phthalonitrile polymers did not show glass transitions below 450 °C in DMA.

Blends of a biphenyl phthalonitrile and the oligomeric resorcinol-based phthalonitrile were investigated by Dominguez and Keller.<sup>23</sup> Specifically the  $n = 4$  oligomeric phthalonitrile was studied, resulting in approximately six aromatic ether linkages in the chain. The two monomers differed significantly in properties. The biphenyl PN monomer had a high degree of crystallinity and high melting point, around 233 °C. The  $n = 4$  PN monomer had a lower degree of crystallinity and much lower melting point, around 40 °C. The biphenyl PN was much more rigid due to the para-substituted biphenyl group. A degree of flexibility is introduced in the meta-catenated aromatic ether groups of the  $n = 4$  PN oligomer. The individual resins have several shortcomings. The biphenyl PN had a small processing window of only 20-30 °C. The  $n = 4$  PN oligomer required high temperatures around 425 °C to be fully cured.

DSC, TGA, and rheology studies were conducted on the polymer blends. It was reported that the biphenyl PN monomer and  $n = 4$  PN oligomer had low complex melt viscosities above 235 °C, around 0.01-1 Pa·s. The melt viscosities of the polymer blends fell between the values of the neat polymers. Higher  $n=4$  PN oligomer contents resulted in larger processing windows, lower crystallinity, and lower melting points. A maximum temperature of 425 °C was needed to fully cure the copolymers. TGA was performed on polymer blends comprised of 75:25, 50:50 and 25:75 biphenyl PN/ $n=4$  PN ratios. In nitrogen atmosphere, polymer blends cured at 375 °C showed a weight loss of 5% at 550, 535 and 493 °C, respectively. In air the 75:25, 50:50 and 25:75 blends exhibited 5% weight loss at 580, 559 and 512 °C, respectively. When cured up to 425 °C, the blends exhibited higher 5% wt. loss temperatures, around 573-577 °C in nitrogen. The decrease of stability with increasing  $n=4$  PN content was explained due to the decrease in cross-linking density. The longer term thermo-oxidative stability of fully cured biphenyl and  $n = 4$  PN polymers and polymer blends was also evaluated. Powdered polymers were aged in the TGA chamber at 260 °C in air for up to 200 hours. The PN blends retained 96-97% of their weight after 100 hours and 91-94% after 200 hours. The biphenyl PN and  $n = 4$  PN materials also showed weight retentions of 98-100% and 95-99% after 100 and 200 hours respectively.

A series of publications focus on the synthesis and processing of oligomeric PEEK-like phthalonitriles containing aromatic ether-ketone linkages.<sup>4-5, 19, 25, 139</sup> In 2005, Laskoski, Dominguez, and Keller<sup>4</sup> report synthesizing one of these compounds also synthesized an aromatic ether-ketone based oligomeric phthalonitrile (abbreviated here as AEK-PN) monomer from

bisphenol A, 4,40-difluorobenzophenone, and 4-nitrophthalonitrile in a two-step reaction. They compared the properties of the AEK-PN to a known resin, 2,2-bis[4-(3,4-dicyanophenoxy)phenyl]propane (BAPh). Polymers were cured with bis[4-(4-aminophenoxy)phenyl]sulfone. The BAPh system had a melting point around 195 °C and began curing with the addition of the curing additive around 250 °C, resulting in a processing window of 55 °C. The curing agent was chosen as *p*-BAPS (bis[4-(4-aminophenoxy)phenyl]sulfone) due to its thermal stability in the processing window of the BAPh polymer. The addition of aromatic ether groups in the chain lowered the softening and melting temperatures of the polymer. The AEK-PN showed a softening temperature of 75 °C, was fully liquid at 145 °C, and had a processing window of 110 °C. DSC confirmed an endothermic softening transition around 75 °C and showed an exothermic curing reaction around 315 °C. For the BAPh polymer, a sharp melting point at 195 °C and an exotherm between 250-275 °C was observed.

Rheometric measurements indicated that the AEK-PN was not fully cured compared with the BAPh. The longer chain of the AEK-PN polymer hindered the reaction with the curing additive. Post-curing the AEK-PN for 4 hours at 375 °C and for 8 hours at 425 °C increased the amount of curing and resulted in an improvement of the storage modulus. TGA was used to investigate the thermal and thermo-oxidative properties of the polymers. The cured AEK-PN and BAPh polymers showed 90% weight retention at 505 and 520 °C in N<sub>2</sub> and 530 and 550 °C in air respectively. The AEK-PN was post-cured for 4 hours at 375 °C and for 8 hours at 425 °C and then tested in nitrogen. Post-curing resulted in a higher thermal stability, with 90% weight retention at 565 °C. The longer term thermo-oxidative stability of AEK-PN was investigated by stepwise heating from 250-375 °C in with 8 hour hold times. A cumulative weight loss around 8% was observed after heating to 375 °C in this manner. It is noted that 5% of this weight loss occurred during the final hold at 375 °C. The AEK-PN polymer showed low water absorption over the course of 50 days immersion. The polymer gained approximately 2.3 wt. % with the water uptake leveling off after around 40 days. It was concluded that the incorporation of ether linkages between terminal PN units results in a lower melting point and easier processing, while maintaining good final polymer properties.<sup>4</sup>

Laskoski and Keller et al.<sup>4</sup> continued their work on oligomeric aromatic ether ketone-based phthalonitriles by replacing the more expensive 4,4'-difluorobenzophenone with a lower cost reactant, 4,4'-dichlorobenzophenone.<sup>5</sup> It was reported that the fluorine unit was more reactive

however, and thus the chlorine group was more difficult to displace. To overcome this, the reaction temperature needed to be 35 °C higher, around 180 °C. The reaction was performed in a high boiling polar aprotic solvent (DMSO), with a small amount of toluene. The addition of toluene allowed the distillation of water, formed as a byproduct.

Mechanical and thermo-oxidative analysis was conducted on the polymer. The phthalonitrile resin possessed a melting point around 70 °C. The viscosity decreased as the resin was heated. The resin showed a viscosity of 275 cP at 150 °C, 75 cP at 200 °C, and to 40 cP at 250 °C. Two curing agents were investigated, including bis[4-(4-aminophenoxy) phenyl]-sulfone (*p*-BAPS) and Cu(II) acetylacetonate (Cu(AcAc))/*p*-toluenesulfonic acid (TsOH). The metal salt, copper acetylacetonate, and the aromatic *p*-toluenesulfonic acid monohydrate (Cu(AcAc)/TsOH) mixture was chosen due to having high solubility in the resin. The *p*-BAPS had been chosen previously due to its high thermal stability, however the lower melting points of the AEK-PN polymer allowed for other choices, such as Cu(AcAc)/TsOH, to be evaluated.

For the phthalonitrile cured with *p*-BAPS (*p*-BAPS-PN), DSC showed exothermic curing reactions starting around 240 °C with a peak at 280 °C. For the phthalonitrile cured with Cu(AcAc)/TsOH, exothermic reactions began around 160 °C and showed three peaks around 190, 263, and 345 °C. The glass transition temperature increased with increasing curing temperature and time. After curing at 350 °C for 2 hours no glass transition was evident for the Cu(AcAc)/TsOH-PN system. For the BAPS-PN polymer a  $T_g$  around 235 °C was observed after curing at 350 °C for 2 hours and the polymer did not show a  $T_g$  after curing at 400 °C for 2 hours. FTIR showed triazine ring and metal-free phthalocyanine formation in the *p*-BAPS-PN polymer. However, the Cu(AcAc)/TsOH system showed mostly the formation of phthalocyanine structures. Weak absorption peaks, attributed to the -CN groups, were more evident in the *p*-BAPS-phthalonitrile. This indicated that the Cu(AcAc)/TsOH system resulted in a more complete cure. The polymers were then post-cured at 375 °C. TGA analysis between 25 and 1000 °C was conducted. Polymers with *p*-BAPS and Cu(AcAc)/TsOH showed 95% weight retention at 490 and 505 °C respectively under an inert atmosphere and 490 and 510 °C respectively under air. Catastrophic degradation was observed between 600 and 800 °C. When the polymers were post-cured to 415 °C for an additional 2 hours, the thermal stability improved for the *p*-BAPS-phthalonitrile. Long-term thermal stability was evaluated using stepwise heating with 8 hour hold

times between 250 and 375 °C in air. It was shown that the Cu(AcAc)/TsOH curing additive accelerated the oxidative degradation. Polymers with *p*-BAPS and Cu(AcAc)/TsOH cured at 375 °C showed cumulative weight losses of 3.9 and 19.5% respectively. When the post-curing temperature was increased to 415 °C, weight losses increased to 21.2 and 61.8% respectively. It was concluded that post-curing at 415 °C temperature resulted in degradation. It was noted that methyl group scission occurs in bisphenol A around these temperatures. After heating in distilled water for 24 hours at 100 °C, both polymers showed a weight gain of 1.5%.

Further work was completed on this chemistry in 2016.<sup>19</sup> The effects of the *p*-BAPS curing additive was contrasted with that of bis[4-(3-aminophenoxy)phenyl] sulfone (*m*-BAPS). Concentration of both additives was varied between 3-5 wt.%. Polymerization occurred at a faster rate with the use of *m*-BAPS and at the higher concentration of 5 wt.%. It was reported that the glass transition and the short-term stability in TGA improved with increasing the post-curing temperature to 415 °C. Conversely, tensile and flexural strength was maximized after curing to 330–350 °C. Maximum tensile and flexural strengths of 71 and 117 MPa respectively were observed. After aging for 100 hours at 302 °C in air, the polymers retained 75-81% of their mechanical properties. The materials also exhibited excellent flammability resistance when compared to cyanate esters and phenolic resins.

Oligomeric phthalonitrile resins containing aromatic ether phosphine oxide were studied by Laskoski, Dominguez, and Keller.<sup>22</sup> Monomers were prepared from bis(4-fluorophenyl)phenylphosphine oxide and excess amounts of either bisphenol A or resorcinol, with of K<sub>2</sub>CO<sub>3</sub> in a N,N-dimethylformamide (DMF)/toluene solvent mixture. These monomers were then end-capped with 4-nitrophthalonitrile. DSC was used to identify glass transitions, melting temperatures, and study exothermic polymerization. TGA was conducted to study the thermo-oxidative stability from 250 to 400 °C. FTIR and <sup>1</sup>H NMR spectroscopies were used to confirm the structures of the monomers. The storage modulus and damping factor were measured using a rheometer.

The oligomeric PN monomers were soluble in common organic solvents including DMF, acetone, toluene, ether, chloroform, and DCM. The monomers exhibited a T<sub>g</sub> around 75-90 °C and were fully melted at 150 °C. Polymerization occurred from 245-260 °C. Polymers cured to 375 °C exhibited 5% weight losses around 490 °C in N<sub>2</sub> and 490-495 °C in air. Longer term thermo-

oxidative stability was analyzed using a stepped heating profile from 250-400 °C, similar to that used in reference<sup>23</sup>. After heating up to 375 °C, the phosphine containing resorcinol and bisphenol A PN materials showed a cumulative weight loss of 3.9 and 4.2% respectively. The corresponding polymers without the aromatic ether phosphine oxide group showed slightly higher weight losses. The non-phosphorous containing resorcinol<sup>26</sup> and bisphenol-A<sup>4</sup> PN showed cumulative weight losses of 4.0 and 7.2% for the same aging conditions. When the phosphine oxide containing resorcinol and bisphenol A PN polymers were heated to 400 °C for an additional 8 hours, weight losses of 4 and 6.6% were measured. The non- phosphine containing resorcinol and bisphenol A materials showed 2-3 times higher weight loss under these conditions. Under SEM microcracks were visible on the surface after aging the polymers.

Many other groups have also investigated the properties of various phthalonitrile polymers. Zhao et al.<sup>95</sup> investigated the thermal properties and water uptake of a naphthyl-based phthalonitrile resin. The 1,6-bis(3,4-dicyanophenoxy) naphthalene monomer was prepared, and 4,4'-diaminodiphenyl ether (ODA) was used as a curing agent. The polymer was cured through addition polymerization at 270 °C for 5 hours and 300 °C for 5 hours. Post-curing conditions were varied. The monomer was observed to have a fairly low melting point (156.7 °C), which along with the high curing temperature gave a large processing window. From TGA and DMA studies, the decomposition temperature was recorded at 488 °C. Three decomposition peaks were observed. These were related to the degradation of first ether linkages, then phenyl structures, and finally phthalocyanine and triazine rings. Increasing the post-curing time and temperature improved the thermal stability.

Badshah et al.<sup>126</sup> synthesized three different ortho-linked phthalonitrile polymers and investigated their thermal properties. It was reported that processability may be improved while maintaining high thermal stability by the incorporation of unsymmetrical units, including meta or ortho-ether-linked aromatic groups. Three monomers were prepared from 2,2 -bis(3,4-dicyanophenoxy)biphenyl, 1,2-bis(3,4-dicyanophenoxy)benzene and 2,2 -bis(3,4-dicyanophenoxy)-1,3,4-oxadiazole. The monomers had a low melt viscosity and melted at 156, 188.7 and 265.7 °C for biphenyl, benzene, and oxadiazole based phthalonitriles respectively. The benzene-based monomer showed the fastest curing behavior at 270 °C. The slower cure of the biphenyl-PN as compared to the benzene-PN was attributed to its bulkier size. The oxadiazole

based material did not cure at 270 °C and required temperatures above 390 °C. This was attributed to the large size and rigid nature of the oxadiazole structure. The high cure temperature and stable melt viscosity of the oxadiazole-PN material provided a large processing window. FTIR confirmed the formation of triazine and phthalocyanine rings. However, it was reported that even after post-curing steric hindrance prevented the full conversion of all cyano groups to triazine rings. The biphenyl-PN exhibited a glass transition around 350 °C, whereas the benzene, and oxadiazole materials had shown transitions higher than 500 °C. The polymers exhibited 5% weight loss at 444, 489.6 and 511.8 °C in N<sub>2</sub> and 436.5, 488 and 500 °C in air for biphenyl, benzene, and oxadiazole based phthalonitriles respectively. The higher stability of the oxadiazole-PN was explained by the polarity, rigidity, and size of the oxadiazole rings. The decreased thermal stability of the biphenyl-PN may be due to the lower stability of the C-C linkage between phenyl groups.

Several groups have incorporated additional cyano groups via functional groups or branched polymers.<sup>7, 21</sup> Tong, Jia, and Liu studied different molecular weight polymers made from poly(arylene ether) nitrile (PEN) end-capped with phthalonitrile.<sup>7</sup> The PEN-PN polymer was intended to combine the thermoplastic properties of the PEN resin and high temperature resistance of a traditional thermosetting phthalonitrile-based resin. It was reported that the thermal stability was improved with increasing curing temperature. FTIR showed the formation of phthalocyanine rings by reactions at phthalonitrile end units and nitrile functional groups. The polymers had a glass transition  $T_g$  greater than 209 °C. TGA results show 5% weight loss at higher than 518 °C in N<sub>2</sub>. Polymers with a number-average molecular weight of 34,000 g/mol exhibited the highest dielectric constant and lowest dielectric loss. The dielectric constant ranged from 3.4-4.6 and the dielectric loss from 0.01-0.025 in the range of 100 Hz to 200 kHz. The polymers had tensile strengths of 90-110MPa and elastic moduli of 2.5-1.7 GPa at room temperature.

Phthalonitrile oligomers containing aromatic ether, ketone, and cyano groups were synthesized and characterized by Liu et al.<sup>21</sup> Polymers with variable main chain length were synthesized from 4,4'-dihydroxybenzophenone, 2,6-difluorobenzonitrile, and end-capped with 4-nitrophthalonitrile. The cyano group on 2,6-Difluorobenzonitrile was included to increase cross-linking amount and rate. The incorporation of flexible linkages has been reported to lower prepolymer melting and glass transition temperatures. It was thus reported that the inclusion of ether

linkages and additional cyano functional groups would result in better processability without a decrease in thermal stability.

The uncured oligomers had good solubility in toluene, THF, chloroform, acetone, DMF, DMSO, N,N-dimethyl acetamide (DMAc), and N-methyl-2-pyrrolidinone (NMP,). Cured polymers were insoluble in these solvents. DSC of the oligomers showed melting transition peaks melted between 109–142 °C. The curing additive, *p*-BAPS was used due to its thermal stability. Polymers were heated at 240 °C for 5 hours, 260 °C for 4 hours, 280 °C for 4 hours, 300 °C for 4 hours, 325 °C for 4 hours, and 350 °C for 4 hours in air. No glass transitions were observed in samples cured by this procedure. DSC also shows that the initial polymerization temperatures increase with increasing chain length and are in the range of 233-245 °C. This results in a processing window of 103–124 °C. FTIR was used after heating to various stages of the cure procedure. After curing at 240 °C, it was observed that the cyano group absorption peak decreased and peaks for phthalocyanine rings and triazine rings appeared. After curing at 300 °C, the cyano peak decreased further and the triazine absorption increased. Little change was observed after curing at 350 °C. A small cyano peak was still present. This indicated that some cyano groups remained unreacted, probably due to steric hindrance. The curing rate was manipulated by controlling the curing additive concentration and curing temperature. The polymers showed 5% weight loss at 507-515 °C in N<sub>2</sub>, and 496-516 °C in air during TGA.

Several groups have investigated self-catalyzed phthalonitrile materials.<sup>88, 97, 122-124</sup> Sheng et al.<sup>124</sup> prepared tri-branched phthalonitrile monomers and characterized their processing and thermal stability. Monomers were prepared from 1,1,1-tris-[4- (3,4-dicyanophenoxy)phenyl]ethane (TDPE). A self-curing material, 4-(aminophenoxy) phthalonitrile (APPH) was used as the curing agent. The curing agent contained a phthalonitrile end cap that was expected to increase the reaction sites. However, APPH contains a lower amine content than other curing additives such as bis[4-(4-aminophenoxy) phenyl]-sulfone (*p*-BAPS). This may explain the relatively higher curing additive content used (20 wt.%). It was reported that the alkyl linkages provide flexibility to the polymer. Increasing the nitrile content of the monomer improved processing by lowering the cure temperature. The TDPE monomer and APPH curing agent exhibited melting points of 105 °C and 136 °C respectively. DSC showed an exothermic self-polymerization peak around 286 °C for pure APPH. The TDPE-APPH polymer showed an

exothermic polymerization peak around 243 °C. The formation of polytriazine and polyindoline structures was observed via FTIR. As also reported by other authors,<sup>21, 126</sup> steric hindrance prevented some CN groups from reacting. The polymer showed low water uptake in immersion studies, reaching a steady state of around 2.9 wt.% after 480 hours immersion.

Zhou et al.<sup>97</sup> compared amine-containing phthalonitriles with a resorcinol-based phthalonitrile of the same structure as produced by Keller and Dominguez.<sup>26</sup> The resorcinol-based phthalonitrile melted around 190 °C and cured in the presence of bis[4-(4-aminophenoxy)phenyl]sulfone (*p*-BAPS) at 195-210 °C after 15-30 minutes. A cure profile of 200 °C for 2 hours, 250 °C for 5 hours, 315 °C for 5 hours, and 375 °C for 5 hours was used for TGA and DMA samples. The 5% weight loss temperature was observed to be 503 °C in air and 495 °C with 72% weight remaining at 900 °C in N<sub>2</sub>. The cured resin exhibited a glass transition at 481 °C. Self-catalyzed amine containing phthalonitriles were also investigated. These included two types, aromatic ether linked monomers and aromatic ether imide linked monomers. Melting points for the aromatic ether amine phthalonitrile ranged from 130.9-172.5 °C depending on the position of the NH<sub>2</sub> group. All amine containing phthalonitriles exhibited 5% weight loss temperatures above 520 °C in N<sub>2</sub> and 510 °C in air. A T<sub>g</sub> was not observed below 560 °C.

Brunovska, Lyona, and Ishida<sup>133</sup> investigated phthalonitrile capped polybenzoxazines. No volatiles are released by the ring-opening polymerization of polybenzoxazines. However, the phenyl group (Ph) on the Mannich bridge (-CH<sub>2</sub>-N(Ph)-CH<sub>2</sub>-) was identified as a thermal weak point in the polymer. The phenyl group was replaced with a phthalonitrile group in the attempt to stabilize the polymer and create further cross-linking. The polymers were cured to a relatively low temperature of 250 °C. Two polymerization mechanisms occurred: the ring opening of the polybenzoxazines and the addition reaction of the phthalonitrile groups.

Polymers cured with a traditional aromatic diamine catalyst showed 5% weight losses from 414-544 °C in N<sub>2</sub> and 390-420 °C in air. The polymers based on monomers with two phthalonitrile groups were more thermally stable than those containing only one group. The high char yields indicated that further polymerization of the nitrile groups occurred at high temperature. During degradation, carbon dioxide, ammonia, and benzene compounds were released by decomposition of the Mannich bridge. In addition, phenolic compounds were released at higher temperatures, from 360-450 °C. It was also attempted to use metal chlorides as curing agents in order to reduce

the processing temperatures. The polymerization temperature was reduced by the addition of FeCl<sub>3</sub>, however a lower degree of nitrile groups reacted, and the thermal stability decreased. The addition of 4,4'-diaminodiphenylether enhanced the conversion of nitrile groups but did not significantly affect the thermal properties.<sup>133</sup>

Zeng et al.<sup>88</sup> investigated directly incorporating an amine in the polymer as opposed to adding an amine curing agent. Nucleophilic displacement of 4-nitrophthalonitrile and 5-aminoresorcinol hydrochloride was used to form a phthalonitrile polymer containing an amino group, 3,5-bis(3,4-dicyanophenoxy)aniline. The structure of the monomer was very similar to that investigated by Keller and Dominguez,<sup>26</sup> except for the addition of an amine group to the central aromatic ring. DSC showed an endothermic melting peak around 214 °C. An exothermic peak was observed 257 °C and 274 °C. This did not correspond to any weight loss in TGA studies as was attributed to a curing reaction. Additional thermal curing was implied but specifics were not given. The polymers exhibited 5% weight loss around 460 °C in N<sub>2</sub>.

Blends of bisphenol phthalonitrile oligomers and benzoxazine phthalonitrile monomers were polymerized by Xu et al.<sup>98</sup> The polymers showed two stages of curing, corresponding to the opening of benzoxazine rings and the formation rings of nitrile groups. The incorporation of benzoxazine phthalonitrile monomers improved the processing of the polymer, with the optimal processing temperature for copolymer about 200 °C. The flexural strength and modulus of composites were also increased. The polymers were stable up to 430 °C in air. The 5% weight loss of composite laminates was reported to occur around 430-465 °C in air. The benzoxazine phthalonitrile showed self-promoted curing and was able to catalyze the polymerization of bisphenol phthalonitrile oligomers.

Branched novolac-phthalonitrile polymers were investigated by Augustine, Mathew, and Nair.<sup>15</sup> Unlike most research, the phthalonitrile units were incorporated as functional groups on a phenolic polymer chain. The presence of phenolic groups accelerated the curing behavior. FTIR showed that the mechanism of polymerization was related to the extent of phthalonitrile substitution, with several possible structures forming. In polymers with high phenol contents, isoindoline groups formed via a phenol-mediated reaction. In phenol deficient polymers, triazine and phthalocyanine groups formed through cross-linking of phthalonitriles. Polymerization

mechanisms for phthalocyanine and triazine were proposed. These mechanisms have been factored into Figure 9.

The phenolic groups increased the interfacial strength of carbon fiber composites and improved their mechanical properties. However, it was reported that the phenolic groups were detrimental to the thermal stability of the polymers. The polymers showed 5% weight loss at 460-510 °C during thermographic analysis. It is worth noting that the phenolic rings are connected by methylene bridges in the novolac chain. The thermal stability of the phenolic chain would be expected to improve if the aromatic rings were connected by an ether linkage instead.

Recently a study was conducted by Koerner et al.<sup>96</sup> The properties of two commercially available phthalonitriles were compared with a representative polyimide. The polymers were aged at high temperatures in air a 329 °C. Some results from this oxidative aging study are provided in Table 6. The two phthalonitrile resins considered exhibited substantially higher weight loss and an earlier onset of cracking, compared with the reference polymer.

*Table 6: Oxidative aging study by Koerner et al.<sup>96</sup>*

<b>Polymer</b>	<b>Approximate wt. loss after 250 hours, %</b>	<b>Approximate wt. loss after 500 hours, %</b>
<b>Phthalonitrile 1</b>	62	-
<b>Phthalonitrile 2</b>	4	15
<b>Reference Polyimide</b>	<1	2

#### 2.2.4.2 Dielectric Properties

As mentioned in the subsection Phthalonitriles (PNs) in the section Classes of High Temperature Polymers, very little information was found on the dielectric properties of phthalonitriles. Tong, Jia, and Liu<sup>7</sup> investigated the dielectric constant and loss of poly(arylene ether) nitrile (PEN) phthalonitriles. Laskoski et al.<sup>6</sup> measured the dielectric properties of phthalonitrile resins containing aliphatic and siloxane linkages. Permittivity values are reported in the range of 2.8-4.6 and dielectric loss around 0.01-0.025 for these systems. Okutan et al.<sup>140</sup> investigated the dielectric properties of 2,3-dicyano-1,4-di[3,4,5-tri(dodecyloxy) phenylcarbonyloxy]benzene in E7 nematic liquid crystals, but did not mention the dielectric properties of the neat polymer. The dielectric anisotropy parameters decreased with the addition of the phthalonitrile derivative. Adam et al.<sup>141</sup> used phthalonitriles along with metallic compounds to

form metallophthalocyanine complexes. These consisted of metal ions trapped within or between phthalocyanine macrocycles. Since the monomers contained only one phthalonitrile group, discrete phthalocyanine molecules formed instead of a polymer network. The electrical and dielectric properties of these phthalocyanine complexes were measured. DC conductivities were in the range of  $3.3 \times 10^{12}$ – $1.4 \times 10^{11}$  S/cm at room temperature. The conductivity increased exponentially with increasing temperature. The real dielectric constant  $\epsilon'$  was in the range of 2-10, decreasing with frequency from 400- $1 \times 10^6$  Hz. Temperature effects became more significant with decreasing frequency. The real part of the dielectric constant increased drastically as temperature increased from 300 to 500K for frequencies below around  $10^3$  Hz. Dielectric loss,  $\epsilon''$  also increased with temperature and decreased with increasing frequency. Pu et al.<sup>142</sup> reported a breakdown strength of 180 kV/mm for a phthalonitrile resin of unspecified chemistry. Liu<sup>8</sup> aged a phthalonitrile resin at 300 °C and tested its dielectric breakdown. Breakdown strengths were initially observed at values higher than 50 kV/mm, however aging longer than 100 hours resulted in degradation and a decrease in breakdown voltage.

In summary, phthalonitrile monomers are usually comprised of short aromatic chains end-capped with phthalonitrile groups. These monomers polymerize in the presence of nucleophilic compounds to form networked structures. Possible structures include phthalocyanine, triazine, diimine, and isoindoline. Since the polymerization occurs via an addition mechanism, no volatiles are evolved. Aromatic ether and other flexible linkages are often incorporated in the monomer backbones in order to decrease the melting temperature, the melt viscosity, and the monomer solubility. Curing usually occurs around 250 °C and post-curing occurs between 370-415 °C. Aromatic amines are commonly used as curing agents due to their thermal stability and solubility in the polymer melt. The amine groups may also be directly added to the monomer structure, yielding self-curing polymers. In addition, the curing temperature may be lowered by the incorporation of amine groups or additional nitrile cross-linking sites to the polymer structure. Fully cured phthalonitrile polymers behave as brittle thermosets with incredible thermal stability. They maintain their mechanical properties and suffer little weight loss up to 325 °C. A glass transition is often not observed below 400 °C. The polymers also show low water absorption and good solvent resistance.

## 2.3 Silicon-Containing Polymers

Applications of high temperature resins demand ever higher thermo-oxidative stability and improved processing. While advances are being made in the organic polymers discussed previously, shortcomings and limitations remain.<sup>31, 33</sup> The incorporation of inorganic moieties into the monomer structure may provide a viable route for improved stability during service at high temperatures in oxidizing environments.<sup>22, 30-44, 143-144</sup> Specifically, the inclusion of silicon linkages has been reported to improve oxidative stability and flammability of high temperature polymers.<sup>31-44, 143-144</sup> As oxygen and free radicals cleave carbon-silicon bonds, siloxy units are formed. These siloxy units may further react to produce SiO<sub>2</sub>. In this case, a silica-rich surface layer forms. This layer can act as a barrier for further degradation and diffusion of oxygen into the bulk.<sup>45-49</sup>

### 2.3.1 Background on Silicon-Containing Polymers

Incorporation of organosilicon linkages into organic high temperature polymers is not trivial, however. To understand the effects and relevant design considerations, silicon-containing polymers are discussed in this section. Focus is initially placed on silanes and siloxanes, before hybrid organic-inorganic polymers are discussed, including carbosilanes, carboxilosilanes, and carboxilosilanes. Polyhedral oligomeric silsesquioxane (POSS) and silazane (Si-N) materials are not focused on in this manuscript and are only mentioned briefly. Representative structures for linkages in silicon-containing polymers are provided in Table 7.

Table 7: Representative linkages for silicon-containing polymers.

Silanes	Silazanes	Siloxanes
$\left[ \begin{array}{cc} R_1 & R_4 \\   &   \\ -Si & -Si- \\   &   \\ R_2 & R_5 \end{array} \right]_n$	$\left[ \begin{array}{cc} R_1 & R_4 \\   &   \\ -Si & -N- \\   & \\ R_2 & \end{array} \right]_n$	$\left[ \begin{array}{c} R_1 \\   \\ -Si-O- \\   \\ R_2 \end{array} \right]_n$
Carbosilanes	Carboxilosilanes	Carboxilosiloxanes
$\left[ \begin{array}{c} R_1 \\   \\ -R_3-Si-R_3 \\   \\ R_2 \end{array} \right]_n$	$\left[ \begin{array}{c} R_1 \\   \\ -R_3-O-Si-O-R_3 \\   \\ R_2 \end{array} \right]_n$	$\left[ \begin{array}{cc} R_1 & R_4 \\   &   \\ -R_3-Si & -O-Si-R_3 \\   &   \\ R_2 & R_5 \end{array} \right]_n \left[ \right]_m$

The groups R<sub>1</sub>, R<sub>2</sub>, R<sub>4</sub>, R<sub>5</sub> represent organic functional groups including hydro, methyl, phenyl, vinyl etc. In the hybrid polymers R<sub>3</sub> denotes organic backbone linkages, usually methylene or phenylene. These structures correspond to basic linear polymers, though variations exist, including star and branched structures. A summary of degradation mechanisms for silicon and organosilicon-containing polymers is provided in section 2.3.1.4.5 A Summary of Degradation Mechanisms of Silicon-Containing Polymers.

#### 2.3.1.1 Silanes

Inorganic silanes are not commonly used for polymers. Instead these materials are most often pyrolyzed at high temperatures to form silicon carbide. Thus, while substantial literature exists on ceramic formation at high temperatures, less literature is available on polymer properties of polysilanes.<sup>145-148</sup> These materials exhibit lower thermal, oxidative and hydrolytic stability than siloxanes and undergo oxidation to siloxanes even at room temperature.<sup>149-150</sup>

Miller and Michl<sup>151</sup> provide an in-depth discussion of silane chemistry, polymerization, molecular and electronic structure, emission and absorption characteristics, and optical properties. West<sup>149, 152</sup> has also provided extensive reviews of polysilane history, synthesis, and chemistry. They report that polysilanes may have glass transitions occurring between -76 °C to greater than 120 °C.<sup>151</sup> Some polysilanes show no weight loss to temperatures up to 300 °C. However chemical degradations may still occur below this temperature. Some aromatic polysilanes, such as poly(methylphenylsilane) act as thermoplastics and are able to be melted without decomposition. However, many others, including sterically hindered bisaryl polysilanes and symmetrically substituted poly(dialkylsilanes), decompose around 200 °C.<sup>151</sup>

Bushnell-Watson et al.<sup>145</sup> investigated the pyrolysis characteristics by modifying conditions during Wurtz-type synthesis. Higher molecular weight roughly corresponded with a higher softening temperature. Softening temperatures were reported in the range of 135 to 225 °C. TGA results show negligible weight loss up to 300 °C. Rearrangement reactions may occur at lower temperatures. Polysilanes decompose to form siloxanes and carbosilanes, and SiO<sub>2</sub> at higher temperature. Functional groups affect their overall thermal stability and solubility, based on bond strengths, flexibility, and steric effects. The delocalization of sigma electrons could result in interesting dielectric properties, making them electronically similar to  $\pi$ -conjugated systems.<sup>61, 153</sup>

This phenomenon is also evident in other silicon-polymers including siloxanes, silazanes, and carbosilanes.

Shukla et al.,<sup>150</sup> Kuřitka et al.,<sup>154</sup> and Bahloul et al.<sup>148</sup> discuss several stages of degradation for the pyrolysis of silanes under inert atmosphere and their conversion to polycarbosilanes and subsequently silicon carbides. These include Si-Si bond cleavage (170-350 °C), elimination of side groups (350-800 °C) and final carbide formation (>450-800 °C). In the first stage of degradation Si-Si bonds underwent homolytic cleavage, resulting in polymer backbone chain shortening and formation of short oligomer units. During the second stage, chain rearrangement and Si-CH<sub>3</sub> and Si-C<sub>6</sub>H<sub>6</sub> bond cleavage occurred, and methylene bridges formed. This resulted in polycarbosilane formation. For some polymers, radical species generated during bond cleavage can react with methyl and aromatic groups. This results in cross-linked SiC<sub>x</sub>H<sub>y</sub> structures. If the polymers are not cross-linked, much of the silicon volatilizes as temperature increases. It has also been reported that the slow process of oxidative cross-linking to form Si-O-Si and Si-O-C bonds, also occurs at room temperature.<sup>151</sup>

Ma et al.<sup>61</sup> investigated the thermal and optical properties of a linear poly(methylphenyl)silane and two branched polysilanes, poly(phenylsilane-dimethylsilane) and poly(phenylsilane-methylphenylsilane). Ozawa theory was applied, which assumes that the activation energy for a reaction is constant. Arrhenius plots of % weight loss lines on log(heating rate) vs 1/temperature were produced and the activation energy was calculated for the decomposition of different polysilanes. It was found that the branched polysilanes possessed a higher activation energy and greater thermal stability than the linear polysilane. The TGA results showed little weight loss below 250-300 °C, agreeing with the results reported by Miller and Michl.<sup>151</sup>

### 2.3.1.2 Silazanes

Silicon-nitrogen bonds make up the backbone of silazane polymers, as shown in Table 7. For this reason, their most common application is pyrolysis to form silicon nitride and other ceramics. Much of the literature focuses on this pyrolysis at very high temperatures (>700 °C) and are thus mostly outside the scope of this research. For example, Birot et al.<sup>147</sup> published an extensive review of polycarbosilanes, polysilazanes, and polycarbosilazanes polymer precursors and their conversion to ceramics.

Silazanes have been used as linkages and additives in high temperature polymers.<sup>11</sup> Polysilazanes degrade by transamination, hydrosilylation, dehydrocoupling, vinyl polymerization, and redistribution reactions. These reactions result in cross-linking, ceramic phase formation, and the release of volatile products.<sup>148, 155</sup> Siloxanes and SiO<sub>2</sub> phases form in oxidizing environments. Some Si<sub>3</sub>N<sub>4</sub> and Si-N compounds also form, both in oxidizing environments and to a greater degree in N<sub>2</sub>. The thermal stability of polysilazanes may be comparable to that of other silicon-based polymers. Reactions began to occur around 180-200 °C. TGA results show 10% weight loss occurs at around 300 °C for short heating times.<sup>148, 155</sup> Little work has been done to look at the dielectric properties of these polymers with respect to frequency or temperature.

### 2.3.1.3 Siloxanes

The most commonly utilized silicon-polymers are polysiloxanes, also known as silicones. Silicon-oxygen bonds comprise the backbone of these materials. Siloxane materials possess very low glass transition temperatures, sometimes below -70 °C. Compared to many common polymers, these materials display high thermal and oxidative stability. They exhibit lower stability compared with polyimides and phthalonitriles but produce inert oxide films and a high amount of char residue when pyrolyzed. Dimethylsiloxanes are able to be used for extended times at 200 °C and for short periods at up to 300 °C. Polysiloxanes containing phenyl groups possess higher thermal stability and may be used for longer periods at 250-300 °C.<sup>156</sup> These materials are also environmentally inert and biocompatible and have good gas permeability.<sup>157</sup> Siloxane polymers also have low surface energy values which hinders surface flashover,<sup>156</sup> as well as low dielectric constant and good breakdown strengths. Their low permittivity, as well as their low water absorption, is due to having low polarizability.<sup>158</sup> The backbone of Polysiloxanes has high static and dynamic flexibility. This results in a low elastic modulus and a high solubility. The polymers are soluble in many common organic solvents such as chloroform, THF, DMF and NMP.<sup>159</sup> Most polysiloxanes are easy to process due to their solubility, low softening points, and easiness of cure. They also possess very flexible chemistry making it easy to tailor their structure.<sup>34</sup> Siloxane materials are used for many applications including automotive applications, food storage products, footwear, electronics, bake-ware, biomedical applications, power cable jointing, encapsulation compounds for power electronics, cable accessories, and interlayers dielectrics for high performance integrated circuits.<sup>160</sup>

Yilgör and Yilgör<sup>34</sup> provide a comprehensive review article on synthesis and properties of siloxane polymers and copolymers. They discussed the effect of composition on structure and properties, including inert and reactive functional groups. Another review was conducted by Goudie et al.<sup>156</sup> who discussed polydimethylsiloxane rubber aging under applied high voltage. Environmental and contamination effects were considered. Aging factors included thermal aging, electrical stress and breakdown, corona effects, moisture adsorption, and UV and chemical attack.<sup>156</sup>

Although silicon and carbon are both group 4A elements, comparing the C-O and Si-O bonds it is evident that there are significant differences in bond lengths, atom electronegativities, and bond character. The carbon atoms radius is much smaller (0.77 Å) than the radius of a silicon atom (1.17 Å). From the Pauling electronegativity scale, carbon has an electronegativity of 2.5, in contrast to silicon's 1.7 and oxygen's 3.5.<sup>34</sup> Using the additivity rule to predict the Si-O bond length by the sum of atomic radii gives a bond length of 1.83 Å. However experimental results show the bond length to be much shorter, around 1.622 Å. This may be explained by: 1) the substantial difference in electronegativity between Si and O, and 2) the partial double bond characteristics due to Silicon  $d_{\pi}$  - Oxygen  $p_{\pi}$  orbital interaction. This yields a bond with higher dissociation energy and partial ionic nature (around 40%).<sup>34, 156</sup>

Si  $d_{\pi}$ -O  $p_{\pi}$  interaction leads to a large, almost linear, bond angle for Si-O-Si linkages. This bond angle also depends on the functional groups attached. For example, hexahydrodisiloxane has a bond angle of 152.7°, and hexamethyldisiloxane has a bond angle of 165.4°. This is in contrast to the  $sp^3$  hybridized carbon analog, dimethyl ether which has a bond angle of 112.3°. The wide bond angle of siloxanes along with the slightly longer bond lengths yield much longer linkages than those present in hydrocarbon and fluorocarbon polymers and greater flexibility from a reduced rotational energy barrier. Polysiloxanes are able to adopt more configurations due to lower steric restrictions.<sup>34, 156</sup> This backbone flexibility results in low elastic modulus, as well as low glass transition temperatures.

Generally, silicon forms only single bonds, however  $\pi$ -bonding may occur at higher temperatures. This may be stabilized at lower temperature by bulky substituent groups. In addition, unlike carbon, silicon may form compounds with a coordination number greater than four. One example of a high coordination silicon compound is  $SiF_6^{2-}$ . Due to their partial ionic character, it

is relatively easy to tailor the siloxane polymer compositions by equilibration or redistribution reactions. Telechelic and functionally terminated polymers, which are able to undergo further reactions, can be produced with controlled molecular weights and reactive end groups. A wide variety of functional groups may be attached to the silicon backbone atom. Inert substituents may include fluoro groups or methyl, phenyl and other hydrocarbon groups. Reactive groups may include hydrogen, vinyl, amino, or epoxy groups.<sup>34</sup> The properties of the polymer are heavily affected by the functional groups. Different substituents yield siloxane polymers with different glass transition temperatures, solubility parameters, thermal stabilities, surface free energies, and dielectric permittivities. For example, in addition to being affected by the backbone flexibility and the molecular weight, the glass transition temperature is also affected by the steric and attractive effects of pendant groups.<sup>156</sup>

One of the most common siloxanes is polydimethylsiloxane (PDMS). The methyl groups affect the polymer properties in multiple ways. Chain interaction is affected by London dispersion forces associated with the pendant methyl groups.<sup>156</sup> PDMS with a high molecular weight shows crystallinity with a melting point around  $-50\text{ }^{\circ}\text{C}$ . For use at temperatures below this it may be necessary to introduce a diphenylsiloxane comonomer, in small amounts. The aromatic groups disrupt the crystallinity and improve flexibility at these temperatures. Phenyl groups also shift the glass transition temperature higher and improve thermal stability at high temperatures. Thus, it is possible to tailor the  $T_g$  and thermal degradation of PDMS by adding diphenylsiloxane to the backbone. Copolymers of this type are also often fabricated to improve the mechanical properties of PDMS. Polydiphenylsiloxane (PDPS) by itself has high thermal stability and may be used for high temperature applications. Phenyl groups may increase the solubility parameters however. Diphenylsiloxanes have a Hildebrand solubility parameter of around  $19.4\text{ (J/cm}^3)^{1/2}$  as compared to dimethyl and methylphenylsiloxanes which possess solubility parameters of around 15.5 and 18.4 respectively.<sup>34</sup>

#### 2.3.1.3.1 Thermal Stability

In general, higher bond energy corresponds to higher thermal stability. The Si-O bond is significantly stronger (400-560 kJ/mol) compared with C-O (350-360 kJ/mol) bonds, C-C bonds (300-360 kJ/mol), Si-Si bonds (220-330 KJ/mol), Si-N bonds (350-460 KJ/mol), or Si-C bonds (320-400 KJ/mol).<sup>161-163</sup> As noted in section 2.1.3 Design of High Temperature Polymers the

apparent decomposition energies are highly affected by the chemical structure of the molecule as well as temperature and environmental factors. Chemical structure and kinetics also play a role in defining the actual degradation mechanism. Thus, it is difficult to observe thermal stability from bond energies alone.<sup>77, 80</sup>

Many authors have investigated the thermal stability of siloxanes and attempted to further improve their thermal properties. Successful methods include: using monomers with different substituents, incorporating phenyl functional groups, the incorporation of phenylene groups into the siloxane backbone, and adding inorganic particles and phases. Many of these focus on inhibiting the unzipping depolymerization by reaction with terminal Si-OH groups.<sup>77-78, 80</sup> The effect of various substituents, end groups, and backbone units on the thermal stability of PDMS and related polymers is reviewed in this section.

Renwick and Reed<sup>164</sup> published a 1953 paper on the development of siloxanes and filled siloxane insulation materials including elastomers and silicone varnishes (solutions of silicone resins in suitable solvents). They report that silicone elastomers undergo degradation after 1000 hours at 250 °C. Thin films of varnishes also degrade with severe cracking from oxidation reactions.

Yao<sup>89</sup> evaluated the short-term and long-term thermal stability of siloxanes, as well as other materials including polyimide and benzocyclobutene polymers. The siloxanes considered were primarily polydimethylsiloxane with a small amount of vinyl groups serving as cross-linking sites. Siloxane degradation occurred after 240 hours of aging at 250 °C in the form of cracking and oxidative cross-linking. It was noted that higher thermal stability naturally corresponded to higher stability of dielectric strength with temperature.

In the review by Goudie et al.<sup>156</sup> it is reported that the partial polar or ionic bond nature of the siloxane bond helps stabilize the methyl groups in PDMS. The result is that a methyl group in the siloxane polymer is more stable than a corresponding methyl group in a hydrocarbon polymer. Methyl splits off under the influence of oxygen, resulting in oxidative cross-linking and hardening. However, depolymerization from the cleavage of the siloxane bond results in the material softening. Oxidative cross-linking dominates in air environments at long exposure times above 200 °C. In inert atmosphere, the depolymerization effect will dominate due to the lack of oxygen. In composite and electronic applications some parts of the polymer may be exposed to oxygen.

However, there may also be areas that are shielded by other materials or that are in the bulk of a sufficiently thick specimen. These areas of the polymer would see limited oxygen and depolymerization is expected to be the dominate decomposition mechanism. There may also be residual catalysts or other impurities that act to accelerate oxidative degradation.

Camino et al.<sup>163</sup> also reviewed and investigated the degradation of polydimethylsiloxane. Kinetic formal treatments and computer simulations are included. It was reported that degradation of PDMS in inert atmosphere or vacuum occurs between 400–650 °C for short heating times. The depolymerization occurred through chain folding and scission of Si–O bonds. Siloxane bond rearrangement occurred, creating cyclic dimethylsiloxane oligomers, and resulting in chain shortening. This reaction is referred to by other authors as unzipping reaction.<sup>80</sup> This folded conformation is favored at higher temperature by the overlapping of empty silicon d-orbitals with oxygen and carbon orbitals.

The formation of cyclic oligomers during depolymerization in N<sub>2</sub> suggested that the stronger Si–O bond fails before the weaker C–Si bond. Thus, Camino et al.<sup>163</sup> concludes that the depolymerization of PDMS should be controlled by molecular and kinetic effects. This evidenced by the observation that degradation took place at lower temperature for lower heating rates. At higher temperatures a small black residue is formed (silicon oxycarbide) in nitrogen atmosphere.

PDMS degrades at much lower temperatures in air or an oxidizing environment. TGA and DSC results for short heating times showed that the peak degradation rate in air occurred around 339 °C, with a second degradation step around 445 °C. This is in contrast to degradation in N<sub>2</sub>, which occurred at 514 °C. The initial degradation occurred around 290 °C, as compared to 400 °C in nitrogen. Oxidation was shown to increase the degradation reaction, producing volatile cyclic oligomers, CO<sub>2</sub>, water, and silica residue. The degradation was reported to occur via a peroxidation mechanism. Here radical species react to form hydroperoxides, which then decompose to release hydrogen. A very fine silica powder was observed floating in the air above 400 °C. This indicated that oxidation also occurs on volatile species. Above 500 °C degradation processes had mostly ceased and a residue of silica remained.<sup>163</sup>

Oxidative cross-linking also occurred by addition of radicals to unreacted methyl groups. This is reported to occur via one of two routes: either 1) methyl groups are oxidized to carboxylic acids, CO<sub>2</sub> is eliminated to form hydrido-silanes, hydrido-silanes are then oxidized and a condensation

reaction occurs to form siloxane bridges<sup>163</sup> or 2) methyl groups are oxidized to hydroperoxide groups, formaldehyde is eliminated to produce silanol groups, which then condense to form siloxane bridges with the elimination of H<sub>2</sub>O.<sup>165</sup> This cross-linking acts to increase thermal stability. In addition, it was proposed that oxidative formation of silica on the polymer surface may also reduce weight loss. Cross-linked structures breakdown at temperatures greater than 400 °C. This occurs by molecular splitting of cyclic oligomers.

In a second publication Camino et al.<sup>166</sup> further studied the degradation of PDMS end-blocked with (CH<sub>3</sub>)<sub>3</sub>Si groups. FTIR and gas chromatography were used to determine the degradation products at various heating rates. At slower heating rates and lower temperatures, cyclic oligomers are formed by Si-O bond scission and chain unzipping. At higher heating rates and temperatures scission of Si-CH<sub>3</sub> occurred in addition to chain unzipping. This resulted in the release of methane followed by the formation of Si-H bonds.

Several groups have investigated the inclusion of phenyl groups into siloxanes. It is reported that the thermal stability increases with the inclusion of bulky aromatic functional groups. This is likely a steric effect, preventing the chain-folding mechanism required for unzipping and rearrangements.<sup>77</sup> While some authors attribute the increase in stability to the electron withdrawing nature of the phenyl group, others report that when attached to silicon, phenyl groups are electron donating. This is due to back-donation of electrons to the empty d orbitals on the silicon acting as acceptors in interactions with the p<sub>π</sub> delocalized system of the aromatic group.<sup>78</sup>

Sun et al.<sup>80</sup> investigated the effect of curing agents on the thermal degradation of polymethylphenylsiloxane (PMPS). Triethanolamine and polysilazane were used as curing agents. Thermal stability was investigated using isothermal heat soaks, TGA, differential thermogravimetry, and FTIR. It was reported that curing agents were required for curing at lower temperatures. TGA results show the PMPS cured with curing agents resulted in higher short-term stability due to increased cross-linking. Also, compared with thermally cured PMPS, the use of polysilazane as a curing agent resulted in much lower mass loss at temperatures lower than 500 °C during isothermal heat soaks for 3 hours. It was reported that the polysilazane reacted with silanol (Si-O-H) groups and prevented unzip degradation of the polymer. Ammonia was generated and released from the reaction. It was also stated that the incorporation of phenyl groups increases the thermal and thermal-oxidative stability of siloxanes. It is of note that hydroxyl groups are also

reported to catalyze the Si-phenyl bond cleavage in methylphenylsiloxanes, resulting in lower effective decomposition energies than what may be predicted.<sup>78</sup>

Sun et al.<sup>167</sup> also investigated the thermal degradation of polymethylphenylsiloxane containing methacryloyl groups (PMPS-M) by TGA. The TGA results showed little weight loss below around 350 °C. Two degradation stages were observed, occurring at around 400 °C and 500 °C. These were correlated to unzipping degradation and rearrangement degradation respectively. Kinetic parameters of the two degradation stages were obtained by various methods. Activation energies, reaction orders, and the Arrhenius pre-exponential factor were found and related to degradation mechanisms. It was concluded that the first degradation stage of PMPS-M followed a three-dimensional diffusion mechanism, described by the Ginstlinge-Brounshtein equation. The second degradation stage followed a nucleation and growth mechanism, described by the Avramie-Erofeev equation. A theoretical background on various degradation models and ways of calculating kinetic parameters was provided.

Zhou et al.<sup>168</sup> compared the thermal degradation of branched and linear polysiloxanes. The effect of phenyl content on the thermal stability of branched polysiloxanes was also considered. TGA results in air showed that branched polysiloxanes were more thermally stable than linear siloxanes. It was proposed that the branched structure promotes cross-linking. Increasing phenyl content improved the mass retention at temperatures around 200-300 °C, however decreased the mass retention at higher temperatures. This is consistent with phenyl preventing Si-O cleavage at lower temperatures and Si-C cleavage occurring at higher temperatures as reported by Yang et al.<sup>77</sup> It was reported that there was little change in initial thermal degradation behavior with phenyl contents exceeding 50%.

Hua et al.<sup>159</sup> explored the properties of polysiloxane with long side chains including carbazole groups and pentafluorophenyl groups. The solubility in common organic solvents, thermal stability, and photonic properties were investigated. Negligible weight loss was observed below 282 °C via thermographic analysis. The polymers also showed good solubility in common organic, such as chloroform, THF, DMF and NMP.

Deshpande and Rezac<sup>169</sup> researched the degradation of vinyl-terminated PDMS and poly(diphenyl-dimethyl)siloxane. The polymers were pyrolyzed under isothermal conditions at temperatures from 325 °C to 400 °C for 5 hours. TGA results show 10% weight loss ranged from

425 °C to 465 °C. Glass transitions ranged between -75 °C and -118 °C. It was reported that PDMS is stable to 300 °C under vacuum and the incorporation of aromatic groups increases the short-term temperature stability to around 400 °C. The thermal stability was significantly improved by the addition of 3–5 mol% of diphenyl substituents. . However, increasing the diphenyl content to roughly 25 mol% actually increased the mass loss. It was noted that this result conflicts with work by other groups.<sup>169</sup>

The pre-exponential factors decreased with increasing phenyl content. This was attributed to the reduced mobility of backbone. Deshpande and Rezac reference work by Chou and Yang, who relate the glass transition temperature to the polymer composition of random copolymers. An empirical formula,  $T_g = 1.95x-123$  was reported where x represents the diphenyl mol%. The calculated activation energies decreased with the incorporation of phenyl groups. This was attributed to additives in the pre-polymer. It was reported that at low temperatures benzene forms as a degradation product, indicating the cleavage of Si-C bonds. At higher temperatures volatile cyclic compounds form.<sup>169</sup>

It is of note that the formula referenced by Deshpande and Rezac<sup>169</sup> predicts the  $T_g$  of polydiphenylsiloxane (100% substitution) as 72 °C. However, Drake et al.<sup>170</sup> report that PDPS has a  $T_g$  around 265 °C. PDPS exhibited a  $T_{10\%}$  at 511 °C. Despite the high thermal stability, it has proved difficult to synthesize high molecular weight polymers of PDPS and the melting point of 540 °C makes processing difficult.<sup>170</sup>

Jovanovic et al.<sup>48</sup> considered the effect of hydrido-substituents and vinyl end-groups on the thermal stability of polymethylsiloxanes. They concluded that these groups decrease the thermal stability by increasing the reactivity of the polymer and changing the degradation mechanism. It was reported that oxygen and free radicals affected that organic substituents instead of attacking the chain directly, yielding oxidation and cleavage of functional groups.

The degradation of vulcanized RTV silicone rubber with polyhedral oligomeric silsesquioxanes as a functional group was studied by Liu et al.<sup>171</sup> POSS cages were attached to the vinyl-functionalized PDMS backbone via a hydrosilylation with the addition of Platinum(0)-1,3-divinyl-1,1,3,3-tetramethyldisiloxane (Pt(dvs)). Their results show that the addition of POSS significantly improved the thermal stability of the siloxane rubber. TGA results show that RTV silicone experienced a 5 wt. % loss around 337 °C in air. In contrast, siloxane polymer with 5 wt. % POSS

showed a 5 wt. % loss around 393 °C. The effect was even greater in nitrogen. Monofunctional phenyl POSS by itself was also investigated, which showed a 5% wt. loss around 503 °C.

The effect of POSS on the thermal stability may be explained by a number of mechanisms, including the high thermal stability of POSS itself. The rigidity and large steric effects of the POSS molecule hindered the chain folding and prevented the formation of cyclic oligomers. In addition, POSS reacted with radical species forming a networked structure. This grafted or cross-linked structure hindered further free radical degradation. Lastly, a protective ceramic char formed on the surface of the siloxane which hindered diffusion and heat transfer.<sup>171</sup>

In summary, siloxane materials are widely used in many applications. The Si-O-Si bonds are longer and stronger, with wider bond angles, than many other polymer bonds. This ease of bond rotation yields flexible polymers. In general, oxidative decomposition of siloxanes begins to occur in the range of 200- 300 °C.<sup>165</sup> Polydimethylsiloxane degrades above 200 °C by oxidative cross-linking or chain folding and unzipping or rearrangement mechanisms. The thermal stability may be improved by the addition of phenyl groups. Aromatic groups sterically hinder chain folding, preventing Si-O scission and unzipping or rearrangement. Instead the Si-C bond cleavage occurs at temperatures above 300 °C. Depending on the surrounding structure, the stability of polymers generally increases with the following trend in functional groups: vinyl < propyl < ethyl < methyl < hydrido < phenyl.<sup>165</sup> Siloxane polymers have a dielectric constant as low as 2.5, and high breakdown strengths.<sup>172 173-174 89 175</sup>

#### *2.3.1.4 Hybrid Polymers with Organic and Silicon Backbone Linkages; Carbosilanes, Carbosilazanes, Carboxysilanes, and Carbosiloxanes*

The addition of silicon-containing linkages is often used to improve the flexibility and oxidative stability of organic polymers. Silicon is also reported to affect a number of other attributes of polymer systems. A variety of organic-inorganic hybrid systems have been produced by incorporating silicon-containing moieties along with organic substituents in the backbone or as pendant groups.

The Si-C bond (322 kJ/mol) is reported to be slightly weaker than the C-C bond (346 kJ/mol).<sup>2, 72-75</sup> However it is also reported that the lower electronegativity of the silicon adds a slightly ionic character to the Si-C bond, increasing its effective thermal stability.<sup>176</sup> The nature of the carbon

substituent also has a significant effect. As discussed in section 2.3.1.3, Siloxanes, when attached to silicon, the phenyl group has been shown to be slightly electron donating. This is due to interaction of the silicon d orbitals with the phenyl group  $\pi$  system.<sup>78</sup> This has a detrimental effect on stability. Thus for example, the dissociation energies of tetraphenylsilane ( $354 \pm 10 \text{ kJ mol}^{-1}$ ) is significantly lower than that of its carbon analogue, tetraphenylmethane ( $404 \pm 5 \text{ kJ mol}^{-1}$ ).<sup>177</sup> This cleavage of Si-phenyl bonds is reported to occur via a free radical mechanism to produce triphenylsilyl products and phenyl radicals.<sup>78, 169, 178</sup> Once cleavage of an Si-phenyl bond occurs, then oxidative crosslinking, disproportionation reactions, chain branching mechanisms, and other rearrangements of the structure are possible.<sup>77-78, 168-169, 178-180</sup> Oxidation of the silicon results in the formation of siloxy units which condense to form siloxane bridges.<sup>48</sup> In systems with higher silicon content, this mechanism is reported to result in the formation of a silica rich region, which serves as a barrier for further oxidation.<sup>163</sup>

While the inclusion of silica fillers can also provide similar resistance to oxygen diffusion, the in-situ formation of a barrier layer from oxidation of organosilicon groups provides the benefit that it can be regenerated if removed by degradation.<sup>33</sup> Additionally, if the use of fillers can be avoided, lower resin viscosity and thus easier processing is maintained.<sup>33</sup> Processing is also often improved by the addition of thermally stable, yet flexible silicon linkages. Aspects that yield high thermal stability rarely contribute to easy processing of the material. Highly thermally stable units, such as aromatic and heterocyclic segments, improve the stability of the polymer but also make the resin difficult to process and the resulting material brittle.<sup>15</sup> These structures increase the melting point and the melt viscosity, and make the material insoluble.<sup>4-5, 124, 133</sup> However, the wide bond angle and strong character of -O-Si- bonds results in flexible and thermally stable backbones. Thus, the inclusion of flexible silicon linkages can provide enhanced processing characteristics without sacrificing the stability of the material.

There are several types of linkages that are commonly incorporated into the backbone of organic high-temperature materials. Examples include carbosilane (-C-Si-C-), carbosiloxane (-C-Si-O-Si-C-), and carboxysilane (-C-O-Si-O-C-). Of these, carbosiloxane is the most commonly used, forming organic-siloxane polymers. Si-O-Si bonds are longer with wide bond angles, than many other polymer bonds.<sup>34, 156</sup> This ease of bond rotation yields very flexible polymers. Carboxysilane also provides wide bond angles and high thermal stability. However, the Si-O-C bond is reported

to be more hydrolytically sensitive than other silicon bonds.<sup>84-85</sup> It is reported that the carboxysilane linkage may be hydrolytically stabilized by increasing the steric bulk of the functional groups on the silicon atom.<sup>52, 82, 86</sup> Carbosilanes are commonly pyrolyzed to form silicon carbide, however less information is available on their degradation at lower temperatures.<sup>145, 151,</sup>  
154

It is of note that in many polymers reported in literature, the silicon linkage is attached to the aromatic backbone via a methylene bridge. However, for optimum thermal stability methylene groups in the backbone should be avoided.<sup>10</sup> Connecting the silicon linkage directly to phenyl groups results in greater resistance to thermal degradation.<sup>77</sup> The incorporation of aromatic functional groups on the silicon also improves thermal stability. For example, polydimethylsiloxane degrades above 200 °C by oxidative cross-linking, or chain folding and unzipping or rearrangement mechanisms.<sup>80, 163</sup> Aromatic groups limit chain-chain interaction and sterically hinder chain folding, preventing Si-O scission and unzipping or rearrangement. Instead the Si-C bond cleavage occurs at temperatures above 300 °C.<sup>34, 80, 153</sup>

Silicon linkages have also been incorporated in other high-temperature materials. Specifically, the addition of silicon linkages has been shown to improve the oxidative stability of polymers similar to phthalonitriles, including cyanate esters.<sup>32-33, 181</sup> In addition to the literature on cyanate esters, a substantial amount of information is available on the incorporation of silicon linkages into polyimide materials.<sup>34-44</sup> Siloxane-imide polymers combine the excellent thermal and thermo-oxidative stability, solvent resistance, and mechanical and electrical properties of high-performance polyimides together with the high flexibility, good solubility, high gas permeability, reduced water absorption and interesting surface properties of siloxanes. Compared with conventional aromatic polyimides, the siloxane-imide copolymers showed improved solubility, stronger adhesion to copper foils, lower moisture absorption, lower elastic modulus, and low dielectric constant, while maintaining high thermal stability. For example, solubility is improved in solvents such as chloroform, DCM, DMF, DMSO, NMP, and DMAc.<sup>182</sup>

While the inclusion of organosilicon moieties into organic polymers can improve their stabilities and many other properties, there are often also some detrimental effects. As mentioned above, the elastic modulus is often decreased. For electronic encapsulation this is often a benefit, however for aerospace composites this is detrimental. The mechanical strength also often

decreases. However, the biggest impact is often on glass transition. Due to the increased length of the Si-C and Si-O bonds, as compared with C-C bonds, additional flexibility is added to the polymer and the glass transition is suppressed. The effect of this must be considered when designing hybrid organosilicon polymers.<sup>33</sup>

#### 2.3.1.4.1 Carbosilane-Imides and Other Carbosilane Polymers

A number of polymers have been produced with carbosilane (-C-Si-C-) linkages. These polymers are most commonly produced with aromatic or heterocyclic backbone linkages and methyl or phenyl functional groups on the silicon.

Tagle and Terraza et al.<sup>176</sup> produced polyimide polymers with dimethyl or diphenyl silane linkages connected directly to aromatic or imide groups in the backbone. The  $T_g$  of these materials was in the range of 107-130 °C. The 10% wt. loss in nitrogen was observed at 420-440 °C. These values are surprisingly low for polyimide materials. Carbosilane-phthalonitrile compounds were also produced,<sup>55</sup> which were converted to poly(ether-imide)s. Dimethyl or diphenyl substituted silicon linkages were included in both the imide and aryl ether sections. Substitution on the silicon were evaluated. Compared with the previously produced polyimides,<sup>176</sup> the poly(ether-imide)s exhibited better thermal properties. This is likely due to a lower degree of polymerization and thus lower molecular weight of the polyimides. Glass transitions of the poly(ether-imide)s were observed in the range of 164 to 184 °C. In nitrogen, the 10% wt. loss occurred at 470- 530 °C. The polymer with full diphenyl substitution exhibited the highest glass transition as expected. However interestingly the polymer with dimethyl substitution exhibited the highest  $T_{10\%}$  value.

Tang et al.<sup>182</sup> produced a bismaleimide polymer with dimethyl-diphenylene silane linkages. For a bismaleimide material it exhibited good thermal and oxidative stability, higher than an organic BMI reference resin.  $T_{5\%}$  was observed in the range of 461-476 °C and 416-445 °C in  $N_2$  and air respectively. Char yield improved from approximately 0% for organic BMI resins to 3-12% for silicon-containing resins. This was attributed to  $SiO_2$  formation.

Guenther et al.<sup>32</sup> produced cyanate esters containing dimethyldiphenylsilane and tetraphenylsilane moieties. A significant reduction of 50% in moisture uptake was observed in the silicon-containing material (SiMCy) as compared with a bisphenol A-based dicyanate ester (BADCy). This was attributed to differences in packing interactions in the two resins. Molecular packing in the BADCy system was governed by hydrogen-bonding attractions between the cyanate

nitrogen atoms and aromatic rings. In contrast, packing in the SiMCy system was dictated by dipole-dipole interactions of the cyanate ester groups. The inclusion of silicon also improved the char yield and thermo-oxidative stability, while lowering the curing temperatures and melting points. The lower curing temperature was attributed primarily to the increased phenolic impurity content of the silicon-containing resins, though the increased flexibility of the organosilicon linkage may have also played a role. The glass transition temperature was substantially affected. The SiMCy polymer exhibited a  $T_g$  of 260 °C as compared with the 320 °C  $T_g$  of BADCy. This was likely due to the increased free volume and increased flexibility of the Si-C linkages.<sup>32-33</sup>

Cyanate ester resins based on methyl[tris(4-cyanatophenyl)]silane and tetrakis(4-cyanatophenyl) silane were also investigated by Guenther et al.<sup>33</sup> The tetrakis(4-cyanatophenyl) silane -cyanate ester resin was also investigated by Zhang et al.<sup>183</sup> Compared with polymers from bis-cyanate esters, the higher crosslink density of the tri and tetrakis-cyanate esters resulted in high glass transition temperatures above 320 °C. Incomplete conversion of tri-functional and tetra-functional cyanate esters was observed, with some cyanate groups remaining un-reacted. This implied the flexible silicon linkages did not overcome the steric hindrance of the system. Interestingly, the tri and tetrakis-cyanate esters showed substantially higher moisture uptake compared with organic BADCy or the silicon-containing bis-cyanate esters SiMCy. This was likely due to the greater free volume as a result of incomplete cyclotrimerization. Substantially greater curing was achieved by co-curing with a bis-cyanate ester monomer, 1,1-bis(4-cyanatophenyl)ethane.<sup>33</sup>

#### 2.3.1.4.2 Silarylene-Siloxanes

The mechanical properties and thermal and oxidative stability of siloxanes may be improved by connecting siloxane segments with rigid organic segments to form a segmented or block copolymer.<sup>184</sup> To this end, several authors have included phenylene linkages into siloxane polymers.<sup>77-78</sup> The inclusion of silphenylene and other aromatic linkages results in higher degrees of crystallinity, melt viscosity, and thermal stability compared with siloxane polymers. The rigid and bulky aromatic groups prevent chain folding and thus hinder rearrangement and unzipping mechanisms.<sup>78</sup>

However, the phenylene moiety, like phenyl functional groups and methylene and ethylene linkages, is electron donating when attached to the silicon. This results in an increase in the electron availability on the oxygen atom in the siloxane backbone, which aids in degradation where oxygen acts as a nucleophile.<sup>78</sup> The effective stability of silarylene-siloxane linkages is contingent on the length of the siloxane segment, functional substitution on the silicon atoms, the identity of the aromatic groups, and additional surrounding chemical structures. As the length of the siloxane segments increase the stability tends to decrease. However, the siloxane segments may be relatively long before unzipping and rearrangement mechanisms become predominant. As the number of arylene groups is increased, the free-radical scission of the silphenylene bond becomes dominating. This is especially true at temperatures above 450 °C.<sup>78</sup>

Beattie<sup>78</sup> produced and analyzed several methyl-phenyl substituted phenylene-siloxane polymers. The *p*-phenylene groups caused chain-branching to occur. This was attributed to an increase in chain rigidity and the electronic effects of the silphenylene linkages. Phenyl substituted phenylene-siloxane polymers were also attempted but could not be produced in high molecular weights.

A series of siloxane resins containing silphenylene units were synthesized by Yang et al.<sup>77</sup> The phenylene groups were reported to inhibit the diffusion and solution of oxygen and hence improve the thermo-oxidative stability. TGA results showed that the introduction of these aromatic moieties increased the degradation onset temperature, as well as the temperature for 5% and 10% mass loss. The onset of degradation ranged between 365-390 °C, with a 5% mass loss between 458 and 486 °C. In contrast a siloxane polymer without silphenylene units experienced a degradation onset around 350 °C and 5% mass loss at 416 °C. However, the temperature at which the maximum mass loss rate occurred was lower for silphenylene-siloxane polymers than standard PDMS.

Initial degradation of siloxane resins without silphenylene groups occurred by dehydration and unzipping reactions of terminal hydroxyl groups. The introduction of silphenylene units was theorized to increase the chain rigidity and inhibit the folding back of the polymer chain, preventing unzipping degradation. This was supported by an increase in glass transition temperature with increasing phenylene units. However, the resin with the highest silphenylene content did not have the highest thermal stability. The temperature of the maximum degradation rate decreased with phenylene content. This was explained as incomplete curing due to a decrease

in chain mobility. This would have resulted in more residual hydroxyl groups, which have been shown to result in cleavage of Si-O and Si-C bonds. In addition, greater phenylene content meant more Si-C bonds in the backbone. As noted previously Si-O bonds are more stable than Si-C bonds or non-aromatic C-C bonds. In aromatic rings the C-C bonds act as a bond and a half due to the hybridization of aromatic structure, resulting in bond strengths of around 460-520 kJ/mol. Thus the Si-C bonds failed before Si-O or C-C bonds in this structure.<sup>77</sup>

#### 2.3.1.4.3 Carbosiloxane-Imides

A significant amount of work is available on polyimides and bismaleimides containing siloxane linkages<sup>36, 93, 102, 184-189</sup> As discussed in the previous section, Classes of High Temperature Polymers, polyimides possess excellent thermal and oxidative stability, glass transition temperatures, resistance to chemical attack, electrical and dielectric properties, and mechanical modulus and strength. However, processing of these materials is difficult and cured materials are insoluble and infusible.<sup>39, 184</sup>

The tendency for polyimides to absorb water is also troublesome, since it causes swelling, increases dielectric constant, and results in diminished hot-wet  $T_g$  and mechanical properties.<sup>36</sup> Siloxanes on the other hand exhibit high solubility, flexibility, transparency to visible and UV light, and gas permeability, and low glass transition temperatures, and surface energies. However siloxanes have low mechanical strength, and while they possess decent resistance to thermal and oxidative degradation, their stability is significantly lower than polyimides.<sup>184</sup>

Siloxane imide materials combine the properties of these two polymer systems.<sup>188</sup> Compared with polyimides, polyimide-siloxane (PIS) copolymers show greater biocompatibility, stronger bonding to metal surfaces, UV stability, ozone resistance, flammability resistance, solubility, and fracture toughness and impact resistance, as well as lower water absorption, mechanical strength and modulus, dielectric constant, glass transition temperatures, and thermal stability.<sup>34, 36, 38, 184, 186-187</sup> The solubility is improved due to the siloxane segments disrupting molecular packing and hydrogen bonding, increasing the free inter-chain volume.<sup>184</sup> The hydrophobicity of the surface is also increased, even at low concentrations of siloxane segments.<sup>187</sup> The decreased dielectric constant is due to the flexible siloxane segments relaxing molecular dipoles by interfering with charge transfer between polar dianhydride moieties and disrupting the conjugated polyimide system.<sup>190</sup> Compared with siloxanes, PIS copolymers exhibit higher thermal stability, dielectric

breakdown strength, elastic modulus, and tensile strength.<sup>184</sup> The nature of copolymer synthesis allows the properties of these materials to be tailored depending on siloxane and imide contents and the chemical structures of each.<sup>38</sup>

PIS materials are specifically of interest for electronic packaging due to their mechanical stability, low permittivity, electrical resistance, lower moisture absorption, and excellent adhesion to copper.<sup>34, 185</sup> These polymers are also of interest for gas-permeable membranes, photosensitive films, and adhesives.<sup>189</sup>

Many groups have connected polydimethylsiloxane linkages to imide groups via a methylene bridge.<sup>35-37, 39, 93, 102, 184-187, 189-193</sup> The impact of specific structures, purity, processing, and experimental test methodology is evident even within these similar polymers.  $T_{5\%}$  values were reported in the range of 410- 487 °C in air<sup>38, 102, 188, 191</sup> and 360- 553 °C in nitrogen.<sup>35-38, 186</sup> The primary glass transition was generally in the range of 150-220 °C,<sup>37-39, 93, 186, 188, 190, 192</sup> but was reported as low as 125 °C<sup>193</sup> and as high as 336 °C.<sup>36</sup> Many groups reported multiple transitions (up to four) due to phase separation.<sup>185</sup> The  $T_g$  of the soft siloxane phase was generally reported in the range of -134 to 29 °C,<sup>36, 38, 189</sup> though was also reported as high as 100 °C.<sup>37</sup> Dielectric constants were measured to be 2.43-3.3,<sup>93, 185-186, 190</sup> as compared with polyimides which are often greater than 3-3.5.<sup>42</sup>

Chang et al.<sup>102, 191</sup> produced PIS copolymers with  $T_{5\%}$  values at 394-422 °C and the maximum decomposition occurring at 598-606 °C in air. It was reported that with increasing siloxane amount the activation energies for degradation decreased in nitrogen and increased in air. This trend conflicts with results by Xi et al.<sup>37</sup> who report that degradation decreased in nitrogen and Cazacu et al.<sup>184</sup> who report that degradation in air increased with increasing siloxane content.

Cazacu et al.<sup>184</sup> produced PIS materials with aliphatic-ester linkages between organic and siloxane groups. The monomers were soluble in DMF, DMSO, NMP, THF, acetone, benzene, and toluene and showed melting points at 204-206 °C. Initial degradation of PIS copolymers occurred at 180-250 °C with  $T_{5\%}$  at 210-270 °C and  $T_{10\%}$  at 260-350 °C in air. The  $T_{10\%}$  decreased with increasing siloxane amount. Compared to results by other authors, this system exhibits very poor stability, likely due to the aliphatic-ester linkages.

Regnier and Guibe<sup>35</sup> produced a bismaleimide-siloxane copolymer from a tetra-substituted aromatic diamine and a maleimide-encapped siloxane. Initial degradation occurred around 320 °C in both air and nitrogen. In air two stages of degradation were observed at 320-500 °C and 540-705 °C with peaks at 440 °C and 650 °C. The second degradation was oxidative in nature, not appearing in inert conditions.

Hamciuc et al.<sup>39</sup> synthesized nitrile-containing PIS copolymers. Solubility increased, and glass transition decreased with increasing siloxane content. The glass transitions were observed at 149–219 °C. polymers were soluble in chloroform, THF, DMAc, NMP, and pyridine. Decomposition temperatures were above 430 °C but decreased with increasing siloxane content.

Adhikari et al.<sup>192</sup> produced linear and crosslinked PIS copolymers. For the crosslinked materials, the  $T_g$  was observed at 175-183 °C. Linear PIS polymers showed glass transitions from 151-171 °C. These values did not change significantly with siloxane content.

Multiple authors observe phase separation and thus multiple glass transitions. The degree of phase separation is dependent on the siloxane content and length of the siloxane and imide segments. Generally, less phase separation occurs with shorter linkages and lower siloxane content. PDMS tends to be immiscible in organic resins, making the production of homogeneous polymers difficult.<sup>185</sup> However, phase separation may be beneficial, since it results in multiple smaller glass transitions, and can preserve the higher  $T_g$  of the hard phase. The higher  $T_g$  of the imide phase results in lower mobility of these regions. Conversely the low  $T_g$  of siloxane segments results in increased mobility. This maneuverability of siloxane segments can result in migration to the surface, which may be beneficial for boundary layer formation.<sup>187</sup>

Ku and Lee<sup>189</sup> synthesized amorphous PIS copolymers and varied the segment lengths and overall content of PDMS and polyimide-poly(arylene ether) blocks. Up to four glass transitions were observed including: the siloxane phase at -134 to 29 °C and the hard, organic phase at 155 to 200 °C, as well as two additional phases at -27 to -74 and 78 °C.

Fitzgerald et al.<sup>36</sup> produced similar PIS phase separated materials with fluorinated polyimide segments. Increasing the siloxane content resulted in a decrease of the glass transition temperature of the imide phase. With increasing siloxane amounts, the size of observed PDMS domains increased but small-angle X-ray scattering data showed that the amount of phase mixing did not

increase. Thus, the change in the  $T_g$  of the imide phase was likely due to decreasing its molecular weight and increasing the flexibility and free volume of the ends of the imide segments. This finding contrasts with the phase mixing explanation as reported by other authors. The siloxane phase  $T_g$  was observed at -115 to -133 °C and the imide phase  $T_g$  at 254-336 °C. The thermal stability also decreased with increasing siloxane amount. This was attributed to the increase in n-propyl linkages between siloxane and imide segments. The  $T_{5\%}$  was observed at 420-510 °C in air.

Ghosh et al.<sup>38</sup> also investigated PIS phase separated materials with fluorinated polyimide segments. Perfectly alternating copolymers were synthesized with segments of varying lengths. The glass transition temperature and elastic modulus of these materials could be tailored based on composition. Polymers were soluble in chloroform, DCM, DMF, THF, DMAc and NMP. The siloxane and imide blocks exhibited glass transitions in the range of 2-12 °C and 132-218 °C respectively. The block copolymer showed a  $T_g$  at 40 °C higher than an analogous random copolymer. This was attributed to increased regularity and decreased size of phase separated morphologies. The  $T_{5\%}$  was observed in at 450-519 °C and 410-487 °C in nitrogen and air respectively. The stability of the block copolymer was recorded at 20 °C higher than the random copolymer. Ghosh et al.<sup>188</sup> also investigated other PIS copolymers.  $T_g$  and oxidative stability both decreased with siloxane content. PIS polymers showed glass transitions at 169-201 °C compared with the  $T_g$  of the homopolyimide at 217 °C. In air, 5 % weight loss occurred at 464-410 °C for PIS copolymers and 515 °C for the homopolyimide.

Additional PIS materials were investigated by Xi et al.<sup>37</sup> It was reported that the  $T_g$  of the siloxane and imide segments were around 100 and 250 °C respectively. With increasing PDMS content, the  $T_g$  of the hard imide block decreased and became less visible. In nitrogen atmosphere, the decomposition temperatures increased with siloxane content.  $T_{5\%}$  was observed in the range of 360-520 °C.

Blends of PDMS or PMPS and polyimide were produced by Tiwari et al.<sup>43</sup> PDMS and PMPS were dissolved in THF and blended with poly (amic-acid) solutions in DMAc. The solutions were then cast, dried, and imidized. Interestingly these blends displayed as high or higher stability than most of the copolymers in literature. Additionally, thermal and oxidative stability increased with siloxane content. For PDMS/imides, 10% weight loss was observed at 604-618 °C in nitrogen and

545-566 °C in air. For PMPS/imides 10% weight loss was observed at 635-682 °C and 563-612 °C in nitrogen and air respectively.

Carbosiloxanes have also been produced by a number of authors with direct attachment of siloxane linkages to aromatic backbones without the use of aliphatic bridges.<sup>40</sup> Damaceanu et al.<sup>41</sup> produced tetramethyldisiloxane-containing poly(oxadiazole-imide)s. The elastic moduli of the materials were 1.5-1.9 GPa.  $T_g$  were observed at 165–183 °C and  $T_{5\%}$  occurred above 440 °C. The dielectric constant in the range of 1 Hz– 1 MHz was measured to be 2.69–2.90.

Tsai et al.<sup>194</sup> produced siloxane imides from poly(amic-acid) solutions endcapped with trioxysilanes. The crosslinking mechanism occurred with hydrolysis of oxysilanes to siloxanes by water produced from imidization reaction. With increasing siloxane content, the  $T_g$  increased from 242 °C up to 250 °C,  $T_{5\%}$  in nitrogen increased from 574 to 589 °C, and CTE decreased from 54 to 47  $\mu\text{m}/(\text{m } ^\circ\text{C})$ . This was explained by siloxane crosslinking. Although the molecular weight of the polyimide blocks was reduced, the degree of crosslinking through terminal oxysilane groups increased.

A similar approach was used by Zhuo.<sup>45, 143</sup> who produced hyperbranched polysiloxane bismaleimide-diallylbisphenol-A and bismaleimide-cyanate ester copolymers. For bismaleimide-cyanate ester resins, phenyltrimethoxysilane was polymerized in the presence of water to form a hyperbranched siloxane network terminated by hydroxyl groups. The hyperbranched siloxane and bismaleimide-cyanate ester were then co-polymerized. The crosslinking mechanism occurred via reaction of the hydroxyl groups with the cyanate ester moiety. For bismaleimide-diallylbisphenol A resins, phenyltrimethoxysilane,  $\gamma$ -aminopropyl triethoxysilane, and hexamethyldisilazane was polymerized in the presence of water to form a hyperbranched siloxane network. The network was terminated with oxyethyl and amine groups. The resins crosslinked via the reaction between amine and maleimide groups. In TGA, 5% weight loss occurred around 370-430 °C in air for both copolymer resins, slightly lower than observed for bismaleimide-diallylbisphenol-A and bismaleimide-cyanate ester homopolymers. Copolymer resins did show decreased dielectric constant and loss, and improved flame retardancy.

A ladder-like polysiloxane, functionalized with amine and phosphaphenanthrene groups, was co-polymerized with a bismaleimide resin by Chen et al.<sup>144</sup> The resin system showed excellent flammability resistance. Compared with the neat BMI resin the thermal stability in nitrogen

improved with addition of up to 20 wt.% siloxane. In fact, the pure ladder-like polysiloxane exhibited the best thermal performance, with initial degradations beginning around 427 °C. The dielectric constant and CTE also decreased by 10-20% with the addition of the siloxane.<sup>144</sup>

Chavez et al.<sup>195</sup> synthesized polyimides containing tetraphenylsilane and hexaphenyldisiloxane linkages. Three different dianhydrides were also used: pyromellitic dianhydride, 3,3',4,4'-tetracarboxylic dianhydride (BTDA), and 4,4'-oxidiphtalic anhydride (OPDA). Tetraphenylsilane containing polymers possessed melting points of 140 °C to greater than 400 °C depending on the flexibility of the anhydride portion and meta or para attachment to the tetraphenylsilane. Hexaphenyldisiloxane-polyimides showed the same trends with melting points of 170 °C to >400 °C. The inclusion of the disiloxane linkage did not necessarily decrease the melting point of the monomer. Hexaphenyldisiloxane compounds with more rigid dianhydride linkages possessed lower melting points than the corresponding tetraphenylsilane compound. However, with more flexible dianhydride linkages the trend reversed, with tetraphenylsilane-imides showing lower melting points. Some polymers, those with more flexible dianhydride linkages and meta substitution, were soluble in DMAc. No phase separation was observed. In general, the polymers displayed 5 wt. % loss in argon at 280-400 °C for meta-substituted compounds and 360-460 °C for para-substituted compounds. The use of the more flexible OPDA resulted in little difference between meta and para substituted compounds. Polymers with OPDA also provided much lower stability than polymers with the other two dianhydride linkages, but also possessed lower melting points. Similarly, ladder-like hexaphenyldisiloxane imides were also produced.<sup>196</sup> Melting points were observed 200 °C to greater than 400 °C. Only polymers with flexible dianhydrides, BTDA and OPDA, showed melting points. The onsets of degradation at occurred at relatively low temperatures of 323-460 °C.

#### 2.3.1.4.4 Carboxysilanes

A number of groups have investigated polymers based on carboxysilane linkages. Whereas for the most part, polymers discussed in the previous sections contain Si-O-Si or Si-C bonds, these materials contain Si-O-C linkages.<sup>85</sup> Similar to the siloxane bond, the carboxysilane bond is very flexible with a wide bond angle of 111-144°.<sup>197</sup> Various synthesis methods for oxysilanes are described by Kawakami<sup>198</sup> as well as Cella and Rubinsztajn.<sup>82</sup> For high temperature applications, focus is generally placed on carboxysilanes where the carbon substituent is aromatic. These

aryloxysilanes provide greater thermal stability in comparison to alkoxy silanes. It is reported that aryloxysilane polymers are also more thermally stable than PDMS materials, with decomposition temperatures above 350 °C.<sup>85, 170</sup> However, the hydrolytic sensitivity of the carboxysilane linkage has been the subject of substantial debate and investigation. Hydrolysis occurs more readily in carboxysilanes as compared with siloxanes.<sup>53, 82-86</sup> Where the Si-O linkage in siloxanes is more ionic, the O-C linkage in oxysilanes is more covalent. The difference in size and electronegativity between carbon and silicon atoms also play a role. Hydrolysis occurs to produce Si-OH and C-OH moieties. The effective hydrolytic stability of this linkage seems to depend on the substituents on the silicon, the nature of the organic moiety, steric hindrance around the linkage, the crosslinked nature of the polymer, and the nature and content of residual impurities. For these reasons, some literature reports polymers with high hydrolytic resistance, while other similar polymers appear to degrade readily.<sup>53, 82</sup>

The rate of this cleavage also depends on moisture content and temperature. While hydrolytic degradation also occurs at room temperatures, it can be especially rapid at processing and service temperatures.<sup>82</sup> There are several ways to improve the hydrolytic and solvolytic degradation. The use of a methylene bridge to produce alkoxy linkages instead of aryloxy linkages results in greater hydrolytic stability.<sup>30, 52, 79</sup> However, this approach sacrifices thermal stability.<sup>10, 36, 133</sup> Hydrolysis and alcoholysis is also acid and base catalyzed, thus acids, bases, or salts present as impurities can expedite degradation. Aryloxysilane linkages are commonly synthesized by condensation reactions with phenols and chlorosilanes. The reaction is catalyzed by a base with the addition of an amine, and ammonium salts are produced as a byproduct. These impurities must be thoroughly removed.<sup>82</sup> By eliminated and avoiding ionic and polar impurities, the rate of degradation may be reduced. Lastly, the rate of hydrolysis or alcoholysis may be retarded substantially by increasing the steric bulk around the Si-O-C linkage. Cella and Rubinsztajn<sup>82</sup> provide a table with relative half-lives of several aryloxysilane linkages subject to methanolysis. Several orders of magnitude difference in rate is observed as a function of increasing bulk of substitution on the silicon and ortho position of aromatic moieties. However, this increasing steric hindrance is also likely to limit the flexibility of the carboxysilane linkage and thus increase the melting points of the monomers.<sup>82</sup> A number of groups have investigated polymers of the type presented in Figure 10.<sup>63, 78, 83-85, 170,</sup>

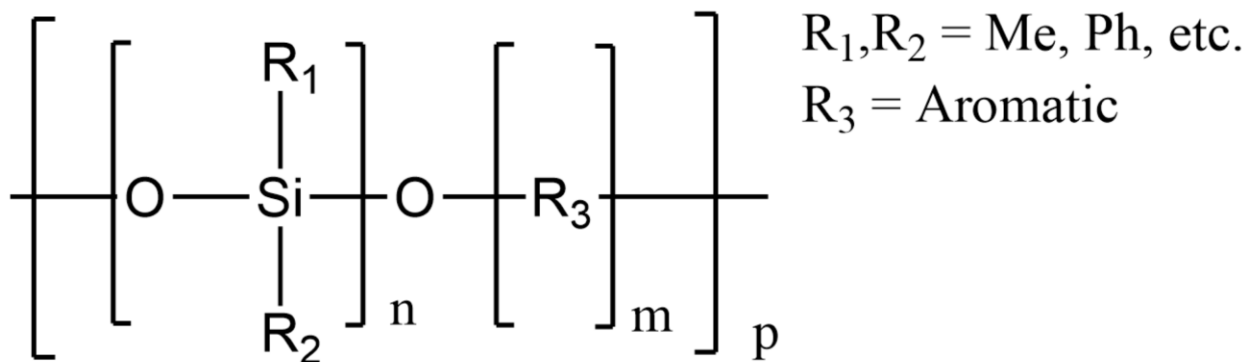


Figure 10: Backbone structure of aryloxysilane polymers.

Noshay and Matzner et al.<sup>83-84</sup> produced a series of block copolymers with polydimethylsiloxane segments linked arylene ethers or cyclobutene hard segments. The polymers showed  $T_{5\%}$  at 380-460 °C in  $\text{N}_2$  and 300-430 °C in air. It was reported that toughness was improved but UV stability decreased. Polymers also showed high hydrolytic stability. Little degradation was observed after 4-8 weeks of immersion in boiling water or more than 2 weeks in 10% aqueous NaOH or 10% aqueous HCl. This was likely due in part to the hydrophobic effects of the PDMS linkages as well as the steric hindrance around the Si-O-C linkage as well as the limited number of Si-O-C linkages in the polymer.

Arsen'eva et al.<sup>85</sup> investigated the hydrolytic and thermo-oxidative polymers incorporating dimethyldiphenoxysilane (DMPS), methylphenyldiphenoxysilane (MPPS) and diphenyldiphenoxysilane (DPPS). Hard sections were produced from the aromatic diols, bisphenol-A and bisphenol-S. The polymers showed softening points of 54-190 °C. The hydrolytic stability was dependent on both the bisphenol and the substitution on the silicon. The polymers produced from DPPS and bisphenol-A displayed high hydrolytic stability, due to the non-polar nature of the bisphenol-A linkage and the steric hindrance of the phenyl functional groups. The sample mass and IR spectra showed no change after immersion in water for 15 days. All other polymers showed some degree of hydrolytic degradation. Methyl-substitution on the silicon and the use of the bisphenol-S linkage resulted in increased hydrolytic degradation, with weight losses up to 9 % after 15 days immersion. The increased degradation of the bisphenol-S containing polymers was likely due to the increased polarity of the sulfonyl group in comparison to the isopropylidene group. In the IR spectrum the bands at 920-945  $\text{cm}^{-1}$  (Si-O-Ph) decreased and peaks formed at 3400, 1225 and 1350  $\text{cm}^{-1}$  (Ph-OH), and 3400 and 880  $\text{cm}^{-1}$  (Si-OH), and 1030-1100

cm<sup>-1</sup> (Si-O-Si). Thermo-oxidative stability was evaluated by heating with a series of 1-hour long steps up to 350 °C. Compared with bisphenol-A polymers, materials with bisphenol-S exhibited higher initial thermal stability but showed higher degradation rates at higher temperatures. During initial decomposition, phenolic end groups were produced from phenoxy linkages. With increasing degradation diol segments and benzene are released. Diol groups resulted from degradation of the polymer backbone. Benzene was produced by cleavage of phenyl functional groups on the silicon. Phenolic end groups and diol segments catalyzed the cleavage of Si-phenyl and Si-O-C linkages. The polymers with DPPS linkages showed the highest stability. After 7 hours at 300 °C, 2% weight loss was observed. In contrast, MPPS and DMPS polymers showed 7% and 10% weight loss respectively.

Beattie<sup>78</sup> synthesized methyl and phenyl substituted aryloxysilane polymers and evaluated their thermal and hydrolytic stability. It was reported that these materials showed similar weight loss to PDMS. Phenyl-substituted aryloxysilanes showed improved thermal performance compared with methyl-substituted polymers. In addition, phenyl substitution was reported to improve compatibility with organic polymers but also increase viscosity. Rearrangement degradation mechanisms were discussed involving nucleophilic attack by oxygen on the silicon.

In work by Curry et al.<sup>199</sup> aryloxydiphenylsilanes were melt polymerized at 200-300 °C under nitrogen. Various diols were considered including hydroquinone, resorcinol, 4,4'-Biphenol, 2,7-Naphthalenediol, and Bisphenol-A. These materials were mostly terminated by phenolic hydroxyl moieties. The polymers showed melting points between 99 °C and greater than 300 °C. The 5 % weight loss was observed at 390-530 °C depending on diol. Dunnivant et al.<sup>202</sup> continued the work by Curry et al.<sup>199</sup> Polymer T<sub>g</sub> values were in the range of 65-155 °C in nitrogen. Crosslinking was observed in air and polymers did not soften below 300 °C. The thermal stability in nitrogen followed the following trend of substitution on the silane: diphenyl > methylphenyl > dimethyl. It was observed that the molecular weight of polymers could be increased by re-heating with the addition of 5% of their monomer. This resulted in tough thermoplastic materials that were soluble in carbon tetrachloride, toluene, THF, 1,2,4 trichlorobenzene, benzene, and DMF. These materials were resistant to hydrolytic degradation in distilled water and 30% aqueous H<sub>2</sub>SO<sub>4</sub> for more than 7 days. Some hydrolysis and absorption were observed after prolonged exposure.

Aryloxysilanes with methyl, phenyl, vinyl, and allyl substitution on the silicon were also produced by Dunnivant et al.<sup>200</sup> Polymers were synthesized by melt-polymerizing dianilinosilanes with p,p'-biphenol. Linear materials exhibited thermoplastic behavior with very low softening temperatures, 50-90 °C. The use of vinyl or allyl functional groups resulted in crosslinked materials with softening points around 300 °C. These materials were able to be melt processed and drawn into fibers. Polymers showed T<sub>5%</sub> values at 370-490 °C and 420-480 °C in nitrogen and air respectively. Above 225 °C, a variety of degradation mechanisms occurred including cleavage of functional groups, backbone cleavage, and crosslinking reactions. Polymers were also aged in air at 200 °C or 300 °C for 21 hours. After aging at 300 °C, polymers retained 85-97% weight. Interestingly, some polymers exhibited higher weight loss after aging at 200 °C than they did at 300 °C. This was likely due to a higher rate of oxidative crosslinking. Polymers had good flammability resistance and were self-extinguishing. Some slow hydrolytic degradation was evident at 200-225 °C in air.

Drake et al.<sup>170</sup> produced aryloxysilanes endcapped with phenyl, phenylethynyl, and 4-fluorophenylethynyl. It was reported that un-encapped polymers produced by condensation of chlorosilanes and bisphenols degrade and crosslink at temperatures above 275 °C through silanol and phenol end groups. This mechanism results in benzene evolution and uncontrolled chain branching and crosslinking. Endcapping to prevent hydroxyl-catalyzed reactions resulted in improved thermal stability and melt stability. The un-encapped and un-crosslinked endcapped polymers showed glass transitions at 100-145 °C. For un-encapped materials, the T<sub>g</sub> was inversely proportional to the molecular weight, since a higher molecular weight meant a lower crosslinking density. Phenylethynyl, and 4-fluorophenylethynyl endcapped polymers were cured at 300 °C. In nitrogen, the T<sub>5%</sub> of un-encapped and endcapped polymers was observed at 500 °C and 510-515 °C respectively. Drake et al.<sup>63</sup> also investigated an additional aryloxysilane containing diacetylene linkages. Before crosslinking, the polymer showed no melting point, a T<sub>g</sub> of 130 °C, and a minimum viscosity at 203 °C. Crosslinking occurred above 260 °C. No T<sub>g</sub> was observed after crosslinking. During TGA, 5% weight loss was observed at 541 °C in N<sub>2</sub> and 522 °C in air. A char yield of 15.7% was observed in air. This value was very close to the theoretical char yield of 15.9% based on conversion of silicon to silicon dioxide.

Several groups have synthesized aryloxysilane-imide polymers. Babanzadeh et al.<sup>44, 203</sup> produced polyimides with diphenylaryloxysilane diamines. The inclusion of flexible ether and oxysilane linkages, as well as the bulky phenyl groups, resulted in amorphous polymers. These materials were soluble in DMF, DMSO, NMP, and DMAc. The materials showed  $T_g$  values of 191 to 220 °C. In nitrogen, the  $T_{10\%}$  was in the range of 390-455 °C. Dielectric constants were measured in the range of 2.96-2.42.

Agrawal and Narula<sup>204</sup> synthesized polyamide-imides produced with a dimethylaryloxysilane diamine. The glass transition temperatures were observed at 254–302 °C. Polymers were soluble in DMF, DMSO, NMP, DMAc, *m*-cresol, pyridine, and H<sub>2</sub>SO<sub>4</sub>, and somewhat soluble in acetone. In nitrogen,  $T_{10\%}$  was observed at 557-575 °C.

Kolahdoozan and Ghoreishi<sup>205</sup> produced dimethyl-substituted aryloxysilanes-copoly(amide-imide)s with different aromatic linkages. Polymers were again soluble in DMF, NMP, DMAc, and H<sub>2</sub>SO<sub>4</sub>. Some polymers were also soluble in ethanol, methanol, ethyl acetate, chloroform, and DCM. The glass transitions were observed at 170-290 °C. TGA in nitrogen revealed  $T_{5\%}$  at 335-460 °C and  $T_{10\%}$  at 445-525 °C.

#### 2.3.1.4.5 A Summary of Degradation Mechanisms of Silicon-Containing Polymers

This section summarizes a number of degradation mechanisms observed in silicon-containing polymers, as mentioned in previous sections. More degradations of silazane and Si-N bonded polymers are discussed by Bahloul et al.,<sup>148</sup> Chang et al.,<sup>206</sup> Kuřitka et al.,<sup>154</sup> and Beattie.<sup>78</sup> The hydrolytic stability of oxysilanes has already been discussed, and is shown in Figure 11.<sup>53, 82-86</sup> Similar hydrolysis reactions also occur with silanes,<sup>50, 149-150</sup> silazanes,<sup>206</sup> and siloxanes.

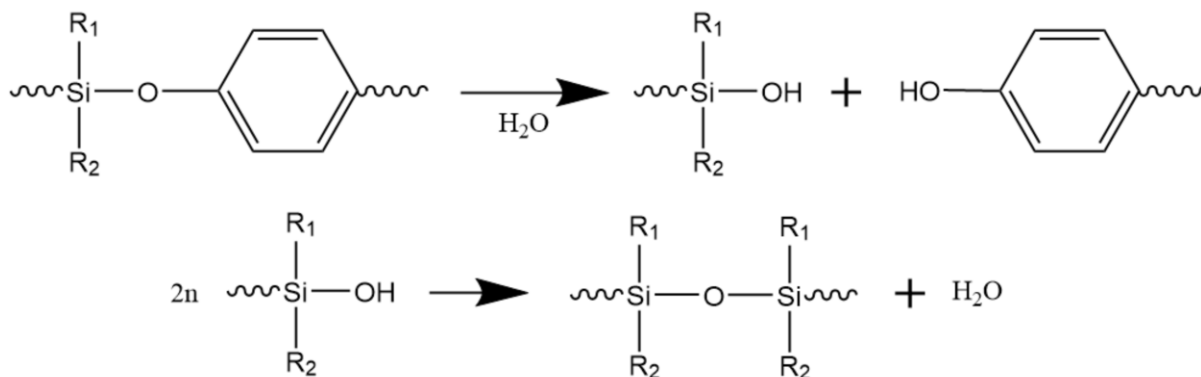


Figure 11: Hydrolysis of oxysilanes.<sup>53, 82-86</sup>

Thermal and oxidative decomposition occurs via several routes, depending on structure. Methyl-siloxanes degrade and form volatile low-molecular weight cyclosiloxanes by unzip or rearrangement mechanisms.<sup>80</sup> This is shown below in Figure 12 and Figure 13, where R represents a methyl or phenyl group. While the decomposition energy of the Si-C bond (322 kJ/mol) is lower than the Si-O bond (397 kJ/mol), energetically favored chain folding or chain-chain interactions and depolymerization result in heterolytic cleavage of the siloxane bond with an effective decomposition energy of only 167 kJ/mol.<sup>2, 72-75, 80</sup> The inclusion of phenyl functional groups is reported to hinder chain folding and prevent these degradations.<sup>34, 80, 153</sup>

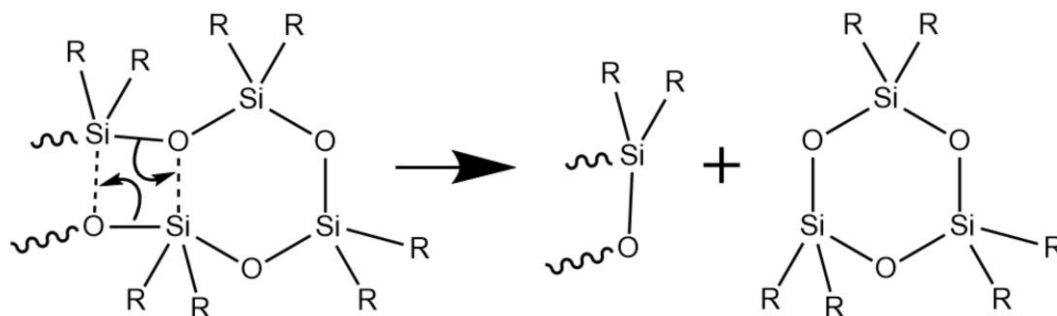


Figure 12: Rearrangement degradation of polydimethylsiloxane.<sup>80</sup>

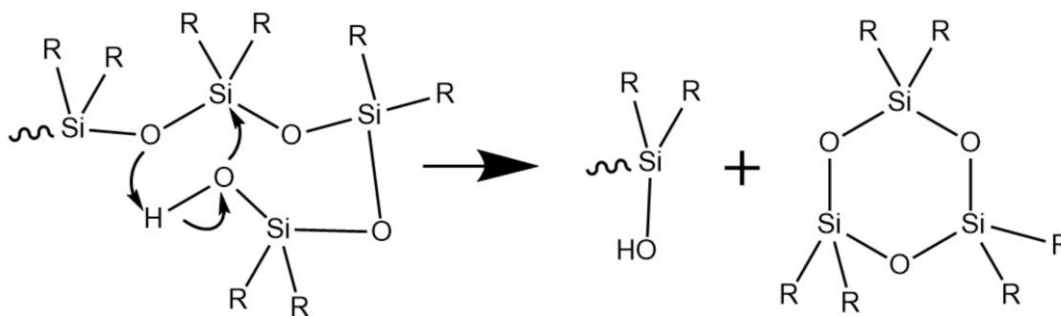


Figure 13: Unzip degradation of polydimethylsiloxane.<sup>80</sup>

Oxidative crosslinking is reported to occur via methyl groups<sup>156, 163, 165</sup> or hydrido groups.<sup>50-51</sup> Oxidation of methyl groups is shown in Figure 14. This reaction does result in stabilization of the polymer, but also releases carbon dioxide and water, and shrinkage or cracking can occur. The phenyl groups is reported to inhibit the oxidation of methyl groups by steric effects.<sup>153</sup>

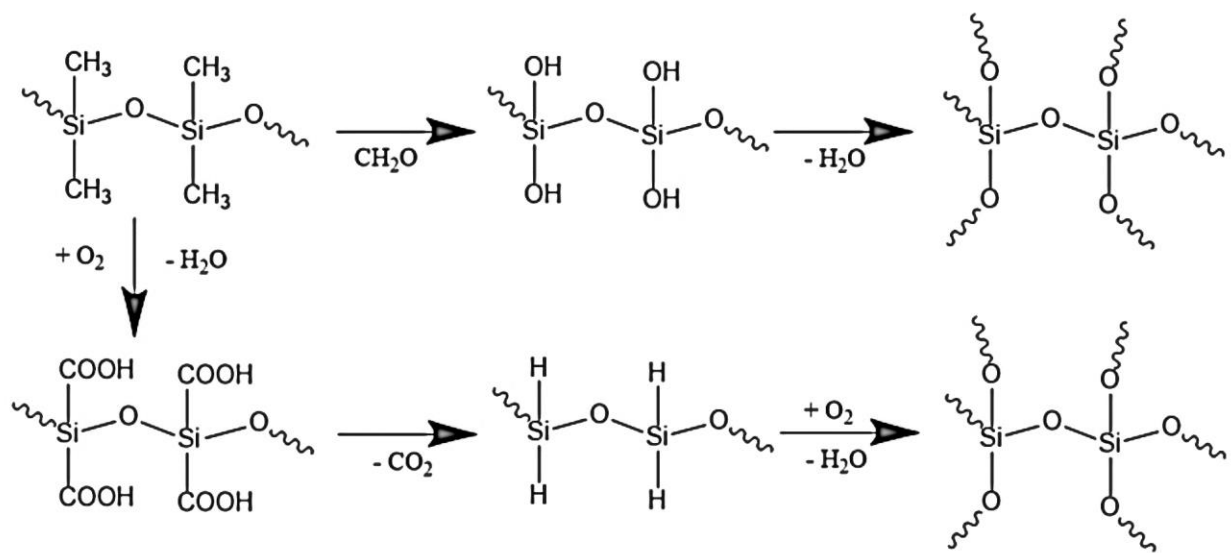


Figure 14: Oxidative crosslinking of polydimethylsiloxane.<sup>156, 163, 165</sup>

Several degradations of phenyl-substituted siloxanes and silanes are described by Beattie,<sup>78</sup> Drake et al.,<sup>170</sup> and Coutant and Levy.<sup>178</sup> Many different reactions are possible depending on steric hindrance, degree of phenyl-silicon (p-d) $\pi$  bonding, presence of oxygen or hydroxyl groups, temperature, and aging time. Hydroxyl groups catalyze the cleavage of phenyl groups from methyl-phenyl and diphenyl substituted organosilicon compounds. This results in crosslinking with the release of benzene and formation of siloxane linkages, as shown in Figure 15 and Figure 16.<sup>78</sup>

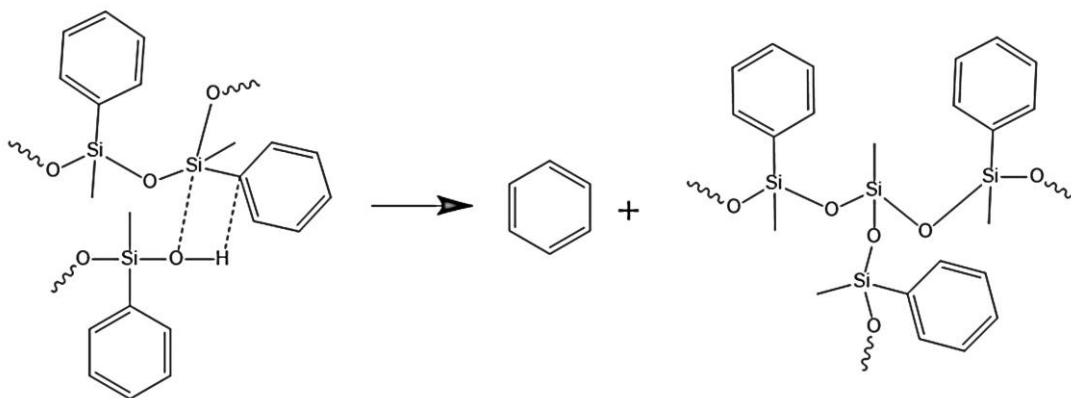


Figure 15: Hydroxyl-catalyzed degradation of methyl-phenyl siloxanes.<sup>78, 170</sup>

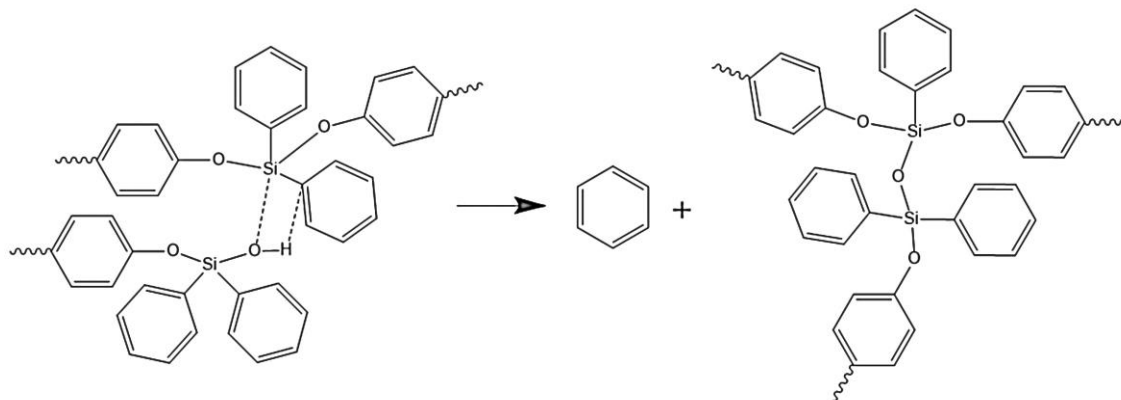


Figure 16: Hydroxyl-catalyzed degradation of diphenyl siloxanes.<sup>78, 170</sup>

The bond energy of the Si-phenyl bond is less than that of Si-O. Siloxane chains are not directly attacked by oxygen and free radicals. Instead thermal cleavage and oxidation of organic groups occurs.<sup>48</sup> Thus, if unzip and rearrangement mechanisms and oxidative crosslinking of methyl groups are avoided, cleavage of the Si-phenyl bond occurs at high temperatures before Si-O cleavage. This is shown in Figure 17.

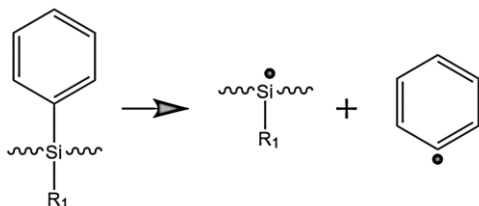


Figure 17: Cleavage of Si-phenyl functional groups at high temperatures.<sup>78</sup>

A variety of subsequent reactions and the formation of various products are then possible depending on environment, temperature, and surrounding structure. Oxidation or hydrogen abstraction from methyl or phenyl groups result in Si-H or siloxy groups, Figure 18 and Figure 19.<sup>78</sup> This cleavage also occurs in polymers with Si-phenylene linkages in the backbone. Above 350 °C, this can result in a chain branching mechanism, the rate of which is proportional to the amount of silphenylene linkages.<sup>78</sup> Cleavage and oxidation of organosilicon groups eventually leads to the formation of a silica phase.<sup>48</sup>

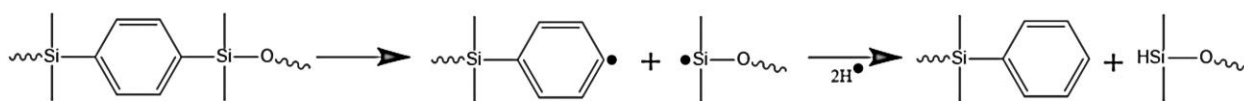


Figure 18: Silphenylene cleavage and hydrogen abstraction to form hydrido-silane groups.<sup>78</sup>

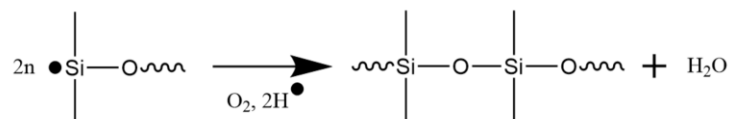


Figure 19 Silphenylene cleavage, hydrogen abstraction, and oxidative crosslinking.<sup>78</sup>

Generally increasing the phenyl-substitution on the silicon results in more thermally stable moieties. For example, poly(tetramethyl-silphenylene-siloxane) (TMPS) is less thermally stable than poly(methylphenyl-silphenylene-siloxane) (MPPS).<sup>78</sup> However this must be balanced with processing and synthesis considerations. For example, polydimethylsiloxane (PDMS) may be more stable than a poly(tetraphenyl-*p*-silphenylene-siloxane) (TPPS) polymer with low molecular weight.<sup>78</sup>

For phenyl or phenylene substituted organosilicon compounds, rearrangement mechanisms can still occur. These rearrangements can occur at temperatures around 300 °C, prior to direct scission of the Si-phenyl or Si-phenylene bond at temperatures above 450 °C.<sup>77-78</sup> In TMPS under inert conditions at lower temperatures, siloxane-silphenyl rearrangements occur as shown in Figure 20. This results in an increase in the polydispersity. At higher temperatures, Si-phenylene cleavage occurs, eventually leading to the formation of hexamethylcyclotrisiloxane.<sup>78</sup>

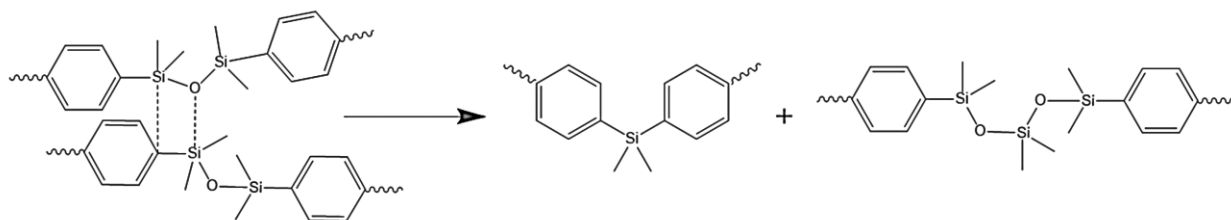


Figure 20: Rearrangement mechanism in poly(tetramethyl-silphenylene-siloxane).<sup>78</sup>

In MPPS under inert conditions, cyclic oligomer formation does not widely occur, due to the rigidity and steric hindrance of the phenylene linkage. Instead linear oligomers terminated with Si-H or Si-phenyl groups are produced. Again, two stages are observed, with rearrangements occurring at lower temperatures and scission of Si-phenyl or Si-phenylene bonds occurring at higher temperatures. At temperatures around 500 °C, the formation of bicyclic compounds is also possible. Rearrangements may occur via interactions of siloxanes moieties with methyl, phenyl, or phenylene groups. When pendant methyl or phenyl groups are involved, these reactions can result in chain-branching, as shown in Figure 21 and Figure 22.<sup>78</sup>

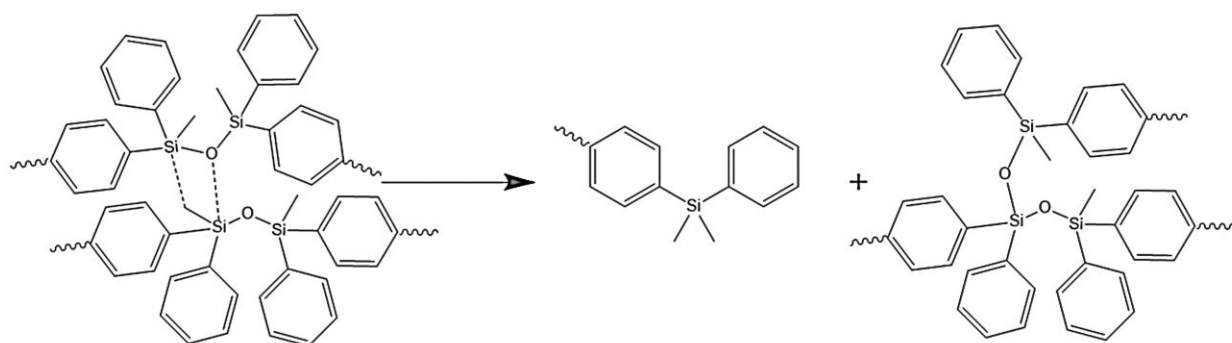


Figure 21: Rearrangements involving methyl functional groups, resulting in chain branching.<sup>78</sup>

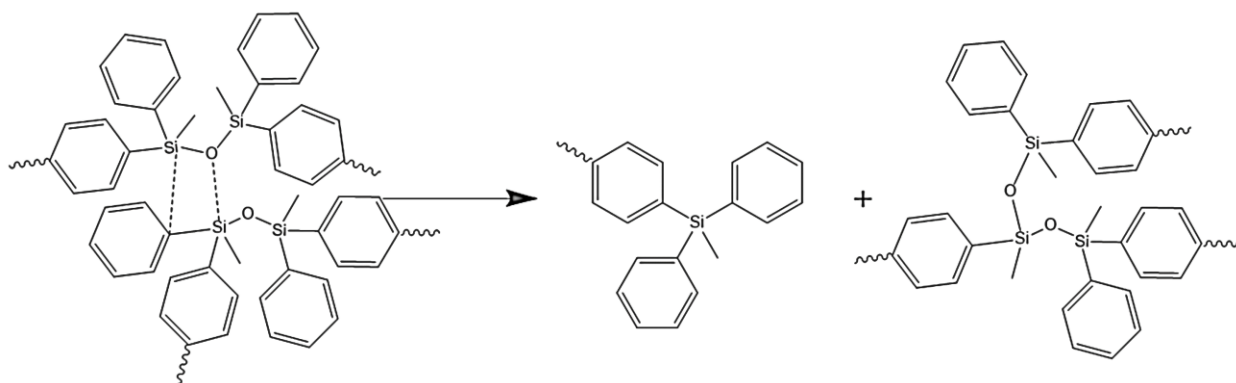


Figure 22: Rearrangements involving phenyl functional groups, resulting in chain branching.<sup>78</sup>

Phenyl-hydridosilanes (mono-, di-, and tri-phenylsilanes) also undergo similar rearrangements of structure at temperatures above 230 °C.<sup>180</sup> This reaction is shown in Figure 23 for a triphenylsilane. These disproportionation reactions are reported to occur via the formation of a four-center activated complex and free radicals are not formed.<sup>178</sup> If the reaction involves phenyl functional groups, chain branching occurs. If it occurs via phenylene linkages, the polydispersity is increased. The presence of chloride salts is reported to catalyze these redistribution reactions.<sup>180</sup>

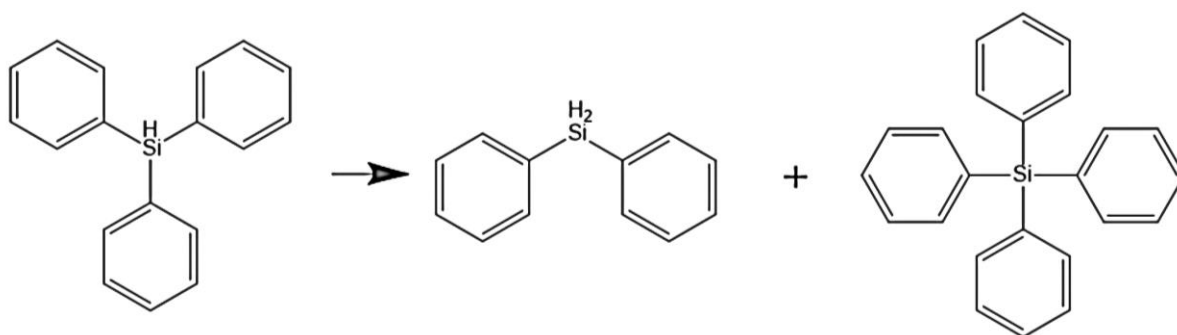


Figure 23: Disproportionation reaction of triphenylsilane.<sup>178, 180, 207</sup>

Under inert conditions at high temperatures, tetraphenylsilane and phenylmethylsilanes undergo free-radical reactions. Silyl, phenyl, and hydrogen radicals and a variety of products are

produced.<sup>178</sup> Coutant and Levy<sup>178</sup> studied the degradation of tetraphenylsilane in the range of 530-663 °C under inert conditions. It was observed that unlike mono, di, and tri-phenylsilanes, tetraphenylsilane first decomposed by cleavage of Si-phenyl bonds. This cleavage was reported to occur via a free radical mechanism to produce triphenylsilyl products and phenyl radicals. These radicals can then interact with the main chain to form several products, including benzene, hydrogen, triphenylsilane, and para, meta, and ortho-biphenyl-triphenylsilane. Additionally, during long-term aging, diphenyl dibenzosilole can also form.<sup>78, 169, 178, 207</sup> Benzene may be produced from phenyl-radicals abstracting hydrogen.<sup>178</sup> In inert atmosphere, the triphenylsilyl radicals may abstract hydrogen to produce triphenylsilane. Triphenylsilane, then decomposes as discussed previously to yield various phenylsilanes, Figure 23. The activation energy for degradation of tetraphenylsilane was reported to be 325 kJ/mol, slightly higher than that of triphenylsilane, 293 kJ/mol.

Roughly 60% of the products were biphenyl structures. Biphenyl-triphenylsilanes are produced from interactions of phenyl radicals or from dehydrogenation of phenyl groups. One example reaction of this type is given in Figure 24. The distribution of products was observed to be 2:4:1 para:meta:ortho isomers.<sup>168, 178, 207</sup>

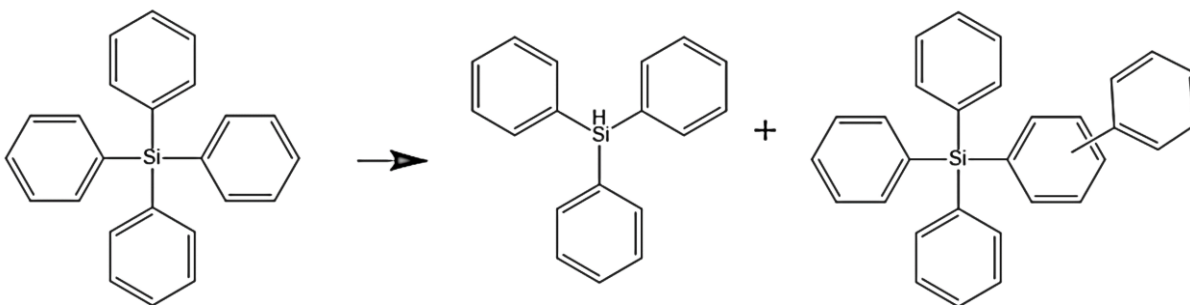


Figure 24: Formation of biphenyl-triphenylsilanes.<sup>178, 207</sup>

During long-term degradation, the formation of 5, 5'-diphenyldibenzosilole and 5, 5'-spirobi(dibenzosilole) were also observed. This cyclization occurred via free-radical reactions. While this reaction was of minor importance in the degradation of tetraphenylsilane, it was described at the primary degradation mechanism for dimethyl-diphenyl silane and methyl-triphenylsilane, as shown in Figure 25.<sup>178</sup>

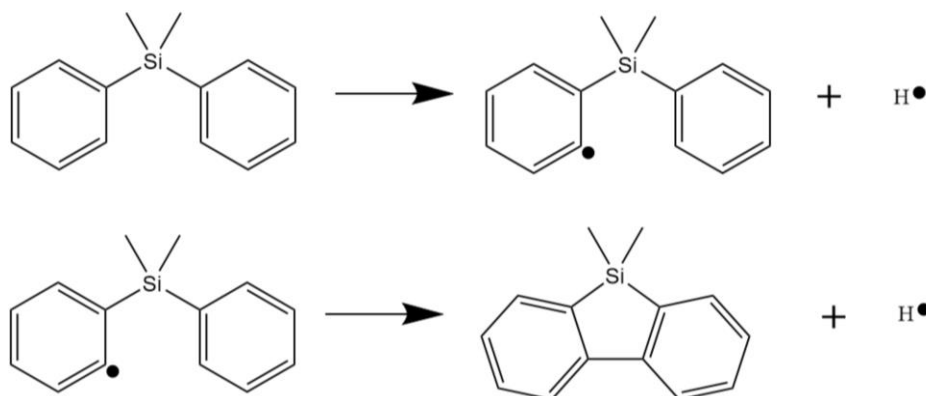


Figure 25: Intermolecular cyclization of dimethyl-diphenylsilane to form 5, 5-dimethyl dibenzosilole.<sup>178, 207</sup>

### 2.3.2 Silicon-Containing Phthalonitriles

Phthalonitriles (PNs) are good candidates for hybridization with organosilicon moieties due to their ease of processing, low moisture absorption, and high glass transition temperatures.<sup>3-8, 15</sup> PN resins are also prone to cracking when exposed to high temperatures and oxidizing environments.<sup>96</sup> The inclusion of organosilicon substituents may provide a viable route to improving the toughness and oxidative stability of these polymers. Until recently, little research existed on silicon-containing phthalonitrile resins. However, since 2015 several groups have produced and characterized silicon-containing phthalonitrile compounds. Examples include silazane,<sup>51</sup> carboxysilane,<sup>30, 52</sup> carbosilane,<sup>50</sup> siloxane,<sup>6, 53</sup> and silsesquioxane groups.<sup>54</sup> Additional groups have synthesized silicon-containing phthalonitrile compounds but did not report the thermal properties of the neat polymers.<sup>55-57</sup>

While not directly phthalonitrile based polymers, materials have been produced with organosilicon linkages and phthalocyanine moieties. A number of siloxane, silane, silazane, and oxysilane linked phthalocyanine polymers were produced in the late 1990's and are covered in a review by McKeown.<sup>106</sup> These materials consisted of phthalocyanine-silicon complexes where the silicon atom connected the organic or siloxane backbone. In 2003, Maya et al.<sup>57</sup> produced phthalocyanines with dimethyl and diphenyl siloxane chains and measured their optical properties and aggregation.

The first known silicon-containing phthalonitrile monomers and polymers were synthesized by Hardict et al.<sup>56</sup> and reported in a dissertation in 2003. These phthalonitriles were blended with novolac resins. While the processing characteristics and thermal properties of the blends were

reported, no information was included on the properties of phthalonitriles containing silane and siloxane by themselves.

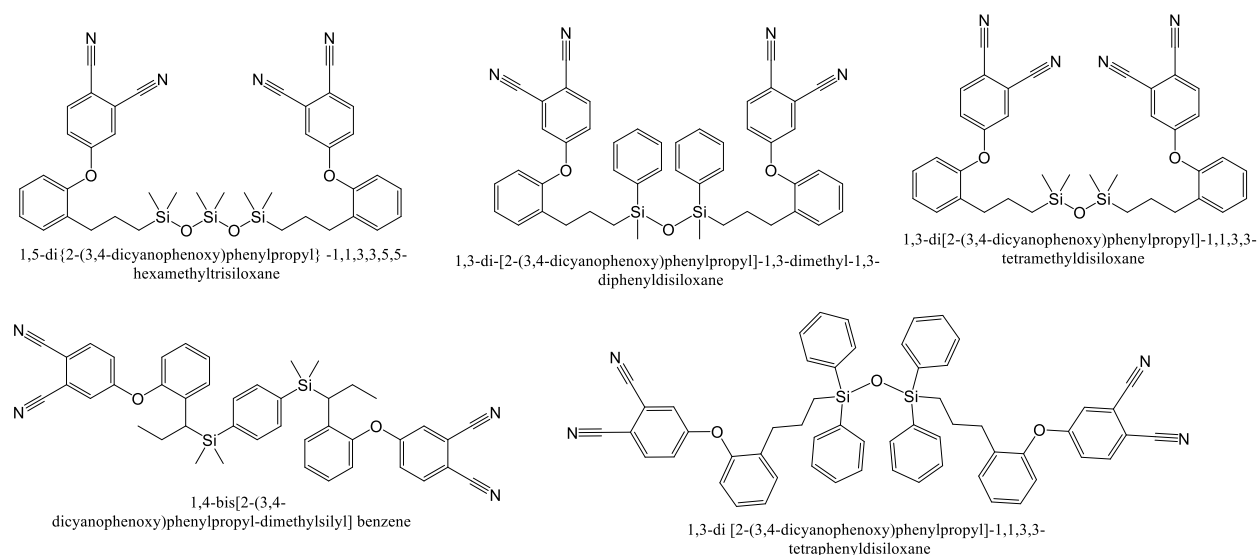


Figure 26: Silicon-containing phthalonitrile monomers produced by Hardrict et al.<sup>56</sup>

In the last few years, several chemistries have been produced and evaluated by Babkin, Bulgakov and their coworkers.<sup>30, 52-53, 79, 208-209</sup> The structures and properties are summarized in Table 8. In 2015, Babkin et al.<sup>30, 52, 79</sup> produced phthalonitriles with dimethyl, methylphenyl, and diphenyl substituted alkoxy silane linkages. The methylene bridge connected to the aromatic backbone via both meta and para substitution. Monomer melting points were not reported but glass transitions were reported at -1 to 27 °C. These alkoxy silane-PN monomers were hydrolytically stable enough to be purified by chromatography. This was explained by steric hindrance from phenyl substitution on the silicon, but was also likely due to the methylene bridge. The para-connected oxysilane with diphenyl substitution started with a low monomer  $T_g$ , but crystallized after heating to 150 °C. This indicates the pure compound possesses a melting point higher than this temperature. Viscosities for other monomers were observed at 0.3-0.6 Pa at 150 °C. Polymers were cured with 4 mol% of 1,3-bis(4-aminophenoxy)benzene (*m*-APB). Heat deflection temperatures in TMA were observed at 413–428 °C. No clear trend was observed in heat deflection temperature with respect to monomer structure.

In TGA, 5 % weight loss was measured at 531-554 °C in argon and 520–527 °C in air.  $T_{10\%}$  was observed in the range of 557-592 °C in argon and at 556 °C in air. Polymers exhibited high residual weight in  $N_2$  of 75-82 wt. % at 900 °C. Char yields in air were 11-13% at 1000 °C. Char

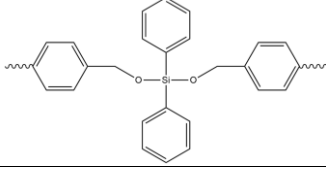
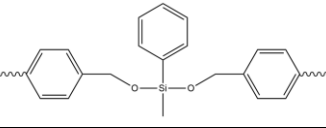
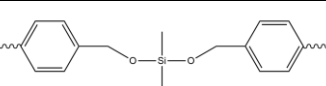
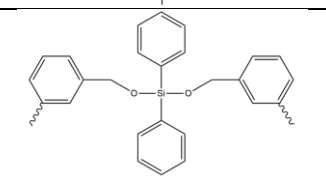
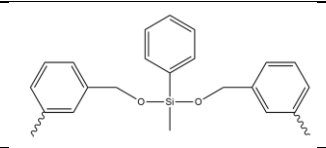
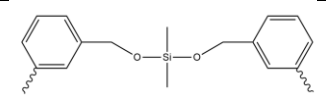
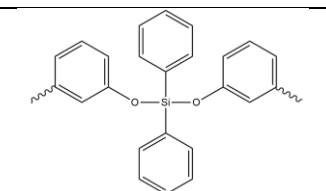
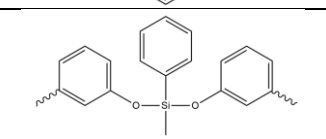
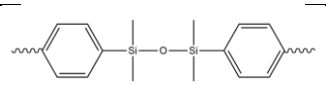
yields in air were 1-4% higher than predicted based on silicon conversion to SiO<sub>2</sub>. Interestingly, higher thermal stability in air was achieved with dimethyl substitution on the silicon and meta substitution on the aromatic backbone. This was attributed to increased flexibility of the monomer resulting in a greater degree of cure or different ratios of curing products. In contrast, polymers with phenyl functional groups and para substitution would have possessed more rigid, sterically hindered backbones, with decreased mobility. Four phthalonitrile groups are involved in phthalocyanine formation and three for triazine. Thus, the backbone must be flexible enough to allow for the formation of these groups. It was also reported that the phenyl group is more labile than the methyl group. In addition, the cleavage of a phenyl group results in more mass loss than loss of a methyl group, due to the difference in mass between benzene and methane. An additional explanation could involve oxidative crosslinking of the methyl groups. In argon, methylphenyl substitution on the silicon led to the highest stabilities. Again, this may be due to the relationship between monomer backbone flexibility and degree and nature of curing or difference in stability and resulting mass loss between Si-methyl and Si-phenyl groups. The observed stabilities were also very close to one another, so it is also possible that differences were within variances. It is unclear whether repeated trials were conducted or what the standard deviations would be. No clear trend was observed based on para/meta substitution on the aromatic backbone.

For the meta-substituted alkoxyasilane-phthalonitrile with methylphenyl functional groups, a flexural strength of 69 MPa was observed. Blends of phthalonitrile resins with 25-30% of this monomer were also considered.<sup>208-209</sup> Blends exhibited flexural strengths of 83±13 MPa and flexural moduli of 5.6±0.1 GPa. At 300 °C, polymers retained 70-85% of their mechanical properties. In flammability studies a limiting oxygen index of >80 was observed indicating excellent flammability resistance.

Babkin et al.<sup>30</sup> then utilized computational modeling was to predict the glass transition temperatures of multiple silicon-containing phthalonitriles. Predicted values were in good agreement with the previously synthesized alkoxyasilane-phthalonitriles. It was assumed that the methylene bridge of previously produced polymers resulted in decreased glass transition temperatures. The synthesis of aryloxyasilane phthalonitrile resins without this alkyl bridge was then attempted. However, it was discovered that the materials underwent rapid hydrolytic degradation. Monomers degraded quickly in solution and in contact with silica or alumina media.

Degradation was also slowly observed in the solid state. NMR was used to confirm the hydrolytic cleavage, with appearance of phenolic OH and polysiloxane peaks, and the disappearance of the water peak.

Table 8: Silicon-containing phthalonitriles synthesized by Babkin and co-workers.<sup>30, 52-53, 79</sup>

Linkage Structure	Monomer T <sub>g</sub> (°C)	Polymer T <sub>hd</sub> (°C)	Argon T <sub>5%</sub> (°C)	Argon T <sub>10%</sub> (°C)	Argon Char 900 °C (wt.%)	Air T <sub>5%</sub> (°C)	Air T <sub>10%</sub> (°C)	Air Char 1000 °C (wt.%)
	27	424	532	557	75	524	556	13
	12	420	537	563	79	520	553	12
	2	432	554	592	82	523	561	12
	21	415	531	585	75	524	556	11
	11	428	549	579	80	524	557	12
	-1	413	545	559	81	527	564	13
	29	-	-	-	-	-	-	-
	28	-	-	-	-	-	-	-
	4	471	503	538	76	495	579	22

A hexamethyldisiloxane was also synthesized in 2016.<sup>53</sup> The monomer was liquid at room temperature with a T<sub>g</sub> of 4 °C. After curing, the polymer exhibited a heat deflection temperature

of 471 °C, as measured using TMA in penetration mode. It is of note that this method usually provides elevated values compared to other measurement techniques. In TGA in argon, the T<sub>5%</sub> was observed at 503 °C and the T<sub>10%</sub> at 538 °C. The residual weight at 900 °C was 76%. In air, the T<sub>5%</sub> was observed at 495 °C, the T<sub>10%</sub> at 579 °C, and char yield at 1000 °C was 22 wt.%. A gradual weight loss was observed at temperatures above 200 °C. This was attributed to slow oxidation of the methyl groups on the disiloxane linkage. This oxidation likely helped stabilize the polymer against further degradation. The char yield in air was 21.8%, which was in good agreement with the 21.1% predicted by conversion of silicon to SiO<sub>2</sub>.

Other groups have also investigated silicon-containing phthalonitrile materials. PN resins with a tetramethyldisiloxane linkage connected to the aromatic segments by a methylene bridge were produced and evaluated by Laskoski et al.<sup>6</sup> The softening point of the resin was around 125 °C. The polymer exhibited a T<sub>5%</sub> at 420 °C in nitrogen and air. These values are very low compared with other phthalonitriles, likely due the dimethylsiloxane, methylene bridge, bisphenol-A linkages, and low maximum curing temperature of 300 °C.

Several groups have produced resins with polyhedral oligomeric silsesquioxane moieties. Li et al.<sup>54</sup> produced resins by co-curing organic bis-phthalonitrile monomer 4,4-bis(3,4-dicyanophenoxy)biphenyl with up to 10 wt. % epoxycyclohexyl and n-phenylaminopropyl POSS and 2 wt. % of the catalyst 4,4-bis(4-aminophenoxy)biphenyl. The oxidative stability improved slightly in TGA with the addition of POSS compounds. The effect was likely limited by the lower stability of linkages produced by the epoxycyclohexyl and n-phenylaminopropyl groups.

Kaliavaradhan and Muthusamy<sup>210</sup> produced a polymer by connecting phthalonitrile groups via oxysilane linkages to an incompletely condensed phenyl silsesquioxane (POSS). The electron withdrawing nature of the phthalonitrile group may have added some stability to the oxysilane linkage. The monomer was dissolved in DMSO and mixed with 3-5 wt. % of 4,4-diaminodiphenyl sulfone. The melting point of the compound was not reported but is expected to be very high due to the high melting points of phenyl-POSS. In TGA, the thermal stability in nitrogen was observed with the T<sub>5%</sub> at 440-470 °C and the T<sub>10%</sub> at 463-520 °C. These values are quite low for phthalonitrile and POSS compounds. It is possible that incomplete curing due to monomer rigidity, or degradation prior to curing via unreacted silanol groups occurred. Phase separation between the monomer and the catalyst was also possible.

Several groups have made use of silazanes or silazane linkages in the curing of phthalonitriles.<sup>50-51, 211</sup> In 2014 Zhang et al.<sup>51</sup> reported on the inclusion of silazane linkages into bis-PN monomers with methylhydro, methylvinyl, or dimethyl functional groups on the silicon atom. The monomers displayed low melting points of 40–60 °C. The monomers were soluble in acetone, DMF, chloroform, DCM, ethyl acetate, and diethylamine. The silazane-linked phthalonitriles exhibited self-curing behavior due to the secondary amine in the silazane linkage. The addition of a catalyst was not needed. The cure reaction occurred at 255–281 °C. Due to the lower basicity of the silazane amine, compared with the primary amines used in PN catalyst compounds, the curing peak shifted to higher temperatures by 6–33 °C. This lower basicity was due to the occupation of the empty silicon d orbital by the lone pair on the nitrogen, producing a  $d\pi-p\pi$  electron withdrawing effect. In addition to standard nitrile curing reactions, in the methylhydro-silazane PN system, dehydrogenation reactions occurred between hydridosilane bonds and amines, as shown in Figure 27. The resins exhibited glass transitions at temperatures greater than 450 °C.  $T_{5\%}$  was observed at 535–570 °C and 543–562 °C in  $N_2$  and air respectively. At 1000 °C, residual char yields were 80.2–82.6 wt.% in  $N_2$  and 10.1–12.5 wt.% in air. The hydridomethyl-substituted polymer possessed the highest stability. This was attributed to the dehydrogenation reaction.

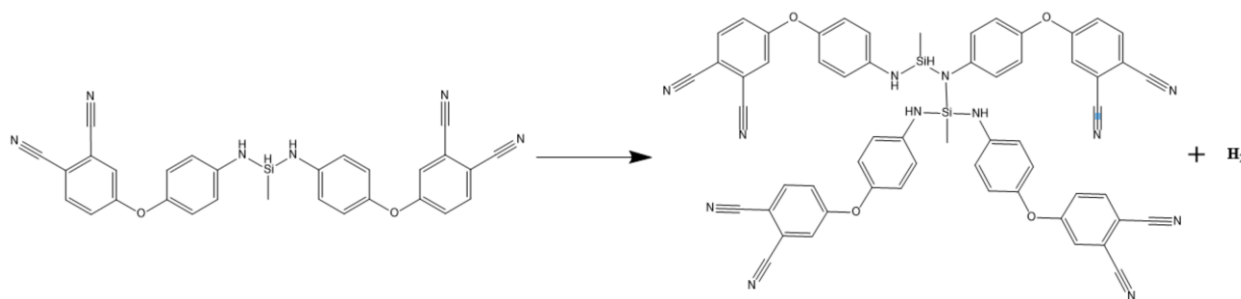


*Figure 27: Crosslinking through dehydrogenation between silazane Si-H and amine N-H bonds.<sup>51</sup>*

Recently, Wang and Ning<sup>50</sup> reported a oligosilylarylnitrile resin of with two methylsilane linkages and nitrile substituted phenylene linkage between terminal phthalonitrile groups. Interestingly the use of a catalyst was not reported, implying the resin exhibited self-catalyzed behavior, likely due to residual impurities or active hydrogen from the Si-H bonds. The resin displayed a softening temperature near 60 °C. Gelation occurred at 160 °C and a curing peak was exhibited at 268 °C. The PN resin was also cured with the addition of 20 wt.%

hydridomethylpolysilazane. The silazane-PN mixture was liquid at room temperature. No phase separation was reported, likely due to the hydridomethyl-silicon moieties in both compounds. For the silazane-PN blend, gelation occurred at 100 °C and a curing peak was observed at 158 °C. Both pure and resin with 20 wt.% polysilazane were cured to a maximum temperature of 200-250 °C for 2 hours, much lower than the traditional postcuring temperature of 375 °C.<sup>50</sup>

The neat oligosilylarylnitrile polymer possessed high stability in TGA with T<sub>5%</sub> observed at 660 °C and 460 °C in nitrogen and air respectively. Very high char yields were also observed at 800 °C with 92.5 wt. % and 55 wt.% in nitrogen and air respectively. It is of note that the values of T<sub>5%</sub> and char yield are likely elevated slightly due to the 20 °C/min ramp rate used in these TGA experiments. It is also unclear whether powders or bulk samples were used. For the oligosilylarylnitrile-silazane blend, T<sub>5%</sub> was observed at 650 °C and 580 °C in N<sub>2</sub> and air respectively. Residue content at 800 °C was 90 wt.% and 74 wt.% in N<sub>2</sub> and air respectively. If these values are correct, they are some of the highest ever reported for phthalonitrile systems. The char yields in air were also much higher than predicted by simple conversion of silicon to SiO<sub>2</sub>. For reference the silicon contents of the neat resin and PN/silazane blend were 12.9 wt.% and 19.2 wt.% respectively, resulting in predicted char yields of 27.6 and 41.1 respectively. Both resins displayed glass transitions above 420 °C. Laminates were produced with silica cloth and provided good mechanical properties on par with other phthalonitriles and polyimides. Greater than 50% retention of mechanical properties was observed at 400 °C.<sup>50</sup>

In addition to traditional phthalonitrile crosslinking mechanisms involving cyano groups (isoindoline, phthalocyanine, and triazine formation), the neat polymer underwent hydrosilylation reactions between C≡N and Si-H moieties, as shown in Figure 28.

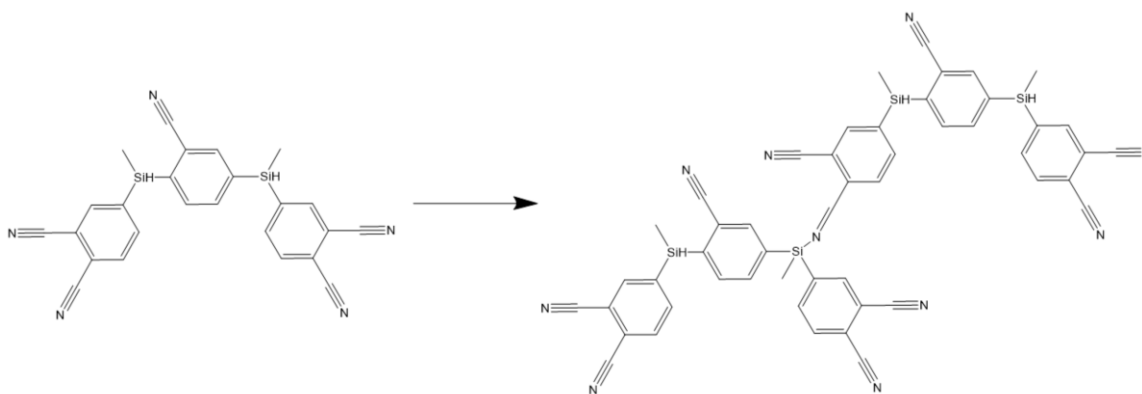


Figure 28: Hydrosilylation between C≡N and Si-H to form a Schiff base structure.<sup>50</sup>

With the addition of silazane, additional curing mechanisms also likely included reactions between cyano groups and N–H groups (Michael reactions) and Si–N groups (nitrosilylation addition reactions). This is shown in Figure 29 and Figure 30.<sup>50</sup>

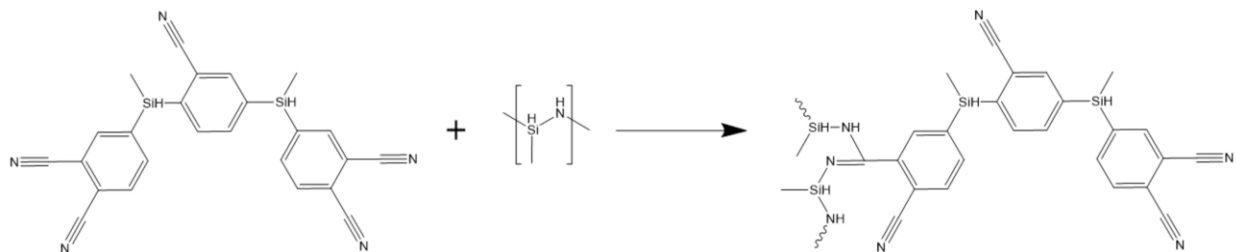


Figure 29: Nucleophilic nitrosilylation of Si–N and C≡N moieties.<sup>50</sup>

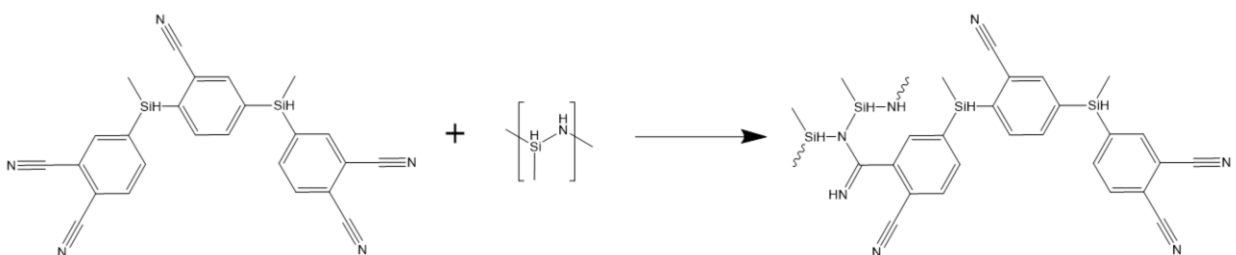


Figure 30: Nucleophilic addition of N–H and C≡N moieties.<sup>50</sup>

The work of Phua et al.<sup>125</sup> is also worth considering. Though their work used SiO<sub>2</sub> fillers instead of molecularly incorporated silicon, many similar interactions between Si, OH, and C≡N groups are discussed, including adducts with isoindoline, triazine, and phthalocyanine. A resorcinol-based phthalonitrile with silica fillers was used for encapsulation of high temperature electronics. DFT calculations found the adduct with isoindoline to be thermodynamically unfavorable but adducts with triazine, and phthalocyanine to be thermodynamically feasible. These interactions are described in Figure 31 and Figure 32.

The addition of silica fillers resulted in improved performance for an encapsulated package. Neat PN encapsulant cracked during exposure to 138 MPa at 250 °C. In contrast, PN resin with the addition of 50 wt.% silica fillers survived, and the package bonds remained intact, after exposure at 190 MPa and 310 °C for 168 hours. This improved performance was attributed not only to thermal stabilization of the PN resin, but also the reduction in CTE with the addition of silica. This resulted in diminished CTE mismatch between encapsulant and package components, which reduced the effective thermal stresses.<sup>125</sup> The dielectric constant of the PN-composite decreased from 7.36 for the neat resin to 3.99 with the addition of 50 wt.% silica. It is of note that the specific curing profile is not discussed, only that the resin was cured at 200 °C for 10 minutes

and the package was subjected to an unspecified heat treatment. The high value of the dielectric constant for the neat PN conflicts with other PN literature<sup>6-7</sup> and may indicate that the resin was not fully cured.

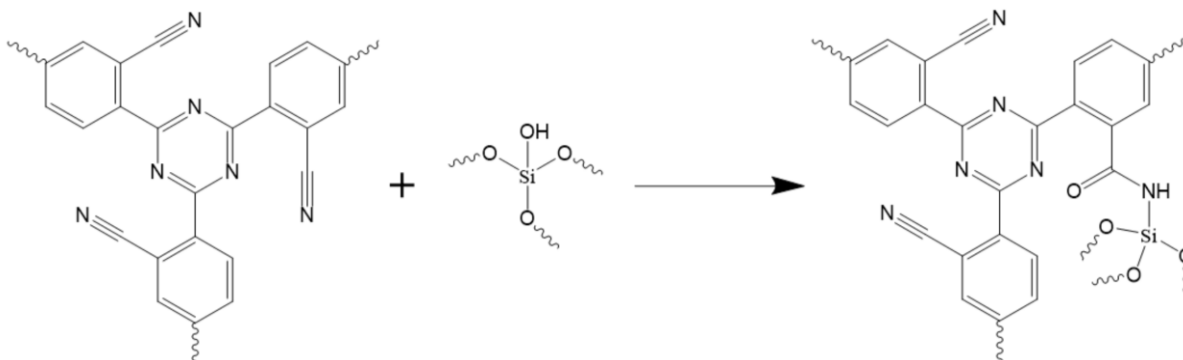


Figure 31: Reaction of silanol groups with cyano groups of the triazine moiety.<sup>125</sup>

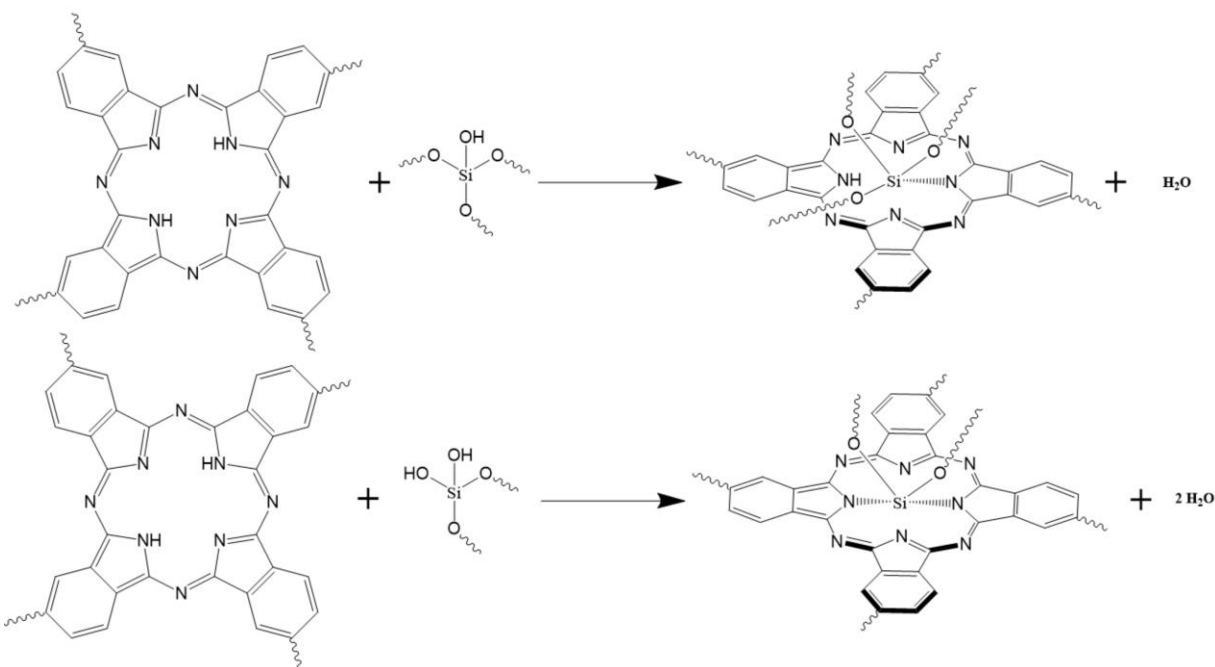


Figure 32: Silanol groups reacting with isoindoline substructures of phthalocyanine moieties.<sup>125</sup>

### 3 Summary of Design Considerations and Research Approach

Literature previously discussed in this manuscript includes various organic high-temperature polymers, as well as organosilicon and hybrid polymers. Building on this literature, several design considerations may be taken into account. Phthalonitrile monomers are commonly designed with thermally stable structures, such as aromatic and heterocyclic rings. Flexible units such as ether linkages commonly connect phthalonitrile groups and other rigid structures. These flexible units improve processing of the pre-polymers and toughness of the resulting polymer.<sup>4, 22</sup>

Until recently, little research has focused on the incorporation of flexible, silicon-containing linkages into phthalonitrile monomers. Zhang et al.<sup>51</sup> incorporated silazane (Si-N) linkages into a phthalonitrile resin and Babkin et al.<sup>30, 52</sup> synthesized similar polymers with carboxysilane linkages. Dzhevakov et al.<sup>53</sup> investigated a disiloxane phthalonitrile with methyl groups. The materials synthesized by these groups showed excellent thermal and thermo-oxidative properties with very low softening points. These results also confirm that phenyl-silicon linkages may be incorporated into phthalonitriles without substantially affecting the glass transition.

While the silicon-phthalonitrile materials synthesized by these groups exhibited high thermal and thermo-oxidative stability, emphasis was generally placed on developing resins with low softening points and long-term stability was not characterized. It is also of note that many polymers reported in literature contain moieties reported to be thermally unstable, Figure 33.

In many of these compounds the silicon linkage is attached to the aromatic backbone via a methylene bridge. This improves processing of the material by lowering the monomer  $T_g$  and melting point. However, methylene and benzylic groups in the backbone should be avoided for optimum thermal stability.<sup>10</sup> This is due to the lower homolytic C-H bond energy of these bonds relative to aromatic C-H bonds. Connecting the silicon linkage directly to phenylene groups results in greater resistance to thermal degradation below 550 °C.<sup>77-78</sup>

The incorporation of aromatic moieties instead of methyl functional groups on the silicon is also reported to improve thermal stability.<sup>63, 80, 163</sup> For example, no decomposition of tetraphenylsilane was reported below 500 °C in inert atmosphere, during short-term experiments.<sup>179, 212</sup>

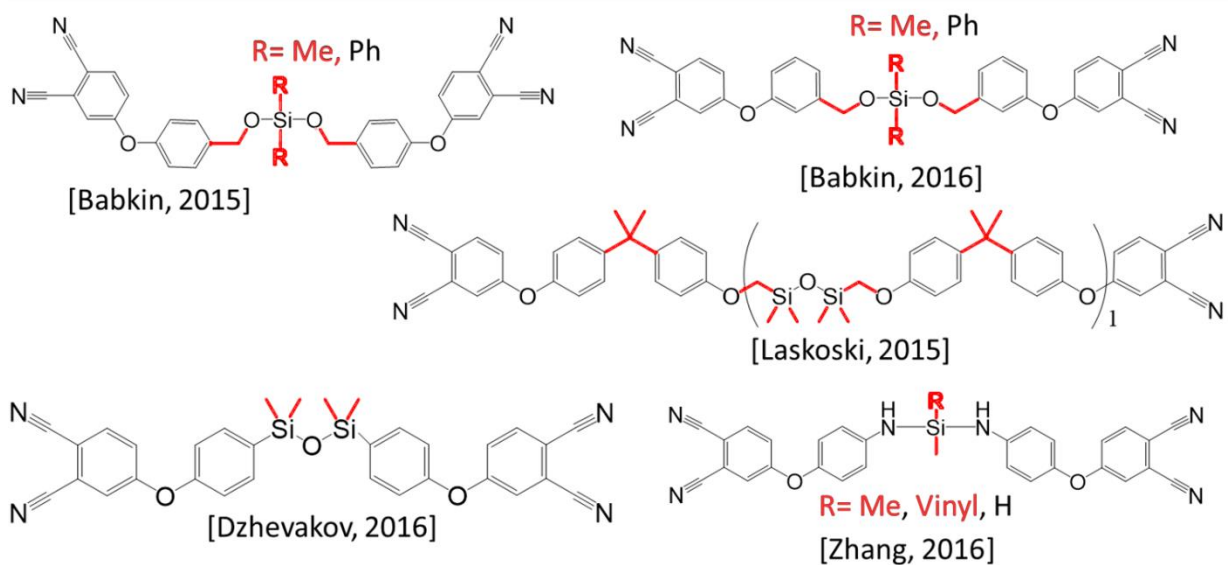


Figure 33: Silicon-containing monomers produced by Babkin et al. 2015,<sup>52, 208-209</sup> Babkin et al. 2016,<sup>79</sup> Laskoski et al. 2015,<sup>6</sup> Dzhevakov et al. 2016,<sup>53</sup> and Zhang et al. 2016.<sup>51</sup> Moieties reported to result in thermally unstable polymers are highlighted in red.

Siloxanes are known for their high resistance to degradation due to the high bond energy and partial polar or ionic nature of the Si-O-Si bonds.<sup>156</sup> Simultaneously, the wide bond angle provides flexibility. However, although the Si-O linkages in siloxane moieties have slightly higher bonding energies (397 kJ/mol) than Si-C bonds (322 kJ/mol) and C-O (354 kJ/mol) in silanes and oxysilanes,<sup>2, 72-75</sup> siloxanes may degrade at lower temperatures. Above 200 °C, Si-O-Si materials often suffer from low temperature degradations due to oxidative cross-linking, or chain folding and unzipping or rearrangement mechanisms.<sup>80, 163</sup> The increased susceptibility of rearrangements is reflected in research on silarylene-siloxane polymers.<sup>78, 170</sup> It is reported that the thermal and oxidative stability decreases with increasing length of siloxane linkages. This is especially true of dimethylsiloxane linkages.<sup>78</sup> These lower-temperature mechanisms may be reduced by keeping the Si-O sections of the aromatic backbone relatively short and limiting chain mobility due to the formation of a highly-linked network, in this case via phthalonitrile groups.<sup>78</sup> It is also reported these mechanisms may be reduced by the inclusion of aromatic functional groups. Bulky substituents chain-chain interaction and sterically hinder chain folding. Instead, the Si-C bond cleavage is reported to occur, with the release of benzene. Generally, this is reported at temperatures above 300 °C but has also been observed as low as 250 °C.<sup>34, 80, 153, 169</sup>

Relevant literature on phenylsiloxanes and phenylsilane compounds provides information on expected degradation modes. Under inert conditions and at high temperatures, tetraphenylsilane

and silphenylene polymers undergo cleavage of Si-phenyl bonds via free-radical mechanisms. The cleavage of a phenyl group from tetraphenylsilane results in the formation of phenyl radicals and triphenylsilyl radicals. Which may react to form a variety of products including benzene and triphenylsilane. Compounds with mono, di, and tri-phenyl substituted silicon moieties may undergo disproportionation reactions to form tetraphenylsilane and lower-substituted hydridophenyl-silanes. This can result in chain branching mechanisms. Under oxidizing atmospheres, the radical species formed from the cleavage of phenyl groups and phenylene linkages, result in the formation of siloxy groups. These siloxy moieties may condense to form siloxane and oxysilane linkages. It is unclear if oxygen catalyzes the cleavage of Si-phenyl bonds or simply interacts with the resulting radicals. Once sufficient cleavage of phenyl groups occurs, siloxane rearrangement mechanisms may be possible via chain-chain interactions. However, unlike other siloxane polymers, cyclic siloxane oligomeric degradation products are not commonly reported in literature for phenylsiloxanes and silphenylenes.<sup>34, 78, 80, 153, 169-170, 179-180</sup>

The presence of hydroxyl groups has been shown to result in cleavage of Si-O and Si-C bonds.<sup>77-78</sup> Phenolic and silanol species may be present as degradation products or as impurities from synthesis. Residual metal, organometallic, ionic, and polar impurities, catalyze degradation mechanisms, especially oxidation mechanisms. For example, salts are commonly produced during synthesis but are detrimental to stability. These impurities must be removed or avoided for optimum thermal performance to be achieved.<sup>78, 82, 180</sup>

The hydrolytic stability is also a concern. The sensitivity of the carboxysilane linkage to moisture has been the subject of substantial debate and investigation. Hydrolysis occurs more readily in carboxysilanes as compared with siloxanes.<sup>53, 82-86</sup> However, most of literature suggests that diphenyl-substituted oxysilane linkages are hydrolytically stable enough to processed.<sup>82-85, 199, 202</sup> It is expected that after curing, the highly crosslinked network will be more resistant to hydrolysis. The use of amino and hydrido groups as substituents on the silicon also result in higher rates of hydrolysis than methyl or phenyl groups.<sup>50, 82</sup>

The longer bond lengths of Si-O and Si-C bonds, and the wide bond angles Si-O-Si and Si-O-C linkages results in a higher degree of flexibility and more free volume than corresponding organic linkages. The increase in backbone flexibility can improve toughness of high temperature polymers.<sup>10, 184</sup> The toughness and resulting damage tolerance is commonly an issue with brittle,

highly crosslinked systems such as phthalonitriles. However, the increased flexibility also lowers the elastic modulus.<sup>34, 41, 156, 159</sup> The inclusion of organosilicon linkages usually also results in a reduction in glass transition temperature. The incorporation of bulky substituents on the silicon atoms, such as phenyl groups, has been shown to limit this effect.<sup>169</sup> Furthermore, due to their high glass transition temperatures, the long-term use temperature of phthalonitriles is often instead limited by degradation. These high  $T_g$  values make PN resins good candidates for hybridization.

In siloxane systems, the use of aromatic functional groups has also been shown to increase the solubility of resins in organic solvents.<sup>77, 80, 91-92</sup> Both phthalonitrile and organosilicon resins are commonly soluble in halogenated and aprotic polar solvents. The softening point of resins is also worth considering. The inclusion of highly flexible organosilicon linkages often results in highly amorphous monomers with low glass transition temperatures. It is of note however, that the increase in steric hindrance from aromatic groups limits the flexibility of linkages. This can increase the melting point of monomers by 50-100 °C.<sup>149</sup> The inclusion of other flexible linkages such as aryl-ether linkages, or asymmetric structures such as ortho and meta-substituted phenylene moieties also decreases monomer glass transition or melting temperatures.<sup>4, 126</sup>

The length of the monomer backbone also affects the softening point, viscosity, and elastic modulus of pre-polymers. Oligomeric compounds with longer backbones between crosslinking groups show slower rates of curing and lower degrees of crosslinking. Lower  $T_g$  values and elastic moduli are observed. Since viscosity increases as curing occurs, the rate of viscosity increase is dependent on the rates of curing reactions.

### 3.1 Research Approach

Objectives for this research were to 1) evaluate the characteristics of silicon-containing PN resins selected for thermal and thermo-oxidative stability and 2) provide insight on how chemistry effects processing, thermo-mechanical properties, and degradation modes. In order to complete these objectives a number of tasks were accomplished: A) a literature review was completed to identify design considerations for high-temperature organosilicon and phthalonitrile polymers and monomer structures were selected, B) synthesis and purification procedures were developed for phthalonitrile compounds with carboxysilane, carbosilane, and carbosiloxane silicon linkages, C) silicon-containing phthalonitrile monomers were synthesized in large scale and high yield and characterized via a variety of methods, D) processing profiles were developed and cured samples

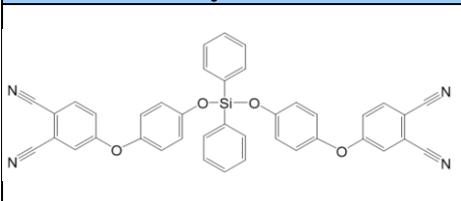
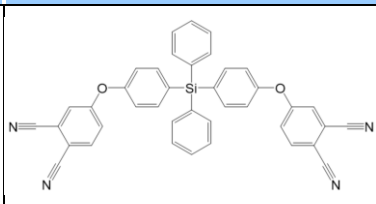
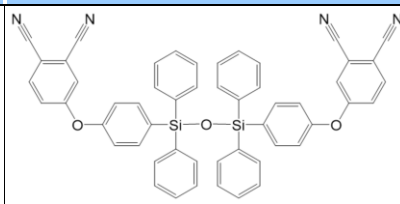
were produced, E) the processing, thermal and oxidative stability, and thermo-mechanical properties of synthesized and commercial phthalonitrile materials were characterized and compared, and F) the degradation behavior and properties of PN materials were reported and opportunities for further improvement were recommended.

Prior to beginning the research presented in this manuscript, little literature existed on silicon-containing phthalonitrile resins. Thus, the majority of the research direction was influenced by literature on phthalonitriles, organosilicon systems, and other hybrid polymers. Since 2015, the work of the groups presented in the section Silicon-Containing Phthalonitriles has shed more light on the inclusion of organosilicon linkages into phthalonitriles. This recent literature has been included in discussion of results, conclusions, and recommendations for future work.

The addition of flexible silicon-containing linkages to phthalonitrile polymers was expected to lower the glass transition temperatures ( $T_g$ ) and elastic moduli, and improve fracture toughness and oxidative stability of polymers, as compared with standard phthalonitriles. These pre-polymers may also possess enhanced solubility, lower the softening points, and lower viscosities at lower temperatures. By attaching the silicon atoms to bulky and rigid aromatic structures, high thermal and oxidative stability and glass transition temperatures should be attained. The oxidative stability is especially of interest as evident by the study by Koerner et al.<sup>96</sup> The formation of siloxy units and subsequent condensation to silica, is likely to result in decreased permeation by oxygen and thus decreased degradation.

Given relevant literature available at the time, three monomer structures were identified, including carboxysilane, carbosilane, and carbosiloxane linkages. These monomer structures are provided in Table 9.

*Table 9: Selected Monomer Structures.*

Carboxysilane-PN	Carbosilane-PN	Carbosiloxane-PN
		

Recently in 2016, the carbosilane PN was produced by Terraza et al.<sup>55</sup> However its polymer properties were not reported. A relatively low melting point of 91–93 °C was reported for this compound. To the author’s knowledge the carboxysilane and carbosiloxane phthalonitriles have not been evaluated.

Procedures are available in literature for the synthesis of similar compounds. The carboxysilane moiety was expected to be produced by the condensation of dichlorodiphenylsilane and the appropriate phenol in the presence of triethylamine.<sup>44, 63, 86, 170, 203, 213-214</sup> The carbosilane and carbosiloxane segments may be produced by reaction of a bromo-aromatic compound with dichlorodiphenylsilane or dichlorohexaphenyldisiloxane and *n*-butyl lithium.<sup>32-33, 183, 195-196, 215-221</sup> The addition of phthalonitrile groups may be accomplished by the standard reaction of phenols with 4-nitro phthalonitrile.<sup>4, 9, 20, 22, 25, 88, 123, 129, 132, 222-223</sup> The monomers and synthesized reactants can be characterized by a variety of characterization techniques to confirm structure, composition, and purity. These include thin-layer chromatography, elemental analysis, differential scanning calorimetry (DSC), Fourier transform infrared (FTIR) spectroscopy, nuclear magnetic resonance spectroscopy (<sup>1</sup>H, <sup>13</sup>C, and <sup>29</sup>Si NMR), and X-ray diffraction crystallography.

Monomers may be mixed with 2-10 wt.% of a typical catalyst. Bis[4-(4-aminophenoxy)phenyl]-sulfone (*p*-BAPS) was selected based on its thermal stability. Alternative amines used in literature include *m*- and *p*-phenylenediamine, 4,4'-mexhylenedianiline, 4-aminophenyl ether, 4,4'-(*p*-phenylenedioxy) dianiline, 4-aminophenyl sulfone, 4'-bis(3-aminophenoxy)diphenyl sulfone (*m*-BAPS), and 1,3-bis(3-aminophenoxy)benzene (*m*-APB).<sup>3</sup> Resin catalyst mixtures may be evaluated by parallel plate rheology and DSC. Curing is accomplished following standard procedures, which involved melting the monomer and catalyst, and heating at 180-200 °C until gelation, followed by a series of steps at 250-375 °C. Compression molding of b-staged pre-polymers can be used to produce resin plaques. Plaques are evaluated by acoustic c-scan analysis to evaluate porosity content.

As-cured polymers can be characterized by FTIR, thermogravimetric analysis (TGA), TGA/FTIR, DSC, dynamic mechanical analysis (DMA), and thermomechanical analysis (TMA). An oxidative aging study may be used to provide information on long-term stability at 250 °C. Volume and weight measurements provide estimates of stability. Appropriate experimental techniques may be used to measure degradation and resultant changes in properties of aged

samples. These include optical microscopy, scanning electron microscopy (SEM) with energy dispersive spectroscopy (EDS), micro-computed X-ray tomography, FTIR, and Knoop hardness characterizations.

## 4 Synthetic Procedures for Silicon-Containing Phthalonitrile Monomers

### 4.1 Introduction

This chapter covers the synthesis, purification, and chemical characterization of three silicon-containing phthalonitrile monomers and their respective precursors. The target chemical structures were selected in the previous chapter, and include carboxysilane, carbosilane, and carbosiloxane linkages. The monomers were intended to avoid specific degradation routes common for silicon-containing compounds as well as address gaps in literature. High-yield synthetic routes are provided in addition to extensive analytical characterization. The melting points and hydrolytic stability of compounds are discussed.

### 4.2 Experimental

#### 4.2.1 Materials and Methods

4-Nitrophthalonitrile (98%) was obtained from Accela Chembio Co. Ltd. Dichlorodiphenylsilane, *n*-butyllithium (*n*-BuLi, 2.5 M in hexanes), 4-bromophenol (>99%), acetic anhydride, and palladium on carbon (10 wt.%) were purchased from Sigma Aldrich. Hydroquinone (99.5%) was purchased from Acros Organics. From Gelest Inc. was obtained 1,3-dichlorotetraphenyldisiloxane. From Oakwood Chemical was purchased 4-benzyloxybromobenzene (low moisture, >99%). Potassium carbonate (K<sub>2</sub>CO<sub>3</sub>, 99%), 4-benzyloxyphenol (>98%), and acetic acid (>99.7%), was purchased from Alfa Aesar. Magnesium sulfate (MgSO<sub>4</sub>, anhydrous, >98%) was obtained from MP Biomedicals. Neutral activated carbon, triethylamine (TEA), tetrahydrofuran (THF), dimethylformamide (DMF), dichloromethane (DCM), ethyl acetate, hexane, and chloroform were purchased from Fisher Chemical. Ethanol was purchased from Decon Laboratories. Toluene was purchased from Spectrum Chemical MFG Corp. Silica gel (40-60 μm, 60 Å) was obtained from VWR International. THF and toluene were each distilled over sodium/ benzophenone ketyl and stored over 4A molecular sieves under nitrogen. DMF was dried with 4A molecular sieves. K<sub>2</sub>CO<sub>3</sub> was dried under vacuum at 80 °C for 24 hours. All other materials were used as received.

<sup>1</sup>H, <sup>13</sup>C, and <sup>29</sup>Si nuclear magnetic resonance (NMR) spectra were recorded on an Agilent U4-DD2 instrument with DMSO-d<sub>6</sub>, CDCl<sub>3</sub>, or acetone-d<sub>6</sub> as the solvent, and tetramethylsilane (TMS) as an internal standard. Correlation spectroscopy (COSY), heteronuclear single-quantum correlation spectroscopy (HSQC), and heteronuclear multiple-bond correlation spectroscopy

(HMBC) were used to assign protons and carbons. Melting point data was obtained by differential scanning calorimetry (DSC) using a TA Instruments Q1000 or Q20 with a ramp rate of 5 °C/min. Elemental analysis was performed by Atlantic Microlab Inc. Fourier transform infrared (FTIR) spectroscopy was conducted using a Thermo Scientific Nicolet 6700 with Spectra Tech Inc. attenuated total reflection (ATR) attachment. Supercritical fluid chromatography (SFC) was conducted using a Thar/Waters Corp. SFC equipped with high pressure pump, a Waters 2990 photodiode array detector, auto-sampler, and a bare silica column. Ultra-performance liquid chromatography mass spec (UPLC/MS) and UV spectroscopy (UPLC/UV) was conducted using a Maldi/Waters SYNAPT G2 with a Waters Acquity UPLC H-class system and Hybrid Quadrupole TOF analyzer, APCI source, and MassLynx software.

#### 4.2.2 Synthesis of the Carboxysilane-Phthalonitrile Monomer

Figure 34 provides a general synthetic scheme for the synthesis of the carboxysilane phthalonitrile monomer and its respective precursor. This synthetic route was chosen due to the hydrolytic sensitivity of the aryloxysilane linkage and the mild conditions needed for the condensation reaction. Furthermore the reaction by-product, triethylamine·HCl salt precipitates out of solution pushing reaction conditions toward completion and allowing easier removal during work-up.<sup>63</sup>

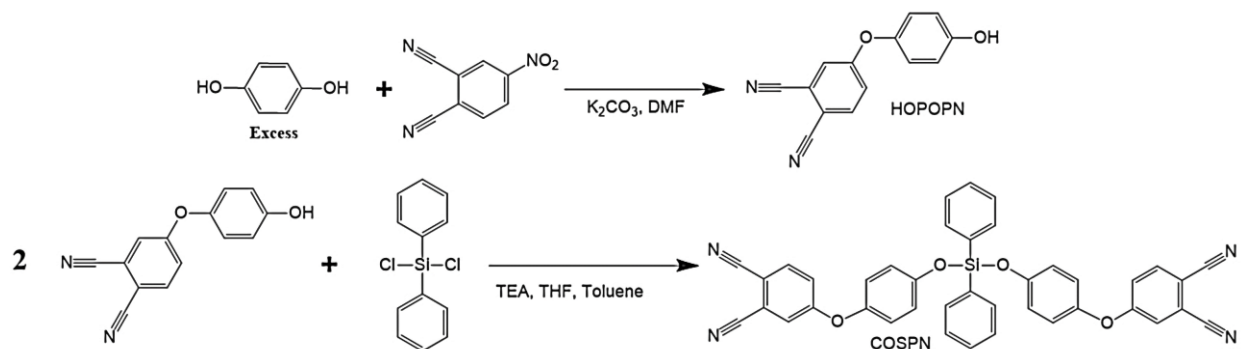


Figure 34: General synthetic scheme for the carboxysilane-phthalonitrile monomer.

##### 4.2.2.1 Synthesis of 4-(4-Hydroxyphenoxy)phthalonitrile (HOPOPN)

A three-necked flask with addition funnel, rubber septum, nitrogen inlet, and stir bar was flame-dried under vacuum and purged with nitrogen. To the vessel was added 80 mL of dry dimethylformamide (DMF) and an excess of hydroquinone (36.9 g, 335 mmol). The reaction was stirred until the hydroquinone dissolved. To the solution was added pulverized, dried potassium carbonate (23.2 g, 168 mmol). The reaction vessel was chilled in an ice water bath and allowed to

stir for fifteen minutes. A solution of DMF (95 mL) and 4-nitrophthalonitrile (14.5 g, 83.8 mmol) was prepared and transferred to the addition funnel. The slowly 4-nitrophthalonitrile solution was added dropwise slowly over approximately one hour. The reaction was allowed to warm to room temperature and left stirring overnight. The reaction was heated to 80 °C for 7 hours. The reaction contents were removed and poured into 1000 mL of 0.1 M HCl. Brown precipitate of the desired product was separated by vacuum filtration through a coarse frit. The precipitate was washed with 200 mL deionized water. The product was then dissolved in 600 mL of DCM and washed with water four times in 400 mL increments (approximately 1.6 L water total). The organic layer was separated and dried with MgSO<sub>4</sub>. The MgSO<sub>4</sub> was removed by vacuum filtration and the solvent was removed by rotary evaporation. The orange/brown product was purified by silica column chromatography (5:12 ethyl acetate: hexane) to produce white powder. The product was dried in a vacuum oven (48 torr at 70-80°C for 24 hours). Extended drying at 70-80 °C caused the product to turn a bluish-green. Yield: 16.1 g, 68.2 mmol, 81%. *R<sub>f</sub>*: 0.36 (SiO<sub>2</sub>, hexanes/ethyl acetate, 3:1). mp: 152 °C (lit. mp 150-151 °C<sup>223</sup>). <sup>1</sup>H NMR (400 MHz, DMSO-d<sub>6</sub>, δ, ppm): 6.80 – 6.89 (m, 2H), 6.97 – 7.06 (m, 2H), 7.28 (dd, J = 8.8, 2.6 Hz, 1H), 7.67 (dd, J = 2.7, 0.4 Hz, 1H), 8.05 (dd, J = 8.8, 0.4 Hz, 1H), 9.62 (s, 1H). <sup>1</sup>H NMR in CDCl<sub>3</sub>, ppm: 6.94 (4H,m), 7.21 (2H, m), 7.70 (1H, d). <sup>13</sup>C NMR (101 MHz, DMSO-d<sub>6</sub>, δ, ppm): 107.31 (ArC), 115.46 (R-C≡N), 116.00 (R-C≡N), 116.54 (ArC), 116.71 (ArC), 120.92 (ArC), 121.72 (ArC), 121.82 (ArC), 136.22 (ArC), 145.30 (ArC), 155.33 (ArC), 162.19 (ArC). IR (ATR, cm<sup>-1</sup>): 3413, 3107, 3077, 3041, 2235, 1592, 1503, 1484, 1442, 1308, 1251, 1197, 1096, 1081, 950, 880, 833, 792. Anal. calcd for C<sub>14</sub>H<sub>8</sub>N<sub>2</sub>O<sub>2</sub>: C, 71.18; H, 3.41; N, 11.86; O, 13.55. Found: C, 71.53; H, 3.41; N, 11.84.

#### 4.2.2.2 *Alternative Synthesis of 4-(4-Hydroxyphenoxy)phthalonitrile (HOPOPAN)*

Prior to using the synthetic route outlined previously for HOPOPAN, an alternative route was utilized, Figure 35. 4-(4-(Benzyloxy)phenoxy)phthalonitrile was first synthesized, followed by cleavage of benzyl groups to form 4-(4-hydroxyphenoxy)phthalonitrile (HOPOPAN). While this method proved successful, the single step route detailed previously in this manuscript yielded excellent results, making the use of a benzyl protecting group unnecessary.

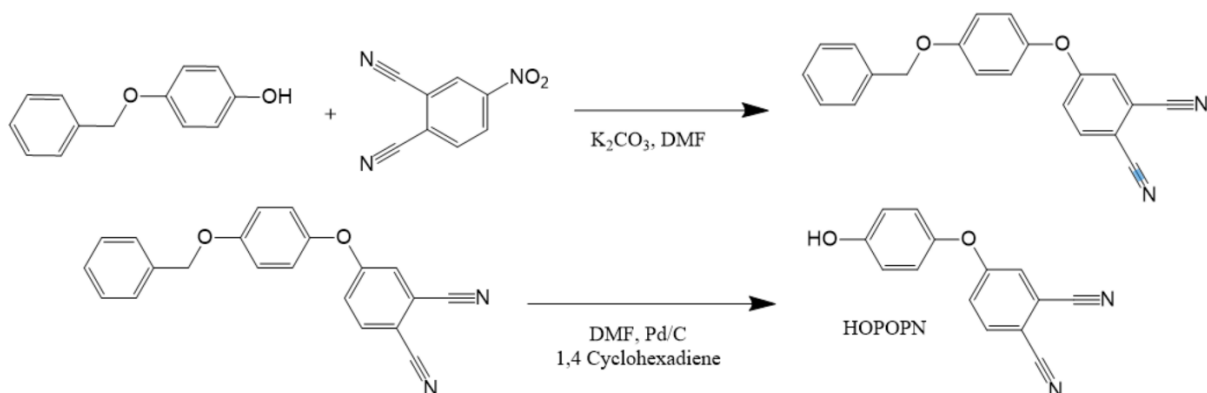


Figure 35: Synthesis of 4-(4-(benzyloxy)phenoxy)phthalonitrile (BOPOPn) and cleavage of benzyl groups to form 4-(4-hydroxyphenoxy)phthalonitrile (HOPOPn).

A three-necked flask with addition funnel, rubber septa, and nitrogen inlet was flame dried under vacuum and purged with nitrogen. The flask was chilled in an ice water bath. The reaction was run under nitrogen atmosphere. To the reaction vessel, 3.00 g (15.0 mmol) of 4-benzyloxyphenol dissolved in 15 mL of dry dimethylformamide (DMF), was added. Pulverized, dried potassium carbonate (2.07 g, 15.0 mmol) of was stirred into solution. 4-nitrophthalonitrile (2.60 g, 15.0 mmol) was dissolved in 7 mL of dry DMF and added dropwise over 30 minutes. The reaction was allowed to warm to room temperature and left stirring overnight. It was then heated at heated at 80 °C for 6 hours while stirring. The reaction contents were poured into 300 mL of iced water. Brown precipitate separated by filtration. The product was then dissolved in DCM (150 mL) and washed with 1 M potassium hydroxide solution in three 50 mL increments. The organic layer was separated and dried with MgSO<sub>4</sub>. The layer was then filtered, and the solvent removed by a rotary evaporator. Off white powder was obtained. Further purification was accomplished by dissolving the product in 2:1 Hexane:DCM and running it through a silica plug. Off-white powder was obtained after removal of solvents by rotary evaporation. Yield: 4.2 g, 13 mmol, 86%; <sup>1</sup>H NMR in DMSO-d<sub>6</sub>, ppm: 5.12 (2H, s), 7.14 (4H, m), 7.31 (1H, dd), 7.35 (1H, m), 7.41 (2H, m), 7.46 (2H, m), 7.71 (1H, d), 8.06 (1H, d)

#### 4.2.2.3 Cleavage of Benzyl Groups to Form 4-(4-Hydroxyphenoxy)phthalonitrile (HOPOPn)

The cleavage of the benzyl protecting groups was accomplished using transfer-hydrogenation with 1,4 cyclohexadiene. Hydrogenation of the nitrile groups was not observed under these conditions. A three-necked flask with addition funnel, rubber septa, and nitrogen inlet was flame dried under vacuum and purged with nitrogen. To the flask was added 0.15 g (0.46 mmol) 4-(4-(benzyloxy)phenoxy) phthalonitrile, 3 mL DMF, 0.055 g (10 %) Pd/C and 1 mL 1,4-

cyclohexadiene. The mixture was allowed to stir at room temperature for 1 hour. The reaction was then heated to 50 °C for 5 hours. An additional 0.2 g Pd/C and 1 mL 1,4 cyclohexadiene were added and the reaction was run for an additional 6 hours. The reaction contents were poured into 100 mL of ethyl acetate and the Pd/C was filtered out. The filtrate was then washed with water (3x 50 mL) and dried with MgSO<sub>4</sub>. The MgSO<sub>4</sub> was removed by vacuum filtration. The solvents were removed by rotary evaporation, yielding an off-white powder. <sup>1</sup>H NMR in DMSO-d<sub>6</sub>, ppm: 6.85 (2H, m), 7.01 (2H, m), 7.28 (1H, dd), 7.67 (1H, d), 8.05 (1H, d), 9.62 (1H, s).

#### 4.2.2.4 *Synthesis of 4,4'-((((Diphenylsilyl)bis(oxy))bis(4,1-phenylene))bis(oxy)) diphthalonitrile (COSPN)*

Figure 34 describes the synthetic procedure for 4,4'-((((diphenylsilyl)bis(oxy))bis(4,1-phenylene))bis(oxy)) diphthalonitrile. A three-necked flask outfitted with an addition funnel, rubber septum, nitrogen inlet, and stir bar, was flame dried under vacuum, and transferred to a glovebox under nitrogen. HOPOP (2.36 g, 10.0 mmol), dry THF (7 mL), dry toluene (1 mL), and TEA (3.8 mL, 27.5 mmol) were added to the reaction vessel. To the addition funnel, dichlorodiphenylsilane (1.05 mL, 5.0 mmol), THF (8.75 mL) and toluene (1.25 mL) were added. The reaction vessel was removed from the glove box and placed under nitrogen in an ice water bath. The HOPOP/THF/ Toluene/TEA solution was stirred for 20 minutes. The dichlorodiphenylsilane solution was added slowly dropwise. The reaction contents were allowed to warm to room temperature and stirred for 24 hours. An additional 0.53 mL (2.5 mmol) dichlorodiphenylsilane, diluted with THF (7 mL) and toluene (1 mL) were added dropwise. After stirring for 20 minutes the addition funnel was removed and replaced with a dry reflux condenser. The reaction mixture was heated to 75 °C for 6 hours. The reaction vessel was then transferred to the glovebox under nitrogen and allowed to cool to room temperature. An additional 100 mL of THF was added. After fifteen minutes contents were filtered to remove triethylammonium salts. The reaction vessel was removed from the glove box and the solvents were removed by rotary evaporation. The yellowish solid product was heated under vacuum (24 torr at 80 °C. for 24 hours to remove solvents and residual impurities. The product was then stored under dry nitrogen. Yield: 3.10 g, 4.70 mmol, 78%. Purity (LCMS): 80%, mp: 168-169 °C. <sup>1</sup>H NMR (400 MHz, CDCl<sub>3</sub>, δ, ppm): 6.88 – 6.93 (m, 4H), 7.02 – 7.07 (m, 4H), 7.13 – 7.20 (4H, m), 7.44 – 7.47 (4H, m), 7.50 – 7.56 (m, 2H), 7.69 (dd, J = 8.7, 0.5 Hz, 2H), 7.76 – 7.81 (4H, m). <sup>13</sup>C NMR (101 MHz, CDCl<sub>3</sub>, δ, ppm): 108.78 (ArC), 115.11 (R-C≡N), 115.51 (R-C≡N), 117.73 (ArC), 121.01, 121.35 (ArC),

121.68 (ArC), 122.05 (ArC), 128.46 (ArC), 130.30 (ArC), 131.60 (ArC), 135.07 (ArC), 135.48 (ArC), 148.12 (ArC), 152.08 (ArC), 162.23 (ArC). IR (ATR,  $\text{cm}^{-1}$ ): 3042, 2929, 2232, 1650, 1584, 1498, 1486, 1429, 1259, 1229, 1214, 1150, 1126, 1103-1012, 1103-1012, 933, 833, 718, 696.

#### 4.2.3 Synthesis of the Carbosilane-Phthalonitrile Monomer

In Figure 36, a general synthetic scheme is provided for the synthesis of the carbosilane phthalonitrile monomer and its respective precursors.

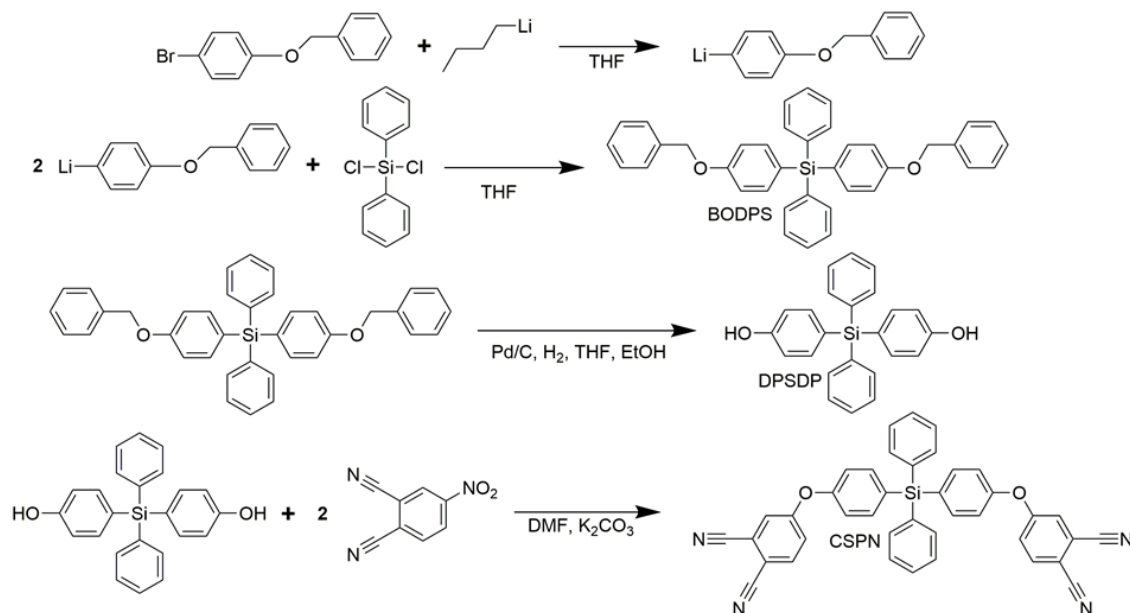


Figure 36: General synthetic scheme for the carbosilane-phthalonitrile monomer.

##### 4.2.3.1 Synthesis of Bis(4-(benzyloxy)phenyl)diphenylsilane (BODPS)

The structure of bis(4-(benzyloxy)phenyl) diphenylsilane (BODPS) is given in Figure 37. A synthetic procedure was followed similar to that reported via Davidsohn et al.<sup>219</sup> Prior to use, all glassware, stir bars, stopcocks, septum, syringes, needles, and cannula were stored in an oven at 100°C overnight. A 1 L three-necked flask with addition funnel, nitrogen inlet, rubber septum, and stir bar was flame-dried under vacuum and purged with nitrogen. To the reaction vessel, 570 mL anhydrous THF and 4-benzyloxybromobenzene (30.0 g, 114 mmol) was added. The reaction vessel was placed in a dry ice/acetone bath and stirred for twenty minutes. To the addition funnel, *n*-BuLi (45.6 mL, 114 mmol) via syringe was transferred. The *n*-BuLi solution was then added slowly dropwise over the course of one hour. The mixture was stirred at -78 °C for thirty minutes. A flame-dried Schlenk flask was transferred to a glove box under nitrogen atmosphere. Then dichlorodiphenylsilane (10.9 mL, 51.8 mmol) and 109 mL THF were transferred to the Schlenk

flask. The flask was removed from the glove box and the silane solution was transferred to an addition funnel via cannula. The silane solution was then added slowly dropwise over the course of approximately two hours. During the addition, dry ice was periodically added to the bath to ensure the temperature remained around -78 °C. The mixture and bath were then allowed to warm up to room temperature slowly over a period of four hours. The mixture was transferred to a round bottom flask and the solvent was removed by rotary evaporation. The resulting product was dissolved in 500 mL DCM and washed with water four times (approximately 2.0 L of water total) to remove lithium salts. The organic layer was separated and dried with MgSO<sub>4</sub>, and the drying agent removed by vacuum filtration. The solvents were removed by rotary evaporation. The product was dissolved in 80 mL of chloroform and recrystallized twice with ethanol (130 mL each time) to yield white powder. For analytical characterization, a small amount was purified via silica column chromatography (2:1 hexane:DCM). Yield: 22.2 g, 0.0424 mol, 82%. *R<sub>f</sub>*: 0.25 (SiO<sub>2</sub>, hexanes/ CH<sub>2</sub>Cl<sub>2</sub>, 2:1). *R<sub>f</sub>*: 0.25 (SiO<sub>2</sub>, hexanes/CH<sub>2</sub>Cl<sub>2</sub>, 2:1). mp: 151 °C (lit. mp 149-150 °C<sup>219</sup>). <sup>1</sup>H NMR (400 MHz, CDCl<sub>3</sub>, δ): 5.09 (s, 4H(9)), 6.95 – 7.05 (m, 4H(7)), 7.30 – 7.47 (m, 16H(1,2,11,12,13)), 7.47 – 7.52 (m, 4H(6)), 7.55 – 7.59 (m, 4H(3)). <sup>1</sup>H NMR (400 MHz, DMSO-*d*<sub>6</sub>, δ): 5.12 (s, 4H), 7.06 – 7.12 (m, 4H), 7.30 – 7.51 (m, 24H). <sup>13</sup>C NMR (101 MHz, CDCl<sub>3</sub>, δ): 69.91 (C9), 114.62 (C7), 125.75 (C5), 127.68 (C11), 127.94 (C2), 128.16 (C13), 128.75 (C12), 129.57 (C1), 135.08 (C4), 136.45 (C3), 137.03 (C10), 138.02 (C6), 160.20 (C8). <sup>29</sup>Si NMR (79 MHz, CDCl<sub>3</sub>, δ): -14.77. IR (ATR, cm<sup>-1</sup>): 3064-2963 (w), 2908 (w; -CH<sub>2</sub>-), 2864 (w; -CH<sub>2</sub>-), 1592 (s), 1565 (m), 1501 (s), **1463** (w; -CH<sub>2</sub>-), 1452 (m), 1428 (m; Si-φ), 1288 (m), 1273 (m), 1241 (s), 1229 (s), 1182 (s), 1110 (s; Si-φ), 1037 (w), 1025 (m), 1010 (m), 830 (m), 821 (m), 747 (m) 736 (m), 700 (s). Anal. calcd. for C<sub>38</sub>H<sub>32</sub>O<sub>2</sub>Si: C, 83.17; H, 5.88; O, 5.83; Si, 5.12. Found: C, 83.01; H, 5.86.

#### 4.2.3.2 Synthesis of 4,4'-(Diphenylsilanediy)diphenol (DPSDP)

The structure of 4,4'-(diphenylsilanediy) diphenol (DPSDP) is provide in Figure 38. A two-necked flask was assembled with a reflux condenser, nitrogen inlet, hydrogen balloon attachment, glass stopper, and stir bar. As to prevent the solvent from interacting with the nitrogen inlet lines or the hydrogen balloon, the reaction vessel was assembled so the nitrogen inlet and hydrogen balloon were connected via the reflux condenser. The reaction vessel was flame dried under vacuum and purged with nitrogen. To the flask was added BODPS (29.6 g, 53.9 mmol), 444 mL THF, 148 mL ethanol, and 2.9 g Pd/C. Vacuum was briefly applied, and the reaction vessel was

purged with hydrogen. This was repeated once to ensure a mostly hydrogen atmosphere. The mixture was stirred at room temperature for 1 hour. The reaction was then heated to 70 °C for three days. The reaction vessel was then removed, and Pd/C was filtered out using vacuum filtration with a Buchner funnel. The solvents were removed via rotary evaporation. The product was purified via silica column chromatography (4:1 hexanes: ethyl acetate). The solvents were removed via rotary evaporation and the product dried under vacuum (48 torr at 50 °C for 24 hours) to yield a white powder. The solvents were removed via rotary evaporation and the product dried under vacuum to yield white powder. Yield: 18.1 g, 49.1 mmol, 90.8%. For analytical characterization, a small amount was recrystallized from toluene.  $R_f$ : 0.16 (SiO<sub>2</sub>, hexanes/ethyl acetate, 4:1). mp: 229 °C (lit. mp 221-222 °C<sup>219</sup>). <sup>1</sup>H NMR (400 MHz, acetone-*d*<sub>6</sub>, δ): 6.88 – 6.93 (m, 4H(7)), 7.34 – 7.44 (m, 10H(1,2,6)), 7.50 – 7.57 (m, 4H(3)), 8.59 (s, 2H(9)). <sup>1</sup>H NMR (400 MHz, DMSO-*d*<sub>6</sub>, δ): 6.74 – 6.92 (m, 4H(7)), 7.21 – 7.34 (m, 4H(6)), 7.35 – 7.53 (m, 10H(1,2,3)), 9.70 (s, 2H(9)). <sup>1</sup>H NMR (400 MHz, CDCl<sub>3</sub>, δ): 4.87 (s, 2H), 6.80 – 6.87 (m, 4H), 7.31 – 7.46 (m, 10H), 7.50 – 7.58 (m, 4H). <sup>13</sup>C NMR (101 MHz, acetone-*d*<sub>6</sub>, δ): 115.99 (C7), 124.47 (C5), 128.54 (C2), 130.10 (C1), 136.25 (C4), 136.88 (C3), 138.57 (C6), 159.69 (C8). <sup>13</sup>C NMR (101 MHz, DMSO-*d*<sub>6</sub>, δ): 115.35 (7), 122.46 (5), 127.92 (2), 129.43 (1), 135.08 (4), 135.73 (3), 137.39 (6), 158.90 (8). <sup>29</sup>Si NMR (79 MHz, acetone-*d*<sub>6</sub>, δ): -14.64. <sup>29</sup>Si NMR (79 MHz, DMSO-*d*<sub>6</sub>, δ): -15.15. IR (ATR, cm<sup>-1</sup>): ν = 3604 (w; OH), 3400 (m, br; OH), 3066-2972 (m), 1597 (m), 1581 (m), 1502 (m), 1428 (m; Si-φ), 1371 (w; φ-OH), 1258 (m), 1238 (m), 1180 (m), 1109 (s; Si-φ), 1048 (m), 826 (m), 742(w), 700 (m). Anal. calcd for C<sub>24</sub>H<sub>20</sub>O<sub>2</sub>Si: C, 78.22; H, 5.47; O, 8.68; Si, 7.62). Found: C, 78.25; H, 5.45.

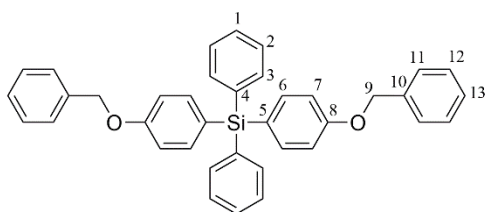


Figure 37: Bis(4-(benzyloxy)phenyldiphenylsilane (BODPS). Numbers correspond to carbons and their respective hydrogens as assigned in NMR.

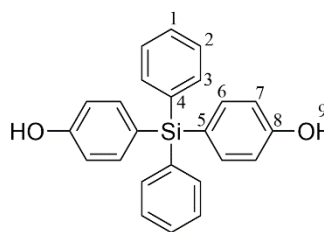


Figure 38: 4,4'-(Diphenylsilanediyl)diphenol (DPSDP). Numbers correspond to carbons and their respective hydrogens as assigned in NMR.

#### 4.2.3.3 Alternative Synthetic Route for 4,4'-(Diphenylsilanediyl)diphenol (DPSDP)

An alternative route for the synthesis of DPSDP, via reaction of 4-bromophenol and dichlorodiphenylsilane is reported by Davidsohn et al,<sup>219</sup> Tagle et al,<sup>224</sup> and Terraza et al.<sup>225</sup> This route was also investigated and is outlined in Figure 39. It was confirmed to produce an identical compound in 40% yield.

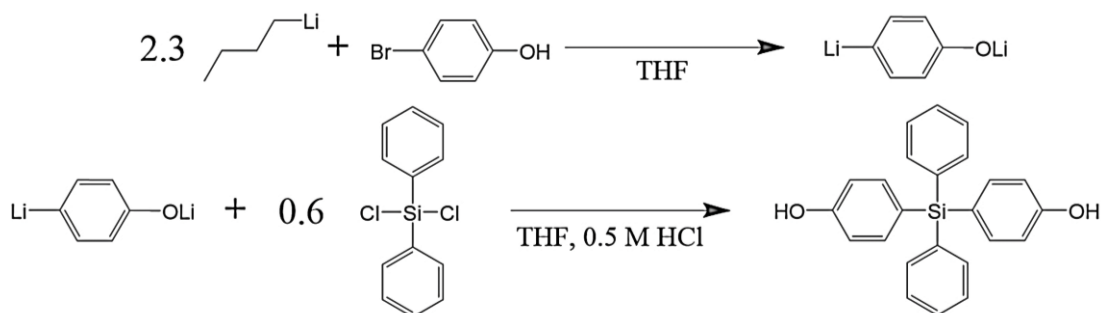


Figure 39: Alternative synthetic route for 4,4'-(diphenylsilanediyl)diphenol (DPSDP).

Prior to use, all glassware, stir bars, stopcocks, septum, syringes, needles, and cannula were stored in an oven at 100 °C overnight. A 250 mL three-necked flask with addition funnel, nitrogen inlet, rubber septum, and stir bar was flame dried under vacuum and purged with nitrogen. To the reaction vessel was added 36.1 mL (90.1 mmol) *n*-BuLi via syringe. The *n*-BuLi solution was cooled to -70 °C. To the addition funnel was added 4-bromophenol (6.78 g, 39.2 mmol) and 108 mL anhydrous THF. The THF/bromophenol solution was added slowly over the course of 1 hour. The reaction mixture was then allowed to warm up slowly to 5 °C. The mixture was then cooled to -60 °C. To a second addition funnel was added 2.64 mL dichlorodiphenylsilane 2.64 mL (12.5 mmol) in 12.5 mL anhydrous THF. The silane/THF solution was added over the course of 20 minutes. The reaction mixture was then allowed to warm up slowly overnight to 10 °C and stirred for 2 hours. The mixture was then removed and poured into 360 mL of 0.5 M HCl. The solvent layer was separated, and the solvents were removed by rotary evaporation. The oily product was then dissolved in diethyl ether and washed with water three times. The organic layer was separated and dried with MgSO<sub>4</sub>. The MgSO<sub>4</sub> was removed by filtration and the solvents were removed by rotary evaporation. The oil was poured into hexane and stirred for 10 minutes. The hexane solution was decanted, and the extraction procedure was repeated. The solvents were removed by rotary evaporation. The resulting product was recrystallized from toluene to yield yellow crystals.

#### 4.2.3.4 Synthesis of 4,4'-(((Diphenylsilanediyl)bis(4,1-phenylene))bis(oxy))diphthalonitrile (CSPN)

Figure 40 provides the structure for 4,4'-(((diphenylsilanediyl) bis(4,1-phenylene))bis(oxy)) diphthalonitrile (CSPN). A three-necked flask with reflux condenser, rubber septum, nitrogen inlet, and stir bar was flame dried under vacuum and purged with nitrogen. DPSDP (22.4 g, 60.8 mmol) and 112 mL of dry DMF was added to the flask. The contents were stirred for 15 minutes to ensure the DPSDP was fully dissolved. Pulverized dried potassium carbonate (26.5 g, 192 mmol) was stirred into solution. The reaction was stirred for an additional 10 minutes. 4-nitrophthalonitrile (22.12 g, 128 mmol) was then added. The reaction was allowed to run at room temperature overnight. The mixture was then heated to 80 °C for 8 hours. The reaction contents were removed and poured into 1 L of dilute HCl (0.1 M). After fifteen minutes, brown precipitate of the desired product was separated by vacuum filtration using a coarse frit. The precipitate was washed with deionized water. The product was then dissolved in 500 mL DCM and washed with water 4 times. The organic layer was separated and dried with MgSO<sub>4</sub> and the solvent was removed by rotary evaporation to yield off-white powder. Yield: 36.25 g, 0.155 mol, 96%. For analytical characterization, a small sample was purified by flash column chromatography (silica, 10:1:10 hexanes: ethyl acetate: chloroform), followed by recrystallization from acetonitrile to yield clear crystals. *R<sub>f</sub>*: 0.23 (SiO<sub>2</sub>, hexanes: ethyl acetate: chloroform, 10:1:10). mp: 223 °C. <sup>1</sup>H NMR (400 MHz, DMSO-*d*<sub>6</sub>, δ): 7.24 – 7.31 (m, 4H(7)), 7.44 – 7.58 (m, 12H(1,2,3,14)), 7.57 – 7.65 (m, 4H(6)), 7.91 (d, *J* = 2.5 Hz, 2H(10)), 8.13 (d, *J* = 8.7 Hz, 2H(13)). <sup>13</sup>C NMR (101 MHz, DMSO-*d*<sub>6</sub>, δ): 108.75 (C12), 115.40 (C15), 115.90 (C16), 116.82 (C11), 119.74 (C7), 122.77 (C14), 123.41 (C10), 128.32 (C2), 130.12 (C1), 130.29 (C5), 133.12 (C4), 135.84 (C3), 136.39 (C13), 138.23 (C6), 155.68 (C8), 160.28 (C9). <sup>29</sup>Si NMR (79 MHz, DMSO-*d*<sub>6</sub>, δ): -14.94. IR (ATR, cm<sup>-1</sup>): ν = 3080-2998 (w), 2234 (m; C≡N), 1585 (s), 1580 (s), 1564 (w), 1487-1483 (s), 1427 (m; Si-φ), 1312 (s), 1307 (m), 1280 (m), 1247 (s; O-φ), 1210 (m), 1175 (m), 1111 (m; Si-φ), 1106 (m; Si-φ), 890 (w), 856 (w), 838 (m), 834 (m), 743 (m), 696 (m). Anal. calcd for C<sub>40</sub>H<sub>24</sub>N<sub>4</sub>O<sub>2</sub>Si: C, 77.40; H, 3.90; N, 9.03; O, 5.15; Si, 4.52. Found: C, 77.11 H, 3.91.

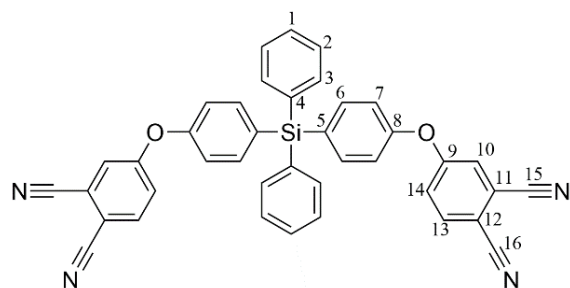


Figure 40: 4,4'-(((Diphenylsilyl)diyl)bis(4,1-phenylene))bis(oxy)diphthalonitrile (CSPN). Numbers correspond to carbons and their respective hydrogens as assigned in NMR.

#### 4.2.4 Synthesis of the Carbosiloxane-Phthalonitrile Monomer

In Figure 41, a general synthetic scheme is provided for the synthesis of the carbosiloxane phthalonitrile monomer and its precursors.

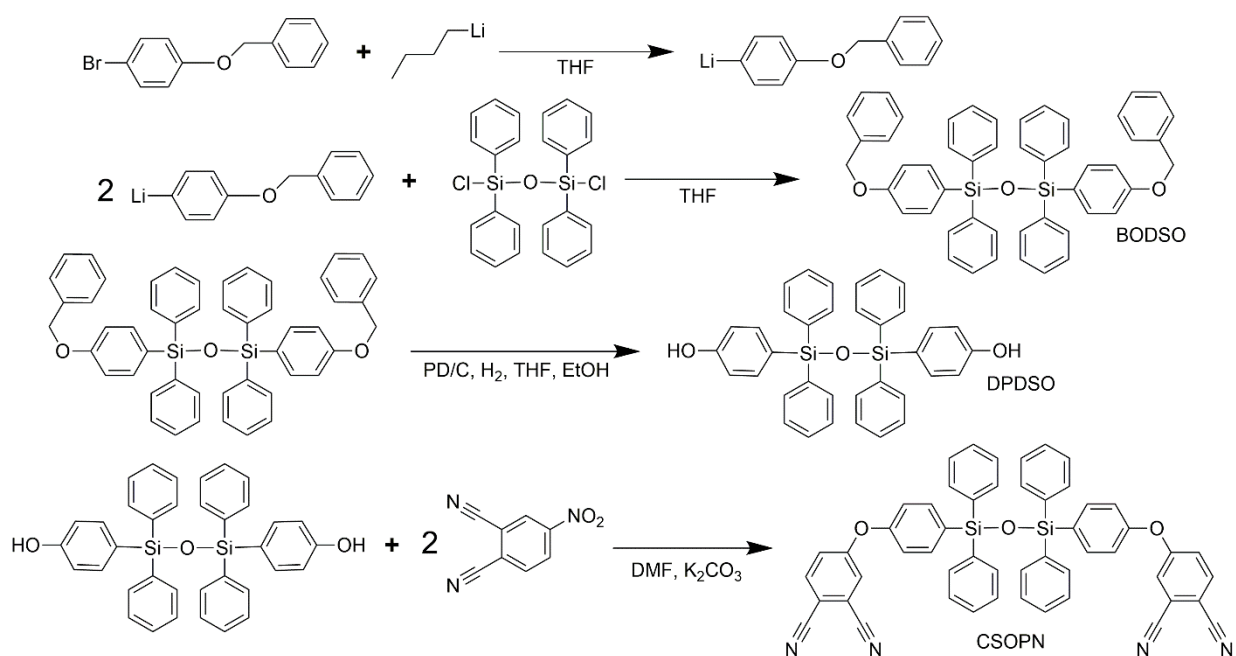


Figure 41: General synthetic scheme for the synthesis of the carbosiloxane phthalonitrile monomer.

##### 4.2.4.1 Synthetic Route for 1,3-Bis(4-(benzyloxy)phenyl)-1,1,3,3-tetraphenyldisiloxane (BODSO)

For the production of BODSO, Figure 42, a synthetic procedure was utilized similar to that reported by Davidsohn et al.<sup>219</sup> for the production of tetraphenylsilane compounds. A three-necked flask with stir bar, rubber septum, addition funnel, and nitrogen inlet, was flame dried under vacuum and charged with dry nitrogen. To the reaction vessel, 190 mL THF and 4-benzyloxybromobenzene (10 g, 38.0 mmol) was added. The reaction vessel was placed in a dry ice/acetone bath. To the solution, *n*-BuLi (16.8 mL, 38.0 mmol) was added slowly dropwise. The

reaction mixture was stirred at -78 °C for thirty minutes. Then 1,3-dichlorotetraphenyldisiloxane (6.53 mL, 7.8 g, 17.3 mmol), diluted with 65 mL THF, was added slowly dropwise. The reaction contents were allowed to warm up to room temperature over a period of four hours. The solvent was removed by rotary evaporation. The product was then dissolved in 300 mL DCM and washed with deionized water four times (approximately 2.0 L of water total). The organic layer was separated and dried with MgSO<sub>4</sub>. The drying agent was removed by vacuum filtration and the solvents were removed by rotary evaporation. The resulting product was purified by silica column chromatography (3:1 Hexane/ DCM) to yield a white powder. Yield: 8.73 g, 38.3 mmol, 68%. mp: 164 °C. *R*<sub>f</sub>: 0.19 (SiO<sub>2</sub>, Hexane/CHCl<sub>3</sub>, 2:1). <sup>1</sup>H NMR (400 MHz, Acetone-*d*<sub>6</sub>, δ, ppm) δ 5.11 (s, 4H(9)), 6.99 – 6.94 (m, 4H(7)), 7.34 – 7.27 (m, 10H(2,13)), 7.44 – 7.34 (m, 12H(1,6,12)), 7.49 – 7.44 (m, 4H(11)), 7.53 – 7.49 (m, 8H(3)). <sup>13</sup>C NMR (101 MHz, Acetone-*d*<sub>6</sub>) δ 70.20 (C9), 115.26 (C7), 127.31 (C5), 128.47 (C11), 128.63 (C2), 128.66 (C13), 129.28 (C12), 130.75 (C1), 135.79 (C3), 136.72 (C4), 137.55 (C6), 138.14 (C10), 161.40 (C8). <sup>29</sup>Si NMR (79 MHz, Acetone-*d*<sub>6</sub>) δ -18.41. IR (ATR, cm<sup>-1</sup>): 3067-3019 (w), 2936 (w; -CH<sub>2</sub>-), 2875 (w; -CH<sub>2</sub>-), 1593 (s), 1560 (w), 1503 (m), 1465 (w; -CH<sub>2</sub>-), 1456 (w), 1430 (m; Si-φ), 1273 (m), 1247 (m), 1182 (m), 1112 (s; Si-φ), 1095 (s; Si-O-Si), 1026 (w), 1011 (m), 998 (w), 861 (w), 831 (w), 821 (w), 741 (m), 700 (s). Anal. calcd for C<sub>50</sub>H<sub>42</sub>O<sub>3</sub>Si<sub>2</sub>: C, 80.39; H, 5.67; O, 6.42; Si, 7.52). Found: C, 80.18; H, 5.62.

#### 4.2.4.2 Synthetic Route for 4,4'-(1,1,3,3-Tetraphenyldisiloxane-1,3-diyl)diphenol (DPDSO)

Figure 43 provides the structure of DPSPD. A two-necked flask was assembled with stir bar, nitrogen inlet, reflux condenser, and hydrogen balloon attachment. The vessel was flame dried under vacuum and purged with dry nitrogen. BODSO (23.4 g, 31.4 mmol), 351 mL THF, 117 mL ethanol, and 2.34 g Pd/C were added to the flask. The reaction vessel was then purged with hydrogen. The mixture was stirred at room temperature for 1 hour. The reaction contents were then heated to 70 °C for four days. The reaction vessel was removed, and Pd/C was removed by filtration. The solvents were removed via rotary evaporation. The product was purified by flash silica column chromatography using 19:1 DCM/ethyl acetate. Solvents were removed via rotary evaporation. The resulting white powder was dried under vacuum (48 torr at 50 °C for 24 hours). Yield: 15.2 g, 26.8 mmol, 86%. A small amount was further purified by recrystallization from toluene for analytical characterization. *R*<sub>f</sub>: 0.08 (SiO<sub>2</sub>, DCM/ethyl acetate, 19:1). mp: 217 °C. <sup>1</sup>H NMR (400 MHz, Acetone-*d*<sub>6</sub>) δ 6.79 – 6.83 (m, 4H(7)), 7.29 (m, 8H(2)), 7.32 – 7.36 (m, 4H(6)), 7.36 – 7.41 (m, 4H(1)), 7.48 – 7.55 (m, 8H(3)), 8.56 – 8.60 (m, 2H(9)). <sup>13</sup>C NMR (101 MHz,

Acetone- $d_6$ )  $\delta$  115.86 (C7), 125.69 (C5), 128.52 (C2), 130.59 (C1), 135.78 (C3), 137.01 (C4), 137.65 (C6), 160.03 (C8).  $^{29}\text{Si}$  NMR (79 MHz, Acetone- $d_6$ )  $\delta$  -18.38. IR (ATR,  $\text{cm}^{-1}$ ):  $\nu$  = 3536 (w, br; OH), 3200-3400 (m, br; OH), 3067-2974 (m), 1598 (m), 1581 (m), 1504 (m), 1428 (m; Si- $\phi$ ), 1372 (w;  $\phi$ -OH), 1263 (m), 1243 (m), 1179 (m), 1114 (s; Si- $\phi$ ), 1091 (s; Si-O-Si), 1047 (m), 828 (m), 738 (w), 712 (m), 699 (s); Anal. calcd for  $\text{C}_{36}\text{H}_{30}\text{O}_3\text{Si}_2$ : C, 76.29; H, 5.34; O, 8.47; Si, 9.91. Found: C, 76.41; H, 5.38.

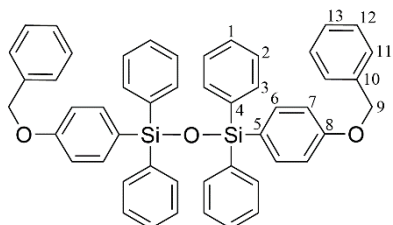


Figure 42: 1,3-Bis(4-(benzyl oxy)phenyl)-1,1,3,3-tetraphenyldisiloxane (BODSO). Numbers correspond to carbons and their respective hydrogens as assigned in NMR.

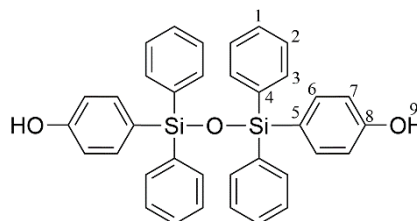


Figure 43: 4,4'-(1,1,3,3-Tetraphenyl disiloxane-1,3-diyl)diphenol (DPDSO). Numbers correspond to carbons and their respective hydrogens as assigned in NMR.

#### 4.2.4.3 Synthetic Route for 4,4'-(((1,1,3,3-Tetraphenyldisiloxane-1,3-diyl)bis(4,1-phenylene))bis(oxy)) diphthalonitrile (CSOPN)

Figure 44 illustrates the structure of CSOPN. A three-necked flask was assembled with stir bar, nitrogen inlet, rubber septum, and reflux condenser. The reaction vessel was flame dried under vacuum and purged with dry nitrogen. DPDSO (15.2 g, 26.8 mmol) was dissolved in 112 mL of dry DMF.  $\text{K}_2\text{CO}_3$  (11.12 g, 80.5 mmol) was stirred into solution. The mixture was allowed to stir for fifteen minutes. Then, 4-nitrophthalonitrile (9.28 g, 53.6 mmol) was stirred into solution. The reaction ran at room temperature overnight and was then heated to 80 °C for 8 hours. The reaction contents were removed and poured into 700 mL of 0.1 M HCl. Precipitate of the desired product was separated by filtration and washed with deionized water. The product was then dissolved in 500 mL DCM and washed with deionized water 4 times (2 L total). The organic layer was separated and dried with  $\text{MgSO}_4$ . The  $\text{MgSO}_4$  was removed by filtration, and the solvent was removed by rotary evaporation. The product was purified by flash silica column chromatography using 10:1:10 hexane/ethyl acetate/chloroform. Yield: 15.4 g, 18.8 mmol, 70 %. For analytical characterization, a small amount was further purified by recrystallization from acetonitrile.  $R_f$ : 0.23 ( $\text{SiO}_2$ , hexane/ethyl acetate/chloroform, 10:1:10). mp: 190-191 °C.  $^1\text{H}$  NMR (400 MHz,  $\text{CDCl}_3$ ,  $\delta$ , ppm): 6.95 – 7.01 (m, 4H(7)), 7.23 – 7.28 (m, 4H(10,14)), 7.30 – 7.35 (m, 8H(2)), 7.41 – 7.46 (m, 4H(1)), 7.48 – 7.53 (m, 8H(3)), 7.54 – 7.58 (m, 4H(6)), 7.71 – 7.76 (m, 2H(13)).  $^{13}\text{C}$  NMR (101

MHz, CDCl<sub>3</sub>, δ, ppm): 109.14 (C12), 114.92 (C15), 115.32 (C16), 117.65 (C11), 119.77 (C7), 121.60 (C14), 121.90 (C10), 127.96 (C2), 130.29 (C1), 133.65 (C5), 134.55 (C4), 135.08 (C3), 135.43 (C13), 137.64 (C6), 155.13 (C8), 161.24 (C9). <sup>29</sup>Si NMR (79 MHz, CDCl<sub>3</sub>) δ -18.50. IR (ATR, cm<sup>-1</sup>): ν = 3098-3000 (w), 2233 (m; C≡N), 1580 (s), 1563 (w), 1495 (m), 1485 (s), 1428 (m; Si-φ), 1311 (s), 1281 (s), 1252 (s; O-φ), 1213 (m), 1175 (m), 1138 (s; Si-φ), 1107 (s; Si-φ), 1086 (s; Si-O-Si), 1054 (w, br; Si-O-Si), 897 (w), 853 (w), 837 (m), 830 (m), 739 (m), 712 (m), 699 (m). Anal. calcd for C<sub>52</sub>H<sub>34</sub>N<sub>4</sub>O<sub>3</sub>Si<sub>2</sub>: C, 76.26; H, 4.18; N, 6.84; O, 5.86; Si, 6.86. Found: C, 76.04; H, 4.23; N, 6.73.

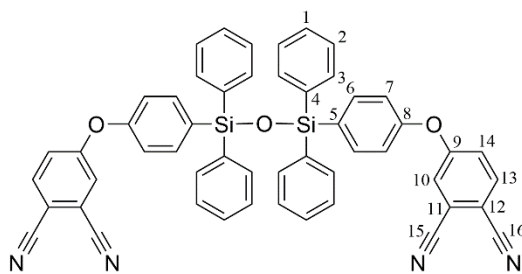


Figure 44: 4,4'-(((1,1,3,3-Tetraphenyldisiloxane-1,3-diyl)bis(4,1-phenylene))bis(oxy))diphthalonitrile (CSPN). Numbers correspond to carbons and their respective hydrogens as assigned in NMR.

## 4.2.5 Crystal Structures

### 4.2.5.1 Crystal Structure of CSPN

Crystals of CSPN were grown from 4:1 hexane: ethyl acetate. The structure was confirmed by X-ray crystallographic analysis, Figure 45. A colorless block (0.17 x 0.29 x 0.35 mm<sup>3</sup>) was centered on the goniometer of a Rigaku Oxford Diffraction Gemini Ultra diffractometer operating with MoK $\alpha$  radiation. The data collection routine, unit cell refinement, and data processing were carried out with the program CrysAlisPro.<sup>226</sup> The Laue symmetry and systematic absences were consistent with the triclinic space group P-1. The structure was solved using SHELXT-2014 and refined using SHELXL-2014 via Olex2.<sup>227-229</sup> The final refinement model involved anisotropic displacement parameters for non-hydrogen atoms and a riding model for all hydrogen atoms. Olex2 was used for molecular graphics generation.<sup>229</sup> Information on the crystal structure of CSPN is provided as follows: 103 K, C<sub>40</sub>H<sub>24</sub>N<sub>4</sub>O<sub>2</sub>Si, triclinic, space group P-1, primitive. Unit cell parameters: a = 9.7711(8) Å, b = 12.4266(11) Å, c = 13.9186(7) Å, alpha = 91.435(6)°, beta = 93.552(5)°, gamma = 104.879(7)°, volume = 1628.7(2) Å<sup>3</sup>.

#### 4.2.5.2 Crystal Structure of CSOPN

Crystals of CSOPN were grown from toluene. The structure was confirmed by X-ray crystallographic analysis, Figure 46. A colorless plank was cut into a prism (0.13 x 0.24 x 0.34 mm<sup>3</sup>) and centered on the goniometer of a Rigaku Oxford Diffraction Gemini E Ultra diffractometer operating with MoK $\alpha$  radiation. The data collection routine, unit cell refinement, and data processing were carried out with the program CrysAlisPro.<sup>226</sup> The Laue symmetry was consistent with the triclinic space groups P1 and P-1. The centrosymmetric space group, P-1, was chosen. The structure was solved using SHELXT-2014 and refined using SHELXL-2014 via Olex.<sup>227-229</sup> The final refinement model involved anisotropic displacement parameters for non-hydrogen atoms and a riding model for all hydrogen atoms. Information on the crystal structure of CSOPN is provided as follows: 101.8(9) K, C<sub>52</sub>H<sub>34</sub>N<sub>4</sub>O<sub>3</sub>Si<sub>2</sub> • C<sub>7</sub>H<sub>8</sub> triclinic, space group P-1, primitive. Unit cell parameters: a = 10.5442(3) Å, b = 19.3888(5) Å, c = 25.4613(6) Å,  $\alpha$  = 110.194(2)°,  $\beta$  = 93.652(2)°,  $\gamma$  = 100.237(2)°, Volume = 4763.3(2) Å<sup>3</sup>.

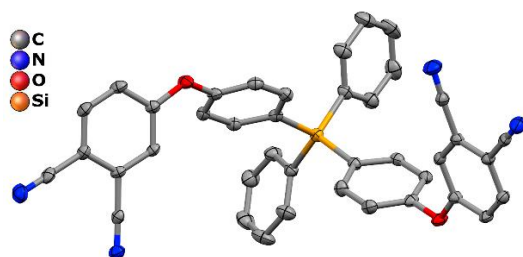


Figure 45: X-ray structure of CSPN.

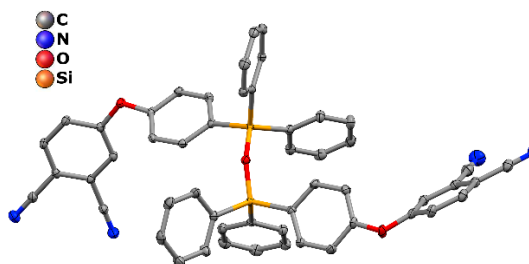


Figure 46: X-ray structure of CSOPN. Solvent molecules are omitted.

#### 4.2.6 Additional Compounds and Synthesis Routes Investigated

Additional synthetic routes were initially investigated in the pursuit of synthesizing the carboxysilane monomer. The intention was to synthesize 4,4'-((diphenylsilylanediyl)bis(oxy))diphenol and react it with 4-nitrophthalonitrile to form the desired monomer. A direct route using hydroquinone, as well as the use of ester and benzyl protecting groups were investigated. However, these routes either did not yield desired results or were found to be less optimal than the procedures previously detailed in this manuscript. Due to the observed hydrolytic sensitivity of the aryloxysilane linkage, the divergent synthesis approach was abandoned in favor of a convergent synthesis route. The following sections detail these investigations. Due to their sub-optimal nature, these methods were not fully characterized.

#### 4.2.6.1 Attempted Synthesis of 4,4'-((Diphenylsilanediyl)bis(oxy))diphenol

A direct synthesis approach using hydroquinone (no protecting group) was attempted, Figure 47. However, this yielded a distribution of products.

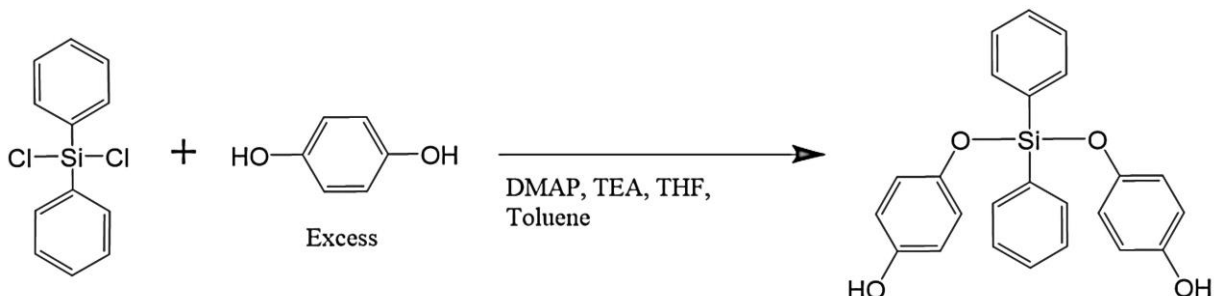


Figure 47: Attempted synthesis of 4,4'-((diphenylsilanediyl)bis(oxy))diphenol.

A three necked flask with addition funnel, rubber septa, and nitrogen inlet was flame dried under vacuum and purged with nitrogen. A mixture of 1.44 g (13.1 mmol) of hydroquinone, 0.46 mL (3.3 mol) of trimethylamine (TEA), a catalytic amount of 4-dimethylaminopyridine (DMAP) 0.016 g (0.13 mol), 23 mL of tetrahydrofuran (THF), and 3.3 mL of toluene were introduced into the three-necked flask. Then 0.35 mL (1.6 mmol) of dichlorodiphenylsilane diluted with 5.5 mL of 7:1 THF: toluene was added into the mixture dropwise while stirring. The reaction mixture was refluxed for 24 hours at 75 °C. Formed solid was removed from the mixture by filtration and the filtrate was concentrated by a rotary evaporator.

#### 4.2.6.2 Synthesis of 4-Hydroxyphenyl Acetate

A protecting group was deemed necessary since the direct synthetic route in Figure 47 yielded a distribution of products. Originally an ester was considered as a protecting group for hydroquinone and 4-hydroxyphenyl acetate was synthesized, Figure 48.

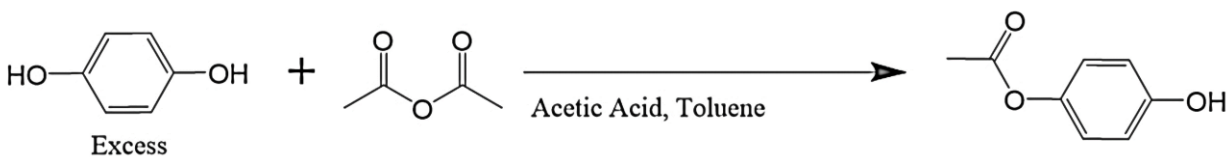


Figure 48: Synthesis of 4-hydroxyphenyl acetate.

To a solution of 30 g (270 mmol) of hydroquinone in 68 mL (1.19 mol) of acetic acid, 12.8 mL (136 mmol) of acetic anhydride was added dropwise over the course of five hours while stirring the solution at 110 °C. The mixture was maintained at 110 °C overnight. The acetic acid was then removed by rotary evaporation under vacuum. Toluene (136 mL) was added to the reaction

mixture and the unreacted excess hydroquinone was filtered and collected. The solvents were removed by rotary evaporation. The product was dissolved in DCM and washed with DI water in a separatory flask. The organic layer containing the product was separated out. the solution was dried with MgSO<sub>4</sub>. The MgSO<sub>4</sub> was removed by vacuum filtration. The product was then purified using a silica column with 1:3 ethyl acetate: hexane mixture. <sup>1</sup>H NMR in CDCl<sub>3</sub>, ppm: 2.27 (3H, s), 6.73 (2H, m), 6.87 (2H, m).

#### 4.2.6.3 Attempted synthesis of ((Diphenylsilanediyl)bis(oxy))bis(4,1-phenylene) Diacetate

Once 4-hydroxyphenyl acetate was synthesized, the following synthesis procedure of the carboxysilane linkage was investigated, Figure 49. However, the ester group proved to be unstable under the conditions required for the synthesis of the carboxysilane linkage. Redistribution of the ester group was observed via NMR, with the formation of hydroquinone and 1,4-phenylene diacetate. It is of note however that a catalytic amount of DMAP was used. This was later found to be unnecessary and detrimental due to the formation of side products. It is possible that the ester group may be stable during reaction conditions without the presence of DMAP, but this was not evaluated. <sup>1</sup>H NMR of hydroquinone in CDCl<sub>3</sub>, ppm: 6.70 (4H, s). <sup>1</sup>H NMR of 1,4-phenylene diacetate in CDCl<sub>3</sub>, ppm: 2.30 (6H, s), 7.10 (4H, s)

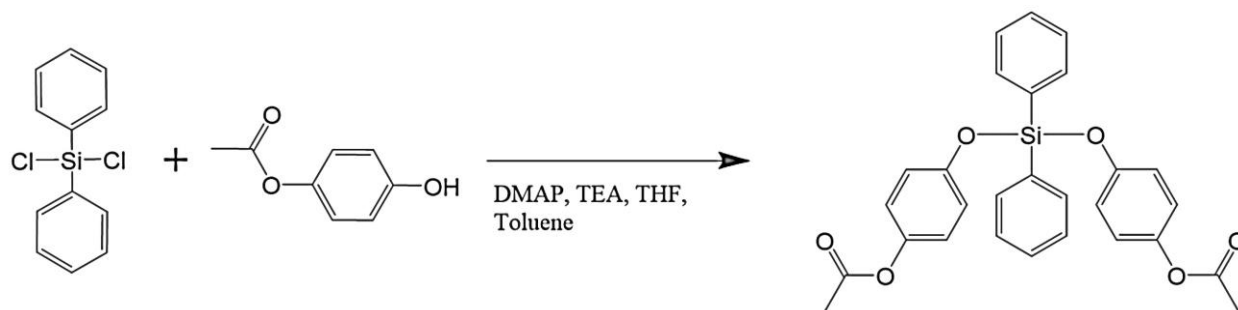


Figure 49: Attempted synthesis of ((diphenylsilanediyl)bis(oxy))bis(4,1-phenylene) diacetate.

A three necked flask with addition funnel, rubber septa, and nitrogen inlet was flame dried under vacuum and purged with nitrogen. The flask was chilled in an ice water bath. A mixture of 0.3 g (2.0 mmol) of 4-hydroxyphenyl Acetate, 0.14 mL (1.0 mmol) of triethylamine (TEA), 3.5 mL of THF, 0.5 mL of toluene and a catalytic amount of DMAP 5.0 mg (0.04 mmol) were introduced into the three-necked flask. Then 0.2 mL (1.0 mmol) of dichlorodiphenylsilane diluted with 3.5 mL THF and 0.5 mL toluene was added dropwise while stirring. The reaction mixture was stirred overnight at room temperature. The reaction mixture was refluxed for an additional 24

hours at 75 °C. Formed solid was removed from the mixture by filtration and the filtrate was concentrated by a rotary evaporator.

#### 4.2.6.4 Synthesis of Bis(4-(benzyloxy)phenoxy)diphenylsilane

Due to the instability of the ester group, a different protecting group was needed. A benzyl protecting group was then investigated. 4-Benzyloxyphenol was reacted with dichlorodiphenylsilane to produce a benzyl protected carboxysilane, Figure 50. This compound was successfully synthesized. However, it hydrolytically degraded during purification via silica column chromatography.



Figure 50: Synthesis of bis(4-(benzyloxy)phenoxy)diphenylsilane.

A three necked flask with addition funnel, rubber septa, and nitrogen inlet was flame dried under vacuum and purged with nitrogen. The flask was chilled in an ice water bath. A mixture of 2g (10 mmol) of 4-benzyloxyphenol, 1.4 mL (1.0 mmol) of TEA, 17.5 mL of THF, and 2.5 mL of toluene were introduced into the three-necked flask. Then 1.05 mL (5.0 mmol) of dichlorodimethylsilane diluted with 4 mL THF was added into the mixture dropwise while stirring. After an hour, a catalytic amount of DMAP 0.05 g (0.40 mmol) was added dissolved in 1 mL THF. The reaction mixture was stirred overnight at room temperature. The reaction mixture was refluxed for an additional 24 hours at 75 °C. Formed solid was removed from the mixture by filtration and the filtrate was concentrated by a rotary evaporator. <sup>1</sup>H NMR in CDCl<sub>3</sub>, ppm: 4.96 (4H, s), 6.78, (4H, m), 6.89 (4H, m), 7.31-7.49 (16H, m), 7.76 (4H, m). Purification was attempted using silica column chromatography with 1:4 ethyl acetate:hexane. However, a significant amount of 4-benzyloxyphenol was obtained indicating hydrolytic degradation.

### 4.3 Results and Discussion

#### 4.3.1.1 Synthesis of Compounds

All analytical characterization supports the formation of the reported compounds. The NMR and IR for HOPOPn agree with literature.<sup>132, 223</sup> The formation of the COSPN monomer is evident

in IR by the disappearance of the 3413  $\text{cm}^{-1}$  (O-H stretching, free), and 3324  $\text{cm}^{-1}$  (OH, H-bonded) peaks, and appearance of peaks at 915-930  $\text{cm}^{-1}$  (Si-O-C). The use of excess TEA was found to be necessary for the formation of C-O-Si linkages. The yield of BODPS was significantly improved by the slow addition of reactants, a slight excess of 4-benzyloxybromobenzene, sufficient stirring to equalize temperature gradients, and a slow warm up to room temperature. The addition of excess *n*-BuLi was found to create side products. The NMR spectra for DPSDP agree with data published by Tagle et al.<sup>224</sup> and Terraza et al.<sup>225</sup> The cleavage of the benzyl groups of BODPS or BODSO, to form DPSDP or DPDSO, is observed in IR with the disappearance of peaks at 1010-1037 and 1270-1288  $\text{cm}^{-1}$  (alkyl-aryl ether C-O stretching), and 1461-1465  $\text{cm}^{-1}$  (methylene C-H bending). This corresponds with the appearance of peaks at 3200-3400  $\text{cm}^{-1}$  (broad, H-bonded O-H), and 3604  $\text{cm}^{-1}$  (free O-H stretching). In  $^1\text{H}$  NMR ( $\text{CDCl}_3$ ), the disappearance of benzyl peaks at 5.08-5.09 ppm is observed. The rate of hydrogenation of the benzyl groups was found to be significantly accelerated by the addition of ethanol, as compared with running the reaction in just THF. Occasionally deprotection reactions to form DPSDP did not proceed, yielding only BODPS starting material. It was assumed this was due to the Pd/C catalyst being poisoned by sulfur contamination. Reactions ran as expected when precautions were taken by avoiding rubber septum and the use of reflux condensers to isolate rubber nitrogen lines and hydrogen balloons. Since the BODPS starting material was stable under the reaction conditions, it was recovered in the event of catalyst poisoning. Product from poisoned reactions was run through a silica plug prior to running the reaction again. The formation of the aryl-aryl ether linkage and addition of the phthalonitrile group to DPSDP to form CSPN, is observed in IR with the disappearance of peaks at 3200-3430 and 3604  $\text{cm}^{-1}$ , and appearance of peaks at 890-897  $\text{cm}^{-1}$  (1,2,4-trisubstituted benzene C-H bending), 1210-1212 and 1280  $\text{cm}^{-1}$  (aryl-aryl ether), and 2231-2233  $\text{cm}^{-1}$  ( $\text{C}\equiv\text{N}$  stretching).

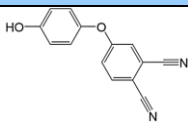
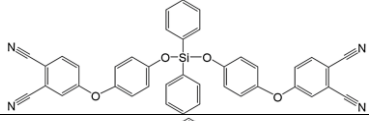
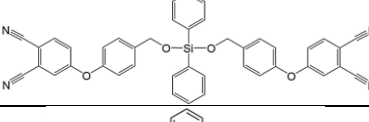
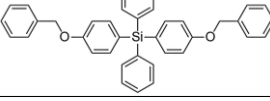
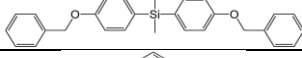
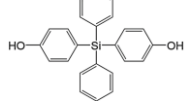
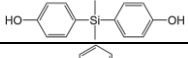
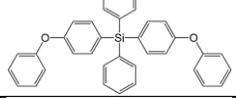
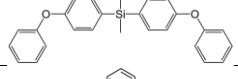
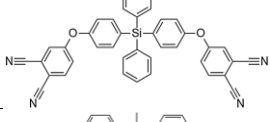
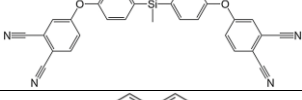
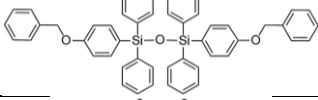
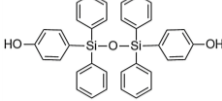
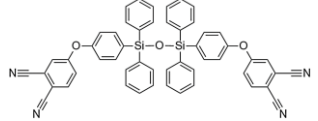
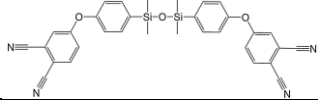
#### 4.3.1.2 Melting Points

Melting points for synthesized compounds are compared with similar compounds from literature in Table 10. The melting points observed in DSC for BODPS and DPSDP agree with work by Davidsohn et al. and Tagle et al.<sup>219,224</sup> The melting points for COSPN, CSPN, and CSOPN monomers are comparable to first generation, highly aromatic phthalonitriles.<sup>6, 21-26</sup> CSPN was also recently reported by Terraza et al.<sup>55</sup> It is interesting to note, that while NMR spectra agree with the published data, Terraza et al. reports the melting point of CSPN to be only 91–93 °C. It

is currently unclear where the discrepancy lies. However, given the melting points of similar compounds reported in this paper and in literature, as well as the well-documented difference between melting points of similar dimethyl and diphenyl silane compounds, the value of 223 °C appears to be more reasonable.<sup>219, 224-225, 230-231</sup>

Melting points are extremely difficult to predict due to complex interactions and large differences in crystal structures resulting from small changes in chemical structure.<sup>232</sup> However, overall trends are often apparent when comparing similar molecules. In general, melting point decreases with increasing flexibility of linkages. For example, decreasing phenyl substitution on the silicon leads to decreased steric hindrance, and thus more flexible linkages and lower melting points. Dimethyl substituted compounds in Table 10 melt at > 40 °C lower than the corresponding diphenyl substituted compounds. If the CSPN monomer is compared with its methyl-substituted analogue (compound F in Table 10) a decrease in the melting point of 130 °C is observed with methyl-substitution. Likewise, the CSOPN monomer may be compared with work by Dzhevakov et al,<sup>53</sup> who synthesized the corresponding methyl-substituted compound (compound G in Table 10). A  $T_g$  of only 4 °C was reported for this tetramethyldiphenyl-disiloxane-containing phthalonitrile. A melting point was not reported for this compound. Comparing COSPN and CSPN monomers, the addition of -O- into the backbone between the silicon and carbon lowered the melting point by 50 °C. It is of note however, that the COSPN monomer was obtained at only 80% purity. The true melting point of the purified compound is likely higher, and thus the difference smaller. The hexaphenyldisiloxane linkage in CSOPN decreased the melting point by 30 °C, as compared the tetraphenylsilane linkage CSPN. However, this effect was smaller in DPDSO and not observed in the case of BODSO. The bisphenol compounds (DPSDP, DPDSO, compound C) have high melting points due to hydrogen bonding. When the phthalonitrile group is attached, the melting point decreases by 6-30 °C for diphenyl-substituted compounds (CSPN and CSOPN) and 80 °C for the dimethyl-substituted compound F, as compared with their corresponding bisphenols. Compared with phenoxy end-capped compounds D and E, the rigid nitrile groups increase the melting point by 20-60 °C. When the COSPN monomer is compared with work by Babkin et al.<sup>52</sup> (compound A in Table 10), the further addition of a methylene linkage to the backbone between the oxygen and carbon, resulted in a  $T_g$  of only 27 °C. A melting point was not reported.

Table 10: Melting points of synthesized and selected literature compounds.

Compound	Structure	mp/T <sub>g</sub> , °C	Reference
HOPOP		150-152	This Work, Liu <sup>223</sup>
CSOPN		168-169	This Work
A		27 (T <sub>g</sub> )	Babkin <sup>52</sup>
BODPS		142-150	This Work, Davidsohn <sup>219</sup>
B		109-110	Davidsohn <sup>219</sup>
DPSDP		221-229	This Work, Davidsohn <sup>219</sup>
C		171-174	Davidsohn <sup>219</sup>
D		162-163	Gilman <sup>230</sup>
E		68-69	Olin-Mathieson <sup>231</sup>
CSPN		223	This Work
F		89-91	Terraza <sup>55</sup>
BODSO		164	This Work
DPDSO		217	This Work
CSOPN		190-191	This Work
G		4 (T <sub>g</sub> )	Dzhevakov <sup>53</sup>

#### 4.3.1.3 Stability of Compounds

The COSPN monomer showed a high sensitivity to hydrolysis. In the presence of moisture, the Si-O-C bond cleaved to produce Si-OH compounds and HOPOPAN starting material. After storing samples in ambient conditions for several days, degradation of the COSPN monomer was observed via NMR with the reappearance of HOPOPAN. COSPN samples stored in a desiccator for 1 year showed emergence of a sharp melting transition around 150 °C, also indicating the formation of HOPOPAN. This was confirmed via FTIR with the appearance of broad a OH band at 3417-3450 cm<sup>-1</sup>.

Due to its hydrolytic instability, purification of the COSPN compound proved difficult. Sublimation was attempted, but decomposition of the compound was observed prior to evaporation. To evaluate the possibility of running a silica column on the COSPN monomer, TLC plates were dried at 100 °C for 48 hours. TLC plates were run with anhydrous solvents in a glove box under nitrogen, however degradation of the COSPN compound was still observed. Similar degradation was observed when purification was attempted via LCUV. Given procedures developed later for CSPN and CSOPN monomers, it is possible that purification of the COSPN monomer could be accomplished with recrystallization in dry acetonitrile or toluene under nitrogen, however this was not attempted.

These results agree with recently published findings by Dzhevakov et al,<sup>53</sup> Bulgakov et al,<sup>30</sup> and Babkin et al.<sup>79</sup> Degradation of similar compounds occurred on silica and alumina TLC plates, as well as in ambient humidity, both in solution and in the solid state. It was reported that steric hindrance by phenyl groups alone does not sufficiently stabilize the Si-O-C linkage. Hydrolytic stability was improved by addition of a methylene linkage; this is however considered detrimental for thermal stability. Results by Cella and Rubinsztajn<sup>82</sup> indicate that further steric hindrance by the addition of functional groups on the phenylene rings may stabilize the linkage, but may also result in a higher degree of rigidity and thus higher melting points.

In contrast to phthalonitriles with carboxysilane linkages, including COSPN and compounds reported in literature,<sup>30, 53, 79</sup> the CSPN and CSOPN monomers show no hydrolytic sensitivity, allowing for aqueous workup. The corresponding benzyl-protected precursors, BODPS and BODSO, also did not exhibit any sensitivity towards hydrolysis. The bis-phenols DPSPD and DPDSO were observed to degrade slowly when stored at room temperature and ambient conditions. While this degradation may be somewhat explained by hydroxyl-catalyzed degradation

of Si-C bonds, the stability of these compounds improved substantially when highly pure and stored in dark, moisture-free conditions.

#### 4.4 Summary and Conclusions

Synthesis and purification procedures were developed, and three monomers and their precursors were produced in high yields. These compounds include four novel compounds not previously published to the authors knowledge. Additional characterization information is included for compounds already present in literature. Carboxysilane compounds showed high sensitivity to water and thus are not commercially viable. The carbosilane and carbosiloxane compounds showed no hydrolytic sensitivity. Increasing phenyl substitution on the silicon resulted in increased steric hindrance, and thus increased melting points, yet is expected to also result in increased thermal and oxidative stability. Melting points for all three monomers were in the range of first-generation, highly-aromatic phthalonitriles.<sup>6, 21-26</sup> This is not ideal since it requires a higher processing temperature, and results in a smaller processing window. In addition, the melting points for all three monomers are significantly higher than reported for silicon-containing phthalonitriles in literature, which report glass transitions in the range of -1 to 30 °C<sup>30, 52-53, 79</sup> or melting points in the range of 35 to 91°C.<sup>6, 51, 55</sup> However, these literature compounds contain either methyl functional groups on the silicon or a methylene bridge, which have been reported as detrimental to thermal and oxidative stability.

## 5 Processing and Characterization of As-Synthesized Carboxysilane and Carbosilane Phthalonitriles

### 5.1 Introduction

This chapter covers processing and characterization of the as-synthesized carboxysilane (COSPN) and carbosilane (CSPN) resins following procedures in Chapter 4-Synthetic Procedures for Silicon-Containing Phthalonitrile Monomers. The structures of COSPN and CSPN monomers are reproduced below for convenience in Figure 51 and Figure 52. These as-synthesized materials are given the suffix “-U”. A subsequent chapter, Chapter 6-Processing and Characterization of Purified CSPN and CSOPN Materials covers processing and characterization carbosilane and carbosiloxane phthalonitriles of high purity. Due to its hydrolytic sensitivity, only limited processing and characterization of the of the carboxysilane (COSPN-U) monomer was performed, and the highly purified monomer was not evaluated.

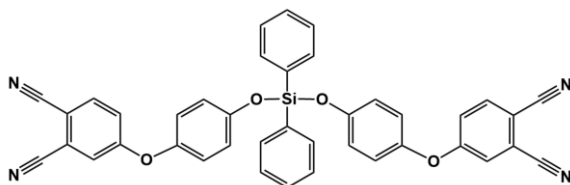


*Figure 51: Carboxysilane-Phthalonitrile (COSPN) Monomer.*

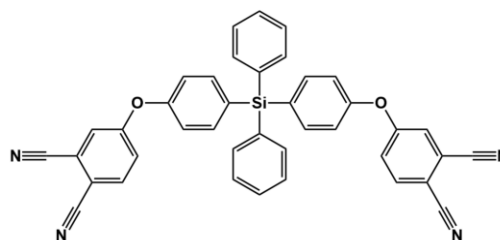


*Figure 52: Carbosilane-Phthalonitrile (CSPN) Monomer.*

CSPN and COSPN monomer/catalyst mixtures were prepared and cured. To provide information related to processing, monomers and pre-polymers were evaluated using differential scanning calorimetry, parallel plate rheology, thermogravimetric analysis, and Fourier transform infrared spectroscopy. The glass transition of cured polymer samples was characterized by dynamic mechanical analysis, thermomechanical analysis, and differential scanning calorimetry. The linear coefficient of thermal expansion was measured using thermomechanical analysis. Thermal stability was evaluated using thermomechanical analysis. Fourier transform infrared (FTIR) spectroscopy of evolved gases from thermomechanical analysis provided insight into degradation reactions.

## 5.2 Experimental

### 5.2.1 Materials and Methods

Bis(4-(4-aminophenoxy)phenyl)sulfone (*p*-BAPS, >98%) was purchased from TCI America. A model 10444 (30 ton) Wabash hydraulic press was used to compression mold resin plaques. Differential scanning calorimetry (DSC) was conducted using a TA Instruments Q1000 with a ramp rate of 5 °C/min. Fourier transform infrared (FTIR) spectroscopy was conducted using a Thermo Scientific Nicolet 6700 with Spectra Tech Inc. attenuated total reflection (ATR) and Thermo Electron Corp. TGA/FT-IR accessories. Parallel plate rheology and torsional dynamic mechanical analysis (DMA) were performed on a TA Instruments Ares G2 with a ramp rate of 5 °C/min. Thermogravimetric analysis (TGA) of powder samples in air and nitrogen was performed using a TA Instruments Q500 or Q50, with a ramp rate of 10 °C/min and a flow rate of 90 mL/min. A TA Instruments Q400 was used for thermomechanical analysis (TMA) with a ramp rate of 5 °C/min. Panels were c-scanned at AFRL/RXAS, Wright Patterson Air Force Base.

### 5.2.2 Preparation of Monomer-Catalyst Mixtures and Pre-Polymer B-staged Resins

The processing profile for COSPN-U resins is given in Figure 53. A catalytic amount (4 wt. %) of *p*-BAPS was added to the COSPN monomer. The mixture was then dissolved in anhydrous THF and cast into aluminum weighing boats. COSPN monomer samples were then placed in an oven under nitrogen at 110 °C for 3.5 hours to remove the THF. The samples were then degassed by slowly increasing temperature up to 200 °C under vacuum over three hours.

A slightly different profile was used for CSPN-U samples, Figure 54. This was due the differing reactivity, lack of hydrolytic sensitivity, and higher melting point of the CSPN-U monomer. CSPN-U monomer samples were added to a Teflon<sup>TM</sup>-lined aluminum weighing boat and placed in an oven at 190 °C under nitrogen atmosphere. Temperature was increased, and the monomer was melted at 210 °C. To the melt, was added 4-6 wt. % of the catalyst *p*-BAPS. The mixture was stirred for two minutes. Vacuum was applied, and the resin was degassed and b-staged for 30 minutes at 220-230 °C. A sample was removed for characterization. The melt-mixing approach was chosen since it was the standard in literature.<sup>4, 22</sup> Other mixing methods produced comparable results including: 1) dry mixing the monomer and catalyst powders and melting the mixture and 2) dissolving the monomer and catalyst in DCM/Chloroform (1:1), removing the solvents by rotary evaporation, degassing the mixture under vacuum at 25 °C for 4 hours, 100 °C for 30 minutes, and

220-230 °C for 30 minutes. To increase the viscosity further for rheology and compression molding, CSPN-U pre-polymer mixtures were heated under nitrogen to 230 °C for an additional 30 minutes, followed by 240-250 °C for thirty minutes. The resin was allowed to cool to room temperature in a desiccator.

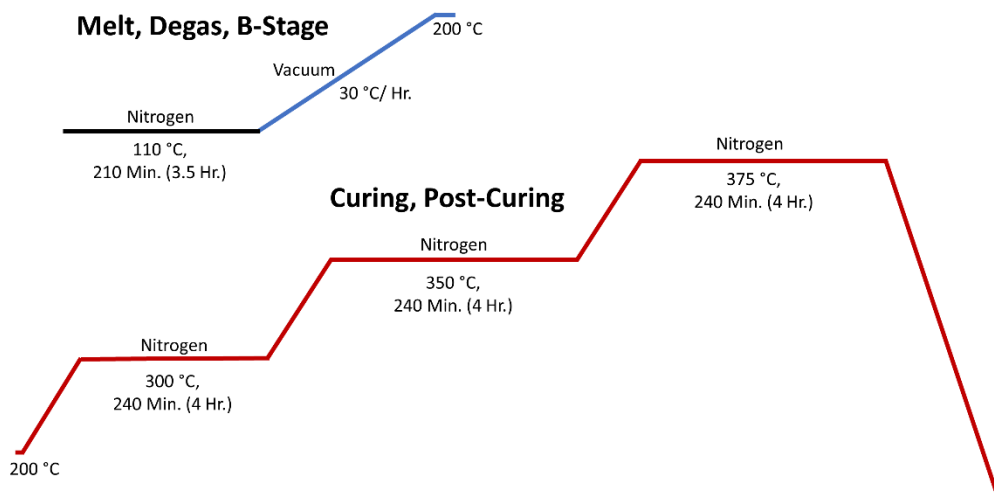


Figure 53: Processing profile for COSPN-U resins with 4 wt. % p-BAPS.

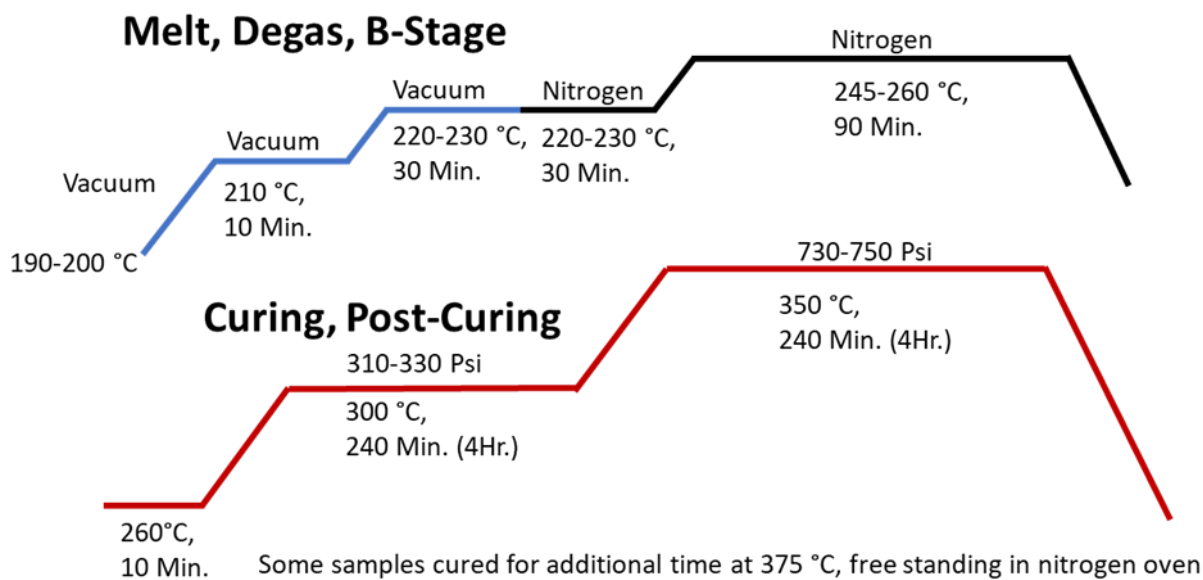


Figure 54: Processing profile for CSPN-U resins with 4-6 wt. % p-BAPS.

### 5.2.3 Fabrication of Cured Samples

COSPN-U samples were then cured under nitrogen at 300 °C for four hours, 350 °C for four hours, and 375 °C for four hours. The cured COSPN samples were then broken up and ground for TGA and DSC measurements, Figure 55.



*Figure 55: Cured COSPN-U polymer, as cast (right) and ground (left).*

To fabricate CSPN polymer samples, the pre-polymer resin was placed in a steel mold. A 3" x 3" x 1/8" steel mold was used for the panel with 6 wt. % *p*-BAPS while a 2" x 2" x 1/8" mold was used for the panel with 4 wt. %. The mold was placed in a hydraulic press at 275 °C and heated at 300 °C for four hours (130-170 psi). A sample was removed for characterization. The plaque was placed back in the press and cured at 350 °C for four hours (290 psi). The polymer panel was then allowed to cool to room temperature. To determine porosity content and distribution, the panel then was c-scanned. A wet saw was then used to cut the plaque into samples for DMA, TMA, and TOS. After cutting, some samples were then further cured under nitrogen at 375 °C for 1-3 hours. All samples were dried under vacuum at 100 °C for three days and stored in a desiccator prior to characterization.

## 5.3 Results and Discussion

### 5.3.1 DSC of Monomers- Curing Exotherms

In DSC, COSPN monomer without any curing additive exhibited a small exotherm at 385 °C, Figure 56. This may be attributed to a curing reaction catalyzed by hydroxyl groups present in

impurities or hydrolytic degradation products. The COSPN-U/*p*-BAPS mixtures exhibited melting endotherms between 131-158 °C. Exothermic peaks occurred between around 265-277 °C. These exothermic peaks likely correspond to curing reactions and the peak values are consistent with those reported in phthalonitrile literature.<sup>17, 22, 139</sup>

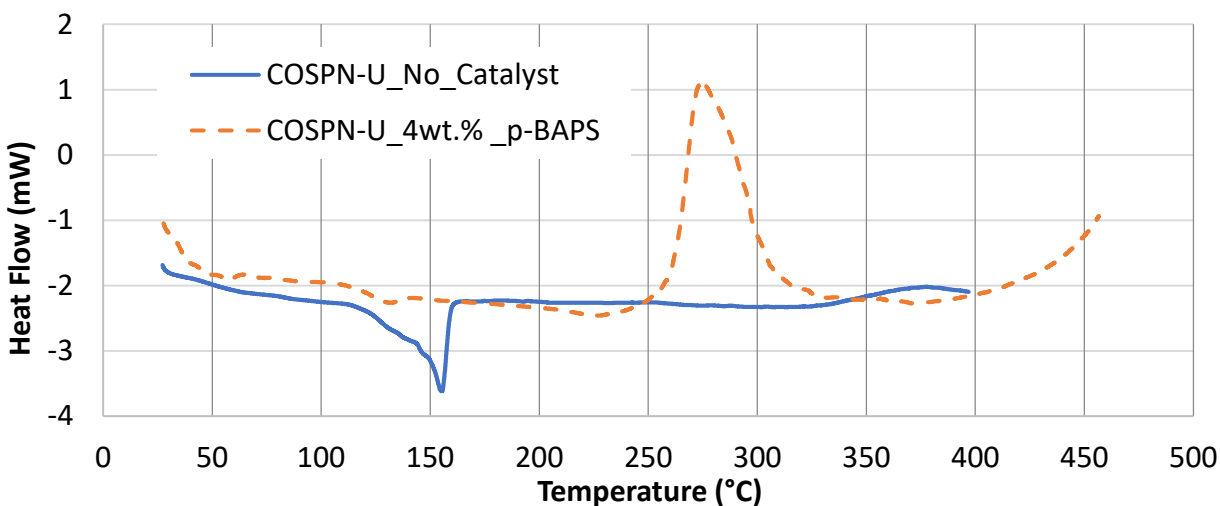


Figure 56: DSC in nitrogen of COSPN neat resin and COSPN with 4 wt. % *p*-BAPS mixture.

Figure 57 provides DSC data in nitrogen for the CSPN-U monomer, monomer with 4 wt.% *p*-BAPS (dry mixed), and monomer/*p*-baps mixture after b-staging to 220 °C. All three exhibited inflections/endotherms in the range of 90-120 °C. The removal of absorbed moisture likely contributes to this endotherm. However, monomer/*p*-BAPS mixture after b-staging also exhibited an inflection at this point during cooling. Thus, it likely also corresponds to a glass transition. The endotherm at 177 °C and exotherm at 185 °C observed in the CSPN-U monomer without *p*-BAPS, is possibly due to an impurity, or a glass transition followed by crystallization prior to melting. The as-synthesized CSPN-U monomer melted at 205-208 °C. Pure Bis(4-(4-aminophenoxy)phenyl)sulfone (*p*-BAPS) melts at 194-198 °C, and is evident as a small endotherm overlapping with the CSPN-U melting endotherm.<sup>24</sup> CSPN-U monomers with 4 wt. % *p*-BAPS exhibited an exotherm at 265 °C corresponding to the curing reaction.<sup>17, 22, 139</sup> The melting endotherms and curing exotherm disappeared after melting, degassing, and b-staging to 220 °C for 30 minutes. A very small exotherm was present at 350 °C, likely corresponding to a curing reaction. This reaction may be a second curing reaction, or residual of the reaction observed at 265

°C but shifted to higher temperatures due to increased steric hindrance from crosslinking. No degradation exotherm was observed up to 400 °C under nitrogen.

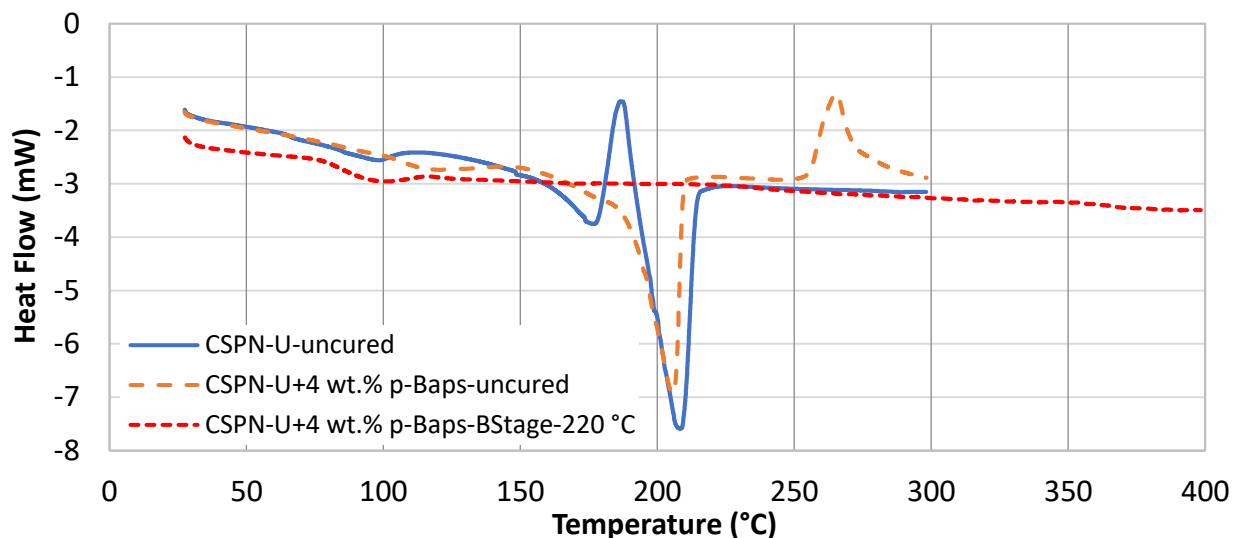


Figure 57: DSC in nitrogen of CSPN-U monomer, monomer with 4 wt.% p-BAPS (dry mixed), and monomer/p-baps mixture after b-staging to 220 °C.

### 5.3.2 Rheology of CSPN Resin

Rheology was performed on CSPN-U samples after degassing to 210 °C and again after b-staging at 220 °C. Results are given in Figure 58, Figure 59, and Table 11. Degassing was required to remove volatile products and achieve useful viscosity data. Softening began at 130 °C. After degassing, the viscosity decreased to 0.3-0.5 Pa\*s between 250-290 °C. After b-staging, the viscosity reached a minimum of 10 Pa\*s between 210-220 °C before increasing. While the CSPN monomer showed a smaller processing window than second generation phthalonitriles the material may still be processed effectively. The very low viscosities, on par with other phthalonitrile resins, facilitate processing by non-autoclave processing techniques.<sup>23</sup> Furthermore, the ability to increase the viscosity is critical in facilitating various processing techniques, including autoclave and hot pressing methods. These results agree with work by Keller and Dominguez,<sup>26</sup> who demonstrated that the viscosity of phthalonitriles can be precisely tailored by changing the curing additive content and b-staging conditions.

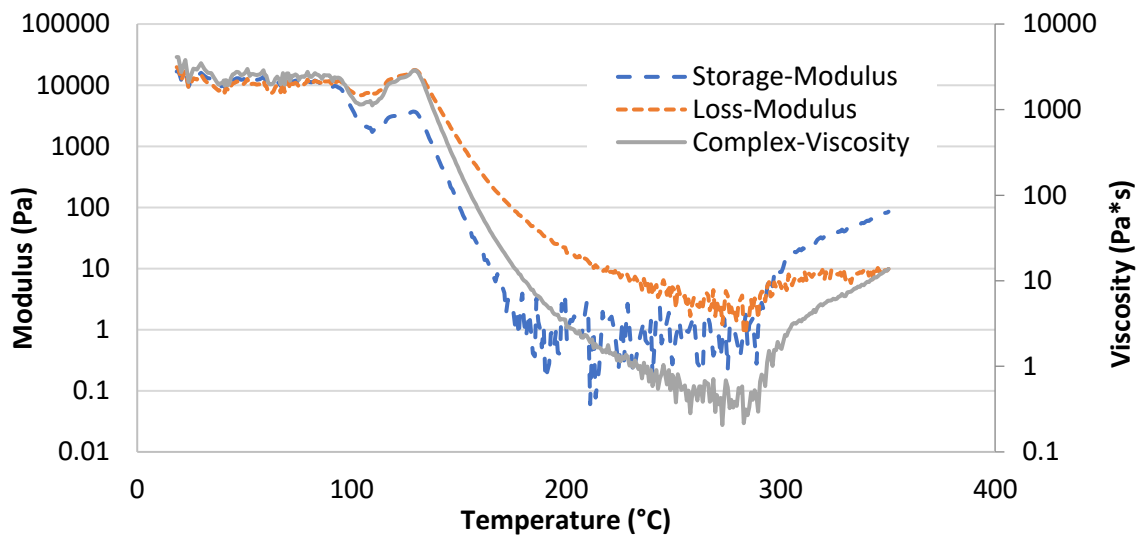


Figure 58: Example rheology curve of CSPN-U with 4 wt.% p-BAPS, after degassing to 210 °C. The ramp rate was 5 °C/min.

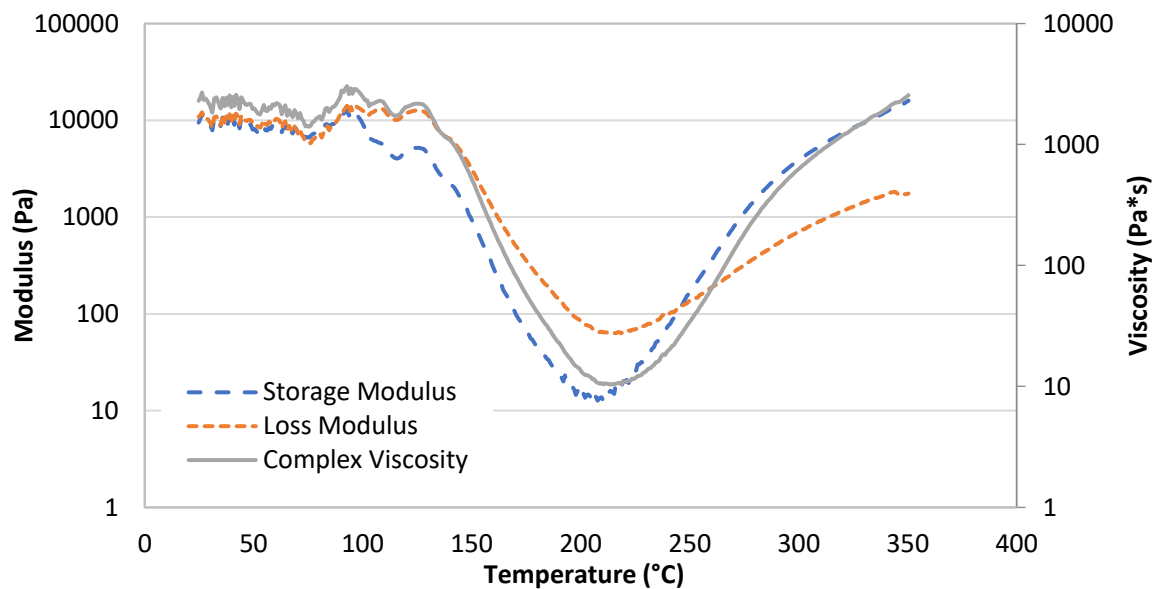


Figure 59: Example rheology curve of CSPN-U with 4 wt.% p-BAPS, after b-staging at 220 °C for 1 hour. The ramp rate was 5 °C/min.

Table 11: Viscosity and processing window information for CSPN-U with 4 wt. % p-BAPS.

Prior Conditioning	Min. Complex Viscosity (Pa·s)	Temperature Range (°C) for Min. Viscosity
Degas to 210 °C	0.3-0.4	256-288
Degas to 210 °C 220 °C-1Hr	10.0-11.0	207-222

### 5.3.3 TGA stability of CSPN Monomer

Figure 60 provides TGA data in nitrogen for CSPN-U monomer mixed with 4 wt. % *p*-BAPS. The as-mixed monomer/*p*-BAPS resin exhibited multiple weight loss peaks in the range of 80-300 °C, most likely from the volatilization of impurities and absorbed moisture. After degassing and b-staging up to 220 °C for 30 minutes, the resin shows no appreciable weight loss up to 300 °C. This data indicates that degassing and b-staging is required to improve stability and remove volatile products that would lead to porosity. The b-staged resin exhibited high thermal stability with 5% weight loss at 416 °C. Thus, substantial degradation was not expected at the processing temperatures of 250-300 °C.

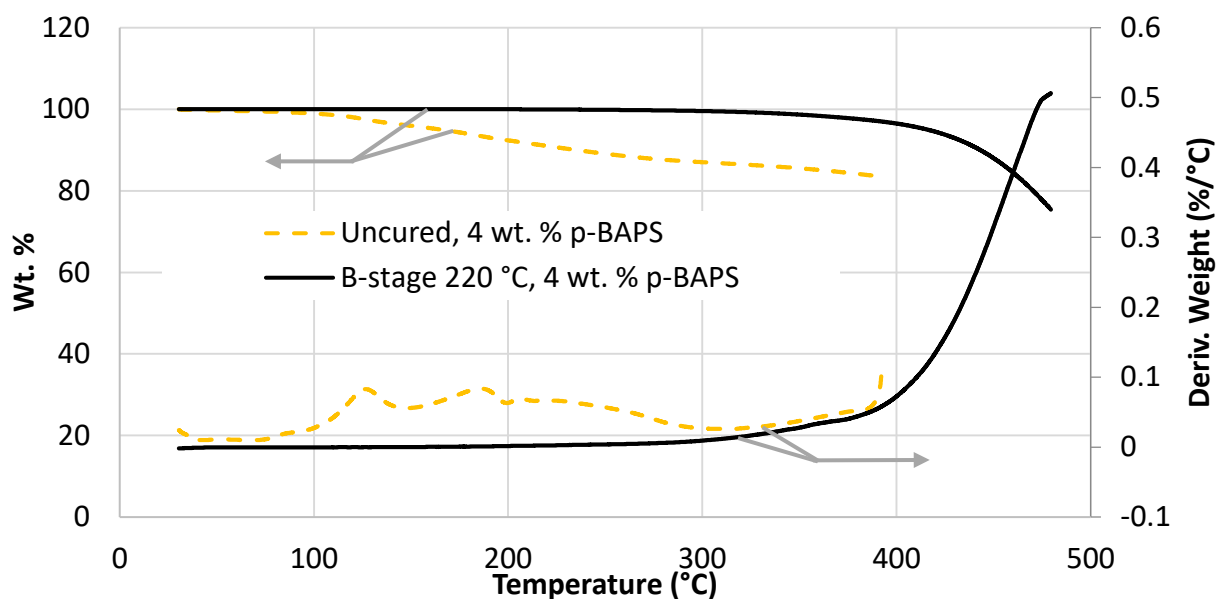


Figure 60: TGA data in nitrogen of CSPN-U with 4 wt. % *p*-BAPS, uncured monomer and after degassing and b-staging to 220 °C. The uncured resin shows multiple derivative weight loss peaks in the range of 80-300 °C and had lost 13% weight by 300 °C. These losses are likely due to absorbed moisture and volatilization of impurities. At 300-400 °C, the uncured and b-staged resin have similar slopes.

### 5.3.4 FTIR of Monomers and Polymers

The FTIR spectra of COSPN-U uncured monomer, pre-polymer with 4 wt.% *p*-BAPS b-staged to 200 °C, and polymer with 4 wt.% *p*-BAPS cured to 375 °C is given in Figure 61. Compared with the uncured monomer, the b-staged pre-polymer exhibits peaks at 1010-1020, 1500 and 1610  $\text{cm}^{-1}$  corresponding to isoindoline or phthalocyanine structures. After curing at 375 °C for 4 hours, peaks at 1356-1360 and 1530  $\text{cm}^{-1}$  corresponding to triazine also appear.<sup>5, 15, 95</sup>

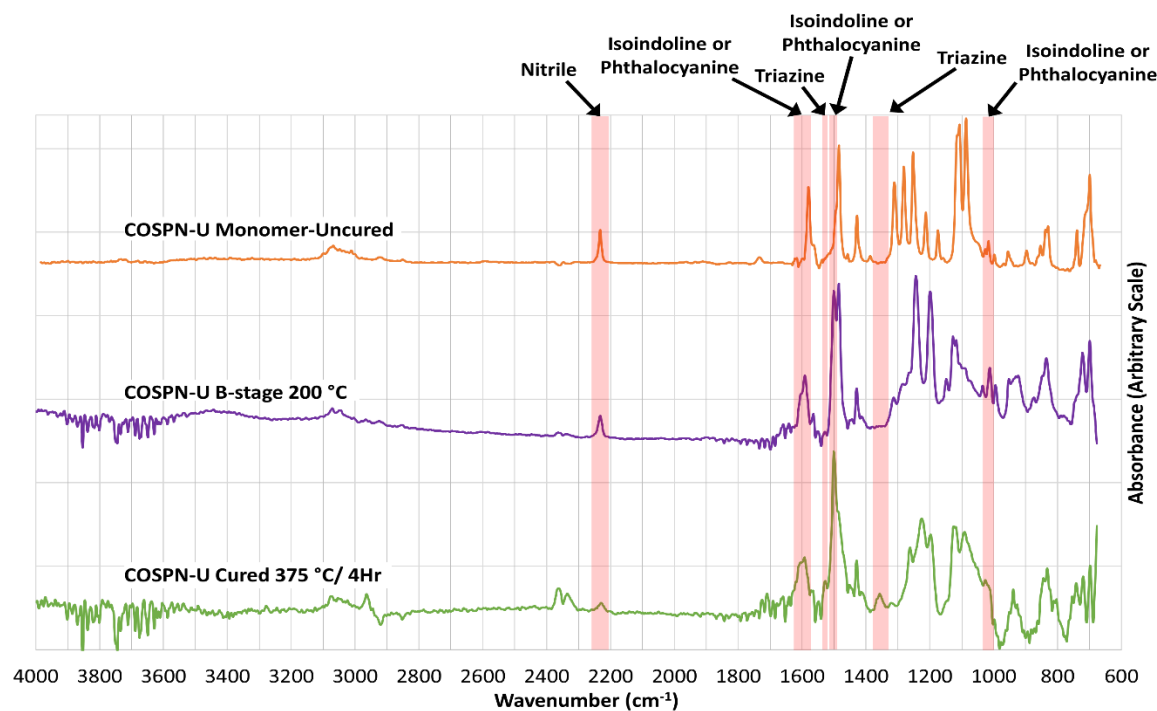


Figure 61: FTIR spectra of COSPN-U uncured monomer, pre-polymer with 4 wt.% *p*-BAPS b-staged to 200 °C, and polymer with 4 wt.% *p*-BAPS cured to 375 °C. The nitrile peak diminishes with additional curing.

Figure 62 provides the FTIR spectra of the CSPN-U monomer and polymers with 6 wt.% *p*-BAPS cured to 350 °C for 4 hours and 375 °C for 0-3 hours. After hot-pressing at 350 °C for 4 hours, CSPN-U polymers showed the formation of triazine with the appearance of characteristic peaks at 1356-1360  $\text{cm}^{-1}$  and 1520-1532  $\text{cm}^{-1}$ .<sup>5, 15, 95</sup> Peaks at 1580-1590  $\text{cm}^{-1}$  could plausibly correspond to isoindoline or phthalocyanine structures. Peaks usually attributed to phthalocyanine at 1015-1016  $\text{cm}^{-1}$  overlap with peaks present in the monomer. However, the green-black color observed in cured samples indicated that some phthalocyanine formation is likely. Figure 63 illustrates triazine and phthalocyanine structures formed during the curing of the CSPN-U resin. Additional curing at 375 °C for 1-3 hours did not result in substantial changes in the IR spectra, indicating that no substantial degradation occurred during post-curing up to 375 °C.

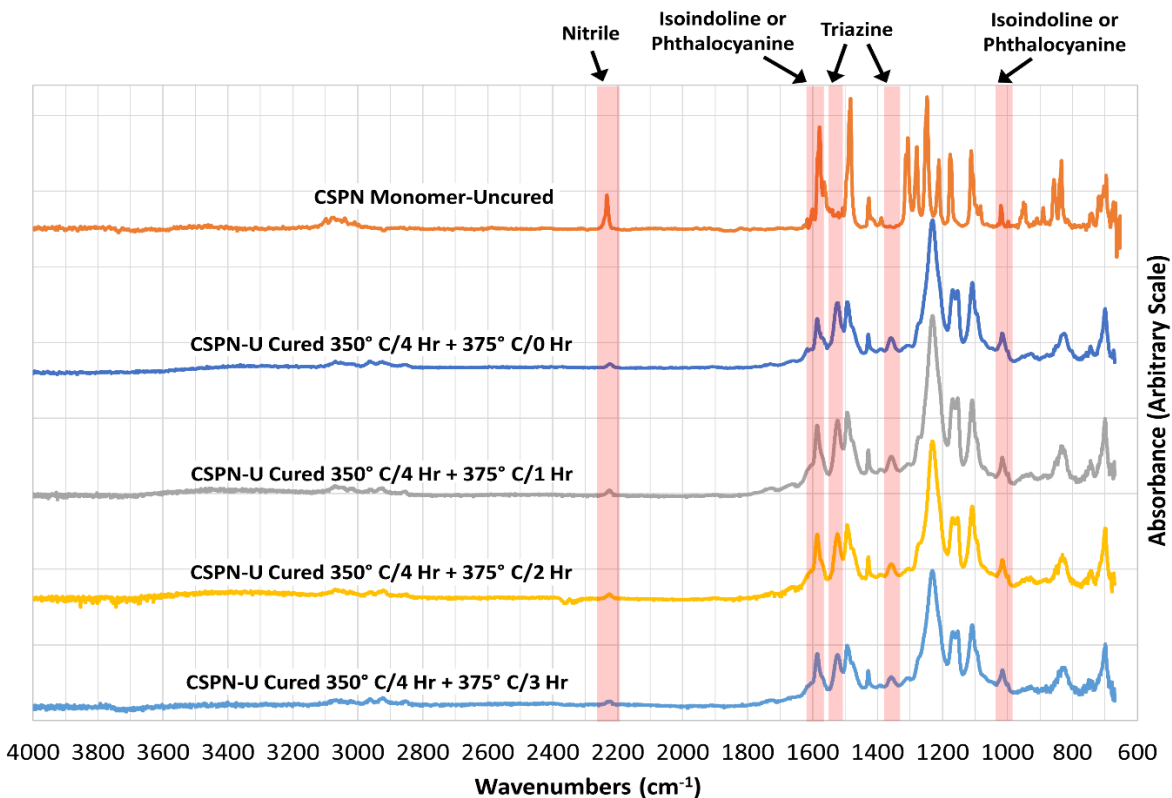


Figure 62: FTIR spectra of CSPN-U uncured monomer and after curing to 350°C for 4 hours and 375 °C for 0-3 hours. The formation of triazine peaks is evident in cured polymers. Isoindoline and phthalocyanine peaks overlap with peaks present in the monomer. No significant differences in spectra were observed for cured polymers.

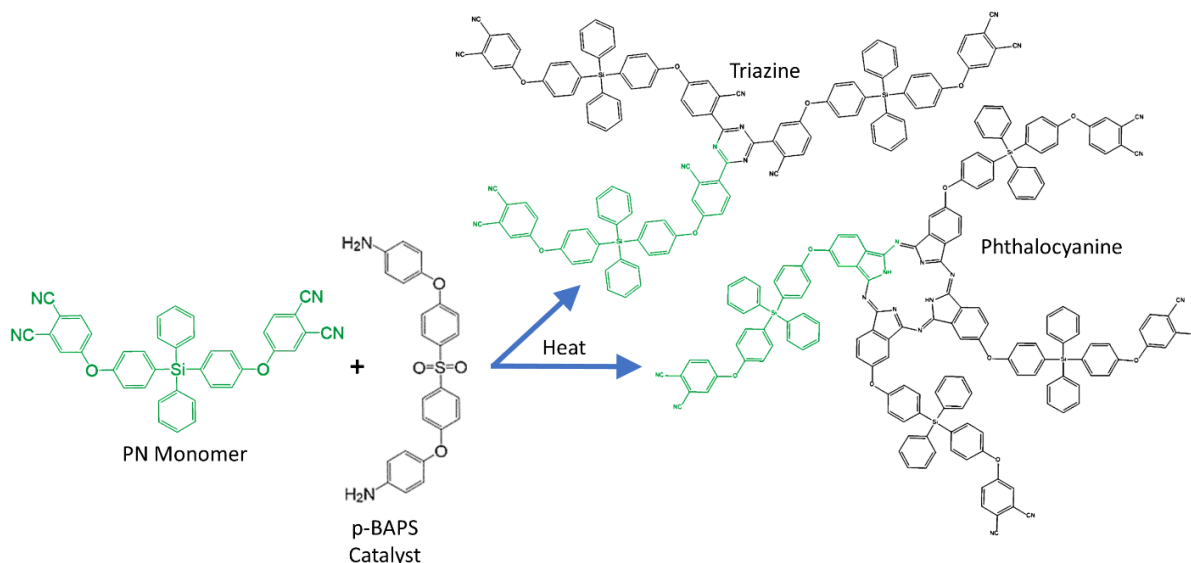
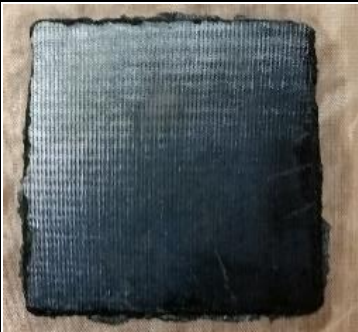
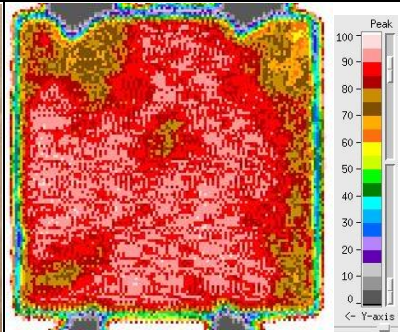
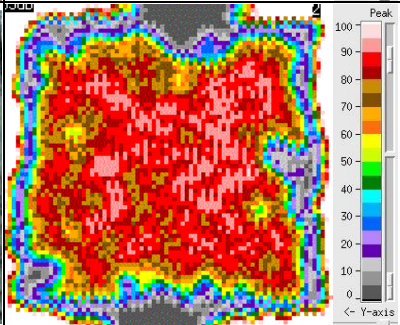


Figure 63: Triazine and phthalocyanine formation from curing reactions of nitrile groups in CSPN resin.

### 5.3.5 CSPN-U Panel Fabrication

CSPN-U pre-polymers were degassed and partially cured to a rubbery state prior to hot pressing. This was necessary in order to avoid porosity and prevent the resin from flowing out of the mold by increasing the viscosity. During degassing and b-staging up to 250 °C the CSPN-U pre-polymers lost approximately 10 % weight. Both 4 and 6 wt. % compositions showed gelation times of around 30 minutes at 250 °C. CSPN-U polymer panels were then fabricated by hot pressing. The results are provided in Table 12. Both panels showed good qualitative strength. The acoustic c-scan data provides a density map of each panel. The 4 wt. % panel exhibited more porosity than the 6 wt. % panel, however this may be due to slight differences in processing conditions. The density map was used to select areas of reasonable density for oxidative stability, TMA, and DMA specimens.

Table 12: CSPN-U polymer panels hot-Pressed to 350 °C for 4 hours. Red and white areas indicate high density.

	<i>p</i> -BAPS	Panel Size	Panel Images	C-Scan Density Map
CSPN-U	6 wt.% 8.4 mol%	3" x 3" x 1/8"		
CSPN-U	4 wt.% 5.7 mol%	2" x 2" x 1/8"		

### 5.3.6 DSC of Cured Polymers

The DSC data in nitrogen for COSPN-U cured to 375 °C for 4 hours is provided in Figure 64. No obvious glass transition was observed. The initiation of degradation was observed with an increase in slope beginning at 395 °C.

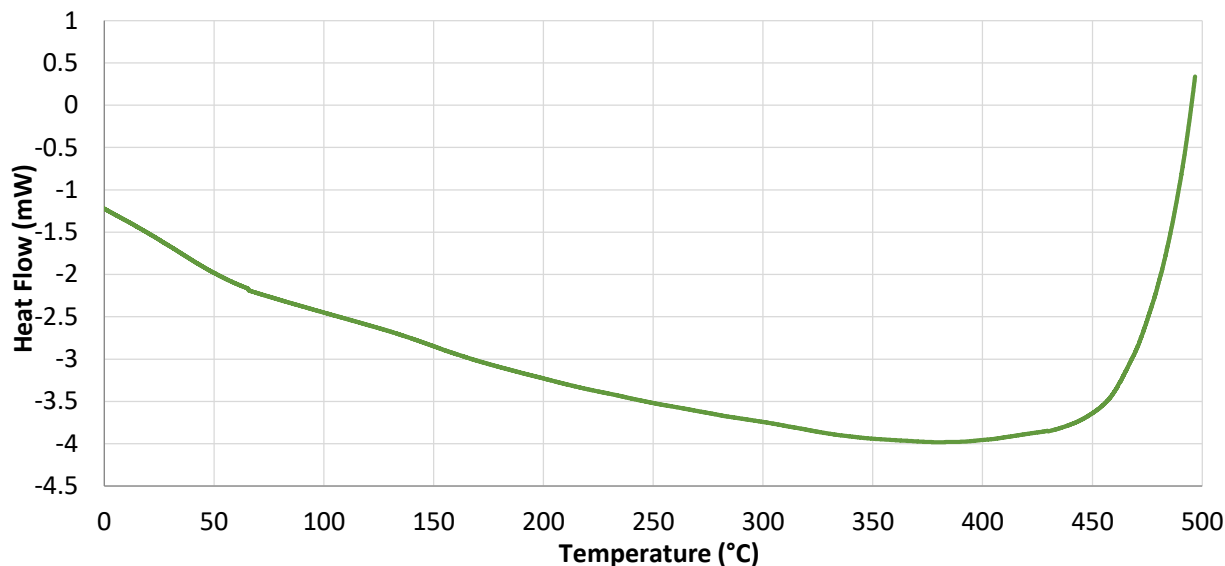


Figure 64: DSC of COSPN-U cured polymer powder in nitrogen. No distinct glass transition is evident.

Figure 65 provides DSC data in nitrogen for CSPN-U cured to 350 °C for 4 hours followed by 375 °C for 0-3 hours. A glass transition ( $T_g$ ) was evident at 344 °C for CSPN-U Cured to 350 °C for 4 hours (375 °C/ 0 hours). After curing to 375 °C for 1-3 hours, the glass transition disappeared, either due to a decrease in magnitude or due to being obscured by the onset of degradation. The onset of degradation was observed with an exothermic increase beginning at 410-420 °C. Thus, different curing times did not result in significant differences in the onset of degradation but did affect the glass transition temperature. Figure 66 provides DSC data for cured CSPN-U polymers in air. As compared with nitrogen, the onset of degradation shifts lower to 250-280 °C.

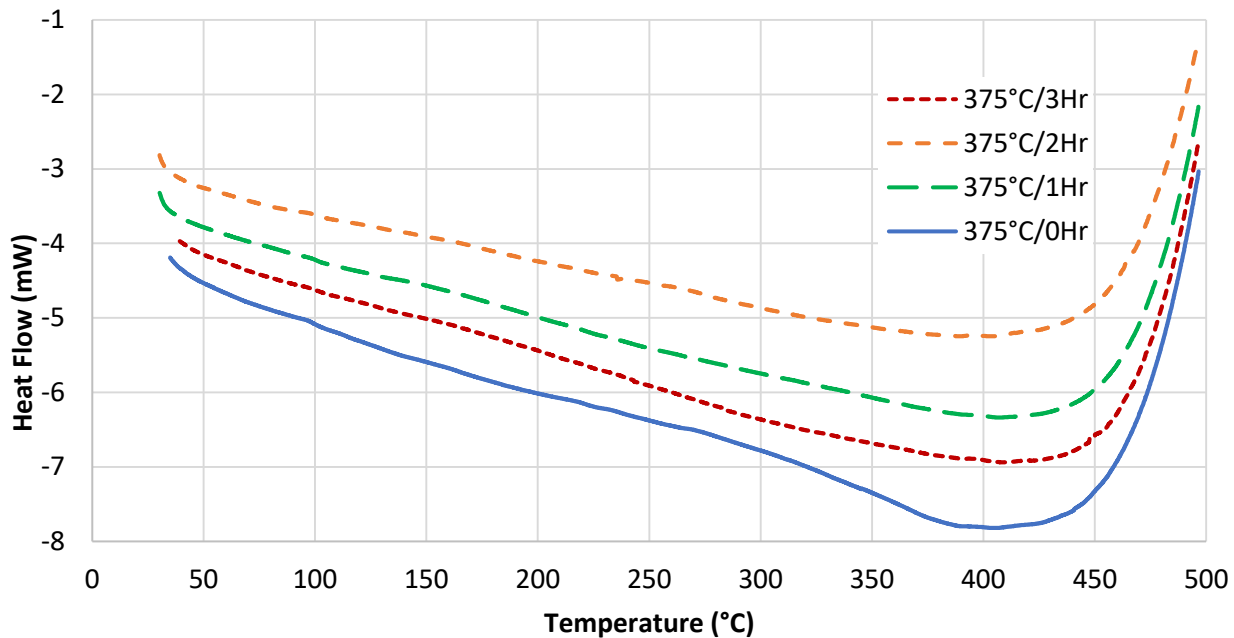


Figure 65: DSC of CSPN-U cured powders (6 wt. % *p*-BAPS) in nitrogen. A  $T_g$  at 344 °C was evident for CSPN cured to 350 °C/4 hours.

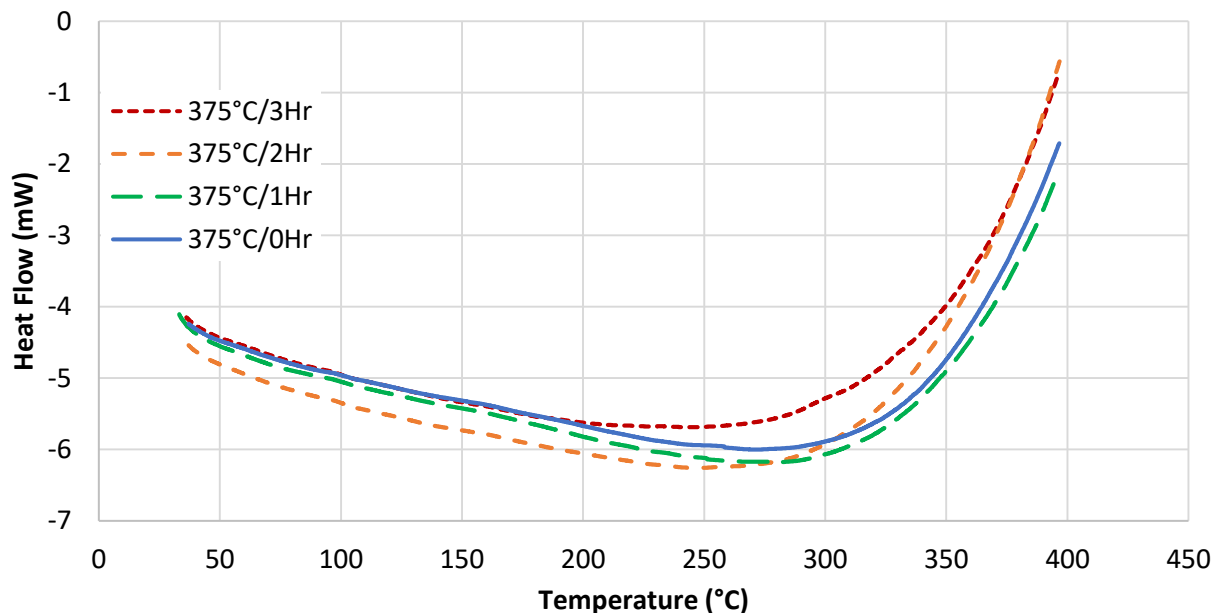


Figure 66: DSC of CSPN-U cured powders (6 wt. % *p*-BAPS) in Air. The Onset of Degradation Occurs Much Earlier Than in Nitrogen.

### 5.3.7 DMA of Cured CSPN Polymers

Figure 67, Figure 68, and Figure 69 provide DMA information for CSPN-U cured to 375 °C for 0, 1, and 3 hours respectively with 6 wt. % *p*-BAPS. The glass transition, as taken by the inflection of the storage modulus ( $G'$ ) was observed at 287 °C after curing at 350 °C/4 hours. After additional curing at 375 °C for 1 and 3 hours the  $T_g$  increased to 310 and 324 °C respectively.

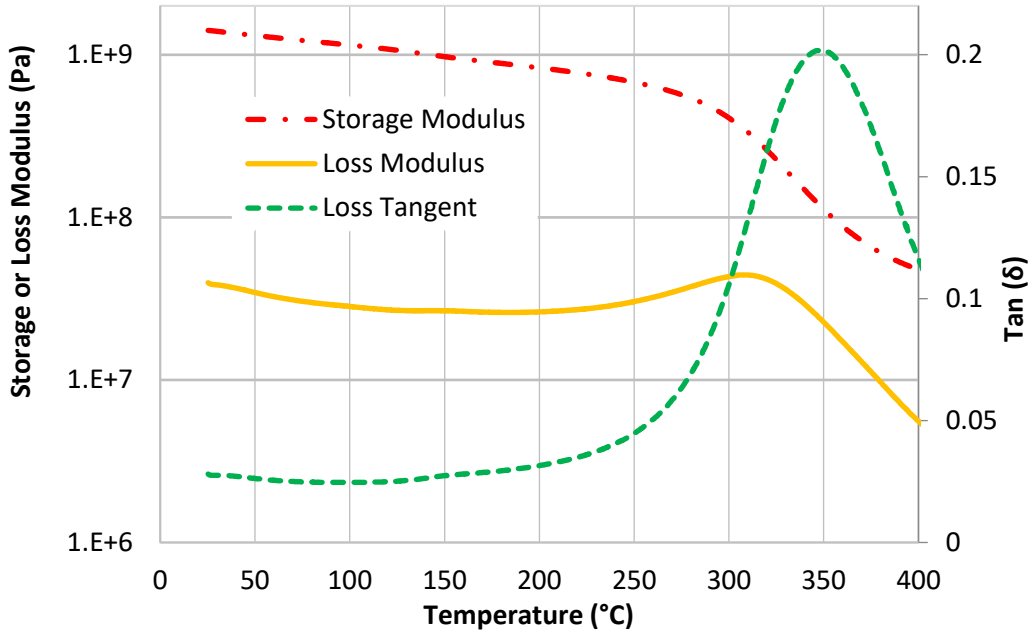


Figure 67: DMA of CSPN-U cured to 350 °C for 4 hours. The glass transition from inflection of the storage modulus was observed at 287 °C. The loss modulus and loss tangent exhibited peaks at 307 °C, and 349 °C.

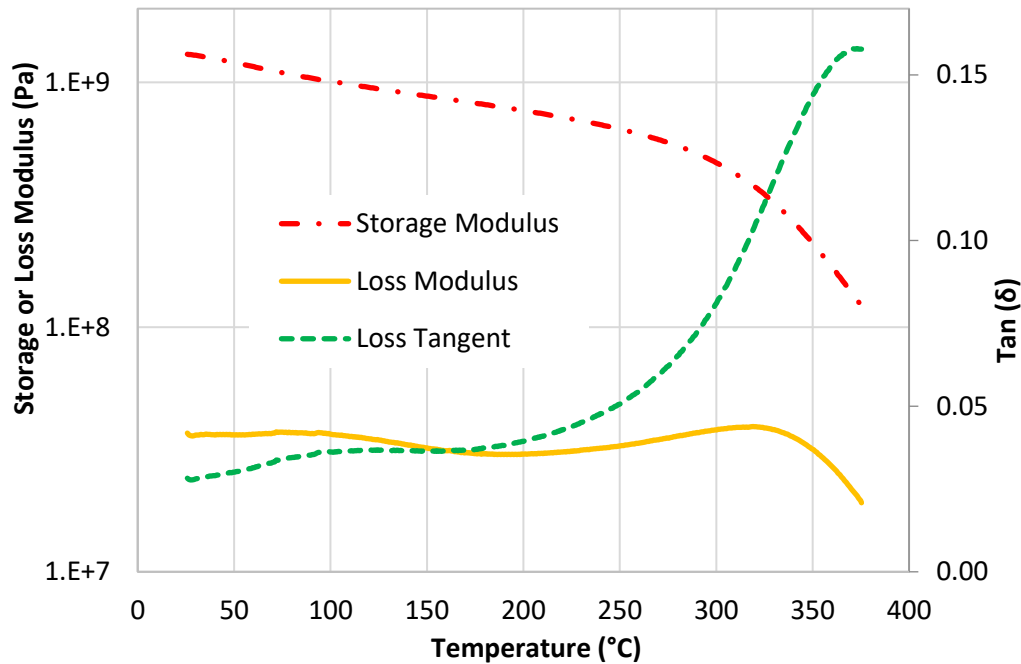


Figure 68: DMA of CSPN-U cured to 375 °C for 1 hour. The glass transition from inflection of the storage modulus was observed at 310 °C. The loss modulus and loss tangent exhibited peaks at 319 °C, and 373 °C.

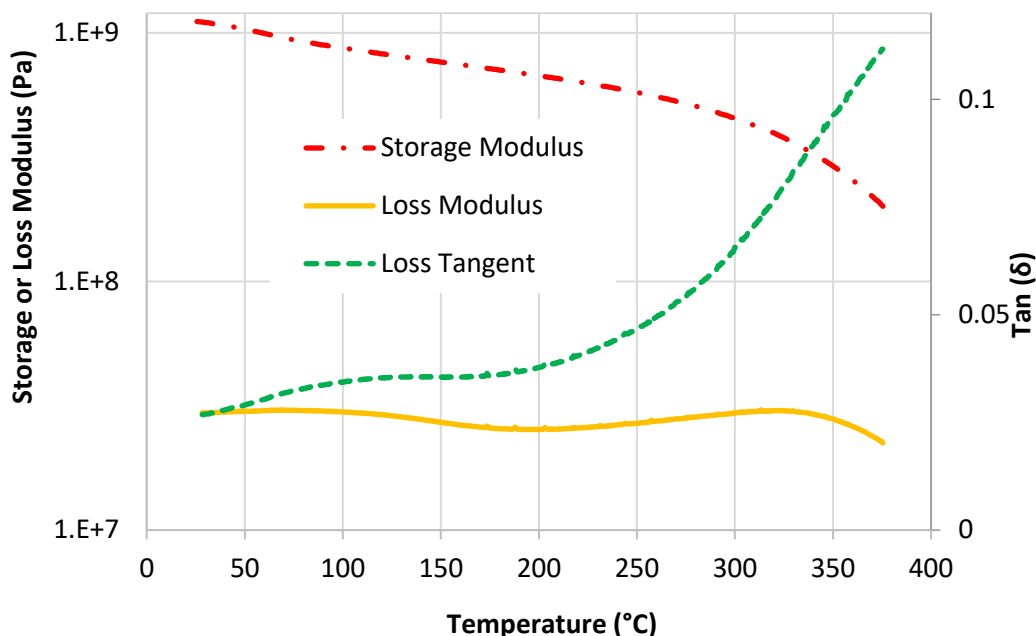


Figure 69: DMA of CSPN-U cured to 375 °C for 3 hours. The glass transition from inflection of the storage modulus was observed at 324 °C. The loss modulus and loss tangent exhibited peaks at 322 °C, and 375 °C.

### 5.3.8 TMA of Cured CSPN Polymers and CTE Information

TMA curves for CSPN-U cured polymers with 6 wt. % *p*-BAPS are given in Figure 70. The glass transition onsets and midpoints were identified as the peaks in the second and first derivatives, respectively. CSPN-U cured to 350 °C/ 4 hours had a  $T_g$  onset at 307 °C and a midpoint of 329 °C. With increasing post-curing time at 375 °C, transitions became smaller and more difficult to define in TMA, eventually disappearing entirely. When cured for an additional hour at 375 °C, CSPN-U showed an onset of the glass transition at 335 °C and midpoint at 390 °C. The glass transition disappeared after curing for 3 hours at 375 °C.

The coefficient of thermal expansion (CTE) is not often reported for phthalonitriles but is critical in designing components with these materials. The CTE was defined as the slope between 50-200 °C in TMA data, normalized by the sample thickness. This data is given in Figure 71. The CTE of CSPN samples cured to 350 °C for 4 hours, was observed in the range of  $77 \pm 1.4 \mu\text{m}/(\text{m } ^\circ\text{C})$ . The CTE decreased to  $75 \pm 1.5 \mu\text{m}/(\text{m } ^\circ\text{C})$ ,  $74 \pm 1.4 \mu\text{m}/(\text{m } ^\circ\text{C})$ , and  $73 \pm 0.9 \mu\text{m}/(\text{m } ^\circ\text{C})$  after additional curing to 375 °C for 1, 2, and 3 hours respectively. These values are higher than observed for other phthalonitrile systems ( $40\text{-}60 \mu\text{m}/(\text{m } ^\circ\text{C})$ ).<sup>96, 233</sup> This difference may be due to increased free volume from the inclusion of C-Si linkages.

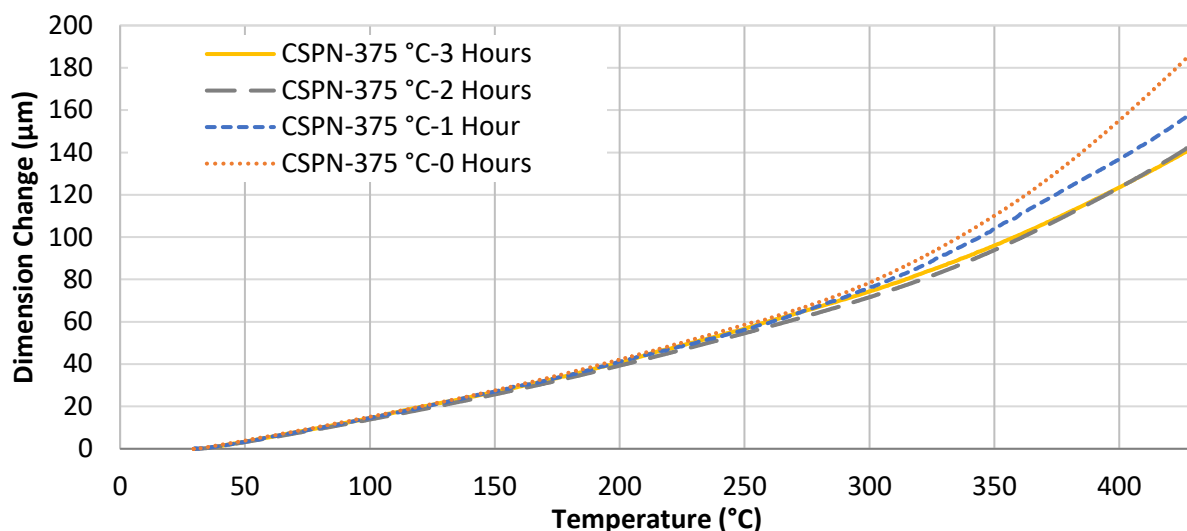


Figure 70: Example TMA curves of CSPN-U samples (6.35 mm x 6.35 mm x 3.3 mm thick) cured to 350 °C for 4 hours and 375 °C for 0-3 hours.

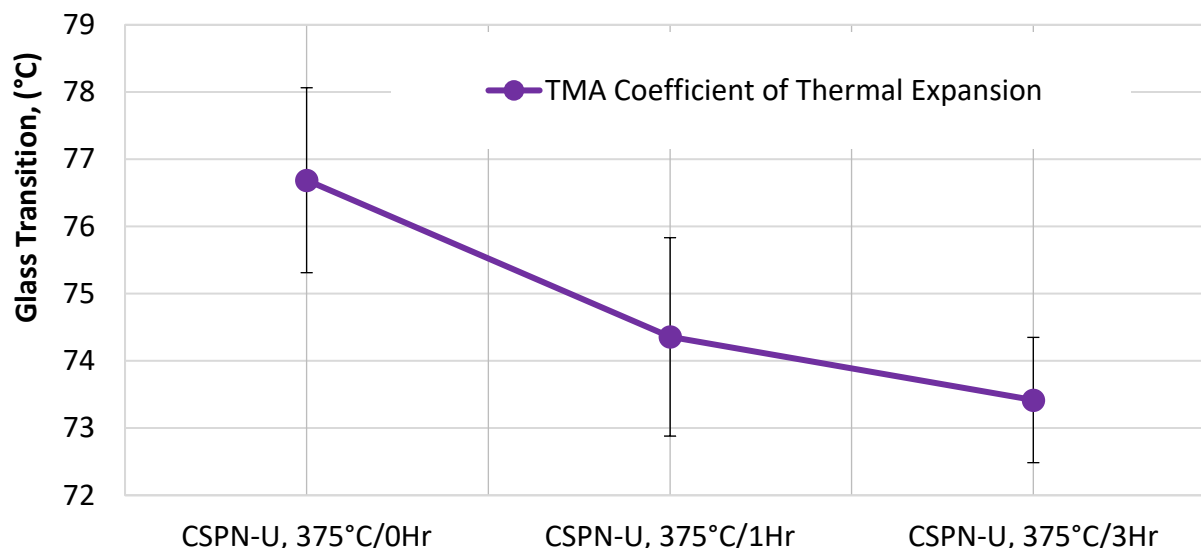


Figure 71: The CTE from TMA (50-200 °C) for CSPN-U samples cured to 350 °C for 4 hours, and 0, 1, or 3 hours at 375 °C.

### 5.3.9 Summary of CSPN-U Glass Transition Measurements

A summary of glass transition information for CSPN-U samples with 6 wt. % *p*-BAPS, is provided in Figure 72. Since glass transitions disappeared in DSC and TMA with additional curing at 375 °C, DMA proved a much more reliable method of measuring the  $T_g$ . The  $T_g$  of CSPN-U polymers was observed to be in the range of 287-324 °C. This glass transition temperature is slightly lower than other phthalonitriles reported in literature, likely due in part to the inclusion of silicon-containing linkages.<sup>6, 19, 24, 26</sup> While the effect of silicon moieties on glass transition is well known and substantial information exists on the inclusion of siloxane linkages, less literature is

available on the inclusion of phenyl-substituted silanes into polymers with high glass transition temperatures.<sup>6, 30, 44, 50-54, 63, 170, 204</sup> The glass transitions observed for CSPN-U are as high or higher than other phenyl-substituted silane or oxysilane polymers.<sup>44, 55, 63, 170, 204</sup>

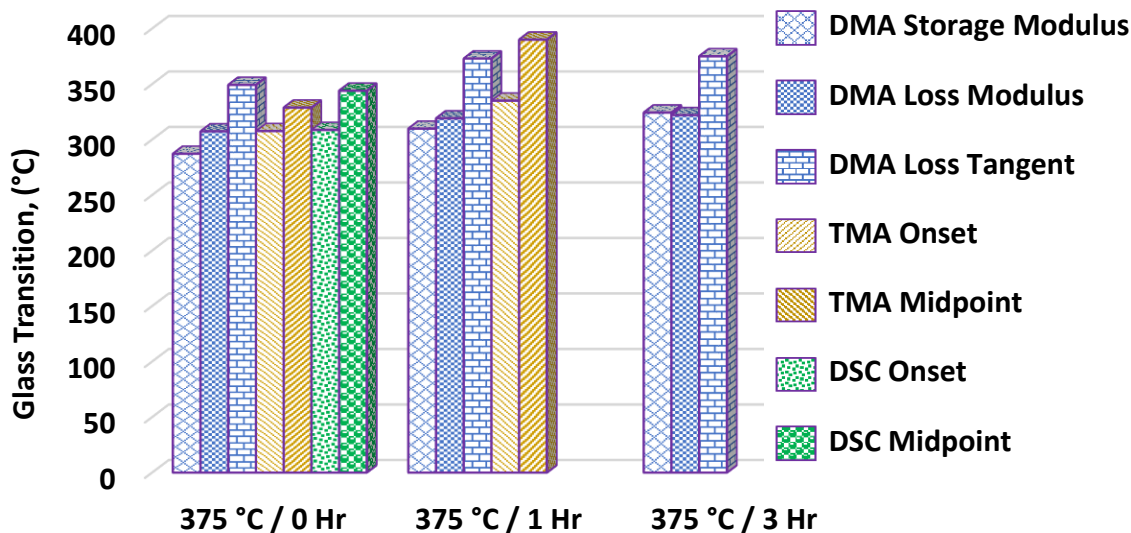


Figure 72: Glass transition of CSPN cured at 350 °C for 4 hours and 375 °C for an additional 0-3 hours. The  $T_g$  increased slightly with post-curing time at 375 °C. Transitions became more difficult to define in DSC and TMA with increasing curing time.

### 5.3.10 Thermal and Thermo-oxidative Stability of Cured Polymers

#### 5.3.10.1 TGA of CSPN-U Polymers

Thermogravimetric analysis was performed in air and nitrogen on CSPN-U polymers. Repeated trials with the same material batch and processing conditions, showed standard deviations in the range of  $\pm 5$  °C for 5 % weight loss ( $T_{5\%}$ ) and 10 % weight loss ( $T_{10\%}$ ) values and  $\pm 0.5$  weight % for the residual weight at 1000 °C. A comparison of the TGA behavior in nitrogen for CSPN-U, with 6 wt. % *p*-BAPS, cured to maximum temperatures of 300 °C and 350 °C is provided in Figure 73. The thermal stability was significantly improved after curing to 350 °C. CSPN-U cured to 300 °C for 4 hours showed a degradation peak at 466 °C. This degradation peak disappeared when cured for an additional 4 hours at 350 °C.

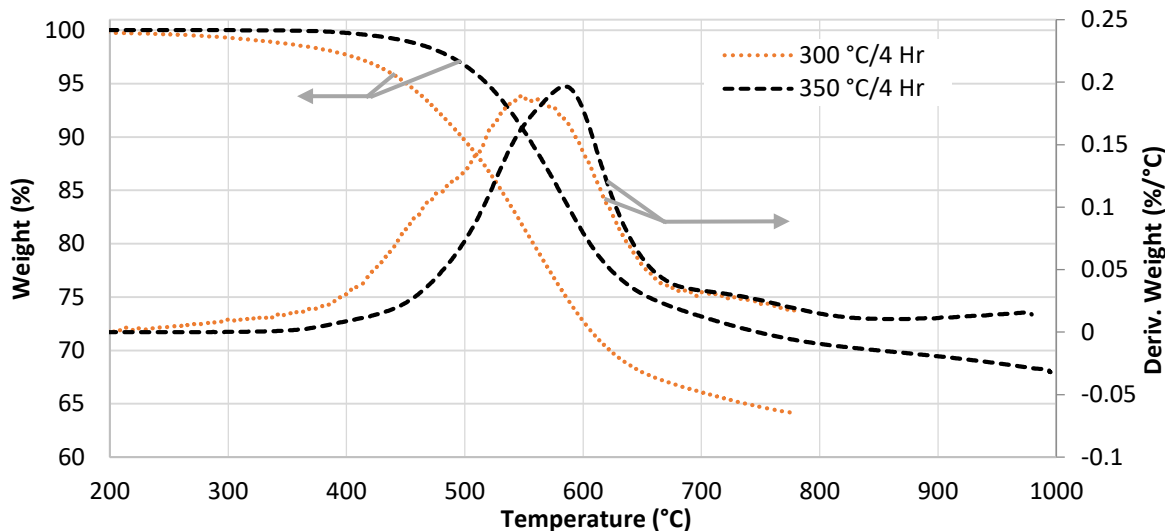


Figure 73: TGA under nitrogen of CSPN-U cured to 300 °C for 4 hours and after curing an additional 350 °C for 4 hours. The sample cured to 300 °C for 4 hours exhibited 5 % and 10 % weight losses at 451 and 498 °C respectively. After curing an additional 4 hours at 350 °C, the 5 % and 10 % weight loss values improved to 519 °C and 553 °C respectively.

Figure 74 and Figure 75 provide TGA data for powder samples in nitrogen and air with 6 wt. % *p*-BAPS. Little change was observed in thermal stability and thermo-oxidative stability after additional post-curing to 375 °C for 1-3 hours. In nitrogen, degradation peaks were evident in the derivative weight loss curves with overlapping peaks at 540-550 °C and 580-585 °C and a small peak at 710-720 °C. In air three degradation peaks were observed at 510-515 °C, 570-580 °C, and 635-650 °C. These degradations are examined in more detail in the following section on FTIR-TGA.

Figure 76 and Figure 77 compare TGA curves for CSPN-U cured to 350 °C for 4 hours with either 4 or 6 wt. % *p*-BAPS in nitrogen and air respectively. In nitrogen, CSPN-U with 4 wt. % showed slightly better initial weight retention but exhibited a lower char yield. With a decrease in *p*-BAPS content from 6 to 4 wt. %, the primary degradation peak shifted from 580 °C to 610 °C. In air, the magnitude of the second and third degradation peaks changed slightly, however the weight loss curves were nearly identical.

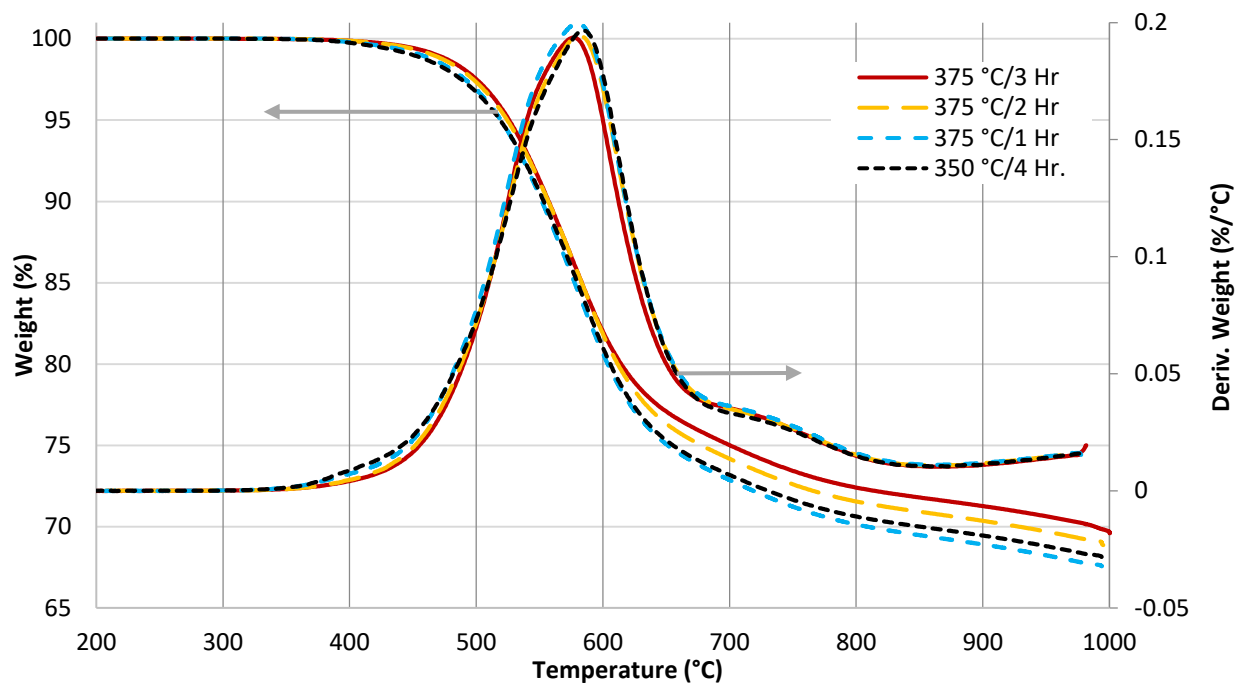


Figure 74: TGA data in  $N_2$  for CSPN-U with 6 wt. % p-BAPS, cured to 350 °C for 4 hours with additional curing at 375 °C for 1-3 hours.

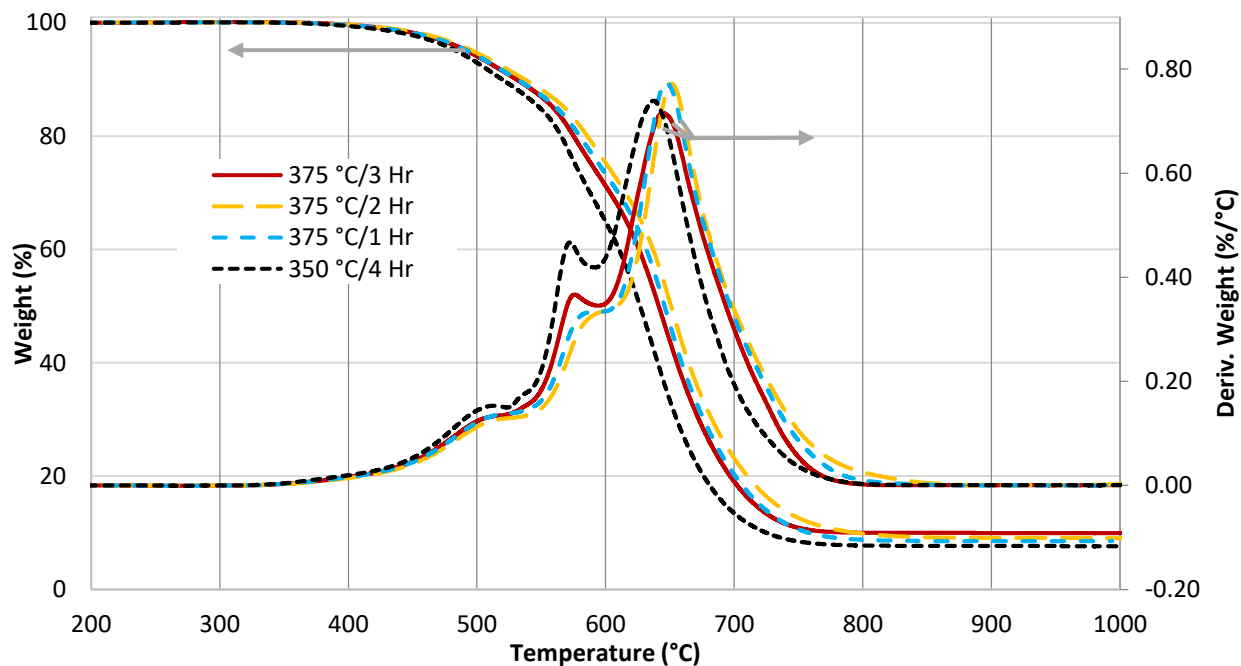


Figure 75: TGA data in air for CSPN-U with 6 wt. % p-BAPS, cured to 350 °C for 4 hours with additional curing at 375 °C 1-3 hours.

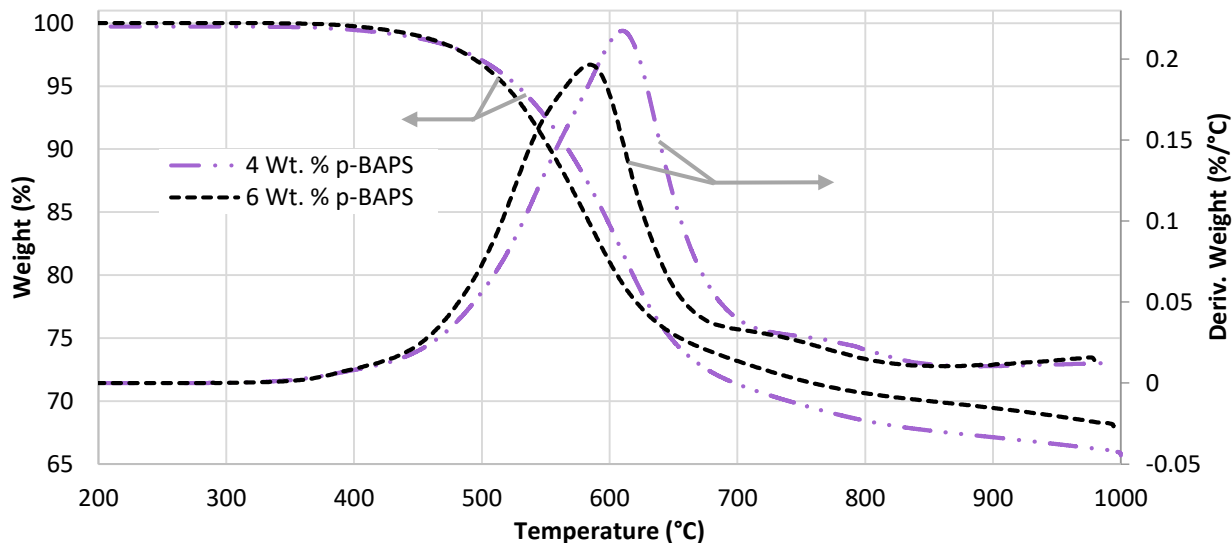


Figure 76: TGA data in nitrogen for CSPN-U cured to 350 °C for 4 hours with 4 or 6 wt. % p-BAPS.

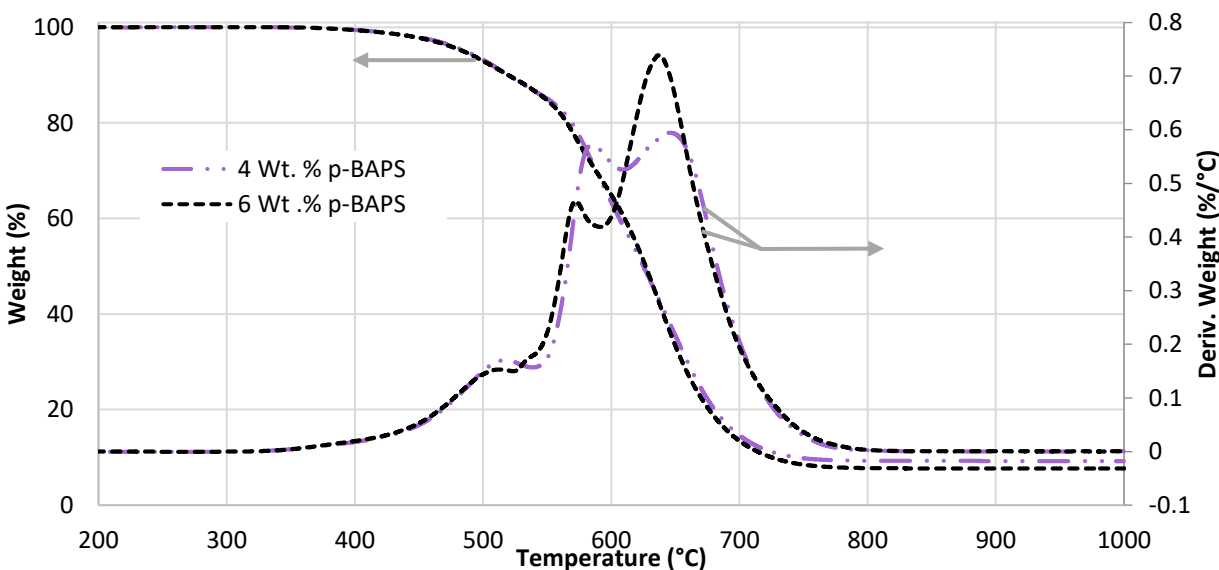


Figure 77: TGA data in air for CSPN-U cured to 350 °C for 4 hours with 4 and 6 wt. % p-BAPS.

### 5.3.10.2 TGA of COSPN-U Polymer

The TGA weight loss and derivative weight loss data for COSPN-U in nitrogen and air is given in Figure 78. Degradation peaks at 530, 590, and 710 °C were evident in the derivative weight curves in nitrogen. In air, degradation peaks in the derivative weight curves were observed at 540, 600, and 645 °C.

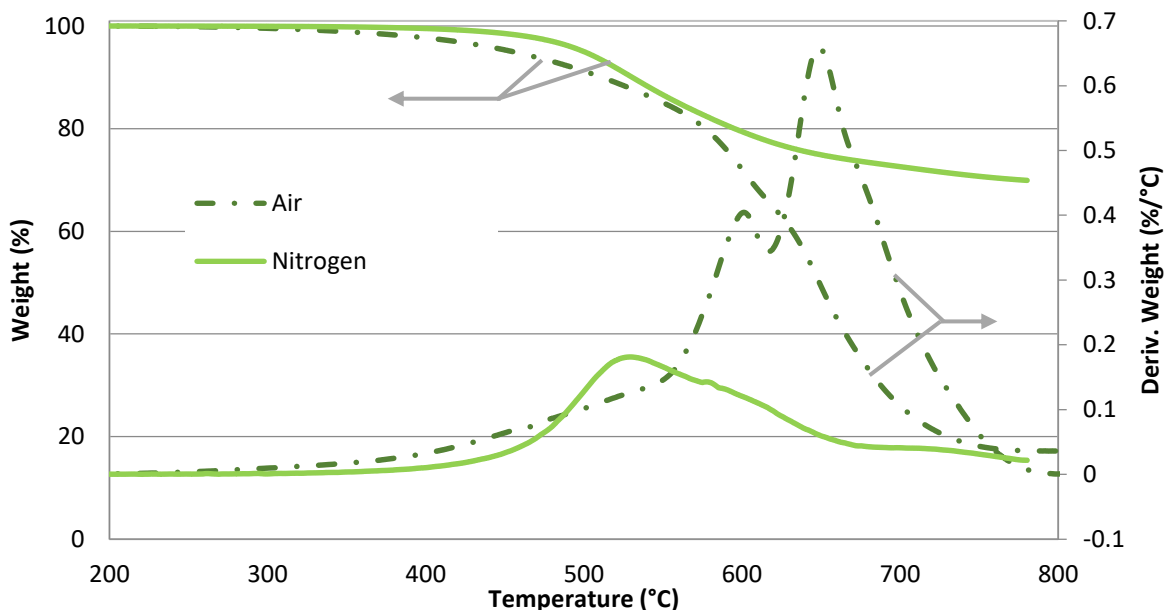


Figure 78: TGA of COSPN-U polymers cured to 375 °C for 4 hours in air and nitrogen.

### 5.3.10.3 Comparison of Thermogravimetric Data for COSPN-U and CSPN-U Polymers

Table 13 provides TGA data in air and nitrogen for cured COSPN-U and CSPN-U in air and nitrogen. The observed values for 5 % and 10 % weight losses were in the range of that observed for other phthalonitrile resins reported in literature.<sup>5, 24, 132, 234</sup> Overall CSPN polymers were more stable than COSPN. This may be due to the structure of the polymer but could also be influenced by differences in purity level, nature of impurities, hydrolytic degradation, and processing conditions. For both chemistries, degradation occurred earlier in air than in nitrogen. The CSPN-U 300 °C trial and the COSPN-U trials were only run to 800 °C, so char yields at 1000 °C are not included. The char yield in nitrogen at for 780 °C was approximately equal for COSPN and CSPN resins. In air the char yield at 780 °C was higher for COSPN-U. Char yields of CSPN monomers at 1000 °C in air were in the range of 7.65-9.05 wt. %. The char yields for organic phthalonitrile polymers in air at 1000 °C are generally close to 0 wt. %. A rough estimate of the char yield of these organosilicon monomers can be determined using

Equation 1. This assumes no volatilization of silicon-containing oligomers and that all silicon in the monomer reacts with oxygen to form SiO<sub>2</sub>. Using equation 1 and theoretical weight percent of silicon (100 % monomer purity), the predicted char yields for COSPN and CSPN materials are 9.20 and 9.67 wt. % respectively. The predicted value for CSPN is within 20% error of all

experimental values for CSPN-U polymers. The observed char yields for COSPN polymers are higher than predicted.

Table 13: TGA data in nitrogen and air for CSPN polymers cured to 350 °C for 4 hours with additional curing at 375 °C.

Polymer	Wt. % <i>p</i> -BAPS	Gas	Max Cure	T <sub>5</sub> wt.% (°C)	T <sub>10</sub> wt.% (°C)	Residual at 780 °C (Wt. %)	Residual at 1000 °C (Wt. %)
COSPN-U	4	N <sub>2</sub>	375 °C/4 Hr.	448	532	69.5	-
COSPN-U	4	Air	375 °C/4 Hr.	455	512	13.6	-
CSPN-U	4	N <sub>2</sub>	350 °C/4 Hr.	528	567	68.9	65.7
CSPN-U	6	N <sub>2</sub>	300 °C/4 Hr.	451	498	64.1	-
CSPN-U	6	N <sub>2</sub>	350 °C/4 Hr.	519	553	71.1	68.0
CSPN-U	6	N <sub>2</sub>	375 °C/1 Hr.	519	552	70.5	67.6
CSPN-U	6	N <sub>2</sub>	375 °C/2 Hr.	525	557	71.9	68.9
CSPN-U	6	N <sub>2</sub>	375 °C/3 Hr.	526	557	72.7	69.7
CSPN-U	4	Air	350 °C/4 Hr.	487	519	9.37	9.23
CSPN-U	6	Air	350 °C/4 Hr.	482	520	8.56	7.65
CSPN-U	6	Air	375 °C/1 Hr.	493	531	8.77	8.51
CSPN-U	6	Air	375 °C/2 Hr.	497	537	9.85	9.05
CSPN-U	6	Air	375 °C/3 Hr.	497	535	8.97	8.49

Equation 1: Predicted Char Yield in Air

$$\text{Wt. \% Char} = \frac{\text{Wt.\% Silicon in Monomer}}{\text{Wt.\% Silicon in SiO}_2} * 100$$

The differences in experimental and predicted values, and the difference between COSPN and CSPN experimental char yields, may be partially accounted for by the nature of impurities in the two systems. Different synthetic routes were used for the production of the two monomers. In the CSPN synthetic route the silane containing moiety was formed first and then purified prior to adding the phthalonitrile moieties. Therefore CSPN-U resins contained more organic impurities and thus a lower actual wt. % of silicon. In COSPN, the oxysilane moiety was formed last and extensive purification was not conducted. COSPN-U resins therefore contained more organosilicon impurities and thus a higher actual wt. % of silicon. This higher than theoretical char yield agrees with literature on carboxysilane-phthalonitriles.<sup>79</sup> TGA curves for COSPN-U cured to 375 °C for 4 hours and CSPN-U cured to 375 °C for 3 hours are provided in Figure 79 and Figure 80 in air and nitrogen respectively. In nitrogen COSPN-U exhibited an earlier onset of degradation and a larger degradation peak at 530 °C. In CSPN this degradation peak was shifted

to 550 °C. Both materials show a degradation peak at 580-590 °C, though the magnitude of the COSPN peak is smaller.

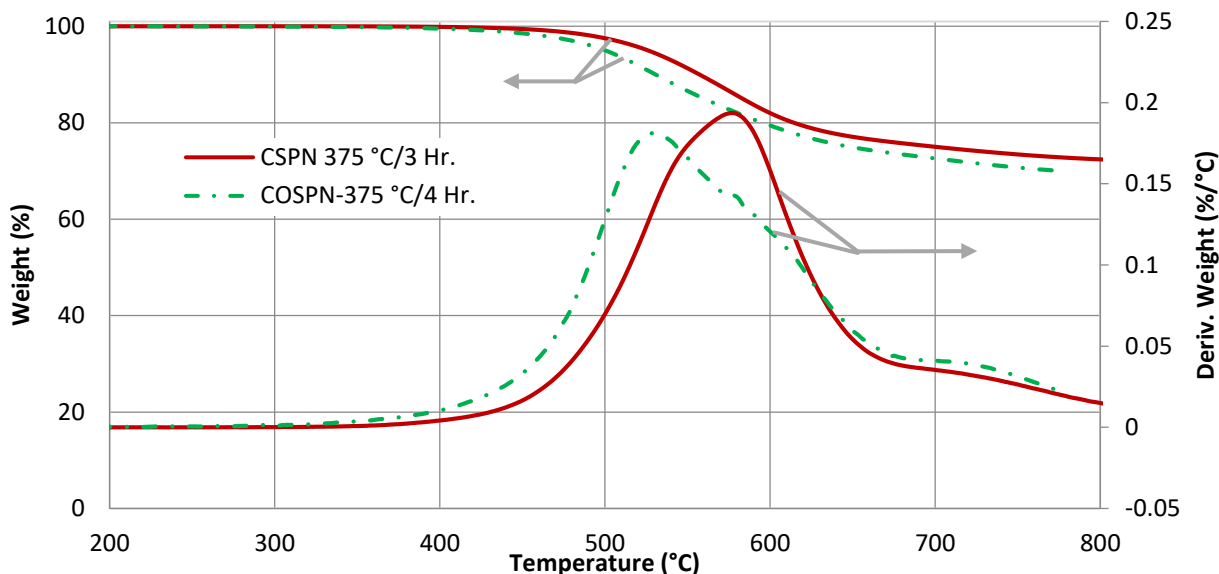


Figure 79: TGA data in nitrogen for COSPN-U cured to 375 °C for 4 hours and CSPN-U cured to 375 °C for 4 hours.

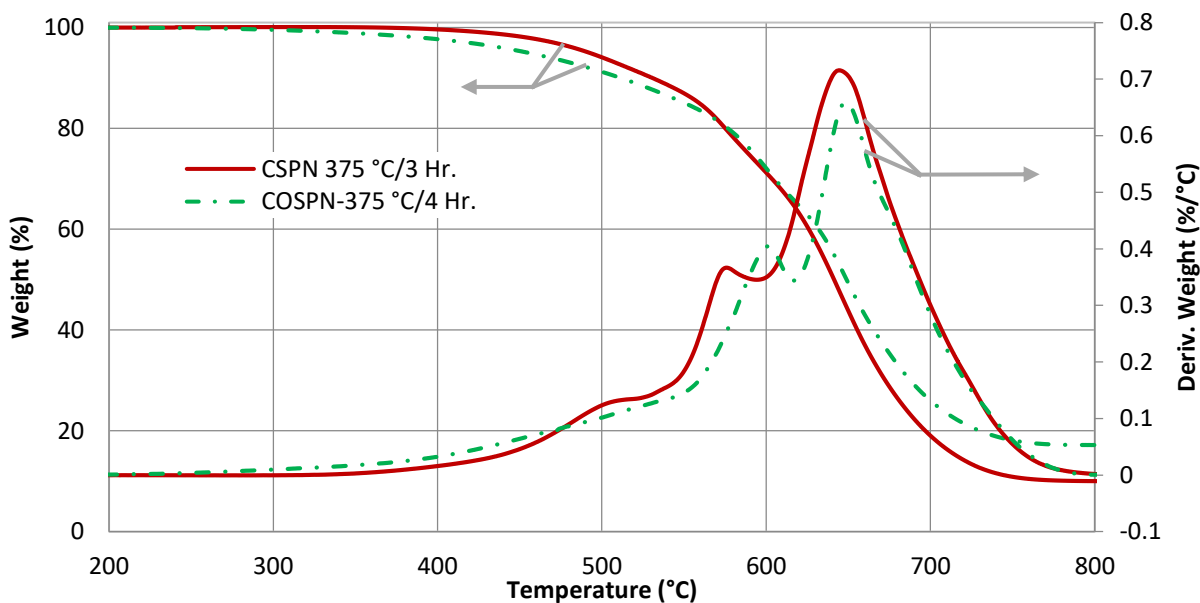


Figure 80: TGA data in air for COSPN-U cured to 375 °C for 4 hours and CSPN-U cured to 375 °C for 4 hours.

In air, COSPN again shows an earlier onset of degradation. Both materials show derivative weight loss curves of similar shape. A difference was exhibited in location of the second degradation peak. This peak was observed at 580 °C for CSPN-U and at for 600 °C COSPN. Phthalonitriles in literature have been shown to exhibit degradation peaks in similar regions at 530-

550 °C, 560-600 °C, and 720-740 °C in nitrogen and 530-540 °C and 620-660 °C in air.<sup>16, 95, 134, 234-235</sup>

### 5.3.10.4 Thermogravimetric Analysis-Fourier Transform Infrared Spectroscopy of CSPN-U Polymers

To gain a better understanding of degradation routes, FTIR was performed on gases evolved during TGA runs on CSPN-U samples. Samples were cured to a maximum temperature of 350 °C for 4 hours with 6 wt. % *p*-BAPS. Figure 81 and Figure 83 compare intensity of IR peaks with TGA curves in nitrogen and air respectively. Intensity maps and selected spectra are provided in Figure 82 and Figure 84 for nitrogen and air, respectively. The intensity of IR spectra correlated well with the derivative weight loss curves.

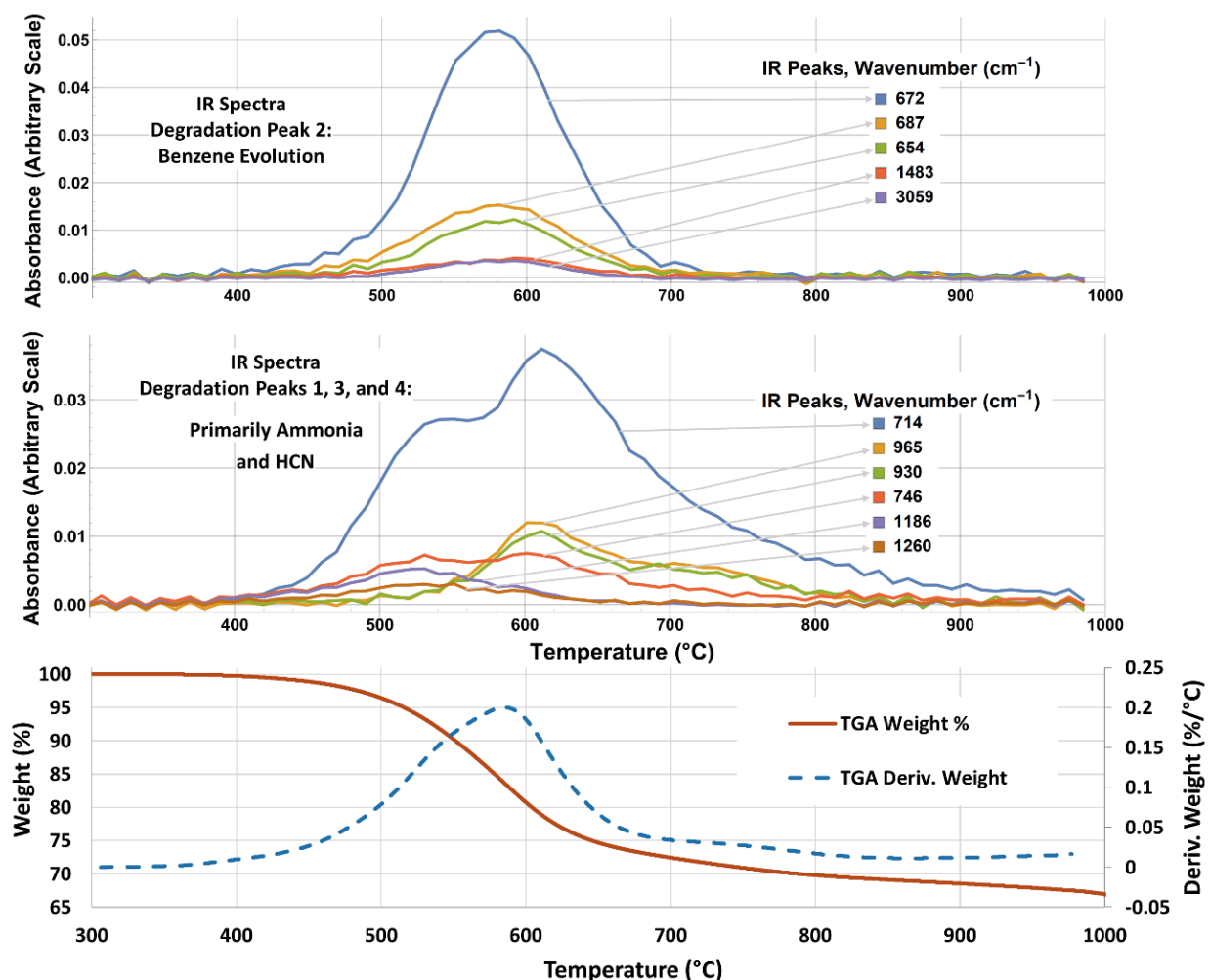


Figure 81: TGA/FTIR in nitrogen of CSPN-U cured to 350 °C for 4 hours. TGA curves (bottom) correlate with IR peaks of evolved gases (top and middle). Several degradations are evident, involving benzene evolution (top) and production of hydrogen cyanide and ammonia.

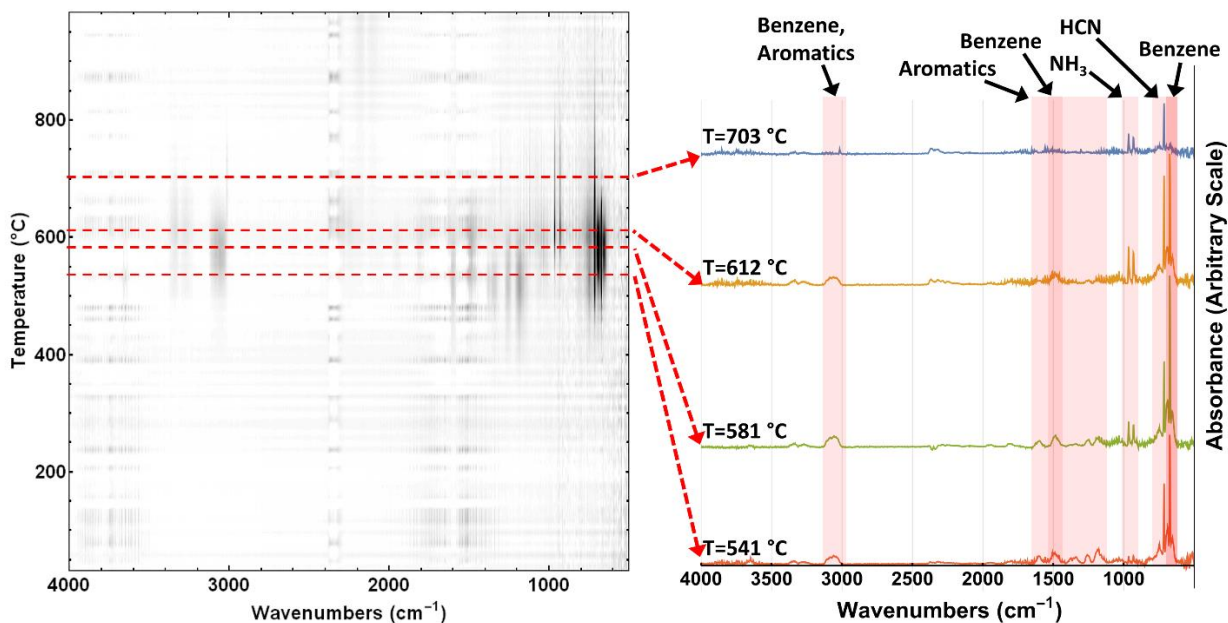


Figure 82: FTIR-TGA spectra in nitrogen (90.0 mL/min) of CSPN-U cured to 350 °C for 4 hours. An intensity map is provided on the left. On the right, selected spectra correspond to degradation peaks shown in Figure 81.

Under nitrogen atmosphere, four overlapping degradations were evident. The peak of the first degradation occurred at 540 °C, with a peak in the IR spectrum at 714  $\text{cm}^{-1}$ , corresponding to the evolution of hydrogen cyanide. Peaks were also observed at 1186, 1261, 1342, 1379, and 1601  $\text{cm}^{-1}$ . These peaks could plausibly correspond to any number of nitrogen-containing aromatic compounds, including isoindoline structures. The second degradation was observed at 580 °C, with peaks at 654, 672, 687, 1483, and 3059  $\text{cm}^{-1}$ , corresponding to the evolution of benzene. The third and fourth degradation peaks occurred at 610 and 700 °C respectively. IR peaks were observed at 714, 930, and 965  $\text{cm}^{-1}$  for both degradations, corresponding to the evolution of ammonia and hydrogen cyanide. The first, third, and fourth degradations likely result from the decomposition and volatilization of the *p*-BAPS curing additive, residual cyano groups, and isoindoline, triazine, or phthalocyanine structures. Residual cyano groups were likely present from both unreacted phthalonitrile groups and as part of triazine structures.

In air, derivative weight curves clearly showed three degradation peaks at 500-520 °C, 570-585 °C, and 635-650 °C. The gas phase spectra for all three degradations corresponded primarily to  $\text{CO}_2$  with lesser amounts of  $\text{H}_2\text{O}$ . This is unsurprising since most organic compounds were likely to combust prior to reaching the IR detector. Hydrogen cyanide was detected in small amounts at 714  $\text{cm}^{-1}$  corresponding to the degradation peaks at 500-520 °C and 570-585 °C. This agrees with

literature, which reports the evolution of hydrogen cyanide in trace amounts (<0.5 ppm) during combustion of phthalonitriles.<sup>127, 236-237</sup> These values are significantly smaller than observed for other resin systems, including cyanate esters (~3 ppm).<sup>238-239</sup> A small amount of benzene was also detected, with a peak at 500 °C. Benzene may be produced at higher temperatures as well but detection may have been limited by combustion. In both nitrogen and air, the production of benzene is expected to occur from the cleavage of Si-phenyl bonds.<sup>34, 77, 80, 153, 169, 240</sup>

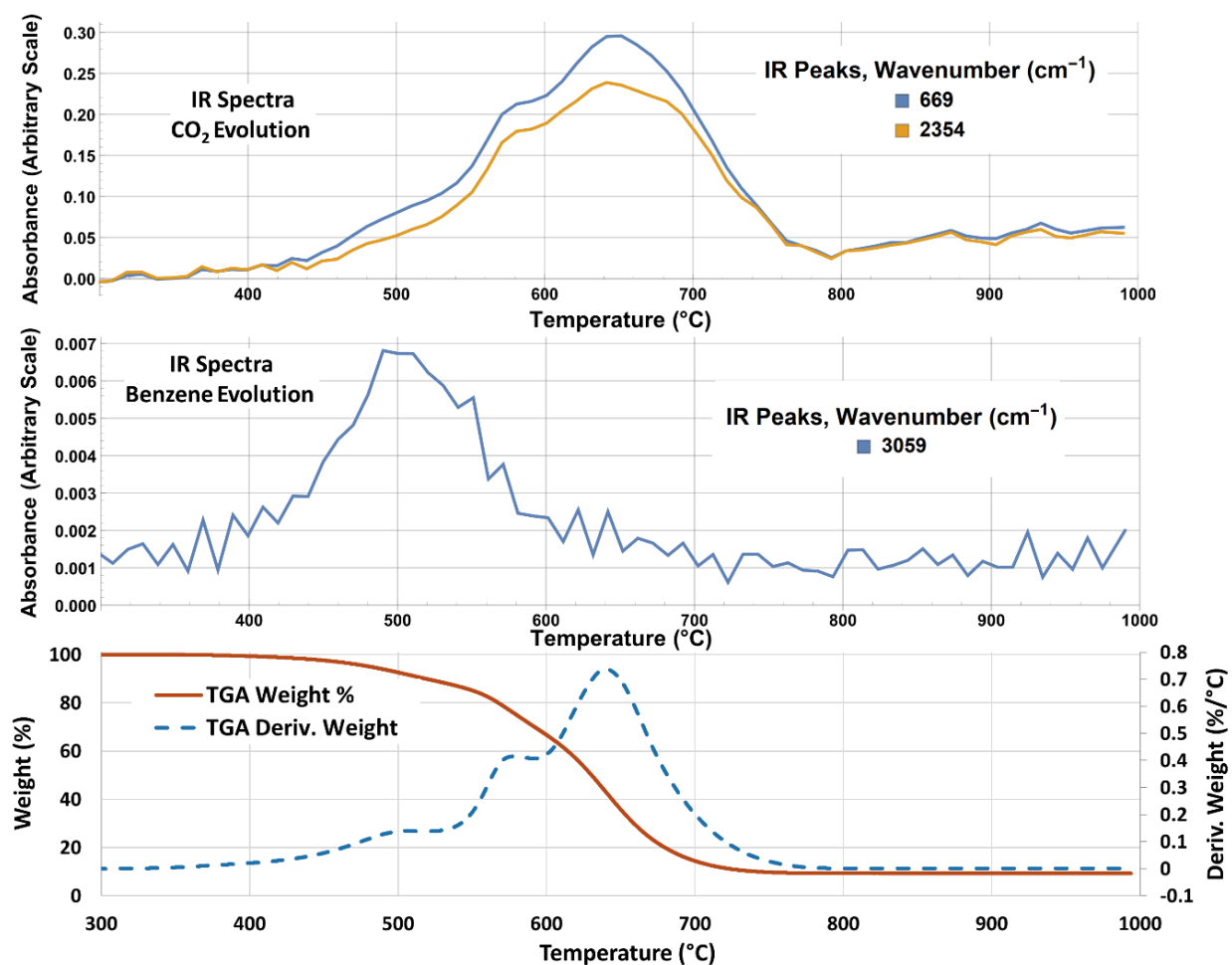


Figure 83: TGA/FTIR in air of CSPN-U cured to 350 °C for 4 hours. TGA curves (bottom) correlate with IR peaks of evolved CO<sub>2</sub> (top) and benzene (middle).

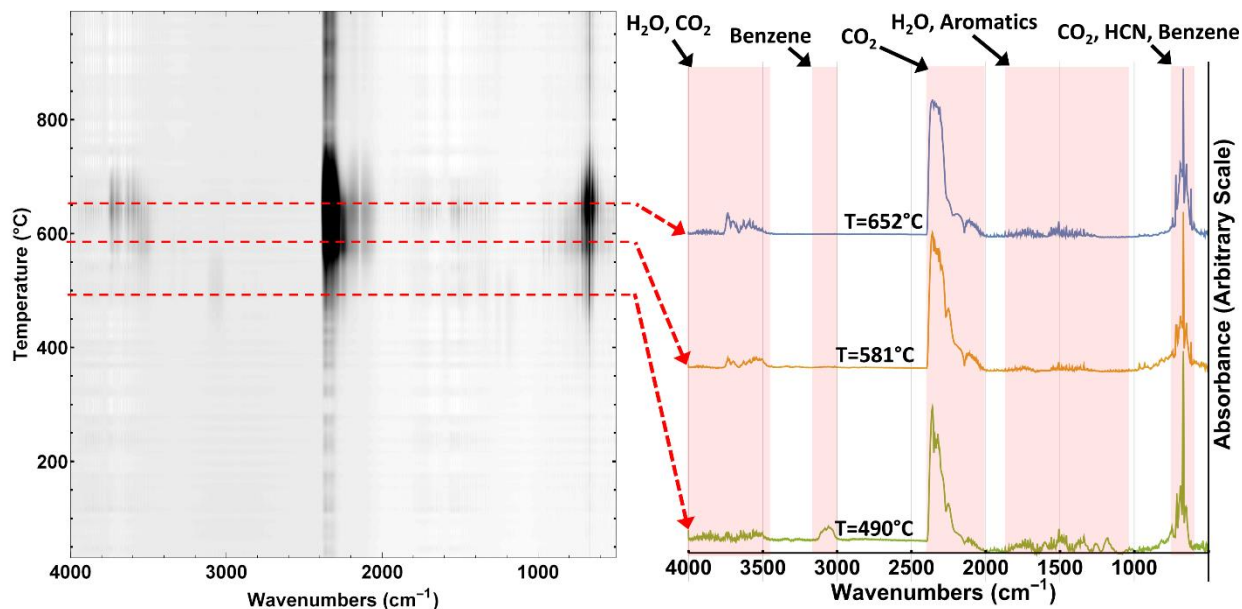


Figure 84: TGA/FTIR in air (90.0 mL/min) of CSPN-U cured to 350 °C for 4 hours. An intensity map is provided on the left. On the right, selected spectra correspond to degradation peaks shown in Figure 83.

## 5.4 Conclusions

Very low viscosities were observed which facilitate processing by non-autoclave processing techniques. Degassing prior to molding was necessary to remove moisture and small molecule impurities. Curing for both COSPN and CSPN materials occurred at temperatures above 200 °C. Curing to 350 °C was necessary to improve the thermal stability of the CSPN-U polymer. Post-curing for additional time at 375 °C was beneficial since it resulted in a decrease in CTE and increase in  $T_g$  for the CSPN-U polymers. DMA provided the most reliable method of measuring the glass transition, since glass transitions disappeared in DSC and TMA after curing at 375 °C. A high glass transition temperature is maintained, however glass transitions were lower than commonly reported for other phthalonitrile systems, presumably due to the inclusion of the organosilicon linkage.<sup>6, 19, 24, 26</sup> While the glass transition of CSPN-U may limit the use in composites to ~280 °C, the  $T_g$  is well above the 250 °C target use-temperature for wide band-gap power electronics. Higher values of CTE were observed for CSPN-U as compared with other phthalonitrile systems. This is likely due to the increased free volume around the silicon.

High values were observed for 5 % and 10 % weight loss temperatures in TGA for both polymers, on par with those observed for other phthalonitrile polymers reported in literature.<sup>5, 24, 132, 234</sup> CSPN-U exhibited higher stability in air and nitrogen than COSPN-U. This may be

explained by the differences in flexibility of the linkages, the effect of any hydrolytic degradation of CSOPN-U polymers, and differing nature of impurities. It is reported that the amine salt byproduct of the carboxysilane synthetic procedure catalyzes degradation at high temperatures if not thoroughly removed.<sup>82</sup> The inclusion of phenyl functional groups avoided lower-temperature degradations commonly observed with methyl and hydro silane moieties and high thermal stability was observed in TGA. However, at higher temperatures and prolonged exposure times, the cleavage of Si-phenyl bonds occurred to release benzene. The presence of HCN in the degradations at 500-540 °C may be due to the *p*-BAPS curing additive but could also imply that decomposition of nitrile derivatives occurred, most likely involving residual cyano groups or isoindoline structures. The use of 4 wt. % *p*-BAPS resulted in slightly higher thermal stability, as compared with 6 wt. %. Since the curing additive most likely does not become incorporated into triazine or phthalocyanine structures, the additive does volatilize and contribute to weight loss at high temperatures. Thus, while a sufficient amount of curing additive is required for curing, an excess of catalyst likely decreases the overall stability.

## 6 Processing and Characterization of Purified CSPN and CSOPN Materials

### 6.1 Introduction

Since it is commonly reported that impurities catalyze the degradation of silicon-containing polymers,<sup>77-78, 82, 180</sup> this chapter covers the processing and characterization of purified carbosilane (CSPN) and carbosiloxane (CSOPN) materials. It was theorized that the inclusion of a short siloxane linkage may provide a lower melting point, and thus larger processing window, while simultaneously maintaining good thermo-oxidative stability.<sup>241</sup> Synthesis of these monomers was covered in Chapter 4. Synthetic Procedures for Silicon-Containing Phthalonitrile Monomers. Characterization of the as-synthesized CSPN material was covered in Chapter 5. Processing and Characterization of As-Synthesized Carboxysilane and Carbosilane Phthalonitriles. It was originally assumed that purity would increase stability, and the as-synthesized carbosiloxane (CSOPN-U) materials were not characterized. The structures of CSPN and CSOPN monomers are reproduced below for convenience in Figure 85 and Figure 86. The carboxysilane (COSPNU) polymer, characterized in the previous chapter, is also occasionally discussed in relation to the materials presented here.

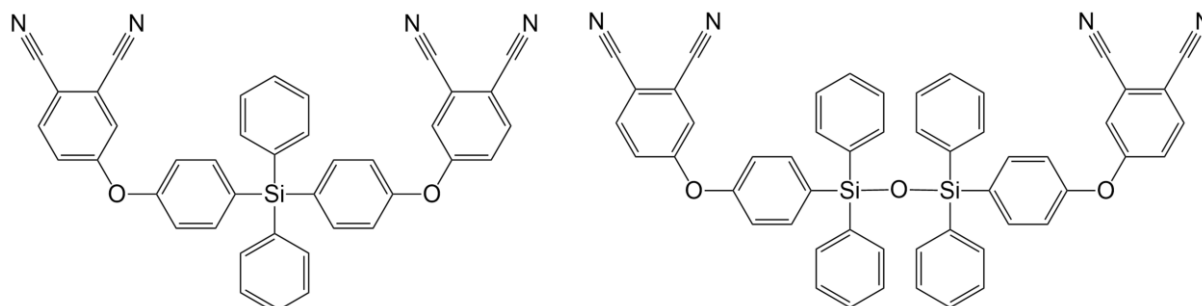


Figure 85: Carbosilane (CSPN) monomer. Figure 86: Carbosiloxane (CSOPN) monomer.

CSPN-P and CSOPN-P monomer/catalyst mixtures were prepared and cured. Monomers and b-staged pre-polymers were characterized using DSC, parallel plate rheology, TGA, and FTIR. The glass transition of cured polymer samples was evaluated by DSC, TMA, and DMA. The CTE was measured using TMA. Short-term thermal and thermo-oxidative stability was evaluated using TGA. The properties of purified CSPN-P and CSOPN-P materials are compared with those observed for as-synthesized CSPN-U and COSPN-U materials as well as several commercial phthalonitriles. FTIR of evolved gases from TGA was used to provide insight into degradation reactions of CSOPN monomers.

## 6.2 Experimental

### 6.2.1 Materials and Methods

Bis(4-(4-aminophenoxy)phenyl)sulfone (*p*-BAPS, >98%) was purchased from TCI America. Parallel plate rheology and torsional dynamic mechanical analysis (DMA) were performed on a TA Instruments Ares G2 with a ramp rate of 5 °C/min. A TA Instruments Q400 was used for thermomechanical analysis (TMA) with a ramp rate of 5 °C/min. Thermogravimetric analysis (TGA) of powder samples in air and nitrogen was performed using a TA Instruments Q500, with a ramp rate of 10 °C/min and a flow rate of 90 mL/min. Differential scanning calorimetry (DSC) was conducted using a TA Instruments Q1000 or Q20 with a ramp rate of 5 °C/min. Fourier transform infrared (FTIR) spectroscopy was conducted using a Thermo Scientific Nicolet 6700 with Spectra Tech Inc. attenuated total reflection (ATR) and Thermo Electron Corp. TGA/FT-IR accessories. A model 10444 (30 ton) Wabash hydraulic press was used to compression mold resin plaques. Panels were c-scanned at AFRL/RXAS, Wright Patterson Air Force Base.

### 6.2.2 Preparation of Monomer-Catalyst Mixtures and Pre-Polymer B-staged Resins

The processing of purified CSPN-P and CSOPN-P resins was dependent on melting point and catalyst concentration. General heating profiles for CSPN-P and CSOPN-P resins are given in Figure 87 and Figure 88. For CSPN-P, The 6 wt. % *p*-BAPS sample was dry-mixed and melted at 220-230 °C. For CSPN-P with 3.5-4 wt. % *p*-BAPS, the monomer and catalyst were co-dissolved in 1:1 DCM/chloroform mixture and then the solvent was removed by rotary evaporation. The mixture was dried under vacuum at room temperature for 4 hours, transferred to a Teflon™-lined aluminum weighing boat, and heated under vacuum from 130 to 220 °C. The resin was degassed under vacuum at 220-230 °C for 30 minutes and 240-250 °C for 25 minutes. The resin was then b-staged under nitrogen atmosphere at 250-260 °C until viscosity increased. The b-staged material was then removed and allowed to cool to room temperature in a desiccator.

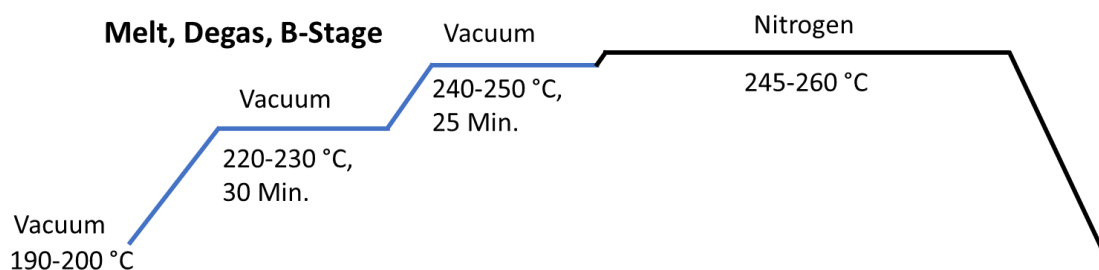


Figure 87: General melting, degassing, and b-staging profile for CSPN-P resin.

For CSOPN-P samples, the monomer samples were added to a Teflon<sup>TM</sup>-lined aluminum weighing boat and melted at 200 °C under nitrogen. The catalyst, *p*-BAPS (2.7 or 4 wt. %) was added. The mixture was stirred for two minutes. Vacuum was applied, and the resin was degassed for 30 minutes. After mixing the monomers and catalyst, the temperature was increased to 220-230 °C for 30 minutes and 240-250 °C for 25 minutes under vacuum. The resin was then b-staged under nitrogen atmosphere at 250-260 °C for until viscosity increased. The b-staged material was then removed and allowed to cool to room temperature in a desiccator.

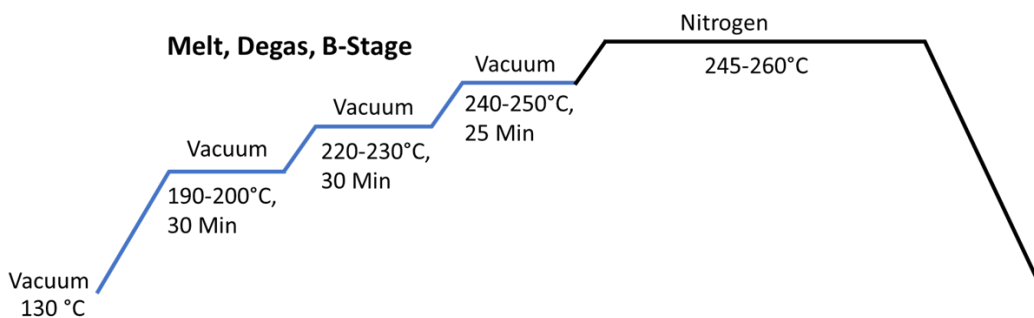


Figure 88: General melting, degassing, and b-staging profile for CSOPN-P resin.

### 6.2.3 Fabrication of Cured Samples

The same hot-pressing profile was used for both CSPN-P and CSOPN-P materials, given in Figure 89. The resins were cooled to room temperature and placed in a 2” by 2” steel mold. The mold was placed in a hydraulic press at 275 °C. Pressure was applied and the press was heated at 300 °C for four hours (130-170 psi) and 350 °C for four hours (290 psi). The polymer panel was then allowed to cool to room temperature. To determine porosity content and distribution, the panel then was c-scanned. A wet saw was used to cut the plaque into samples for DMA, TMA, and TOS. Additional curing of some CSOPN-P polymer samples was accomplished in an oven under nitrogen at 375 °C for 1-3 hours. Prior to characterization, samples were dried under vacuum at 100 °C for three days and stored in a desiccator.

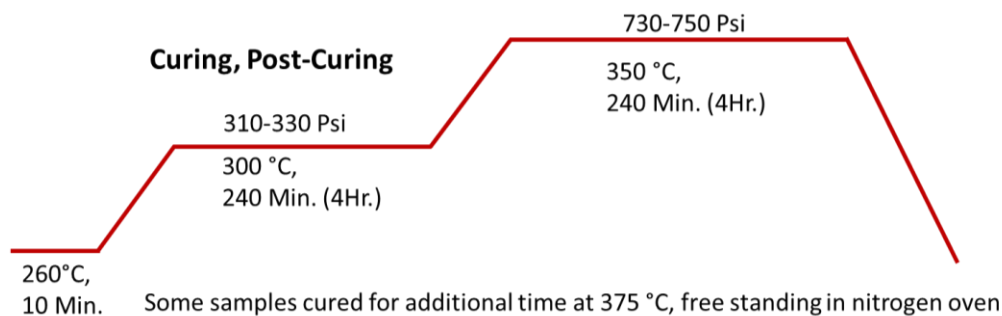


Figure 89: Curing and post-curing profile used for CSPN-P and CSOPN-P resins.

## 6.3 Results and Discussion

### 6.3.1 Preparation of Monomer-Catalyst Mixtures and Pre-Polymer B-staged Resins

Table 14 provides the time until visible viscosity increase was observed vs. *p*-BAPS content. The high melting temperature of the purified CSPN resin required higher initial processing temperatures, as compared to CSPN-U or CSOPN-P. This complicated the processing of the CSPN-P resins since the melting temperature of 223 °C overlapped with curing. When the CSPN-P monomer was dry-mixed with 6 wt. % *p*-BAPS, the mixture cured as it was melting. Subsequently, CSPN-P mixtures with 3.5 and 4 wt. % *p*-BAPS were first co-dissolved in DCM/chloroform to ensure complete mixing. The two-solvent system was intended to spread out the release of volatiles during heating, due to the difference in the boiling points of the two solvents. Approximately 3.5-4 wt. % (5.0-5.6 mol%) *p*-BAPS was required to achieve visible increase in viscosity within a reasonable amount of time. At a lower concentration of 2.1 wt.%, (3.0 mol%) *p*-BAPS, the melt did not substantially increase in viscosity even after heating for more than 12 hours at 250-260 °C. Comparing the CSPN-P and CSPN-U resins with 4.0 wt.% *p*-BAPS, gelation occurred in approximately the same timeframe.

Table 14: Working time at 250-260 °C for CSPN and CSOPN resins.

Sample	<i>p</i> -BAPS Content	Time Until Visible Gelation at 250-260 °C
CSPN-U	6.0 wt.% (8.4 mol%)	~1 hour
CSPN-U	4.0 wt.% (5.6 mol%)	~1 hour
CSPN-P	2.1 wt.% (3.0 mol%)	Did not gel at >12 Hours
CSPN-P	3.5 wt.% (5.0 mol%)	~4 hours at to gel
CSPN-P	4.0 wt.% (5.6 mol%)	~40 min
CSPN-P	6.0 wt.% (8.4 mol%)	Cured immediately (did not fully melt)
CSOPN-P	1.6 wt.% (3.0 mol%)	Did not gel at >12 Hours
CSOPN-P	2.7 wt.% (5.0 mol%)	~13 hours to gel
CSOPN-P	4.0 wt.% (7.3 mol%)	~1.5 hours to gel

The CSOPN-P/*p*-BAPS mixtures softened at around 180 °C, approximately 40 °C lower than the CSPN-P/*p*-BAPS mixtures. This allowed for a lower initial processing temperature. The larger processing window also facilitated more complete mixing and easier control of viscosity. The

CSOPN-P mixtures followed a similar trend with *p*-BAPS content as did CSPN-P. At 4.0 wt.% *p*-BAPS it took approximately 90 minutes for viscosity to increase to a rubbery state. Conversely the sample with 2.7 wt.% *p*-BAPS took around 13 hours to for the viscosity to increase substantially. The sample with 1.6 wt.% *p*-BAPS did not gel within a reasonable timeframe.

### 6.3.2 DSC of Monomers with 4 wt. % *p*-BAPS

Figure 90 provides DSC data in nitrogen for the CSOPN-P monomer, monomer with 4 wt.% *p*-BAPS (dry mixed), and monomer/*p*-BAPS mixture after b-staging to 220 °C. With the addition of the catalyst, the melting temperature decreased from 191 °C to 181 °C. An exothermic peak corresponding to the curing reaction was observed in the CSOPN-P/*p*-BAPS mixture at 285-327 °C, with overlapping peaks at 290 and 310 °C. After melting and degassing to 220 °C no melting peak is evident, and the curing peak shifted to 310-340 °C with overlapping peaks at 313 and 323 °C. A possible glass transition of the melted mixture is observed around 60 °C.

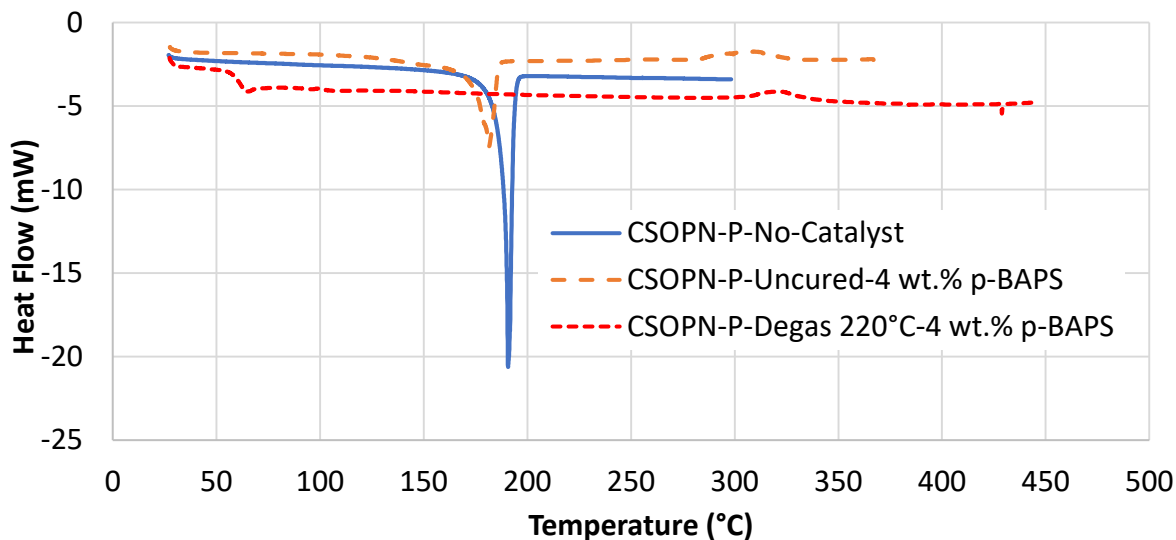


Figure 90: DSC of CSOPN-P resins with no catalyst, dry-mixed with 4 wt. % *p*-BAPS, and after melting and degassing to 220 °C with 4 wt. % *p*-BAPS. The addition of *p*-BAPS decreased the melting temperature by 10 °C. A curing peak was observed in the CSOPN-P/*p*-BAPS mixture at 285-327 °C, which shifted to 310-340 °C after heating to 220 °C.

Figure 91 provides DSC data for CSPN-P resins with no catalyst and dry-mixed with 4 wt. % *p*-BAPS. The melting point of the CSPN-P/*p*-BAPS mixture was observed at 220 °C, very close to the melting point of CSPN-P without *p*-BAPS (223 °C).

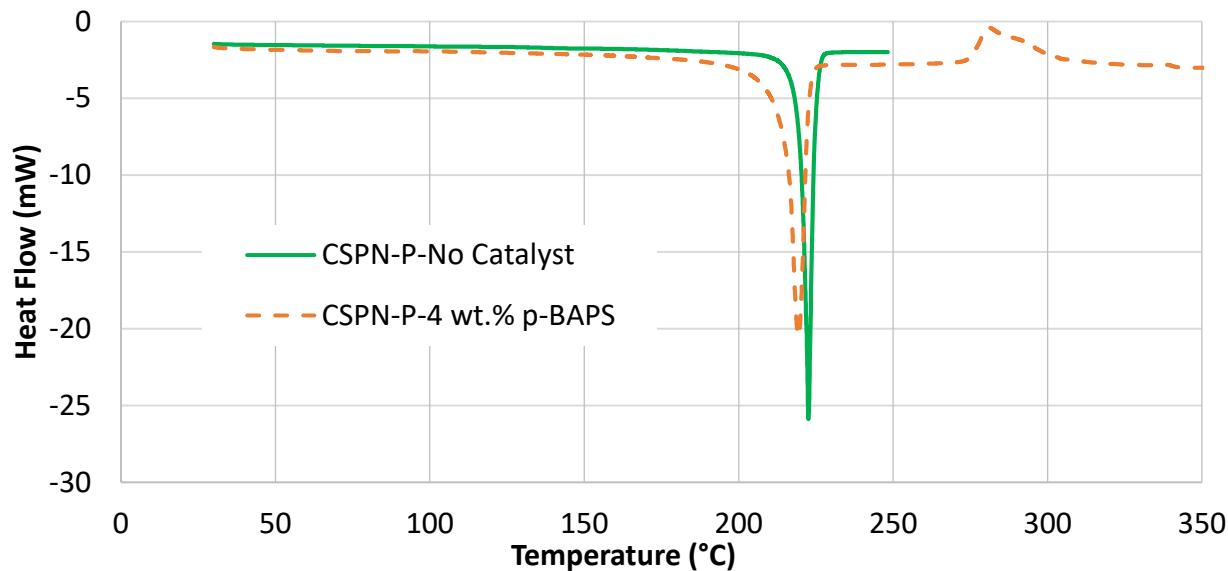


Figure 91: DSC of CSPN-P resins with no catalyst and dry-mixed with 4 wt. % p-BAPS. The endothermic melting transitions of CSPN-P and CSPN-P/p-BAPS were observed at 223 °C and 220 °C, respectively.

A comparison of as-synthesized and purified CSPN resins with 4 wt. % p-BAPS is given in Figure 92. The CSPN-P/p-BAPS mixture displayed an exothermic curing reaction at 275-300 °C with overlapping peaks at 281 and 293 °C. In contrast, in the CSPN-U/p-BAPS mixture the curing reaction occurred at lower temperatures, 255-278 °C, with overlapping peaks at 260 and 266 °C.

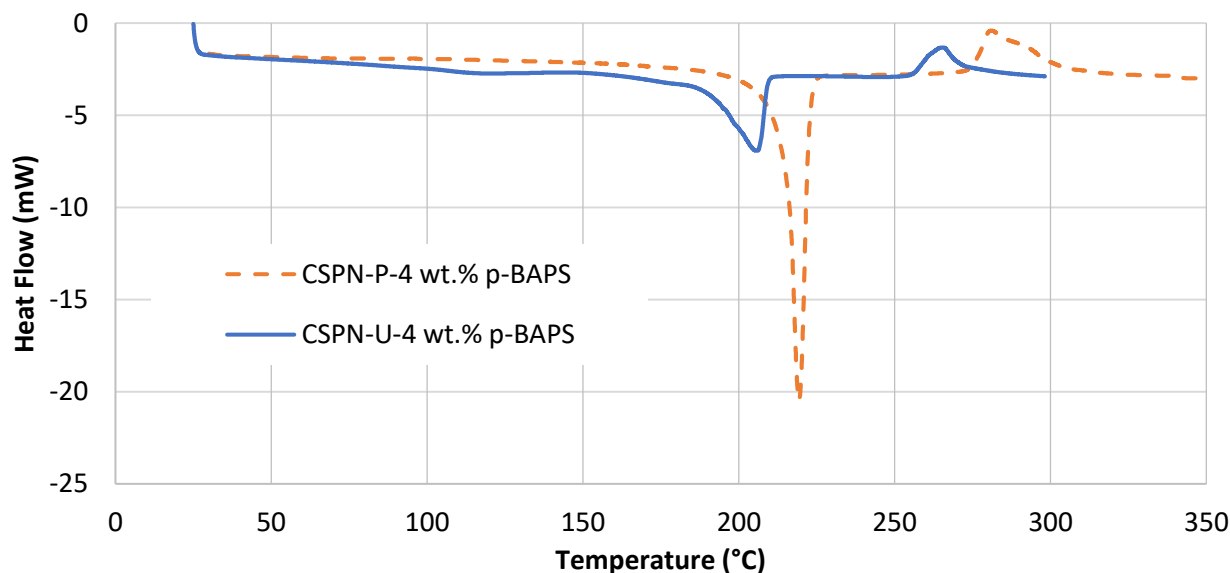


Figure 92: DSC of purified and unpurified CSPN resins, dry-mixed with 4 wt. % p-BAPS. The CSPN-P/p-BAPS and CSPN-U/p-BAPS mixtures displayed exothermic curing reactions at 275-300 °C and 255-278 °C, respectively.

### 6.3.3 Rheology of Monomers

Table 15 summarizes the viscosity data for CSPN and CSOPN samples with 4 wt.% *p*-BAPS. Figure 93 provides data on the change in complex viscosity vs. time of CSPN-P after degassing to 230 °C and b-staging at 235 °C for approximately 40 minutes. The sample was heated at a rate of 5 °C/min and held at 250 °C. Softening for CSPN-P began to occur at 190 °C, in contrast with CSPN-U which softened beginning at 130 °C. The minimum viscosity dropped sharply to 0.2 Pa·s beginning around 220 °C. Viscosity ( $\eta$ , Pa·s) increased in a roughly exponential manner with time ( $t$ , min.) at 250 °C, which could be empirically fit to the equation  $\eta = 10^{-4} \cdot e^{0.1492 \cdot t}$ . Working time at viscosities lower than 1 Pa·s was 18 minutes at 250 °C. At viscosities lower than 10 Pa·s, working time was approximately 33 minutes at 250 °C.

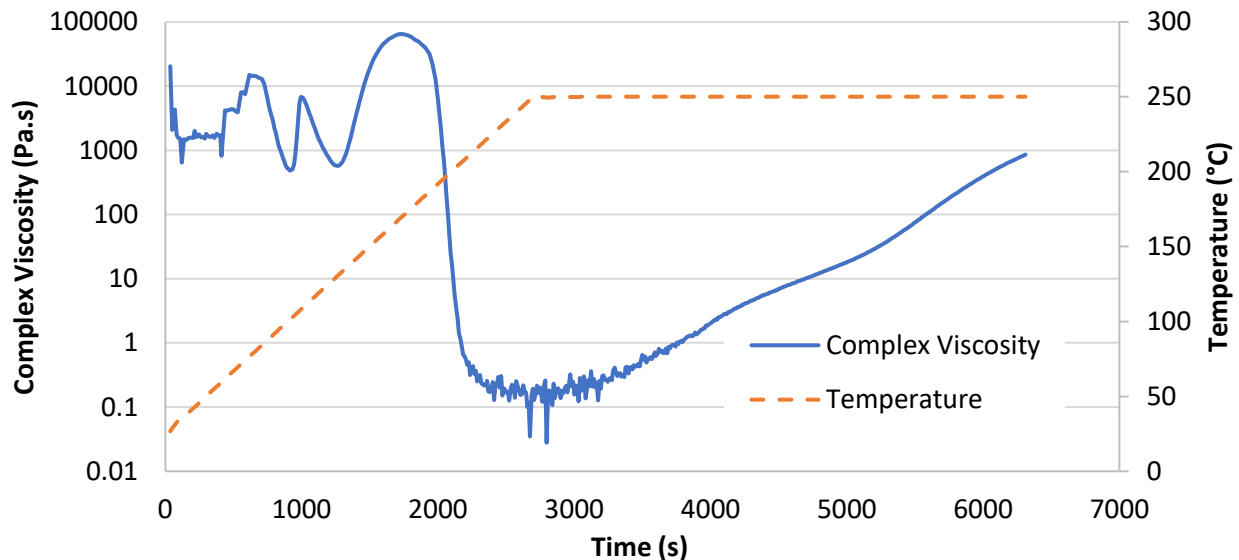


Figure 93: Parallel plate rheology of CSPN-P with 4 wt. % *p*-BAPS, after b-staging at 235 °C for 30 minutes. The material was heated at a rate of 5 °C/min and held at 250 °C.

Figure 94 gives information on the change in complex viscosity over time at 250 °C for CSOPN-P. CSOPN-P samples began to soften at 100 °C and showed a gradual decrease in viscosity. The viscosity was observed as low as 0.09-0.1 Pa·s beginning at 170 °C. Considering resin transfer molding (RTM), which requires  $< 10$  Pa·s,<sup>58</sup> this would result in a processing window beginning at approximately 120 °C. In contrast to the CSPN-P resin, the viscosity increase was not linear on a semi-log scale for CSOPN-P. Working time at 250 °C was 15 minutes and 20 minutes at viscosities of  $< 1$  Pa·s and  $< 10$  Pa·s, respectively.

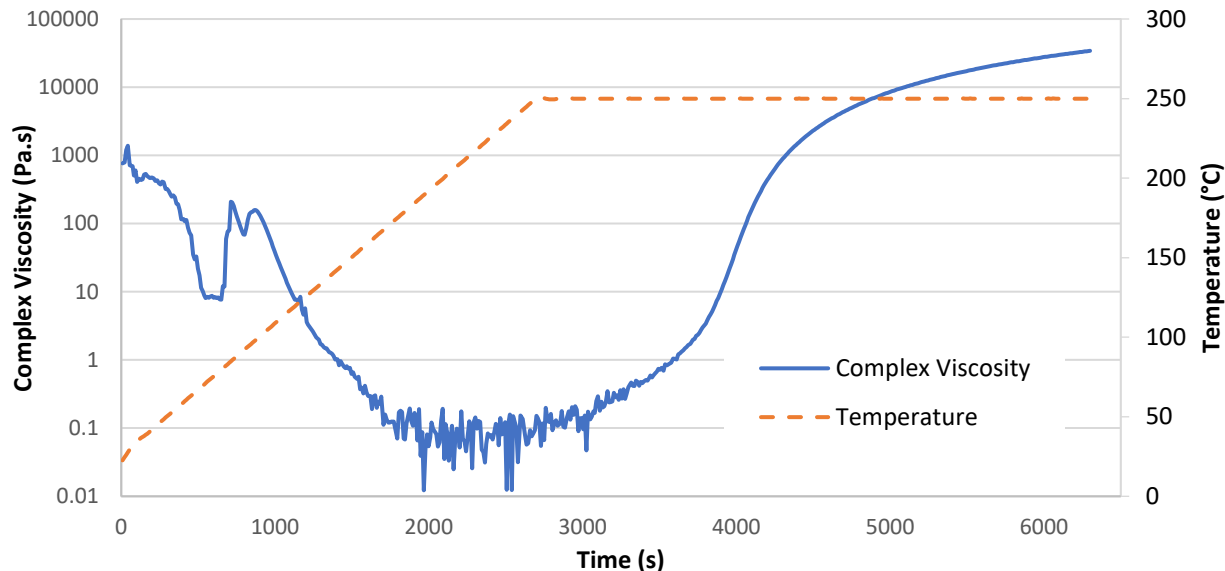


Figure 94: Parallel plate rheology of CSOPN with 4 wt.% p-BAPS, after b-staging at 230 °C for 30 min. The material was heated at a rate of 5 °C/min and held at 250 °C.

Table 15: The minimum viscosity and corresponding temperature range from rheometric data for CSPN and CSOPN resins.

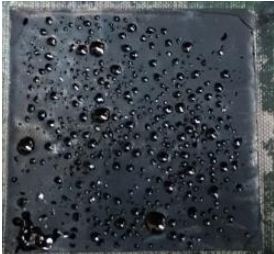
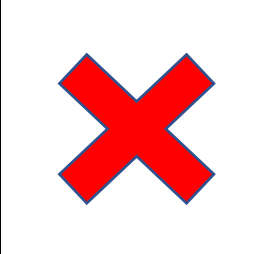
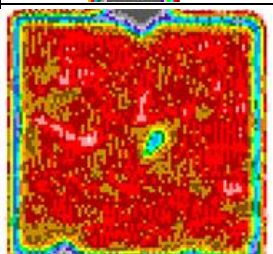
Sample, 4 wt. % p-BAPS	Prior Conditioning	Min Complex Viscosity (Pa·s)	Temperature Range (°C)
CSPN-I	Degas to 210 °C	0.3-0.4	256-288
CSPN-I	Degas to 210 °C, 220 °C-1 Hr.	10.0-11.0	207-222
CSPN-P	Degas to 230 °C, 235 °C-30 Min.	0.2	220-250*
CSPN-P	Degas to 230 °C, 250 °C-30 Min.	175	250*
CSOPN-P	Degas to 210 C, 220 °C-30 Min.	0.1-0.5	180-250
CSOPN-P	Degas to 210 °C, 250 °C-1 Hr.	0.4-0.5	220-260
CSOPN-P	Degas to 210 °C, 230 °C-30 Min.	0.6-0.7	185-250*
CSOPN-P	Degas to 210 °C, 235 °C-25 Min.	0.09-0.1	170-250*

\*Ramped and held at 250 °C

### 6.3.4 Panel Fabrication

Table 16 and Table 17 provide the results of panel fabrication experiments as a function of *p*-BAPS content for CSPN-P and CSOPN-P panels. The qualitative hardness and strength of the materials was observed during de-molding panels, cutting samples for TMA, DMA, and TOS, and grinding powder samples for TGA and DSC characterizations. For CSPN-P, it was determined that 3.5-4 wt.% of *p*-BAPS was required to achieve desirable processing of the material. At a *p*-BAPS concentration of 3.5 wt.%, the material took substantially longer (4 hours) to gel at 250-260 °C as compared to the resin with 4 wt.% (40 minutes). As mentioned previously, when dry-mixed with 6 wt. % *p*-BAPS, the material began curing while it was melting. A panel produced from this batch was highly porous, qualitatively weak, and cracked at the edges.

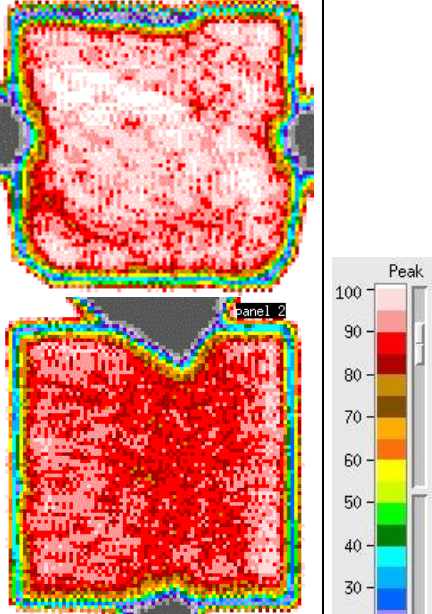
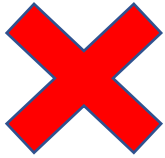
Table 16: Fabrication of CSPN-P panels.

<i>p</i> -BAPS	Panel Result	Images (Front and Back)		C-Scan
<b>6.0 wt.%, 8.4 mol%</b>	Bad finish, porosity, soft/weak			
<b>3.5 wt.%, 5.0 mol%</b>	Mediocre finish, good hardness/strength, low porosity			
<b>4.0 wt.%, 5.7 mol%</b>	Good finish, hard/strong, low porosity			

CSOPN-P provided similar processing results. Samples with 4 wt.% *p*-BAPS exhibited good panels with high qualitative strength and hardness, glossy finish, and low porosity. The sample with 2.7 wt.% (5.0 mol%) produced a panel that was cracked, and qualitatively weak and soft, with a

hazy finish. For both CSPN-P and CSOPN-P the lower quality of panels at lower *p*-BAPS concentration was likely due to a lower overall degree of cure and degradation of the monomer from longer exposure to curing temperatures in the un-crosslinked state.

Table 17: Fabrication of CSOPN-P panels.

<i>p</i> -BAPS	Panel Result	Images	C-Scan
4.0 wt.%, 7.3 mol%	Good finish, hard/strong, low porosity		
2.7 wt.%, 5.0 mol%	Bad finish, cracks, soft/weak		

### 6.3.5 FTIR of cured CSOPN polymers

The IR spectra of the CSOPN-P monomer and cured polymers with is provided in Figure 95. After hot pressing with 4 wt.% *p*-BAPS to 350 °C for 4 hours, the formation of triazine peaks are observed at 1356-1360 cm<sup>-1</sup> and 1520-1532 cm<sup>-1</sup>.<sup>5, 15, 95</sup> Peaks for isoindoline or phthalocyanine structures at 1580-1590 cm<sup>-1</sup> and 1015-1016 cm<sup>-1</sup> were possible but overlapped with peaks present in the monomer. It is likely that some phthalocyanine structured formed due to the appearance of

the green-black color. To evaluate the effect of additional post-curing, samples were cured to 350 °C for 4 hours and then at 375 °C for an additional 0-3 hours under nitrogen atmosphere. The observed spectra for all samples were identical. Thus, it can be assumed that no substantial degradation occurred during post-curing up to 375 °C.

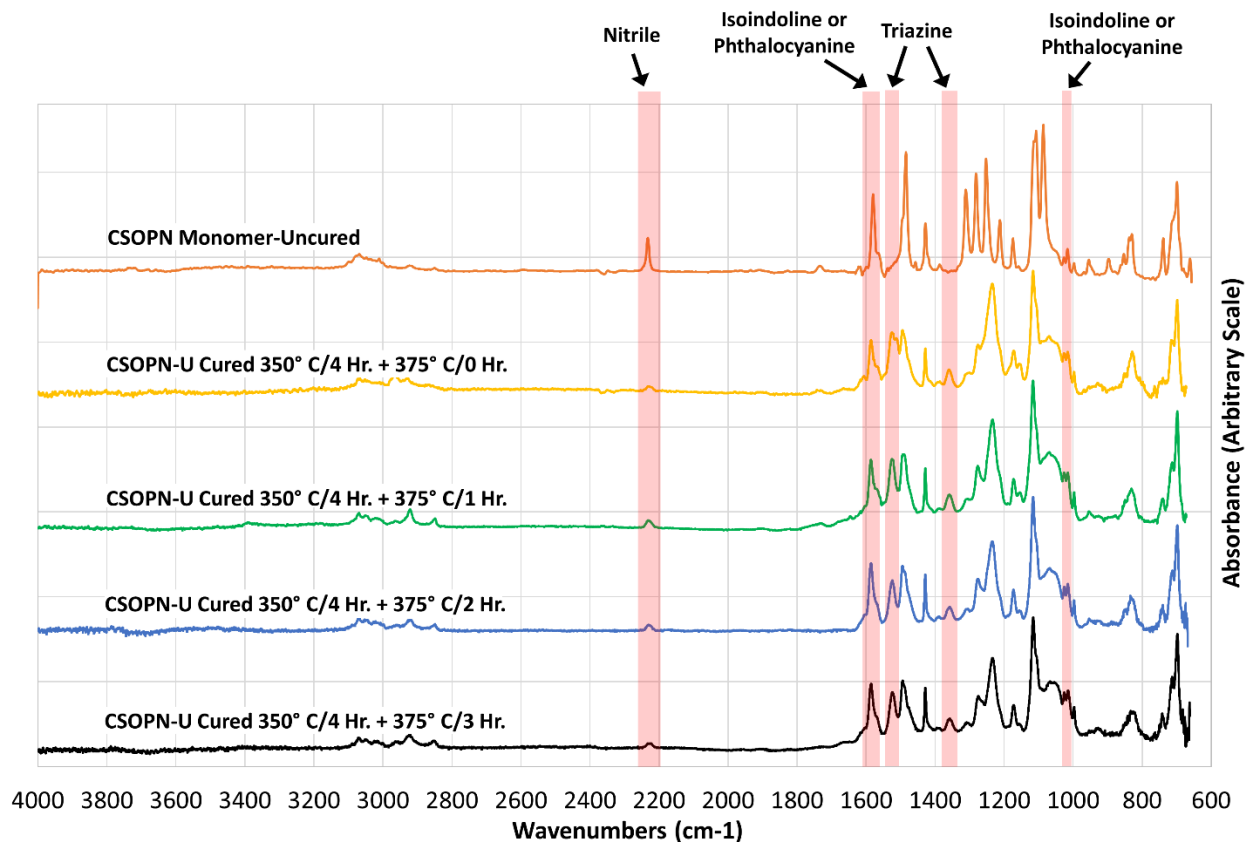


Figure 95: FTIR spectra of CSOPN uncured monomer and after curing to 350 °C for 4 hours and 375 °C for 0-3 hours. The formation of triazine peaks is evident in cured polymers. Isoindoline and phthalocyanine peaks overlap with peaks present in the monomer. No significant differences in spectra were observed for cured polymers.

### 6.3.6 DSC of Cured Polymers

Figure 96 compares the DSC curves for CSPN-U and CSPN-P in nitrogen. CSPN-P showed an onset of the glass transition at 161 °C and a midpoint at 180 °C. Conversely, CSPN-U exhibited a  $T_g$  onset at 309 °C and a midpoint at 344 °C.

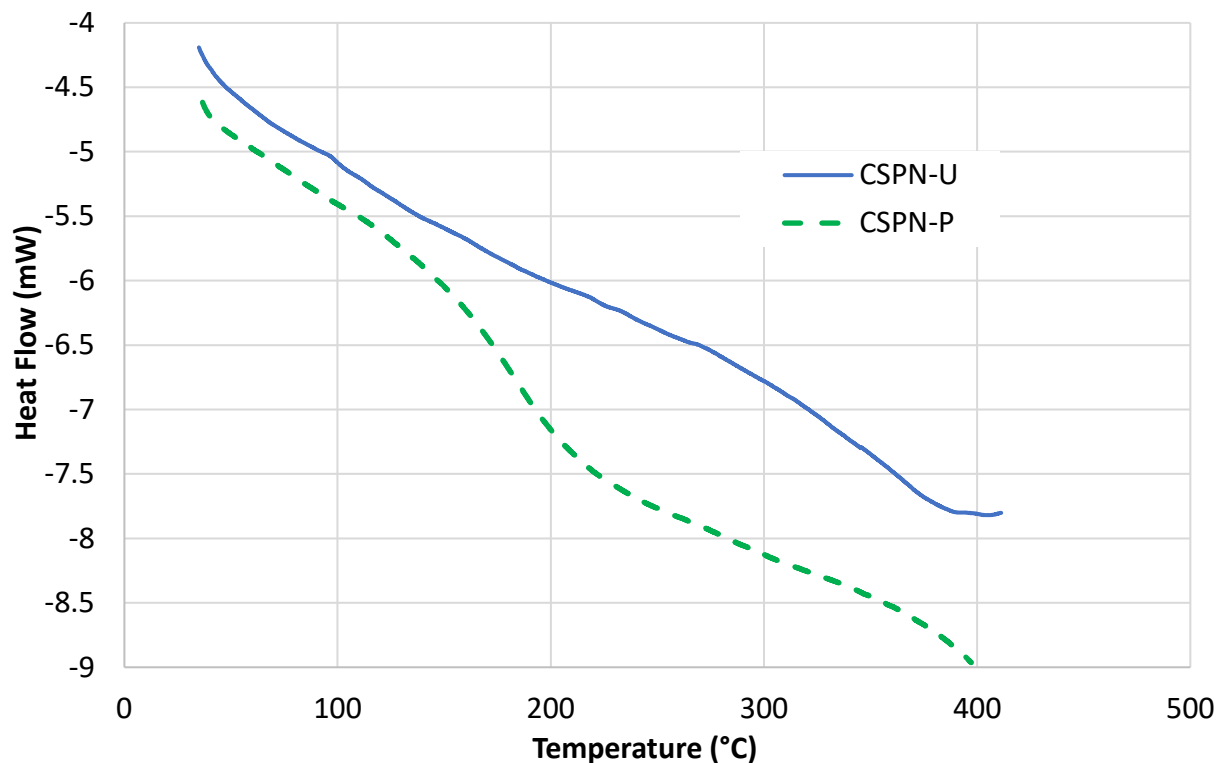


Figure 96: Comparison of DSC curves for CSPN-U and CSPN-P. Glass transitions were observed at 344 °C and 180 °C for CSPN-U and CSPN-P respectively.

Figure 97 and Figure 98 provide DSC data for CSOPN-P polymers in nitrogen and air respectively. Materials were hot pressed to 350 °C and post-cured to 375 °C for 0-3 hours. Table 18 provides glass transition temperatures. The  $T_g$  of CSOPN-P was observed at 170-197 °C, in the same range as CSPN-P but significantly lower than CSPN-U. The onset of degradation was defined as the beginning of positive slope as part of the exothermic degradation process. Under inert conditions the onset of degradation occurred at 390-425 °C. Conversely in air, the onset occurred much earlier, at 230-250 °C.

Table 18: Glass transition data from DSC for CSOPN-P polymers.

CSOPN-P	DSC $T_g$ Onset in N <sub>2</sub> (°C)	DSC $T_g$ Midpoint in N <sub>2</sub> (°C)
350 °C/4 Hr.+375 °C/0Hr.	154	170
350 °C/4 Hr.+375 °C/1Hr.	169	192
350 °C/4 Hr.+375 °C/2Hr.	165	191
350 °C/4 Hr.+375 °C/3Hr.	168	197

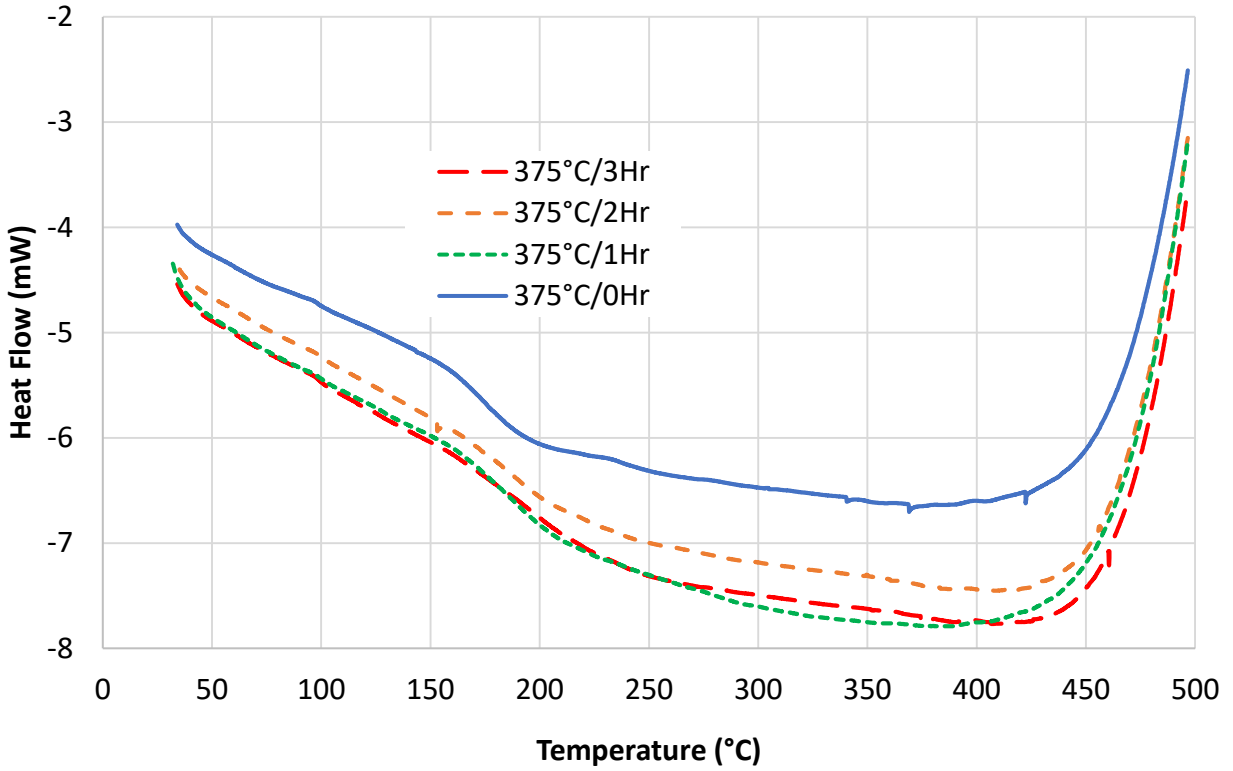


Figure 97: DSC of CSOPN-P under nitrogen. Glass transitions were observed at 170-197 °C. Onset of degradation occurred at 400-430 °C.

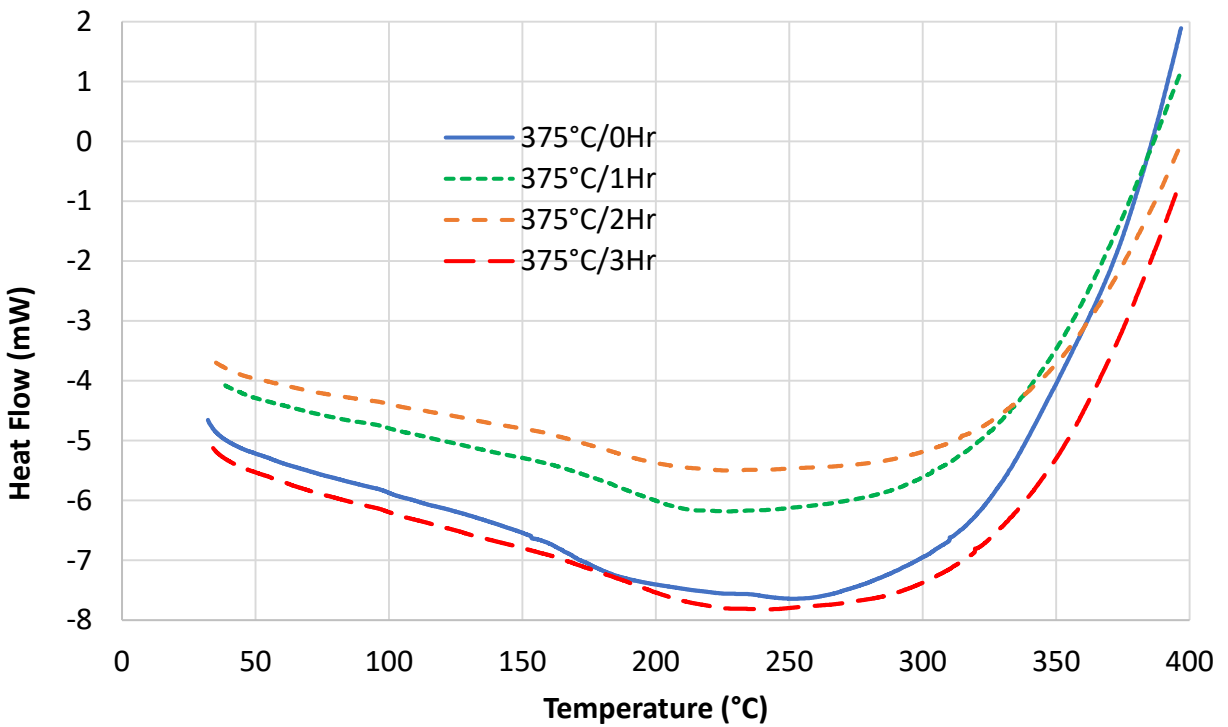


Figure 98: DSC of CSOPN-P in air. Onset of degradation occurred around 250 °C.

### 6.3.7 DMA of Cured CSOPN Polymers

Figure 99, Figure 100, and Figure 101 provide DMA data for CSOPN-P cured to 350 °C for 4 hours and 375 °C for 0, 1, or 3 hours respectively. Table 19 provides the glass transition temperatures as measured by the inflection point of the storage modulus ( $G'$ ), and peaks of the loss modulus ( $G''$ ) and loss tangent ( $\tan(\delta)$ ). The glass transition as measured by  $G'$  increased slightly from 188 °C to 199-200 °C after curing to 375 °C. Post-curing at 1 and 3 hours resulted in nearly identical transition temperatures.

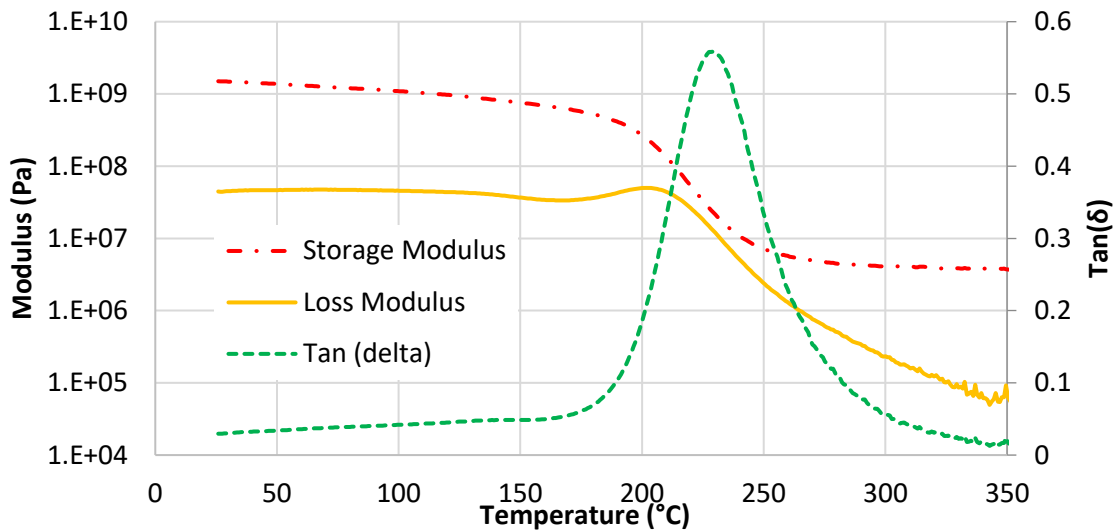


Figure 99: DMA of CSOPN-P, with 4 wt. % p-BAPS, hot-pressed to 350 °C for 4 hours.

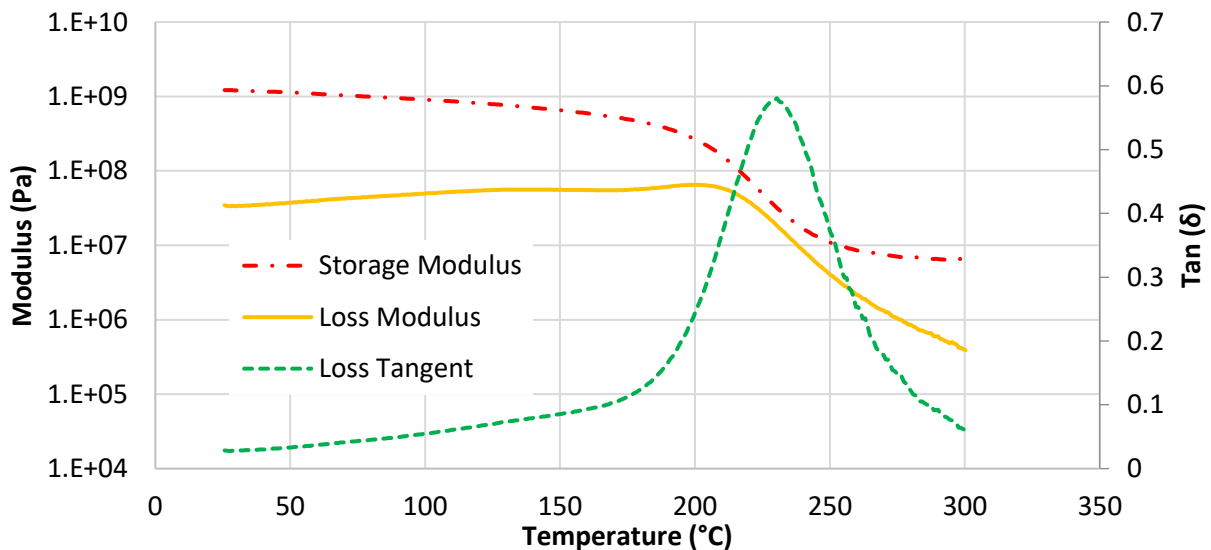


Figure 100: DMA of CSOPN-P, with 4 wt. % p-BAPS, hot-pressed to 350 °C for 4 hours and 375 °C for 1 hour.

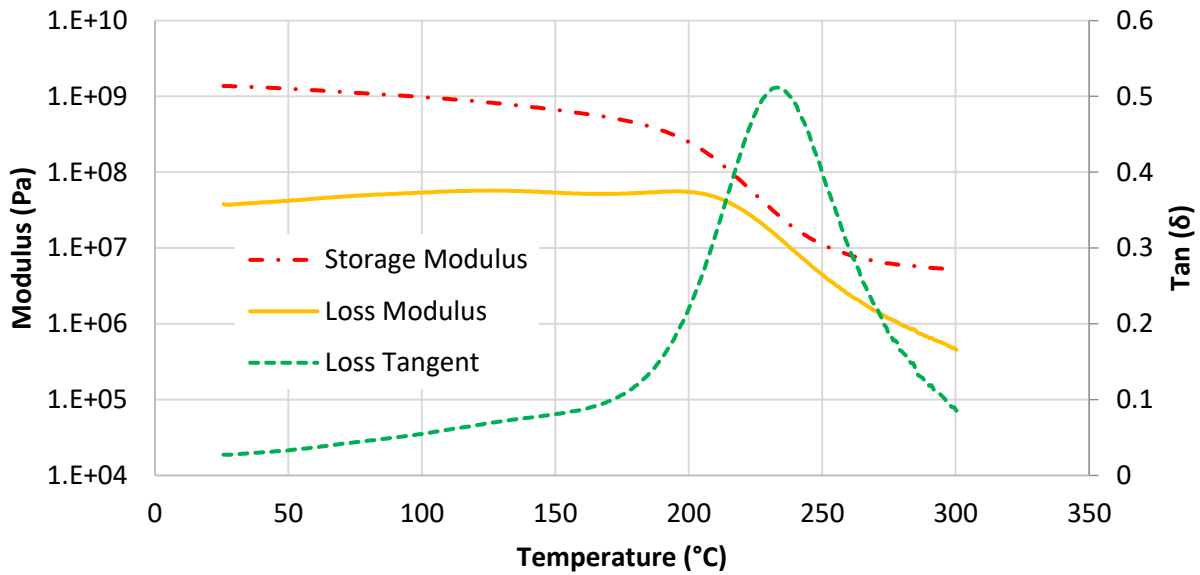


Figure 101: DMA of CSOPN-P, with 4 wt. % p-BAPS, hot-pressed to 350 °C for 4 hours and 375 °C for 3 hours.

Table 19: Glass transitions of CSOPN-P as measured by DMA.

CSOPN	DMA Storage Modulus T <sub>g</sub> (°C)	DMA Loss Modulus T <sub>g</sub> (°C)	DMA Loss Tangent T <sub>g</sub> (°C)
<b>350 °C/4 Hr.+375 °C/0Hr.</b>	188	192	221
<b>350 °C/4 Hr.+375 °C/1Hr.</b>	200	200	230
<b>350 °C/4 Hr.+375 °C/2Hr.</b>	Not Measured	Not Measured	Not Measured
<b>350 °C/4 Hr.+375 °C/3Hr.</b>	198	195	234

### 6.3.8 TMA of Cured CSOPN Polymers and CTE Information

TMA curves are given in Figure 102 and Figure 103 for CSOPN-P polymers with 4 wt. % p-BAPS, cured to 350 °C and 375 °C respectively. Table 20 provides T<sub>g</sub> and CTE data for CSOPN-P from TMA measurements. Standard deviations for the T<sub>g</sub> and CTE were in the range of 1.0-7.4 °C and 0.9-2.8 μm/(m°C), respectively. The glass transition onsets and midpoints were identified as the peaks in the second and first derivatives, respectively. With increasing post-curing time at 350 °C or 375 °C, the glass transitions became slightly smaller but did not disappear as with CSPN-U. Additionally, the glass transitions increased in temperature slightly, with onsets increasing from 176 °C to 191 °C and midpoints increasing from 197 °C to 212 °C, with increasing curing time at 350 °C. After curing at 375 °C, the T<sub>g</sub> onsets increased to 180-196 °C and midpoints to 205-223 °C. While the T<sub>g</sub> midpoints increased with curing time at 375 °C, the T<sub>g</sub> onsets first increased before decreasing. This may indicate degradation of the compound was occurring.

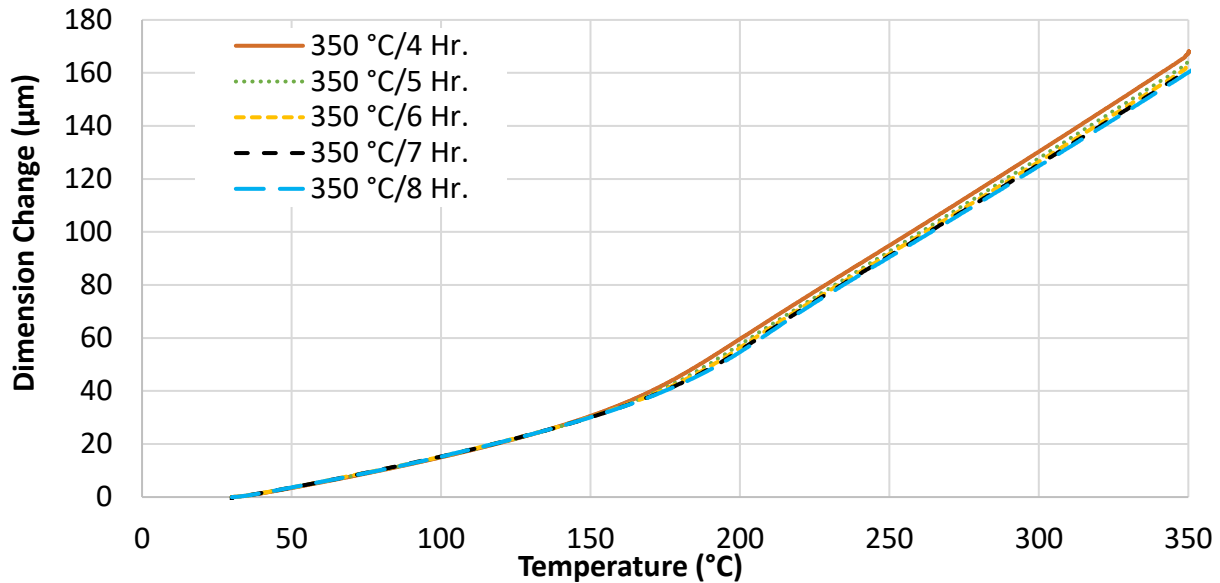


Figure 102: TMA curves of CSOPN-P cured to 350 °C for 4-8 hours.

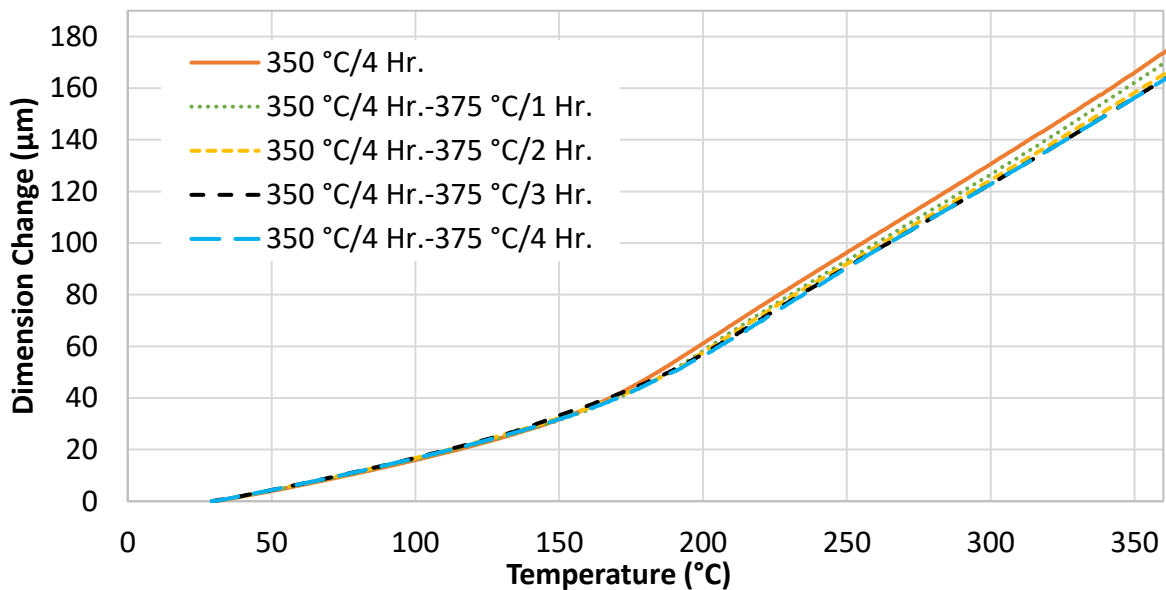


Figure 103: TMA curves of CSOPN-P cured to 350 °C for 4 hours and 375 °C for 0-4 hours.

The CTE was defined as the slope between 50-150 °C in TMA data, normalized by the sample thickness. This was slightly lower than the range used for CSPN-U (50-200 °C) due to the substantially lower  $T_g$  of the CSOPN-P material. The CTE for CSOPN-P was measured in the range of 77.7-79.7 ( $\mu\text{m}/(\text{m}^\circ\text{C})$ ) and generally increased with curing time at 350 °C or 375 °C. This is contrary to what was observed with CSPN-U, where the CTE decreased with curing temperature at 375 °C. Additionally CSPN-U exhibited a slightly lower CTE as compared to CSOPN-P. A

summary of CTE data for CSPN-U, CSOPN-P, and several reference materials is provided in Figure 104.

Table 20:  $T_g$  and CTE of CSOPN-P after various curing cycles as measured by TMA.

Curing	TMA Onset ( $^{\circ}\text{C}$ )	TMA Midpoint ( $^{\circ}\text{C}$ )	CTE ( $\mu\text{m}/(\text{m}^{\circ}\text{C})$ )
350 $^{\circ}\text{C}$ /4 Hr.	176	197	77.7
350 $^{\circ}\text{C}$ /5 Hr.	178	204	78.6
350 $^{\circ}\text{C}$ /6 Hr.	185	207	78.5
350 $^{\circ}\text{C}$ /7 Hr.	189	210	78.7
350 $^{\circ}\text{C}$ /8 Hr.	191	212	78.2
350 $^{\circ}\text{C}$ /4 Hr.+375 $^{\circ}\text{C}$ /1Hr.	189	205	77.9
350 $^{\circ}\text{C}$ /4 Hr.+375 $^{\circ}\text{C}$ /2Hr.	196	212	79.0
350 $^{\circ}\text{C}$ /4 Hr.+375 $^{\circ}\text{C}$ /3Hr.	191	222	79.6
350 $^{\circ}\text{C}$ /4 Hr.+375 $^{\circ}\text{C}$ /4Hr.	180	223	79.7

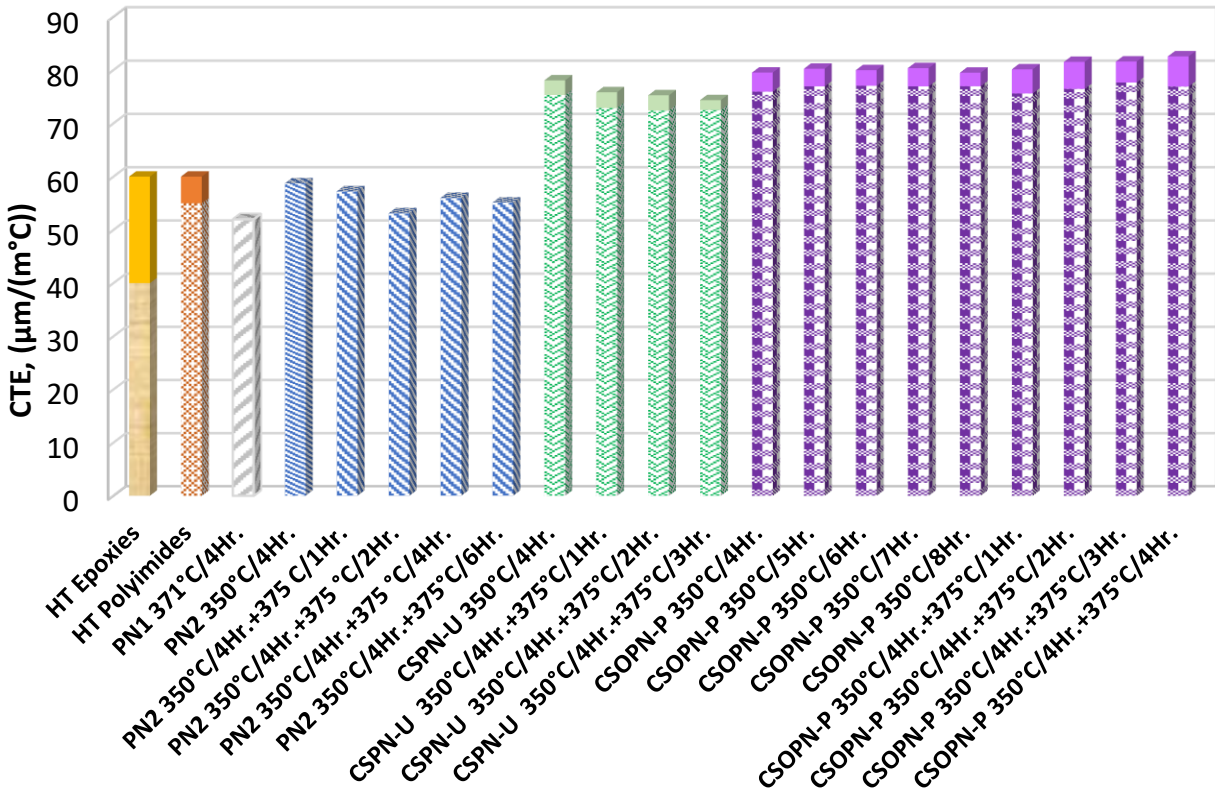


Figure 104: Summary of CTE data for CSPN-U, CSOPN-P and two commercial phthalonitrile resins (PN1 and PN2). General ranges for high temperature epoxies and polyimides are also provided for reference. Some data is included from Koerner and Gibson et al.<sup>96, 138</sup>

Commercially available phthalonitriles and reference polyimides showed CTE values in the range of 50-60 ( $\mu\text{m}/(\text{m}^{\circ}\text{C})$ ). This is substantially lower than the CTE values observed for the

CSPN-U and CSOPN-P polymers. This may be due to a possible lower degree of cure, and greater free volume due to bulky phenyl pendant groups and longer Si-C and Si-O bonds.

### 6.3.9 Summary of Glass Transition Measurements

Figure 105 provides a summary of glass transition measurements for CSPN-U, CSPN-P, and CSOPN-P, and commercial phthalonitrile PN2 from DSC, DMA, and TMA. The  $T_g$  of purified CSPN-P and CSOPN-P are observed in the same range. A significant difference of 99-174 °C is observed between purified CSPN or CSOPN polymers and the as-synthesized CSPN, depending on sample and measurement method. In turn, CSPN-U and PN2 show  $T_g$  in the same range when cured to 350 °C for 4 hours. However, when cured to 375 °C the  $T_g$  of PN2 is increased at a greater rate than CSPN-U.

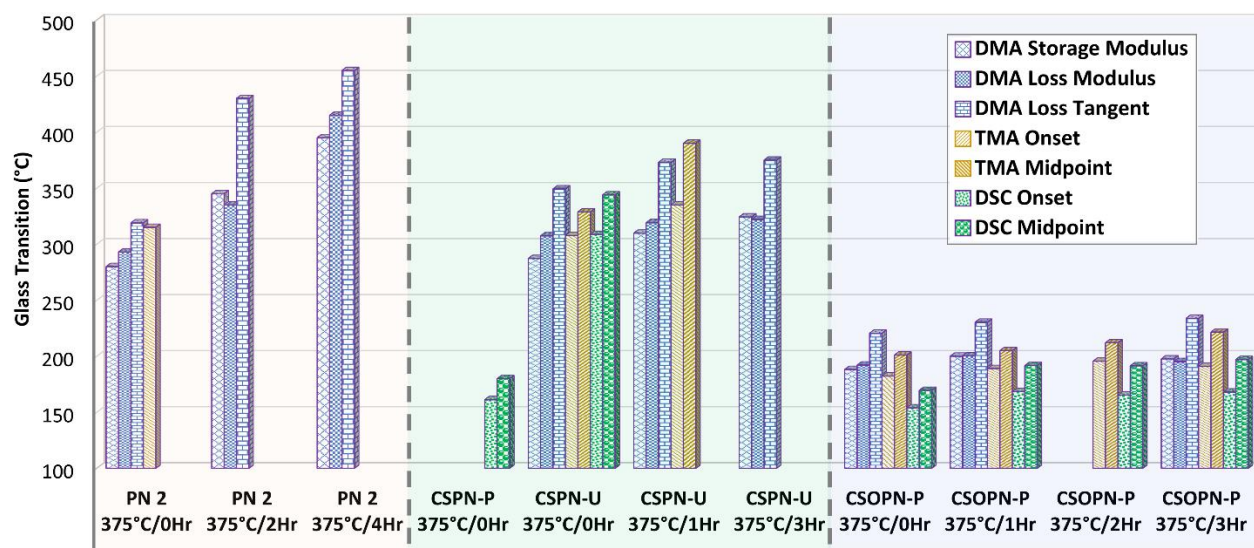


Figure 105: Summary of glass transition data for CSPN-U, CSPN-P, and CSOPN-P, and commercial phthalonitrile PN2. Data on PN2 is included from Koerner and Gibson et al.<sup>96, 138</sup>

### 6.3.10 Thermal and Thermo-oxidative Stability of Cured Polymers

#### 6.3.10.1 TGA of CSPN Polymers

The TGA results for CSPN-P and CSPN-U polymers with 4 wt.% p-BAPS are compared in Figure 106 and Figure 107 for nitrogen and air atmospheres. CSPN-P exhibited lower stability in nitrogen with  $T_{5\%}$  at 487 °C,  $T_{10\%}$  at 516 °C, and final char yield at 1000 °C of 60.3 wt.%. In comparison, CSPN-U exhibited  $T_{5\%}$  at 528 °C,  $T_{10\%}$  at 567 °C, and final char yield at 1000 °C of 65.7 wt.%. For the CSPN-P polymer, degradation peaks in nitrogen occurred at 533 °C and 580

°C, as compared with a single degradation peak at 610 °C for CSPN-U. The degradations of the CSPN-P polymer were in the same temperature range as observed with the CSPN-U (6 wt.% *p*-BAPS) polymer, which showed overlapping degradations at 540-550 °C, 580-585 °C, and 730-740 °C. There is likely also a degradation at 600-610 °C, as indicated in the FTIR-TGA data of CSPN-U, provided in the previous chapter. For the CSPN-P (4 wt.% *p*-BAPS) polymer, the greatest rate of degradation occurred at the 533 °C peak, in comparison with the CSPN-U (6 wt.% *p*-BAPS) polymer which showed the highest degradation at the 610 °C peak. FTIR-TGA data of CSPN-U showed both degradations corresponded to decomposition of nitrogen-containing compounds from phthalonitrile curing derivatives. The results here indicate a lower degree of cure for the CSPN-P system, with less thermally stable structures being formed.

In air, the CSPN-P showed  $T_{5\%}$  at 461 °C,  $T_{10\%}$  at 492 °C, and char at 1000 °C was 8.42 wt.%. In comparison, CSPN-U showed higher values of  $T_{5\%}$  at 487 °C,  $T_{10\%}$  at 519 °C, and char at 1000 °C was 9.23 wt.%. CSPN-P showed degradation peaks at 485, 519, 582, and 645 °C. In comparison, CSPN-U did not show the degradation peak at 485 °C but did show the other three degradations. This supports the hypothesis of a lower degree of cure, with more unreacted or incomplete (isoindoline) curing products present.

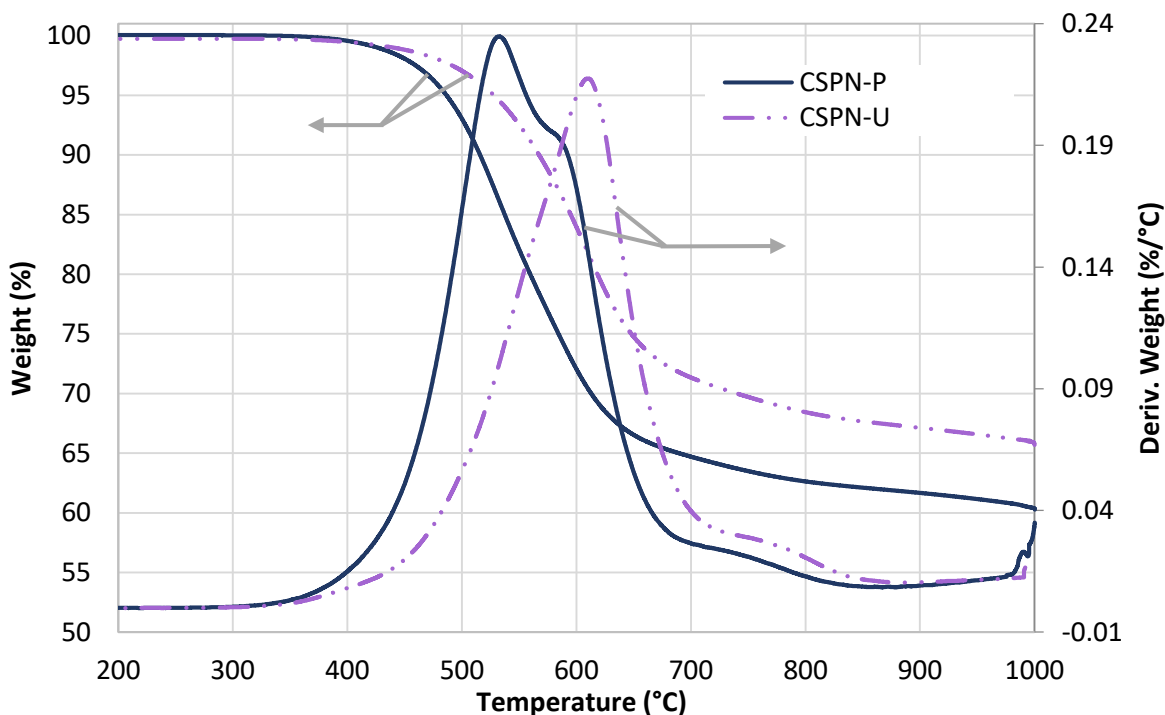


Figure 106: Comparison of TGA data in  $N_2$  of CSPN-P and CSPN-U cured to 350 °C for 4 hours with 4 wt.% *p*-BAPS.

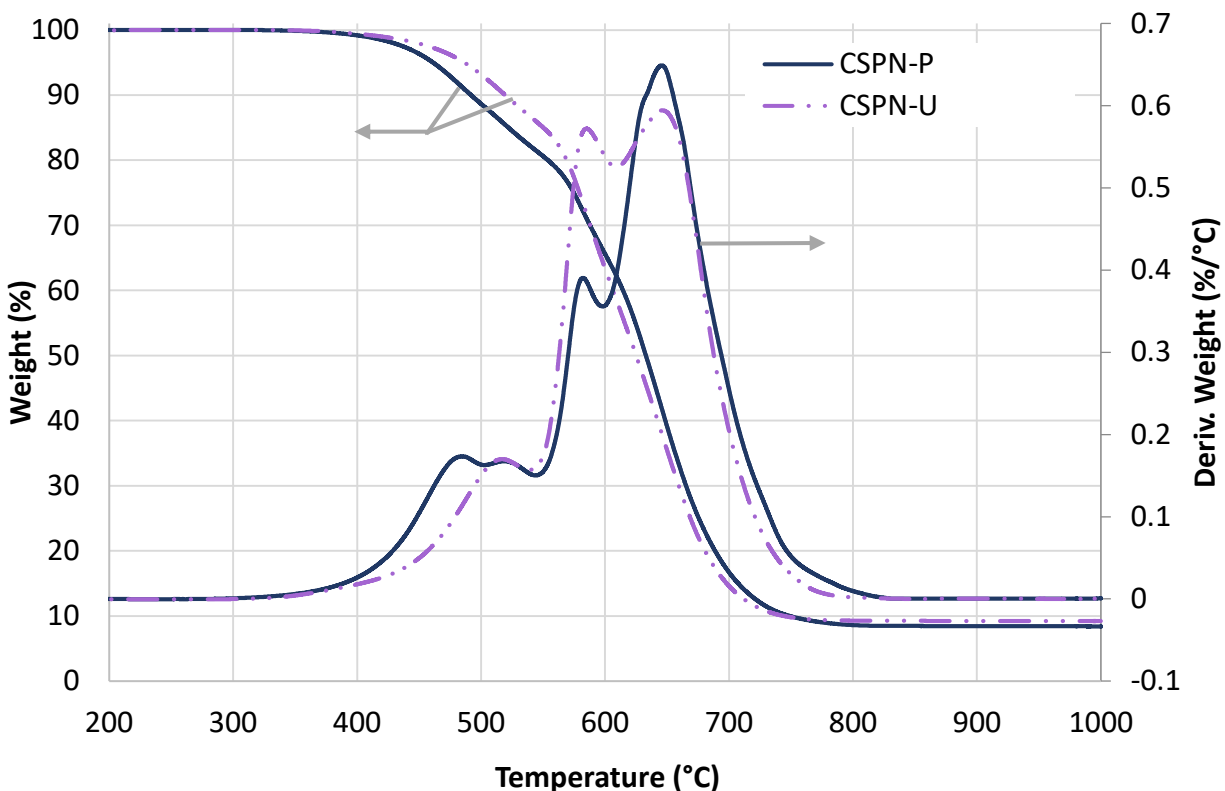


Figure 107: Comparison of TGA data in air of CSPN-P and CSPN-U cured to 350 °C for 4 hours with 4 wt.% p-BAPS.

### 6.3.10.2 TGA of CSOPN-P Polymers

Comparisons of CSOPN-P cured at 350 °C for 4 hours and 375 °C for 0-3 hours are given in Figure 108 and Figure 109 for nitrogen and air atmospheres respectively. Numerical data is provided in Table 21 including T<sub>5%</sub>, T<sub>10%</sub>, and residual char yield at 780 °C and 1000 °C. In both nitrogen and air, stability in TGA increased slightly with additional curing at 375 °C. In nitrogen final char yield increased with curing time but a clear trend was not observed in air. In nitrogen, CSOPN-P showed degradation peaks at 525-530 °C, 594-596 °C, and 740-750 °C. After curing to 375 °C, the 525-530 °C peak decreased, whereas the 594-596 °C peak increased slightly. In air degradation peaks were observed at 480-490 °C, 518-523 °C, 590-603 °C and 656-665 °C. A clear trend in peak heights with increasing curing time was not evident. Greater analysis of degradation peaks is provided in the following subsection: Thermogravimetric Analysis-Fourier Transform Infrared Spectroscopy of CSOPN-P Polymers.

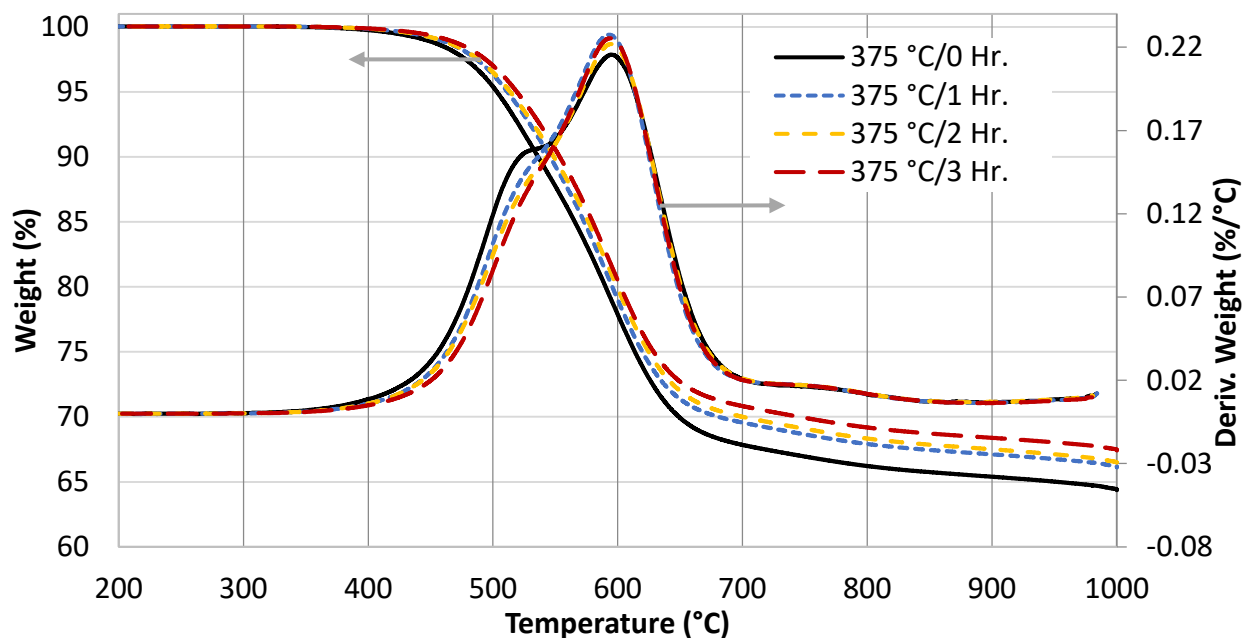


Figure 108: TGA of CSOPN-P with 4 wt.% p-BAPS in nitrogen atmosphere.

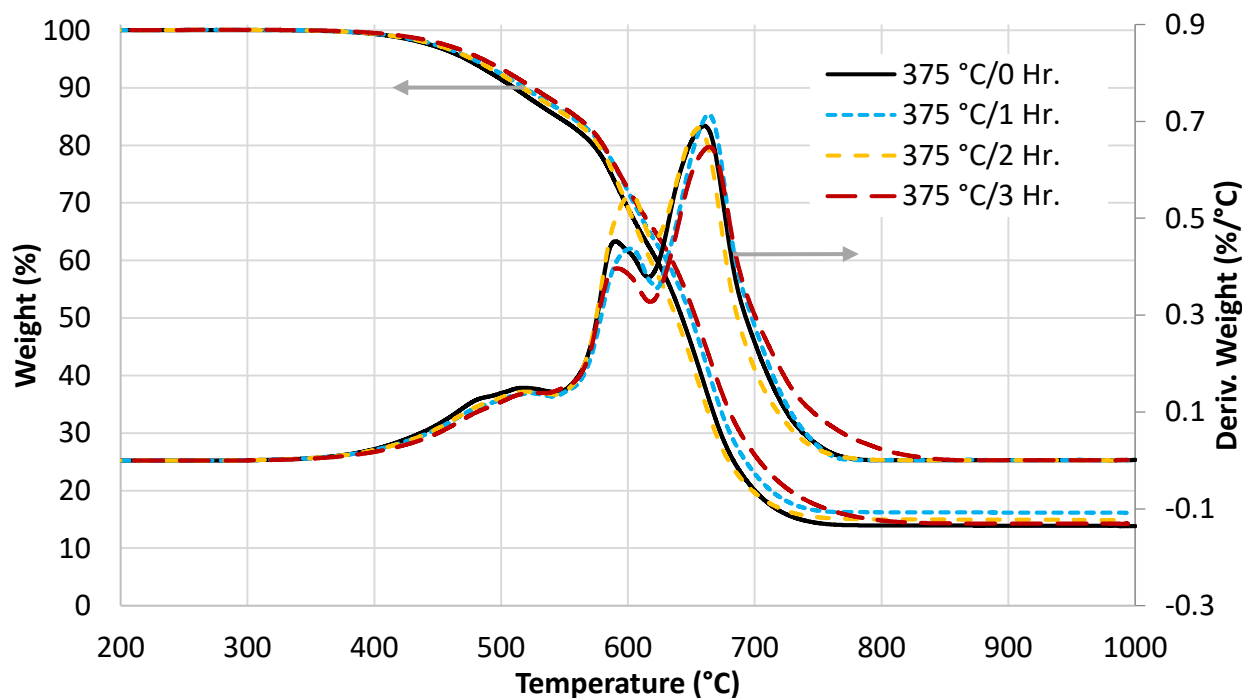


Figure 109: TGA of CSOPN-P with 4 wt.% p-BAPS in air atmosphere.

The predicted char yield in air, as estimated by conversion of silicon to SiO<sub>2</sub>, is 14.7 wt.% for CSOPN-P. The observed values are within 10 % error of the predicted value and appear to approach the predicted value with increasing curing time. CSPN-P and CSOPN-P with 4 wt. % p-

BAPS, cured to 350 °C for 4 hours, are compared in Figure 110 and Figure 111 respectively. CSOPN-P exhibited higher stability in both air and nitrogen, however similar degradation peaks were observed in both polymers. The peak heights differed in nitrogen, with CSPN-P exhibiting greater degradation at 520-530 °C and CSOPN-P displaying greater degradation in the range of 585-595 °C. In air the CSOPN-P showed lower degradations at 480-490 °C and 520 °C, while higher degradation peaks at higher temperatures were observed for the 580-600 °C and 645-665 °C degradations.

Table 21: TGA data for CSOPN-P with 4 wt.% p-BAPS in air and nitrogen.

Atmosphere	Max Cure	T <sub>5%</sub> (°C)	T <sub>10%</sub> (°C)	Residual at 780 °C (Wt. %)	Residual at 1000 °C (Wt. %)
N <sub>2</sub>	350 °C/4 Hr.	504	538	67.8	64.8
N <sub>2</sub>	375 °C/1 Hr.	512	546	68.2	66.2
N <sub>2</sub>	375 °C/2 Hr.	514	549	68.6	66.5
N <sub>2</sub>	375 °C/3 Hr.	519	554	69.4	67.5
Air	350 °C/4 Hr.	471	507	13.7	13.2
Air	375 °C/1 Hr.	478	518	16.3	16.1
Air	375 °C/2 Hr.	478	517	15.1	14.9
Air	375 °C/3 Hr.	485	527	15.5	14.8

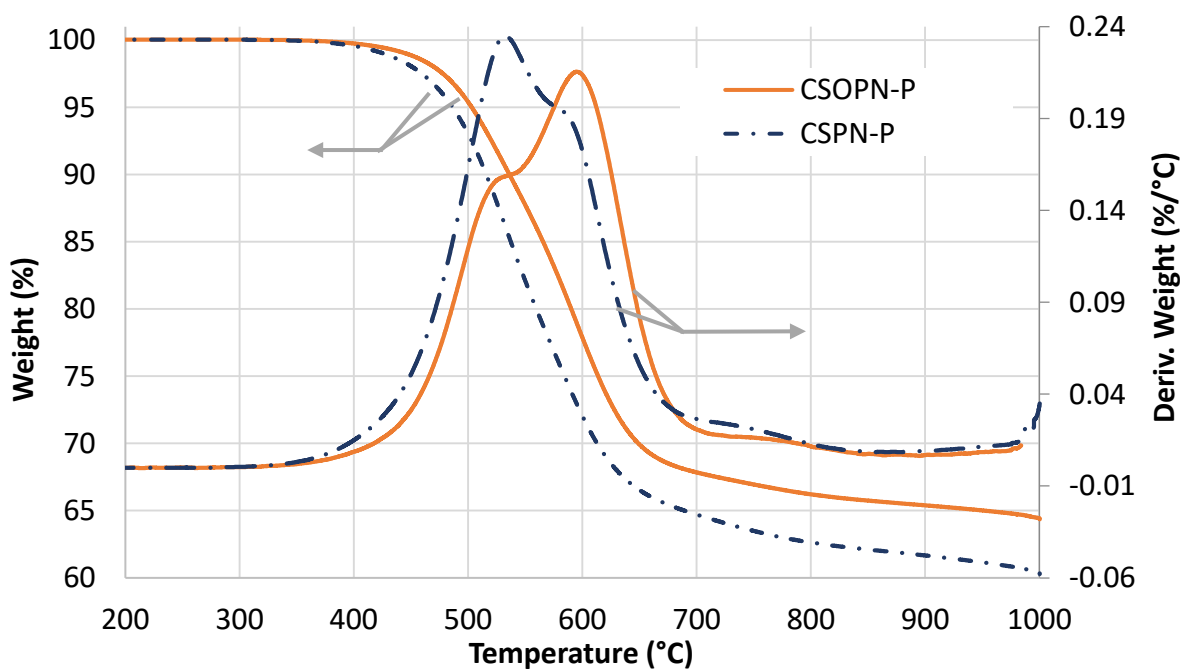


Figure 110: Comparison of TGA results in nitrogen of CSPN-P and CSOPN-P cured to 350 °C for 4 hours.

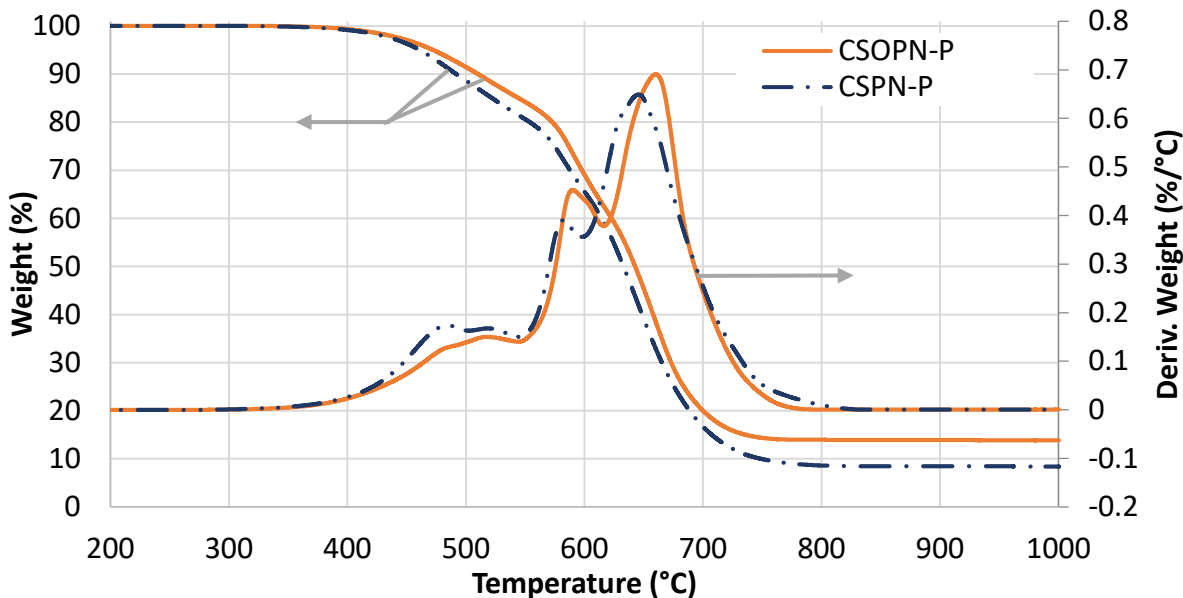


Figure 111: Comparison of TGA results in air of CSPN-P and CSOPN-P cured to 350 °C for 4 hours.

### 6.3.10.3 Comparison of Thermogravimetric Data

A summary of TGA data in air and nitrogen is given in Figure 112. A table of  $T_{5\%}$ ,  $T_{10\%}$ , and char yields may be found in Appendix B: Thermogravimetric Data. A comparison of TGA curves is provided in Figure 113 and Figure 114 for CSPN-U and CSOPN-P cured to 375 °C for 3 hours and PN1 and PN2 cured to 375 °C.

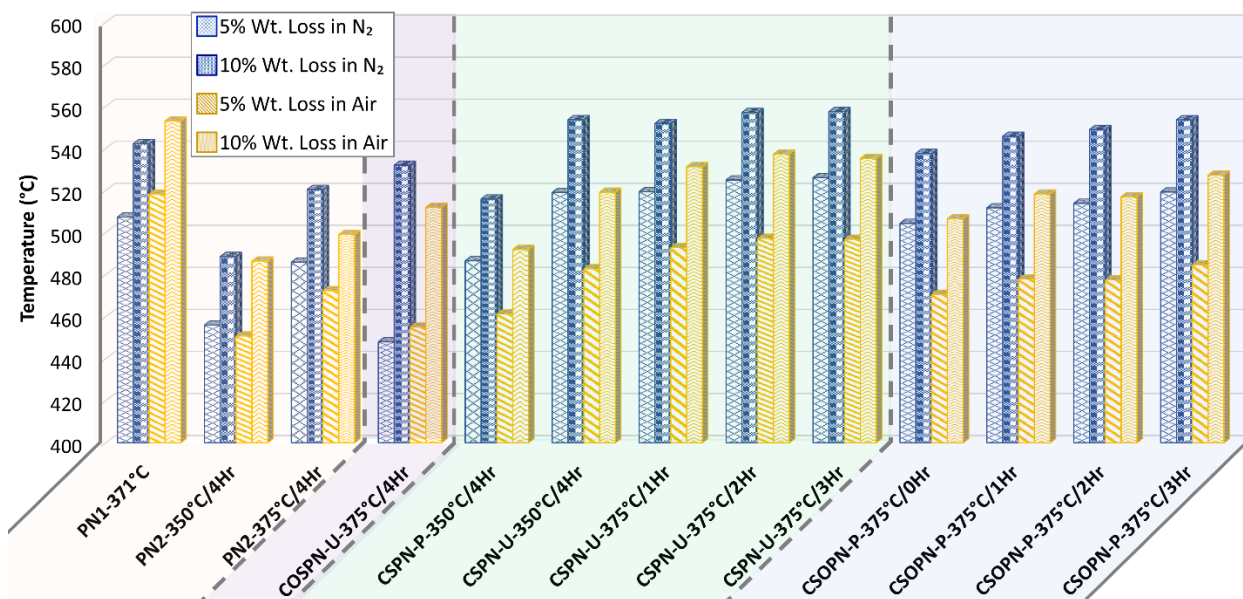


Figure 112: Summary of TGA data for COSPN-U, CSPN-P, CSPN-U, CSOPN-P, and commercial PN1 and PN2 polymers in air and nitrogen. Some data on commercial phthalonitriles PN1 and PN2 is included from Koerner and Gibson et al.<sup>96, 138</sup>

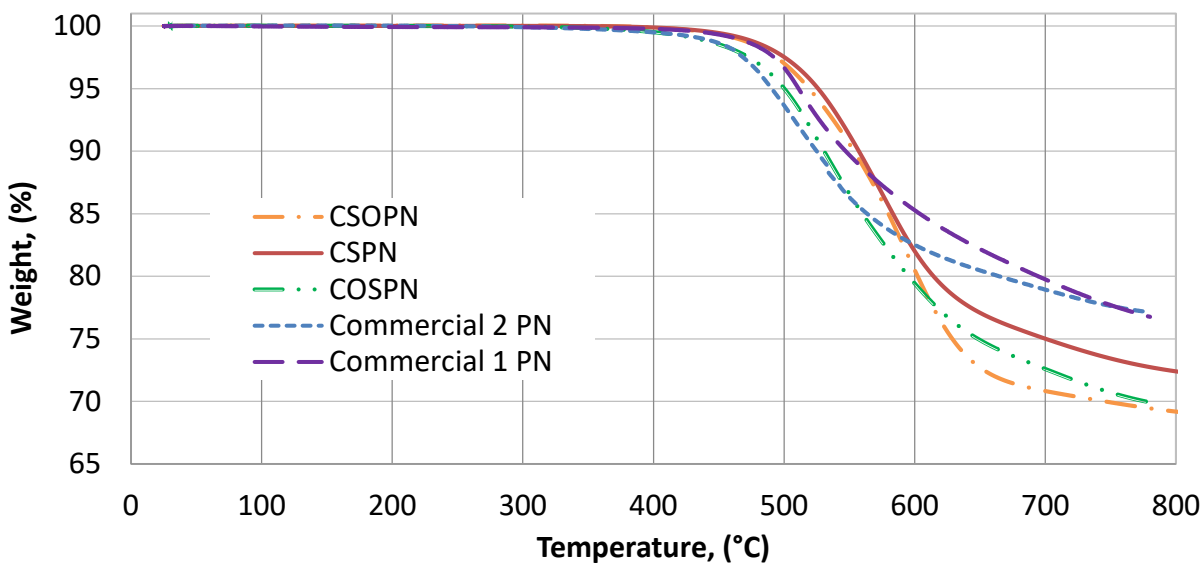


Figure 113: Comparison of TGA curved in nitrogen for phthalonitrile polymers cured to 375 °C. Data on commercial phthalonitriles PN1 and PN2 is included from Koerner and Gibson et al.<sup>96, 138</sup>

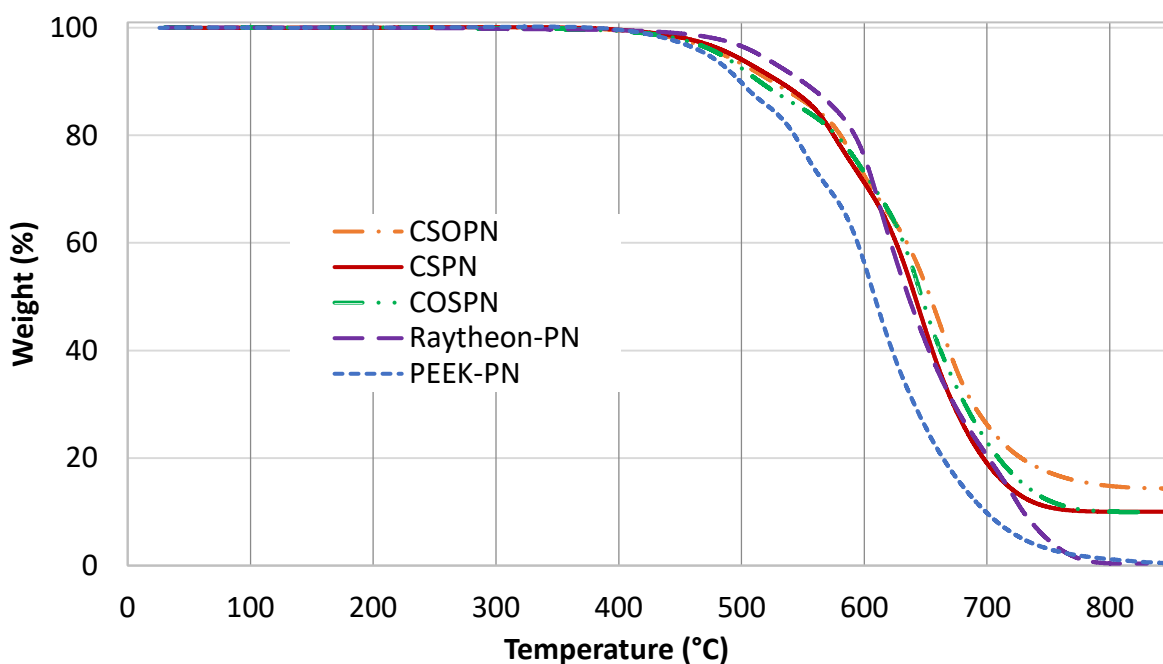


Figure 114: Comparison of TGA curved in air for phthalonitrile polymers cured to 375 °C. Data on commercial phthalonitriles PN1 and PN2 is included from Koerner and Gibson et al.<sup>96, 138</sup>

For all polymers, performance in TGA improved with increasing curing time and temperature. For similar curing cycles, the stability of the silicon-containing polymers followed the trend CSPN-U > CSOPN-P > COSPN-U > CSPN-P. Purified CSPN exhibited much lower stability than the as-synthesized polymer. Although the resin was purified, CSOPN-P exhibited very good

performance in TGA. Commercial PN1 showed high stability and was the only polymer to show greater stability in air as compared to nitrogen. Commercial PN2 showed lower stability than other materials considered. Char yields for silicon-containing phthalonitriles were lower than that of commercial organic PN polymers under nitrogen, but higher in air. The higher char yield in air of silicon-containing PN materials is almost entirely dependent on conversion of silicon to SiO<sub>2</sub>. Conversely their lower char yield in air, as compared with organic PN polymers, may be explained by the difference in the Si-C and C-C bond strengths.

#### 6.3.10.4 Thermogravimetric Analysis-Fourier Transform Infrared Spectroscopy of CSOPN-P Polymers

To better understand the degradation routes of CSOPN-P, FTIR was performed on gases evolved during TGA runs. Samples were cured with 4 wt. % *p*-BAPS to a maximum temperature of 350 °C for 4 hours. Figure 115 and Figure 117 provide intensity maps and selected spectra for nitrogen and air, respectively. The intensity of IR peaks is compared with weight loss and derivative TGA curves in nitrogen and air respectively in Figure 116 and Figure 118 respectively. The derivative weight loss curves correlate well with the intensity of IR peaks.

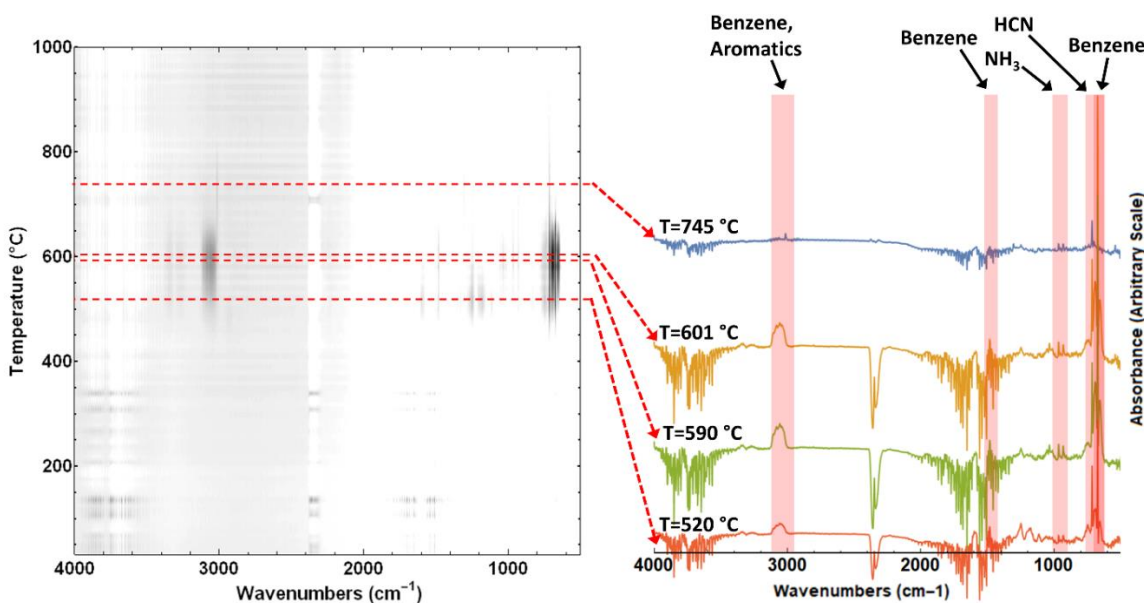


Figure 115: FTIR-TGA spectra in nitrogen (90.0 mL/min) of CSOPN-P cured to 350 °C for 4 hours. An intensity map is provided on the left. On the right, selected spectra correspond to degradation peaks shown in Figure 116.

The degradation peaks of CSOPN-P were nearly identical to those observed in CSPN-U in both air and nitrogen. In nitrogen, four overlapping degradations were observed in IR spectra at 520 °C, 590 °C, 601 °C, and 745 °C. In comparison, CSPN-U showed the same evolutions at 540 °C, 580 °C, 610 °C, and 700 °C. The first degradation correlated with IR peaks corresponding to HCN (714  $\text{cm}^{-1}$ ) and what is plausibly isoindoline structures or other nitrogen-containing aromatics (1342, 1379, and 1601  $\text{cm}^{-1}$ ). The second degradation at 590 °C correlated with the evolution of benzene (654, 672, 687, 1483, and 3059  $\text{cm}^{-1}$ ). The benzene evolution peak of CSOPN-P is roughly twice the intensity of that observed in CSPN-U. This is due to the presence of twice the number of pendant phenyl rings in the backbone. The evolution of ammonia (930, and 965  $\text{cm}^{-1}$ ) and hydrogen cyanide (714  $\text{cm}^{-1}$ ) were likely from the decomposition of triazine and phthalocyanine structures.

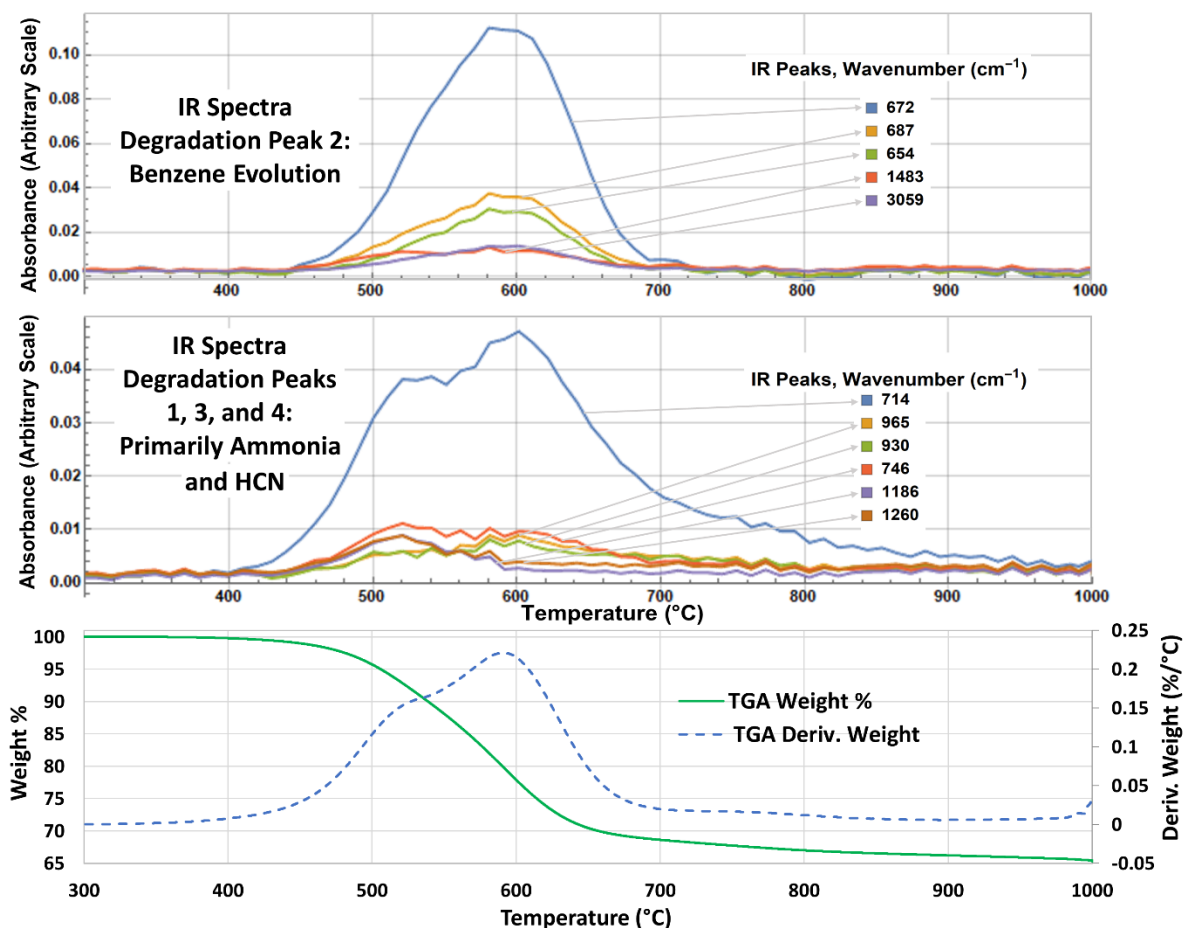


Figure 116: TGA/FTIR in nitrogen of CSOPN-P cured to 350 °C for 4 hours. TGA curves (bottom) correlate with IR peaks of evolved gases (top and middle). Several degradations are evident, involving benzene evolution (top) and production of hydrogen cyanide and ammonia.

In air, three degradations were observed with peaks at 515°C, 575°C, and 645 °C. All three degradations corresponded primarily with the evolution of CO<sub>2</sub> and H<sub>2</sub>O. This result may be expected due to combustion of the organic polymer and degradation products, prior to reaching the IR detector. Hydrogen cyanide was detected in small amounts at 714 cm<sup>-1</sup>. It is of note that the HCN peak overlaps with the CO<sub>2</sub> peak, making the signal intensity appear greater. A trace amount of ammonia was also observed, corresponding to the degradation peak at 575 °C. Trace amounts of benzene were also detected at 500-520 °C. It is likely that benzene and ammonia peaks extend to higher temperatures but are truncated by combustion of these species prior to reaching the detector.

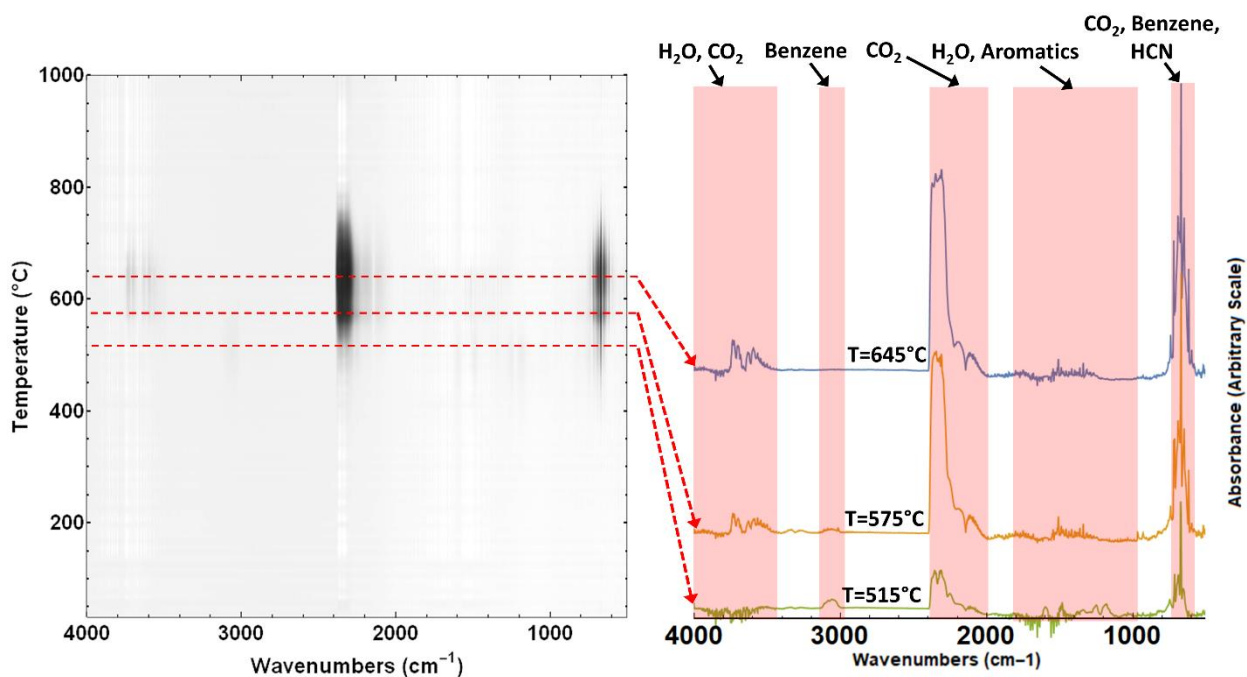


Figure 117: TGA/FTIR in air (90.0 mL/min) of CSOPN-P cured to 350 °C for 4 hours. An intensity map is provided on the left. On the right, selected spectra correspond to degradation peaks shown in Figure 118.

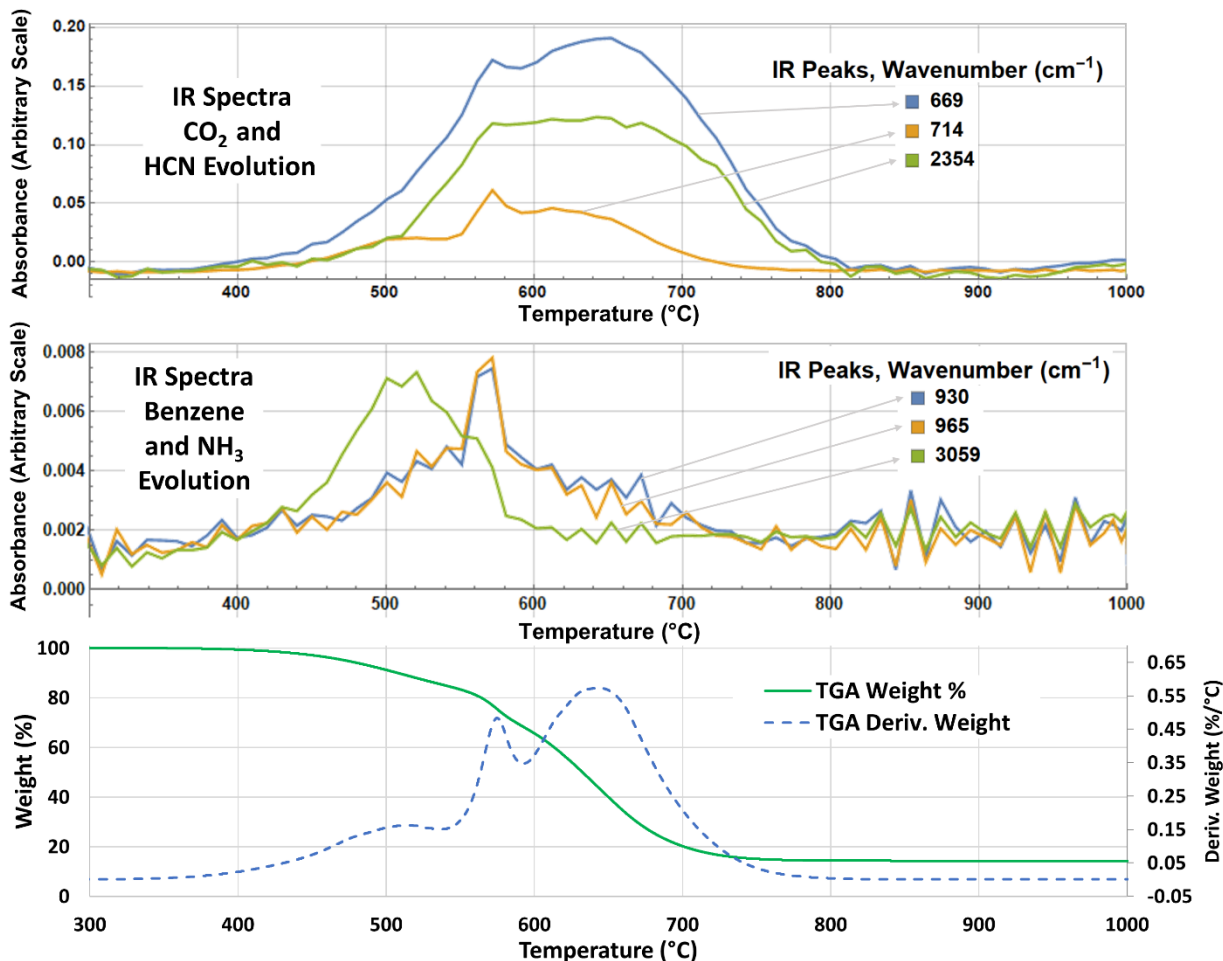


Figure 118: TGA/FTIR in air of CSOPN-P cured to 350 °C for 4 hours. TGA curves (bottom) correlate with IR peaks of evolved CO<sub>2</sub> and HCN (top), and benzene and NH<sub>3</sub> (middle).

## 6.4 Summary and Conclusions

While it could be assumed that the presence of impurities would result in increased degradation of the silicon-containing phthalonitriles, the opposite appears to be true. Increasing purity is observed to have an extremely detrimental effect on the processing, qualitative hardness and strength, glass transition temperature, and stability of these silicon-containing phthalonitrile resins. This effect may be explained by several considerations. First, the softening point increases with purity, resulting in higher initial processing temperatures and small processing windows. Volatile entrapment and monomer degradation are more likely to occur. In contrast, impurities disrupt crystallinity and act as plasticizers, allowing greater chain motion at lower temperatures. Simultaneously, many impurities, including metal salts, amines, and compounds with hydroxyl

groups, catalyze the phthalonitrile curing reaction. This greater chain mobility and catalytic effect result in an increased degree of cure. The greater processing window and slightly lower curing temperature of as-synthesized resin resulted in less volatile entrapment and monomer degradation. This and the higher greater degree of cure resulted in higher stability and  $T_g$ .

Post-curing to 375 °C was beneficial for purified resins since it increased the  $T_g$  and stability in air and nitrogen. However additional curing after initial 1-hour exposure to 375 °C did not result in substantial improvements in properties and in some cases, properties worsened. This was likely due to increasing degradation of the material. CSPN and CSOPN resins appear to follow nearly identical degradation routes. The peak heights varied slightly, likely due to different distributions of curing products and different Si-Phenyl content. Although the CSOPN-P resin was purified, it exhibited high thermal stability, as compared with CSPN-P. This is likely due to the increased monomer backbone flexibility, which facilitates a larger processing window and greater degree of cure. The CSOPN-P resin also exhibited better processing characteristics, on par with CSPN-U. The increased backbone flexibility resulted in decreased softening temperatures and more gradual softening.

For all silicon-containing resins, the CTE was higher than for commercial organic PN resins and the  $T_g$  was lower. This was likely caused by greater free volume due to bulky phenyl pendant groups, longer Si-C and Si-O bonds. The  $T_g$  of CSOPN-P and CSPN-P were observed in the same range. Conversely these purified materials showed substantially lower glass transition temperatures as compared with CSPN-U or commercial phthalonitrile polymers. Assuming the low  $T_g$  of the CSOPN-P polymer is primarily due to the effect of purity, as indicated by CSPN results, a significantly higher  $T_g$  may be expected for the as-synthesized CSOPN-U polymer. Given the results presented here, it would also be expected that CSOPN-U would exhibit improved processability and stability in comparison to CSOPN-P. Given that the CSOPN-P system provided easier processing and better TGA stability in comparison to CSPN-P, the CSOPN-U system remains highly attractive.

## 7 Long-Term Thermo-Oxidative Stability of Phthalonitrile Polymers

### 7.1 Introduction

#### 8 Given the intended applications of aerospace composites and wide-bandgap semi-conductor power modules, it is of interest to evaluate the long-term thermo-oxidative stability at temperatures of 250 °C or greater. As discussed in Chapter 1 Introduction

The inclusion of organosilicon moieties into phthalonitrile resins may provide a feasible route to maintaining processing characteristics while improving thermo-oxidative stability for high temperature applications.

Since the onset of research into high temperature polymers in the 1950's, work has been governed by technological need, economic opportunity, and academic pursuit. Today, high temperature materials are a small but critical class of polymers, present in many applications that touch our daily lives. Applications for thermally and environmentally stable polymers include: 1) aerospace composites 2) electronics and microelectronics. 3) space applications 4) optoelectronics and other optical applications 5) structural reinforcements, 6) automotive parts including composites for high performance vehicles, brake pads binders, and filters, 7) other filters and membranes 8) structural and insulating foams, 9) fire resistant materials, 11) tooling, 12) moldings, 13) coatings, 14) gaskets, sealants, tubing, and pipes, and 15) components for the energy sector including geothermal, nuclear, and petroleum systems.<sup>1-9</sup>

Specifically, in this work, motivation is derived from aerospace composites and wide band-gap power modules. For aerospace composites, polymer matrix materials are needed for long-term use above 300 °C. High temperature polymers and polymer composites are required for advancement of supersonic and hypersonic aircraft as well as subsonic civilian transport.<sup>10</sup> Replacement of metal structures with polymer composites results in valuable weight savings, and in turn improvements in performance and fuel efficiency.<sup>11</sup> Similarly, polymer encapsulation compounds are an enabling technology for wide band-gap power modules for use above 250 °C. Such devices promise improved thermal and mechanical durability, lower power losses, higher switching speeds and current densities, increased durability and reliability, greater resistance to ionizing radiation, and reduced weight.<sup>12-14</sup> The operating temperatures for both applications are well above the useful range for other polymers including silicones and epoxies.

In polymers, continuous exposure at elevated temperatures or intermittent exposure to extreme temperatures results in chemical and physical aging and decomposition. Mass loss, volume shrinkage, cracking, discoloration, and a degradation of thermo-mechanical and mechanical properties can occur.<sup>10</sup> High temperature polymers must be able to resist degradation of their properties during operation in extreme environments with long exposure times, cyclic heating, and intense temperature spikes.

Many different chemistries have been evaluated and developed including polyimides, bismaleimides, phenolics and benzoxazines, fluorinated polymers, poly(arylene ethers), cyanate esters, and phthalonitriles. However, opportunities for improvement exist as applications demand greater temperature capabilities and improved processing. Resins are sought with reduced cost, good solubility in common solvents, low softening temperatures, stable and easily controllable melt viscosities, large processing windows, lower cure temperatures, and minimal volatile evolution. For processed polymers, even greater thermal and oxidative stability, higher glass transition temperatures, improved toughness, excellent mechanical strength and modulus, and improved retention of mechanical properties at elevated temperatures are desired. A greater understanding of degradation and aging mechanisms is also needed.<sup>10</sup>

One resin system currently growing in popularity is phthalonitriles (PNs). PN based resins show great promise for high temperature applications and easier processing. Research into phthalonitrile polymers began in earnest at the U.S. Naval Research Lab in the 1980's. Phthalonitrile monomers possess low melt viscosities and are soluble in many common solvents. Curing occurs at elevated temperatures with the addition of a catalyst, usually a thermally stable aromatic amine. The curing reaction progresses by addition polymerization via the phthalonitrile cyano groups and does not produce volatile by-products, facilitating the fabrication of dense components.<sup>15</sup> State-of-the-art cured resins possess high flammability resistance, excellent mechanical and dielectric properties, and low water absorption.<sup>9, 16-19</sup>

Although these materials show exceptional thermal and oxidative stability in thermogravimetric experiments and during hours of exposure at temperatures between 250-400 °C,<sup>6, 9, 20-28</sup> their long-term thermo-oxidative stability requires improvement to meet the challenging demands of the extreme applications. During longer exposures to air at high temperatures, many phthalonitrile polymers experience significant weight losses, volume shrinkage and cracking.<sup>4, 19, 22-23, 26, 29</sup>

Furthermore, oxidative aging studies of durations longer than 48 hours and subsequent analysis of degradation regions, are rarely reported in phthalonitrile literature. Such experiments are critical in gaining an understanding of material degradation modes and behavior in service.

The incorporation of inorganic groups into the organic monomer backbone of polymers often provides a viable route for improved stability and toughness during service at high temperatures in oxidizing environments.<sup>22, 30</sup> The inclusion of silicon moieties has been reported to improve oxidative stability and flammability of high temperature polymers including cyanate ester,<sup>31-33</sup> and polyimide systems.<sup>34-44</sup> As oxygen and free radicals cleave carbon-silicon bonds, siloxy units are formed. These siloxy moieties may interact to produce the inert phase SiO<sub>2</sub>. In this case, a silica-rich surface layer forms. This layer can act as a barrier, reducing the rates of degradation of the surface and oxygen diffusion into the bulk.<sup>45-49</sup>

Thus, it is of interest to evaluate the effects of the inclusion of silicon-containing linkages on the properties of high temperature polymers, including phthalonitriles. Phthalonitriles are good candidates for hybridization with organosilicon moieties due to their ease of processing and high glass transition temperatures.<sup>3-8, 15</sup> Prior to beginning investigations for this dissertation, little research existed on silicon-containing phthalonitrile resins. However, in the last few years several groups have produced and characterized silicon-containing phthalonitrile compounds. Examples include silane,<sup>50</sup> silazane,<sup>51</sup> oxysilane,<sup>30, 52</sup> siloxane,<sup>6, 53</sup> and silsesquioxane moieties.<sup>54</sup> Additional groups have synthesized silicon-containing phthalonitrile compounds but did not report their properties as neat phthalonitrile resins.<sup>55-57</sup> While the silicon-phthalonitrile materials synthesized by these groups exhibited high thermal and thermo-oxidative stability in short-term thermogravimetric experiments, emphasis was generally placed on developing resins with low softening points and long-term stability was not characterized.

Design of hybrid organic-inorganic polymers is not a trivial matter however. Inclusion of organosilicon moieties does not in itself guarantee improvements. Literature suggests there are a number of design considerations to keep in mind to achieve desirable properties. For example, avoiding the use of benzylic or methylene bridges, the presence of phenyl functional groups on the silicon, and limiting the length of silicon-containing linkages are a few approaches reported to achieve higher glass transitions and thermo-oxidative stabilities.

The purpose of this work is to investigate the processing, properties, and degradations of the silicon-containing phthalonitrile resins for high temperature applications. Background is provided on relevant properties and measurement techniques, high temperature polymers in general, phthalonitriles, and several classes of organosilicon polymers. While a plethora of similar compounds to those discussed in this dissertation have been synthesized and evaluated in literature for other purposes, focus here is placed primarily on high temperature applications. Thus, this work is not intended to be comprehensive of all related compounds and chemistries. In addition, focus was placed on silane, oxysilane, and siloxane chemistries. While polymers containing poly octahedral silsesquioxane (POSS) or silazane (Si-N) linkages are discussed briefly, they are mostly outside the scope of this work. A thorough investigation of various chemical synthesis techniques is also not included, though some information is provided for phthalonitriles and polyimides.

Based on available literature, three monomer structures were selected containing carboxysilane (C-O-Si-O-C), carbosilane (C-Si-C), and carbosiloxane linkages (C-Si-O-Si-C). The processing and properties of these silicon-containing phthalonitriles were evaluated. While similar compounds with diphenyl-substitution have been recently investigated in literature the three monomers considered in this manuscript have not been investigated.<sup>30, 51-52</sup> Furthermore, this manuscript addresses the complex degradation mechanisms of silicon-containing phthalonitriles. It also includes information not often reported for phthalonitrile resins, such as coefficient of thermal expansion and long-term (~4000 hour) oxidative aging behavior. Synthetic routes were developed, and the monomers and their precursors were synthesized in high yields. Compounds were analyzed by nuclear magnetic resonance spectroscopy, Fourier transform infrared spectroscopy, elemental analysis, X-ray crystallography, and differential scanning calorimetry. The monomers were mixed with a catalytic amount of bis(4-(4-aminophenoxy)phenyl)sulfone. The pre-polymer mixtures were analyzed by differential scanning calorimetry and parallel plate rheology. The effect of purity and catalyst content were considered. The resins were cured to 350-375 °C under nitrogen. Cured polymer samples were characterized by acoustic density scans, Fourier transform infrared spectroscopy, differential scanning calorimetry, thermo-mechanical analysis, dynamic mechanical analysis, thermogravimetric analysis, infrared spectroscopy-thermogravimetric analysis, and an oxidative aging study. Glass transitions, coefficients of thermal expansion, and degradations in air and nitrogen are reported. After exposure to air for 5000 hours at 250 °C, aged carbosilane-phthalonitrile samples were removed and analyzed by optical

microscopy, energy dispersive spectroscopy, Fourier transform infrared spectroscopy, Knoop hardness measurements, and X-ray micro-computed tomography. Four zones of degradation were identified. Chemical and physical changes were observed providing insight into degradation routes.

Background Information, extended exposure to high service temperatures results in chemical and physical aging. Mass loss, volume shrinkage, cracking, discoloration, and a degradation of thermo-mechanical and mechanical properties can occur.<sup>10</sup> Kinetically slow processes may dominate that are not evident in TGA experiments. Oxidative degradation is limited by the rate of diffusion of oxygen into the sample. Additionally, the mode or rate of degradation at isothermal conditions may change over time with the formation of cracks or a silica-rich boundary layer. Other oxidative crosslinking reactions and further curing is also possible due to the increased time for backbone motion. Additionally, while dynamic TGA experiments are generally concerned with degradation at higher temperatures (for high temperature polymers > 350 °C), actual service temperatures are usually below these temperatures. However, the modes of degradation may also change with temperature. In some rare cases polymers may even experience greater weight losses at lower temperatures (i.e. 200 °C) during isothermal experiments than they do at higher temperatures (i.e. 300 °C)<sup>200</sup> This may occur due to further curing of the material or the formation of silica. For these reasons, polymers may not show the same trends in stability when comparing dynamic TGA experiments and isothermal aging data. Thus, if the material in service will see high temperatures for long durations, short-term or accelerated tests may not provide accurate data. For the most accurate predictions of behavior, aging conditions should be selected to mimic expected service conditions.<sup>1</sup>

Specifically, many phthalonitrile polymers experience significant weight losses, volume shrinkage and cracking during extended exposure to air at high temperatures.<sup>4, 19, 22-23, 26, 29</sup> Furthermore, oxidative aging studies of durations longer than 48 hours and subsequent analysis of degradation regions, are rarely reported in phthalonitrile literature. Such experiments are critical in gaining an understanding of material degradation modes and behavior in service.

Samples were aged in circulating air at 250 °C. Weight and volume changes were tracked during several thousand hours of exposure. To investigate the degradation modes of aged silicon-containing PN polymers, CSPN-U (6 wt.% *p*-BAPS) samples were removed after exposure for

5000 hours. These samples were analyzed by optical microscopy, SEM/EDS, FTIR, micro-CT, and Knoop hardness measurements. Four zones of degradation were identified.

## 8.1 Experimental

### 8.1.1 Materials and Methods

Samples of commercial phthalonitriles PN1, PN2, and PN3 were supplied by the Air Force Research Laboratory Polymer Matrix Composites Group. CSPN-U, CSPN-P, and CSOPN-P samples were cut from panels produced in previous chapters of this work. For thermo-oxidative stability (TOS) characterization, 12.7 mm x 12.7 mm x 3.3 mm samples were aged in air at 250 °C using a thermocouple-controlled Blue-M Ultra-Temp oven. Fourier transform infrared (FTIR) spectroscopy was conducted using a Thermo Scientific Nicolet 6700 with Spectra Tech Inc. attenuated total reflection (ATR) accessory and Thermo Electron Corp. Nicolet Continuum microscope. Energy dispersive spectroscopy (EDS) was conducted at 5 kV and 20 μm aperture using a Zeiss Gemini 500 with an Oxford Instruments X-Max Extreme detector. Optical microscopy was performed using a Nikon Eclipse LV100. Hardness testing was conducted using a Phase II model 900-390 micro-Vickers hardness tester equipped with a Knoop indenter. Micro X-ray computed tomography (Micro-CT) was conducted with a Zeiss Versa XRM 520 with 0.4x and 4x optics, and 1601 projections at 60 kV/5 W. Images were reconstructed with filtered-back projections (FBP) and processed with Dragonfly software.

## 8.2 Results and Discussion

### 8.2.1 Long-Term Thermo-Oxidative Stability (TOS) Study

The aging temperature of 250 °C was selected based on the needs of the power electronics industry and results of the phthalonitrile aging study performed by Koerner et al.,<sup>96</sup> where PN polymers exhibited cracking and significant degradation within 150 hours at 329 °C. Figure 119 and Figure 120 and provide weight loss and volume loss data, respectively. Table 22 provides data on the time until 5% or 10% weight loss was observed, and the steady state slope after the initial 1500 hours. It is of note that commercial PN polymers were removed before reaching 10% weight loss. PN2 was removed after 4400 hours due to extensive cracking. Phthalonitrile PN1 retained 92% weight after 10,000 hours.

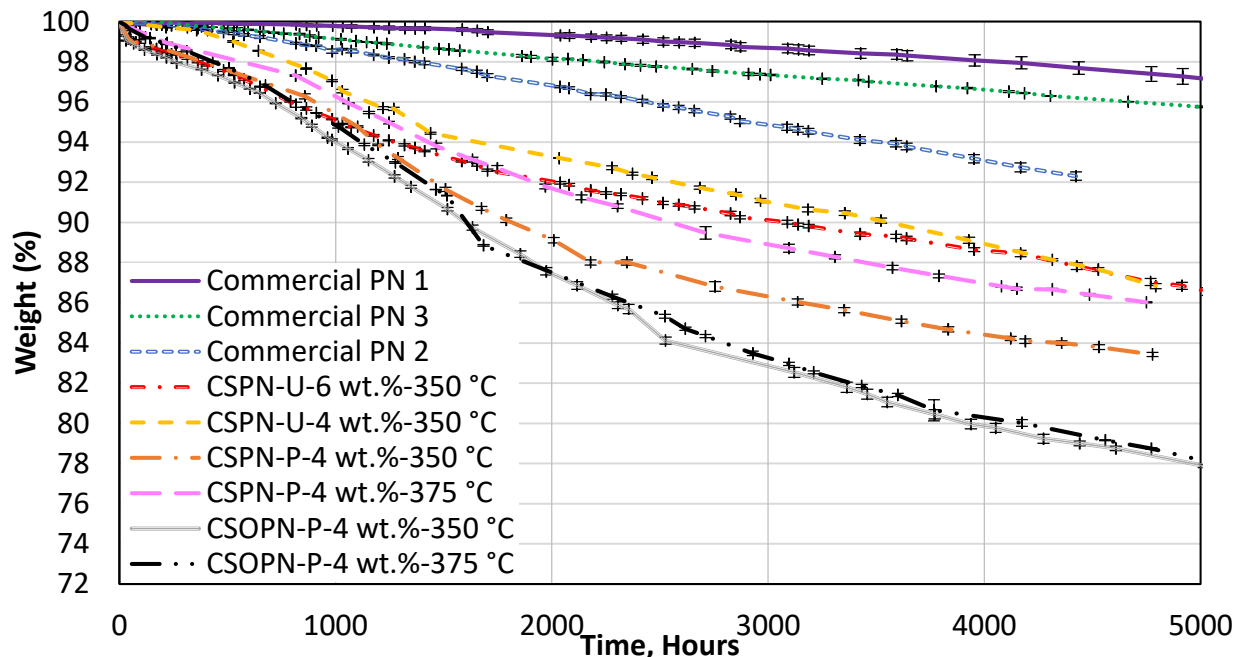


Figure 119: Weight change of silicon-containing and commercial phthalonitriles during oxidative aging in air at 250 °C. CSPN and CSOPN polymers were cured to 350 °C for 4 hours and 0 or 3 hours at 375 °C. Sample nomenclature is as follows: monomer - wt.% p-BAPS- max curing temperature. Data is included on PN3 from AFRL.<sup>242</sup>

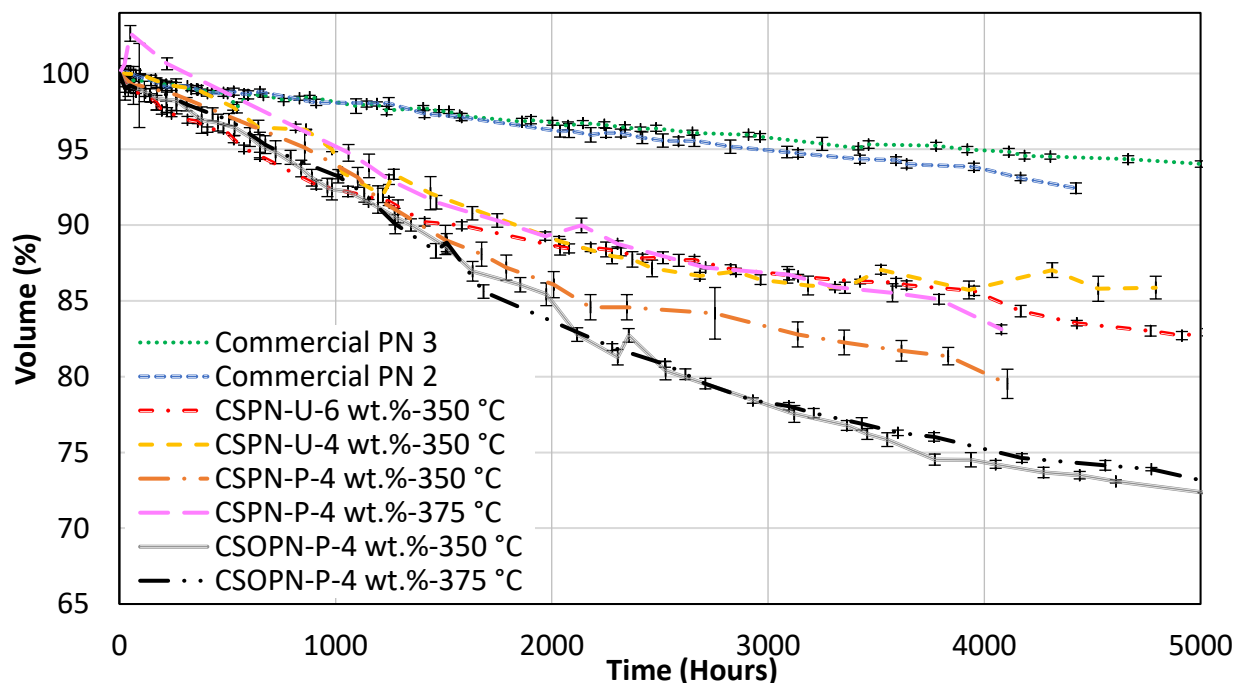


Figure 120: Volume change of silicon-containing and commercial phthalonitriles during oxidative aging in air at 250 °C. CSPN and CSOPN polymers were cured to 350 °C for 4 hours and 0 or 3 hours at 375 °C. Sample nomenclature is as follows: monomer - wt.% p-BAPS- max curing temperature. Data is included on PN3 from AFRL.<sup>242</sup>

Table 22: Oxidative aging results of phthalonitrile resins. The times until 5% and 10% weight loss are provided as  $t_{5\%}$  and  $t_{10\%}$ . The steady state slope was calculated using data after the initial 1500 hours of exposure. The time until cracking was first observed in at least one sample is provided as  $t_{Crack}$ . Weight and volume % at the onset of cracking is also provided.

Polymer	$t_{5\%}$ (Hr.)	$t_{10\%}$ (Hr.)	Slope (Wt.%/Hr.)	$t_{Crack}$ (Hr.)	Wt. % at $t_{Crack}$	Vol. % at $t_{Crack}$
Commercial PN1	7030	-	-0.0009	-	-	-
Commercial PN2	2900	-	-0.0019	2400	96.1	95.8
Commercial PN3*	5990	-	-0.0008	7500	93.5	91.5
CSPN-U-6 wt.%-350 °C	1010	3090	-0.0018	3900	88.6	85.7
CSPN-U-4 wt.%-350 °C	1360	3560	-0.0022	4300	88.1	87.0
CSPN-P-4 wt.%-350 °C	1070	1810	-0.0023	3600	85.1	81.7
CSPN-P-4 wt.%-375 °C	1240	2550	-0.0024	3600	87.8	85.5
CSOPN-P-4 wt.%-350 °C	870	1600	-0.0033	4800	75.8	71.0
CSOPN-P-4 wt.%-375 °C	970	1610	-0.0030	5300	77.6	71.5

\*Includes unpublished data from reference <sup>242</sup>

Among polymers, the same general trends in stability were observed in weight changes and volume changes. Overall, CSPN and CSOPN polymers experienced significantly more weight and volume losses than commercial organic resins. Their steady state weight loss rates were also higher. Commercial resins followed roughly linear trends in weight and volume loss. In contrast, silicon-containing resins showed relatively repeatable S-shaped curves, becoming roughly linear only after ~1500 hours. This may indicate shifts in degradation mechanisms as reacting species were generated and consumed and diffusion limits are reached. Interestingly CSPN-P-4 wt.%-375 °C showed an initial increase in volume. The cause of this is unknown, especially given that the residual stresses of these samples should have been relieved after post-curing above the  $T_g$ . Ignoring this initial increase in volume of CSPN-P-4 wt.%-375 °C, CSPN-P polymers showed substantially higher losses than CSPN-U. This agrees with previously observed TGA behavior. While there is some initial difference in CSPN-U with 4 and 6 wt.% *p*-BAPS, overall the two polymers showed similar degradation rates, both reaching 13% mass loss after 4800 hours. The lower initial value of CSPN-U with 6 wt.% *p*-BAPS may be due to greater mass loss from volatilization of the curing additive. The less negative steady state slope of CSPN-U with 6 wt.% *p*-BAPS is likely due to an increased degree of cure.

CSPN-P polymers showed lower losses than CSOPN-P polymers. Several considerations may explain this difference in stability. It has been reported that triphenyl-substituted silanes undergo

rearrangement mechanisms, whereas tetraphenylsilane must first undergo free-radical cleavage of an Si-Phenyl bond.<sup>178</sup> The activation energies for degradation of tetraphenylsilane and triphenylsilane were reported to be 325 kJ/mol and 293 kJ/mol, respectively. It is interesting that the ratio of these energies ( $E_{\text{tetraphenylsilane}}/E_{\text{triphenylsilane}} = 1.1$ ) corresponds well with the ratios of the steady state slopes of CSPN and CSOPN materials (1.1-1.2). The difference in stability may also be explained by the presence of 4 phenyl functional groups in CSOPN as compared with 2 in CSPN. Assuming cleavage of Si-Phenyl bonds plays a key role in the degradation of these polymers, then the increase in Si-Phenyl content would result in increased mass loss. The observed difference in mass loss rate is less than what would be expected if the cleavage of Si-Phenyl was the sole degradation mechanism. This is of course due in part to the presence of additional degradation mechanisms involving other portions of the polymer chain. CSOPN-P polymers cured to 350 °C and 375 °C exhibited nearly identical behavior. Some initial difference was observed in CSPN-P polymers, but steady state degradation rates were similar.

Cracking was observed in all resins except PN1. The weight and volume changes did not directly correlate with cracking. CSPN samples showed minor cracking after 3600-4300 hours. Example images of CSPN-U with 6 wt.% *p*-BAPS, cured to 350 °C for 4 hours, are provided in Figure 121. Conversely CSOPN-P samples did not exhibit cracks until after 4800-5300 hours, despite experiencing greater weight and volume losses. PN2 exhibited much lower weight and volume change as compared with CSPN and CSOPN polymers, but showed severe pitting and cracking, Figure 122. CSPN-U survived longer without cracking as compared with CSPN-P. Curing to 375 °C did not affect the aging time before cracking for CSPN-P, but did increase the time for CSOPN-P.

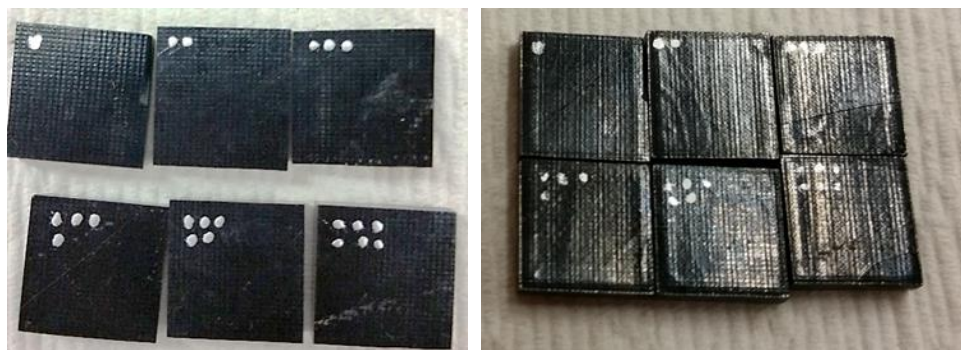


Figure 121: Samples of CSPN-U with 6 wt.% *p*-BAPS cured to 350 °C for 4 hours; aged at 250 °C for 0 hours (left) and 4400 hours (right).



Figure 122: Samples of PN2 cured to 350 °C for 4 hours; aged at 250 °C for 0 hours (left), 720 hours (middle) and 4200 hours (right).

### 8.2.2 Analysis of Aged CSPN-U samples

CSPN-U-6 wt.%-350 °C samples were removed after 5000 hours and FTIR (ATR) was performed on the surface and crack morphology was characterized by micro-CT. Some samples were cross-sectioned, mounted in epoxy, and polished. Polished samples were characterized by optical microscopy, FTIR microscopy, and Knoop hardness testing. Additional samples were coated with Au/Pd and used for SEM/EDS characterization. FTIR, Knoop hardness, and EDS measurements were also completed on unaged samples. No cracks, visible boundaries, or compositional or chemical gradients were observed in unaged specimens. Figure 123 and Figure 124 provide optical micrographs of aged samples. A boundary was evident between a surface degradation region and inner core at a depth of 700-950  $\mu\text{m}$ . Macro-cracks penetrated 400-700  $\mu\text{m}$  into the degradation region, running perpendicular to the surface, but did not penetrate the inner core. Micro-cracks were also observed running parallel to the surface at a depth of 50-100  $\mu\text{m}$ . Micro-crack thicknesses were on the order of 4-16  $\mu\text{m}$ . In some cases, it appeared at the micro-cracks did not connect with the surface or macro-cracks.

Micro-CT was conducted to investigate whether these micro-cracks were present in the degraded material or were formed during sectioning and polishing. Example projections are provided in Figure 125. Some microcracks were observed connecting macro-cracks. However, the micro-cracks observed at 50-100  $\mu\text{m}$  in optical microscopy were not evident in CT data. This indicates that the cracks formed during sample preparation. Yet, the presence of these cracks in polished samples still indicate a degraded and weaker region. Regions with cracks were avoided when taking hardness, EDS, or FTIR measurements. SEM/EDS data is provided in Figure 126, Figure 127, and Table 23. The atomic composition of the unoxidized inner core matched that of

unaged samples. The atomic percent of silicon and oxygen were higher near the surface, and carbon atomic percent diminished. This agrees with oxidation and formation of  $\text{SiO}_2$  near the surface. As expected the atomic % of carbon and oxygen show inverse trends as a function of depth into the sample, Figure 126. This is due to oxidation of organic and volatilization of groups. Interestingly the atomic % of silicon and nitrogen are roughly inversely proportional. This indicates volatilization of the nitrogen-containing portions of the chain, including isoindoline, triazine, phthalocyanine, and residual phthalonitrile and cyano groups.



Figure 123: Mounted and polished cross-section after aging for 5000 hours at 250 °C, taken with 2.5x objective lens. The surface layer measured approximately 0.7-0.95 mm thick.

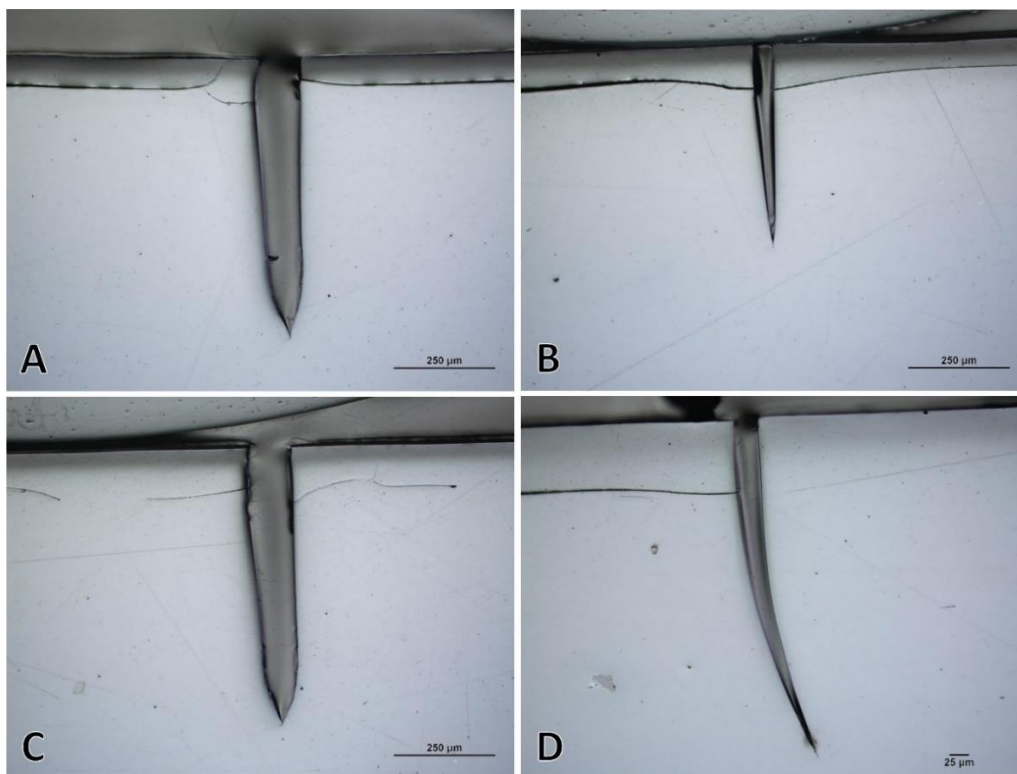


Figure 124: Optical microscopy of cracks in aged samples. Images A, B, and C were taken with a 10x objective, image D was taken using a 20x objective. Larger cracks run perpendicular to the surface (top of images) with crack lengths of 430-650  $\mu\text{m}$ . Microcracks run parallel at a depth of 50-100  $\mu\text{m}$ .

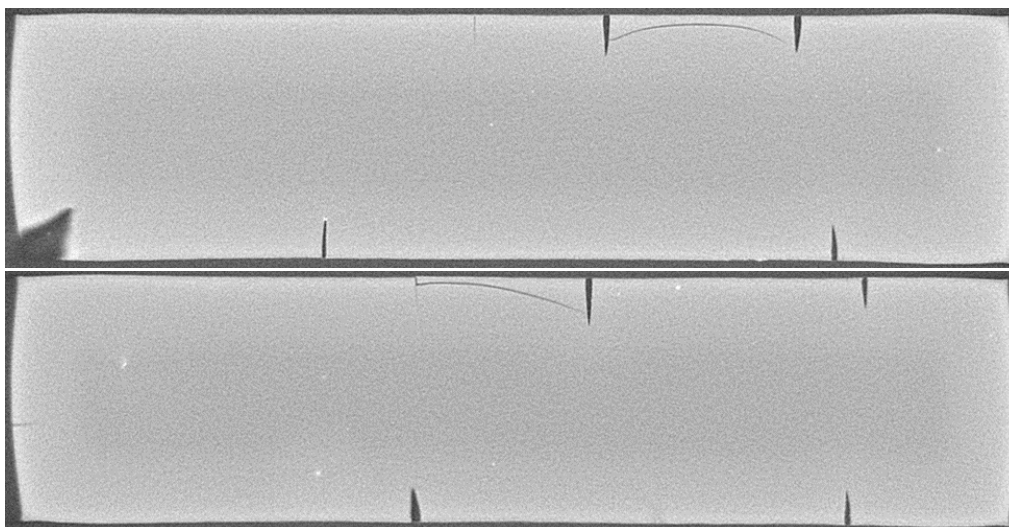


Figure 125: Two example micro X-ray CT projections showing slightly darker inner core, macro-cracks perpendicular to the surface, and micro-cracks between macro-cracks.

Table 23: Semi-quantitative EDS data in atomic % of areas near the surface and in the center of CSPN samples cured at 350 °C for 4 hours and aged at 250 °C for 5000 hours.

	C (At. %)	N (At. %)	O (At. %)	Si (At. %)
<b>Aged-Surface Layer</b>	58.3	15.4	21.7	4.63
<b>Aged-Inner Core</b>	75.6	15.4	6.40	2.65
<b>Unaged</b>	76.34 ± 1.16	15.02 ± 0.95	5.98 ± 0.27	2.66 ± 0.19

An FTIR microscopy map with a resolution of 25 μm is provided in Figure 128. The disappearance of Si-Phenyl peaks is observed along with the formation of siloxy and siloxane groups. The formation of carbonyl and hydroxyl groups were also observed near the surface. Figure 129 provides representative spectra of the surface of unaged samples, the surface of aged samples prior to sectioning, and at various locations in the bulk. The FTIR-ATR spectra of the unaged sample matches the FTIR-microscopy spectra of the center of the aged samples. The ATR spectra of the aged surface prior to sectioning matches the FTIR-microscopy spectra of the surface after sectioning, mounting, and polishing. Knoop hardness data is provided in Figure 130. In the inner core region observed in optical microscopy the hardness is constant. At the edge of the inner core, hardness begins to first increase before decreasing at the surface. Figure 131 provides a compilation of Knoop hardness and EDS atomic % data (top) and heights of selected IR peaks (bottom) as a function of distance from the surface.

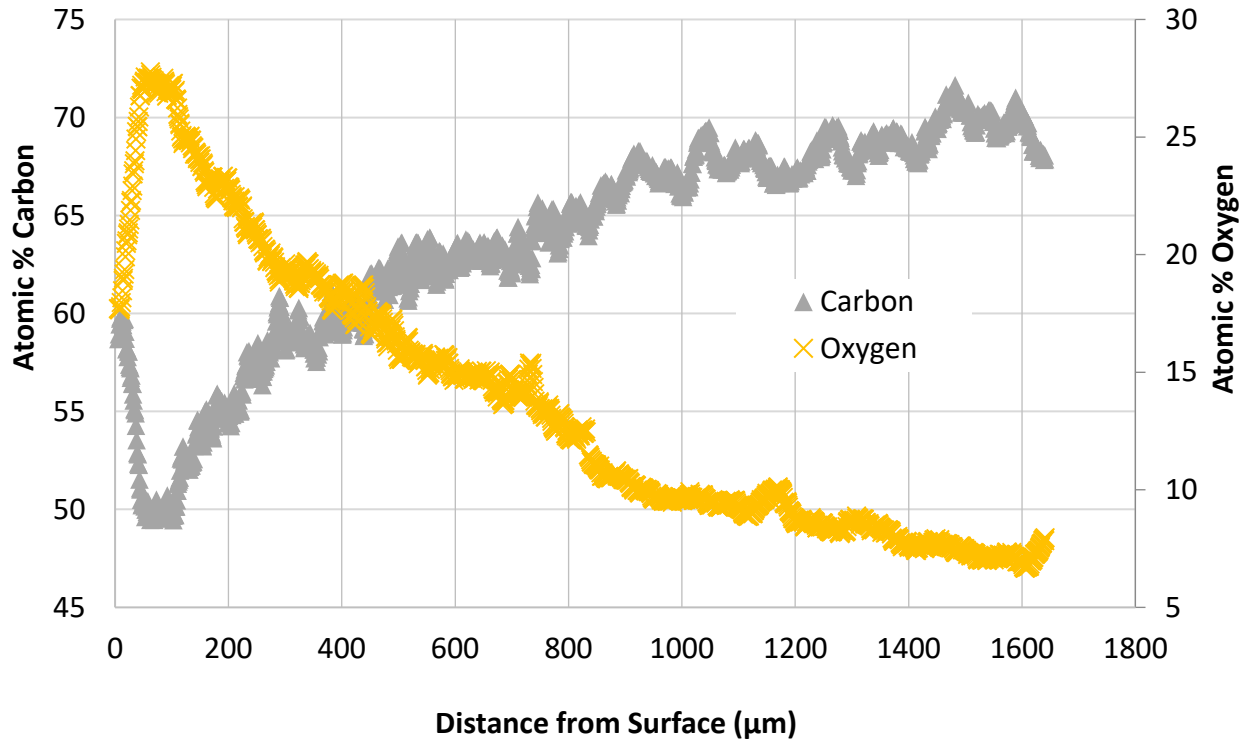


Figure 126: SEM/EDS data for atomic % of carbon and oxygen as a function of depth into the sample (distance from the surface). Trends in carbon and oxygen percent are roughly inversely proportional.

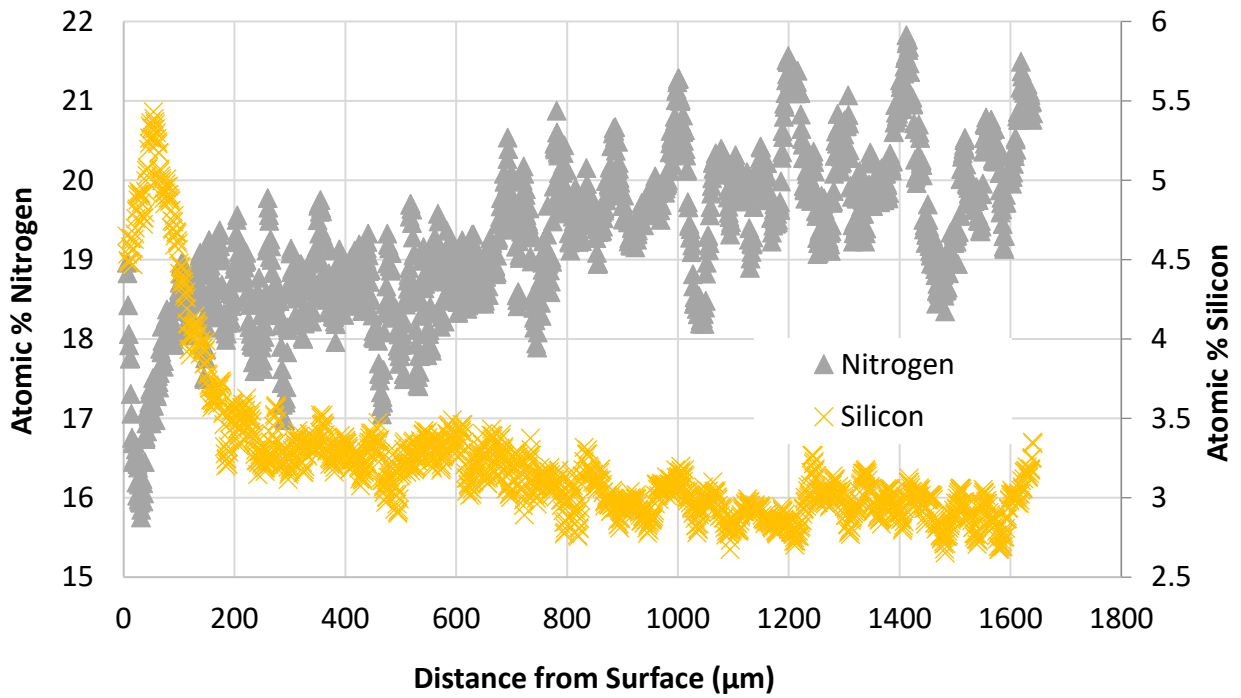


Figure 127: SEM/EDS data for atomic % of nitrogen and silicon as a function of depth into the sample (distance from the surface). Trends in nitrogen and silicon percent are roughly inversely proportional.

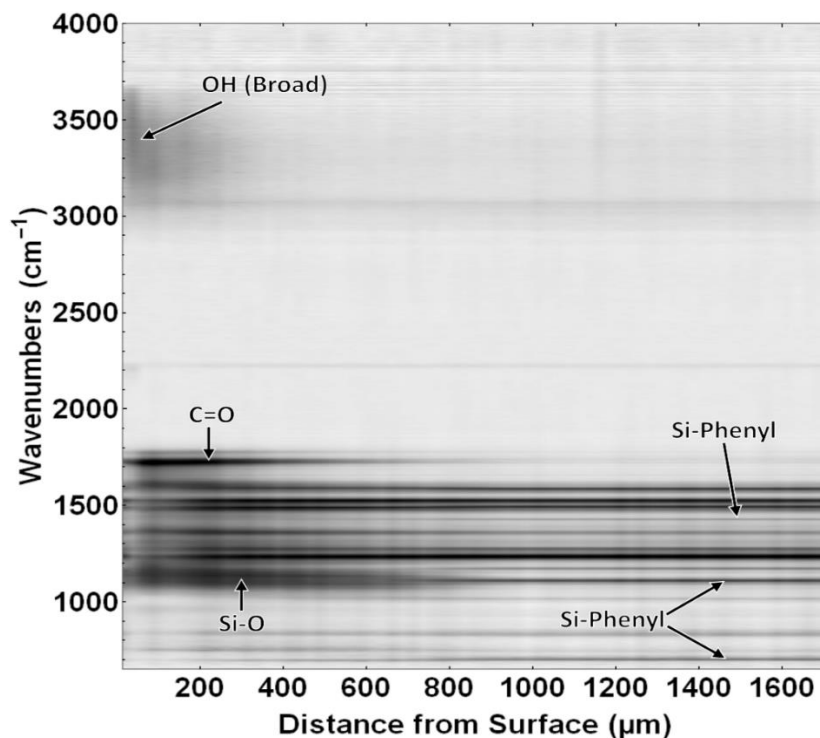


Figure 128: Intensity map of IR spectra as a function of depth from the surface of aged CSPN samples. Samples were cured at 350 °C for 4 hours and aged at 250 °C for 5000 hours. Darker regions correspond to greater absorbance.

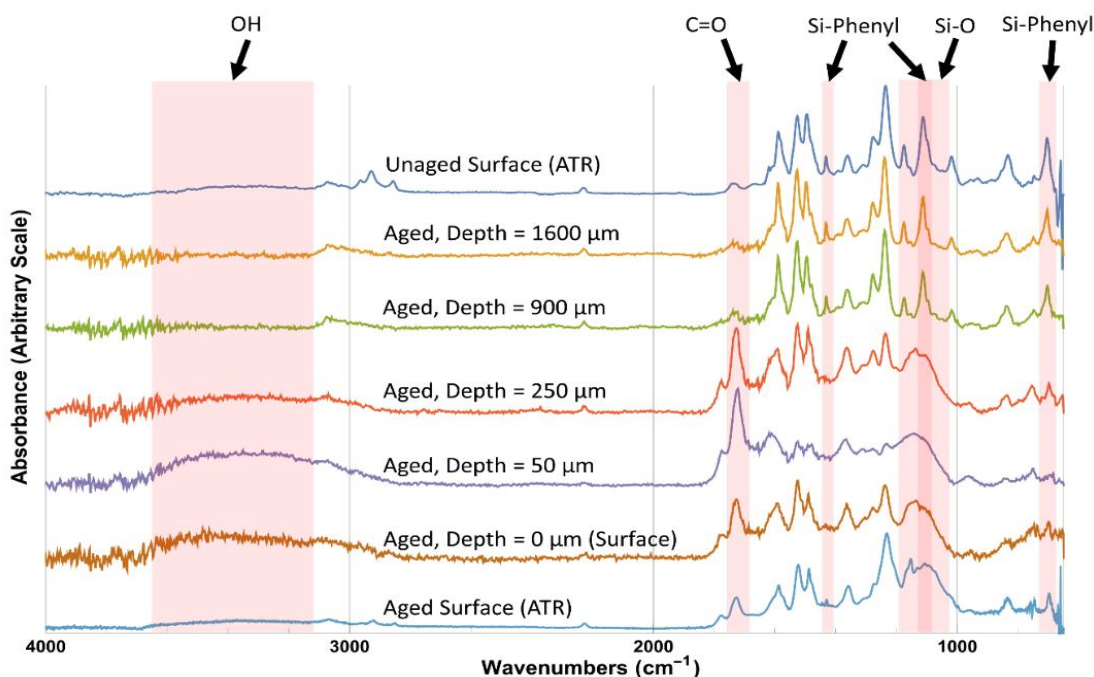


Figure 129: IR microscopy (diffuse reflectance) was used to produce representative spectra at varying depths from the surface of aged CSPN samples. IR spectra (ATR) of the aged and unaged sample surfaces, taken prior to mounting and polishing, are also provided for reference. Samples were cured at 350 °C for 4 hours and aged at 250 °C for 5000 hours.

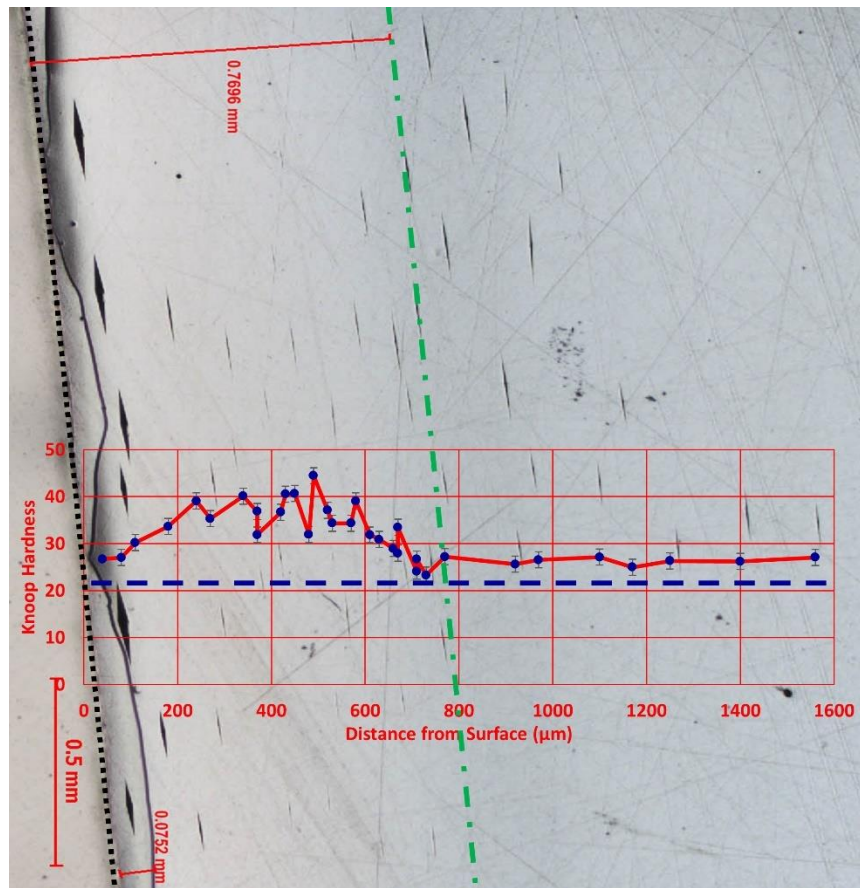


Figure 130: Knoop hardness data of aged CSPN sample. Data points were discarded if the indentation was within 40 μm of cracks, the sample edge, or other indentations. The edge of the sample is denoted by a black dotted line. The green dot-dashed line denotes the boundary of the inner core observed optically. Unaged samples exhibited hardness values of  $21.4 \pm 1.7$ , as denoted by the blue dashed line.

In Figure 131, four distinct zones were assigned to the data. Zones 1-3 generally agree with regions defined in the three-zone thermo-oxidative degradation model, but with the addition of oxidative crosslinking mechanisms in the active zone.<sup>62</sup> Zone 1 (>920 μm) corresponds to the unoxidized region where little degradation was observed. The IR spectra and EDS atomic composition generally matched that of unaged samples. A slight decrease in carbon with corresponding increase in oxygen was observed, indicating some diffusion of oxygen into the bulk and subsequent oxidation. The hardness of zone 1,  $26.2 \pm 0.7 \text{ kgf} \cdot \text{mm}^{-2}$ , was slightly higher than unaged samples, which gave values of  $21.4 \pm 1.7 \text{ kgf} \cdot \text{mm}^{-2}$ . This increase in hardness likely indicates additional curing occurred during aging. The boundary between zones 1 and 2 agrees with the boundary visible in optical microscopy.

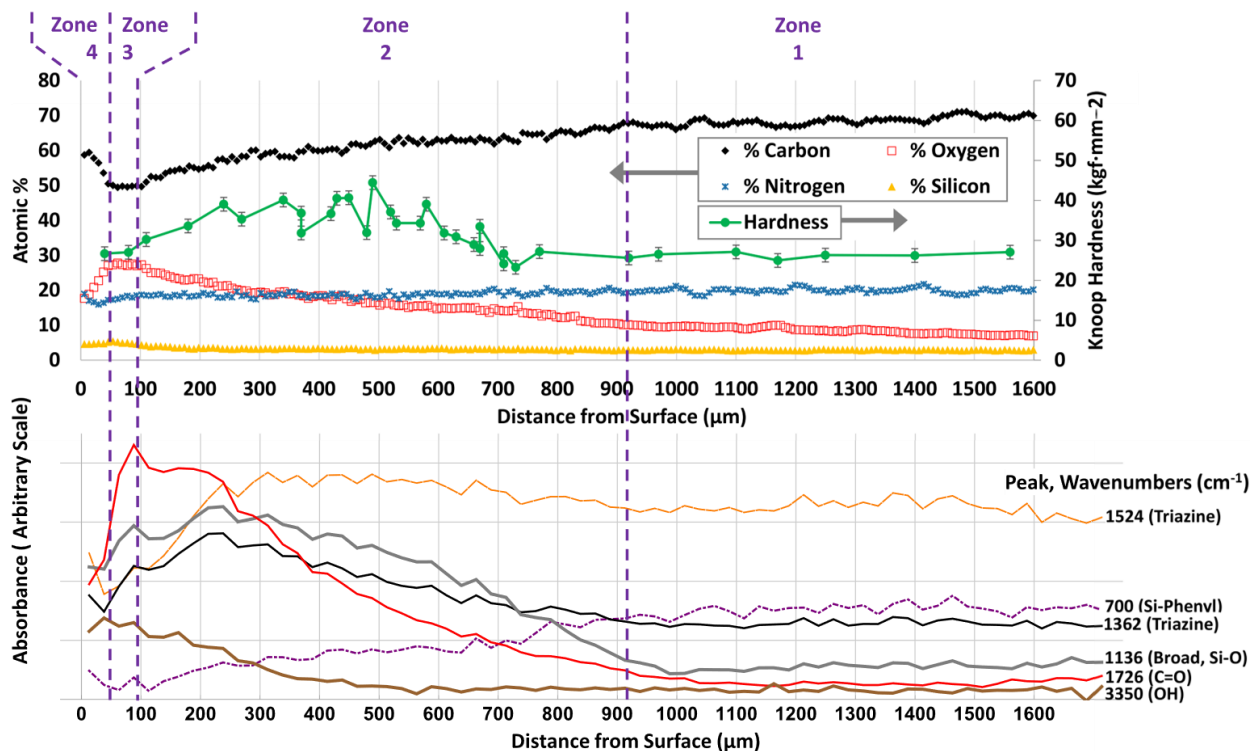


Figure 131: Compilation of property changes of an aged and cross-sectioned CSPN sample, as a function of depth from the surface (left) into the bulk (right). Knoop hardness and EDS atomic % data are included in the top portion of the graph. Hardness is denoted by the connected line and corresponds to the right vertical axis. The left vertical axis denotes atomic % of C, O, Si, and N, given as points. In the bottom graph, the intensities of selected IR wavenumbers are presented. Each wavenumber peak is labeled on the right. Four distinct zones are assigned. Dashed vertical lines denote boundaries of the assigned zones. Zone 4 corresponds to the very surface (0-50  $\mu\text{m}$  depth). Zone 3 (50-100  $\mu\text{m}$ ) corresponds to the degraded region. The active region coincides with zone 2 (100-920  $\mu\text{m}$ ). The unoxidized bulk is observed at depths >920  $\mu\text{m}$ , zone 1.

In the active zone, zone 2 (100-920  $\mu\text{m}$ ), several trends were visible approaching the surface from the bulk. A gradient of decreasing atomic percent of carbon and increasing atomic percent of oxygen was evident. A slight decrease in atomic percent of nitrogen and increase in silicon was also observed. From 100-740  $\mu\text{m}$ , hardness increased with values of 32-45  $\text{kgf}\cdot\text{mm}^{-2}$ . In the IR spectra, decreases were observed for peaks related to Si-phenyl at 700  $\text{cm}^{-1}$  and aromatic C=C at 1587  $\text{cm}^{-1}$ . Increases were observed in the characteristic peaks for triazine at 1360 and 1520  $\text{cm}^{-1}$ , the Si-O system at 1000-1150  $\text{cm}^{-1}$ , C=O peaks at 1730  $\text{cm}^{-1}$ , and a broad OH peak at 3350  $\text{cm}^{-1}$ . The increase in hardness may be explained by crosslinking reactions through the formation of Si-O-Si bonds, as well as additional crosslinking from nitrile groups. Crosslinking via the formation of Si-phenyl-Si linkages by proton abstraction with benzene evolution, or Si-biphenyl-Si linkages by phenyl dehydrogenation was also possible.<sup>168</sup> The formation of Si-O phases required cleavage

of Si-phenyl bonds in the tetraphenylsilane moiety. The Si-phenyl bond strength is reported to be lower than what may be expected. When attached to silicon, the phenyl group has been shown to be slightly electron donating. This is due to interaction of the silicon d orbitals with the phenyl group  $\pi$  system.<sup>78</sup> Thus, the dissociation energies of tetraphenylsilane ( $354 \pm 10 \text{ kJ}\cdot\text{mol}^{-1}$ ) is significantly lower than that of its carbon analogue, tetraphenylmethane ( $404 \pm 5 \text{ kJ}\cdot\text{mol}^{-1}$ ).<sup>177</sup>

This cleavage of Si-phenyl bonds was reported to occur via a free radical mechanism to produce triphenylsilyl products and phenyl radicals.<sup>78, 169, 178</sup> Once cleavage of an Si-phenyl bond occurred, then oxidative crosslinking, disproportionation reactions, chain branching mechanisms, and other rearrangements of the structure were possible.<sup>77-78, 168-169, 178-180</sup> Oxidation of the silicon resulted in the formation of siloxy units which condensed to form siloxane bridges.<sup>48</sup> In systems with higher silicon content, this mechanism is reported to result in the formation of a silica rich region. It is likely however, that the silicon content of this system was too small to effectively form a protective boundary layer.

In the fully oxidized region, zone 3 (50-100  $\mu\text{m}$ ), the material was significantly degraded and depolymerization dominated. In EDS data, approaching the surface, the gradient of decreasing atomic % of carbon and increasing atomic % oxygen continued. A slight increase in silicon corresponded to slight decrease in nitrogen, indicating some volatilization of organic sections of the polymer structure leaving a higher concentration of organosilicon moieties. Hardness decreased in this zone to values of 26-27  $\text{kgf}\cdot\text{mm}^{-2}$ . In IR spectra, C=O and OH dominated, while all other peaks decreased. C=O formation results from oxidation of organic portions of the chain, while the OH broad system was likely a combination of C-OH and Si-OH.

An interesting phenomenon was observed close to the surface in zone 4 (0-50  $\mu\text{m}$ ), with the reversal of EDS and IR trends, giving the appearance of reduced degradation near the surface. The zone was repeatable with multiple scans on different samples. This behavior may be explained by polishing effects, such as debris building up at the edge or becoming lodged in cracks and porous regions. However, the ATR spectra of the surface taken prior to mounting and polishing, matches the IR microscopy spectra at depth = 0, refuting this explanation. It is also possible that a surface region could have formed during processing, prior to aging. However, no such zone was observed in IR microscopy of mounted and polished unaged samples. One possible explanation may be the formation of a condensation zone from thermal cycling. Samples were removed from the oven

each time a measurement was performed. Since the surface of the sample cooled faster than the bulk, condensation of volatilized species present in the resin or atmosphere may have occurred in this region. An alternative explanation may be provided by differing chemical and thermo-mechanical properties between the surface and zone 2. This could have resulted in a region of higher stress present in zone 3, and thus increased degradation. This explanation is supported by the occurrence of micro-cracks running parallel to the surface at a depth of 50-100  $\mu\text{m}$  after sectioning. Additional experimentation is required to fully explain the existence of this zone.

### 8.3 Conclusions

Weight and volume retention during oxidative aging followed the trend of  $\text{PN1} > \text{PN3} > \text{PN2} > \text{CSPN-U} > \text{CSPN-P} > \text{CSOPN-P}$ . PN1 exhibited the overall highest stability, retaining 91.6 wt.% after more than 1 year of exposure. The greater weight losses of the CSPN and CSOPN polymers could be attributed to homolytic cleavage of Si-phenyl bonds due to the lower Si-C bond energy. Alternatively, the increased weight and volume loss could also be due to a potentially lower degree of cure from either steric hindrance of the bulky and rigid phenyl-substituted backbone, or lower effective reactivity of the catalyst/monomer system possibly due to phase separation. Unpurified CSPN performed better than purified CSPN. This agrees with TGA results observed in the previous chapter. A minor improvement in stability is observed after curing to 375 °C. The onset and degree of cracking did not directly correlate with magnitude of weight or volume loss.

A toughening effect may be observed as CSPN and CSOPN polymers exhibited greater weight and volume losses before the onset of cracking, as compared to PN2 and PN3. This may be due to the formation of flexible siloxane linkages or a lower initial crosslinking density. Cracking in silicon-containing PNs occurred after PN2, but before PN3. PN1 did not crack after over 1 year of exposure.

Four zones were identified in aged samples. First, the core of samples consisted of a region where oxidation was not present but some physical/chemical aging occurred. Second, an active zone existed where oxygen diffused into the sample and interacted with reacting species. Competing crosslinking and degradation mechanisms result in chemical and physical gradients in this region. Towards the bulk, crosslinking mechanisms are prominent while nearer to the surface

oxidation and cleavage dominates. The formation of Si-O phases was observed, however there was likely insufficient silicon content to form a protective barrier layer and inhibit further diffusion of oxygen. Third, a significantly degraded region was observed where reacting species had been consumed, and composition and properties were constant. These three regions generally agree with previously published literature on the three-zone degradation model, with the addition of oxidative crosslinking in the active zone.<sup>62</sup> Interestingly, a fourth zone was observed at the surface where trends in the chemistry and composition reversed. Additional experimentation is required to fully explain the existence of this region.

## 9 Summary and Conclusions

### 10 Overall, polymer exhibited high thermal and oxidative stability as compared with much of the organosilicon literature discussed in Chapter 1 Introduction

The inclusion of organosilicon moieties into phthalonitrile resins may provide a feasible route to maintaining processing characteristics while improving thermo-oxidative stability for high temperature applications.

Since the onset of research into high temperature polymers in the 1950's, work has been governed by technological need, economic opportunity, and academic pursuit. Today, high temperature materials are a small but critical class of polymers, present in many applications that touch our daily lives. Applications for thermally and environmentally stable polymers include: 1) aerospace composites 2) electronics and microelectronics. 3) space applications 4) optoelectronics and other optical applications 5) structural reinforcements, 6) automotive parts including composites for high performance vehicles, brake pads binders, and filters, 7) other filters and membranes 8) structural and insulating foams, 9) fire resistant materials, 11) tooling, 12) moldings, 13) coatings, 14) gaskets, sealants, tubing, and pipes, and 15) components for the energy sector including geothermal, nuclear, and petroleum systems.<sup>1-9</sup>

Specifically, in this work, motivation is derived from aerospace composites and wide band-gap power modules. For aerospace composites, polymer matrix materials are needed for long-term use above 300 °C. High temperature polymers and polymer composites are required for advancement of supersonic and hypersonic aircraft as well as subsonic civilian transport.<sup>10</sup> Replacement of metal structures with polymer composites results in valuable weight savings, and in turn improvements in performance and fuel efficiency.<sup>11</sup> Similarly, polymer encapsulation compounds are an enabling technology for wide band-gap power modules for use above 250 °C. Such devices promise improved thermal and mechanical durability, lower power losses, higher switching speeds and current densities, increased durability and reliability, greater resistance to ionizing radiation, and reduced weight.<sup>12-14</sup> The operating temperatures for both applications are well above the useful range for other polymers including silicones and epoxies.

In polymers, continuous exposure at elevated temperatures or intermittent exposure to extreme temperatures results in chemical and physical aging and decomposition. Mass loss, volume shrinkage, cracking, discoloration, and a degradation of thermo-mechanical and mechanical

properties can occur.<sup>10</sup> High temperature polymers must be able to resist degradation of their properties during operation in extreme environments with long exposure times, cyclic heating, and intense temperature spikes.

Many different chemistries have been evaluated and developed including polyimides, bismaleimides, phenolics and benzoxazines, fluorinated polymers, poly(arylene ethers), cyanate esters, and phthalonitriles. However, opportunities for improvement exist as applications demand greater temperature capabilities and improved processing. Resins are sought with reduced cost, good solubility in common solvents, low softening temperatures, stable and easily controllable melt viscosities, large processing windows, lower cure temperatures, and minimal volatile evolution. For processed polymers, even greater thermal and oxidative stability, higher glass transition temperatures, improved toughness, excellent mechanical strength and modulus, and improved retention of mechanical properties at elevated temperatures are desired. A greater understanding of degradation and aging mechanisms is also needed.<sup>10</sup>

One resin system currently growing in popularity is phthalonitriles (PNs). PN based resins show great promise for high temperature applications and easier processing. Research into phthalonitrile polymers began in earnest at the U.S. Naval Research Lab in the 1980's. Phthalonitrile monomers possess low melt viscosities and are soluble in many common solvents. Curing occurs at elevated temperatures with the addition of a catalyst, usually a thermally stable aromatic amine. The curing reaction progresses by addition polymerization via the phthalonitrile cyano groups and does not produce volatile by-products, facilitating the fabrication of dense components.<sup>15</sup> State-of-the-art cured resins possess high flammability resistance, excellent mechanical and dielectric properties, and low water absorption.<sup>9, 16-19</sup>

Although these materials show exceptional thermal and oxidative stability in thermogravimetric experiments and during hours of exposure at temperatures between 250-400 °C,<sup>6, 9, 20-28</sup> their long-term thermo-oxidative stability requires improvement to meet the challenging demands of the extreme applications. During longer exposures to air at high temperatures, many phthalonitrile polymers experience significant weight losses, volume shrinkage and cracking.<sup>4, 19, 22-23, 26, 29</sup> Furthermore, oxidative aging studies of durations longer than 48 hours and subsequent analysis of degradation regions, are rarely reported in phthalonitrile literature. Such experiments are critical in gaining an understanding of material degradation modes and behavior in service.

The incorporation of inorganic groups into the organic monomer backbone of polymers often provides a viable route for improved stability and toughness during service at high temperatures in oxidizing environments.<sup>22, 30</sup> The inclusion of silicon moieties has been reported to improve oxidative stability and flammability of high temperature polymers including cyanate ester,<sup>31-33</sup> and polyimide systems.<sup>34-44</sup> As oxygen and free radicals cleave carbon-silicon bonds, siloxy units are formed. These siloxy moieties may interact to produce the inert phase SiO<sub>2</sub>. In this case, a silica-rich surface layer forms. This layer can act as a barrier, reducing the rates of degradation of the surface and oxygen diffusion into the bulk.<sup>45-49</sup>

Thus, it is of interest to evaluate the effects of the inclusion of silicon-containing linkages on the properties of high temperature polymers, including phthalonitriles. Phthalonitriles are good candidates for hybridization with organosilicon moieties due to their ease of processing and high glass transition temperatures.<sup>3-8, 15</sup> Prior to beginning investigations for this dissertation, little research existed on silicon-containing phthalonitrile resins. However, in the last few years several groups have produced and characterized silicon-containing phthalonitrile compounds. Examples include silane,<sup>50</sup> silazane,<sup>51</sup> oxysilane,<sup>30, 52</sup> siloxane,<sup>6, 53</sup> and silsesquioxane moieties.<sup>54</sup> Additional groups have synthesized silicon-containing phthalonitrile compounds but did not report their properties as neat phthalonitrile resins.<sup>55-57</sup> While the silicon-phthalonitrile materials synthesized by these groups exhibited high thermal and thermo-oxidative stability in short-term thermogravimetric experiments, emphasis was generally placed on developing resins with low softening points and long-term stability was not characterized.

Design of hybrid organic-inorganic polymers is not a trivial matter however. Inclusion of organosilicon moieties does not in itself guarantee improvements. Literature suggests there are a number of design considerations to keep in mind to achieve desirable properties. For example, avoiding the use of benzylic or methylene bridges, the presence of phenyl functional groups on the silicon, and limiting the length of silicon-containing linkages are a few approaches reported to achieve higher glass transitions and thermo-oxidative stabilities.

The purpose of this work is to investigate the processing, properties, and degradations of the silicon-containing phthalonitrile resins for high temperature applications. Background is provided on relevant properties and measurement techniques, high temperature polymers in general, phthalonitriles, and several classes of organosilicon polymers. While a plethora of similar

compounds to those discussed in this dissertation have been synthesized and evaluated in literature for other purposes, focus here is placed primarily on high temperature applications. Thus, this work is not intended to be comprehensive of all related compounds and chemistries. In addition, focus was placed on silane, oxysilane, and siloxane chemistries. While polymers containing poly octahedral silsesquioxane (POSS) or silazane (Si-N) linkages are discussed briefly, they are mostly outside the scope of this work. A thorough investigation of various chemical synthesis techniques is also not included, though some information is provided for phthalonitriles and polyimides.

Based on available literature, three monomer structures were selected containing carboxysilane (C-O-Si-O-C), carbosilane (C-Si-C), and carbosiloxane linkages (C-Si-O-Si-C). The processing and properties of these silicon-containing phthalonitriles were evaluated. While similar compounds with diphenyl-substitution have been recently investigated in literature the three monomers considered in this manuscript have not been investigated.<sup>30, 51-52</sup> Furthermore, this manuscript addresses the complex degradation mechanisms of silicon-containing phthalonitriles. It also includes information not often reported for phthalonitrile resins, such as coefficient of thermal expansion and long-term (~4000 hour) oxidative aging behavior. Synthetic routes were developed, and the monomers and their precursors were synthesized in high yields. Compounds were analyzed by nuclear magnetic resonance spectroscopy, Fourier transform infrared spectroscopy, elemental analysis, X-ray crystallography, and differential scanning calorimetry. The monomers were mixed with a catalytic amount of bis(4-(4-aminophenoxy)phenyl)sulfone. The pre-polymer mixtures were analyzed by differential scanning calorimetry and parallel plate rheology. The effect of purity and catalyst content were considered. The resins were cured to 350-375 °C under nitrogen. Cured polymer samples were characterized by acoustic density scans, Fourier transform infrared spectroscopy, differential scanning calorimetry, thermo-mechanical analysis, dynamic mechanical analysis, thermogravimetric analysis, infrared spectroscopy-thermogravimetric analysis, and an oxidative aging study. Glass transitions, coefficients of thermal expansion, and degradations in air and nitrogen are reported. After exposure to air for 5000 hours at 250 °C, aged carbosilane-phthalonitrile samples were removed and analyzed by optical microscopy, energy dispersive spectroscopy, Fourier transform infrared spectroscopy, Knoop hardness measurements, and X-ray micro-computed tomography. Four zones of degradation were identified. Chemical and physical changes were observed providing insight into degradation routes.

Background Information.<sup>35-37, 39, 77-78, 80, 93, 102, 148-150, 155-156, 184-187, 189-193</sup> However, polymers presented in this work possessed lower  $T_g$ , lower long-term thermo-oxidative stability, and higher CTE and softening points, when compared with commercial phthalonitrile polymers. For silicon-containing polymers stability followed the trends CSPN-U > CSOPN-P > COSPN-U > CSPN-P in dynamic TGA, and CSPN-U > CSPN-P > CSOPN-P in TOS. A toughening effect was observed as CSPN and CSOPN polymers exhibited greater weight and volume losses before the onset of cracking, as compared to commercial phthalonitriles PN2 and PN3. This was likely due in part to the formation of flexible siloxane linkages. The use of oxysilane linkages is not recommended due to their lower hydrolytic stability. The shelf life of such materials would be limited by hydrolytic degradation of pre-polymer feedstock during extended storage. Furthermore, the hydrolytic degradation of pre-polymers and polymers would adversely affect thermal stability. This may explain the lower performance of COSPN-U. Given the performance of CSOPN-P, CSPN-P, and CSPN-U polymers, the behavior of as-synthesized CSOPN-U may be predicted. Compared to CSPN-U, it is expected that CSOPN-U would exhibit higher performance in TGA, slightly lower TOS, similar  $T_g$ , and improved processing due to a significantly lower softening point.

The lower stability and  $T_g$  of CSPN-P and CSOPN-P polymers was in large part due to purity. Organosilicon literature indicates that the presence of a variety of impurities, such as metal salts, organometallics, and hydroxyl groups, can catalyze the degradation of Si-O, Si-N, and Si-C bonds.<sup>77-78, 82, 180</sup> Furthermore, low molecular weight species are likely to volatilize at high temperatures, increasing weight loss and porosity formation, and decreasing density. Thus, it was originally assumed that increasing purity would result in increased stability. However, it was found that highly pure monomers resulted in severely decreased performance in comparison to as-synthesized CSPN. The presence of some residual reactants and reaction by-products may improve the processing and performance of phthalonitrile resins in two ways. First, a decreased purity results in more amorphous materials with lower melting points. This increases the processing window and allows for the use lower initial temperatures. This improved the ability to produce dense, homogeneous parts. Second, a variety of impurities may act to catalyze the reaction of phthalonitrile groups, resulting in a higher degree of cure. Since aromatic amines, secondary amines such as silazanes, amine salts, transition metals and their salts, strong organic acids and their salts, and hydroxyl compounds have been used as catalysts it is expected that impurities of such nature would also exhibit this effect.<sup>50-51, 88</sup> Thus, the rate and degree of curing is increased

and curing occurs at lower temperatures. Additionally, if impurities contain one or more phthalonitrile groups, they are likely to become chemically incorporated into the polymer network, preventing volatilization. Impurities that contain both phthalonitrile and catalytic groups may thus remain active at higher temperatures.

In this manner, additional curing at 375 °C was affected by purity. The  $T_g$  and stability of as-synthesized CSPN-U continued to improve with additional curing time at 375 °C. Conversely the properties of CSOPN-P and CSPN-P improved with initial 1-hour exposure to 375 °C, however little improvement was observed with additional curing time and in some cases, properties decreased. This limited curing of purified systems may be explained by degradation and volatilization of the curing additive. Conversely the CSPN-U polymer also contained impurities, which could have catalyzed curing and may not have volatilized.

Despite literature indicating that phenyl groups disrupt crystallinity,<sup>34, 44, 76, 203</sup> the monomers were crystalline solids with high melting points. The high melting points were comparable to those of other highly aromatic phthalonitriles<sup>6, 21-26</sup> and similar organosilicon compounds.<sup>219, 230-231</sup> Most similar silicon-containing bis-phthalonitriles reported in literature were amorphous monomers/oligomers with glass transitions between -1 and 60 °C. This difference is likely due to impurity levels as well as steric hindrance of the silicon linkage. The inclusion of hydrido or methyl groups on the silicon results in greater flexibility than when phenyl substituted, reducing the softening temperatures significantly.

Much of literature reports that thermal and oxidative stability is improved by the inclusion of phenyl substitution on the silicon,<sup>63, 77-78, 80, 85, 156, 163, 167, 199</sup> but the results of many authors disagree with this assertion.<sup>30, 33, 52-53, 77, 169, 176, 195</sup> It is likely highly dependent on exposure conditions<sup>168</sup> and the chemistry of the remainder of the polymer system.<sup>77</sup> The discrepancy of findings in literature shows that the use of di, tri, and tetra-phenyl substituted organosilicon compounds do not necessarily result in more stable polymers. Likewise, literature reports the inclusion of phenyl-functional groups on the silicon increases the glass transition temperature.<sup>1, 34, 169-170</sup> However, even after curing to 375 °C, the glass transitions of CSPN-U materials were lower than commonly reported in organic phthalonitrile literature.<sup>26, 29, 95</sup> While this effect was expected based on organosilicon literature, the magnitude of  $T_g$  suppression was larger than anticipated. For instance,

the observed glass transition temperatures were lower than reported for the  $T_g^{51}$  and  $T_{hd}^{30, 52-53, 79}$  of other silicon-containing phthalonitrile polymers.

Two considerations may explain the variance of findings observed in organosilicon literature and the performance of COSPN, CSPN, and CSOPN materials. Several authors have reported that highly-rigid and sterically bulky polymer structures hinder polymerization and result in incomplete curing with lower molecular weights and crosslink densities.<sup>21, 30, 33, 52, 77-79, 100, 124, 126</sup> A lower degree of cure can result in diminished stability and  $T_g$ . This effect of steric hindrance may be especially potent in phthalonitrile polymers, where 3 or 4 phthalonitrile groups must interact to form triazine or phthalocyanine structures respectively. An alternative explanation is possible by considering electronic homogeneity of the moiety. For example, in methyl-phenyl substituted organosilicon compounds, the methyl-silicon moiety is reported to be electron withdrawing with respect to the phenyl group which enhances  $p\pi$ - $d\pi$  bonding. Conversely no such effect is observed in electrically symmetric compounds such as tetraphenylsilane.<sup>78, 178</sup>

The improvement in stability and  $T_g$  with increasing phenyl substitution occurs more consistently in siloxane polymers as opposed to polymers with hybrid organic-organosilicon backbones. Specifically, mono, or di-phenyl substituted hybrid polymers often show improvements over similar tri and tetra-phenyl substituted materials. Di-phenyl substitution may be in the form of phenyl pendant groups as part of flexible siloxane, oxysilane, or silazane linkages or as phenylene backbone groups with smaller functional groups such as methyl or hydrido groups as the remaining substituents on the silicon. This approach seems to more commonly result in better performance, possibly due to optimal backbone rigidity or electronic distribution.<sup>30, 51-53, 78, 85, 199</sup>

All polymers considered performed well in oxidative testing, and phthalonitriles remain attractive candidates for use in aerospace composites and high temperature electronics. However, the expected higher thermo-oxidative stability of silicon-containing polymers was also not achieved as compared with organic systems. This decreased performance may be due to several reasons: 1) the homolytic cleavage of Si-phenyl bonds occurred at lower temperatures than C-C bonds due to the lower Si-C bond energy, 2) the loss of a phenyl group results in significantly more weight loss and volume change, as compared with the loss of a methyl or hydrido group, 3) while phenylene linkages are reported to result in decreased oxygen diffusion,<sup>77</sup> conversely the

increase in intra-chain spacing from phenyl functional groups<sup>1</sup> may increase the diffusivity of oxygen, 4) while oxidative crosslinking through siloxane and subsequently silica formation occurred, it is likely that the silicon content of these polymers is insufficient to form an effective barrier layer, and 5) the polymers likely exhibited a lower degree of cure with less triazine and phthalocyanine formation. Two plausible explanations for this lower degree of cure would be A) steric hindrance, as discussed previously, or B) incompatibility of the amine catalyst and silicon-containing monomer. If phase separation occurred, the catalyst would exhibit a lower effective reactivity. However, further work is required to identify any potential phase separation and quantify the degree of cure.

The IR-TGA data of CSPN-U and CSOPN-P and characterizations of oxidatively aged CSPN-U samples, provide useful information on degradation modes. In IR-TGA under nitrogen, the degradation at 520-540 °C likely corresponds to residual cyano groups and isoindoline structures. The degradation peak at 580-590 °C corresponds to the cleavage of Si-phenyl bonds and the release of benzene. In air an overall degradation peak is also observed at 570-590 °C with the detection of CO<sub>2</sub> and H<sub>2</sub>O. Furthermore, a small benzene peak is observed in air corresponding to the same range as the onset of benzene evolution in nitrogen. Since benzene was likely to combust prior to reaching the IR detector it may be assumed that this peak was truncated, and benzene evolution continued at temperatures correlating with the 570-590 °C peak. This indicates the Si-phenyl cleavage reaction is likely not catalyzed by oxygen but occurs via free-radical homolytic cleavage. These free radical species then interact with oxygen to form siloxy groups, which condense to form siloxane linkages.<sup>48</sup> In nitrogen, the degradations at 601-610 °C and 710-750 °C most likely correspond to triazine and phthalocyanine decomposition respectively. These occur to a much greater degree in air, most likely as part of overlapping degradations at 570-650 °C. Since there is a significant difference in the magnitude of degradations of the phthalonitrile derived structures in air vs. nitrogen, phthalonitrile resins remain good candidates for hybridization.<sup>31, 33</sup>

In oxidatively aged CSPN-U samples, four zones of degradation were identified. Three of these zones correlate well with the three-zone degradation model.<sup>62</sup> Additional triazine formation and oxidative crosslinking through siloxane bridges was observed. Triazine formation was observed at the same depths into the sample as siloxane formation but at greater depths than -OH. The reaction may be free radically catalyzed by siloxy groups. Closer to the surface, the triazine reaction is

likely also catalyzed by silanol and phenolic groups following a similar mechanism as reported for phenolic compounds.<sup>15</sup> The interaction of silanol groups with nitriles was proposed by Phua et al.<sup>125</sup> and discussed earlier in this work in Section 2.3.2. Silicon-Containing Phthalonitriles. An alternative explanation of additional triazine formation would simply be that the chain mobility was increased due to Si-phenyl bond cleavage.

Oxidative crosslinking and chain branching routes occur via the cleavage of Si-phenyl bonds and rearrangement or subsequent oxidation of organosilicon moieties.<sup>77-78, 168-169, 178-180</sup> An example CSPN polymer linkage with triazine structures is used to illustrate a few possible reaction routes. Figure 132 provides homolytic free-radical cleavage of Si-phenyl bonds. The silyl radicals then react with oxygen to form siloxy groups. While many possible crosslinking and chain branching routes involving the condensation of siloxy groups to form siloxane bridges may occur, a few examples are provided in Figure 133. This mechanism would continue to form silsesquioxane moieties and finally silicon dioxide. The formation of biphenyl structures was not observed in this system.

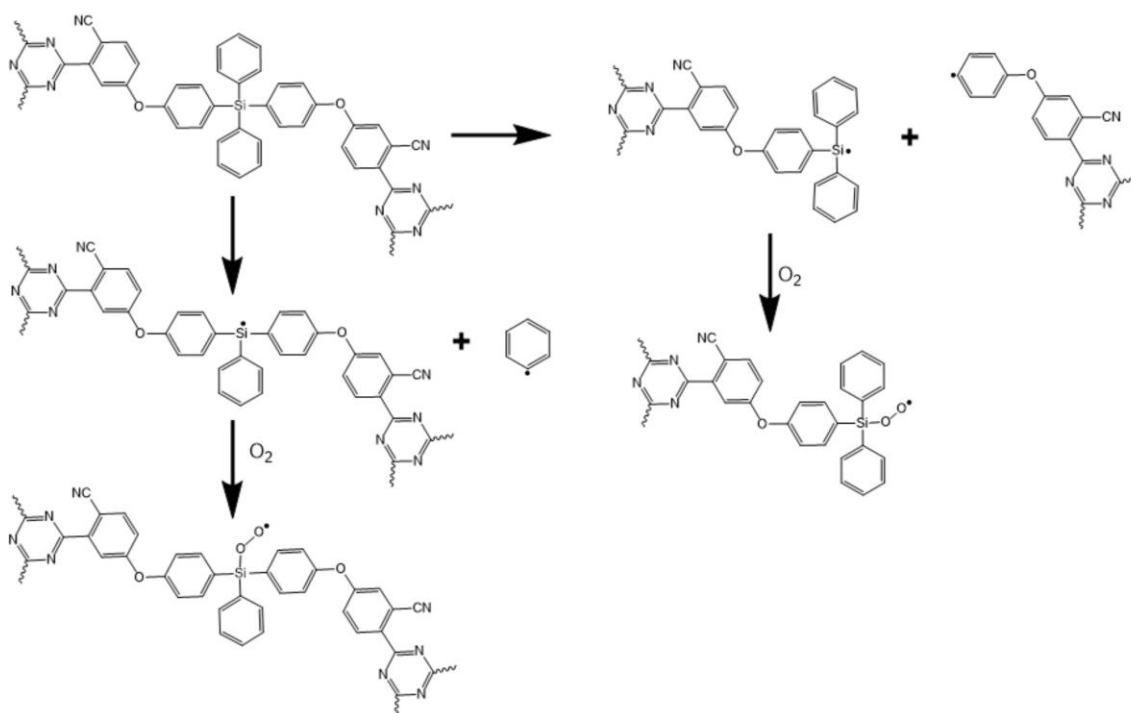


Figure 132: Cleavage of Si-phenyl groups and Si-phenylene linkages followed by oxidation to form siloxy groups.

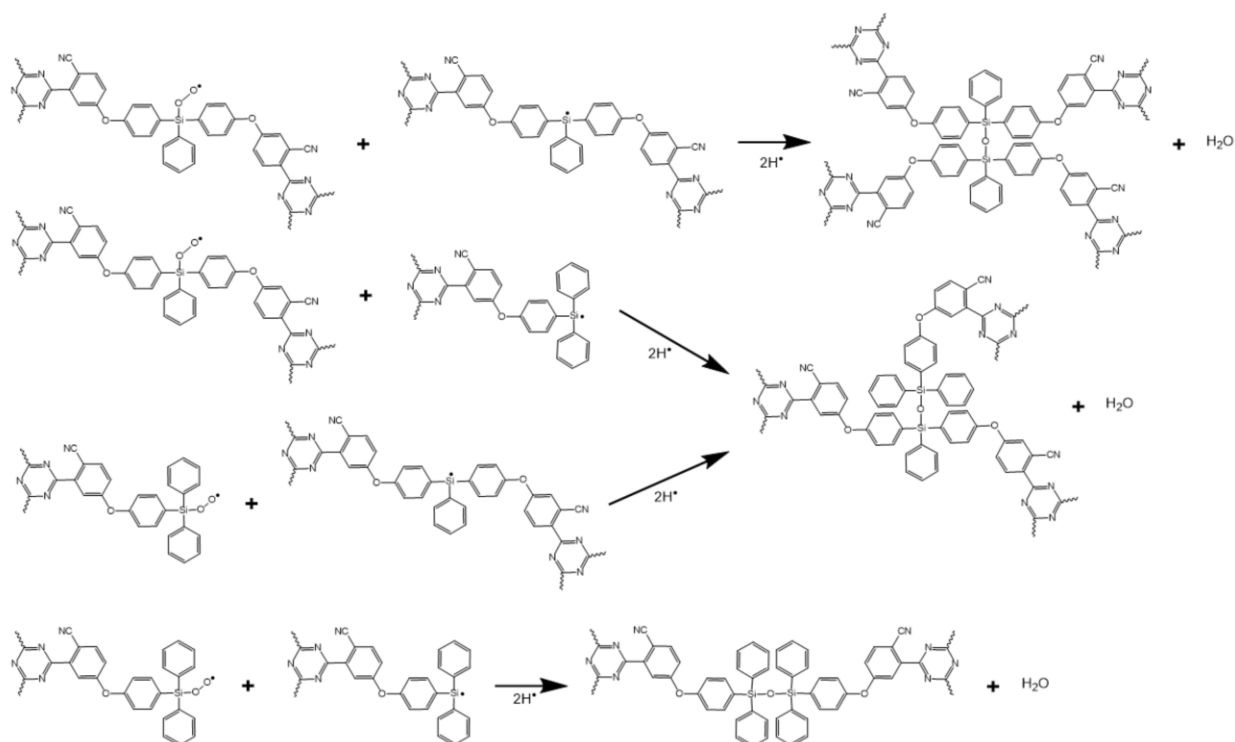


Figure 133: Example possible routes for condensation of siloxy groups and silyl radicals.<sup>78</sup>

Rearrangement reactions involving free radical displacement of phenyl groups may have also occurred. The tetraphenylsilane moiety is expected to undergo cleavage of a Si-phenyl bond prior to rearrangement. The triphenyl substituted moieties in the hexaphenyldisiloxane linkage may be able to directly interact with a silyl radical and undergo rearrangements of structure. While many possible structures may be generated in this manner, two examples are provided in Figure 134.

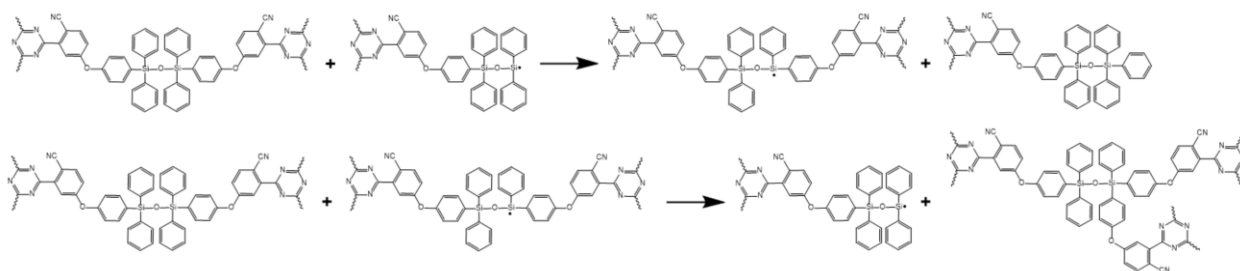


Figure 134: Example disproportionation reactions of a triphenyl-substituted silicon moiety in reaction with a silyl radical.<sup>178, 180, 207</sup>

Overall, this work supports that oxidative stability may be improved by the inclusion of silicon-containing moieties, and subsequent formation of Si-O phases. However, approaches which increase the  $T_g$  and stability of siloxanes are not guaranteed to increase the  $T_g$  and stability of hybrid systems. Specifically, increasing the phenyl substitution and the avoidance of impurities

did not result in better performance of silicon-containing phthalonitriles. Regarding the degree of phenyl substitution, hybrid systems may already avoid the lower temperature unzipping and rearrangement mechanisms found in siloxanes. For this reason, further steric hindrance may be not only unnecessary but actually detrimental. For improved processing and stability, a balance must be found in the backbone rigidity and steric bulk. Optimal results require alternative strategies for the inclusion and stabilization of silicon moieties into polymers for extreme temperature performance.

## 11 Opportunities for Future Work

Some improvements may be obtained in polymers similar to CSPN and CSOPN by the use of asymmetric linkages, the reduction in aromatic substitution, and the use of additional phenylene-linked cyano crosslinking or amine catalytic sites instead of non-functionalized pendant phenyl groups. Selecting a different organic curing additive and modifying the processing profile may also result in greater stability. However, greater enhancements are likely obtained by alternative approaches which increase the silicon content of the monomer, include additional crosslinking via Si-H and N-H mechanisms, and incorporate more thermally stable organosilicon structures such as silole or polyoctahedral silsesquioxane (POSS) groups. Increasing the silicon content, through the use of silazane, or POSS structures would result in improved SiO<sub>2</sub> barrier layer formation.

There are several opportunities for improvement of silicon-containing phthalonitriles in general. The effects of various impurities on the properties of phthalonitriles stands to be better understood. While industrially it is advantageous to not require extensive purification, there is surely a level of impurity that is detrimental. Furthermore, it may be that some specific impurities are harmful, while others are beneficial. Thus, it is of interest to understand the composition and nature of common contaminants and their role as plasticizers and catalysts.

A greater understanding of oxidative degradation of isoindoline, triazine, and phthalocyanine structures at high temperatures is also warranted. The specific degradation pathways are likely complex with multiple reactions occurring at once. However, understanding the most common degradation mechanisms may provide some insight into the design of PN polymers.

The dielectric properties of silicon-containing phthalonitriles have not been reported to the authors knowledge. Since the addition of silicon is known to lower the dielectric permittivity,<sup>1, 34, 158, 185</sup> and organic phthalonitriles have exhibited high breakdown strengths, these materials are of great interest for high temperature electronics.<sup>8, 142</sup> Permittivity measurements may be conducted by a variety of techniques, including those with bulk samples such as free space or waveguide methods. However, the measurement of dielectric breakdown usually requires films on the order of 10-100  $\mu\text{m}$  thick. However, a high level of difficulty is involved in the fabrication of defect and crack-free phthalonitrile thin films, due to the high degree of adhesion, high processing temperatures, and brittle nature of the polymer. The choice of appropriate conductive substrate or proper release system is critical. Initial work was conducted by the author on PN2 and CSPN-P

thin films. The CTE and surface energy of the substrate, as well as changes in curing profile resulted in significant differences in film quality. Thin films of PN2 were produced by spreading of monomer-solvent solutions via a doctor blade. The monomer was soluble in acetone, benzene, chloroform, DCM, DMF, DMSO, DCM, ethyl acetate, and THF. Silver-coated and fluorine-doped indium-tin oxide (FTO) coated glasses were investigated as substrates. Best results were achieved in benzene, chloroform, and DCM with FTO substrates. High quality monomer films were produced. However, films experienced melt flow, discoloration, delamination, and cracking during high temperature processing. Despite the lower quality of films, DC breakdown strengths of 171-854 kV/mm were measured. Using lessons learned from PN2 films, CSPN films were fabricated by autoclave processing of degassed and b-staged polymers on polished steel and aluminum substrates. Steel substrates provided better results due to better wettability and adhesion. However, difficulties were still experienced with porosity, cracking, and adhesion to the Teflon<sup>TM</sup> release layer. Despite significant optimization of processing techniques, high quality thin films were not able to be obtained. Further work is required to produce defect free PN films.

It is also desirable to quantify the degree of cure of these systems and the distribution of curing products. The degree of formation of various products, including isoindoline, triazine, and phthalocyanine, directly relates to the properties of the resulting polymer. The degree of conversion of cyano groups to these species is likely affected by purity, curing additive reactivity and compatibility, backbone mobility, and thermal curing profile. For low degrees of cure the material may still be somewhat soluble and thus liquid state NMR may be used. Solid state NMR may provide information on cured polymer samples. X-ray photoelectron spectroscopy, and ultraviolet–visible spectroscopy may be used to provide additional information.

For a variety of reasons, it is also of interest to investigate curing at lower temperatures (< 200 °C) for longer times (>24 hours). In this work, curing was accomplished at temperatures up to 350-375 °C with holds of  $\leq 4$  hours. However, curing temperatures in excess of 300-325 °C may be undesirable for many applications with 250 °C service temperatures, including wide band-gap power modules. Furthermore, better performance may be achieved using longer curing holds at temperatures near 250 °C. Greater isoindoline formation at this temperature would likely correlate with greater phthalocyanine formation at higher temperatures.<sup>79</sup> This is advantageous since phthalocyanine structures result in greater stability and reduced evolution of toxic volatiles. In

contrast residual cyano groups, either as unreacted phthalonitrile or as pendant groups on triazine moieties, likely result in HCN evolution during degradation. It has also been reported that maintaining the curing temperatures below the current glass transition temperature can result in decreased part shrinkage.<sup>53</sup>

Similarly, it is desirable to reduce the temperatures required for the curing reactions to occur. This may be accomplished via a variety of methods including 1) the use of combinations of catalysts,<sup>4, 58, 133</sup> 2) the inclusion of additional cyano crosslinking sites,<sup>7, 21, 50, 124</sup> 3) the addition of catalytic groups such as amine or silazane substituents in the monomer structure<sup>21, 51, 88, 97, 122-124</sup> and 4) the use of silazane resins as a curing additive.<sup>50</sup>

It is likely that the curing additive must be tailored to the chemistry of the pre-polymer resin for optimal results. It is possible that phase separation of the amine catalyst occurred in CSPN and CSOPN systems, resulting in lower reactivity. Other commonly used amines including 4,4'-bis(3-aminophenoxy)diphenyl sulfone (*m*-BAPS) or 1,3-bis(4-aminophenoxy) benzene (*m*-APB) would likely have higher solubility and reactivity. Alternatively, silicon-containing amines or silazane resins with appropriate organic functionality will likely provide improved solubility in silicon-containing phthalonitriles, while simultaneously increasing the silicon content. Very few silicon-containing amines are commercially available which possess high enough thermal stability to survive the curing conditions without extensive degradation and volatilization. Two compounds that may prove acceptable are triphenylaminosilane and octa(aminophenyl)-t8-silsesquioxane.

Silazanes may also prove effective curing additives for organic phthalonitrile resins, with the added benefit of increasing the silicon content. However the organic substituents on the silicon and composition of the organic monomer backbone must be carefully selected, otherwise phase separation occurs. This was observed in preliminary studies by the author. Commercial PN2 was mixed with varying amounts of a silazane resin and curing was attempted. The mixture phase separated and did not cure as intended. A silazane functionalized with 4,4'-(perfluoropropane-2,2-diyl)bis(2-aminophenol) did result in curing, but still separation occurred. However, even with phase separation, excellent results were obtained in TGA under nitrogen, as included in Appendix B: Thermogravimetric Data.

The inclusion of methyl or hydrido groups on the silicon may likely provide improved processing and properties. Instead of attempting to avoid oxidative degradations, an improved

approach may be to encourage oxidative crosslinking while limiting weight loss. Rearrangements of structure are likely but not necessarily detrimental. This approach, in conjunction with use of a silazane resin was recently shown to be highly effective.<sup>50</sup> In addition to traditional phthalonitrile crosslinking mechanisms involving cyano groups (isoindoline, phthalocyanine, and triazine formation), the interactions of C≡N, Si-H, and N-H groups result in hydrosilylation, nucleophilic Michael reactions, and nitrosilylation addition reactions.<sup>50</sup> Additionally transamination, dehydrocoupling, Si-H and N-H bond exchange, formation and insertion of N=Si species, and other structural rearrangements may occur.<sup>148</sup>

Since the silicon-organic connection appears to often be a weak link in the polymer structure, it is of interest to consider alternate ways of attaching organosilicon moieties to improve stability. The Si-phenyl linkage is still expected to have higher stability than Si-CH<sub>2</sub>-phenyl or Si-O-phenyl linkages.<sup>35-37, 39, 93, 102, 184-187, 189-193</sup> Thus phenylene linkages are likely still one of the best ways of attaching the aromatic backbone to the silicon moiety. The use of electron withdrawing substituents on the silicon has been shown to improve the strength of the Si-phenyl bonds.<sup>78, 178, 210</sup> Since cyano groups are strongly electronically withdrawing, attaching the phthalonitrile moiety directly to the silicon may also result in slightly improved properties.

The use of multiple attachments or additional organic linkages in the backbone would also likely result in improved stability. For example, silole and dibenzo-silole structures incorporate the silicon as part of a heterocyclic ring. It has been reported that benzo-siloles are more thermally stable than phenylsilanes. In fact dibenzo-siloles may be formed from the decomposition of dimethyldiphenylsilane structures.<sup>78, 178</sup> When considering 5,5-diphenyl-5H-dibenzo[b,d]silole, it may be assumed that the melting point would increase due to the increased rigidity from the additional bi-phenyl bond. However, the asymmetry of the dibenzo-silole structure results in a significant decrease in melting point (146-149 °C)<sup>243</sup> as compared to tetraphenylsilane (236-237 °C).<sup>244</sup> The dimethyl-substituted compound, 5,5-dimethyl-5H-dibenzo[b,d]silole, exhibits an even lower melting point of 57-61 °C.<sup>243</sup>

Lastly, polyhedral oligomeric silsesquioxanes are also of interest due to the extremely high decomposition temperatures and high silicon content. POSS moieties may be incorporated as pendant groups, backbone structures, or curing additives. However, most POSS compounds, especially polyphenylsilsesquioxanes show very high melting points, often above 500 °C.<sup>196</sup> It is

desirable to reduce this melting point without the use of thermally detrimental structures. Low-melting point POSS-PN polymers with sufficiently improved stability have yet to be demonstrated.

## 12 Bibliography

1. Hergenrother, P. M., The Use, Design, Synthesis, and Properties of High Performance/High Temperature Polymers: An Overview. *High Performance Polymers* **2003**, *15* (1), 3-45.
2. Connell, J. W. In *The Design, Synthesis and Properties of High Performance/High Temperature Polymers*, High Temperature Polymeric Laminates (High Temple) Workshop, Plam Springs, CA, Jan. 29- Feb. 1, 2018; Plam Springs, CA, 2018.
3. Keller, T. M.; Price, T. R., Amine-Cured Bisphenol-Linked Phthalonitrile Resins. *Journal of Macromolecular Science: Part A - Chemistry* **1982**, *18* (6), 931-937.
4. Laskoski, M.; Dominguez, D. D.; Keller, T. M., Synthesis and properties of a bisphenol A based phthalonitrile resin. *Journal of Polymer Science Part A: Polymer Chemistry* **2005**, *43* (18), 4136-4143.
5. Laskoski, M.; Neal, A.; Keller, T. M.; Dominguez, D.; Klug, C. A.; Saab, A. P., Improved synthesis of oligomeric phthalonitriles and studies designed for low temperature cure. *Journal of Polymer Science Part A: Polymer Chemistry* **2014**, *52* (12), 1662-1668.
6. Laskoski, M.; Neal, A.; Schear, M. B.; Keller, T. M.; Ricks-Laskoski, H. L.; Saab, A. P., Oligomeric aliphatic–aromatic ether containing phthalonitrile resins. *Journal of Polymer Science Part A: Polymer Chemistry* **2015**, *53* (18), 2186-2191.
7. Tong, L.; Jia, K.; Liu, X., Novel phthalonitrile-terminated polyarylene ether nitrile with high glass transition temperature and enhanced thermal stability. *Materials Letters* **2014**, *128* (0), 267-270.
8. Liu, Y. Packaging of Silicon Carbide High Temperature, High Power Devices - Processes and Materials. Auburn University, Auburn, Alabama, 2006.
9. Dominguez, D. D.; Keller, T. M., Low-melting Phthalonitrile Oligomers: Preparation, Polymerization and Polymer Properties. *High Performance Polymers* **2006**, *18* (3), 283-304.
10. Tant, M., R.; McManus, Hugh, L. N.; Rogers, Martin, E. , High-Temperature Properties and Applications of Polymeric Materials. In *High-Temperature Properties and Applications of Polymeric Materials*, Martin R. Tant, J. W. C., Hugh L. N. McManus, Ed. American Chemical Society: Washington, DC, 1995; Vol. 603, pp 1-20.
11. Hilmar Koerner, T. P. *High Temp Hybrid Polymers*; AFRL Composite Materials Branch (RXCC), Materials and Manufacturing Directorate: WPAFB, September 19 2014.
12. Valdez-Nava, Z.; Kozako, M.; Dinculescu, S.; Omura, I.; Hikita, M.; Lebey, T. In *Packaging of SiC-SBD for high temperature operation*, Electronic Materials and Packaging (EMAP), 2012 14th International Conference on, 13-16 Dec. 2012; 2012; pp 1-4.
13. Thomas, T.; Becker, K. F.; Braun, T.; Dijk, M. v.; Wittler, O.; Lang, K. D. In *Assessment of high temperature reliability of molded smart power modules*, Electronics System-Integration Technology Conference (ESTC), 2014, 16-18 Sept. 2014; 2014; pp 1-7.
14. Khazaka, R.; Mendizabal, L.; Henry, D.; Hanna, R.; Lesaint, O. In *Assessment of dielectric encapsulation for high temperature high voltage modules*, 2015 IEEE 65th Electronic Components and Technology Conference (ECTC), 26-29 May 2015; 2015; pp 1914-1919.

15. Augustine, D.; Mathew, D.; Nair, C. P. R., Phenol-containing phthalonitrile polymers - synthesis, cure characteristics and laminate properties. *Polymer International* **2013**, *62* (7), 1068-1076.
16. Peng, X.; Sheng, H.; Guo, H.; Naito, K.; Yu, X.; Ding, H.; Qu, X.; Zhang, Q., Synthesis and properties of a novel high-temperature diphenyl sulfone-based phthalonitrile polymer. *High Performance Polymers* **2014**, *26* (7), 837-845.
17. Matthew, L.; S., C. J.; Arianna, N.; G., H. B.; L., R. L. H.; Judson, H. W.; N., D. M.; R., S. A.; M., K. T., Sustainable High-Temperature Phthalonitrile Resins Derived from Resveratrol and Dihydroresveratrol. *ChemistrySelect* **2016**, *1* (13), 3423-3427.
18. Pandey, M. K.; Khan, A. R.; Saxena, A. K., Synthesis and thermal analysis of phosphonitrile-core-bearing aromatic nitriles for high-temperature applications. *Journal of Thermal Analysis and Calorimetry* **2017**, *129* (3), 1453-1462.
19. Keller, T. M.; Dominguez, D. D.; Laskoski, M., Oligomeric bisphenol A-based PEEK-like phthalonitrile-cure and polymer properties. *Journal of Polymer Science Part A: Polymer Chemistry* **2016**, *54* (23), 3769-3777.
20. Sheng, H.; Zhao, F.; Yu, X.; Naito, K.; Qu, X.; Zhang, Q., Synthesis and thermal properties of high-temperature phthalonitrile polymers based on 1,3,5-triazines. *High Performance Polymers* **2016**, *28* (5), 600-609.
21. Liu, T.; Yang, Y.; Wang, T.; Wang, H.; Zhang, H.; Su, Y.; Jiang, Z., Synthesis and Properties of Poly(aryl ether ketone)-Based Phthalonitrile Resins. *Polymer Engineering and Science* **2014**, *54* (7), 1695-1703.
22. Laskoski, M.; Dominguez, D. D.; Keller, T. M., Synthesis and properties of aromatic ether phosphine oxide containing oligomeric phthalonitrile resins with improved oxidative stability. *Polymer* **2007**, *48* (21), 6234-6240.
23. Dominguez, D. D.; Keller, T. M., Properties of phthalonitrile monomer blends and thermosetting phthalonitrile copolymers. *Polymer* **2007**, *48* (1), 91-97.
24. Laskoski, M.; Keller, T. M.; Ricks-Laskoski, H. L.; Giller, C. B.; Hervey, J., Improved Synthesis of Oligomeric Sulfone-Based Phthalonitriles. *Macromolecular Chemistry and Physics* **2015**, *216* (17), 1808-1815.
25. Laskoski, M.; Schear, M. B.; Neal, A.; Dominguez, D. D.; Ricks-Laskoski, H. L.; Hervey, J.; Keller, T. M., Improved synthesis and properties of aryl ether-based oligomeric phthalonitrile resins and polymers. *Polymer* **2015**, *67*, 185-191.
26. Keller, T. M.; Dominguez, D. D., High temperature resorcinol-based phthalonitrile polymer. *Polymer* **2005**, *46* (13), 4614-4618.
27. Zhao, E.; Hu, J.; Wang, J.; Shi, M.; Wang, Z.; Zeng, K.; Yang, G., Preparation and properties of phthalonitrile resins promoted by melamine. *High Performance Polymers* **2018**, *30* (5), 561-570.
28. Liu, T.; Yan, W.; Su, Y.; Yu, H.; Zhao, N.; Yang, Y.; Jiang, Z., Synthesis and characterization of hyperbranched poly(aryl ether ketone) terminated with phthalonitrile group. *High Performance Polymers* **2016**, *28* (3), 263-270.
29. Warzel, M. L.; Keller, T. M., Tensile and fracture properties of a phthalonitrile polymer. *Polymer* **1993**, *34* (3), 663-666.
30. Bulgakov, B. A.; Babkin, A. V.; Dzhevakov, P. B.; Bogolyubov, A. A.; Sulimov, A. V.; Kepman, A. V.; Kolyagin, Y. G.; Guseva, D. V.; Rudyak, V. Y.; Chertovich, A. V., Low-melting phthalonitrile thermosetting monomers with siloxane- and phosphate bridges. *European Polymer Journal* **2016**, *84*, 205-217.

31. Andrew J Guenther, V. V., Timothy S Haddad, Josiah T Reams, Kevin R Lamison, Christopher M Sahagun, Sean M Ramirez, Gregory R Yandek, Joseph M Mabry *Silicon-Containing Tri-and Tetra-Functional Cyanate Esters: Synthesis, Cure Kinetics, and Network Properties*; Air Force Research Lab Aerospace Systems Directorate: Edwards AFB CA, 2014; p 58.
32. Guenther, A. J.; Yandek, G. R.; Wright, M. E.; Petteys, B. J.; Quintana, R.; Connor, D.; Gilardi, R. D.; Marchant, D., A New Silicon-Containing Bis(cyanate) Ester Resin with Improved Thermal Oxidation and Moisture Resistance. *Macromolecules* **2006**, *39* (18), 6046-6053.
33. Guenther, A. J.; Vij, V.; Haddad, T. S.; Reams, J. T.; Lamison, K. R.; Sahagun, C. M.; Ramirez, S. M.; Yandek, G. R.; Suri, S. C.; Mabry, J. M., Silicon-containing trifunctional and tetrafunctional cyanate esters: Synthesis, cure kinetics, and network properties. *Journal of Polymer Science Part A: Polymer Chemistry* **2014**, *52* (6), 767-779.
34. Yilgör, E.; Yilgör, I., Silicone containing copolymers: Synthesis, properties and applications. *Progress in Polymer Science* **2014**, *39* (6), 1165-1195.
35. Regnier, N.; Guibe, C., Methodology for multistage degradation of polyimide polymer. *Polymer Degradation and Stability* **1997**, *55* (2), 165-172.
36. Fitzgerald, J. J.; Tunney, S. E.; Landry, M. R., Synthesis and characterization of a fluorinated poly(imide-siloxane) copolymer: a study of physical properties and morphology. *Polymer* **1993**, *34* (9), 1823-1832.
37. Xi, K.; Meng, Z.; Heng, L.; Ge, R.; He, H.; Yu, X.; Jia, X., Polyimide–polydimethylsiloxane copolymers for low-dielectric-constant and moisture-resistance applications. *Journal of Applied Polymer Science* **2009**, *113* (3), 1633-1641.
38. Ghosh, A.; Banerjee, S.; Komber, H.; Schneider, K.; Häußler, L.; Voit, B., Synthesis and characterization of fluorinated poly(imide siloxane) block copolymers. *European Polymer Journal* **2009**, *45* (5), 1561-1569.
39. Hamciuc, E.; Hamciuc, C.; Cazacu, M.; Ignat, M.; Zarnescu, G., Polyimide–polydimethylsiloxane copolymers containing nitrile groups. *European Polymer Journal* **2009**, *45* (1), 182-190.
40. Saxena, K.; Bisaria, C. S.; Kalra, S. J. S.; Saxena, A. K., Synthesis of some novel silicone-imide hybrid inorganic–organic polymer and their properties. *Progress in Organic Coatings* **2015**, *78*, 234-238.
41. Damaceanu, M.; Rusu, R.; Bruma, M.; Mu, x; ller, A. In *Thin polyimide films for dielectric interlayer application*, Semiconductor Conference, 2009. CAS 2009. International, 12-14 Oct. 2009; 2009; pp 351-354.
42. Damaceanu, M.-D.; Musteata, V.-E.; Cristea, M.; Bruma, M., Viscoelastic and dielectric behaviour of thin films made from siloxane-containing poly(oxadiazole-imide)s. *European Polymer Journal* **2010**, *46* (5), 1049-1062.
43. Tiwari, A.; Nema, A. K.; Das, C. K.; Nema, S. K., Thermal analysis of polysiloxanes, aromatic polyimide and their blends. *Thermochimica Acta* **2004**, *417* (1), 133-142.
44. Babanzadeh, S.; Mahjoub, A. R.; Mehdipour-Ataei, S., Novel soluble thermally stable silane-containing aromatic polyimides with reduced dielectric constant. *Polymer Degradation and Stability* **2010**, *95* (12), 2492-2498.
45. Zhuo, D. X.; Gu, A. J.; Liang, G. Z.; Hu, J. T.; Cao, L.; Yuan, L., Flame retardancy and flame retarding mechanism of high performance hyperbranched polysiloxane modified bismaleimide/cyanate ester resin. *Polymer Degradation and Stability* **2011**, *96* (4), 505-514.

46. Morgan, A. B.; Putthanarat, S., Use of inorganic materials to enhance thermal stability and flammability behavior of a polyimide. *Polymer Degradation and Stability* **2011**, *96* (1), 23-32.
47. Yudasaka, I.; Tanaka, H.; Miyasaka, M.; Inoue, S.; Shimoda, T., 27.2: Poly-Si Thin-Film Transistors Using Polysilazane-Based Spin-On Glass for All Dielectric Layers. *SID Symposium Digest of Technical Papers* **2004**, *35* (1), 964-967.
48. Jovanovic, J. D.; Govedarica, M. N.; Dvornic, P. R.; Popovic, I. G., The thermogravimetric analysis of some polysiloxanes. *Polymer Degradation and Stability* **1998**, *61* (1), 87-93.
49. Khazaka, R.; Locatelli, M. L.; Diahm, S.; Bidan, P., Effects of mechanical stresses, thickness and atmosphere on aging of polyimide thin films at high temperature. *Polymer Degradation and Stability* **2013**, *98* (1), 361-367.
50. Wang, M.; Ning, Y., Oligosilylarylnitrile: The Thermoresistant Thermosetting Resin with High Comprehensive Properties. *ACS Applied Materials & Interfaces* **2018**, *10* (14), 11933-11940.
51. Zhang, Z. B.; Li, Z.; Zhou, H.; Lin, X. K.; Zhao, T.; Zhang, M. Y.; Xu, C. H., Self-Catalyzed Silicon-Containing Phthalonitrile Resins with Low Melting Point, Excellent Solubility and Thermal Stability. *Journal of Applied Polymer Science* **2014**, *131* (20), 40919.
52. Babkin, A. V.; Zodbinov, E. B.; Bulgakov, B. A.; Kepman, A. V.; Avdeev, V. V., Low-melting siloxane-bridged phthalonitriles for heat-resistant matrices. *European Polymer Journal* **2015**, *66* (0), 452-457.
53. Dzhevakov, P. B.; Korotkov, R. F.; Bulgakov, B. A.; Babkin, A. V.; Kepman, A. V.; Avdeev, V. V., Synthesis and polymerization of disiloxane Si-O-Si-linked phthalonitrile monomer. *Mendeleev Communications* **2016**, *26* (6), 527-529.
54. Li, X.; Yu, B.; Zhang, D.; Lei, J.; Nan, Z., Cure Behavior and Thermomechanical Properties of Phthalonitrile-Polyhedral Oligomeric Silsesquioxane Copolymers. *Polymers* **2017**, *9* (8), 334.
55. Terraza, C. A.; Tagle, L. H.; Tundidor-Camba, A.; Gonzalez-Henriquez, C. M.; Sarabia-Vallejos, M. A.; Coll, D., Synthesis and characterization of aromatic poly(ether-imide)s based on bis(4-(3,4-dicarboxyphenoxy)phenyl)-R,R-silane anhydrides (R = Me, Ph) - spontaneous formation of surface micropores from THF solutions. *RSC Advances* **2016**, *6* (55), 49335-49347.
56. Hardict, S. N. Novel Novolac-Phthalonitrile and Siloxane-Phthalonitrile Resins cured with low melting Novolac Oligomers for Flame Retardant Structural Thermosets. Virginia Polytechnic Institute and State University, Blacksburg, VA, 2003.
57. Maya, E. M.; Snow, A. W.; Shirk, J. S.; Pong, R. G. S.; Flom, S. R.; Roberts, G. L., Synthesis, aggregation behavior and nonlinear absorption properties of lead phthalocyanines substituted with siloxane chains. *Journal of Materials Chemistry* **2003**, *13* (7), 1603-1613.
58. Lau, K. S. Y., 10 - High-Performance Polyimides and High Temperature Resistant Polymers. In *Handbook of Thermoset Plastics (Third Edition)*, Dodiuk, H.; Goodman, S. H., Eds. William Andrew Publishing: Boston, 2014; pp 297-424.
59. McKeen, L. W., 3 - Introduction to the Physical, Mechanical, and Thermal Properties of Plastics and Elastomers. In *The Effect of Long Term Thermal Exposure on Plastics and Elastomers*, McKeen, L. W., Ed. William Andrew Publishing: Oxford, 2014; pp 43-71.
60. Li, L. Dielectric properties of aged polymers and nanocomposites. Iowa State University, Ames, Iowa, 2011.
61. Ma, N.; Yu, Y.; Sun, Z.; Huang, S., Comparative study on the optical properties and stability of linear and branched polysilanes. *Journal of Luminescence* **2007**, *126* (2), 827-832.
62. Pochiraju, K. V.; Tandon, G. P., Modeling Thermo-Oxidative Layer Growth in High-Temperature Resins. *Journal of Engineering Materials and Technology* **2005**, *128* (1), 107-116.

63. Drake, K.; Mukherjee, I.; Mirza, K.; Ji, H.-F.; Bradley, J.-C.; Wei, Y., Novel Diacetylinic Aryloxysilane Polymers: A New Thermally Cross-Linkable High Temperature Polymer System. *Macromolecules* **2013**, *46* (11), 4370-4377.
64. Dunson, D. L. Synthesis and Characterization of Thermosetting Polyimide Oligomers for Microelectronics Packaging. Virginia Polytechnic Institute and State University, 2000.
65. Kasap, S. O., Ch. 7 Dielectric Materials and Insulation In *Principles of Electronic Materials and Devices*, 3rd ed.; McGraw-Hill: New York, NY, 2006; pp 583-684.
66. Agilent Technologies, I. Basics of Measuring the Dielectric Properties of Materials 2014, p. 1-34.
67. Ul Haq, S.; Raju, G. G., DC breakdown characteristics of high temperature polymer films. *Dielectrics and Electrical Insulation, IEEE Transactions on* **2006**, *13* (4), 917-926.
68. ASTM, D149 – 09 (Reapproved 2013) Standard Test Method for Dielectric Breakdown Voltage and Dielectric Strength of Solid Electrical Insulating Materials at Commercial Power Frequencies.
69. ASTM, D3755 – 14 Standard Test Method for Dielectric Breakdown Voltage and Dielectric Strength of Solid Electrical Insulating Materials Under Direct-Voltage Stress.
70. Dissado, L. A.; Fothergill, J. C., *Electrical Degradation and Breakdown in Polymers*. Institution of Engineering and Technology: 1992.
71. Van Krevelen, D. W.; Te Nijenhuis, K., Chapter 11 - Electrical Properties. In *Properties of Polymers (Fourth Edition)*, Elsevier: Amsterdam, 2009; pp 319-354.
72. Cottrell, T. L., *The strengths of chemical bonds*. Butterworths: London, 1958.
73. OpenStax, 7.5 Strengths of Ionic and Covalent Bonds. In *Chemistry*, BC Campus ed.; OpenStax CNX: Rice University, 2016.
74. Yoder, C. Common Bond Energies (D )and Bond Lengths (r) 2018. [http://www.wiredchemist.com/chemistry/data/bond\\_energies\\_lengths.html](http://www.wiredchemist.com/chemistry/data/bond_energies_lengths.html).
75. Bond Energies. In *Encyclopedia of Inorganic Chemistry*, R. B. King, R. H. C., C. M. Lukehart, D. A. Atwood and R. A. Scott, Ed. 2006.
76. McKeen, L. W., 1 - Introduction to Plastics and Polymers. In *The Effect of Long Term Thermal Exposure on Plastics and Elastomers*, McKeen, L. W., Ed. William Andrew Publishing: Oxford, 2014; pp 1-16.
77. Yang, Z.; Han, S.; Zhang, R.; Feng, S.; Zhang, C.; Zhang, S., Effects of silphenylene units on the thermal stability of silicone resins. *Polymer Degradation and Stability* **2011**, *96* (12), 2145-2151.
78. Beattie, S. R. The Thermal Decomposition of Some Silphenylene-Siloxane Polymers. University of Glasgow, Glasgow, UK, 1981.
79. Babkin, A. V.; Zodbinov, E. B.; Bulgakov, B. A.; Kepman, A. V.; Avdeev, V. V., Thermally stable phthalonitrile matrixes containing siloxane fragments. *Polymer Science Series B* **2016**, *58* (3), 298-306.
80. Sun, J. T.; Huang, Y. D.; Cao, H. L.; Gong, G. F., Effects of ambient-temperature curing agents on the thermal stability of poly(methylphenylsiloxane). *Polymer Degradation and Stability* **2004**, *85* (1), 725-731.
81. McKeen, L. W., 01-Introduction to Plastics and Polymers. In *The Effect of Long Term Thermal Exposure on Plastics and Elastomers*, McKeen, L. W., Ed. William Andrew Publishing: Oxford, 2014; pp 1-16.

82. Cella, J.; Rubinsztajn, S., Preparation of Polyaryloxysilanes and Polyaryloxysiloxanes by B(C6F5)<sub>3</sub> Catalyzed Polyetherification of Dihydrosilanes and Bis-Phenols. *Macromolecules* **2008**, *41* (19), 6965-6971.
83. M. Matzner, A. N., L. M. Robeson, C. N. Merriam, R. Barclay, Jr., and J. E. McGrath,, Block Copolymer Elastomers From Polysiloxanes and High Temperature Resistant Segments. *Polymeric Materials for Unusual Service Conditions* **1973**, *Applied Polymer Symposia NO. 22*, 143-156.
84. Noshay, A.; Matzner, M., Hydrolytic stability of the Si·O·C linkage in organo-siloxane block copolymers. *Die Angewandte Makromolekulare Chemie* **1974**, *37* (1), 215-218.
85. Arsen'eva, E. D.; Aulova, N. V.; Fromberg, M. B.; Gashnikova, N. P.; Grozdov, A. G., Hydrolytic and thermal stability of polyoxyarylenesilanes. *Polymer Science U.S.S.R.* **1972**, *14* (1), 239-245.
86. Church, A. C. Synthesis of Functionalized Polycarbosilanes Via Acyclic Diene Metathesis (ADMET) Polymerization. University of Florida, 2001.
87. Black, S. Are high-temp thermosets ready to go commercial? *High Performance Composites* [Online], 11/1/2004
88. Zeng, K.; Zhou, K.; Tang, W. R.; Tang, Y.; Zhou, H. F.; Liu, T.; Wang, Y. P.; Zhou, H. B.; Yang, G., Synthesis and curing of a novel amino-containing phthalonitrile derivative. *Chinese Chemical Letters* **2007**, *18* (5), 523-526.
89. Yao, Y. Thermal Stability of Al<sub>2</sub>O<sub>3</sub>/Silicone Composites as High-Temperature Encapsulants. Virginia Polytechnic Institute and State University, Blacksburg, Va, 2014.
90. Yao, Y. Thermal Stability of Silicone-Based Composites for High-Temperature Encapsulation Virginia Tech, Blacksburg, Va, 2013.
91. Yang, F.; Li, Y.; Ma, T.; Bu, Q.; Zhang, S., Synthesis and characterization of fluorinated polyimides derived from novel unsymmetrical diamines. *Journal of Fluorine Chemistry* **2010**, *131* (7), 767-775.
92. Liaw, D.-J.; Wang, K.-L.; Huang, Y.-C.; Lee, K.-R.; Lai, J.-Y.; Ha, C.-S., Advanced polyimide materials: Syntheses, physical properties and applications. *Progress in Polymer Science* **2012**, *37* (7), 907-974.
93. Wang, H.; Tao, X.; Newton, E., Dielectric Properties and Relaxation Behavior of Polymethylsiloxane-imide Films. *High Performance Polymers* **2003**, *15* (1), 91-103.
94. Scheel, L. D.; Lane, W. C.; Coleman, W. E., The Toxicity of Polytetrafluoroethylene Pyrolysis Products—Including Carbonyl Fluoride and a Reaction Product, Silicon Tetrafluoride. *American Industrial Hygiene Association Journal* **1968**, *29* (1), 41-48.
95. Zhao, F.; Liu, R.; Kang, C.; Yu, X.; Naito, K.; Qu, X.; Zhang, Q., A novel high-temperature naphthyl-based phthalonitrile polymer: synthesis and properties. *Rsc Advances* **2014**, *4* (16), 8383-8390.
96. Hilmar Koerner, T. G., G. P. Tandon, & Heritage Weems In *Phthalonitriles (PN): Thermo-Oxidative Stability (TOS) Study*, High Temple Workshop, Charleston, SC, January 23-26; Charleston, SC, 2017.
97. Heng Zhou, F. L., Yuehai Li, Tong Zhao, Thermal and Mechanical Properties of Several Phthalonitrile Resin System. *Institute of Chemistry, Chinese Academy of Sciences, Beijing* **2011**.
98. Xu, M.; Liu, M.; Dong, S.; Liu, X., Design of low temperature self-cured phthalonitrile-based polymers for advanced glass fiber composite laminates. *J. Mater. Sci.* **2013**, *48* (23), 8108-8116.

99. McKeen, L. W., 6 - Polyimides. In *The Effect of Long Term Thermal Exposure on Plastics and Elastomers*, McKeen, L. W., Ed. William Andrew Publishing: Oxford, 2014; pp 117-137.
100. Keller, T. M., Imide-containing phthalonitrile resin. *Polymer* **1993**, *34* (5), 952-955.
101. Zelmat, S.; Locatelli, M.-L.; Lebey, T.; Diaham, S., Investigations on high temperature polyimide potentialities for silicon carbide power device passivation. *Microelectronic Engineering* **2006**, *83* (1), 51-54.
102. Chang, T. C.; Wu, K. H., Characterization and degradation of some silicon-containing polyimides. *Polymer Degradation and Stability* **1998**, *60* (1), 161-168.
103. Achar, B. N.; Fohlen, G. M.; Parker, J. A., Phthalocyanine polymers. III. Poly(nickel phthalocyanine)benzimidazole as a novel high-temperature-resistant polymer. *Journal of Polymer Science: Polymer Chemistry Edition* **1982**, *20* (8), 2073-2079.
104. Liao, M. S.; Kuo, K. T., Phthalocyanine Polymers II. Synthesis and Characterization of Fused Metal Phthalocyanine Polymers. *Polymer Journal* **1993**, *25*, 947.
105. Wöhrle, D.; Schulte, B., Polymeric phthalocyanines and their precursors, 10. Thermal stability of polymeric phthalocyanines and their low molecular analogues. *Die Makromolekulare Chemie* **1985**, *186* (11), 2229-2245.
106. McKeown, N. B., Phthalocyanine-containing polymers. *Journal of Materials Chemistry* **2000**, *10* (9), 1979-1995.
107. McKeen, L. W., 10 - High-Temperature/High-Performance Polymers. In *The Effect of Long Term Thermal Exposure on Plastics and Elastomers*, McKeen, L. W., Ed. William Andrew Publishing: Oxford, 2014; pp 209-238.
108. Wen, S.; Jun, G.; Lei, Z.; Lily, Z.; Fengxiang, W.; Guangning, W. In *Study on mechanism and characteristics of dielectric breakdown in polyimide film*, Solid Dielectrics, 2004. ICSD 2004. Proceedings of the 2004 IEEE International Conference on, 5-9 July 2004; 2004; pp 908-911 Vol.2.
109. Wu, S.; x; Yang; Denton, D. D., Dielectric modeling of polyimide exposed to environmental stress. *Electrical Insulation, IEEE Transactions on* **1992**, *27* (2), 362-373.
110. McConnel, V. P. Resins for the Hot Zone, Part II: BMIs, CEs, benzoxazines and phthalonitriles 2009. <https://www.compositesworld.com/articles/resins-for-the-hot-zone-part-ii-bmis-ces-benzoxazines-and-phthalonitriles>.
111. Scofield, J. *Wide Temperature Power Electronics-Package Reliability Hurdles-*; Power Electronics Section, Propulsion Directorate, Air Force Research Laboratory: 2010.
112. Hopkins, D. C.; Bowers, J. S. In *Characterization of advanced materials for high voltage/high temperature power electronics packaging*, Applied Power Electronics Conference and Exposition, 2001. APEC 2001. Sixteenth Annual IEEE, 2001; 2001; pp 1062-1067 vol.2.
113. Zelmat, S.; Diaham, S.; Decup, M.; Locatelli, M. L.; Lebey, T. In *Weibull Statistical Dielectric Breakdown in Polyimide up to 400°C*, Electrical Insulation and Dielectric Phenomena, 2008. CEIDP 2008. Annual Report Conference on, 26-29 Oct. 2008; 2008; pp 583-586.
114. Khazaka, R.; Mendizabal, L.; Henry, D.; Hanna, R., Survey of High-Temperature Reliability of Power Electronics Packaging Components. *IEEE Transactions on Power Electronics* **2015**, *30* (5), 2456-2464.
115. Yiyang, Y.; Guo-Quan, L.; Zheng, C.; Boroyevich, D.; Ngo, K. D. T. In *Assessment of encapsulants for high-voltage, high-temperature power electronic packaging*, Electric Ship Technologies Symposium (ESTS), 2011 IEEE, 10-13 April 2011; 2011; pp 258-264.

116. Braun, T.; Becker, K. F.; Koch, M.; Bader, V.; Aschenbrenner, R.; Reichl, H., High-temperature reliability of Flip Chip assemblies. *Microelectronics Reliability* **2006**, *46* (1), 144-154.
117. Dent, C. E.; Linstead, R. P., 215. Phthalocyanines. Part IV. Copper phthalocyanines. *Journal of the Chemical Society (Resumed)* **1934**, (0), 1027-1031.
118. Marvel, C. S.; Rassweiler, J. H., Polymeric Phthalocyanines1. *Journal of the American Chemical Society* **1958**, *80* (5), 1197-1199.
119. Liepins, R.; Campbell, D.; Walker, C., 1,2-Dinitrile polymers. I. Homopolymers and copolymers of fumaronitrile, maleonitrile, and succinonitrile. *Journal of Polymer Science Part A-1: Polymer Chemistry* **1968**, *6* (11), 3059-3073.
120. Liepins, R., 1,2-dinitrile polymers. II. Homopolymers and copolymers of diphenylmaleonitrile, meso- and dl-diphenylsuccinonitrile, phthalonitrile. *Die Makromolekulare Chemie* **1968**, *118* (1), 36-44.
121. ISI Web of Knowledge. Clarivate Analytics: <http://www.webofknowledge.com/>, 2018.
122. Jiang, M.; Xu, M.; Jia, K.; Liu, X., Copolymerization of self-catalyzed phthalonitrile with bismaleimide toward high-temperature-resistant polymers with improved processability. *High Performance Polymers* **2016**, *28* (8), 895-907.
123. Chen, X.; Liu, J.; Xi, Z.; Shan, S.; Ding, H.; Qu, X.; Zhang, Q., Synthesis and thermal properties of high temperature phthalonitrile resins cured with self-catalytic amino-containing phthalonitrile compounds. *High Performance Polymers* **2017**, *29* (10), 1209-1221.
124. Sheng, H.; Peng, X.; Guo, H.; Yu, X.; Tang, C.; Qu, X.; Zhang, Q., Synthesis and thermal properties of a novel high temperature alkyl-center-trisphenolic-based phthalonitrile polymer. *Materials Chemistry and Physics* **2013**, *142* (2-3), 740-747.
125. Phua, E. J. R.; Liu, M.; Cho, B.; Liu, Q.; Amini, S.; Hu, X.; Gan, C. L., Novel high temperature polymeric encapsulation material for extreme environment electronics packaging. *Mater. Des.* **2018**, *141*, 202-209.
126. Badshah, A.; Kessler, M. R.; Heng, Z.; Hasan, A., Synthesis and characterization of phthalonitrile resins from ortho-linked aromatic and heterocyclic monomers. *Polymer International* **2014**, *63* (3), 465-469.
127. Satya B. Sastri, J. P. A., and Teddy M. Keller In *Flame Resistant Phthalonitrile Composites*, International Fire and Cabin Safety Research Conference Atlantic City, NJ, Atlantic City, NJ, 1998.
128. Yang, J.; Yang, X.; Zhan, Y.; Zou, Y.; Zhao, R.; Liu, X., Synthesis and properties of crosslinked poly(arylene ether nitriles) containing pendant phthalonitrile. *Journal of Applied Polymer Science* **2013**, *127* (3), 1676-1682.
129. Zhang, H.; Liu, T.; Yan, W.; Su, Y.; Yu, H.; Yang, Y.; Jiang, Z., Synthesis and properties of cross-linkable poly (aryl ether ketone) oligomers terminated with phthalonitrile group. *High Performance Polymers* **2014**, *26* (8), 1007-1014.
130. Yuan, P.; Liu, Y.; Zeng, K.; Yang, G., Synthesis and characterization of a new imide compound containing phthalonitrile and phenylethynyl end-groups. *Designed Monomers and Polymers* **2015**, *18* (4), 343-349.
131. Jiang, M.; Zou, X.; Huang, Y.; Liu, X., The effect of bismaleimide on thermal, mechanical, and dielectric properties of allyl-functional bisphthalonitrile/bismaleimide system. *High Performance Polymers* **2017**, *29* (9), 1016-1026.

132. Zhao, F.; Liu, R.; Yu, X.; Naito, K.; Qu, X.; Zhang, Q., A high temperature polymer of phthalonitrile-substituted phosphazene with low melting point and good thermal stability. *Journal of Applied Polymer Science* **2015**, *132* (39), n/a-n/a.
133. Brunovska, Z.; Lyon, R.; Ishida, H., Thermal properties of phthalonitrile functional polybenzoxazines. *Thermochimica Acta* **2000**, *357–358* (0), 195-203.
134. Zong, L.; Liu, C.; Guo, Y.; Wang, J.; Jian, X., Thermally stable phthalonitrile resins based on multiple oligo (aryl ether)s with phenyl-s-triazine moieties in backbones. *Rsc Advances* **2015**, *5* (94), 77027-77036.
135. Bulgakov, B. A.; Sulimov, A. V.; Babkin, A. V.; Kepman, A. V.; Malakho, A. P.; Avdeev, V. V., Dual-curing thermosetting monomer containing both propargyl ether and phthalonitrile groups. *Journal of Applied Polymer Science* **2017**, *134* (18).
136. Yang, Y.; Min, Z.; Yi, L., A novel addition curable novolac bearing phthalonitrile groups: synthesis, characterization and thermal properties. *Polymer Bulletin* **2007**, *59* (2), 185-194.
137. Guangxing, W.; Ying, G.; Zheng, L.; Shuangshuang, X.; Yue, H.; Zhenhua, L.; Li, Y.; Heng, Z.; Tong, Z., Synthesis and properties of phthalonitrile terminated polyaryl ether nitrile containing fluorene group. *Journal of Applied Polymer Science* *0* (0), 46606.
138. Hilmar Koerner, T. G., Timothy Pruyn, Heritage Weems, Sarah Izor, Personal Communication on Thermal Properties of Commercial Phthalonitriles. Monzel, J., Ed. 2017.
139. Matthew Laskoski, T. M. K., Dawn D. Dominguez In *High Temperature Phthalonitrile Resins/Polymers For Advanced Applications*, SAMPE, Long Beach, CA, May 23-26; Long Beach, CA, 2016.
140. Okutan, M.; Yakuphanoglu, F.; Köysal, O.; Durmuş, M.; Ahsen, V., Dielectric spectroscopy analysis in employing liquid crystal phthalonitrile derivative in nematic liquid crystals. *Spectrochimica Acta Part A: Molecular and Biomolecular Spectroscopy* **2007**, *67* (2), 531-535.
141. Adam, N.; Uğur, A. L.; Altındal, A.; Erdoğan, A., Synthesis, characterization and dielectric properties of novel phthalocyanines bearing an octa-peripherally substituted mercaptoquinoline moiety. *Polyhedron* **2014**, *68* (0), 32-39.
142. Pu, Z.; Tong, L.; Feng, M.; Jia, K.; Liu, X., Influence of hyperbranched copper phthalocyanine grafted carbon nanotubes on the dielectric and rheological properties of polyarylene ether nitriles. *RSC Advances* **2015**, *5* (88), 72028-72036.
143. Zhuo, D. X.; Gu, A. J.; Liang, G. Z.; Hu, J. T.; Yuan, L.; Chen, X. X., Flame retardancy materials based on a novel fully end-capped hyperbranched polysiloxane and bismaleimide/diallylbisphenol A resin with simultaneously improved integrated performance. *Journal of Materials Chemistry* **2011**, *21* (18), 6584-6594.
144. Chen, X. X.; Ye, J. H.; Yuan, L.; Liang, G. Z.; Gu, A. J., Multi-functional ladderlike polysiloxane: synthesis, characterization and its high performance flame retarding bismaleimide resins with simultaneously improved thermal resistance, dimensional stability and dielectric properties. *Journal of Materials Chemistry A* **2014**, *2* (20), 7491-7501.
145. Bushnell-Watson, S. M.; Morris, M. J.; Sharp, J. H., Effect of processing variables on the properties of polysilane ceramic precursors. *Polymer* **1996**, *37* (11), 2067-2076.
146. Abu-eid, M. A.; Bruce King, R.; Kotliar, A. M., Synthesis of polysilane polymer precursors and their pyrolysis to silicon carbides. *European Polymer Journal* **1992**, *28* (3), 315-320.
147. Birot, M.; Pillot, J.-P.; Dunogues, J., Comprehensive Chemistry of Polycarbosilanes, Polysilazanes, and Polycarbosilazanes as Precursors of Ceramics. *Chemical Reviews* **1995**, *95* (5), 1443-1477.

148. Bahloul, D.; Pereira, M.; Gerardin, C., Pyrolysis chemistry of polysilazane precursors to silicon carbonitride. *Journal of Materials Chemistry* **1997**, 7 (1), 109-116.
149. West, R., The polysilane high polymers. *Journal of Organometallic Chemistry* **1986**, 300 (1-2), 327-346.
150. Shukla, S. K.; Tiwari, R. K.; Ranjan, A.; Saxena, A. K.; Mathur, G. N., Some thermal studies of polysilanes and polycarbosilanes. *Thermochimica Acta* **2004**, 424 (1-2), 209-217.
151. Miller, R. D.; Michl, J., Polysilane high polymers. *Chemical Reviews* **1989**, 89 (6), 1359-1410.
152. Robert, W.; Jim, M., Polysilane High Polymers: An Overview. In *Inorganic and Organometallic Polymers*, American Chemical Society: 1988; Vol. 360, pp 6-20.
153. Chen, M.; Zhou, B.; Liao, Y.; Huang, S., Synthesis and investigation of the properties of a star-shaped polysilane. *Materials Letters* **2009**, 63 (23), 2032-2034.
154. Kuřitka, I.; Horváth, P.; Schauer, F.; Zemek, J., Thermal stability of plasma deposited polysilanes. *Polymer Degradation and Stability* **2006**, 91 (12), 2901-2910.
155. Gardelle, B.; Duquesne, S.; Vu, C.; Bourbigot, S., Thermal degradation and fire performance of polysilazane-based coatings. *Thermochimica Acta* **2011**, 519 (1-2), 28-37.
156. Goudie, J. L.; Owen, M. J.; Orbeck, T. In *A review of possible degradation mechanisms of silicone elastomers in high voltage insulation applications*, Electrical Insulation and Dielectric Phenomena, 1998. Annual Report. Conference on, 25-28 Oct 1998; 1998; pp 120-127 vol. 1.
157. Rey, T.; Chagnon, G.; Le Cam, J. B.; Favier, D., Influence of the temperature on the mechanical behaviour of filled and unfilled silicone rubbers. *Polymer Testing* **2013**, 32 (3), 492-501.
158. Jun, Y.; Mingfei, S.; Yuanrong, C.; Fei, X. In *Study of benzocyclobutene-functionalized siloxane thermoset with a cyclic structure*, Electronic Packaging Technology and High Density Packaging (ICEPT-HDP), 2011 12th International Conference on, 8-11 Aug. 2011; 2011; pp 1-6.
159. Hua, J.; Li, Z.; Qin, J.; Li, S.; Ye, C.; Lu, Z., Synthesis and characterization, second-order nonlinear optical and photorefractive properties of new multifunctional polysiloxane with broad optical transparent pentafluorophenyl azo chromophore. *Reactive and Functional Polymers* **2007**, 67 (1), 25-32.
160. Postava, K.; Yamaguchi, T.; Horie, M., Estimation of the dielectric properties of low-k materials using optical spectroscopy. *Applied Physics Letters* **2001**, 79 (14), 2231-2233.
161. Connor, J. A.; Finney, G.; Leigh, G. J.; Haszeldine, R. N.; Robinson, P. J.; Sedgwick, R. D.; Simmons, R. F., Bond dissociation energies in organosilicon compounds. *Chemical Communications (London)* **1966**, (6), 178-179.
162. Walsh, R. Bond Dissociation Energies in Organosilicon Compounds. (accessed Accessed 12/8/2014).
163. Camino, G.; Lomakin, S. M.; Lazzari, M., Polydimethylsiloxane thermal degradation Part 1. Kinetic aspects. *Polymer* **2001**, 42 (6), 2395-2402.
164. Renwick, W. J.; Reed, J. R., Silicone resins, fluids and elastomers in insulation for use at power frequencies. *Proceedings of the IEE - Part IIA: Insulating Materials* **1953**, 100 (3), 239-246.
165. Rhein, R. A. *Thermally Stable Elastomers: A Review*; Ordnance Systems Department, Naval Weapons Center China Lake, California: 1983.
166. Camino, G.; Lomakin, S. M.; Lageard, M., Thermal polydimethylsiloxane degradation. Part 2. The degradation mechanisms. *Polymer* **2002**, 43 (7), 2011-2015.

167. Sun, J. T.; Huang, Y. D.; Gong, G. F.; Cao, H. L., Thermal degradation kinetics of poly(methylphenylsiloxane) containing methacryloyl groups. *Polymer Degradation and Stability* **2006**, *91* (2), 339-346.
168. Zhou, W.; Yang, H.; Guo, X.; Lu, J., Thermal degradation behaviors of some branched and linear polysiloxanes. *Polymer Degradation and Stability* **2006**, *91* (7), 1471-1475.
169. Deshpande, G.; Rezac, M. E., Kinetic aspects of the thermal degradation of poly(dimethyl siloxane) and poly(dimethyl diphenyl siloxane). *Polymer Degradation and Stability* **2002**, *76* (1), 17-24.
170. Drake, K.; Mukherjee, I.; Mirza, K.; Ji, H.-F.; Wei, Y., Phenylethynyl and Phenol End-Capping Studies of Polybiphenyloxydiphenylsilanes for Cross-Linking and Enhanced Thermal Stability. *Macromolecules* **2011**, *44* (11), 4107-4115.
171. Liu, Y.; Shi, Y.; Zhang, D.; Li, J.; Huang, G., Preparation and thermal degradation behavior of room temperature vulcanized silicone rubber-g-polyhedral oligomeric silsesquioxanes. *Polymer* **2013**, *54* (22), 6140-6149.
172. Hans-Jörg Winter, J. L., Roland Bärsch In *On the measurement of the dielectric strength of silicone elastomers*, Universities Power Engineering Conference (UPEC), 2010 45th International, Aug. 31 2010-Sept. 3 2010; 2010; pp 1-5.
173. Finis, G.; Claudi, A.; Malin, G. In *Dielectric breakdown strength of silicone gel under various environmental conditions*, Power Tech, 2005 IEEE Russia, 27-30 June 2005; 2005; pp 1-6.
174. Finis, G.; Claudi, A., On the dielectric breakdown behavior of silicone gel under various stress conditions. *Dielectrics and Electrical Insulation, IEEE Transactions on* **2007**, *14* (2), 487-494.
175. Zhang, B. J.; Zhuo, D. X.; Gu, A. J.; Liang, G. Z.; Hu, J. T.; Yuan, L., Preparation and properties of addition curable silicone resins with excellent dielectric properties and thermal resistance. *Polymer Engineering and Science* **2012**, *52* (2), 259-267.
176. Tagle, L. H.; Terraza, C. A.; Leiva, A.; Valenzuela, P., Poly(amides) and poly(imides) containing silicon and germanium in the main chain: Synthesis, characterization and thermal studies. *Journal of Applied Polymer Science* **2006**, *102* (3), 2768-2776.
177. Steele, W. V., The standard enthalpy of formation of tetraphenylsilane and the Ph-M mean bond-dissociation energies of the Group IV elements. *The Journal of Chemical Thermodynamics* **1978**, *10* (5), 445-452.
178. Coutant, W. R. L., Arthur A *Kinetic Study of the Thermal Decomposition of Selected Cyclohexyl and Phenylsilanes*; Battelle Memorial Inst Columbus Ohio Columbus Labs: Air Force Research Laboratories, Office of Aerospace Research, Wright Patterson Air Force Base, Ohio, 1969.
179. Lee E. Nelson, N. C. A., Donald R. Weyenberg, The Free Radical-Catalyzed Disproportionation of Arylsilanes. A New Homolytic Aromatic Displacement Reaction. *Journal of the American Chemical Society* **1963**, *85* (17), 2662-2663.
180. Gilman, H.; Miles, D., Communications - Disproportionation Reaction of Diphenylsilane in the Absence of Any Added Catalyst. *The Journal of Organic Chemistry* **1958**, *23* (2), 326-328.
181. Andrew J Guenther, V. V., Timothy S Haddad, Josiah T Reams, Kevin R Lamison, Christopher M Sahagun, Sean M Ramirez, Gregory R Yandek, Joseph M Mabry, Silicon-Containing Tri- and Tetra-Functional Cyanate Esters: Synthesis, Cure Kinetics, and Network Properties. *AIR FORCE RESEARCH LAB EDWARDS AFB CA AEROSPACE SYSTEMS DIRECTORATE* **2104**.

182. Tang, H.; Song, N.; Chen, X.; Fan, X.; Zhou, Q., Synthesis and properties of silicon-containing bismaleimide resins. *Journal of Applied Polymer Science* **2008**, *109* (1), 190-199.
183. Zhang, B.; Wang, Z., Building ultramicropores within organic polymers based on a thermosetting cyanate ester resin. *Chemical Communications* **2009**, (33), 5027-5029.
184. Cazacu, M.; Racles, C.; Vlad, A.; Marcu, M., Segmented poly(siloxane-ester-imide)s. *European Polymer Journal* **2001**, *37* (12), 2465-2473.
185. Othman, M. B. H.; Ramli, M. R.; Tyng, L. Y.; Ahmad, Z.; Akil, H. M., Dielectric constant and refractive index of poly (siloxane-imide) block copolymer. *Mater. Des.* **2011**, *32* (6), 3173-3182.
186. Ku, C.-K.; Ho, C.-H.; Chen, T.-S.; Lee, Y.-D., Synthesis and characterization of pyridine-containing poly(imide-siloxane)s and their adhesion to copper foil. *Journal of Applied Polymer Science* **2007**, *104* (4), 2561-2568.
187. Novák, I.; Sysel, P.; Zemek, J.; Špírková, M.; Velič, D.; Aranyosiová, M.; Florián, Š.; Pollák, V.; Kleinová, A.; Lednický, F.; Janigová, I., Surface and adhesion properties of poly(imide-siloxane) block copolymers. *European Polymer Journal* **2009**, *45* (1), 57-69.
188. Ghosh, A.; Sen, S. K.; Dasgupta, B.; Banerjee, S.; Voit, B., Synthesis, characterization and gas transport properties of new poly(imide siloxane) copolymers from 4,4'-(4,4'-isopropylidenediphenoxy)bis(phthalic anhydride). *Journal of Membrane Science* **2010**, *364* (1-2), 211-218.
189. Ku, C.-K.; Lee, Y.-D., Microphase separation in amorphous poly(imide siloxane) segmented copolymers. *Polymer* **2007**, *48* (12), 3565-3573.
190. Wang, H. M.; Tao, X. M.; Newton, E., Dielectric properties of fluorine-containing polymethylsiloxane-imide films. *High Performance Polymers* **2002**, *14* (3), 271-283.
191. Chang, T. C.; Wu, K. H.; Liao, C. L.; Lin, S. T.; Wang, G. P., Thermo-oxidative degradation of siloxane-containing polyimide and unmodified polyimide. *Polymer Degradation and Stability* **1998**, *62* (2), 299-305.
192. Adhikari, R.; Dao, B.; Hodgkin, J.; Mardel, J., Synthesis, structures and membrane properties of siloxane-imide co-polymers produced by aqueous polymerization. *European Polymer Journal* **2011**, *47* (6), 1328-1337.
193. Shi, L. T., Characterization of a polyimide siloxane by thermal analysis. *Thermochimica Acta* **1990**, *166* (0), 127-136.
194. Tsai, M.-H.; Chiang, P.-C.; Whang, W.-T.; Ko, C.-J.; Huang, S.-L., Synthesis and characteristics of polyimide/siloxane hybrid films for reliability adhesion. *Surface and Coatings Technology* **2006**, *200* (10), 3297-3302.
195. Chavez, R.; Ionescu, E.; Fasel, C.; Riedel, R., Silicon-Containing Polyimide-Based Polymers with High Temperature Stability. *Chemistry of Materials* **2010**, *22* (13), 3823-3825.
196. Chavez, R.; Ionescu, E.; Fasel, C.; Riedel, R., Imide-containing ladder polyphenylsilsesquioxanes with high thermal stability and thermoplastic properties. *Journal of Applied Polymer Science* **2014**, *131* (7).
197. Kwart, H.; King, K., *d-Orbitals in the Chemistry of Silicon, Phosphorus and Sulfur*. Springer Berlin Heidelberg: 2012.
198. Kawakami, Y.; Li, Y., Approaches to polymers containing a silicon-oxygen bond in the main chain. *Designed Monomers and Polymers* **2000**, *3* (4), 399-419.
199. Curry, J. E.; Byrd, J. D., Silane polymers of diols. *Journal of Applied Polymer Science* **1965**, *9* (1), 295-311.

200. Dunnavant, W. R.; Markle, R. A.; Sinclair, R. G.; Stickney, P. B.; Curry, J. E.; Byrd, J. D., p,p'-Biphenol-Dianilinosilane Condensation Copolymers. *Macromolecules* **1968**, *1* (3), 249-254.
201. Pacansky, T. J.; Schank, R. L.; Gruber, R. J.; Brandt, K. A.; Bernardo, M., Synthesis and thermomechanical properties of alternating copolymers containing bisphenol-A. *Journal of Polymer Science: Polymer Chemistry Edition* **1980**, *18* (10), 3119-3127.
202. Dunnavant, W. R.; Markle, R. A.; Stickney, P. B.; Curry, J. E.; Byrd, J. D., Synthesis of polyaryloxysilanes by melt-polymerizing dianilino- and diphenoxysilanes with aromatic diols. *Journal of Polymer Science Part A-1: Polymer Chemistry* **1967**, *5* (4), 707-724.
203. Babanzadeh, S.; Mehdipour-Ataei, S.; Mahjoub, A. R., Preparation and Characterization of Novel Polyimide/SiO<sub>2</sub> Nano-hybrid Films by In Situ Polymerization. *Journal of Inorganic and Organometallic Polymers and Materials* **2012**, *22* (6), 1404-1412.
204. Agrawal, S.; Narula, A., Facile synthesis of new thermally stable and organosoluble polyamide-imides based on non-coplaner phosphorus and silicon containing amines. *J Chem Sci* **2014**, *126* (6), 1849-1859.
205. Kolahdoozan, M. G., Monir S. , Synthesis, characterization and properties of novel thermally stable copoly(amide-imide)s containing dimethylsilane moieties. *e-Polymers* **2011**, *008*.
206. Chang, T. C.; Tsai, T. M.; Liu, P. T.; Chen, C. W.; Yan, S. T.; Aoki, H.; Chang, Y. C.; Tseng, T. Y., CMP of ultra low-k material porous-polysilazane (PPSZ) for interconnect applications. *Thin Solid Films* **2004**, *447-448* (0), 524-530.
207. Coutant, W. R. L., *Arthur A Kinetic Study of the Thermal Decomposition of Selected Cyclohexyl and Phenylsilanes*; Battelle Memorial Institute: Aerospace Research Laboratories, Columbus Ohio, 1965.
208. Bulgakov, B. A.; Sulimov, A. V.; Babkin, A. V.; Afanasiev, D. V.; Solopchenko, A. V.; Afanaseva, E. S.; Kepmana, A. V.; Avdeeva, V. V., Flame-retardant carbon fiber reinforced phthalonitrile composite for high-temperature applications obtained by resin transfer molding. *Mendeleev Communications* **2017**, *27* (3), 257-259.
209. Bulgakov, B. A.; Babkin, A. V.; Bogolyubov, A. A.; Afanas'eva, E. S.; Kepman, A. V., Mechanical and physicochemical properties of matrices for fiber reinforced plastics based on low-melting phthalonitrile monomers. *Russian Chemical Bulletin* **2016**, *65* (1), 287-290.
210. Kaliavaradhan, K.; Muthusamy, S., Studies on novel tri-phthalonitrile phenyl polyhedral oligomeric silsesquioxane and the phthalonitrile-epoxy blends. *High Performance Polymers* **2015**, *28* (3), 296-308.
211. Toru, H. U. M. M. P. Y. R. S. N. T., Convenient synthesis of phthalocyanines with disilazanes under mild conditions. *ARKIVOC-Archive for Organic Chemistry* **2004**, *2005* (11), 17-23.
212. C., L. D.; Tobias, H.; A., K. B., The Role of Precursor-Decomposition Kinetics in Silicon-Nanowire Synthesis in Organic Solvents. *Angewandte Chemie International Edition* **2005**, *44* (23), 3573-3577.
213. Naghash, H. J.; Massah, A. R.; Kalbasi, R. J.; Arman, M., Crosslinked methyl methacrylate/ethylene glycol dimethacrylate polymer compounds with a macroazoinitiator. *Journal of Applied Polymer Science* **2010**, *116* (1), 382-393.
214. Shao, Y.; Li, Y. F.; Wang, X. L.; Guo, J. S.; Zhao, X., Synthesis of a new siloxane-containing diamine and related polyimide. *Chinese Chemical Letters* **2007**, *18* (6), 762-763.
215. Fournier, J.-H.; Wang, X.; Wuest, J. D., Derivatives of tetraphenylmethane and tetraphenylsilane: Synthesis of new tetrahedral building blocks for molecular construction. *Canadian Journal of Chemistry* **2003**, *81* (5), 376-380.

216. Nishide, K.; Ohsugi, S.-i.; Miyamoto, T.; Kumar, K.; Node, M., Development of Odorless Thiols and Sulfides and Their Applications to Organic Synthesis. *Monatshefte für Chemie / Chemical Monthly* **2004**, *135* (2), 189-200.
217. Fujii, S.; Miyajima, Y.; Masuno, H.; Kagechika, H., Increased Hydrophobicity and Estrogenic Activity of Simple Phenols with Silicon and Germanium-Containing Substituents. *Journal of Medicinal Chemistry* **2013**, *56* (1), 160-166.
218. Beele, B.; Guenther, J.; Perera, M.; Stach, M.; Oeser, T.; Blumel, J., New linker systems for superior immobilized catalysts. *New Journal of Chemistry* **2010**, *34* (12), 2729-2731.
219. Davidsohn, W.; Laliberte, B. R.; Goddard, C. M.; Henry, M. C., Organometallic bis(p-hydroxyphenyl) derivatives of group IV elements and related compounds. *Journal of Organometallic Chemistry* **1972**, *36* (2), 283-291.
220. Brenzovich, W. E.; Brazeau, J.-F.; Toste, F. D., Gold-Catalyzed Oxidative Coupling Reactions with Aryltrimethylsilanes. *Organic Letters* **2010**, *12* (21), 4728-4731.
221. Hirano, K.; Biju, A. T.; Piel, I.; Glorius, F., N-Heterocyclic Carbene-Catalyzed Hydroacylation of Unactivated Double Bonds. *Journal of the American Chemical Society* **2009**, *131* (40), 14190-14191.
222. Sheng, L.; Zeng, J.; Xing, S.; Yin, C.; Yang, J.; Yang, Y.; Xiao, J., A new resin with improved processability and thermal stability. *High Performance Polymers* **2017**, *29* (1), 13-25.
223. Liu, X.-Q.; Jikei, M.; Kakimoto, M.-a., Synthesis and Properties of AB-Type Semicrystalline Polyimides Prepared from Polyamic Acid Ethyl Ester Precursors. *Macromolecules* **2001**, *34* (10), 3146-3154.
224. Tagle, L. H.; Vega, J. C.; Diaz, F. R.; Radic, D.; Gargallo, L.; Valenzuela, P., Polymerization by Phase Transfer Catalysis. 25. Synthesis of Polycarbonates and Polythiocarbonates Derived from Diphenols Containing Germanium and Silicon in the Main Chain. *Journal of Macromolecular Science, Part A* **2000**, *37* (9), 997-1008.
225. Terraza, C. A.; Tagle, L. H.; Concha, F.; Poblete, L., Synthesis and characterization of new bi-functional monomers based on germerylene or silarylene units: 4,4'-(R1R2-silylene)bis(phenyl chloroformates) and 4,4'-(R1R2-germylene)bis(phenyl chloroformates). *Designed Monomers and Polymers* **2007**, *10* (3), 253-261.
226. *CrysAlisPro Software System*, v1.171.37.35; Rigaku Oxford Diffraction: Rigaku Corporation, Oxford, UK., 2015.
227. Sheldrick, G. M., SHELXT – Integrated space-group and crystal structure determination. *Acta Cryst.* **2015**, (A71), 3–8.
228. Sheldrick, G. M., Crystal structure refinement with SHELXL. *Acta Cryst.* **2015**, C71, 3-8.
229. Dolomanov, O. V. B., L. J.; Gildea, R. J.; Howard, J. A. K.; Puschmann, H. , *J. Appl. Cryst.* **2009**, *42*, 339–341.
230. Gilman, H.; Goodman, J. J., Some Monomeric Organosilicon Compounds of High Thermal Stability. *The Journal of Organic Chemistry* **1957**, *22* (1), 45-47.
231. Schnabel, W. J. Bis-Aryloxyphenyl-Dialkylsilanes. June 5, 1959, 1961.
232. Andrew J. Guenther, K. B. G., Jerry A. Boatz, Denisse Soto In *Melting Points by Design in High Temperature Thermosetting Monomers*, High Temperature Polymeric Laminates (High Temple) Workshop, Palm Springs, CA, Jan 30 2018; Palm Springs, CA, 2018.
233. Liu, T.; Wang, Y.; Su, Y.; Yu, H.; Zhao, N.; Yang, Y.; Jiang, Z., Preparation and properties of film materials of poly(aryl ether ketone)-based phthalonitrile resins. *Polymer Engineering & Science* **2015**, *55* (10), 2313-2321.

234. Tong, L.; Pu, Z.; Huang, X.; Chen, Z.; Yang, X.; Liu, X., Crosslinking behavior of polyarylene ether nitrile terminated with phthalonitrile (PEN-t-Ph)/1,3,5-Tri-(3,4-dicyanophenoxy) benzene (TPh) system and its enhanced thermal stability. *Journal of Applied Polymer Science* **2013**, *130* (2), 1363-1368.
235. Ji, S.; Yuan, P.; Hu, J.; Sun, R.; Zeng, K.; Yang, G., A novel curing agent for phthalonitrile monomers: Curing behaviors and properties of the polymer network. *Polymer* **2016**, *84*, 365-370.
236. Gibson, A. P. M. a. A. G., *Fire Properties of Polymer Composite Materials*. Springer: Dordrecht, The Netherlands, 2006; Vol. 143.
237. Sorathia, U., 19 - Flame Retardant Materials for Maritime and Naval Applications. In *Advances in Fire Retardant Materials*, Horrocks, A. R.; Price, D., Eds. Woodhead Publishing: 2008; pp 527-572.
238. Properties of Unreinforced Cyanate Ester Matrix Resins. In *Chemistry and Technology of Cyanate Ester Resins*, 1 ed.; Hamerton, I., Ed. Chapman & Hall: Department of Chemistry University of Surrey, 1994; pp 193-229.
239. Lyon, R. E.; Walters, R. N.; Gandhi, S., Combustibility of Cyanate Ester Resins. *Fire and Materials* **2006**, *30* (2), 89-106.
240. Deshpande, G.; Rezac, M. E., The effect of phenyl content on the degradation of poly(dimethyl diphenyl) siloxane copolymers. *Polymer Degradation and Stability* **2001**, *74* (2), 363-370.
241. Pawlenko, S., *Organosilicon Chemistry*. Walter de Gruyter: Berlin, 1986.
242. Pruynt, T., TOS of PN Resins Monzel, W. J., Ed. 2017-2018.
243. Gilman, H.; Gorsich, R. D., Cyclic Organosilicon Compounds. I. Synthesis of Compounds Containing the Dibenzosilole Nucleus. *Journal of the American Chemical Society* **1958**, *80* (8), 1883-1886.
244. Gilman, H.; Oita, K., Cleavage of Some Organosilicon Compounds by Formic Acid. *Journal of the American Chemical Society* **1955**, *77* (12), 3386-3387.

## 13 Appendix A: Analysis of Synthesized Compounds

### 13.1 $^1\text{H}$ NMR Spectra

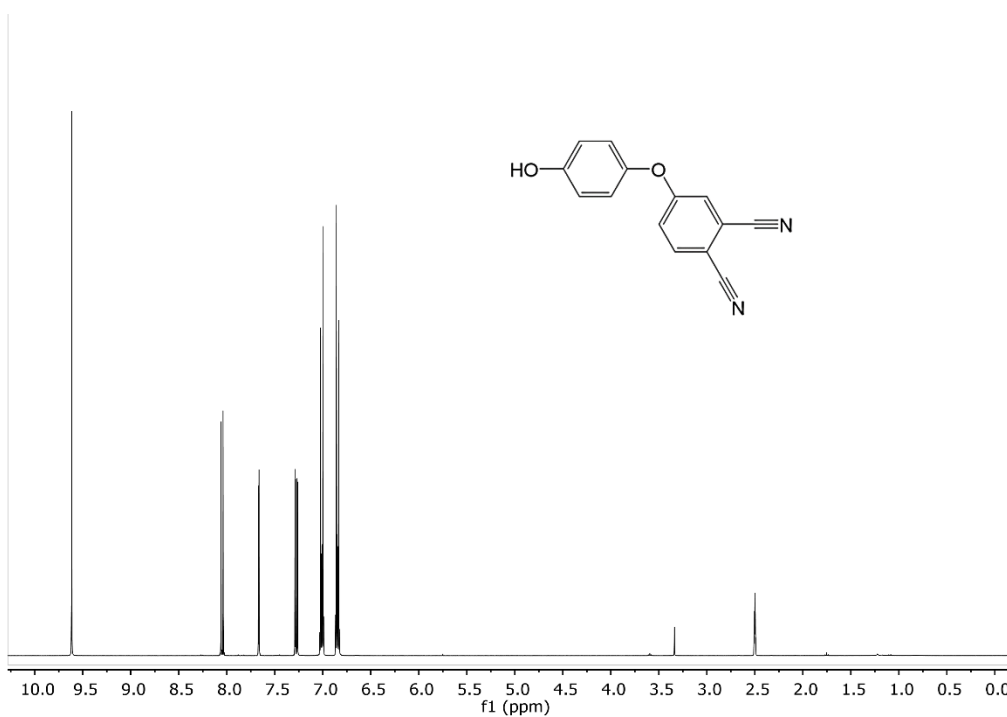


Figure 135:  $^1\text{H}$  NMR of 4-(4-hydroxyphenoxy)phthalonitrile (HOPOPN) in  $\text{DMSO-d}_6$ .

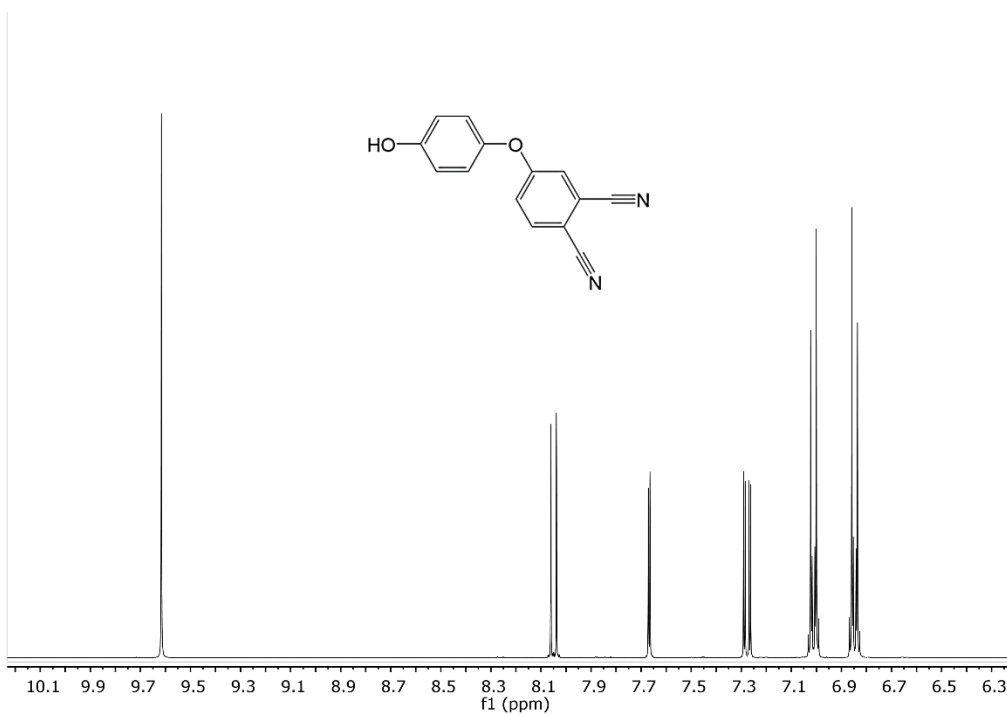


Figure 136: Excerpt of molecule peaks,  $^1\text{H}$  NMR of 4-(4-hydroxyphenoxy)phthalonitrile (HOPOPN) in  $\text{DMSO-d}_6$ .

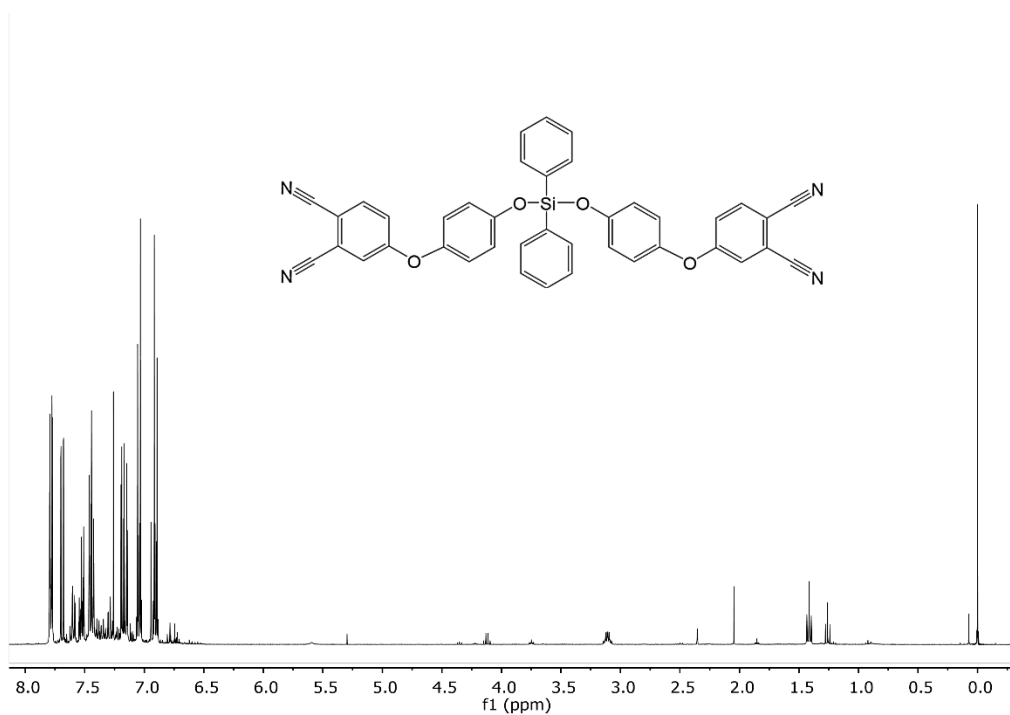


Figure 137: <sup>1</sup>H NMR of 4,4'-(((diphenylsilyl)bis(oxy))bis(4,1-phenylene))bis(oxy)diphthalonitrile (COSPN) in CDCl<sub>3</sub> with TMS.

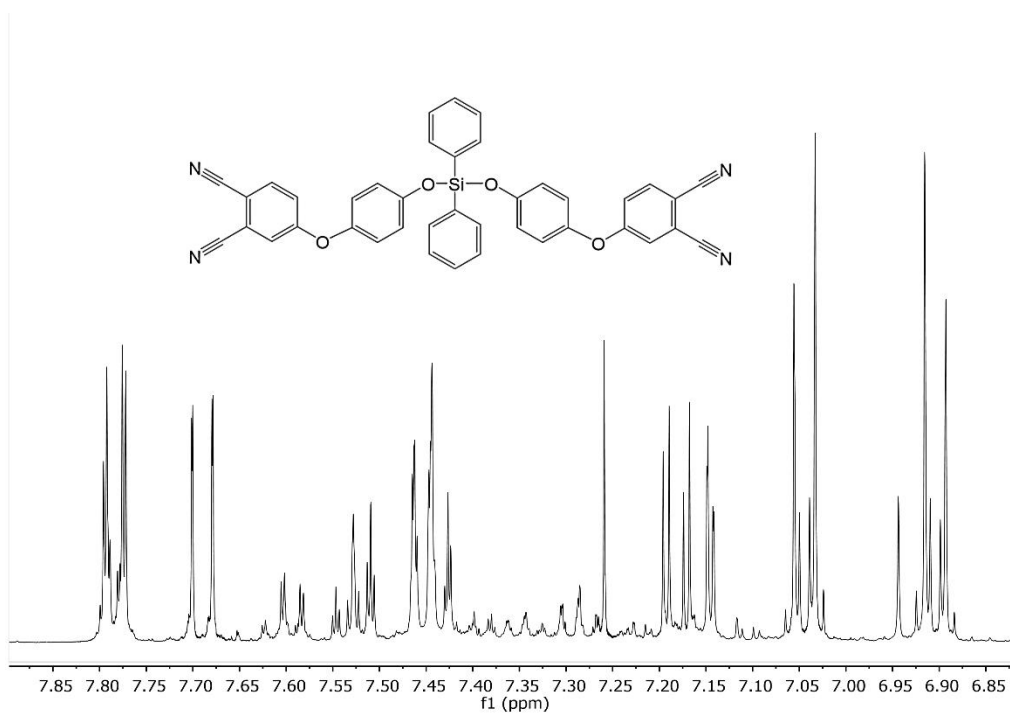


Figure 138: Excerpt of monomer peaks, <sup>1</sup>H NMR of 4,4'-(((diphenylsilyl)bis(oxy))bis(4,1-phenylene))bis(oxy)diphthalonitrile (COSPN) in CDCl<sub>3</sub>.

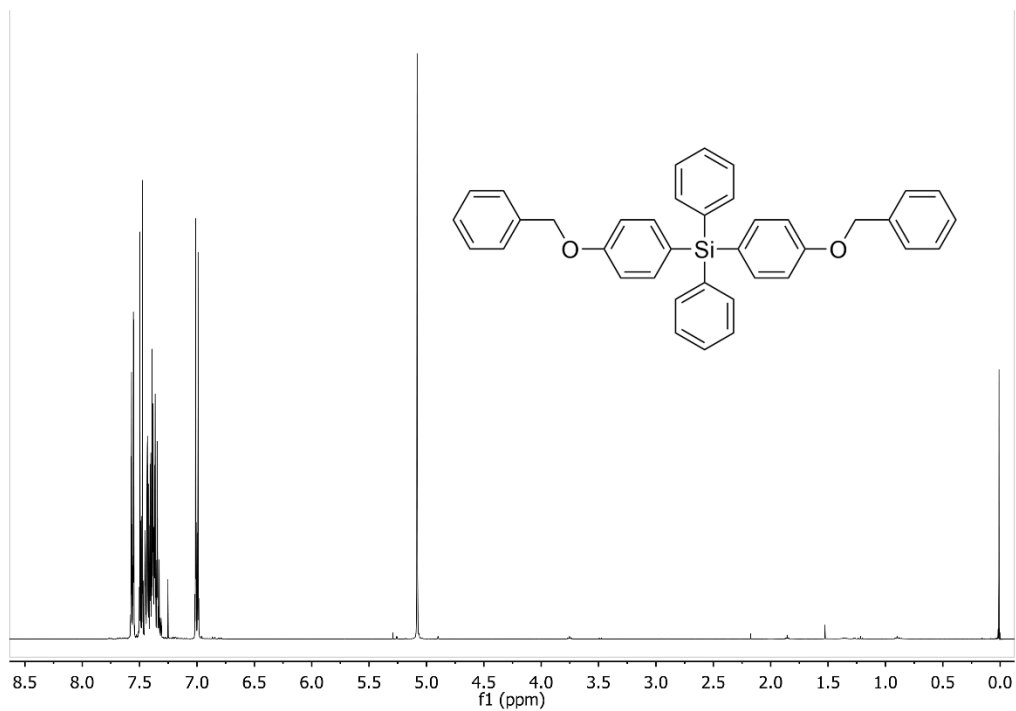


Figure 139:  $^1\text{H}$  NMR of bis(4-(benzyloxy)phenyl)diphenylsilane (BODPS) in  $\text{CDCl}_3$  with TMS.

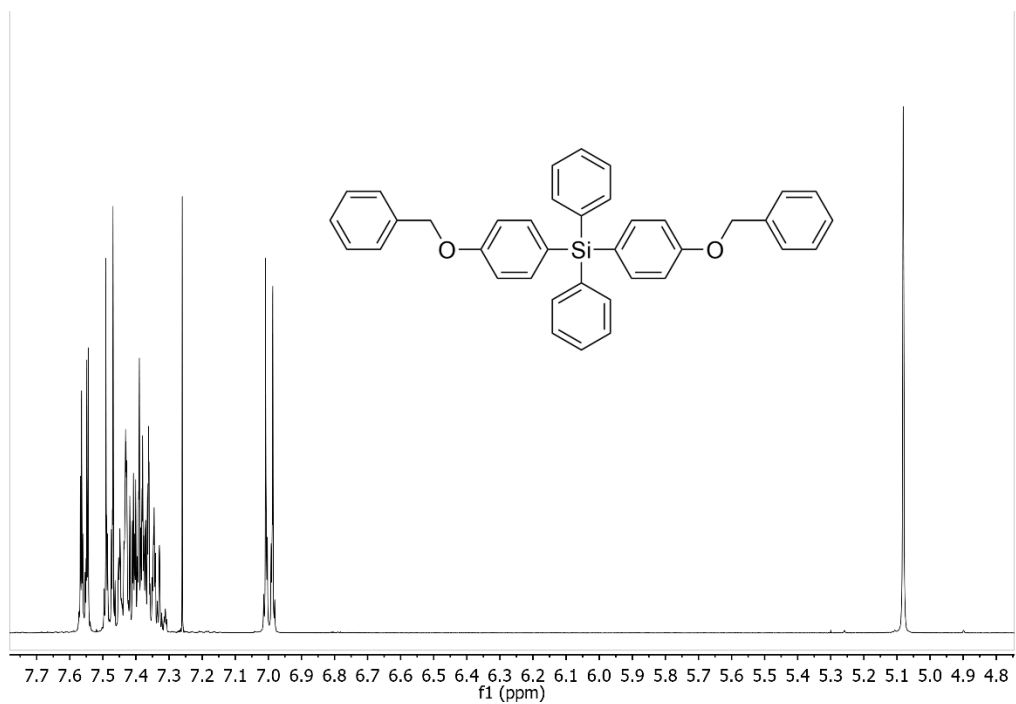


Figure 140: Excerpt of molecule peaks,  $^1\text{H}$  NMR of bis(4-(benzyloxy)phenyl)diphenylsilane (BODPS) in  $\text{CDCl}_3$  with TMS.

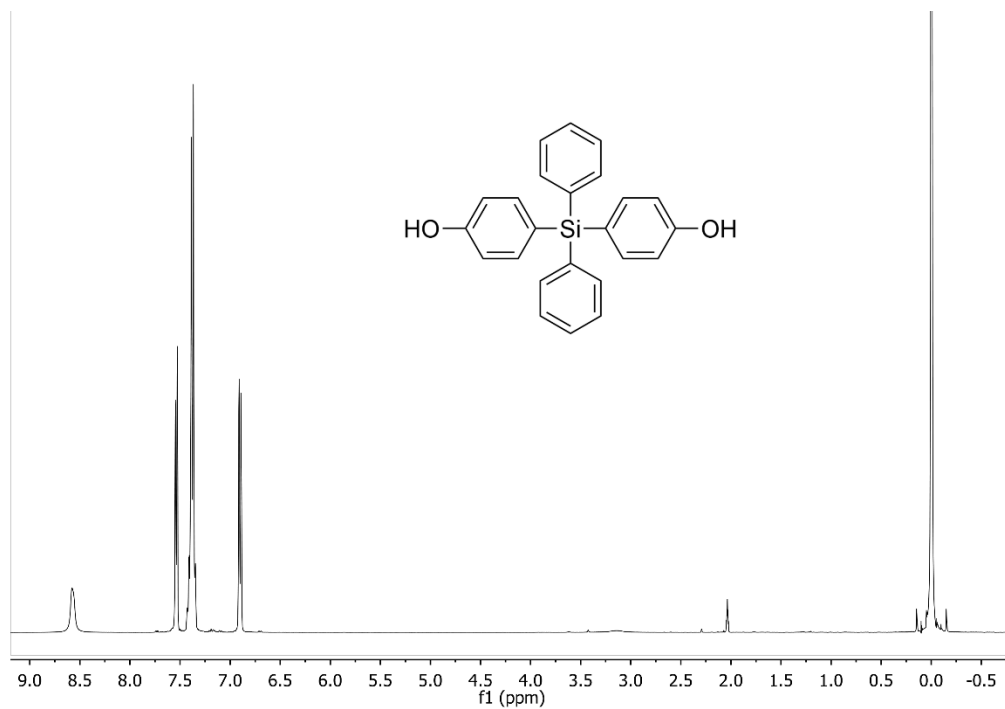


Figure 141: <sup>1</sup>H NMR of 4,4'-(diphenylsilyl)bisphenol (DPSDP) in acetone-d<sub>6</sub> with TMS.

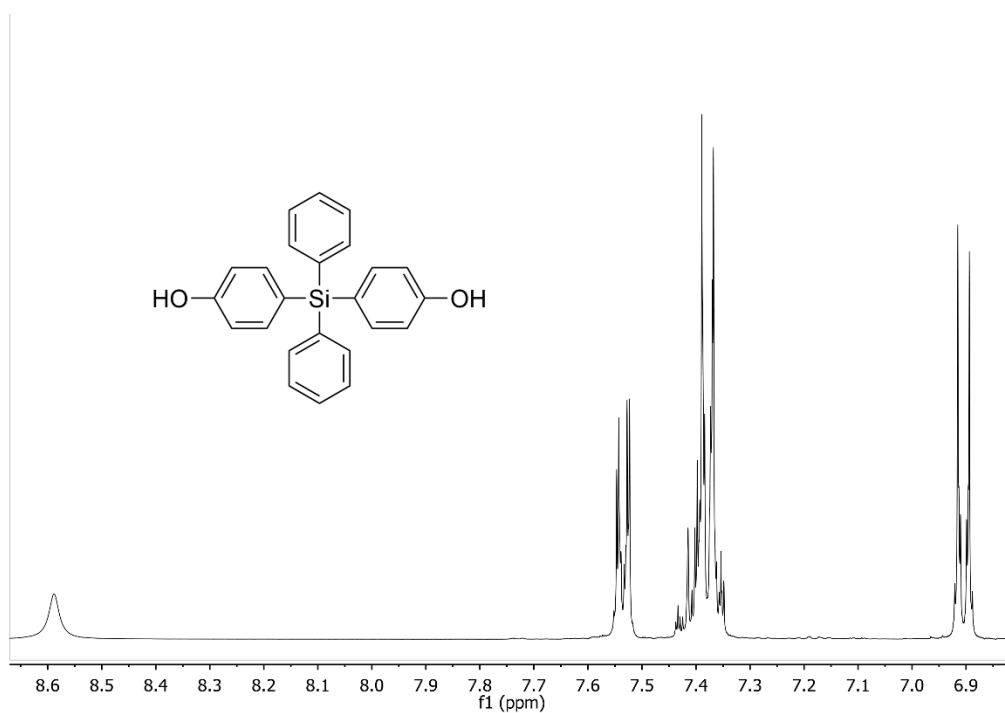


Figure 142: Excerpt of molecule peaks, <sup>1</sup>H NMR of 4,4'-(diphenylsilyl)bisphenol (DPSDP) in acetone-d<sub>6</sub> with TMS.

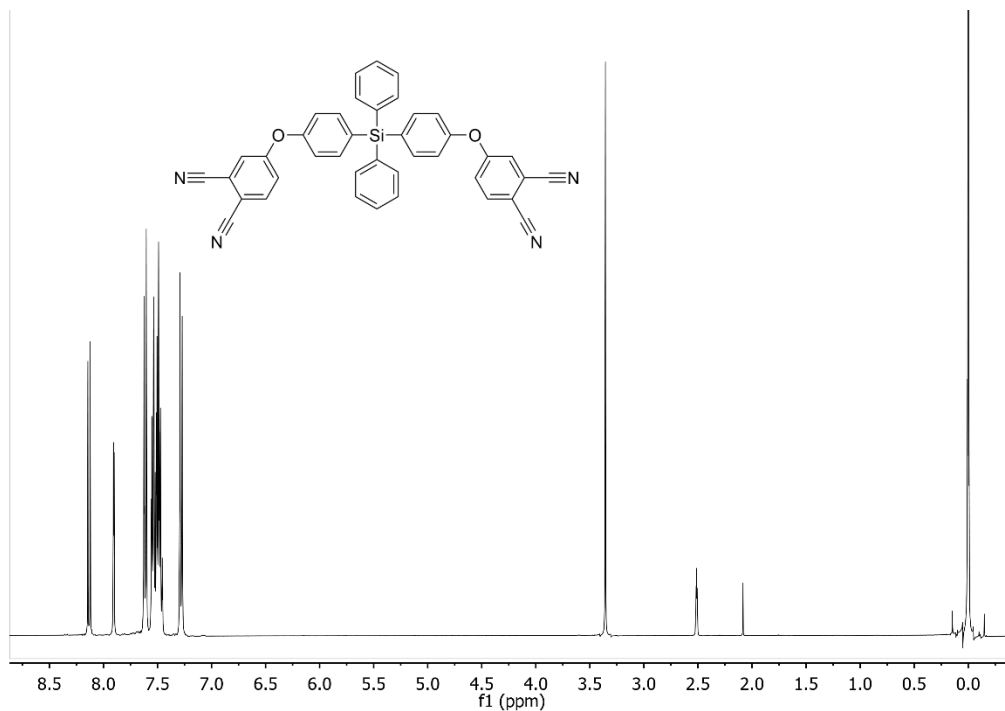


Figure 143: <sup>1</sup>H NMR of 4,4'-(((diphenylsilanediyl)bis(4,1-phenylene))bis(oxy))diphthalonitrile (CSPN) in DMSO-d<sub>6</sub> with TMS. Peaks at 3.33 and 2.05 correspond to water and acetonitrile respectively.

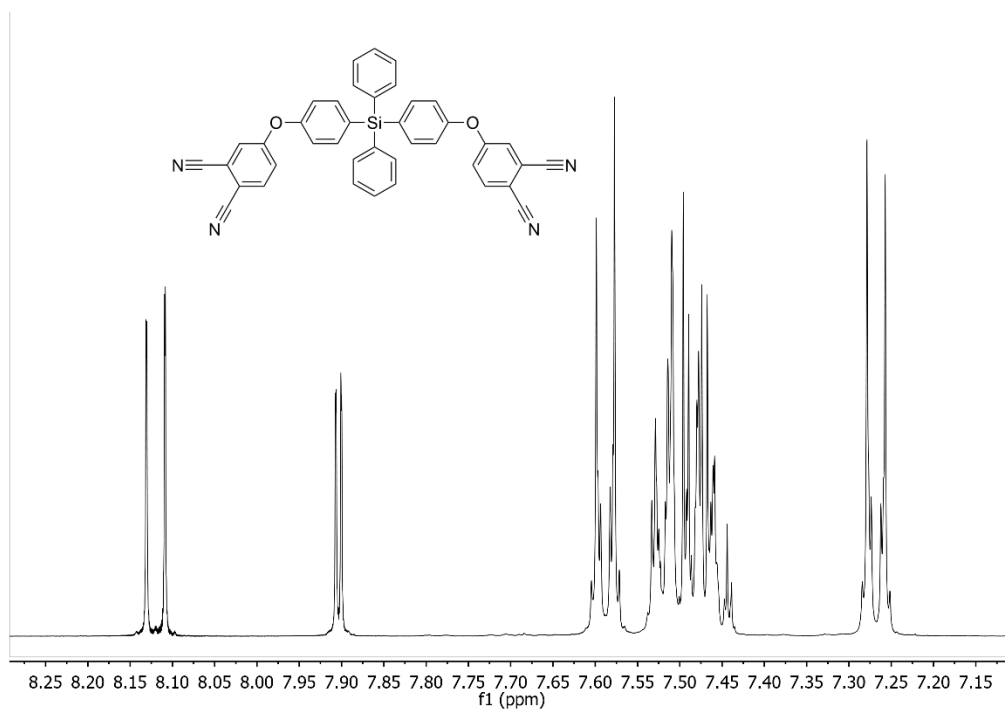


Figure 144: Excerpt of monomer peaks, <sup>1</sup>H NMR of 4,4'-(((diphenylsilanediyl)bis(4,1-phenylene))bis(oxy))diphthalonitrile (CSPN) in DMSO-d<sub>6</sub> with TMS.

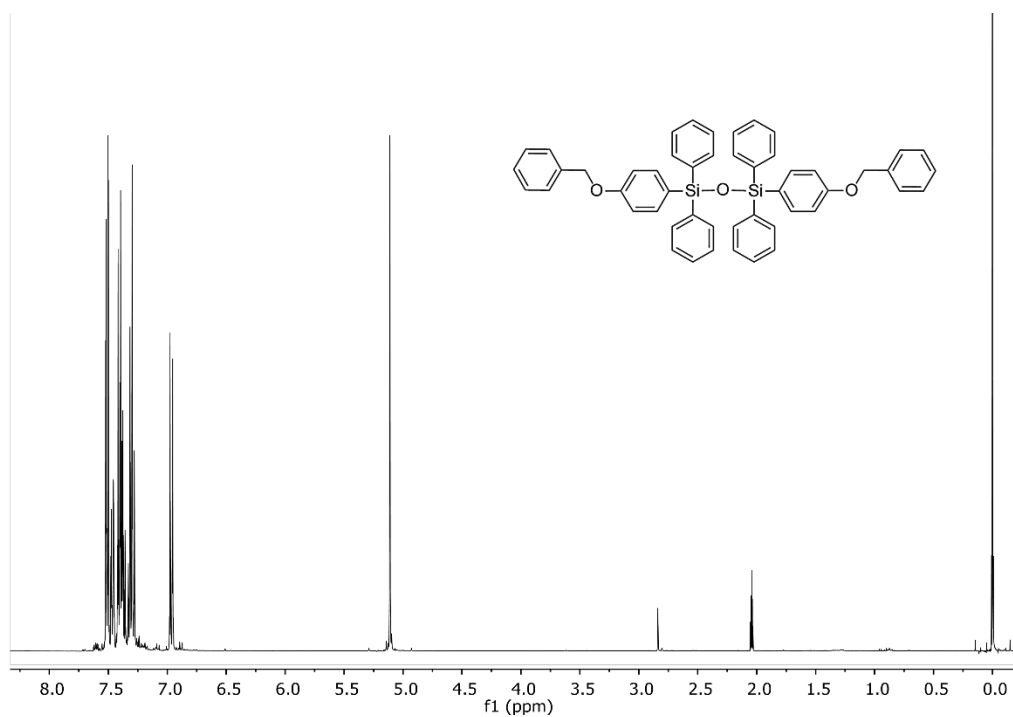


Figure 145:  $^1\text{H}$  NMR of 1,3-bis(4-(benzyloxy)phenyl)-1,1,3,3-tetraphenyldisiloxane (BODSO) in  $\text{CDCl}_3$  with TMS.

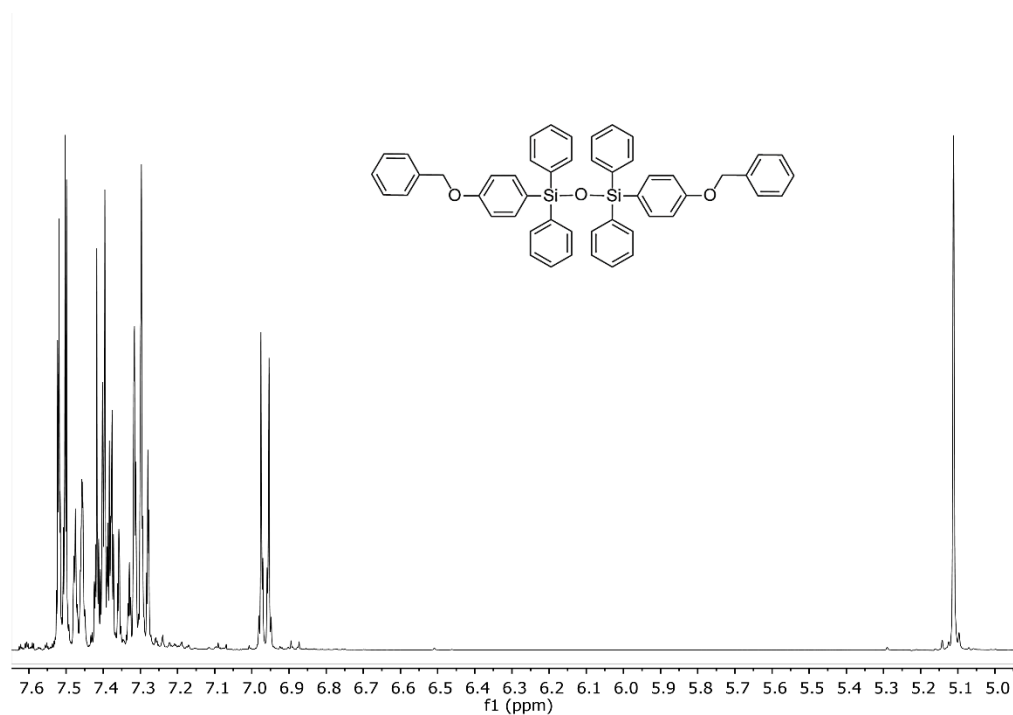


Figure 146: Excerpt of molecule peaks,  $^1\text{H}$  NMR of 1,3-bis(4-(benzyloxy)phenyl)-1,1,3,3-tetraphenyldisiloxane (BODSO) in  $\text{CDCl}_3$  with TMS.

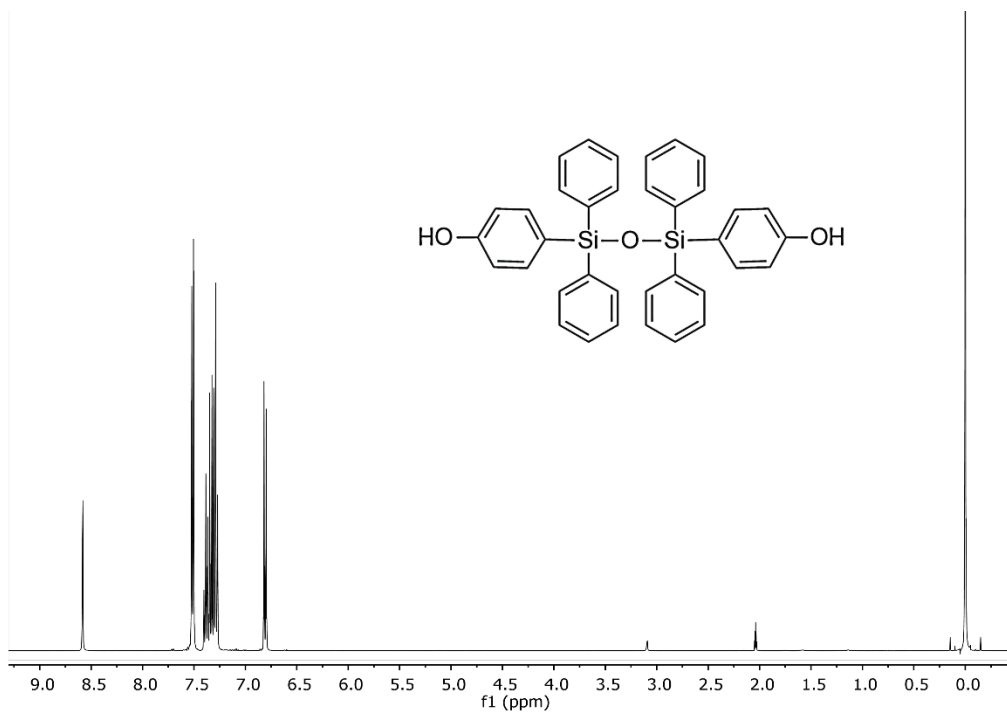


Figure 147:  $^1\text{H}$  NMR of 4,4'-(1,1,3,3-tetraphenyldisiloxane-1,3-diyl)diphenol (DPDSO) in  $\text{acetone-}d_6$  with TMS.

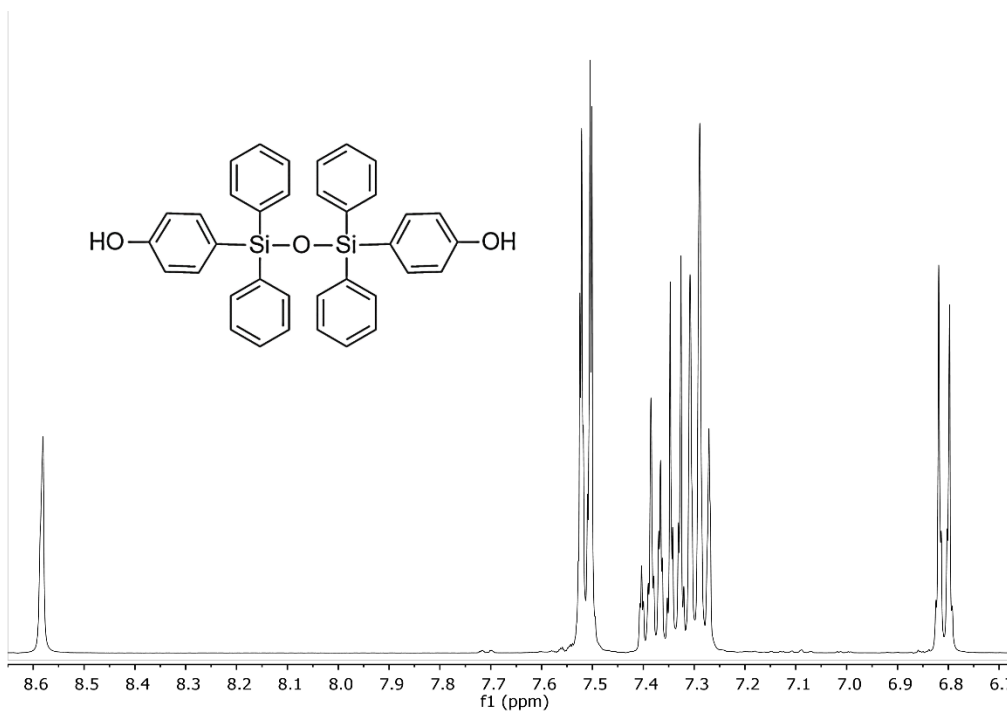


Figure 148: Excerpt of molecule peaks,  $^1\text{H}$  NMR of 4,4'-(1,1,3,3-tetraphenyldisiloxane-1,3-diyl)diphenol (DPDSO) in  $\text{acetone-}d_6$  with TMS.

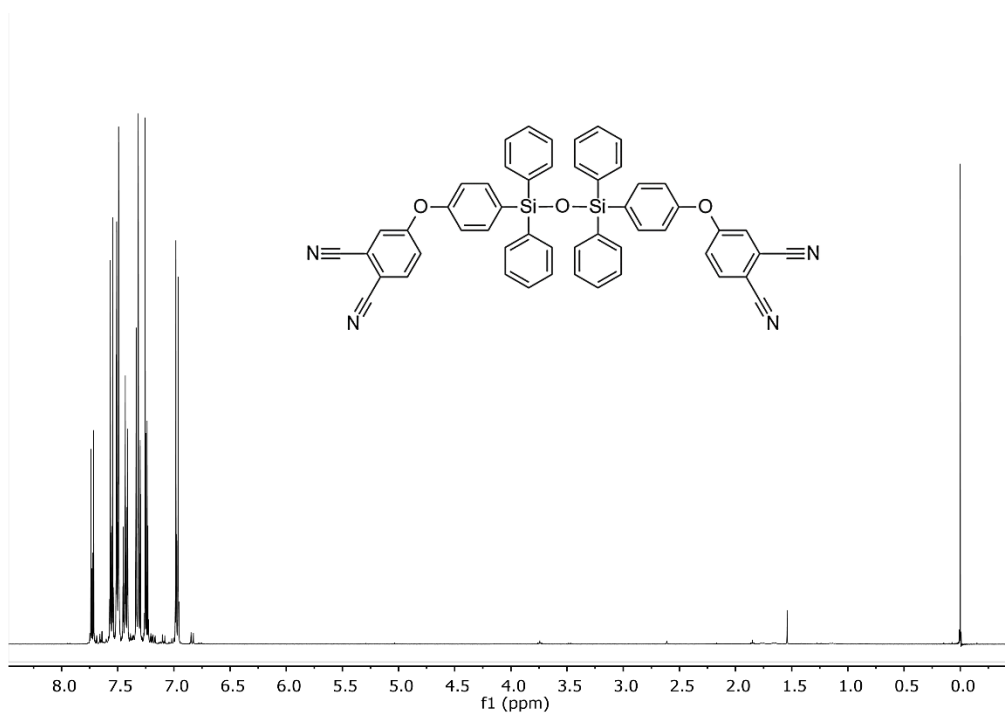


Figure 149:  $^1\text{H}$  NMR of 4,4'-(((1,1,3,3-tetraphenyldisiloxane-1,3-diyl)bis(4,1-phenylene))bis(oxy))diphthalonitrile (CSOPN) in  $\text{CDCl}_3$  with TMS.

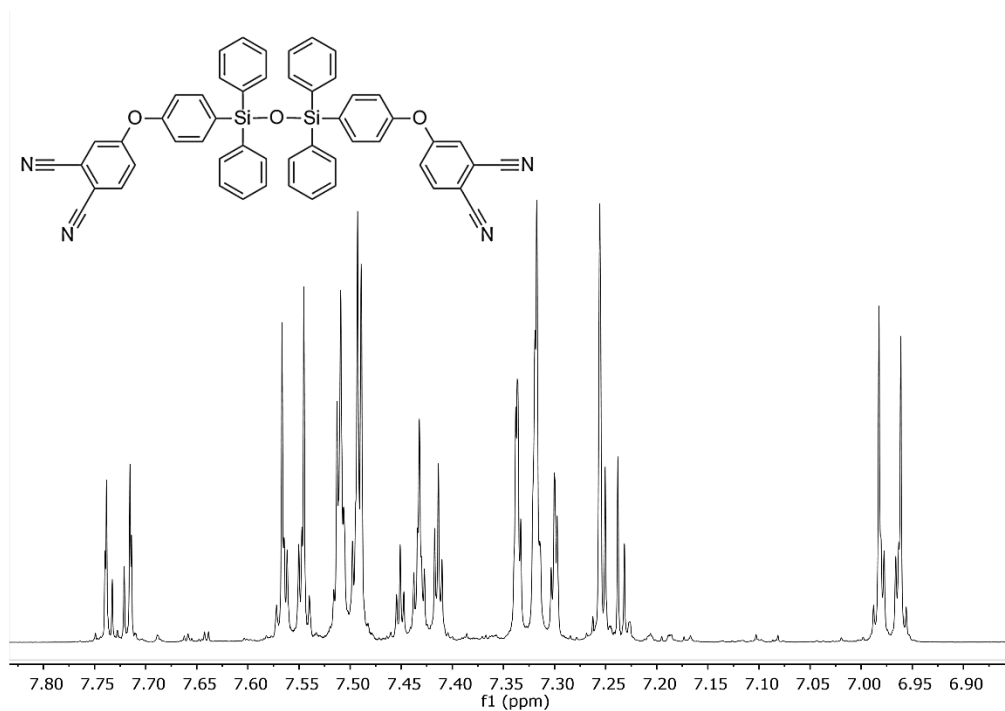


Figure 150: Excerpt of monomer peaks,  $^1\text{H}$  NMR of 4,4'-(((1,1,3,3-tetraphenyldisiloxane-1,3-diyl)bis(4,1-phenylene))bis(oxy))diphthalonitrile (CSOPN) in  $\text{CDCl}_3$  with TMS.

## 13.2 Correlation Spectroscopy (COSY) NMR Spectra

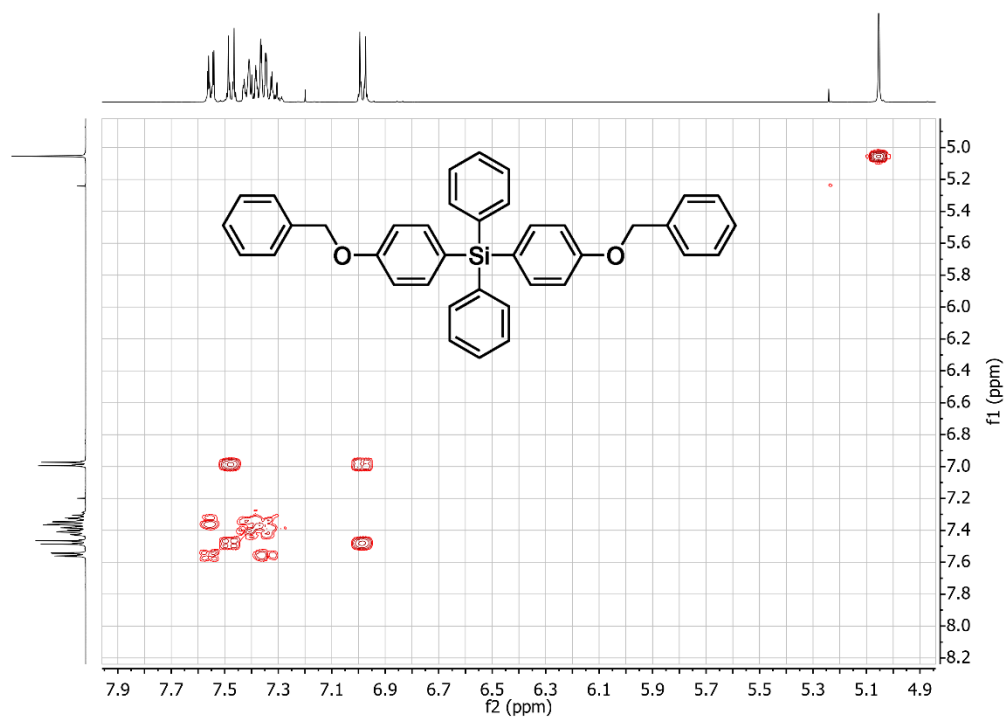


Figure 151: COSY NMR of bis(4-(benzyloxy)phenyl)diphenylsilane (BODPS) in  $CDCl_3$  with TMS.

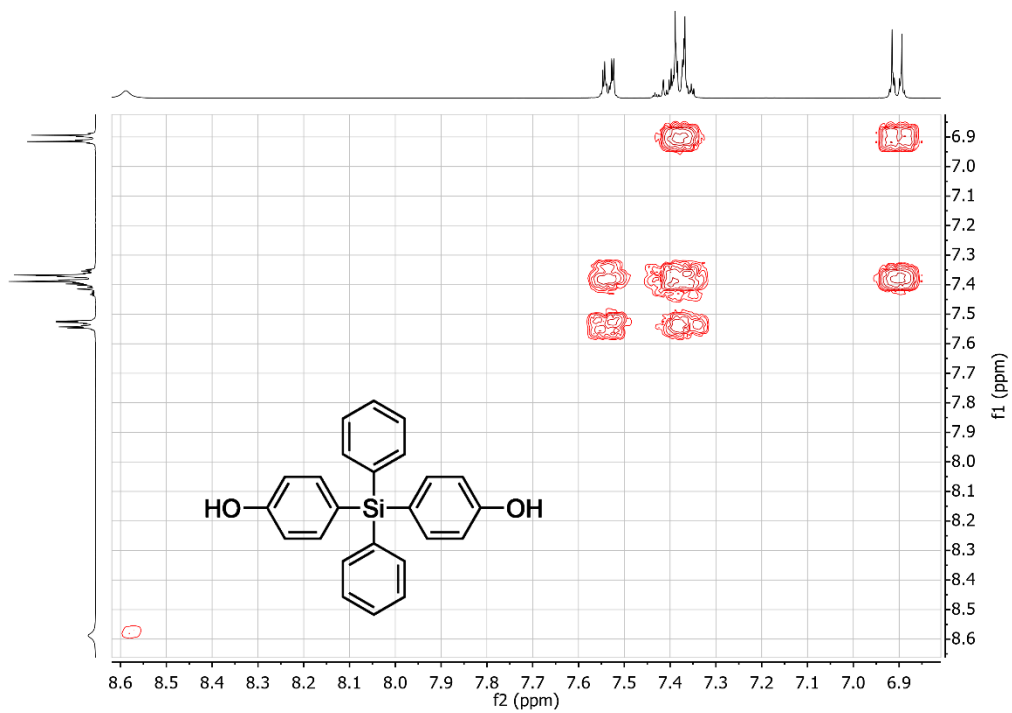


Figure 152: COSY NMR of 4,4'-(diphenylsilanediyl)diphenol (DPSDP) in  $acetone-d_6$  with TMS.

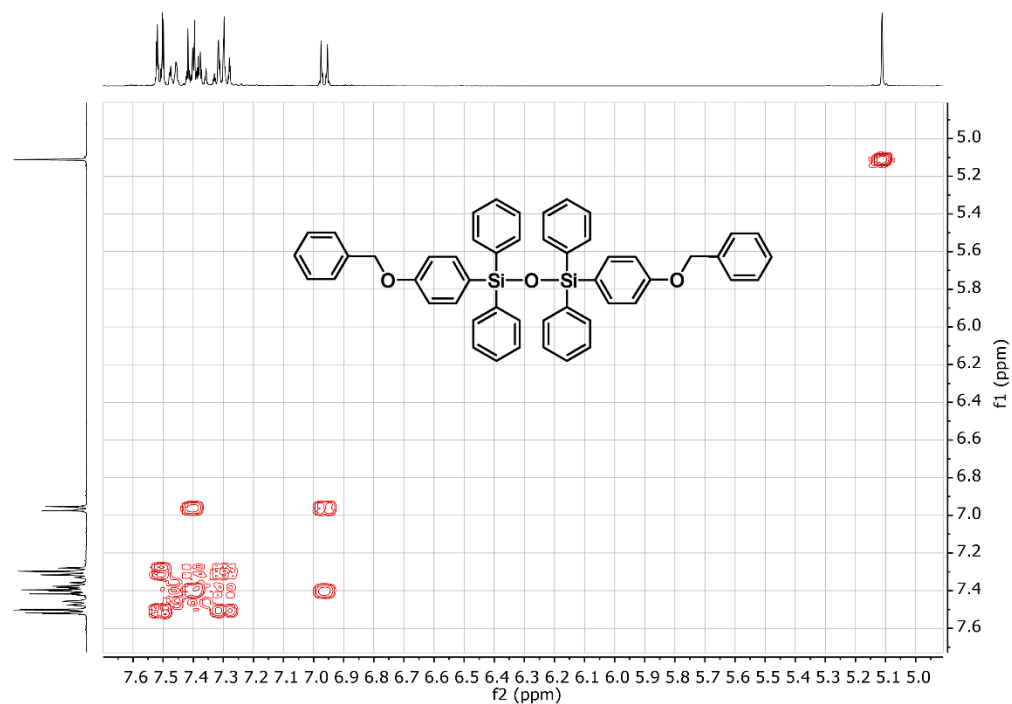
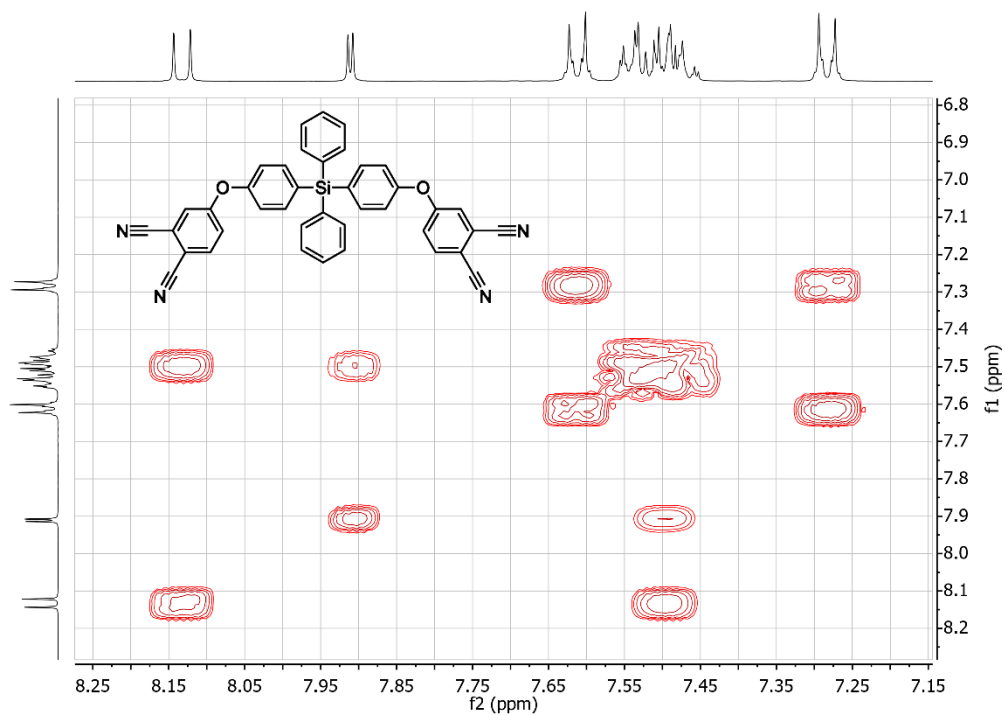


Figure 154: COSY NMR of 1,3-bis(4-(benzyloxy)phenyl)-1,1,3,3-tetraphenyldisiloxane (BODSO) in  $CDCl_3$  with TMS.

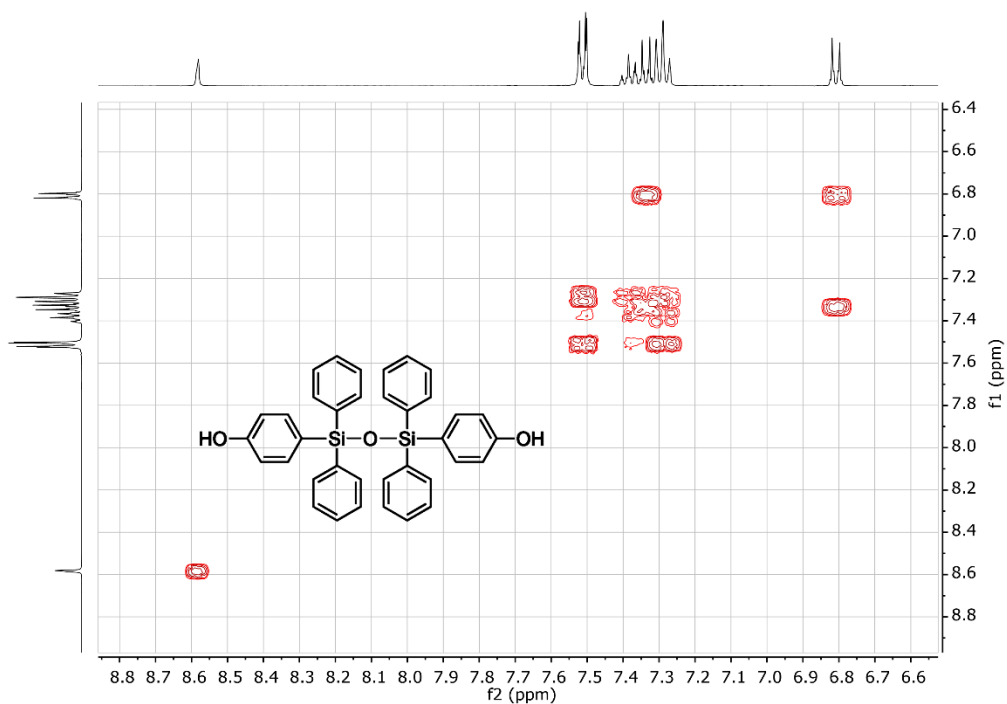


Figure 155: COSY NMR of 4,4'-(1,1,3,3-tetraphenyldisiloxane-1,3-diyl)diphenol (DPDSO) in acetone- $d_6$  with TMS.

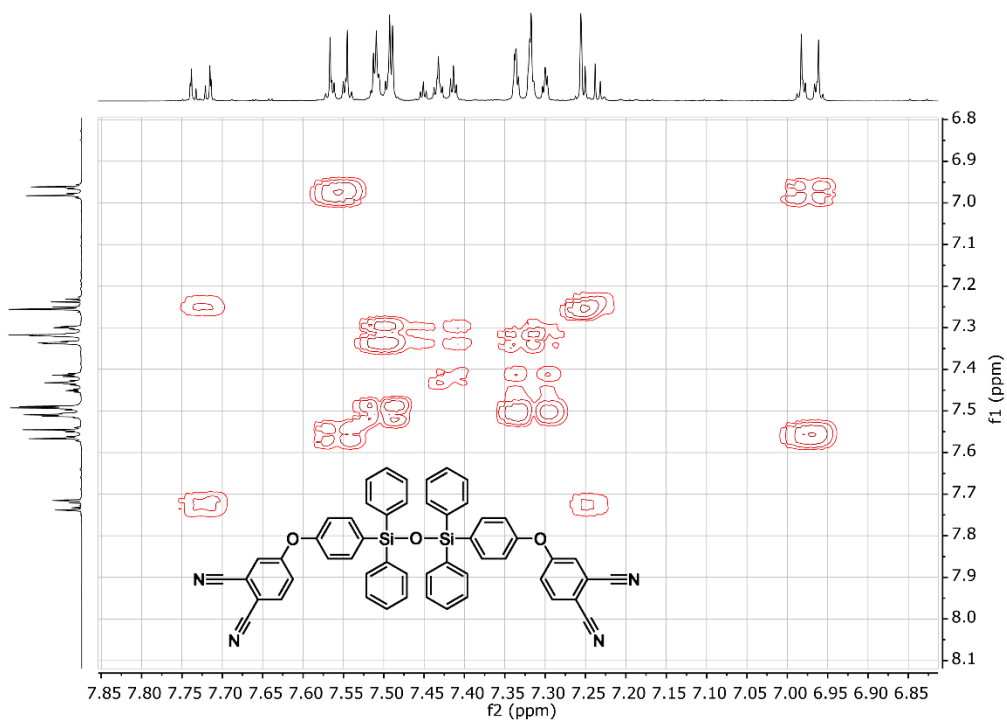


Figure 156: COSY NMR of 4,4'-((1,1,3,3-tetraphenyldisiloxane-1,3-diyl)bis(4,1-phenylene))bis(oxy)diphthalonitrile (CSOPN) in  $CDCl_3$  with TMS.

### 13.3 $^{13}\text{C}$ NMR Spectra

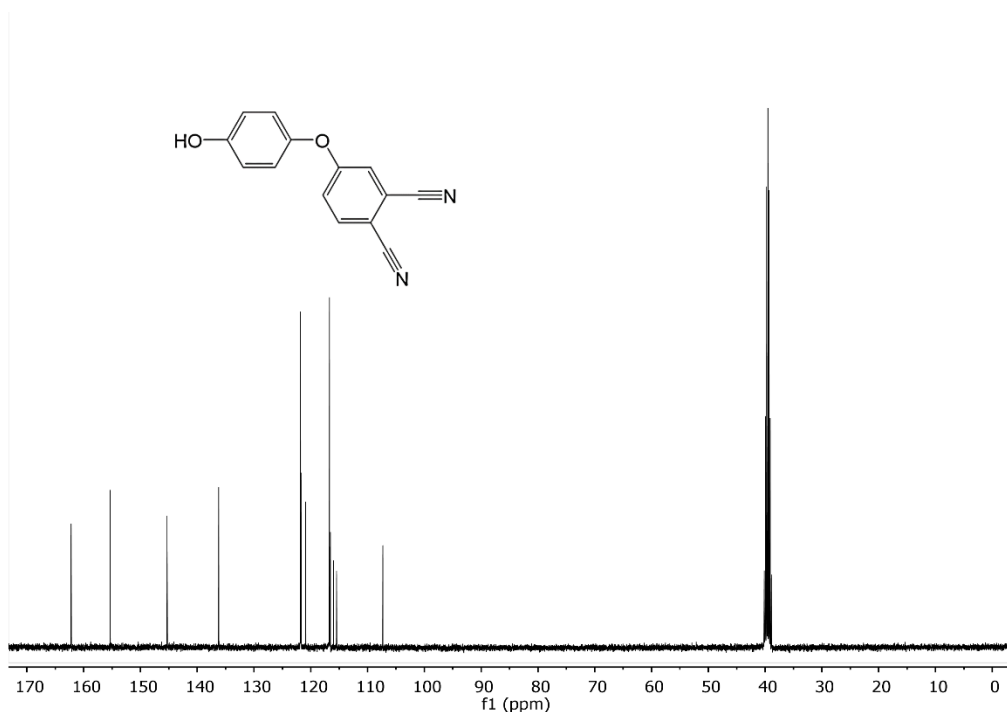


Figure 157:  $^{13}\text{C}$  NMR of 4-(4-hydroxyphenoxy)phthalonitrile (HOPOPN) in DMSO- $d_6$ .

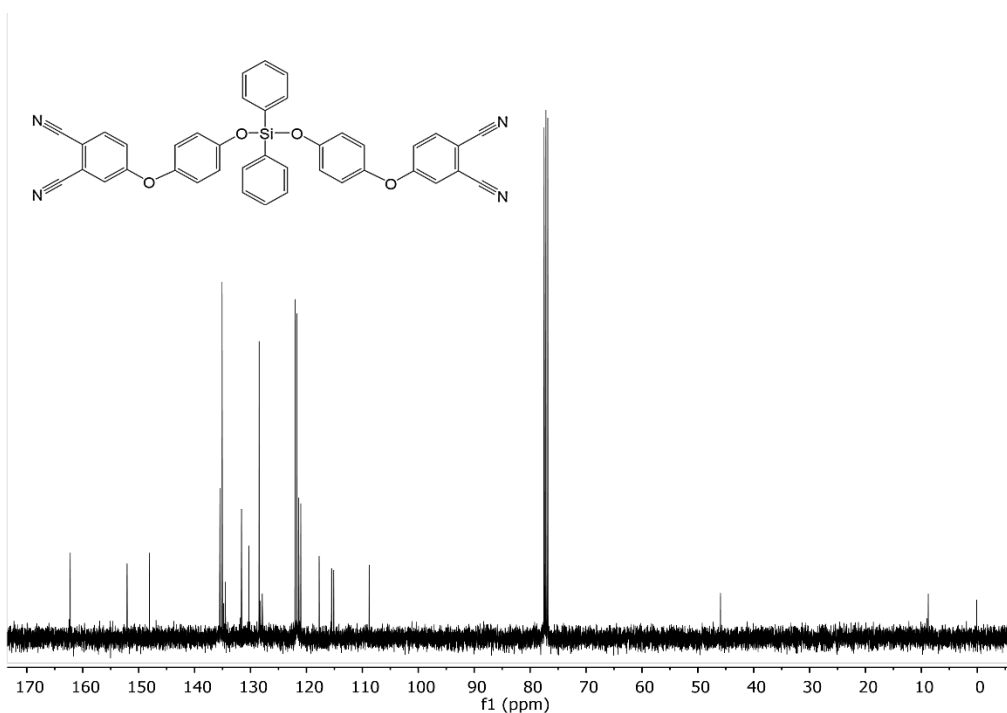


Figure 158:  $^{13}\text{C}$  NMR of 4,4'-(((diphenylsilyl)diyl)bis(oxy))bis(4,1-phenylene))bis(oxy)diphthalonitrile (COSPN) in CDCl<sub>3</sub> with TMS.

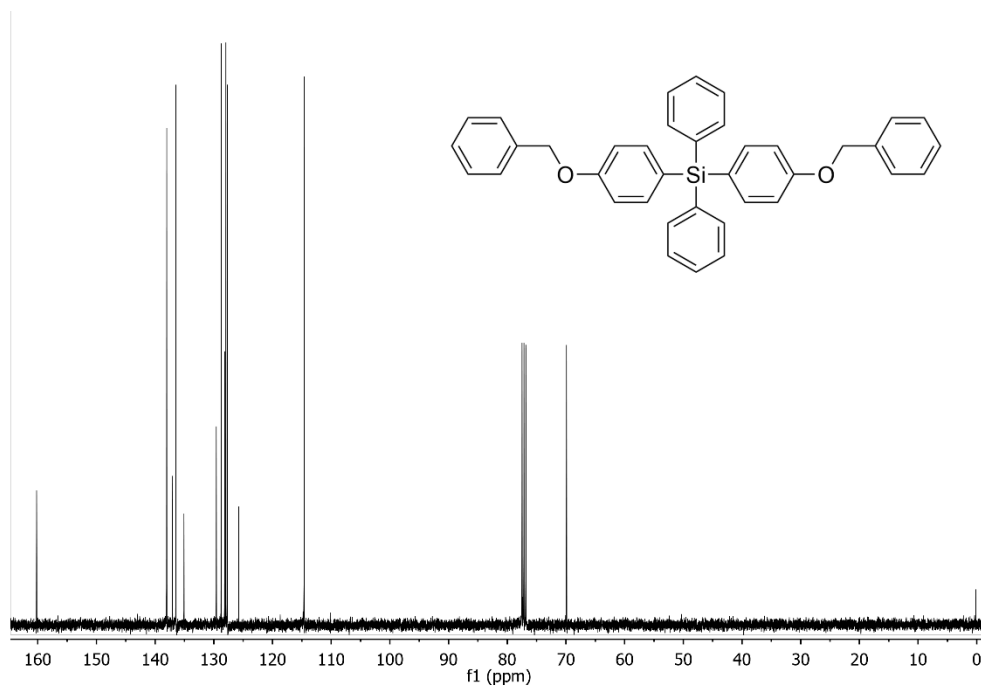


Figure 159:  $^{13}\text{C}$  NMR of Bis(4-(benzyloxy)phenyl)diphenylsilane (BODPS) in  $\text{CDCl}_3$  with TMS.

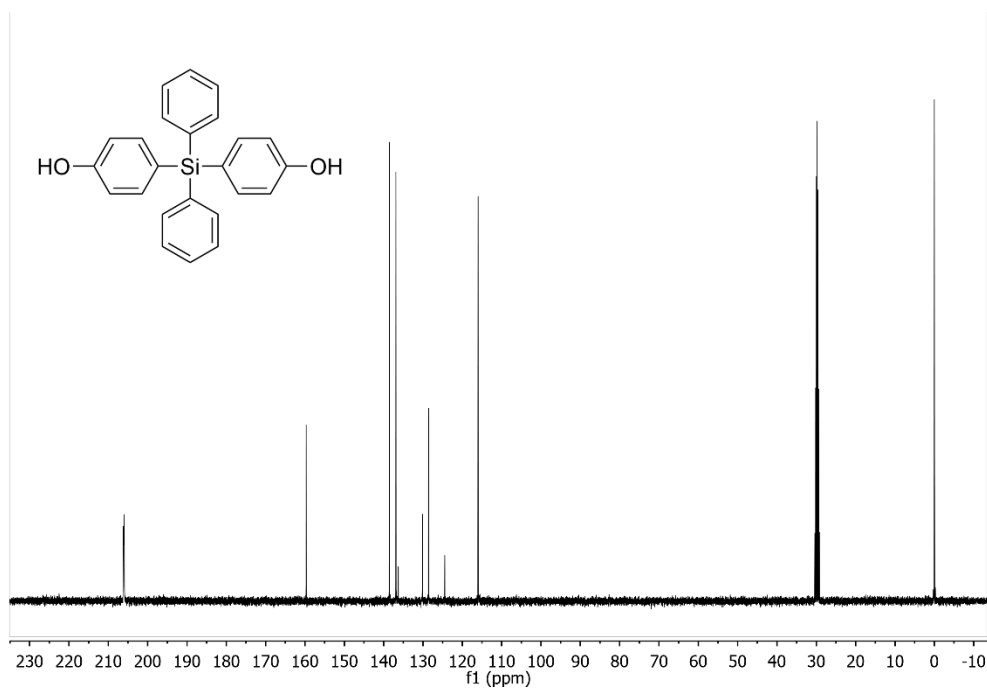


Figure 160:  $^{13}\text{C}$  NMR of 4,4'-(diphenylsilyl)diphenol (DPSDP) in  $\text{Acetone-}d_6$  with TMS.

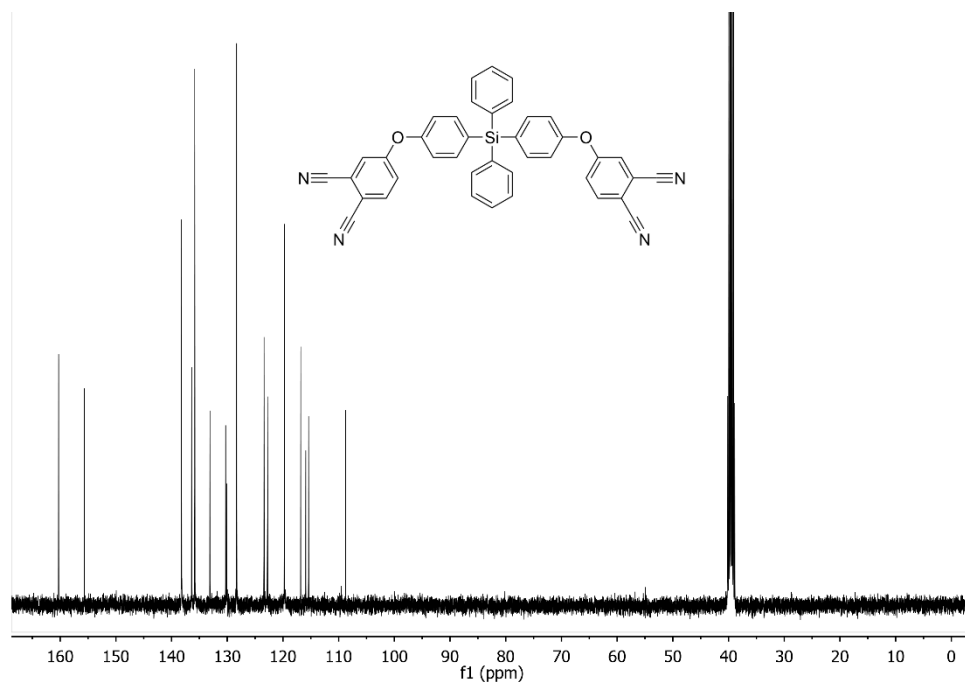


Figure 161:  $^{13}\text{C}$  NMR of 4,4'-(((diphenylsilanediyl)bis(4,1-phenylene))bis(oxy))diphthalonitrile (CSPN) in  $\text{CDCl}_3$ .

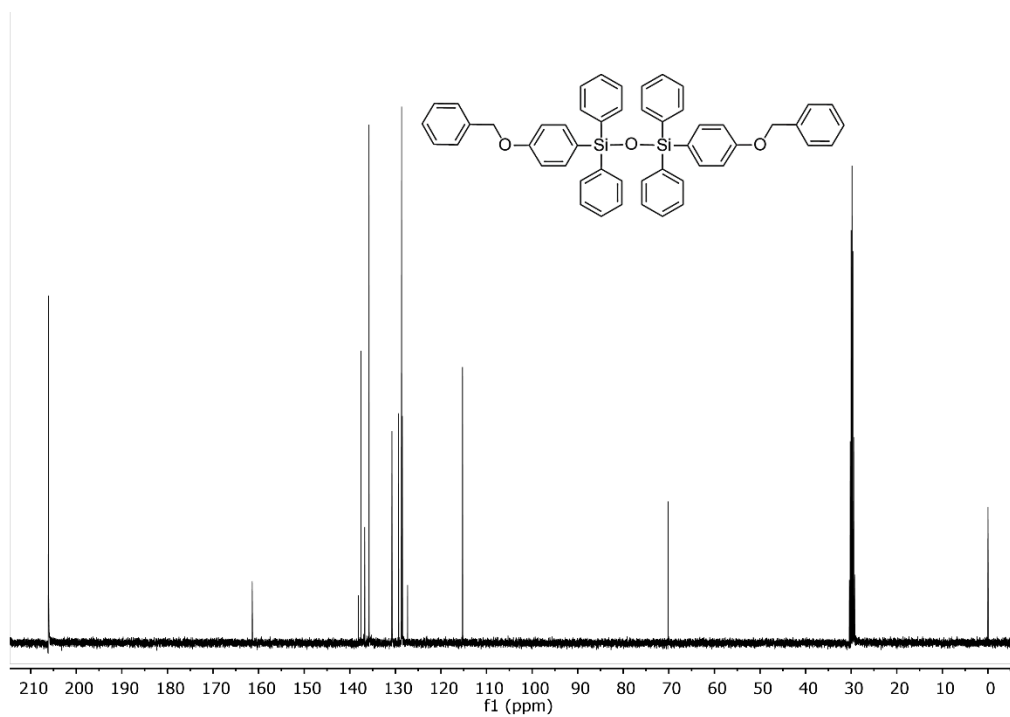


Figure 162:  $^{13}\text{C}$  NMR of 1,3-bis(4-(benzyloxy)phenyl)-1,1,3,3-tetraphenyldisiloxane (BODSO) in  $\text{CDCl}_3$  with TMS.

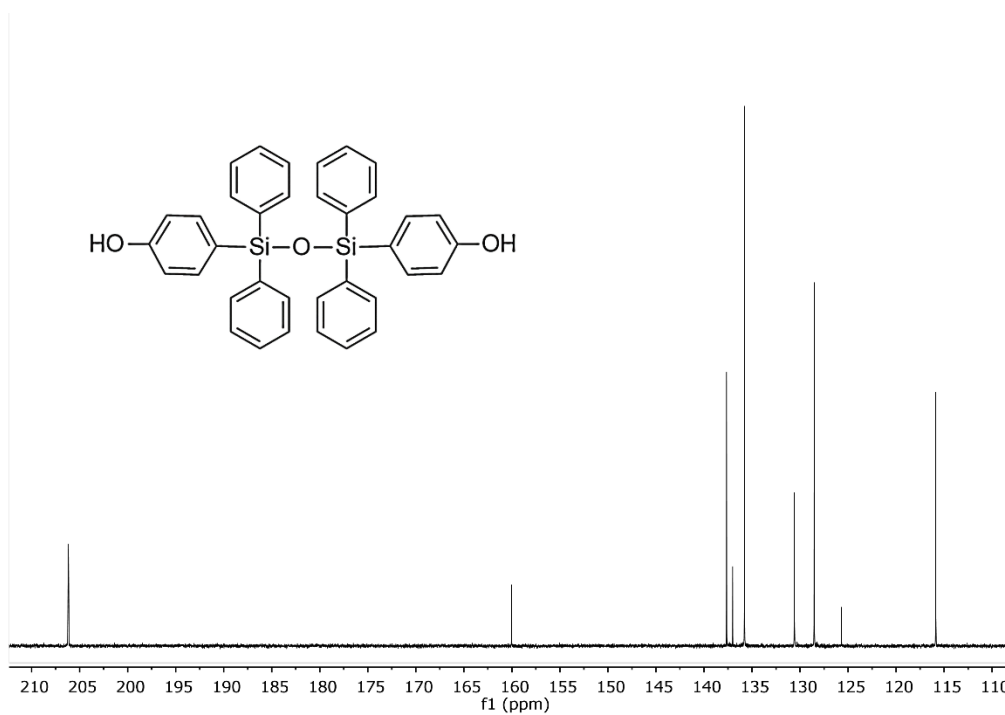


Figure 163:  $^{13}\text{C}$  NMR of 4,4'-(1,1,3,3-tetraphenyldisiloxane-1,3-diyl)diphenol (DPDSO) in acetone- $d_6$  with TMS.

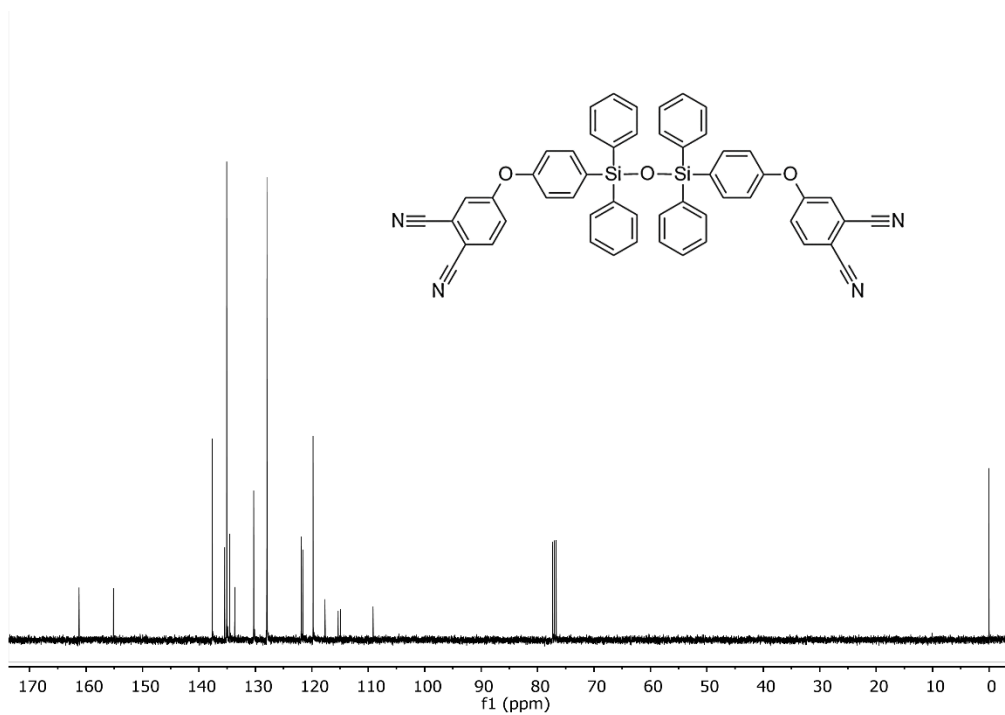


Figure 164:  $^{13}\text{C}$  NMR of 4,4'-(((1,1,3,3-tetraphenyldisiloxane-1,3-diyl)bis(4,1-phenylene))bis(oxy))diphthalonitrile (CSOPN) in  $\text{CDCl}_3$  with TMS.

### 13.4 Heteronuclear Single-Quantum Correlation Spectroscopy (HSQC) NMR Spectra

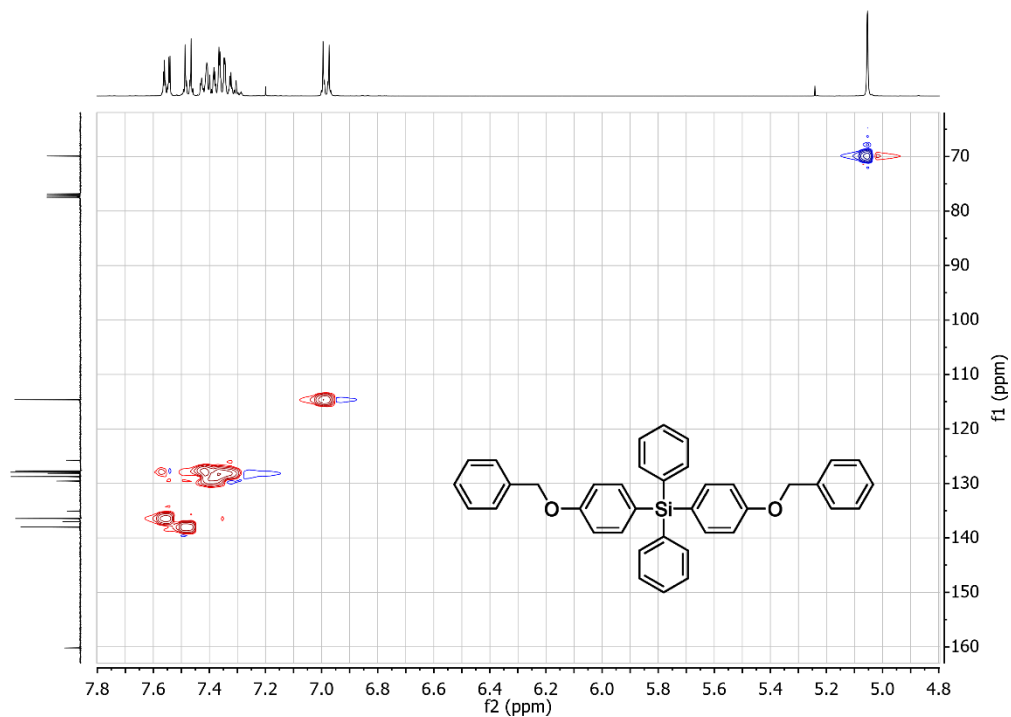


Figure 165: HSQC NMR of bis(4-(benzyloxy)phenyl)diphenylsilane (BODPS) in  $CDCl_3$  with TMS.

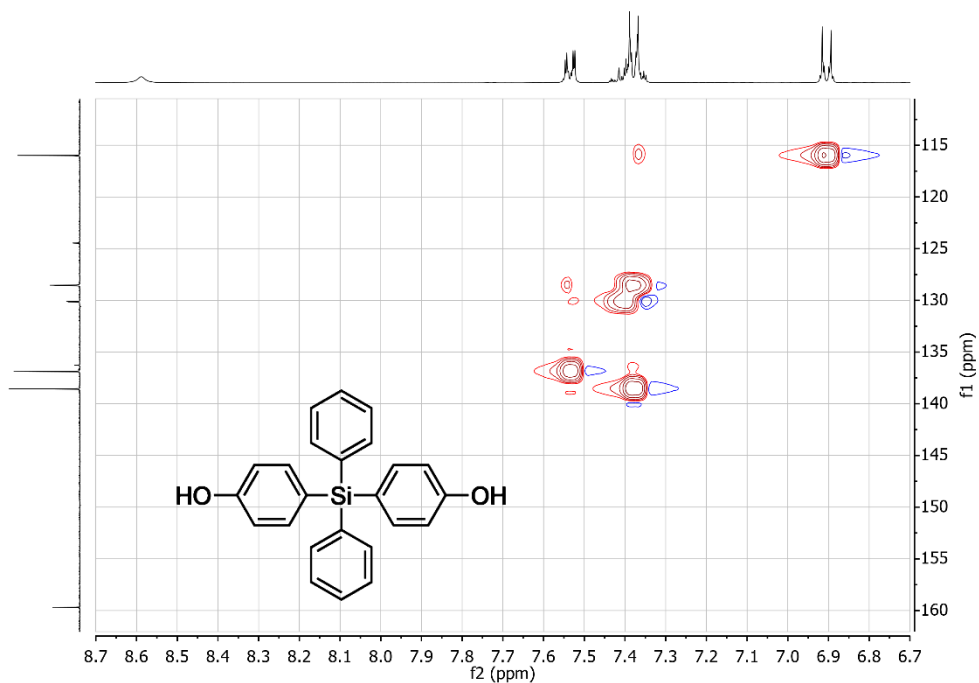


Figure 166: HSQC NMR of 4,4'-(diphenylsilanediyl)diphenol (DPDSO) in  $acetone-d_6$  with TMS.

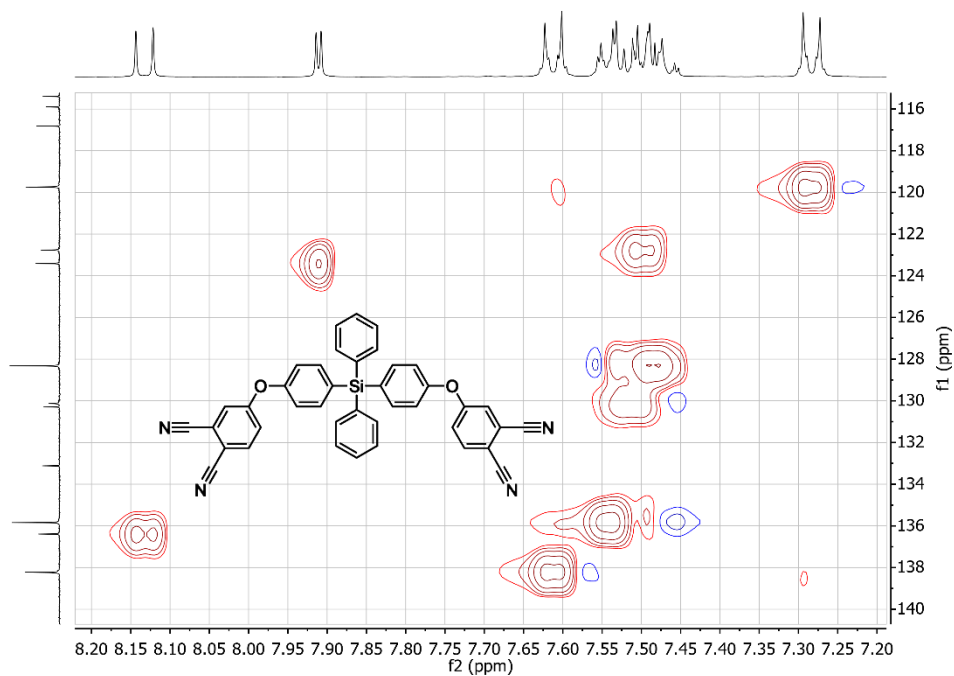


Figure 167: HSQC NMR of 4,4'-(((diphenylsilanediyl)bis(4,1-phenylene))bis(oxy))diphthalonitrile (CSPN) in  $\text{CDCl}_3$  with TMS.

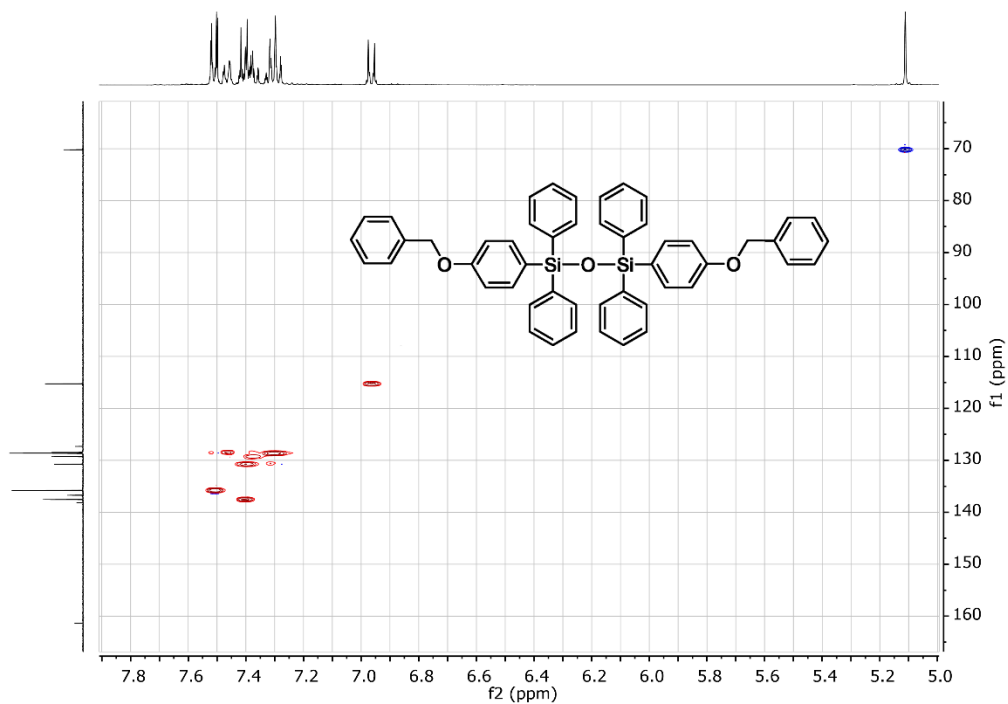


Figure 168: HSQC NMR of 1,3-bis(4-(benzyloxy)phenyl)-1,1,3,3-tetraphenyldisiloxane (BODSO) in  $\text{CDCl}_3$  with TMS.

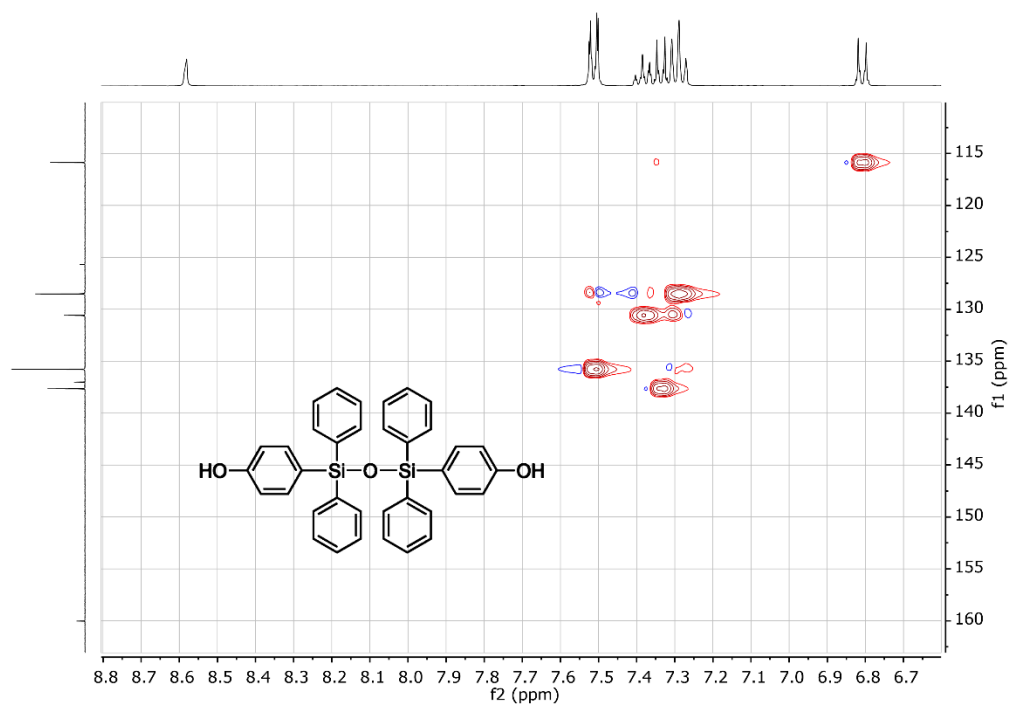


Figure 169: HSQC NMR of 4,4'-(1,1,3,3-tetraphenyldisiloxane-1,3-diyl)diphenol (DPDSO) in acetone- $d_6$  with TMS.

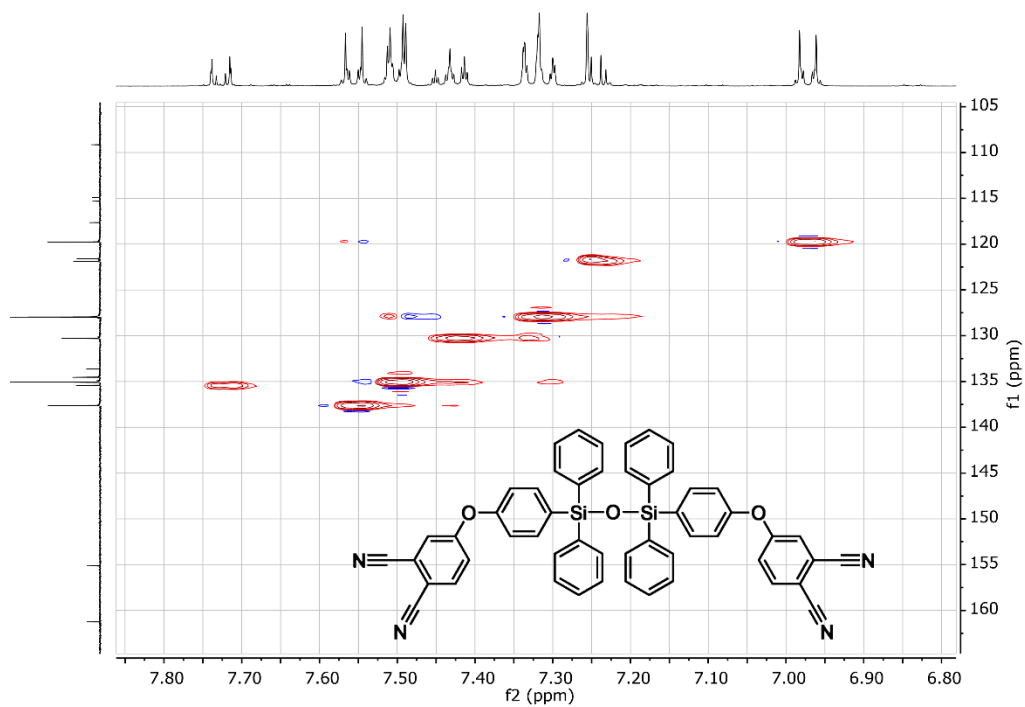


Figure 170: HSQC NMR of 4,4'-(((1,1,3,3-tetraphenyldisiloxane-1,3-diyl)bis(4,1-phenylene))bis(oxy))diphthalonitrile (CSOPN) in  $CDCl_3$  with TMS.

### 13.5 Heteronuclear Multiple-Bond Correlation Spectroscopy (HMBC) NMR Spectra

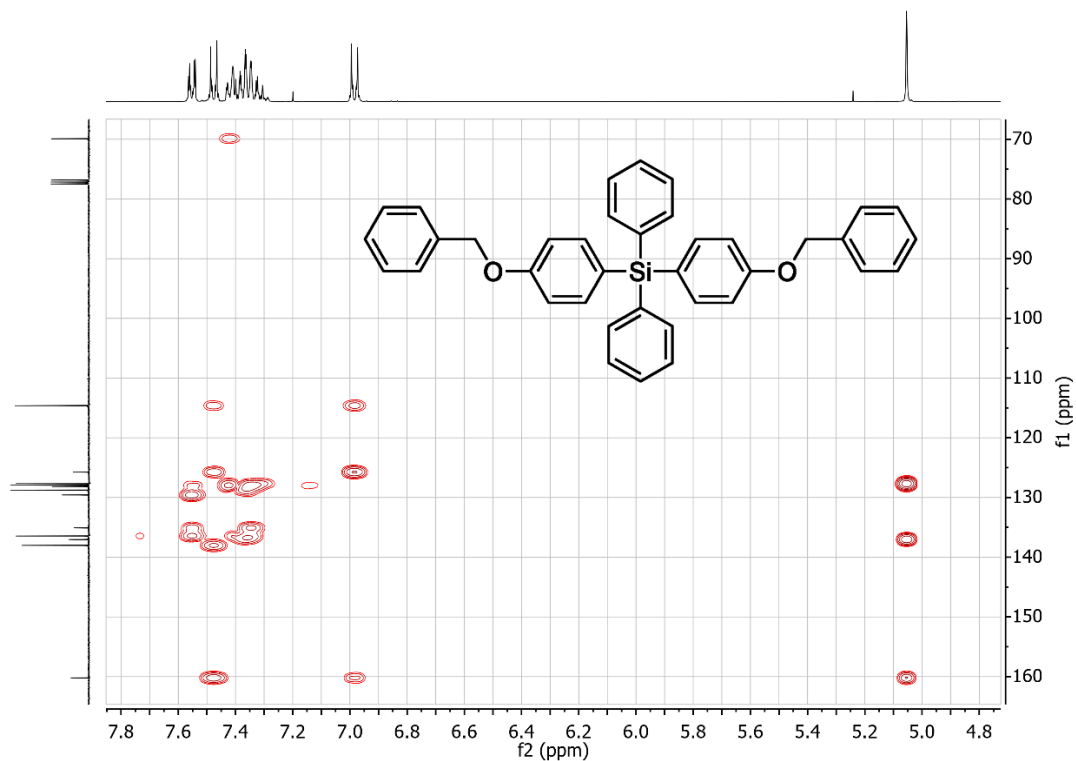


Figure 171: HMBC NMR of bis(4-(benzyloxy)phenyl)diphenylsilane (BODPS) in  $CDCl_3$  with TMS.

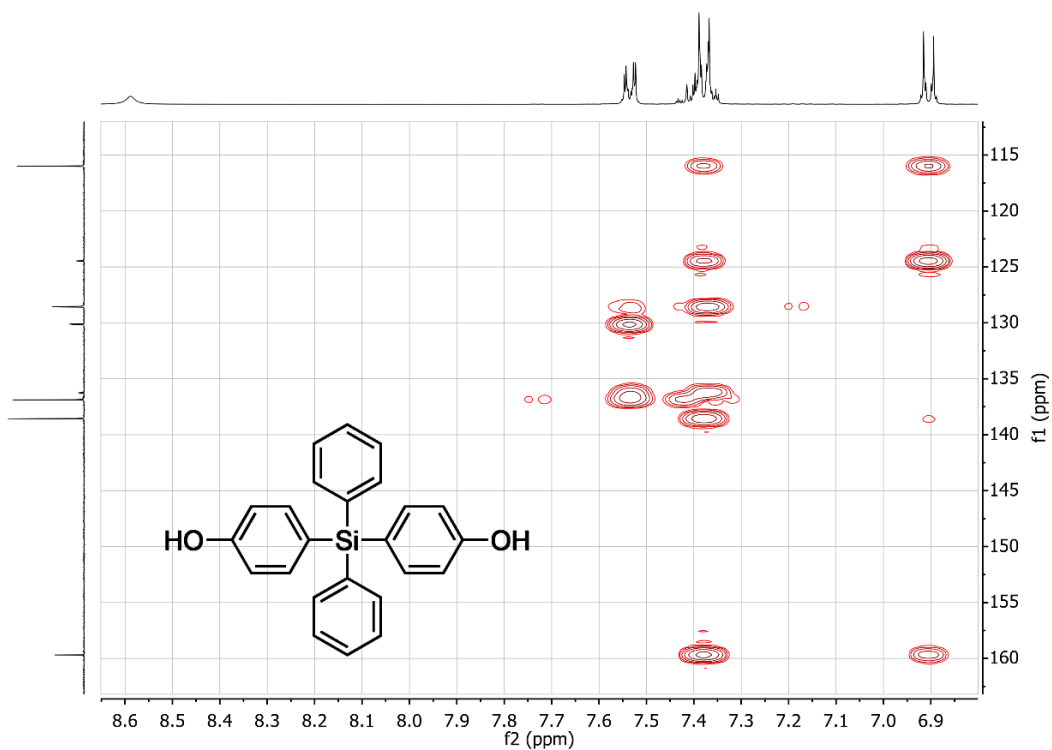


Figure 172: HMBC NMR of 4,4'-(diphenylsilanediyl)diphenol (DPSDP) in  $acetone-d_6$  with TMS.

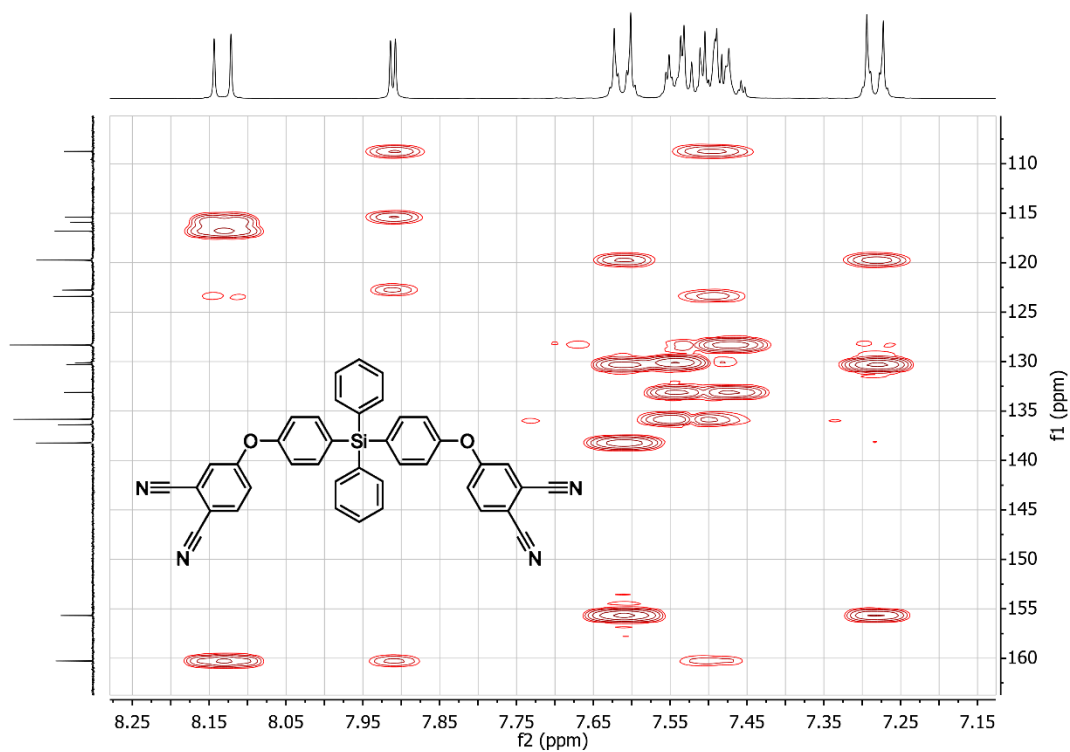


Figure 173: HMBC NMR of 4,4'-(((diphenylsilanediyl)bis(4,1-phenylene))bis(oxy))diphthalonitrile (CSPN) in CDCl<sub>3</sub> with TMS.

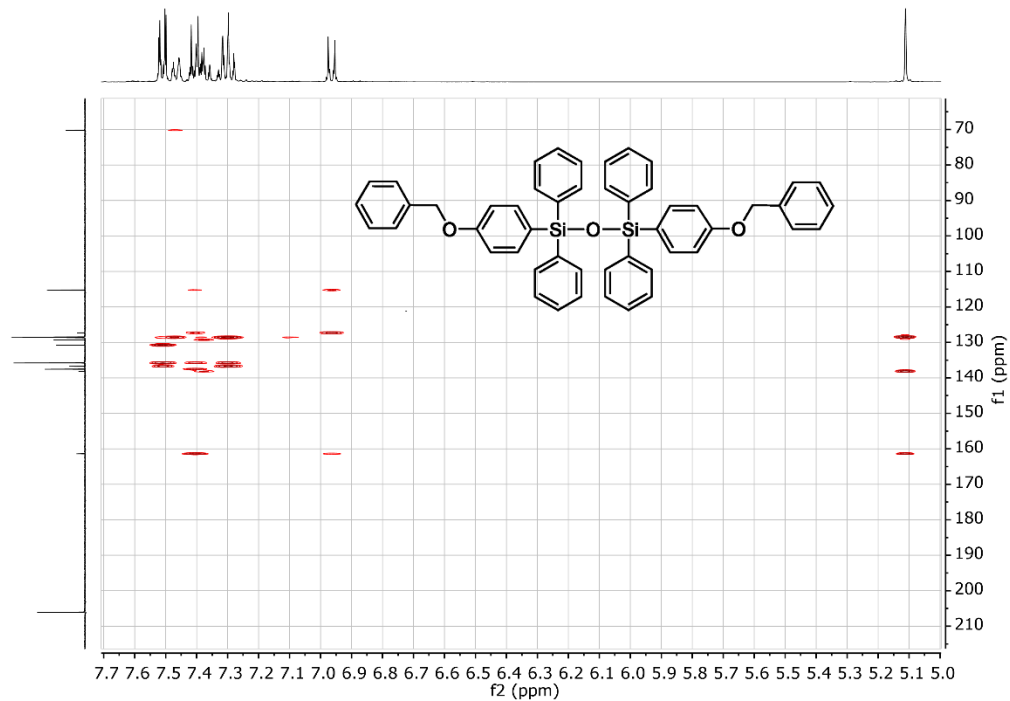


Figure 174: HMBC NMR of 1,3-bis(4-(benzyloxy)phenyl)-1,1,3,3-tetraphenyldisiloxane (BODSO) in CDCl<sub>3</sub> with TMS.

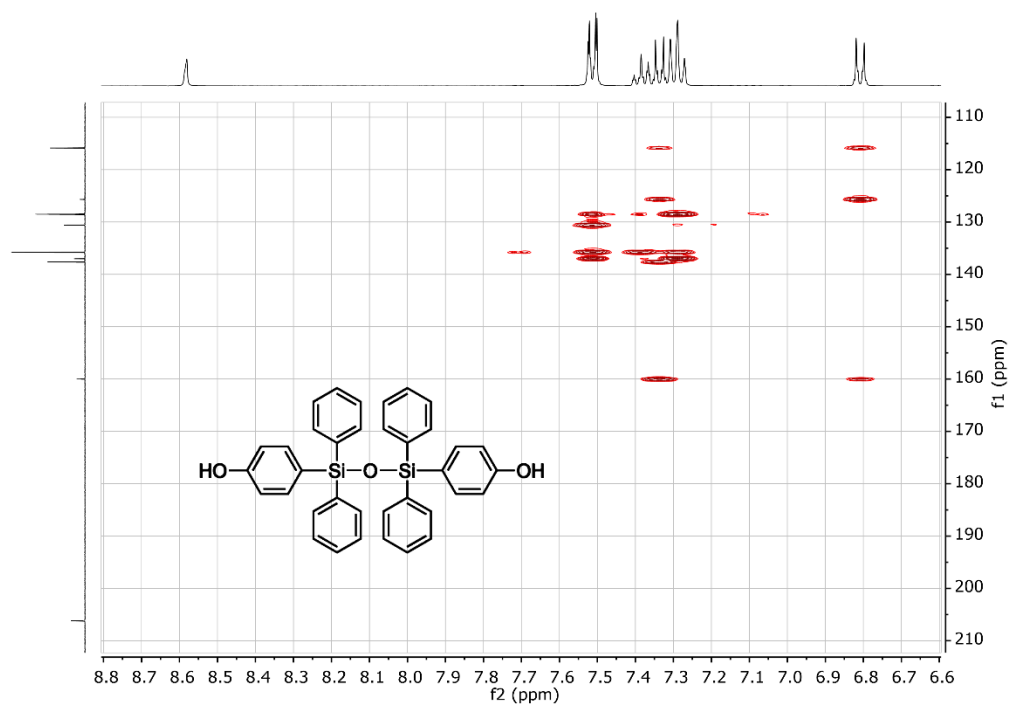


Figure 175: HMBC NMR of 4,4'-(1,1,3,3-tetraphenyldisiloxane-1,3-diyl)diphenol (DPDSO) in acetone- $d_6$  with TMS.

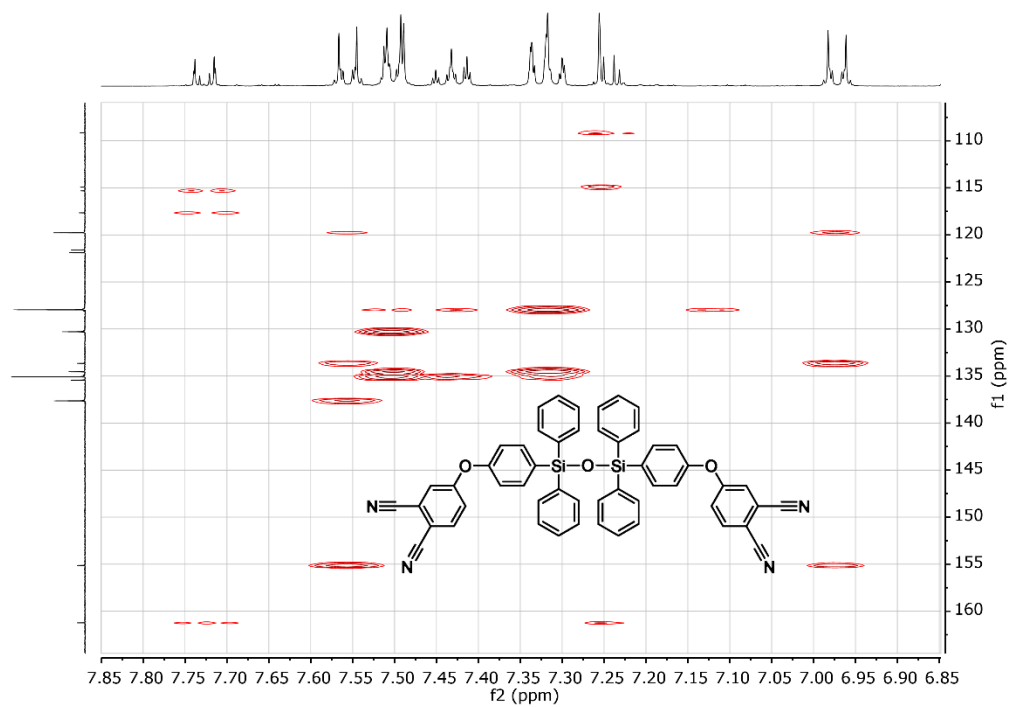


Figure 176: HMBC NMR of 4,4'-(((1,1,3,3-tetraphenyldisiloxane-1,3-diyl)bis(4,1-phenylene))bis(oxy))diphthalonitrile (CSOPN) in  $CDCl_3$  with TMS.

## 13.6 FTIR Spectra

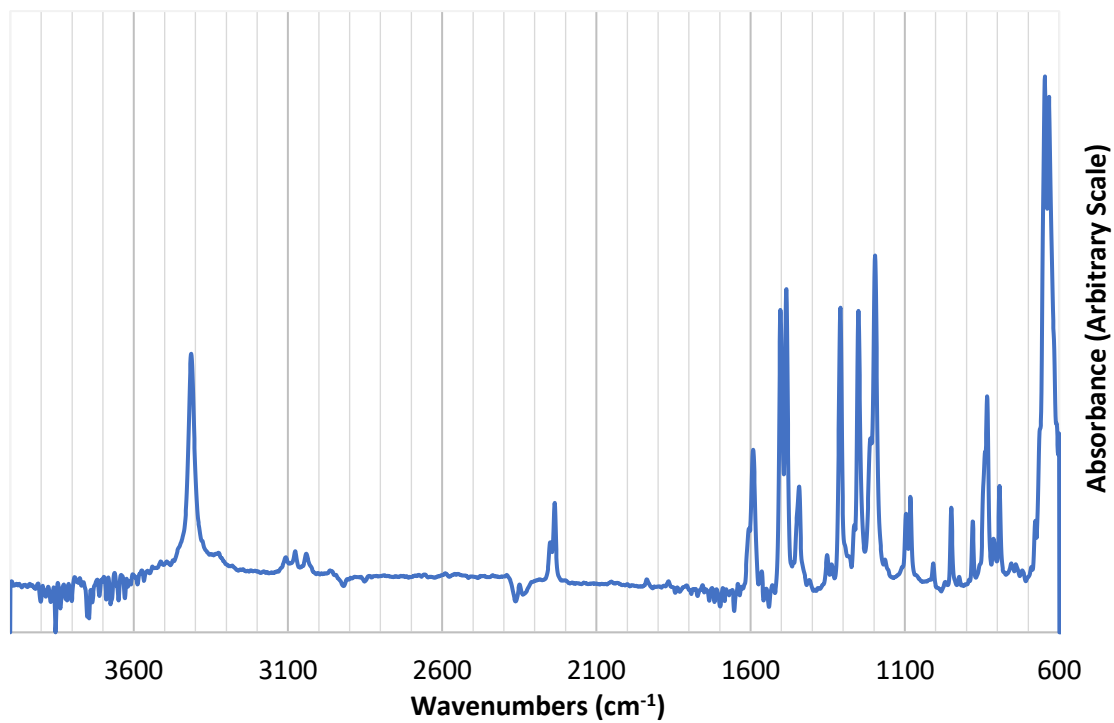


Figure 177: FTIR spectra of 4-(4-hydroxyphenoxy)phthalonitrile (HOPOPn).

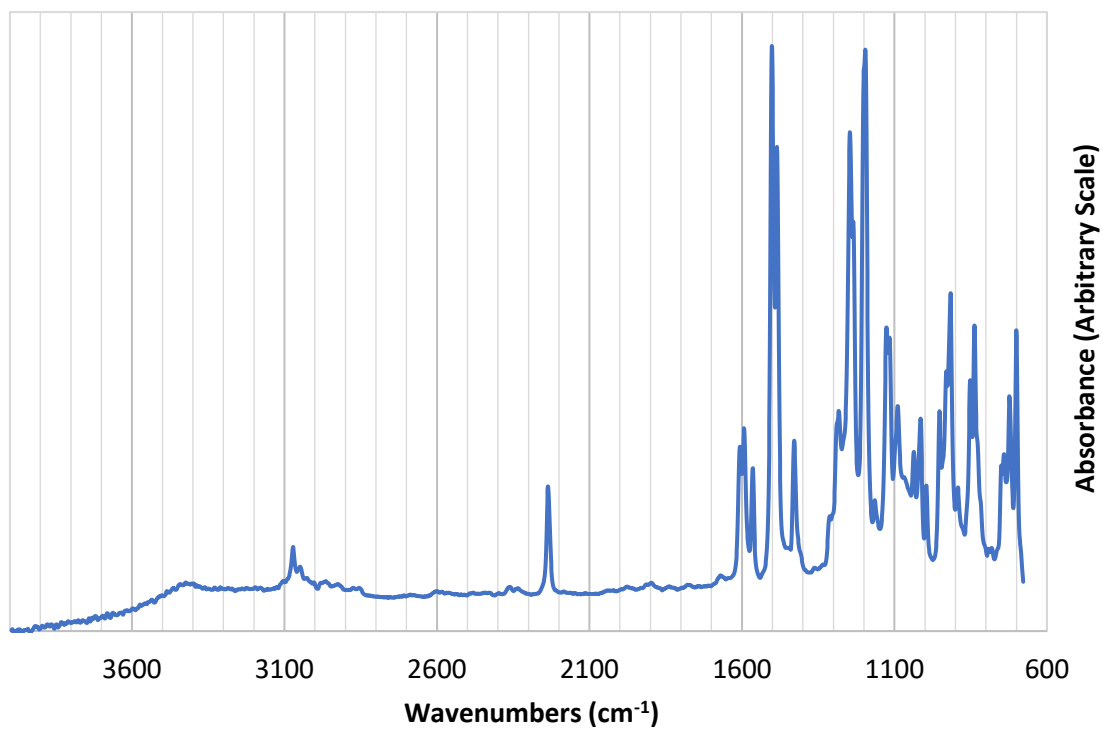


Figure 178: FTIR spectra of 4,4'-(((diphenylsilanediyl)bis(oxy))bis(4,1-phenylene))bis(oxy)diphthalonitrile.

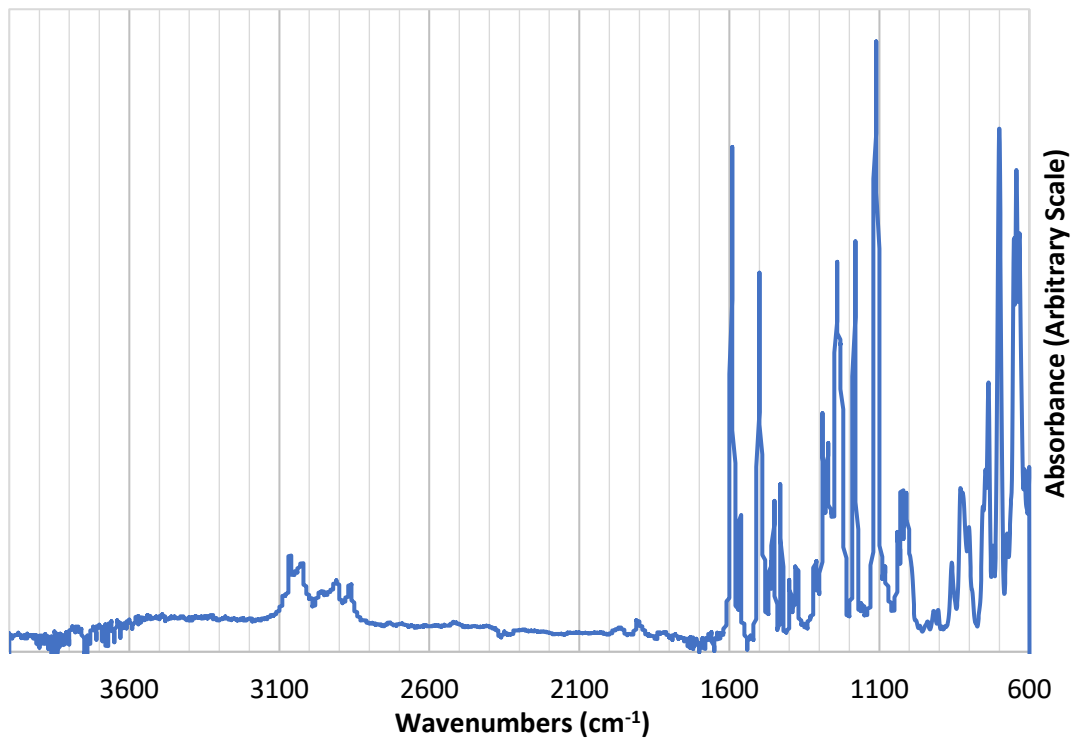


Figure 179: FTIR spectra of bis(4-(benzyloxy)phenyl)diphenylsilane (BODPS).

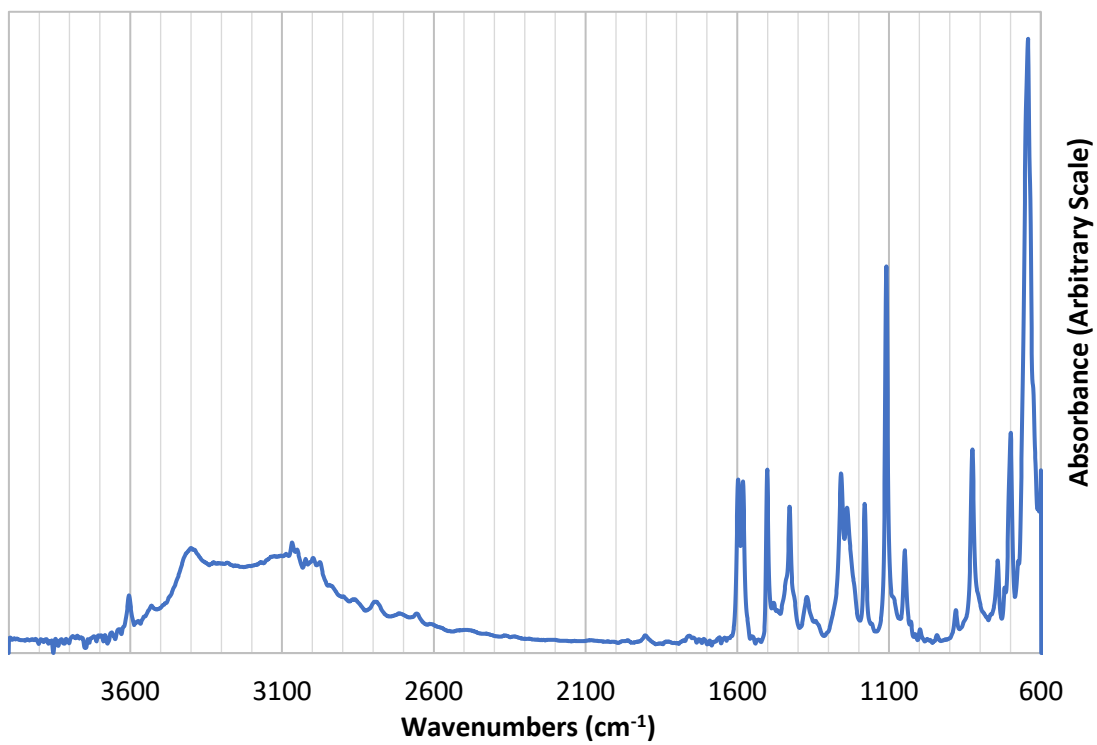


Figure 180: FTIR spectra of 4,4'-(diphenylsilanediyl)diphenol (DPSDP).

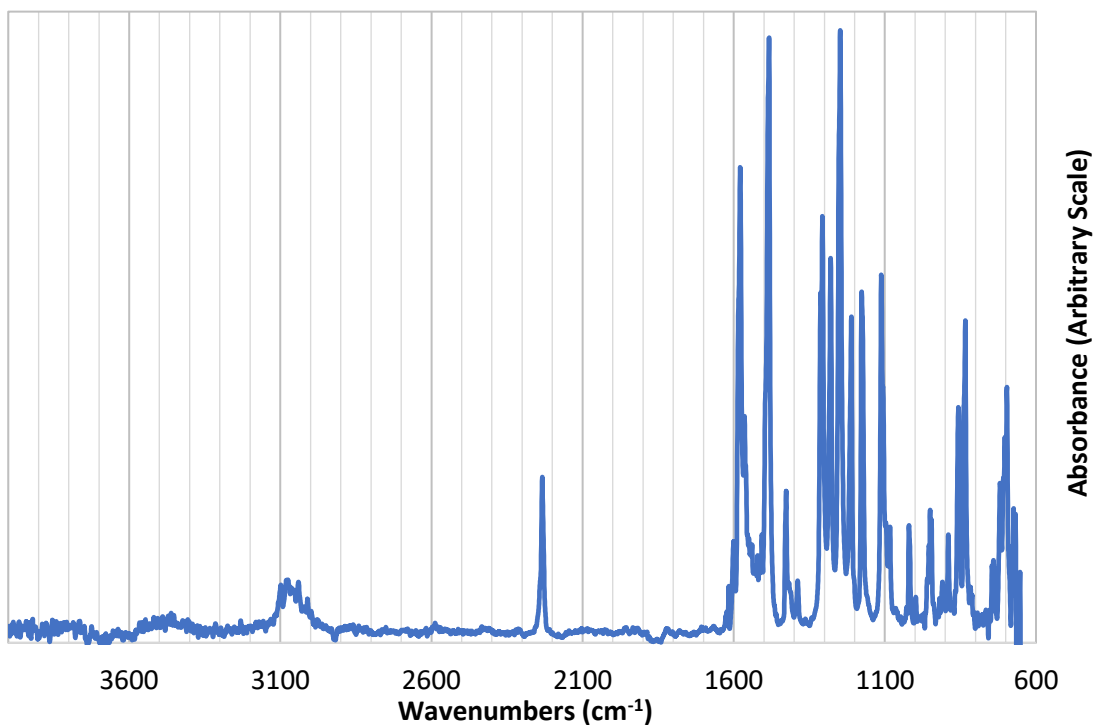


Figure 181: FTIR spectra of 4,4'-(((diphenylsilyl)bis(4,1-phenylene))bis(oxy))diphthalonitrile (CSPN).

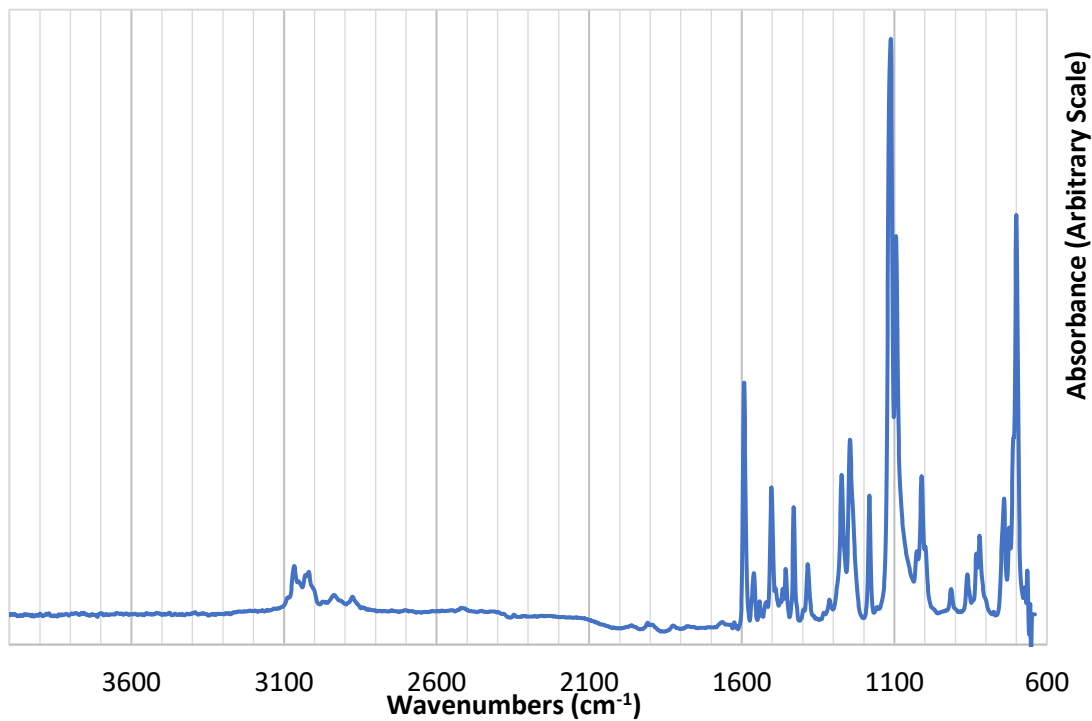


Figure 182: FTIR spectra of 1,3-bis(4-(benzyloxy)phenyl)-1,1,3,3-tetraphenyldisiloxane (BODSO).

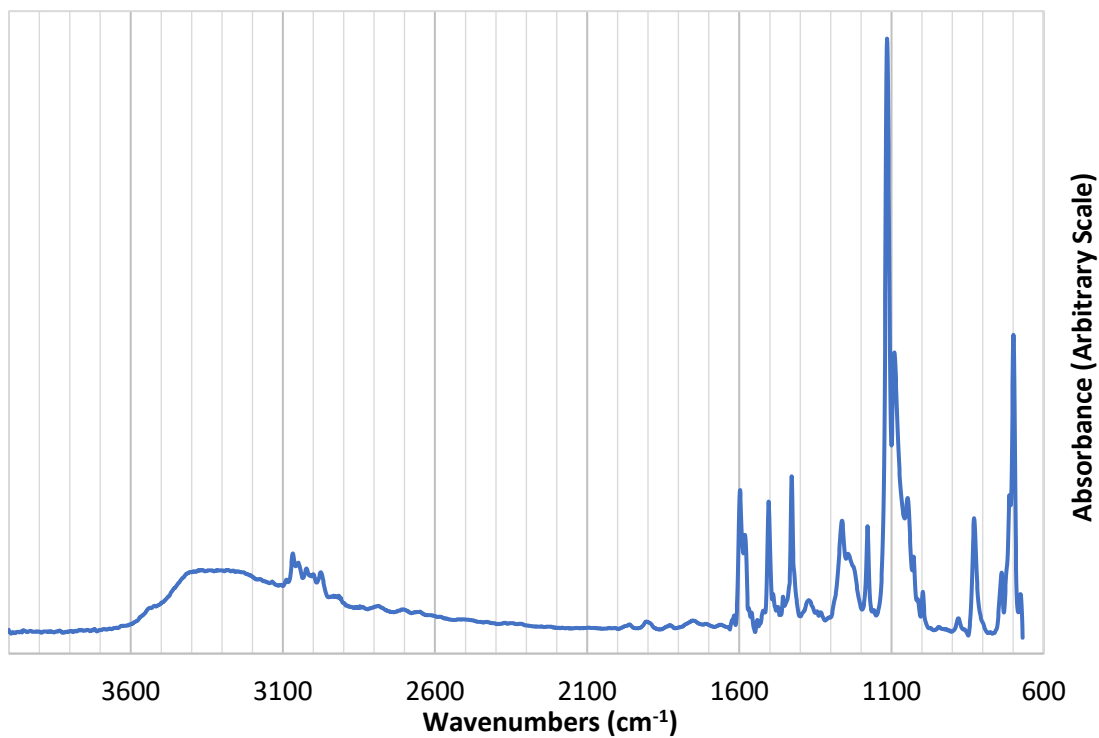


Figure 183: FTIR spectra of 4,4'-(1,1,3,3-tetraphenyldisiloxane-1,3-diyl)diphenol (DPDSO).

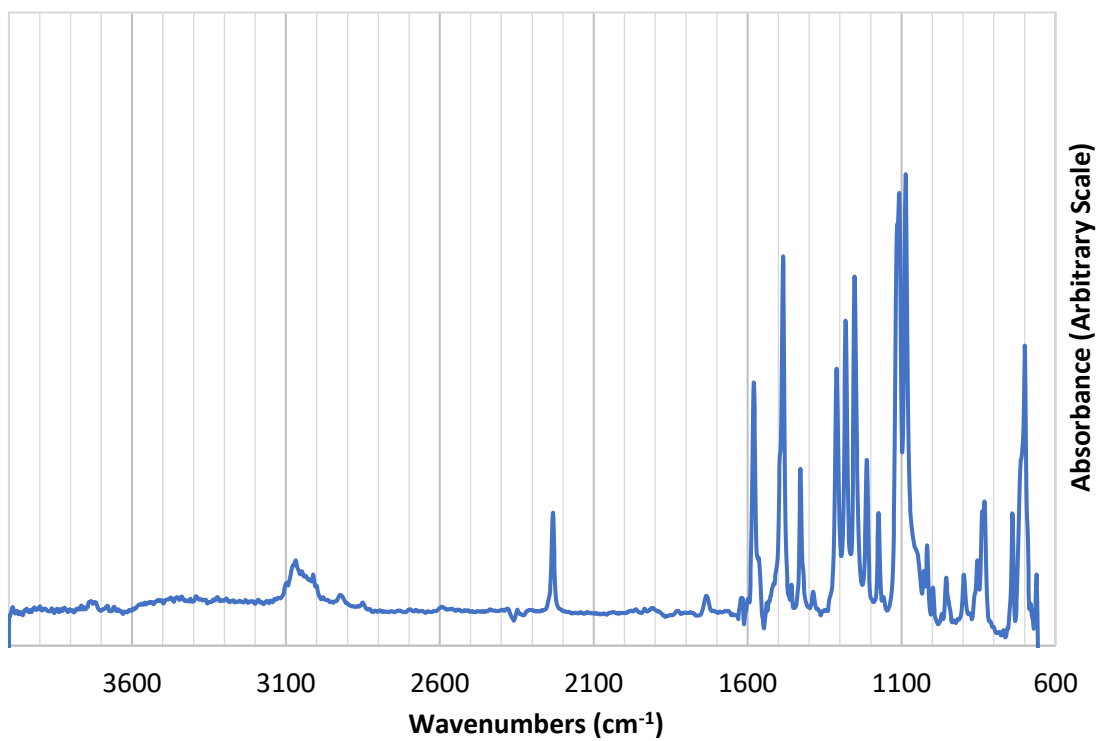


Figure 184: FTIR spectra of 4,4'-(((1,1,3,3-tetraphenyldisiloxane-1,3-diyl)bis(4,1-phenylene))bis(oxy))diphthalonitrile (CSOPN).

### 13.7 DSC Curves

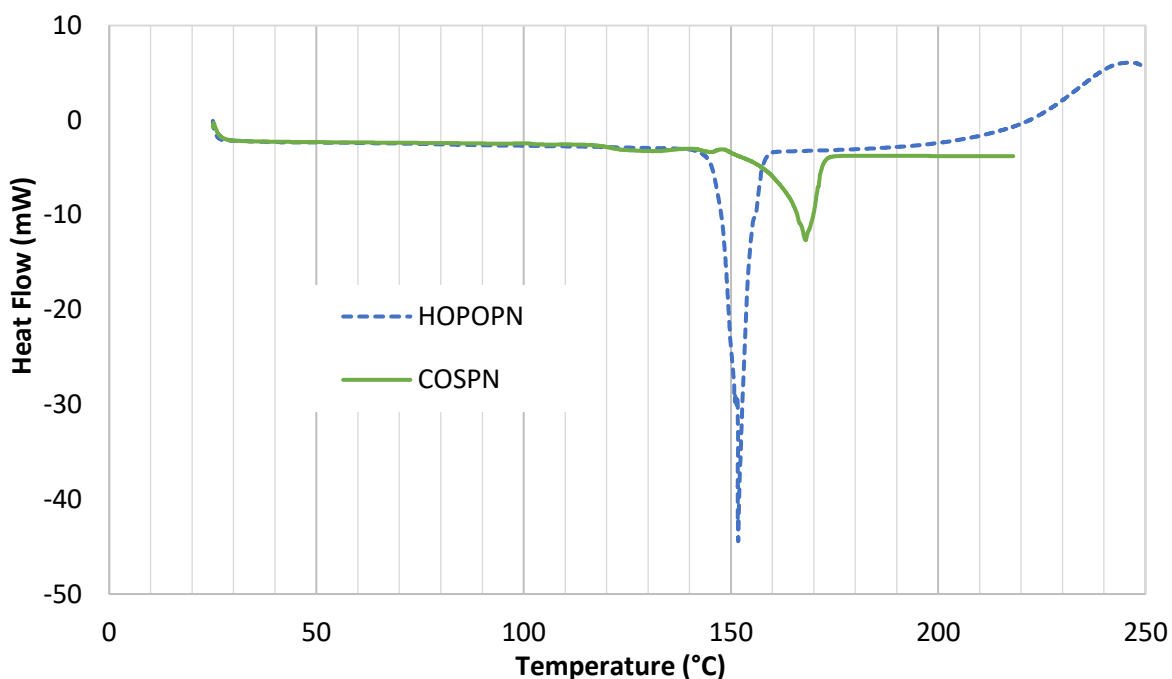


Figure 185: DSC data providing endothermic melting peaks for HOPOP (152 °C) and COSPN (169 °C). The melting peak for the COSPN monomer was broader and of lesser magnitude due to the presence of impurities. The exothermic peak observed for HOPOP at 245 °C likely corresponds to curing of the nitrile groups catalyzed by hydroxyl groups.

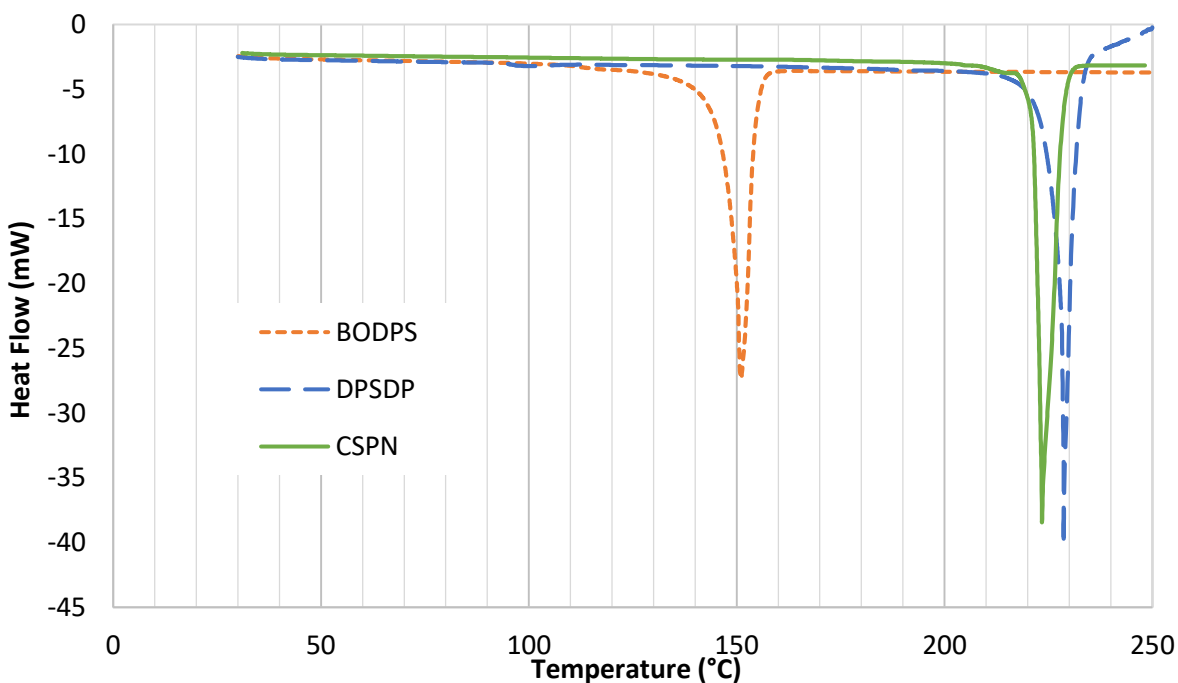


Figure 186: DSC data providing endothermic melting peaks for BODPS (151 °C), DPSDP (229 °C), and CSPN (223 °C). The exothermic peak above the melting point of DPSDP likely corresponds to degradation.

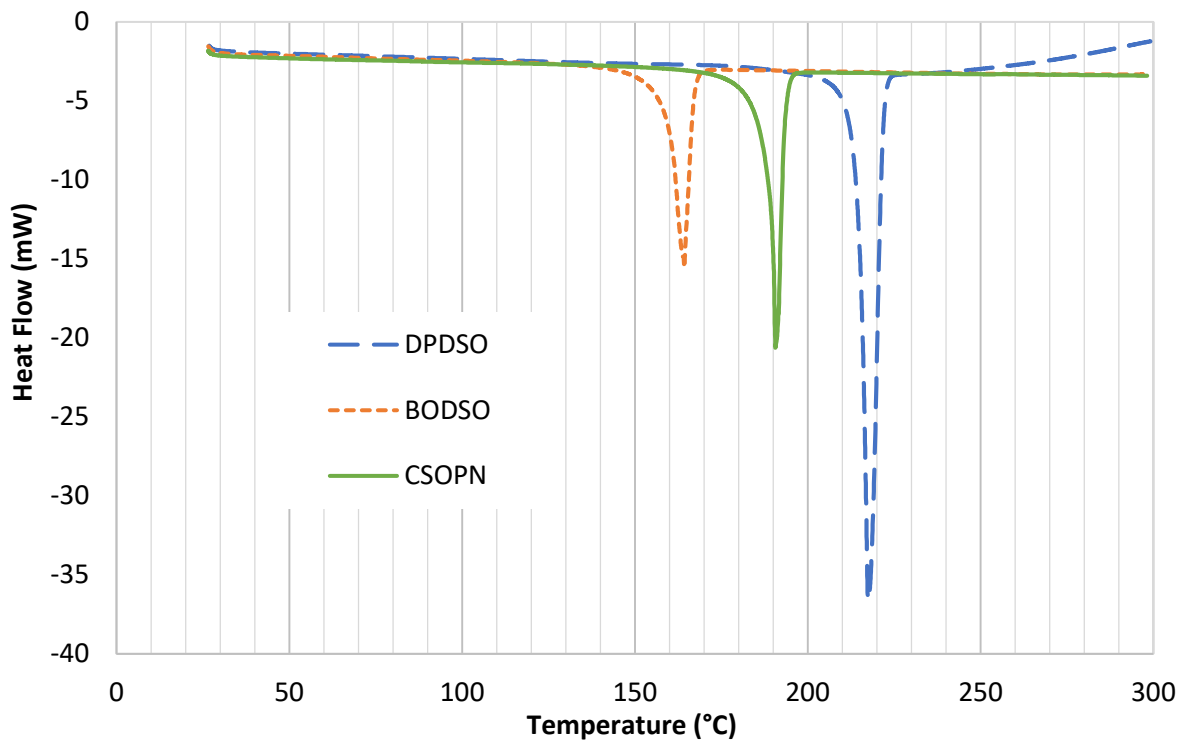


Figure 187: DSC data providing endothermic melting peaks for BODSO (164 °C), DPDSO (217 °C), and CSOPN (191 °C). The exothermic peak above the melting point of DPDSO likely corresponds to degradation.

### 13.8 SFC, LCMS and LCUV of COSPN

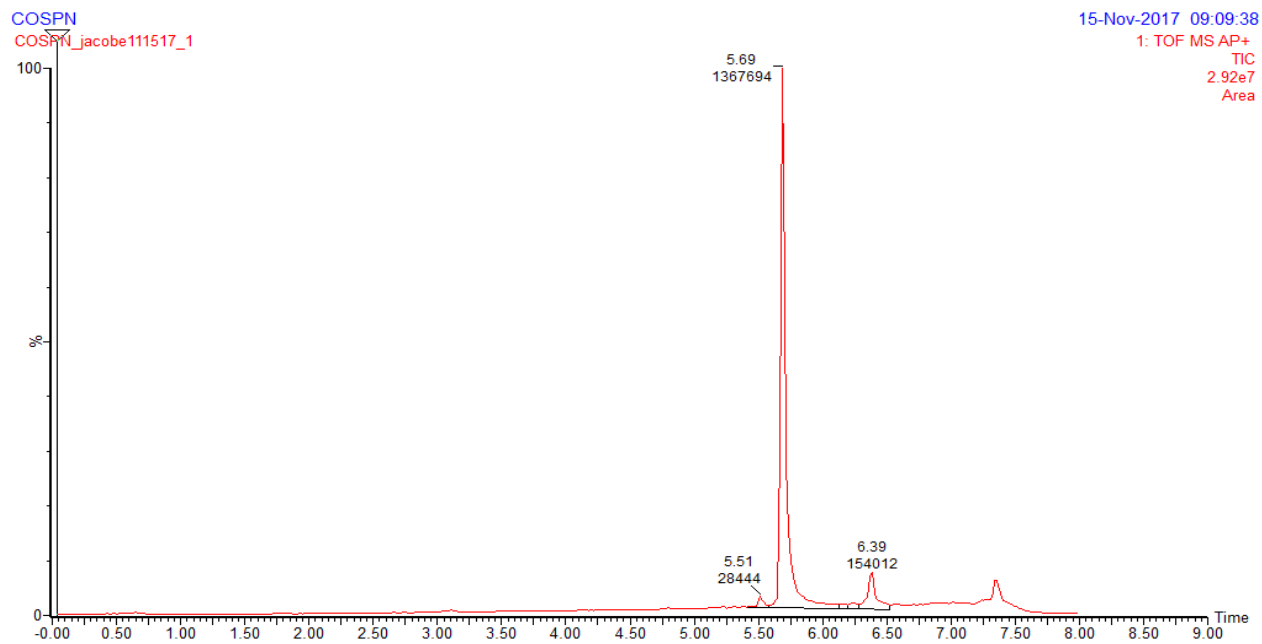


Figure 188: LC/MS (APCI) of COSPN showing 80% purity.

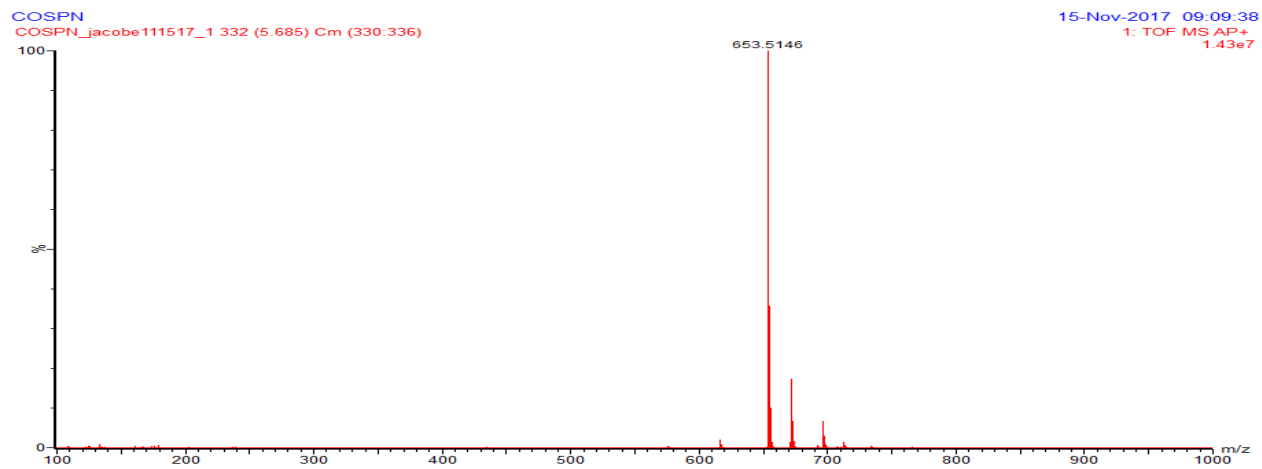


Figure 189: COSPN MS spectrum of peak with retention time of 5.69 min confirming molecular weight.

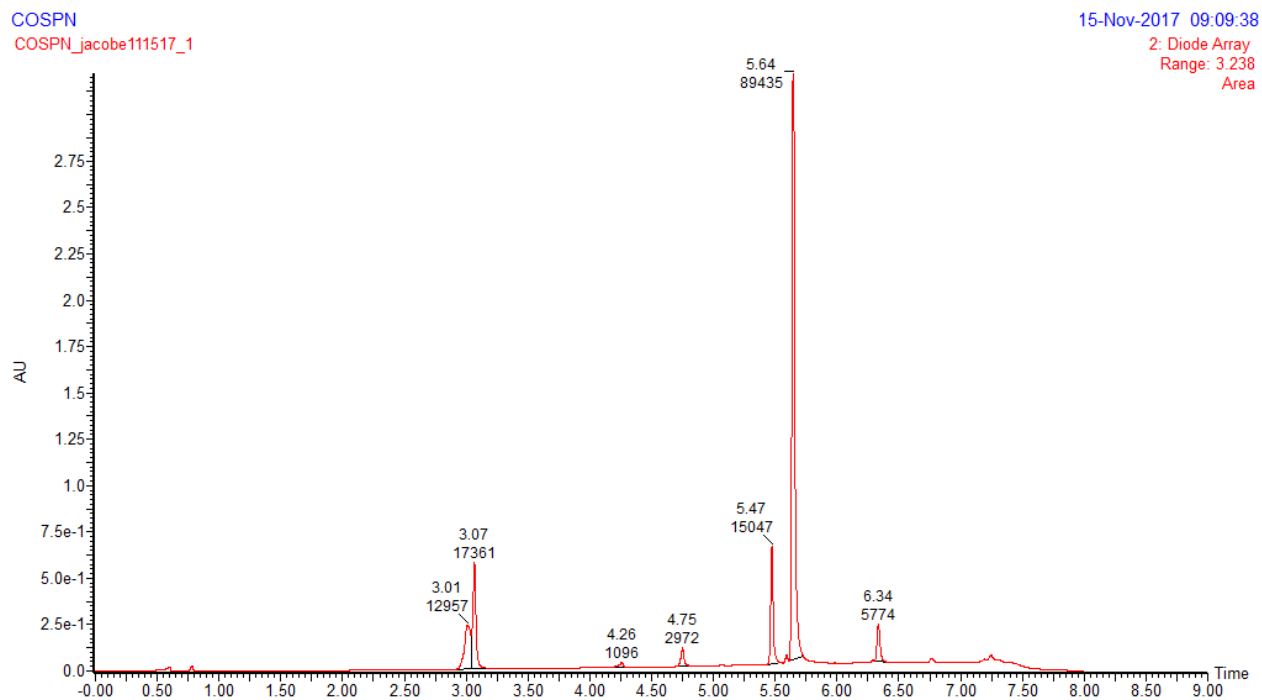


Figure 190: LC/UV (EtOH/Hexane) of COSPN showing degradation.

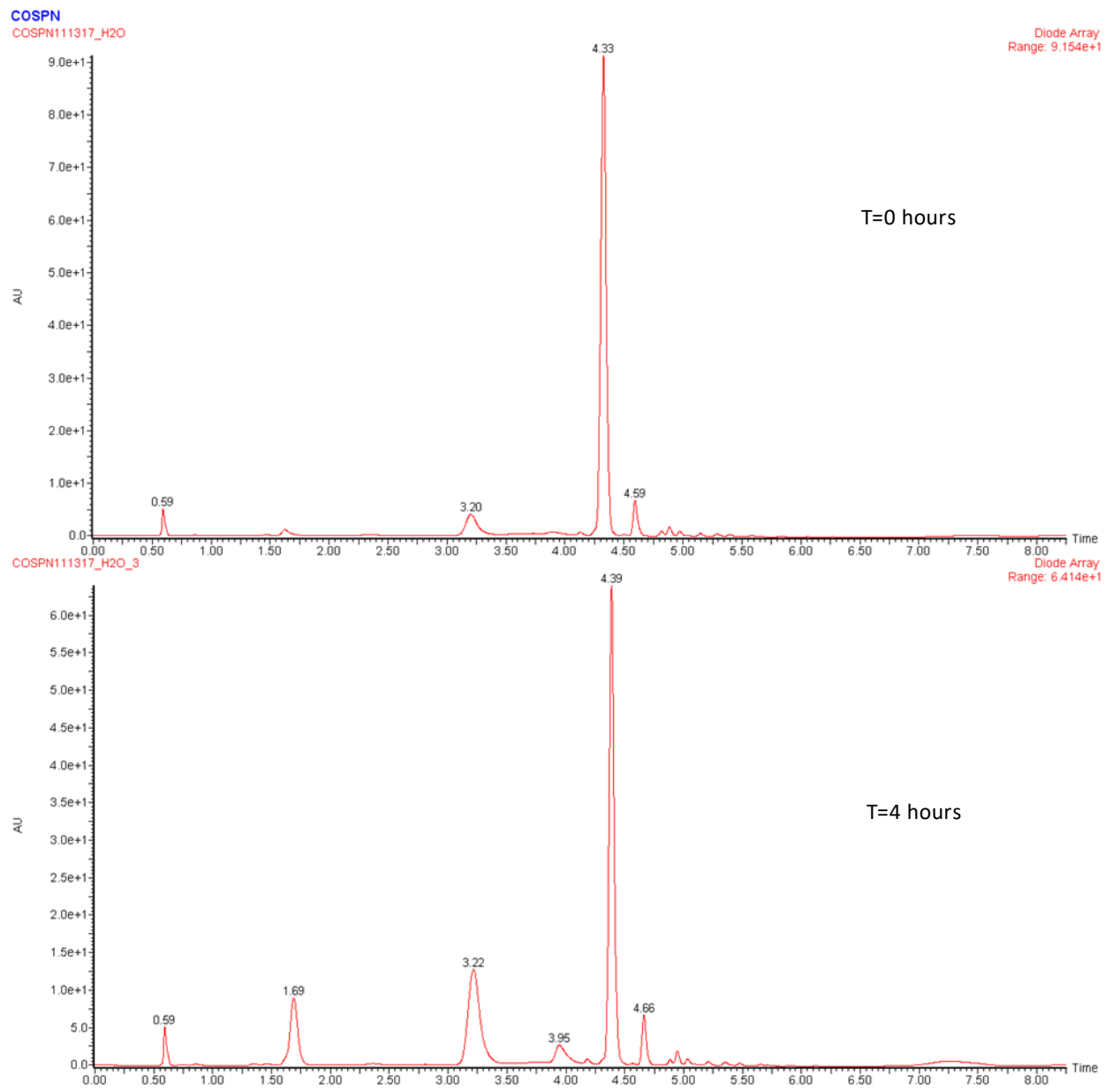


Figure 191: Supercritical fluid chromatography (EtOH/Hexane) of COSPN showing degradation in wet solvent; top: initial, bottom: after 4 hours.

## 14 Appendix B: Thermogravimetric Data

Table 24: Dynamic TGA of PN materials.

Polymer	Wt. % <i>p</i> -BAPS*	Gas	Max Cure	T <sub>5%</sub> (°C)	T <sub>10%</sub> (°C)	Residual at 780 °C (Wt. %)	Residual at 1000 °C (Wt. %)
COSPN-U	4	N <sub>2</sub>	375 °C/4 Hr.	448	532	69.5	-
COSPN-U	4	Air	375 °C/4 Hr.	455	512	13.6	-
CSPN-U	4	N <sub>2</sub>	350 °C/4 Hr.	528	567	68.9	65.7
CSPN-U	6	N <sub>2</sub>	300 °C/4 Hr.	451	498	64.1	-
CSPN-U	6	N <sub>2</sub>	350 °C/4 Hr.	519	553	71.1	68.0
CSPN-U	6	N <sub>2</sub>	375 °C/1 Hr.	519	552	70.5	67.6
CSPN-U	6	N <sub>2</sub>	375 °C/2 Hr.	525	557	71.9	68.9
CSPN-U	6	N <sub>2</sub>	375 °C/3 Hr.	526	557	72.7	69.7
CSPN-U	4	Air	350 °C/4 Hr.	487	519	9.37	9.23
CSPN-U	6	Air	350 °C/4 Hr.	482	520	8.56	7.65
CSPN-U	6	Air	375 °C/1 Hr.	493	531	8.77	8.51
CSPN-U	6	Air	375 °C/2 Hr.	497	537	9.85	9.05
CSPN-U	6	Air	375 °C/3 Hr.	497	535	8.97	8.49
CSPN-P	4	N <sub>2</sub>	350 °C/4 Hr.	487	516	62.9	60.3
CSPN-P	4	Air	350 °C/4 Hr.	461	492	8.91	8.42
CSOPN-P	4	N <sub>2</sub>	350 °C/4 Hr.	504	538	67.8	64.8
CSOPN-P	4	N <sub>2</sub>	375 °C/1 Hr.	512	546	68.2	66.2
CSOPN-P	4	N <sub>2</sub>	375 °C/2 Hr.	514	549	68.6	66.5
CSOPN-P	4	N <sub>2</sub>	375 °C/3 Hr.	519	554	69.4	67.5
CSOPN-P	4	Air	350 °C/4 Hr.	471	507	13.7	13.2
CSOPN-P	4	Air	375 °C/1 Hr.	478	518	16.3	16.1
CSOPN-P	4	Air	375 °C/2 Hr.	478	517	15.1	14.9
CSOPN-P	4	Air	375 °C/3 Hr.	485	527	15.5	14.8
PN1*	-	N <sub>2</sub>	371 °C	507	542	76.4	-
PN1*	-	Air	371 °C	518	553	0.97	-
PN2*	-	N <sub>2</sub>	350 °C/4 Hr.	456	489	63.9	62.5
PN2*	-	N <sub>2</sub>	375 °C/4 Hr.	486	520	76.6	-
PN2*	-	N <sub>2</sub>	400 °C/2 Hr.	502	537	79.0	-
PN2*	-	Air	350 °C/4 Hr.	451	486	2.34	-
PN2*	-	Air	375 °C/4 Hr.	472	499	1.70	-
1:1 PN2/ Silazane	-	N <sub>2</sub>	375 °C/5 Hr.	518	548	78.5	77.2

Includes data from Koerner and Gibson et al.<sup>96, 138</sup>

\*If applicable. Polymers with – in this column used other catalysts.